

Healthy rice products - understanding the effect of protein-starch matrices during digestion.

A thesis submitted to the University of Nottingham for the Degree of Doctor of Philosophy

Qingsu Liu

PhD Chemical Engineering, H80P

Faculty of Engineering, Research Group: Food, water and waste

Abstract

White rice is one of the most cultivated and consumed rice types worldwide and is growing in popularity as an ingredient in gluten-free products. However, white rice consumption can significantly affect glycaemic homeostasis due to its high and rapidly digestible starch content, which may pose health risks if not managed properly. There is an increasing need to understand better how rice microstructure may influence rice starch's conversion to glucose during digestion and the relationship between rice microstructure and its health-benefiting properties. Therefore, this thesis presents a comprehensive investigation of the relationship between the cooked white rice microstructure and the *in vitro* digestibility. An emphasis is placed on the influence of the rice protein network, which entraps starch granules in "protein-starch matrices," on controlling starch digestibility. Moreover, the addition of low acyl gellan gum (LAGG) was evaluated as an innovative approach to further reduce starch digestibility upon rice cooking by simulating the starch entrapment mechanism used by the proteins in the protein-starch matrices. The primary objectives of this study were i) to investigate the complex interaction between the microstructure of white rice and *in vitro* starch digestion and ii) to identify the feasibility of developing innovative rice-based formulations with a low-glycaemic index potential.

This study begins with investigating how microstructure influences the textural characteristics and *in vitro* oral starch digestion of two types of white rice, non-parboiled white jasmine rice (JR) and parboiled white rice (PR), from high- and low-glycaemic index (GI) categories, respectively. Despite the similar total starch content, PR had higher amylose and protein content than JR; moreover, PR had more compact protein-starch matrices than JR, which has limited starch gelatinisation capacity during the cooking process. Additionally, LAGG addition was investigated for its effects on the physicochemical and microstructural attributes of cooked rice. LAGG induces a distinct viscosity increase of JR and a change in its thermal properties by hindering starch gelatinisation. Microstructural alterations, such as the formation of β-sheet structures and V-type starch-LAGG complexes,

were also observed, with microscopic analysis confirming a coating on the rice grain surface. All these changes were less evident in PR, perhaps due to the already partially denatured protein network and pre-gelatinised starch, forming more compact protein-starch matrices. This increased compactness of the matrices in PR can act as a physical barrier between digestive enzymes and starch, thus decreasing starch digestibility, and modifying the starch digestion kinetics. In parallel, the addition of LAGG on cooked JR or PR resulted in promising for reducing starch digestibility by mirroring the encapsulating effect of a protein network.

The study extends to the digestion kinetics, which were quantitatively evaluated by a static *in vitro* digestion model combined with a multi-enzyme system which progressively removed rice protein networks, revealing two-phase starch digestion patterns. Starch digestibility became higher when the protein network was previously physically disintegrated by homogenisation. As the homogenisation process was prolonged, the degree of granular-scale disintegration was increased, as well as enzymatic accessibility and protein and starch digestibility.

It is important to note that starch digestibility is affected by the *in vitro* digestion conditions adopted. In this thesis, a semi-dynamic *in vitro* digestion model, characterised by controlled pH changes in the gastric phase and simulated peristalsis, was also used. Compared to the static digestion model, the effect of homogenisation (oral processing simulation) on starch digestibility became less evident in the semi-dynamic model due to the constant structure disintegration provided by the simulated peristalsis. However, LAGG-cooked rice displayed lower starch digestibility under both digestion models than non-LAGG controls, indicating LAGG multi-functionality (viscosity increase- and physical barrier properties) in mitigating starch digestibility.

Based on the above findings, a gluten-free orzo-shaped pasta with low predicted glycaemic index (pGI) potential was developed from rice flour, incorporating rice protein and/or LAGG. Formulations including LAGG and/or protein exhibited altered pasting properties due to limited starch gelatinisation and formation of starch/LAGG

complexes, resulting in reduced starch digestibility and improved cooking quality and texture.

Overall, this collective research provided insight into the role of rice microstructure (specifically the protein-starch matrices) and the addition of LAGG in controlling starch digestibility. This approach would offer a pathway to innovate and develop healthier rice-based products.

Keywords: rice-based product, low acyl gellan gum, protein-starch matrices; *in vitro* digestibility.

Acknowledgement

It has been a great experience for me to complete this PhD thesis after four years of work at the University of Nottingham, as well as a remarkable chapter in my life. Towards the end of my PhD journey, I would like to express my gratitude to all who contributed to its realisation.

I would like to express my sincere gratitude to my supervisor team, Prof. Nicholas James Watson, Dr. Vincenzo Di Bari and Dr. Eleanor Binner for the continuous support of my PhD study and related research, for their patience, motivation, and immense knowledge. Their guidance helped me in all the time of research and writing of this thesis. I could not have imagined having a better advisor and mentor for my PhD study.

I would also like to thank my thesis committee: Dr. Joanne Gould, and Dr. Tom Mills for their insightful comments and encouragement, but also for the hard questions which incented me to widen my research from various perspectives.

I am very grateful to University of Nottingham for funding my research, Food, Water, Waste Research Group, Faculty of Engineering and Division of Food Sciences for providing me with the resources and facilities needed for this study.

A special thanks to my family. Words cannot express how grateful I am to my mother, father for all of the sacrifices that you've made on my behalf. Your support for me was what sustained me thus far. I would also like to thank Dr. Gleb Yakubov. My friends and colleagues Dr. Wang Yan (Luby), Dr. Filippo Bramante, Dr. Daniel Amor, Dr-to-be. Malgorzata Walczak, and Ms. Farrah Humberstone for their encouragement, support, and for always being there for me. I am grateful for Lieutenant Columbo's presence as my white noise throughout the day and night when I was working on my thesis. The final point that I would like to make is that I acknowledge with deep reverence all those who have supported me in their own special manner throughout my life. This thesis is dedicated to all of you.

Qingsu Liu 

Table of Contents

Abstract i
Acknowledgement iv
Table of Contents v
Table of Figures ix
List of Tables xi
Table of abbreviations xiii
1 General introduction 1
1.1 Introduction 1
1.2 Research aims and objectives 5
1.3 Thesis overview 6
1.4 References 7
2 Literature review 11
2.1 Introduction 11
2.2 Structure of rice grain 12
2.3 Can white rice pose a health risk? 14
2.4 Rice bolus to digesta: oral-gastrointestinal digestion and grain structural disintegration 16
2.4.1 Enzymatic reactions 17
2.4.2 Macroscopic level 18
2.4.3 Mesoscopic level 22
2.4.4 Nanoscopic level 24
2.5 The role of GI in diet: measurement *in vivo*, applications and limitations 25
2.5.1 Physiological definition of GI (in vivo) 25
2.5.2 Physiological effects of low-GI diet on health 26
2.5.3 Current understanding of GI data 28
2.5.4 Limitations of the in vivo GI measurements 28
2.6 *In vitro* digestion models 29
2.6.1 Model types, applications, and limitations 29
2.6.2 Kinetic models for characterising starch digestion behaviour 39
2.7 Recent trends in rice-based food design with a reduced GI potential 41
2.7.1 Rice varieties with slow starch digestibility 41
2.7.2 Imitating the food matrices to reduce starch digestibility 42
2.7.3 Providing low-GI properties to white rice by structuring with hydrocolloids - an example of low acyl gellan gum (LAGG) 43
2.8 Summary of literature review 46
2.9 References 47
3 Materials and methods 59
3.1 Materials: sample selection 59
3.2 Sample preparation 62
3.2.1 Rice flour production and respective starch isolation 62
3.2.2 Morphological properties of rice flour and starch 63
3.3 Physicochemical properties 64
3.3.1 Pasting properties measured with Rapid Visco Analyser (RVA) 64
3.3.2 Thermal properties of rice measured by Differential Scanning Calorimetry (DSC) 66
3.3.3 Hydration properties of rice 68
3.4 Rice cooking method 69
3.5 Proximate composition analysis 70

3.6 Microstructural properties 71
3.6.1 Fourier Transform Infrared Spectroscopy (FTIR) 71
3.6.2 X-ray diffraction (XRD) 73
3.6.3 Morphological observations 73
3.7 Textural properties 75
3.8 *In vitro* digestion models 75
3.8.1 Simulated digestion fluid preparation. 75
3.8.2 Oral phase 76
3.8.3 Rice bolus disintegration 77
3.8.4 Static in vitro digestion model 78
3.8.5 Semi-dynamic digestion model 81
3.8.6 Quantitative evaluation of digested starch 85
3.8.7 Quantitative evaluation of digested protein 85
3.8.8 Analyses of starch digestion kinetics and predicted glycaemic indexes. 87
3.9 Statistical analysis 90
3.10 References 90
4 The physicochemical and microstructural effects of low acyl gellan gum on the protein-starch matrices of cooked white rice: Impact on textural properties 95
Abstract 96
Highlights 97
4.1 Introduction 98
4.2 Materials and methods 101
4.2.1 Materials 101
4.2.2 Rice flour production and extraction of starch 101
4.2.3 Morphological Properties of rice flour and starch 102
4.2.4 Preparation of cooked rice with and without LAGG 102
4.2.5 Thermal properties 105
4.2.6 Hydration properties 105
4.2.7 Microstructural properties 106
4.2.8 Textural properties of cooked rice samples 108
4.2.9 Statistical analysis 110
4.3 Results 110
4.3.1 Proximate composition and morphological properties of raw rice 110
4.3.2 Pasting properties of rice dispersion with and without LAGG 112
4.3.3 Thermal properties of rice dispersion with and without LAGG 117
4.3.4 Hydration properties of rice dispersion with and without LAGG 121
4.3.5 The secondary structure of rice protein and the short-range ordered structure of starch 123
4.3.6 Crystalline structure 129
4.3.7 Proximate composition and morphological properties of cooked rice 132
4.3.8 Textural profile and oral digestion (in vitro) of cooked rice. 138
4.4 Conclusions 142
4.5 References 144
5 An evaluation of *in vitro* digestion of protein-starch matrices in cooked rice containing low acyl gellan gum using a multi-enzyme approach 153
Abstract 154
Highlights 155
5.1 Introduction 156
5.2 Materials and methods 159
5.2.1 Material 159
5.2.2 Preparation of cooked rice samples 160
5.2.3 Proximate analysis of cooked rice samples with and without LAGG 160

5.2.4 In vitro digestion experiments 161
5.2.5 Quantitative evaluation of starch and protein digestion 165
5.2.6 Analyses of starch digestion kinetics and predicted glycaemic index 167
5.2.7 170
5.2.8 Measurement of the particle size distribution in digested fluid 170
5.2.9 Statistical analysis 170
5.3 Results 171
5.3.1 Sample condition 171
5.3.2 Protein digestion 173
5.3.3 Food model case 1: starch digestibility of cooked grain 182
5.3.4 Food model case 2: Protein and starch digestibility of cooked and homogenised rice 191
5.3.5 Starch digestibility profiles and predicted GI 192
5.4 Conclusion 195
5.5 References 196
5.6 Supplementary material 202
6 An *in vitro* study of protein and starch digestibility in rice cooked with low acyl gellan gum evaluated using static and semi-dynamic digestion models 214
Abstract 215
Highlights 216
6.1 Introduction 217
6.2 Materials and methods 219
6.2.1 Materials 219
6.2.2 Preparation of cooked rice samples 220
6.2.3 Proximate composition of cooked rice with and without LAGG 221
6.2.4 Morphological structure of cooked rice with and without LAGG 221
6.2.5 Oral in vitro digestion of cooked rice with and without LAGG 222
6.2.6 In vitro digestion models 223
6.2.7 Quantitative evaluation of digested starch 231
6.2.8 Quantitative evaluation of digested protein 232
6.2.9 Analyses of starch digestion kinetics and predicted glycaemic indexes. 233
6.2.10 Rice bolus disintegration 234
6.2.11 Statistical analysis 234
6.3 Results 236
6.3.1 Proximate composition and granular morphology of cooked grains 236
6.3.2 Morphology of cooked rice with and without LAGG 236
6.3.3 Texture properties of cooked rice with and without LAGG 238
6.3.4 In vitro oral digestion of cooked rice with and without LAGG 240
6.3.5 Rice bolus disintegration behaviour 243
6.3.6 In vitro digestion of cooked rice with and without LAGG 247
6.4 Conclusions 258
6.5 References 258
7 Understanding the structure, texture, and digestion of rice-based formulations incorporated with rice protein and low acyl gellan gum 264
Abstract 265
Highlights 266
7.1 Introduction 267
7.2 Materials and Methods 270
7.2.1 Materials 270
7.2.2 Preparation of rice flour (RF) 271
7.2.3 Preparation of orzo pasta using a Rice-based formula 271
7.2.4 Pasting properties of orzo pasta 273

7.2.5 Orzo pasta cooking method and evaluation of cooking quality 274
7.2.6 Proximate analysis of cooked orzo pasta..... 274
7.2.7 Structural properties of cooked orzo pasta..... 275
7.2.8 Texture properties of cooked orzo 277
7.2.9 Oral processing simulation and granulometry distribution analysis..... 277
7.2.10 In vitro digestion and quantitative evaluation of protein and starch digestion 278
7.2.11 Quantification of digested protein and starch..... 279
7.2.12 Statistical analysis..... 280
7.3 Results 280
7.3.1 Proximate composition and cooking quality of orzo pasta..... 280
7.3.2 Pasting properties of rice-based formulations..... 284
7.3.3 IR characterisation of structural differences in cooked orzo..... 288
7.3.4 XRD pattern of cooked orzo 292
7.3.5 Morphology of cooked orzo 293
7.3.6 Textural properties of cooked orzo 296
7.3.7 In vitro digestion (static model) 299
7.3.8 In vitro digestion (semi-dynamic model)..... 304
7.4 Conclusion 308
7.5 References 308
8 General discussions, conclusions, and recommendations for future work ... 316
8.1 General discussions and conclusions.....316
8.1.1 The protein-starch matrices play a role in regulating rice starch digestibility in vitro 317
8.1.2 Disruption of the macroscopic-scale structure in rice increased starch digestibility during in vitro digestion..... 319
8.1.3 Modifying the protein-starch matrices microstructure may affect in vitro starch digestibility..... 319
8.1.4 LAGG addition decreased starch digestibility. 320
8.1.5 A food model system (rice-based orzo pasta) with reduced pGI was produced based on the findings in this thesis 320
8.2 Novelty of the research 321
8.3 Recommendation of future work.....322
8.4 References 325

Table of Figures

Fig. 2.1. Rice grain structure. 13
Fig. 2.2. Schematic of the anatomical hierarchy of rice structures in nature and the disassembly of these structures during human digestion and *in vitro* digestion model (based on the INFOGEST procedure). 17
Fig. 2.3. Mechanism of Enzyme Action. 18
Fig. 2.4. Multi-scale structure of rice and starch. 19
Fig. 2.5. The protein-starch matrices observed in cereals. 20
Fig. 2.6. Physiological benefits associated with the consumption of low-GI foods. 27
Fig. 2.7. Schematic illustration of the three possible starch digestion patterns in a heterogeneous environment. 41
Fig. 2.8. The molecular structure of (A) high acyl gellan gum and (B) low acyl gellan gum. 45
Fig. 2.9. A schematic illustration of how low acyl gellan gum undergoes conformational transitions 46
Fig. 3.1. PCA scores and loading plots of GI and main nutrient contents of the six white rice types. 60
Fig. 3.2. Flowchart of the starch and protein separation process from rice flour used in this study. 63
Fig. 3.3. Pasting profile of rice measured using the standard American Association of Cereal Chemists (AACC) method. 65
Fig. 3.4. Working mechanism of a DSC instrument. 67
Fig. 3.5. Schematic of bolus disintegration model. 77
Fig. 3.6. Overview of the semi-dynamic *in vitro* digestion model setup. 81
Fig. 3.7. Schematic of the change in gastric pH during semi-dynamic gastric phase. 84
Fig. 3.8. Kinetic models applied on starch digestibility curve. 88
Fig. 4.1. Morphology of raw flour and starch isolates. 111
Fig. 4.2. RVA profiles of rice with and without 1-3 % LAGG. 113
Fig. 4.3. DSC curves. 118
Fig. 4.4 (Part I). The amide I and starch fingerprint region spectra taken from the FTIR spectra. 124
Fig. 4.4 (Part II). The amide I and starch fingerprint region spectra taken from the FTIR spectra. 125
Fig. 4.5 (Part I). XRD diffraction patterns. 130
Fig. 4.5 (Part II). XRD diffraction patterns (following by P147). 131
Fig. 4.6. SDS-PAGE profile of JR and PR proteins from rice raw and cooked with 0-3 % LAGG. 135
Fig. 4.7. Morphology of JR cooked with 0-3 %LAGG. 136
Fig. 4.8. Morphology of PR cooked with 0-3 %LAGG. 137
Fig. 4.9. Textural properties (hardness, cohesiveness, adhesiveness, and chewiness) of JR (A) and PR (B) cooked in 0-3 % (w/w) LAGG dispersions in water. 138
Fig. 4.10.Distribution of particle sizes in bolus of cooked JR and PR with 0-3 % (w/w) LAGG addition after homogenization for 10 s (A) or 20 s (B). 140
Fig. 4.11. Starch digestibility after the *in vitro* oral phase 141
Fig. 5.1. Schematic representation of the seven static *in vitro* digestion sets. 162
Fig. 5.2. Schematic of kinetic models applied on starch digestibility curve. 168
Fig. 5.3. SDS-PAGE patterns of rice proteins under (A) non-reducing and (B) reducing conditions. 172

Fig. 5.4. Microstructural comparison of JR grain (upon gastric digestion with pepsin) following 2h incubation with (B) (Set 6_PTA) or without (A) (Set 5_PTA_con) trypsin proteolysis. 177
Fig. 5.5. *In vitro* starch digestion of cooked JR grains. 184
Fig. 5.6. Scanning electron micrograph of (A) JR, (B) JR_1LA, (C) PR and (D) PR_1LA. 190
Fig. 5.7. pGI (A), imaging (B), and particle size distribution (C) of cooked digested rice, non-homogenised or homogenised for 20 seconds, as evaluated after Set 7_HPP. 193
Fig. 6.1. Overview of the semi-dynamic *in vitro* digestion model setup. The image shows blank fluid (solution with enzyme, but no sample) within the system. 227
Fig. 6.2. An illustration of the gradual change in gastric pH during the semi-dynamic gastric phase 230
Fig. 6.3. Schematic representation of bolus disintegration model. 234
Fig. 6.4. Morphology of cooked rice grains. 238
Fig. 6.5. Radar charts showing the textural characteristics of cooked rice with and without LAGG. 239
Fig. 6.6. The particle size distribution of cooked rice with and without LAGG after oral processing *in vitro* simulation. 241
Fig. 6.7. *In vitro* oral phase starch digestibility of cooked rice grain with and without 1 % LAGG after homogenisation (0 s, 10 s and 20 s). 243
Fig. 6.8. Rice bolus disintegration of cooked rice with and without LAGG in the simulated acidic (pH 3) gastric-like environment. The overlaid images of the bolus were captured at the beginning and end of the stay in the experiment site before falling off. 246
Fig. 6.9. Starch digestibility of cooked grains with and without LAGG. 247
Fig. 6.10. Protein digestion in cooked rice grains with and without LAGG. 248
Fig. 6.11. *In vitro* semi-dynamic starch digestibility of cooked grains with and without LAGG. 253
Fig. 6.12. *In vitro* semi-dynamic protein digestibility of cooked grains with and without LAGG 254
Fig. 7.1. Schematic of the orzo formation and cooking process. 273
Fig. 7.2 Pasting profile (cP) of rice-based formulations incorporated with RP and LAGG as a function of time (s). 284
Fig. 7.3 The characteristic FTIR spectra patterns of cooked GFO made with rice-based formula incorporated with RP and LAGG (D). 288
Fig. 7.4. XRD patterns for cooked GFO incorporated with RP and/or LAGG samples. 293
Fig. 7.5. Morphology of cooked GFO incorporated with RP and/or LAGG. 295
Fig. 7.6 Radar chart of the texture profiles of GFO made with rice-based formula incorporated with RP and LAGG. 297
Fig. 7.7 Particle size distribution curves of cooked rice-based GFO pasta obtained after 20 s homogenisation (*in vitro* oral process simulation). 297
Fig. 7.8. Oral and gastric starch digestibility of cooked orzo evaluated after 20 s homogenisation. 299
Fig. 7.9 *In vitro* digestion curves (the concentration of digested starch over time) obtained for cooked rice-based GFO incorporated with RP and LAGG (via dough-making or cooking) 302
Fig. 7.10 Evolution of the digesta viscosity and *in vitro* starch digestion versus time in the gastric and intestinal phase. 306
Fig. 8.1. Schematic of the orzo pasta microstructure, inspired by PR and cooked with LAGG in six different formulations. 321

List of Tables

Tab. 2.1. Comprehensive comparison between *in vitro* and *in vivo* models. 33
Tab. 2.2. Multicompartmental dynamic *in vitro* models (main dynamic features, applications, and limitations). 36
Tab. 3.1. Nutritional information (as listed on the food label) and GI of the six commercial white rice types. 61
Tab. 3.2. Simulated fluid formulations (stocks, 1.25X concentration). 75
Tab. 3.3. Example of a static *in vitro* digestion experiment 79
Tab. 4.1.Chemical composition of raw JR and PR flour and their isolated starch (g/100g). 111
Tab. 4.2. Pasting properties of rice starch and rice flour with and without LAGG addition. 114
Tab. 4.3. Thermal properties upon heating (Section 4.2.) of JR and PR flours in 0-3 % LAGG dispersions and of JRS and PRS in water. 120
Tab. 4.4. Thermal properties upon cooling (Section 4.2.) of JR and PR flours in 0-3 % LAGG dispersions and of JRS and PRS in water. 121
Tab. 4.5. Hydration properties, SP (g/g) and WSI (%), of JR and PR flours in 0-3 % LAGG dispersions and JRS and PRS in water. 122
Tab. 4.6 Secondary protein and starch structure values taken from normalised FTIR spectra of cooked JR and PR with and without 1-3 % LAGG (w/w). 128
Tab. 4.7. Proximate composition (g/100 g total sample) and morphological properties of cooked JR and PR with and without 1-3 % (w/w) LAGG..... 133
Tab. 5.1. Product code and experimentally measured activity for salivary α-amylase, pepsin, pancreatic α-amylase, trypsin, and pancreatin (consisting of pancreatic α-amylase and trypsin) used in this study. 160
Tab. 5.2. Proximate analysis (g/100g) and mechanical properties of cooked JR, JR_1LA, PR, and PR_1LA..... 172
Tab. 5.3. Kinetic parameters of DSPF (BCA method) and DH (OPA method) in cooked rice digested under different conditions, evaluated by fitting a pseudo-first-order association model (Case 1: intact rice)..... 175
Tab. 5.4. Kinetic parameters of DSPF (BCA method) and DH (OPA method) in cooked rice digested under different conditions, evaluated by fitting a pseudo-first-order association model (Case 2: homogenised rice). 180
Tab. 5.5. Kinetic fitting (LoS and CPS) with constant rates fitting for JR and PR with and without 1 % LAGG addition (intact rice)..... 185
Tab. 6.1. Product code, batch number and activity (measured in our labs) for salivary α-amylase, pepsin, and pancreatin (consisting of α-amylase and trypsin) used in this study. 220
Tab. 6.2. Example of a static *in vitro* digestion experiment for 5 g of cooked sample. 225
Tab. 6.3. Description of the semi-dynamic digestion model components..... 228
Tab. 6.4. Nutritional composition of cooked rice with and without 1 % LAGG (g/100g)... 236
Tab. 6.5. Fitting of the kinetic models for *in vitro* digestion (static model) cooked rice with and without LAGG after oral-gastrointestinal processing simulations (0 s, 10 s, 20 s)..... 252
Tab. 6.6. Fitting of the kinetic models for *in vitro* digestion (semi-dynamic model) cooked rice samples with and without LAGG under different oral processing simulations (0 s, 10 s, 20 s). 257
Tab. 7.1. Formulation design of the experiment..... 272
Tab. 7.2. Proximate composition (g/100 g total weight) and cooking quality of GFO made with studied formulas. 283

Tab. 7.3. Pasting properties of rice-based formulations incorporated with RP and LAGG through dough preparation (RF_1LA_1 and RFRP_1LA_1) and cooking (RF_1LA_2 and RFRP_1LA_2).....285
Tab. 7.4. Kinetic models for *in vitro* digestion (static model) of cooked orzo incorporated with RP and LAGG under oral processing simulations (20s homogenisation). 303
Tab. 7.5. Kinetic models for *in vitro* digestion (semi-dynamic digestion model) of cooked orzo incorporated with RP and LAGG under oral processing simulations (20s homogenisation).....307

Table of abbreviations

A.U.	Arbitrary units
AACC	American Association of Cereal Chemists
AGE	Advanced glycation end products
AM	Amylose
ANOVA	Analysis of variance
AOAC	Association of Official Agricultural Chemists
AP	Amylopectin
AUC	Area under the curve
BCA	Bicinchoninic acid
BD	Breakdown viscosity
BSA	Bovine serum albumin
CL	Cooking loss
CPS	Combination of parallel and sequential
DH	Degree of protein hydrolysis
DOC	Degree of crystallinity
DSC	Differential scanning calorimetry
DSPF	Digested soluble protein fragment
DTAF	5-(4,6-Dichlorotriazinyl) Aminofluorescein
ES	Enzyme-substrate
ESEM	Environmental scanning electron microscopy
ESIN	Engineered stomach and small intestinal
FAO	Food and Agriculture organisation
FDA	Food and drug administration
FTIR	Fourier transform infrared spectroscopy
FV	Final viscosity
GF	Gluten-free
GFO	Gluten-free orzo
GI	Glycaemic index
GIT	Gastrointestinal tract
GL	Glycaemic load
HI	Hydrolysis index
HTT	hydrothermally treated
IVD	*In vitro* digestion
JR	Jasmine white rice
JRS	Jasmine rice starch
LAGG	Low acyl gellan gum
LoS	Logarithmic of slope
MC	Moisture content
NCD	noncommunicable diseases
OCT	Optimal cooking time
OECD	Organisation for Economic Cooperation and Development

OPA	O-phthaldialdehyde
PAHBAH	P-hydroxybenzoic acid hydrazide
PCA	Principal component analysis
PR	Parboiled white rice
PRS	Parboiled rice starch
PT	Peak temperature
PV	Peak viscosity
RC	Random coils
RDS	Rapidly digestible starch
RDS	Rapidly digestible starch
RP	Rice protein
RR	Relative risk
RS	Resistant starch
RVA	Rapid viscos analyser
SD	Standard deviation
SAXS	Small angle X-ray scattering
SB	Setback viscosity
SDS	Slowly digestible starch
SDS-PAGE	Sodium dodecyl sulphate-polyacrylamide gel electrophoresis
SGF	Simulated gastric fluid
SHIME	Simulator of the Human Intestinal Microbial Ecosystem
SIF	Simulated intestinal fluid
SP	Swelling power
SSF	Simulated salivary fluid
TAME	Toluene-sulfonyl-L-arginine methyl ester
TP	Peak temperature
TPA	Texture profile analysis
TS	Total starch
WSI	Water solubility index
XRD	X-ray diffraction

1 General introduction

1.1 Introduction

Food's profound influence on human well-being has long been acknowledged, as highlighted by the popular adage "You are what you eat," attributed to Brillat-Savarin's seminal work, “Physiologie du Gout, ou Meditations de Gastronomie Transcendante” (The Physiology of Taste, or Meditations on Transcendental Gastronomy), which outlined the following: "Tell me what you eat, and I will tell you what you are". This phrase's contemporary resonance underscores the critical role of diet in shaping our physical composition and our behavioural and personality traits, transcending cultural and temporal boundaries (Han & Dingemanse, 2017; Chi et al., 2021). Nowadays, food occupies a middle ground between industrial/natural products, nutrition, and science. Most individuals expect that eating a healthy, balanced diet will improve or maintain physical and mental well-being. Unfortunately, due to the high consumption of refined and ultra-processed foods in today's society, diet-related health issues cause enormous economic losses and life quality impoverishment (Monteiro et al., 2018; Monteiro & Cannon, 2019; Dicken & Batterham, 2022). It has become necessary to know what, why, and how to eat due to these conflicts between health concerns and the availability of food products.

Therefore, there is an increasing scientific consensus on promoting plant-forward diets (diets with a high percentage of plant-based ingredients) to achieve positive health outcomes (Gibbs & Cappuccio, 2022). However, these diets tend to be high in carbohydrates due to high proportions of grains, legumes, and fruit. It is, therefore, unlikely that a plant-forward diet will provide the blood sugar control that many people experience while following a low-carbohydrate diet. A typical example is the consumption of white rice, a habitat staple food for more than half of the world's population (Jeevetha, 2014; van Dam, 2020). There is evidence that white rice contributes to nearly half of the daily caloric intake, with a greater proportion of this food in some plant-forward diets (Mohan et al., 2014; Bhavadharini et al.,

2020). Its remarkable commercial value and consumer acceptance are mostly due to its promising cooking qualities, appealing sensory properties, and long shelf life (Malabadi et al., 2022; Kasote et al., 2022). However, rice's high proportion of starch, which is rapidly digestible, can induce an acute glycaemic response while digested. This response makes rice a high-glycaemic index (GI) food and can be associated with increased risks for diabetes and diabetes-related conditions (Oba et al., 2010; Khosravi-Boroujeni et al., 2013; Bhavadharini et al., 2020).

The functional properties of food materials are mainly related to their nutrient digestibility and bioactivity. A growing body of knowledge has revealed the importance of assessing the nutritional value of foods by analysing their nutrients and considering how food structure impacts nutrient digestion and the health implications. It is becoming increasingly apparent that food microstructure is closely related to its functionality. Emerging evidence has suggested that the structure of plant-based food at various length scales (e.g., molecule, cell, tissue, and organ) is responsible for the digestion and accessibility of nutrients and bioactive molecules. The microstructural complexities of the food matrices, as well as the interactions among its constituents that occur during processing and digestion, provide a framework for evaluating physical (such as thermal, pasting) and sensory (textural, bolus-forming) properties as well as nutritional contributions (such as releasing nutrients and bioactive compounds as necessary). Knowing the relationship between food structure and function can contribute to designing and fabricating food structures that resemble nature to deliver nutrients with predictable bioaccessibility and bioadaptability. Similar concepts, such as "bio-mimic plant foods" (Do et al., 2018) or the food matrices reorganisation to facilitate nutrient delivery (Capuano et al., 2018; Aguilera, 2019; Li et al., 2021; Mondal et al., 2022) were proposed.

Natural plant-based foods offer many examples of fascinating biomimetic structures, which have been studied extensively. Research on microstructural features in starchy foods with low-GI, such as brown rice, legumes, or wholegrain pasta, has demonstrated that protein networks entrap starch granules and limit

starch digestion *in vitro* (Zou et al., 2016; Khatun et al., 2020; Do et al., 2023). The role of the starch structure in the modulation of enzymatic digestion has been the subject of intense research (Zhang et al., 2006; Zhang & Hamaker, 2009; Li et al., 2023). These findings have been used to develop starch-based products with reduced starch digestibility through the incorporation of proteins and their hydrates, using modified slowly digestible starch, as well as altering cooking techniques to maintain the protein-starch matrices integrity (Laleg et al., 2016; Lili et al., 2020; Culetu et al., 2021; Miraji et al., 2021).

Performing *in vivo* nutrient delivery evaluations is essential, but they can be challenging in a reproducible and accurate manner because of individual differences, especially in human subjects. Monitoring digestion during the gastrointestinal tract is highly complex, technically demanding, ethically restricted, and costly. Thus, most research (e.g., that referenced above) prefers to use *in vitro* models to simulate digestion for a better understanding of the digestion behaviour, nutrient bioaccessibility and bioacceptability.

Digestion systems exhibit a high level of physicochemical complexity but are still based on mechanical movements, similar to those used in food processing (Bornhorst & Singh, 2012; Bornhorst et al., 2016). For example, chewing and mixing in the upper digestive tract are analogous to the food industry's crushing, grinding, and homogenising processes. *In vitro* digestion models have evolved in many ways over the past three decades. The transition is from simplified static digestion, focusing on the enzymatic hydrolysis of nutrients and related kinetics, to dynamic models that mimic the anatomy, morphology, mechanical movement, and biochemical conditions of the human gastrointestinal tract (Bohn et al., 2018; Wu & Chen, 2020; Wang et al., 2021).

However, there is a need for a deeper understanding of how we eat. The complexity of food matrices and the further changes occurring during food cooking have significantly impacted nutrient digestion. For example, Tamura et al. (2016) investigated the necessity of simulating oral processing for starch digestion of cooked rice. They found that the rate of starch digestion increased significantly in

correlation with grain damage during cooking. Hardness-induced differences in bolus (chewed food mass before swallowing) have been demonstrated to affect starch and digestion kinetics in wheat (Wu & Warren, 2023) and wheat pasta (Blanquet-Diot et al., 2021; Li et al., 2021) and sorghum flour (Xu et al., 2022).

Recent advances have been made in understanding the influence of microstructural and biomimetic protein networks constraints on starch digestion in rice-based food products. However, the role of the intact protein-starch matrices presented in edible form (i.e., the cellular units, protein network, and starch granule) and their interactions limiting starch digestibility remain unclear and warrant further investigation. There is also little scientific evidence to explore the possibility of designing low-glycaemic foods by understanding the inhibitory effects of these structural properties on starch digestion. Within the scope of the thesis topic, the research studies focused on developing white rice-based foods with reduced GI potential by i) observing the protein-starch matrices of two specific white rice types with distinct GI; ii) examining and understanding the strength and performance of their protein-starch matrices in cooked rice form in inhibiting starch digestion under simulated digestion conditions; iii) serve as mimic models for developing rice-based foods that inhibit starch digestion. The rice models were selected as they demonstrated differences in starch digestion properties and provided a chance to study protein and starch component factors affecting starch digestibility.

The research presented in this thesis compares two rice types from low and high-GI categories in detail to understand how the characteristics of protein, starch, and the combined matrices limit starch digestibility *in vitro*. Regarding the *in vitro* digestion system, besides considering different oral processing modes (only swallow, normal and fine mastication), a static model with multiple enzyme settings was also used to understand the general effect of protein hydrolysis on starch digestibility. An integrated semi-dynamic digestion model that incorporates gastric pH changes, peristalsis movement simulations, and viscosity monitoring was developed to provide more complex digestion conditions to evaluate the capability of the protein-starch matrices to reduce starch digestibility. This work presents an opportunity to

design better-informed food products that contain nature-like structures that can potentially reduce starch digestibility and GI.

1.2 Research aims and objectives

White rice and rice-based products are associated with many postprandial physiological effects. However, the mechanisms behind these effects still need to be fully understood, especially for cooked rice. The protein-starch matrices represent the predominant structure of white rice grains, and it should be studied at various structural levels, ranging from macroscopic down to nanoscopic/molecular level. It has been suggested that cooked rice structure may profoundly affect its degradation mechanism during digestion; however, the degradation mechanisms require better understanding.

The hypothesis underlying this thesis is that during digestion, white rice types that have different microstructures exhibit different physicochemical responses to each digestion phase (oral, gastric, and intestinal), resulting in different starch kinetics of hydrolysis in each phase.

Therefore, this thesis aimed to develop a low-GI rice-based food by imitating the native protein-starch matrices of cooked rice, known for its low-GI properties, and preserving the recreated structure using low acyl gellan gum. In this study, it was important to understand the role that the rice protein-starch matrices play in controlling the gelatinisation of starch, followed by enzymatic hydrolysis. Considering the relationship between rice structure and digestibility, the objectives of this thesis were:

- To understand the effect of cooking on the characteristics of the protein-starch matrices to starch digestibility in white rice (**Chapter 4**)
- To understand the effect of protein hydrolysis on the impact of starch digestibility in white rice (**Chapter 5**)
- By utilising a semi-dynamic digestion system to create a complex digestion scenario to understand the digestive response of cooked white rice (**Chapter 6**)

- To study the role of low acyl gellan gum in preserving the microstructure of white rice upon cooking.
- Based on the results of chapters 4, 5, and 6, develop a formulation to imitate the protein-starch matrices and create food with low-GI properties (**Chapter 7**)

1.3 Thesis overview

Chapter 2 provides a brief overview of the literature regarding the hierarchical assembly of rice grains and their structural disassembly during processing and human digestion. The chapter then explains the role of grain structure in controlling starch digestion at different hierarchical levels and length scales, from nanoscale to macroscale level, including molecular, cellular, and tissue levels. This chapter also reviews the literature about developing rice products with nature-like functionality to modulate macronutrient digestion and physiological response. An overview of the materials, technology, and methodology used to prepare the investigated samples is proposed in **Chapter 3**. Methods for analysing physicochemical (pasting, thermal and hydration) and microstructural properties of food models and the *in vitro* digestion systems used are also described in Chapter 3. Chapters 4 to 7 are the main results chapters of this thesis.

In **Chapter 4**, the role of the protein-starch matrices in two white rice types (high and low-GI) is studied to understand its effect on the physicochemical and microstructural changes occurring in rice before and after cooking. In addition, a food-grade hydrocolloid (low acyl gellan gum, LAGG)-water dispersion was used in formulations and/or as a cooking medium. Its potential effect on reducing protein-starch matrices disintegration was studied. Although advances have been made in understanding the protein-starch matrices in cooked rice (**Chapter 4**), the structure and mechanism of slow starch digestion remain unclear. The comprehensive investigation of rice protein network breakdown has been, to our knowledge, conducted for the first time and discussed in **Chapter 5**, utilising physical homogenisation (oral processing simulation) and a novel multi-enzyme iterative *in vitro* digestion method (gradual enzymatic hydrolysis closely resembling digestion

conditions *in vivo*). In addition to assessing protein digestion, starch digestibility resulting from these protein digestion processes was also evaluated. Furthermore, rice was also cooked with LAGG to evaluate the function of LAGG in preserving the integrity of the protein-starch matrices and reducing the digestibility of cooked rice starch and protein.

Chapter 6 presents a novel semi-dynamic digestion system capable of simulating more complex digestion processes (including pH changes in the gastric phase, peristalsis movement, and viscosity monitoring). Detailed information on viscosity provides new insights into the mechanisms underlying slow starch digestion involving increased viscosity that interferes with enzyme mass transfer. Also, rice cooked with LAGG was produced to evaluate the hydrocolloid role in reducing starch digestibility by increasing viscosity and preserving the integrity of the protein-starch matrices and the starch and protein in cooked rice.

Based on the three previous results chapters, the suggestions about the role of protein and LAGG in inhibiting starch digestion were used to develop rice-based products with low-GI potential. Therefore, **Chapter 7** investigates the effect of rice protein and LAGG on *in vitro* starch digestion in four different formulations of rice-based gluten-free orzo pasta (rice shape pasta), consisting of i) white rice flour, ii) a two-component mixture of white rice flour and LAGG; iii) a two-component mixture of white rice flour and rice protein isolates, iv) a three-component mixture of white rice flour, rice protein and LAGG. For these formulations, two cooking media, distilled water or LAGG- distilled water dispersion, were used.

Chapter 8 provides a general discussion of experimental results, conclusions, and future work directions.

1.4 References

Aguilera, J. M. (2019). The food matrix: implications in processing, nutrition and health. *Critical Reviews in Food Science and Nutrition*, *59*(22), 3612–3629. doi.org/10.1080/10408398.2018.1502743

Bhavadharini, B., Mohan, V., Dehghan, M. et al., (2020). White Rice Intake and Incident Diabetes: A Study of 132,373 Participants in 21 Countries. *Diabetes Care*, *43*(11), 2643. doi.org/10.2337/DC19-2335

Bohn, T., Carriere, F., Day, L. et al., (2018). Correlation between *in vitro* and *in vivo* data on food digestion. What can we predict with static *in vitro* digestion models? *Critical Reviews in Food Science and Nutrition*, *58*(13), 2239–2261. doi.org/10.1080/10408398.2017.1315362

Bornhorst, G. M., Gouseti, O., Wickham, M. S. J.et al., (2016). Engineering Digestion: Multi-scale Processes of Food Digestion. *Journal of Food Science*, *81*(3), R534–R543. doi.org/10.1111/1750-3841.13216

Bornhorst, G. M., & Singh, R. P. (2012). Bolus Formation and Disintegration during Digestion of Food Carbohydrates. *Comprehensive Reviews in Food Science and Food Safety*, *11*(2), 101–118. doi.org/10.1111/j.1541-4337.2011.00172.x

Bornhorst, G. M., & Singh, R. P. (2013). Kinetics of *in vitro* Bread Bolus Digestion with Varying Oral and Gastric Digestion Parameters. *Food Biophysics*, *8*(1), 50–59. doi.org/10.1007/s11483-013-9283-6

Capuano, E., Oliviero, T., Fogliano, V., & Pellegrini, N. (2018). Role of the food matrix and digestion on calculation of the actual energy content of food. *Nutrition Reviews*, *76*(4), 274–289. doi.org/10.1093/nutrit/nux072

Chi, X. (2021). You Are What You Eat: Predictive Model of Eating Habits and Health Outcomes. *Communications in Computer and Information Science*, *1513 CCIS*, 260–270. doi.org/10.1007/978-981-16-8885-0_21

Culetu, A., Duta, D. E., Papageorgiou, M.et al.,(2021). The Role of Hydrocolloids in Gluten-Free Bread and Pasta; Rheology, Characteristics, Staling and Glycemic Index. *Foods*, *10*(12). doi.org/10.3390/FOODS10123121

Dicken, S. J., & Batterham, R. L. (2022). Ultra-processed food: a global problem requiring a global solution. *The Lancet Diabetes and Endocrinology*, *10*(10), 691–694. doi.org/10.1016/S2213-8587(22)00248-0

Do, D. T., Singh, J., Johnson, S.et al.,(2023). Probing the Double-Layered Cotyledon Cell Structure of Navy Beans: Barrier Effect of the Protein Matrix on *In vitro* Starch Digestion. *Nutrients*, *15*(1). doi.org/10.3390/NU15010105

Do, D. T., Singh, J., Oey, I. et al.,(2018). Biomimetic plant foods: Structural design and functionality. In *Trends in Food Science and Technology* (Vol. 82, pp. 46–59). Elsevier Ltd. doi.org/10.1016/j.tifs.2018.09.010

Gibbs, J., & Cappuccio, F. P. (2022). Plant-Based Dietary Patterns for Human and Planetary Health. *Nutrients*, *14*(8). doi.org/10.3390/NU14081614

Han, C. S., & Dingemanse, N. J. (2017). You are what you eat: Diet shapes body composition, personality and behavioural stability. *BMC Evolutionary Biology*, *17*(1), 1–16. doi.org/10.1186/s12862-016-0852-4

Jeevetha, S. (2014). Relationship between Amylose Content and Glycemic Index of Commonly Consumed White Rice. *IOSR Journal of Agriculture and Veterinary Science*, *7*(9), 12–18. doi.org/10.9790/2380-07931218

Kasote, D., Sreenivasulu, N., Acuin, C. et al.,(2022). Enhancing health benefits of milled rice: current status and future perspectives. *Critical Reviews in Food Science and Nutrition*, *62*(29), 8099–8119. doi.org/10.1080/10408398.2021.1925629

Khatun, A., Waters, D. L. E., & Liu, L. (2020). The impact of rice protein on *in vitro* rice starch digestibility. *Food Hydrocolloids*, 109.doi.org/10.1016/J.FOODHYD.2020.106072

Khosravi-Boroujeni, H., Sarrafzadegan, N., Mohammadifard, N., et al., (2013). White rice consumption and CVD risk factors among Iranian population. *Journal of Health, Population and Nutrition*, *31*(2), 252–261. doi.org/10.3329/jhpn.v31i2.16390

Laleg, K., Barron, C., Santé-Lhoutellier, V., et al., (2016). Protein enriched pasta: structure and digestibility of its protein network. *Food & Function*, *7*(2), 1196–1207. doi.org/10.1039/C5FO01231G

Li, C. (2023). Starch fine molecular structures: The basis for designer rice with slower digestibility and desirable texture properties. *Carbohydrate Polymers*, *299*, 120217. doi.org/10.1016/j.carbpol.2022.120217

Li, H. T., Li, Z., Fox, G. P., Gidley, M. J., & Dhital, S. (2021). Protein-starch matrix plays a key role in enzymic digestion of high-amylose wheat noodle. *Food Chemistry*, *336*. doi.org/10.1016/j.foodchem.2020.127719

Malabadi, R., Kolkar, K., & Chalannavar, R. (2022). White and Brown Rice-Nutritional value and Health benefits: Arsenic Toxicity in Rice plants. *International Journal of Innovation Scientific Research and Review*, *4*, 3065–3082.ISSN2582-6131

Miraji, K. F., Linnemann, A. R., Fogliano, V., et al.(2021). Dry-heat processing at different conditions impact the nutritional composition and *in vitro* starch and protein digestibility of immature rice-based products. *Food and Function*, *12*(16), 7527–7545. doi.org/10.1039/D1FO01240A

Mohan, V., Spiegelman, D., Sudha, V., Gayathri, R., et al., (2014). Effect of Brown Rice, White Rice, and Brown Rice with Legumes on Blood Glucose and Insulin Responses in Overweight Asian Indians: A Randomized Controlled Trial. *16*(5), 317–325. doi.org/10.1089/dia.2013.0259

Mondal, D., Awana, M., Aggarwal, S., et al., (2022). Microstructure, matrix interactions, and molecular structure are the key determinants of inherent glycemic potential in pearl millet (Pennisetum glaucum). *Food Hydrocolloids*, *127* (2021), 107481. doi.org/10.1016/j.foodhyd.2022.107481

Monteiro, C. A., & Cannon, G. J. (2019). The role of the transnational ultra-processed food industry in the pandemic of obesity and its associated diseases: problems and solutions. *World Nutrition*, *10*(1), 89–99. doi.org/10.26596/WN.201910189-99

Monteiro, C. A., Cannon, G., Moubarac, J. C., et al., (2018). The UN Decade of Nutrition, the NOVA food classification and the trouble with ultra-processing. *Public Health Nutrition*, *21*(1), 5–17. doi.org/10.1017/S1368980017000234

Oba, S., Nagata, C., Nakamura, K., et al., (2010). Dietary glycemic index, glycemic load, and intake of carbohydrate and rice in relation to risk of mortality from stroke and its subtypes in Japanese men and women. *Metabolism*, *59*(11), 1574–1582. doi.org/10.1016/J.METABOL.2010.02.004

Tamura, M., Singh, J., Kaur, L., et al.,(2016). Impact of structural characteristics on starch digestibility of cooked rice. *Food Chemistry*, *191*, 91–97. doi.org/10.1016/j.foodchem.2015.04.019

Van Dam, R. M. (2020). A Global Perspective on White Rice Consumption and Risk of Type 2 Diabetes. *Diabetes Care*, *43*(11), 2625–2627. doi.org/10.2337/DCI20-0042

Wang, L., Zhao, S., Kong, J., et al., (2020). Changing cooking mode can slow the starch digestion of colored brown rice: A view of starch structural changes during cooking.

International Journal of Biological Macromolecules, *155*, 226–232. doi.org/10.1016/J.IJBIOMAC.2020.03.203

Wang, R., Mohammadi, M., Mahboubi, A., et al., (2021). *In vitro* digestion models: a critical review for human and fish and a protocol for *in vitro* digestion in fish. *Bioengineered*, *12*(1), 3040. doi.org/10.1080/21655979.2021.1940769

Wu, P., & Chen, X. D. (2020). On designing biomimic *in vitro* human and animal digestion track models: ideas, current and future devices. *Current Opinion in Food Science*, *35*, 10–19. doi.org/10.1016/J.COFS.2019.12.004

Wu, J., & Warren, F. J. (2023). The impact of the soluble protein fraction and kernel hardness on wheat flour starch digestibility. Food Chemistry, 406, 135047. doi.org/10.1016/J.FOODCHEM.2022.135047

Zhang, G., & Hamaker, B. R. (2009). Slowly digestible starch: Concept, mechanism, and proposed extended glycemic index. *Critical Reviews in Food Science and Nutrition*, *49*(10), 852–867. doi.org/10.1080/10408390903372466

Zhang, G., Venkatachalam, M., & Hamaker, B. R. (2006). Structural basis for the slow digestion property of native cereal starches. *Biomacromolecules*, *7*(11), 3259–3266. doi.org/10.1021/bm060343a

Zou, W., Sissons, M., Warren, F. J., et al.,(2016). Compact structure and proteins of pasta retard *in vitro* digestive evolution of branched starch molecular structure. *Carbohydrate Polymers*, *152*, 441–449. doi.org/10.1016/J.CARBPOL.2016.06.016

2 Literature review

2.1 Introduction

Rice (Oryza sativa) is one of the most essential food commodities in the world, with a cultivation history spanning over 80 centuries (Spengler et al., 2021). A staple food in Asian cuisine, it is also rapidly increasing in the Western diet due to its taste, nutritional value, and versatility. The Food and Agriculture Organisation (FAO) reported that rice supply has remained over 80 kilograms/capita/per year for the last decade since records were kept (FAO, 2021). Data from the Organisation for Economic Cooperation and Development (OECD) and FAO show that per capita consumption of rice is about 55 kilograms per year, equivalent to about 20 % of the calorie intake of the world's population and 50 % for people living in poverty (OECD, 2021). Among all rice varieties, white rice is the predominant form consumed worldwide (Kaur et al., 2015). post-harvest processes can further improve the texture and flavour of cooked white rice by facilitating starch gelatinisation during cooking and starch hydrolysis to maltose during chewing (Toutounji et al., 2019). The nutritional benefits of rice are not limited to its low-fat and sodium content, gluten-free nature makes it an ideal alternative to wheat flour, which is commonly used in baked goods such as bread, pasta, and foods for babies (Alvarez-Jubete et al., 2010; Kamlesh et al., 2010; Toutounji et al., 2019). It has been demonstrated that the hydrolysates and peptides produced by rice protein (glutelin and albumin) digestion are suppressive of proinflammatory cytokines, hyperglycemia and cholesterol levels (Yang et al., 2012; Kubota et al., 2013; Hoogenkamp et al., 2017). Rice also presents a more significant potential for new food products due to its versatility, as it can be eaten as whole grains, boiled or steamed. Alternatively, rice can be milled into flour or fermented to produce a variety of foods, such as desserts or yoghurt (Witczak et al., 2016).

However, the effects of its digestible starch on the glycaemic response (measured by the glycaemic index, GI) of humans have been linked to many metabolic syndromes. Besides the intrinsic characteristics of rice, different food processing

techniques are also known to impact its GI. As the GI of white rice has become an increasingly important marketing factor for manufacturers and consumers, current research focuses on producing functional rice products with reduced GI.

The chapter begins with a summary of the hierarchical structure characterising rice grains (**Section 2.2**), followed by a description of how the digestion of rice occurs in the oral-gastrointestinal tract. Different methods are discussed that can influence the physicochemical characteristics of rice to mitigate its starch digestibility. Evaluation *in vivo* of the glucose response to starch intake is inevitable, although there are limitations on the validity, reliability, and reproduction of the results, along with high costs and ethical concerns. *In vivo* systems exhibit a high level of physical-chemical complexity, but they are still based on mechanical movements similar to those already available in food processing (Bornhorst et al., 2016). Therefore, both *in vitro* and *in vivo* approaches are necessary to gain a deeper understanding of how food constituents contribute to digestibility, and they will be discussed in **Sections 2.4, 2.5,** and **2.6** of this chapter.

2.2 Structure of rice grain

Mature rice is harvested as paddy grains, i.e., a caryopsis where the endosperm is enclosed by hulls (husk) (Blakeney & Matheson, 1984). The caryopsis, known as brown rice (**Fig. 2.1**), is refined into the more widely consumed polished white rice. As a result of processing and milling, the outer layers of the caryopsis (represented by the husk and the bran) and the germ are removed. The bran layer is rich in fat, dietary fibres, minerals, and vitamin B complex; the germ is also rich in dietary fibre and fat. White rice grains can be further polished to improve their appearance, physicochemical, and eating quality. The removed aleurone layer contains fats, vitamins, minerals, and protein (Zhou et al., 2002; An et al., 2020), although in lower amounts than the bran. The endosperm is rich in starch (80 g/100 g), protein (7-8 g/100 g), fat (3 g/100 g) and fibre (3 g/100 g) (Elaine et al., 2006).

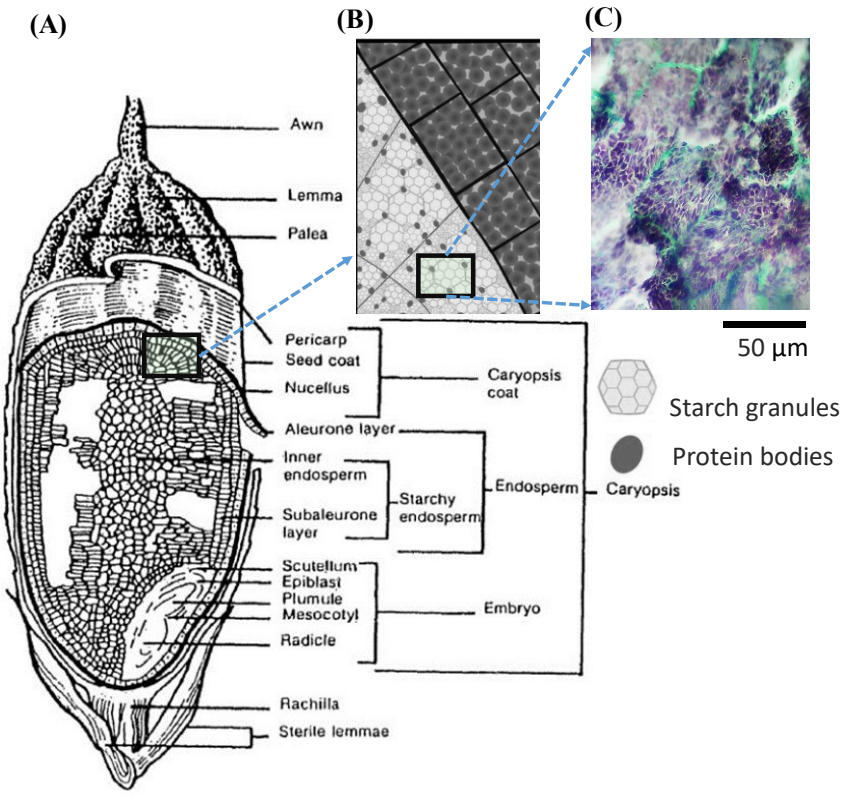


Fig. 2.1. Rice grain structure. Structures of: (A) paddy grain (Blakeney & Matheson, 1984), (B) endosperm (An et al., 2020), (C) protein-starch matrices (green in protein and purple in starch) of inner endosperm (white rice).

White rice, also known as milled rice, is the product of a paddy harvest that undergoes a series of processes, including dehulling, milling, and polishing. A variety of fractions are removed, including hulls, brans (which contain most of the lipids), and aleurone layers, resulting in a loss of lipid, protein, crude fibre, minerals, and vitamins while increasing the percentage of starch content (Shobana et al., 2011).

The hierarchical structure of a modular system (such as rice grains) can typically be classified into three different length scales (macroscopic, mesoscopic, and nanoscopic), which represent populations of food components, and are used as examples in this thesis. The macroscopic scale (100 μm-over 7.5 mm) is related to the whole rice grain or fractions of it; the mesoscopic scale (0.1-100 μm) is associated with single cells and their protein-starch matrices structures; the nanoscopic scale (less than 0.1 μm) refers from the whole organisation of starch granules, protein bodies, and lipid nanoparticles to the primary constituents of each (monosaccharides, amino acids, and fatty acids respectively). An understanding of

how the hierarchical structure is assembled would provide insight into the fate of rice during digestion (microstructural disintegration). This reduction in size of rice during digestion has been demonstrated in previous research (Bornhorst et al., 2013; Li et al., 2021). When rice enters the oral phase (macroscopic level, related to the whole rice grain or its fractions), its structural complexity and large particle size are dramatically reduced during mastication. Disintegration (mesoscopic level, associated with the single cells and their protein-starch matrices) of structural elements proceeds during gastrointestinal digestion, both mechanically and enzymatically. Starch digestion, therefore, occurs as a consequence of the rice grain being broken down into multiple cellular systems containing starch, allowing the liberation of the starch granules and conversion into monosaccharides eventually.

2.3 Can white rice pose a health risk?

Millions of people around the world rely upon rice for their primary source of energy and nutrition. However, this grain contains high levels of rapid-digestible starch, which has been linked to glycemic spikes and related health complications (Boers et al., 2015; Madhu et al., 2017). In fact, Bhavadharini et al. (2020) reported on the association of white rice consumption with the risk of diabetes based on the data of 132,373 participants in 21 countries. Based on the findings of the study, higher consumption of white rice (450 g per day, 3 cups of cooked white rice) is related to an increased risk of diabetes, compared with consumption of lower quantities of white rice (150 g per day, one cup of cooked white rice). White rice consumption was found to be associated with diabetes with the strongest correlation in South Asia, while in other regions, such as North America, Europe, and Africa, this association was modest or not significant. The type of white rice grown in these three regions, along with post-harvest practices such as parboiling and quick-cooking, may play a role in reducing the amount of rapidly digestible starch and alleviating the health risks associated with white rice consumption (Boers et al., 2015; Hamad et al., 2018; Sivakamasundari et al., 2020; Ngo et al., 2023). As part of its effort to simplify the understanding of how digestible properties of intrinsic starch contribute to postprandial glycemic response, FAO/WHO have suggested

using the glycemic index (GI) for categorising starch-rich foods such as white rice. The glycaemic index (GI) is a way to rank carbohydrate-containing foods and beverages according to how quickly they increase glucose levels in the bloodstream compared with a reference (glucose or white bread, with 100 % relative starch digestibility, i.e., GI equal to 100). Foods are normally classified as high (≥70), medium (56-69), and low (≤55) GI (details in **Section 2.4**).

It has been shown in several studies that high-GI foods may cause oxidative stress, hypersecretion of Insulin, and dyslipidaemia, all of which are associated with a wide range of health complications (Anderson et al., 2018; Lambadiari et al., 2020; Pawlak et al., 2001). Diet-related chronic diseases such as obesity, diabetes, cardiovascular disease, and certain cancers are more likely to develop in people who consume high-GI foods (Kaur & Singh, 2016; Saneei et al., 2017; Carcea et al., 2021).Meanwhile, a growing body of evidence supports that intake of staple foods with a low or medium GI positively impacts health and contributes to the prevention of commonly occurring non-communicable diseases (Jenkins et al., 2008; Schwingshackl & Hoffmann, 2013; Jukanti et al., 2020; Miller et al., 2024). As for white rice, the international GI table by Atkinson et al. (2021) revealed that the majority of varieties (cooked) have GI scores of 70 or higher, but that low-GI varieties, e.g., Bangladeshi rice, are also available.

Cooked rice's GI and its relationship to its starch digestion rate are influenced by a variety of intrinsic and extrinsic factors. Rice grain structure intrinsic characteristics, especially starch architecture, play a crucial role. A number of extrinsic factors are discussed in this study, which are related to post-harvest processes (industrial and domestic) and in particular physical processing, which can alter the grain microstructure of rice. Finally, how rice interacts with other components in food during digestion (food matrix effects) affects the digestibility of rice starch and further GI level.

2.4 Rice bolus to digesta: oral-gastrointestinal digestion and grain structural disintegration

The digestion process of rice starts with the mechanical rupture of the grains by chewing and mixing with saliva, contributing to the initial starch enzymatic degradation by α-amylase from human saliva. The rice "bolus" (the mass at the end of the chewing step) is then delivered to the stomach, where further degradation occurs by the combined effect of low pH, mixing by peristalsis and enzymatic action of pepsin (rice protein hydrolysis). Eventually, the rice "chyme" (the mass at the end of the gastric phase) is delivered to the intestine, where it undergoes the enzymatic action of pancreatin by which the food mass is decomposed into more basic components (such as glucose, amino acid or triglycerides). In the digestion process (as shown in **Fig. 2.2**), most of the rice grain structure is progressively degraded from the hierarchical macroscopic level during the oral phase to the macroscopic-mesoscopic level during the gastric phase and the nanoscopic level at the end of the intestinal phase. At the nanoscopic level, the compounds are ready to be absorbed by the intestine and contribute to an increase in the glycaemic response, which can be represented by the glycaemic index from a food digestion perspective (Kaur et al., 2016). Starch constitutes most of the dry weight of rice; it is the most abundant component in cooked rice (80-90 %) and is the main factor regulating digestion at the three observation levels.

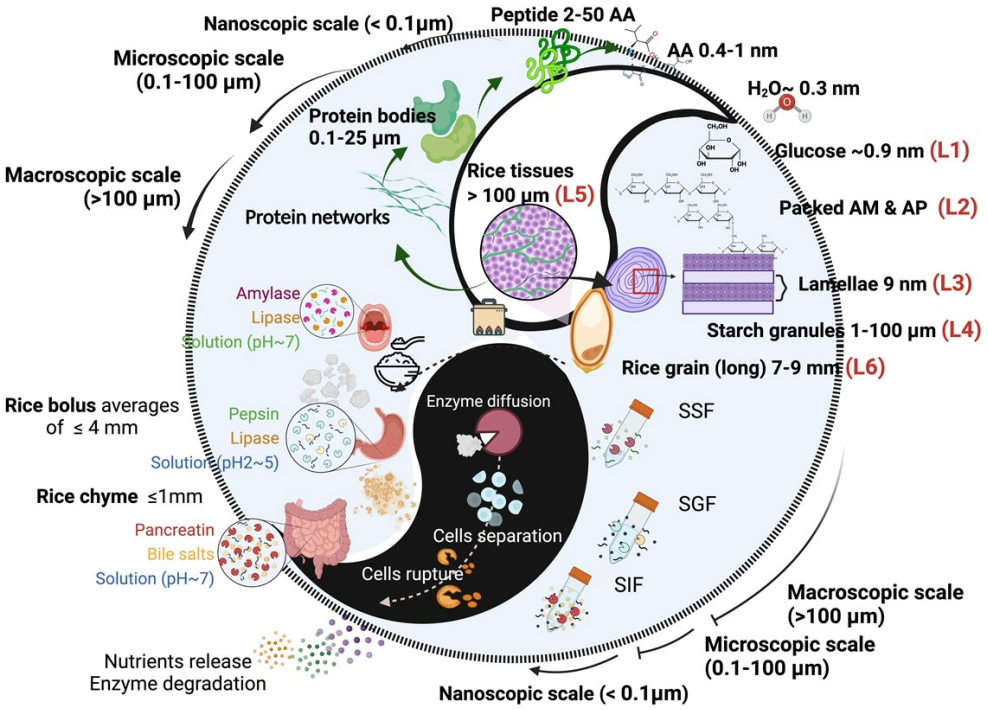


Fig. 2.2. Schematic of the anatomical hierarchy of rice structures in nature and the disassembly of these structures during human digestion and *in vitro* digestion model (based on the INFOGEST procedure).

2.4.1 Enzymatic reactions

Enzymes are protein-based complexes that play a vital role in the oral-gastrointestinal digestive system. As biological catalysts, enzymes accelerate chemical reactions that break down large food molecules into "building block" constituent parts. On a chemical level, enzymes are similar to other catalysts, i.e., they do not alter the thermodynamic equilibrium of chemical reactions and are mostly not consumed during the reaction (Shen et al., 2022). Unlike most other catalysts, enzymes possess a much greater degree of specificity. *In vivo*, different enzymes usually work together in systems, e.g., converting carbohydrates (substrates) into energy (products) (Chandel et al., 2021). Enzymes speed up the reaction through activation energy reduction. During most reactions, an unstable and highly energetic transition state is formed when substrates are converted into products. Enzymes also serve as templates for reactions, binding to each substrate and holding them in the proper position for the reaction. The enzyme also surrounds the substrate with reactive groups, stabilising the transition state and facilitating the reaction process (Tester et al., 2004). **Fig.2.3** depicts the role of enzymes (α-amylase)

in converting starch to maltose and dextrin. Despite being complex, enzymatic reactions *in vivo* can be characterised by three steps: enzymatic diffusion and adsorption, the formation of enzyme-substrate (ES) complexes stabilised by interactions including non-covalent or transient-covalent bonds, and the catalytic reaction (Butterworth et al., 2011). In this regard, the rate at which the glycaemic level rises could be regulated at any of these three steps.

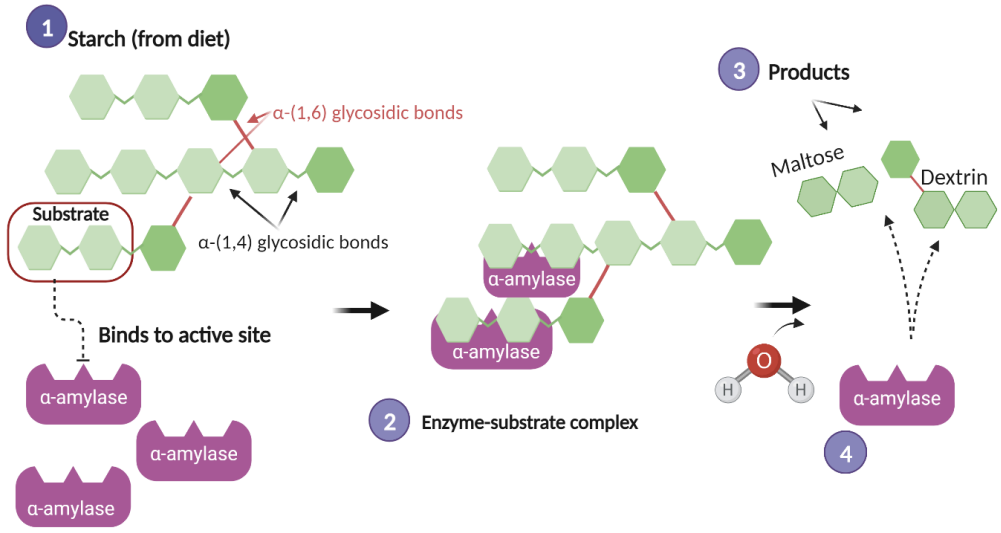


Fig. 2.3. Mechanism of Enzyme Action. Schematic showing the structure of an enzyme, including its active site, to which a substrate molecule binds to form an enzyme-substrate complex. When the reaction occurs, products are released from the active site.

2.4.2 Macroscopic level

At the macroscopic level (100 μm-over 7.5 mm), the substrate for starch digestive enzymes (amylases) is the intact rice grains or fractions. In the rice grain, the pores in the peripheral layer and interior channels (**Fig. 2.4a**) contribute to the speed and range of enzyme diffusion into the granules, thus affecting hydrolysis rates and extents.

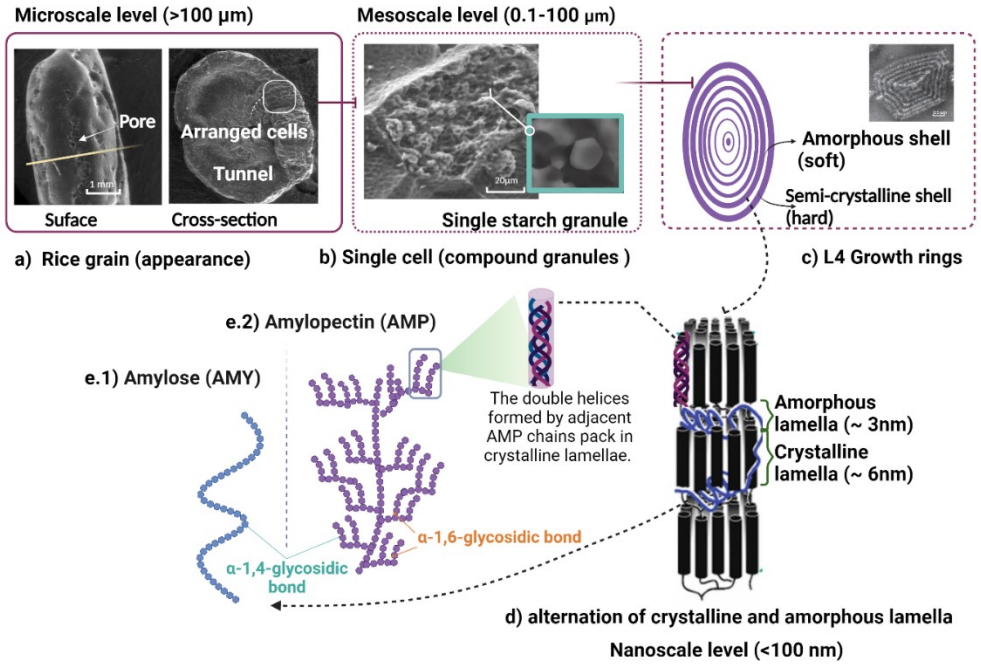


Fig. 2.4. Multi-scale structure of rice and starch. (a) intact rice grain (length 5-7 mm, width 1.5-3.0 mm, thickness 1.5-2.1 mm); (b) rice starch granules (1-100 μm); (c) starch amorphous (in white) and semi-crystalline (in purple) growth rings (or shells; 120–400 nm); (d) magnified detail of the semi-crystalline growth ring (9 nm), made of crystalline (6 nm) and amorphous (3 nm) lamellae; (e) amylopectin double helices forming the crystalline lamella, and amylose molecular structure forming the amorphous lamella (0.1–1 nm);. Adapted from Bao (2018) and Chi et al. (2021).

Therefore, processes that damage the surface and enlarge those tunnels increase the accessibility towards starch granules by exposing more α-glucan chains to α-amylase (Wolever et al., 1986). It has been documented that particle microstructure (size and morphology) of starch granules plays a role in determining the mesoscopic size of starch (0.1-100 μm). As shown in **Fig. 2.5**, the image illustrates the morphology of a cooked white rice grain (A), showing starch granules arranged in cells with a polyhedral shape and approximately 2-7 mm in size.

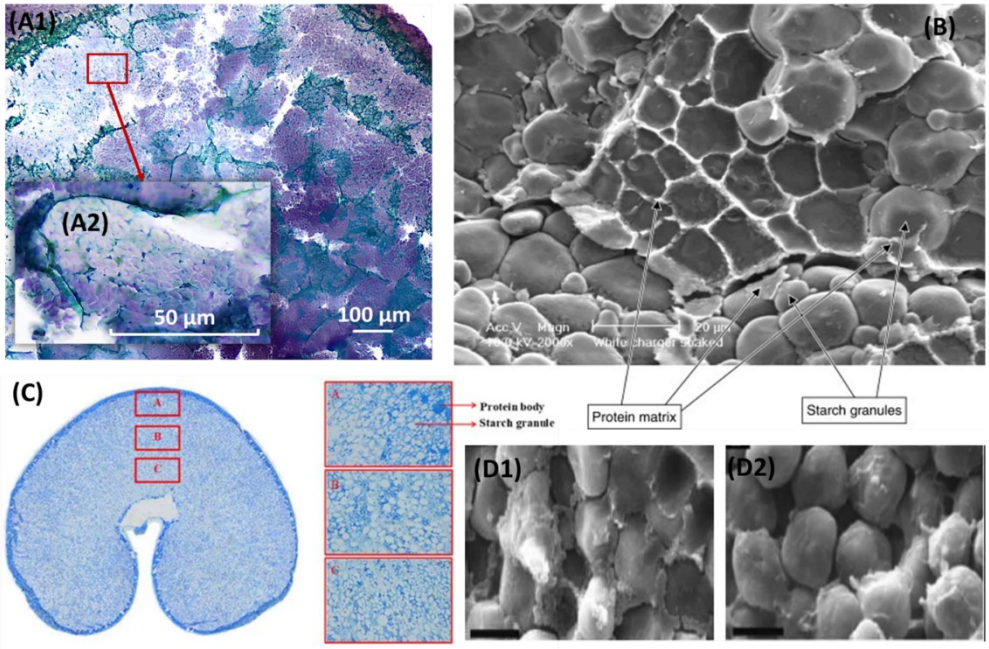


Fig. 2.5. The protein-starch matrices observed in cereals. Protein-starch matrices of cooked white rice grain (A1) and in an individual cellular unit (A2); rice starch granules (purple) arranged and trapped within a protein network (green), scale bar =50 μm. (B) An electron micrograph of the starch granules encapsulated in the protein networks of the sorghum endosperm (Black, 2004). (C) Cross-section of wheat grain (only protein stained with Coomassie bright blue G250) (Zhong et al., 2023). (D) The matrices of high- (D1) and low- (D2) protein content encapsulating corn starch granules (Gibbon et al., 2003).

The size of rice starch granules is smaller than that in most cereal grains (such as wheat) and legumes, which leads to a higher surface-to-volume ratio for the substrate and an increased likelihood of ES complex formation. It is also interesting that results reported by Sujka et al. (2010) demonstrated that starch digestibility could be similar, whether in the form of single and large granules or in agglomerates of small granules. This suggests that starch hydrolysis does not simply follow an "inside-out" pattern, where α-amylase hydrolyses the outer boundary layers of granules. It is also possible that the enzyme could also diffuse within the granules through natural pores and interior channels ("side-by-side pattern"). An early study using human subjects concerning starch digestibility and granule size was published by Langworthy et al. (1922). The digestibility of starch derived from various sources (raw rice, arrowroot, canna, cassava, taro, tree fern, and potato) was used as an ingredient for frozen puddings (100g/day over 3 days). By measuring the amount of undigested starch in faeces detected by iodine testing, the authors determined that

starch digestibility was negatively related to granule size and was species dependent. Large grains, such as potatoes or canna, had starch molecules still detectable in the faeces. However, smaller grains, such as rice, corn, and wheat, showed no traceable starch molecules in the faeces, suggesting they had been completely digested. Another structural factor affecting the α-amylase accessibility is the growth ring density within the starch granules (**Fig. 2.4c**). The growth rings mainly comprise blocklets built up by alternate semi-crystalline and amorphous lamellas. The effects will be discussed in detail in the mesoscopic scale-related (**Section 2.3.3**).

The structural organisation of non-starch components (proteins, lipids, fibres) interacting with starch granules at this level also affects the accessibility of α-amylase. Protein networks encapsulating the starch granules moderate the digestion process in two ways. First, microstructural analyses reveal that proteins and lipids were supposedly attached to the surfaces of starch granules in native rice flour. Similar to those reported in various cereals (e.g. wheat, corn sorghum), rice grains contain compact and ordered protein-starch matrices (**Fig. 2.5**) (Gibbon et al., 2003; Black, 2004; Sujka & Jamroz, 2010; Zhong et al., 2023). Functioning as physical barriers, rice protein networks can facilitate the stability of starch structure, thereby reducing the level of hydration and enzymatic accessibility. Therefore, starch digestibility increased significantly after protein removal (Ye et al., 2018). The results of an *in vitro* study conducted by Li et al. (2021) demonstrated that the digestion rate coefficient (k) of cooked rice flour was significantly lower than that of either cooked starch isolates or a mixture of isolated starch and protein.

Secondly, rice protein is subjected to different stages of proteolysis upon consumption. The process of protein hydrolysis is initiated by pepsin at low pH during the gastric phase and by trypsin during the intestine phase (Rivera Del Rio et al., 2021). The resulting water-soluble fragments of digested protein and the hydrolysate produced showed a substantial inhibitory effect on starch digestibility (Amagliani et al., 2017; Ina et al., 2019). Residues of the water-insoluble fragments

could remain bound to starch granules, reducing enzyme accessibility due to steric hindrances (Ma et al., 2020; Lu et al., 2022).

Starch digestion may be reduced in the presence of lipids because of a physical interaction between the lipids and starch granules (Wang et al., 2017; Cai et al., 2021). However, the amount of lipid in white rice is relatively low (3 %), and the milling process also removes a significant portion, further reducing the lipid content to 0.5-1 % (Morrison, 1988). It is also confirmed by published reviews (Godber & Juliano, 2004; Wang et al., 2020; Chi et al., 2022)

2.4.3 Mesoscopic level

As a result of digestion, starch undergoes irreversible ordered-to-disordered transitions, including the disassembly of molecular structures (crystalline and helical structures). Starch self-structural features (lamellae ordering, thickness, fractal nature) are instrumental in determining starch digestibility in this scale range. The growth rings in rice starch granules are organised in layers, alternating between semi-crystalline and amorphous regions (fractal structure), each of them with a thickness of 400 nm (Patindol et al., 2014). The semi-crystalline regions consist of a series of concentric crystalline (double-helix chains) and amorphous (amylopectin branch points) lamellae with thicknesses of 6 nm and 3 nm, respectively (Dome et al., 2020) (**Fig. 2.4d**).

The degree of crystallinity, crystal size, and compactness of the starch fractals can be characterised by X-ray diffraction (XRD) and small angle X-ray scattering (SAXS), especially if the information on the short-range starch chains (less than 1 nm) is required (Tang et al., 2006). Different plant sources of rapid and slowly digestible starches (wheat, corn, rice, chickpea) have different density profiles, which can be used to study digestive behaviour and predict GI before consumption from the starch structural inherent patterns (Wang & Copeland, 2013; Wang et al., 2016; Dome et al., 2020; Li et al., 2020; Chi et al., 2021). Specifically, Li et al. (2021) studied the *in vitro* digestion rate of 11 rice starch varieties and their structures within the mesoscopic level, finding a negative correlation between the compactness of starch fractals and the rate and extent of digestion. It has been found that the slower and

less digestible starches exhibit a high degree of crystallinity and compactness while their lamellae are thinner. Based on the findings reported above, several methods have been explored to reduce the starch digestibility in cooked rice by applying physical processes such as heat-moisture treatments (Puncha-Arnon & Uttapap, 2013; Zhou et al., 2020) or parboiling (Manful et al., 2008; Tian et al., 2018), or by selecting varieties with finer fractal density and higher crystallinity (Wang et al., 2018; Chi et al., 2018; He et al., 2021; Li et al., 2021).

It is worth mentioning that the reduced digestibility of certain starches can be attributed to two aspects of such fractal characteristics and the way in which α-amylase penetrates through the pores on the starch granules. One would expect that amorphous regions of the surface would be hydrolysed more rapidly than ordered crystallites. It may be because the crystalline regions are composed of amylopectin with double helices that are not digestible unless untwisted (Gallant et al., 1992; Li et al., 2020). However, the amorphous regions are also thought to contribute to reducing the enzyme's ability to digest ordered crystalline lamellas. A study by Zhang et al. (2006), which compared corn starch before and after linearisation with mild acid (to reduce amorphous regions), demonstrated that the amorphous regions are densely packed and that the proximity of the crystalline and amorphous regions inhibited digestive enzymes from performing favourable hydrolysis.

The molecular structure organisation density (represented by the degree of crystallinity) can affect the *in vitro* digestibility of rice starch, which is consistent with the finding that amylopectin crystallites must untwist before digestion (Gallall et al., 1992). Since the rotation of amylopectin double helices during the unwinding process is a kinetic limiting step in digestion (Zhang et al.,2006; Li et al., 2020). In addition, digestion kinetics showed a positive correlation with crystalline and amorphous lamellar thickness. It has been observed that the amorphous lamellae are thicker in the absence of amylose (i.e., in waxy starch) than in its presence, while the crystalline lamellae are thinner. Longer spacers within thicker amorphous lamellas would promote rapid dissociation due to their increased flexibility during

digestion (Jenkins & Donald., 1995; Bertoft, 2017). Li et al. (2020) suggested that several characteristics of the structural organisation provided are critical to consider collectively rather than individually when assessing the digestibility of a supramolecular polymer such as starch. Examples of these characteristics are compactness (the degree of crystallinity), size (chain length of amylose and amylopectin), and the weight of the semi-crystalline lamellas within starch granules.

2.4.4 Nanoscopic level

Starch consists of two glucose polymers that comprise rice starch: amylopectin (AP, more extensive and highly branched molecules) and amylose (AM, smaller and more linear molecules) (**Fig. 2.4e**). The effect of AM content, AM/AP ratios, and chain lengths on starch digestibility have been studied previously (Chung et al., 2011; Jeevetha, 2014; Dhital et al., 2016; Wang et al., 2017; Guillén et al., 2018). Most of the rice starch is composed of AP (65-85 % weight); generally, the majority of AP is composed of short (1-4) chains, which are further linked by 4-6 % of (1-6) bonds (Vandeputte et al., 2003). Conversely, AM comprises α (1-4) bonds with a few branches linked by α (1-6) bonds. AM content varies among rice varieties, ranging from 1-2 % in waxy white rice to over 30 % in high-amylose starch varieties. It has been shown that AM is related to rice hydrolysation by α-amylase in different food models (including grains, flour, and isolated starch). However, some contradictory results have been reported. For example, the GI of cooked rice containing high amounts of AM appears to be lower regardless of the method of cooking (Miller et al., 1992; Wang et al., 2017). Reed et al. (2013) examined the effect of different cooking methods on rice categorised by different AM contents. The RS content differed for the same rice type depending on the cooking method. Likewise, different rice types cooked with the same method presented different levels of RS; this was attributed to the different initial AM content among the rice types. Another factor responsible for the different RS content in the samples could be the initial AP structure and how it changes during cooking and digestion. The study conducted by Syahariza et al. (2013) investigated the correlation between the starch digestibility of cooked rice flour and its molecular (AM and AP) structural features. The digestion

rate appears to be related to the chain length of long AM branches, as well as to the ratio of long to short AP branches and the ratio of long AM branches to short AP branches. However, the correlation results are rather suggestive. The effect might be more concentrated and noticeable at higher levels of hierarchy.

In addition to AP content (the AM/AP ratio), AP chain length also affects the digestion rate. The study of Benmoussa et al. (2007) examined the relationship between AP delicate structures (chain length and branching characteristics) and starch digestion rate. Statistical analysis revealed a strong positive correlation between the proportion of rapidly digestible starch (RDS) and the proportion of very short AP linear chains. In contrast, there was a strong negative correlation between RDS and the proportion of long and intermediate/short linear chains of AP.

2.5 The role of GI in diet: measurement *in vivo*, applications and limitations

2.5.1 Physiological definition of GI (*in vivo*)

The definition of GI indicates how quickly the blood glucose concentration increases in the first 2 hours after food ingestion. As shown in **Eq. 2.1**, the GI is calculated as the ratio (%) of the area under the glycaemic response curve (AUC; i.e., blood glucose concentration over time) of a test food and the AUC of a reference food (usually a glucose drink or white bread). A mass of 50 g is used for both the test and reference food (Brand et al., 1991; Wolever et al., 2008).

$$\mathbf{GI} = \frac{\mathbf{AUC_{Test\ food}}}{\mathbf{AUC_{Reference\ food}}} \times \mathbf{100}\ \% \quad \textbf{(Eq.2.1)}$$

The glycaemic load (GL) was further developed to comprehensively consider the total amount of carbohydrates consumed, which can be calculated from **Eq. 2.2** (Salmeron et al., 1997; Foster-Powell et al., 2002). The GL of food represents the amount of blood glucose increase after consumption of a specific mass of food with a specific GI, describing the cumulative exposure to postprandial glycaemia (Monro and Shaw, 2008).

$$\mathbf{GL} = \frac{\mathbf{GI}}{\mathbf{100}} \times \mathbf{P} \times \mathbf{Wt} \quad \textbf{(Eq.2.2)}$$

Where:

P is the proportion of the digested and absorbed carbohydrates in the test food.

W_t is the sample food weight.

The effectiveness of these two definitions has also been evaluated by systematic review and dose-response meta-analysis (Ojo et al., 2018; Zafar et al., 2019). Results showed there is a positive correlation between GI and relative risk factors (RRs) of noncommunicable diseases (NCDs) such as type 2 diabetes (T2DM). The GI values also more sensitive to predict the RRs than GL (less required for an increase in RR per 5 units/day of GI than for per 20 units/day of GL). thus, GI was included in the guide to daily select starchy food (Greenwood et al., 2013). Meanwhile, GL was more capable of explaining the variability in glucose response than GI (68 % vs 49 %) (Sheard et al., 2004). In addition, both values can explain approximately 90 % of the total variability in glucose response following starchy foods consumption, indicating their cumulative impact on the rate and extent of glycaemic increases (Wolever & Bolognesi, 1996a, 1996b).

2.5.2 Physiological effects of low-GI diet on health

In recent years, there has been a growing interest in the clinical implications and metabolic changes associated with the low-GI diet and whether it may possess long-term health benefits. The following list illustrates the benefits that can be derived from a low-GI diet during the carbohydrate metabolism process (0-6 h following ingestion), as shown in **Fig. 2.6** (Ludwig et al., 2002; Ball et al., 2003; Wolever et al., 2006; Du et al., 2006; Alfenas et al., 2007; Esfahani et al., 2009; Gao & Chilibeck, 2018):

i. Early stage (0-2 hours after ingestion) of glucose metabolism (early postprandial period): An attenuation of the acute hormone response caused by less bioavailable (digested, and ready to absorb) glucose from digested starch.

ii. Middle stage (2-4 hours after ingestion) of glucose metabolism (mid-postprandial period): reduced fluctuations in blood glucose levels and increased fat oxidation (break down triglycerides to provide energy); attenuation of the hormone (like insulin) response. A reduction in the levels of inflammatory factors, such as high-sensitivity C-reactive protein, a marker of systemic inflammation (shown in **Fig. 2.6**).

iii. Late-stage (4-6 hours after ingestion) of glucose metabolism (late postprandial period): The development of sensory-specific satiety; the maintenance of stable blood glucose levels is associated with a delay the return of hunger and restricts caloric intake; facilitate the release of fats from adipocytes into the bloodstream for energy supply

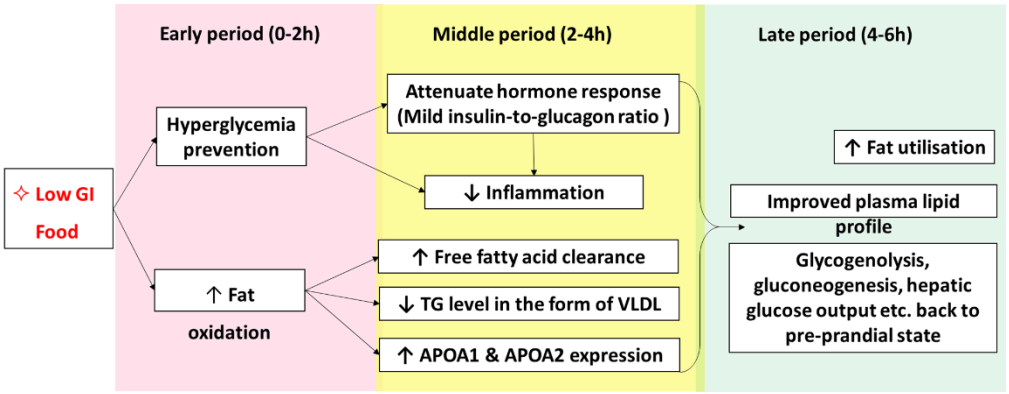


Fig. 2.6. Physiological benefits associated with the consumption of low-GI foods.

Reducing advanced glycation end products (AGEs) is also essential for the long-term health benefits of low-GI food. It has been demonstrated that AGEs play an essential role in the pathophysiological process of ageing and metabolic disorders (Chen et al., 2000; Arasteh et al., 2014; Aljahdali & Carbonero, 2017). AGEs are a complex molecule group that forms primarily from a non-enzymatic glycation reaction. This is a prolonged reaction process and involves a reducing sugar (such as glucose) used to condense with an amine group of proteins (such as collagen, albumin, and haemoglobin in blood) (Ziaee et al., 2011; Henning & Glomb, 2016). By switching to a low-GI diet model, the synthesis of AGEs is restricted due to the deficiency of free glucose (Whitcomb et al., 2015; Guilbaud et al., 2016). Furthermore, low-GI foods can alleviate a series of adverse biomedical impacts, such as adipogenesis (hyperplasia and hypertrophy of adipose cells), reactive oxidative stress and low-

level immunoreaction (Rondeau & Bourdon, 2011; Anguizola et al., 2013; Boyer et al., 2015).

2.5.3 Current understanding of GI data

Two decades after GI introduction, a series of *in vivo* research has identified the potential importance of a low-GI diet in ameliorating disease progression in patients with NCDs (Mirrahimi et al., 2012; Augustin et al., 2015). Multiple world health organisations such as WHO and Diabetes UK have gradually considered the benefits of a low-GI diet by reviewing the available research evidence and evaluating the use of GI on food labels in many countries (such as Australia, New Zealand, and South Africa). However, the employment of the GI data remains very limited in both dietary guidelines and food products. The American Diabetes Association is still hesitant about using food GI data as a measure of food healthiness, and the assessment from the Health Canada Organisation suggested cancelling plans of adding the GI of food to labels (Connor et al., 2003; Sheard et al., 2004; Mann et al., 2007; Atkinson et al., 2008).

The GI calculators are not as popular as calorie calculators, as the user experience of these applications may be sub-optimal (Hoad et al., 2004; Sujka & Jamroz, 2010). The insufficient use of GI calculators can be attributed to three main factors: i) limited food data available; ii) difficulty in calculating GI concerning calorie calculation if the food matrices is altered by complex food material or cooking process, especially starch microstructure; iii) strong dependency of GI values on the glycaemic/physical status of the consumer (in contrast to calories calculated from the food material components).

2.5.4 Limitations of the *in vivo* GI measurements

Because the GI value was originally designed for diabetic patients, *in vivo* measurements were initially the ideal method. However, as research increased in the area, there was criticism about the validity of *in vivo* methods due to low accuracy and precision. The current *in vivo* methodology of GI value lacks comprehensive consideration of inter-individual variability and intra-individual

reproducibility (Vega-López et al., 2007). Participants from different ethnic backgrounds, for example, have shown significantly different GI values (61 ± 6 in healthy Caucasians vs 77 ± 12 in healthy Asians) for the same rice type, making it difficult to provide a precise GI classification (Venn et al., 2010). However, the limited number of subjects and samples may also be responsible for these statistical biases. It is challenging to acquire enough participants, as the GI measurement is expensive and complex, and healthy subjects (e.g., those with no diabetes) are required for standard measurements. Furthermore, invasive methods would be needed to accurately investigate the digestive fates of starchy food (e.g., collecting biological material from the gastrointestinal tract or sacrificing animals), which poses ethical challenges.

Although GI measurements *in vivo* are critical to determining the glycaemic response in an objective digestion process, they lack a comprehensive consideration of the food matrices. Therefore, researchers are engineering *in vitro* analysis techniques that simulate digestion.

Unlike *in vivo* analysis, which measures glucose concentrations absorbed and carried through the bloodstream, an *in vitro* analysis measures the glucose released from relevant food substrates, providing more information on food digestion behaviour for creating new food products.

2.6 *In vitro* digestion models

2.6.1 Model types, applications, and limitations

In vitro digestion models are generally divided into static and dynamic categories. The difference between the two is based on the type of mechanical movement and physiological changes adopted. *In vitro* static models are usually mono-compartmental (one single reaction vessel), while dynamic models can be single or multicompartmental (several reaction vessels connected).

2.6.1.1 Static digestion model

A basic static model simulates the enzymatic reaction during the digestion process. It usually comprises sequence oral, gastric, and intestinal phases, but only single

intestinal or gastrointestinal phases are used. Although defined as “static,” these models include rotators, shaking incubators, and magnet stirrers, with the only aim of obtaining a homogeneous dispersion of the enzyme-substance mixture. Specifically, in this thesis, glycaemic index prediction with the *in vitro* static model was performed by measuring the concentration of intermediate or endpoint products, i.e., maltose released from starchy food due to hydrolysis by α-amylase. There are many variations of static models to suit different food types, limiting the results' comparability and reproducibility. For example, there have been more than 36 protocols of static digestion reported in carbohydrate digestion (Woolnough et al., 2008). Likewise, methods to study protein digestion also vary.

To standardise the digestion parameters, the COST action INFOGEST set up an international and standardised protocol published in 2014 (Minekus et al., 2014) and further refined in 2019 (Brodkorb et al., 2019). Based on this consensus, static models have become a standard method, and 89 % of *in vitro* digestion experiments have been accomplished using static models (Lucas-González et al., 2018). The advantages of static digestion models are numerous. They are simple, cost-effective methods and can provide good lab-to-lab reproducibility of results. Comparisons of standardised static models have shown promising correlations with *in vivo* methods in carbohydrate, protein, and lipid degradation (Goñi et al., 1997; Brandon et al., 2006; Egger et al., 2017). Moreover, with the help of numerical and computational methods, the kinetics of biochemical dissociation in food matrices can be analysed. The concentration of the endpoint products, such as glucose, free fatty acids, and amino acids, can be measured at more key time points than *in vivo* experiments. Depending on the purpose of the study, the impact of initial conditions, such as pH, enzyme types, enzyme concentration, mechanical stress, and fluid flow, can be considered independently or in combinations in each digestion phase. Static models mainly focus on the upper GIT by simulating its physiological conditions to study the deformation, delivery, or release of functional ingredients from the food matrices. Nevertheless, these models can also be extended to the lower GIT if combined with

membrane-based models, cell-culture, and fermentation models (Deferme et al., 2007) to study active molecules' absorption, bioaccessibility and bioavailability.

However, static models have limitations as digestion is a complex and dynamic process. They fail to imitate dynamic changes in pH or enzyme activities. Static models also lack the inclusion of mass transfer and characteristics such as separate cavities for different digestion phases, motion patterns, and transfer flow.

2.6.1.2 Dynamic digestion models

Dynamic digestion models are designed to simulate the mechanical aspect of digestion and include real-time changes in the biochemical conditions. The relevant design generally includes three main features: configuration, biochemical environment, and physical forces. For the configuration of the digestion equipment, it is essential to have a realistic size and shape of the gastrointestinal tract (such as a "J" shape stomach and tube-like small intestine) and resistant materials able to manage complex materials (which may wear or degrade the equipment) and mechanical forces. The biochemical environment includes pH regulation, real-time control of enzymes, bile concentration, and digesta flow. The physical forces considered in the model refer to the peristaltic contractions, which can be obtained with the use of low-speed pumps or Teflon rollers (Marciani et al., 2001; Moxon et al., 2016; Bohn et al., 2018; Lucas-González et al., 2018).

Single-compartment dynamic models usually reproduce one digestive phase and can provide information related to that specific digestive phase. For example, mouth models can replicate mastication and bolus formation and analyse the breakdown of food matrices and the release of volatile compounds (Salles et al., 2007; Benjamin et al., 2012). Gastric systems, such as a Human Gastric Simulator, a dynamic gastric model, and a dynamic *In vitro* Rat Stomach series, can mimic the flow of food, gastric secretions and emptying (Wu et al., 2017). 3D model engineering and morphology have been employed to simulate the actual stomach shape and screen the digestive progress (Zhang et al., 2018). Intestinal systems, such as the Dynamic Duodenum Model and Human Duodenum Model, can mimic the constant peristaltic movement and provide simple absorption methods (Tharakan et al., 2010; Hussain et al., 2015).

To investigate the entire food digestion process, more phases of dynamic models (e.g., oral and gastric) can be connected; moreover, different phases of the dynamic model can be connected with static models and become semi-dynamic models. As depicted in **Tab. 2.2**, semi-dynamic models provide inhomogeneous and localised biochemical environments, allowing researchers to study the digestive process of food in more realistic circumstances (Kong & Singh, 2010; Vardakou et al., 2011). These models are quite delicate and need significant labour and time for preparation and post-experiment cleaning. Repeatability is another concern, as parameters are validated for one particular type of food, which may not be suitable for others (Dupont et al., 2019).

Tab. 2.1. Comprehensive comparison between *in vitro* and *in vivo* models.

	Content	In vitro	In vivo
Overall process	Measuring endpoints/targets	Hydrolysed products, intermediates, and active molecules released during digestion	Indirect observations and endproducts of metabolism (body fluid, faeces, tissue, cells)
	Process	Static/intermittent/dynamic	Real-time/dynamic
	Objects	Numerous types and concentrations of food/drug matrices, such as homogenised/intact materials, isolated or purified compounds, cooked/uncooked materials	Limited types and concentrations of matrices: - Natural oral feeding: usually using complex matrices (e.g., beverages or cooked meals) - Forced-feeding: only matrices that can be directly swallowed
Oral phase	Mechanical force	Grinder (e.g., meat mincer) High-shear mixing	Buccal mastication, 50-150 N Lips - soft, flexible closures Tongue - muscle-type mixer Teeth - incisors, canines, and molars
	Buffer	Neutral electrolyte solutions	Salivary electrolyte fluid
	Temperature	Usually fixed at 37℃	The average 37℃ may be changed by external stimuli, e.g. hot or cold beverages.
	pH	6.9-7.0	6.2-7.4
	Time	2 - 5 mins.	Max 15 mins.
	Enzyme	Salivary α-amylase from different origins	Ptyalin, human salivary α-amylase
	Portion	5-50 g, based on the system scale	Usually 50 g; possible variations
Mass trans_1	Particle size	< 2mm; possibly larger for soft particles	< 2mm for optimal swallowing, possibly higher for soft food
	Tunnel	Usually, a silica gel tube (diameter 3 ± 0.10 cm), if present	Oesophagus (2-3 seconds)
	Force	A pulley with attached weight mass (2-4 N) to reproduce a swallowing model	Weak creep force and gravity

Gastric Phase	**Mechanical force**	**A rotator/shaking incubation (static models); more complicated techniques in dynamic models.**	**Pyloric sphincter**
	Buffer	Neutral electrolyte solutions	Succus gastric (gastric juice)
	Temperature	37°C	Average 37°C
	Enzymes	Pepsin from the porcine pancreas is mainly used; Gastric lipase from rabbits is commonly used.	Pepsin and gastric lipase
	pH	Start at pH 3 in static models; Gradual acidification from 5 to 3 can be achieved in dynamic models.	It can change from 2.0 to 6.5 depending on the stages of gastric emptying.
	Time	Between 30-120 mins, fixed time	50 % of stomach emptying takes 2.5-3 hours and 4-5 hours for total emptying
	Portion	Residual materials from the oral stage=bolus	Residual materials from the oral stage=bolus
Mass trans_2	Particle size	< 2 mm	< 2 mm to pass the pyloric valve
	Tunnel	Teflon membrane with 2 mm holes	Pyloric sphincter
	Force	Peristatic valve-pump	Weak creep force

Small intestinal phase	**Force**	**Outside wall contraction**	**Brush border force (inside the intestine) and rhythmic muscular contractions**
	Buffer	Neutral electrolyte solutions	Sodium hydrogen carbonate neutralising gastric acidity, and other electrolyte fluids composed of sodium, potassium, chloride, and bicarbonate
	Temperature	37°C	Average 37°C
	Enzymes	Can use: i) Individual pancreatic enzymes or related combination (trypsin, chymotrypsin, α-amylase, lipase, and colipase); ii) Porcine pancreatin	Pancreatin
	pH	6.9-7.0	~8
	Time	Approx. 2-3 h, can be prolonged for specific study propose	2.5-3 h for 50 % chyme emptying
	Portion	Residual materials from the stomach stage	Residual materials from the stomach stage
Timing in total		Based on INFOGEST, it takes 3 to 18 hours for one digestion set from the preparation of solutions to the end of digestion.	Inconclusive data. The preparation process, including ethics approvals, recruitment, and training of both animals and humans, could take weeks.
References		(Araya et al., 2002; Petitot, Abecassis and Micard, 2009; Aravind, Sissons and Fellows, 2011; Minekus et al., 2014; T. Bohn et al., 2018; Brodkorb et al., 2019)	(Jenkins et al., 1981; Goñi, Garcia-Alonso and Saura-Calixto, 1997; Vega-López et al., 2007; Tappy et al., 2010; Mills, Norton & Bakalis, 2013)

Tab. 2.2. Multicompartmental dynamic *in vitro* models (main dynamic features, applications, and limitations).

Model	Dynamic features	The system has been applied and further improved upon…	Developed by
DIDGI®	pH monitors and controls (pH electrode and perforated loop). The flow of digestive secretions (redox sensors). Rhythmic peristaltic pumps. Gastric emptying, sieving, and mass transfer (Teflon membrane and StoRM® software). Anaerobic condition (nitrogen purging).	Classic examples are digestion of dairy products, human milk and infant formula. The following areas can be improved: • The addition of oral phase simulation. • Only basic stirring (propeller) is used in the stomach phase. • Fundus exposed to air (open top).	INRA
TIM-1 Simplified model: Tiny-TIM Large-intestinal model: TIM-2	Pre-set peristaltic valve pumps. Rhythmic contractions for mixing (flexible walls in water pressure); pH monitors and controls. Flow of digestive secretions and gastric emptying rates are programmable in variable conditions. We digested products transit to two systems—semi-permeable membranes dialysis (water-soluble) and 50 nm filter (lipophilic products).	Studies on macronutrients, fat- and water-soluble vitamins, minerals and functional compounds (such as probiotics, prebiotics, and antioxidants). Thanks to in silico modelling, TIM can further: - Predict the glycaemic response curve and insulin response. - Stability and bioaccessibility of amino acids, water- and fat-soluble vitamins (such as folate). The following areas can be improved : • Considering the lack of intestinal mucosa, absorption needs to be examined in cell cultures or tissues. • Bioavailability of functional compounds released from food matrices can be predicted using in silico models	Institute of Food Research (Norwich, UK)

SHIME®	Peristaltic pumps in a drafted amount of nutritional medium. The flow of digestive secretions and pH are controllable using tailor-made software. Stirring reactors are applied in duodenum, jejunum, and ileum compartments. Different reactors with faecal microbiota inoculation.	The SHIME model is more applied in colon-region-specific research. Thanks to modules and in silico modelling, it can further: - Conduct dialysis - imitate conditions in host cells (HMI module with epithelial or immune cells) The following areas can be improved: • Only basic stirrers mainly conduct mixing in the last three compartments.	Ghent University (Belgium)
ESIN	Flow of digestive secretions, pH, transit time, and chyme mixing rates are controllable. Different gastric emptying of solids and liquids (piston movement and biphasic pumps)	The ESIN model is more applied to liquid foods and can be further used to digest real-size food matrices. The following areas can be improved: • More applications and validation tests are necessary.	University of Auvergne (Clermont-Ferrand, France)

2.6.1.3 Semi-dynamic digestion model

Semi-dynamic models usually have one main compartment (vessel) that simulates the actual physiological conditions of one specific digestive phase. The other digestion phases may be excluded or remain the same as the static approach. The semi-dynamic gastric model was developed by the Institute of Food Research (Norwich, UK) (Mulet-Cabero et al., 2017). This semi-dynamic model is simple to manipulate and has developed dynamic simulation features such as gradual acidification; it also imitates the gastric emptying process and the sequential addition of gastric fluid and complex enzymes. Another advantage of this model is that it allows image/video recording to study macrostructural changes during digestion. There are some limitations to the compatibility of the process parameters and sample loss during the manual and stepwise emptying.

Simulations of oral processes have proven instrumental in improving practical knowledge of starch digestibility from the perspective of structural integrity (Blanquet-Diot et al., 2021). This is evidenced by a dramatic reduction in the particle size of solid food (e.g., whole rice grain) after chewing, as well as salivary α-amylase remaining active in the human stomach (Van & Shorten., 2014; Wang et al., 2019). Studies in normal and fine mastication cases would be helpful to assist in the development and selection of foods and diet strategies that have low-GI potential.

To conclude, static, dynamic and semi-dynamic *in vitro* digestion models offer diverse methods to study digestion, including the digestive fate of food formulations in verified circumstances. Furthermore, a series of analytical methods (such as morphology, rheology, and spectrometry) and *in silico* modelling can consolidate the insights of food digestion. However, the popularity of dynamic models is still limited, and there is a need for a validation standard between different types of these models before more widespread use. So far, cooperation platforms have been introduced between different models (e.g., SATIN–Satiety Innovation project). Other improvements for the models would be considering the frequency of food ingestion, satiation signals, and food blockage (such as ileal brake) on the decrease of food intake. Most of the *in vitro* models are based on *in vivo* data from healthy

adults, and it would add more value if different age, gender, and health condition groups were also considered.

2.6.2 Kinetic models for characterising starch digestion behaviour

In vitro digestion models provide a reproducible approach, reducing the need to consider individual variations or ethical authorisation (Minekus et al., 2014). These methods can be coupled with kinetic models to quantify the digestibility of starch and determine its health impact (Hasjim et al., 2010). However, it is necessary to couple *in vitro* digestion with an appropriate *in vivo* study to confirm the health impact of digested starch.

Several kinetic models have been employed to characterise starch digestion behaviour. One of the most widely used systems is Englyst's, a method which classifies starch as rapidly digestible (within 20 mins), slowly digestible (20 - 120 mins), and resistant (not digested after 120 mins – end of the experiment time) (Englyst et al., 1992). It must be noted that resistant starch can still be fermented in the colon under physiological conditions, but it does not contribute to the GI values.

Another method to predict GI is based on the hydrolysis index (HI) of starch digestibility, which is obtained by dividing the area under the hydrolysis curve of the tested food between 0-120 mins or 0-180 mins with that of white bread (reference food), as shown in **Eq. 2.3**.

$$\mathbf{HI} = \frac{\mathbf{AUC90_{sample}}}{\mathbf{AUC90_{reference}}} \times \mathbf{100} \quad \textbf{(Eq. 2.3)}$$

The predicted glycaemic index (pGI) is then calculated by placing the HI value into **Eq. 2.4** (Goñi et al., 1997).

$$\mathbf{pGI} = \mathbf{39.71} + (\mathbf{0.549} \times \mathbf{HI}) \quad \textbf{(Eq. 2.4)}$$

Both methods may be limited to detecting and quantifying the changes in the digestion rate when starch is part of complex foods (Hasjim et al., 2010; Man et al., 2012). The HI method is less effective for revealing mechanistic details of digestograms with multiple digestible fractions (Edwards et al., 2014). A way to overcome this limitation is by using an improved first-order kinetics model, as shown in **Eq. 2.5**.

$$\mathbf{C_{(t)} = C_0 + C_\infty\left(1 - e^{-kt}\right)} \quad \textbf{(Eq.2.5)}$$

Where,

$C_{(t)}$ represents the quantity of ingested starch digested at the time

C_∞ represents the potentially digestible starch fraction

k is the rate constant of the starch digestible fraction

t is the chosen time

A Logarithm of Slope (LoS) plot is obtained by expressing the first derivative of the first-order equation in logarithmic form (**Eq. 2.5**) based on the description by Edwards et al. (2014), as shown in **Eq. 2.6**.

$$\mathbf{\ln\left(\frac{dc}{dt}\right) = \ln(C_\infty k) - kt} \quad \textbf{(Eq. 2.6)}$$

The slope of a digestibility curve through several time points was determined: the slope was estimated from the digestion fraction ($\Delta C/ \Delta t$), such as $(C_2 – C_1)/(t_2 – t_1)$, and the natural logarithms were plotted against the meantime, i.e., $(t_2 + t_1)/2$. This gives a linear plot in which the values of digestibility constants, k and C_∞, are calculated from the slope (−k) and y-intercept $\ln(C_\infty k)$, respectively.

In the most practical starchy food models, the overall digestive process is not “unified” as only one rate constant. From a LoS plot, the digestion process can be described by two separate first-order reactions with different rate constants, revealing the rapid-to-slow digestion rate phenomenon. This approach estimates the rate constants (k) represented by the negative slope of each linear plot, and the total starch digested (C_∞) is calculated from the y-axis intercept of the plot.

To avoid bias in identifying numerical derivatives, additional non-linear least squares refinement may be required (Yu et al., 2018). In this model, only sequentially digestible fractions of starch are considered. The slowly digestible phase begins only after all the rapid-digestible fractions have been digested (Li et al., 2019). One typical case is the starch digestion of pasta. The outer protective layer of pasta contains fully gelatinised starch, which is digested more rapidly than the almost intact starch in the centre zone (Zou et al., 2015). As described above, the digestion scenario is

similar to that of intact rice grains, and the model showed good fitting in results presented in **Chapters 5** and **6** ($R^2 > 0.90$).

A parallel first-order kinetic model is also suggested, considering starch systems containing rapidly and slowly digestible starch (RDS and SDS), which will undergo simultaneous degradation. (Li et al., 2019). In some cases, however, a digestion system that combines parallel and sequential (CPS) patterns, referred to as "CPS kinetics", is also considered, as shown in **Fig. 2.7**. The CPS kinetics were used in the thesis to study digestion in a rice bolus (chewed mass before swallowing). This model helps determine which digestion pattern (sequential, parallel, or CPS) occurs in the rice bolus, which is crucial for investigating the relationship between structural properties and starch digestive characteristics.

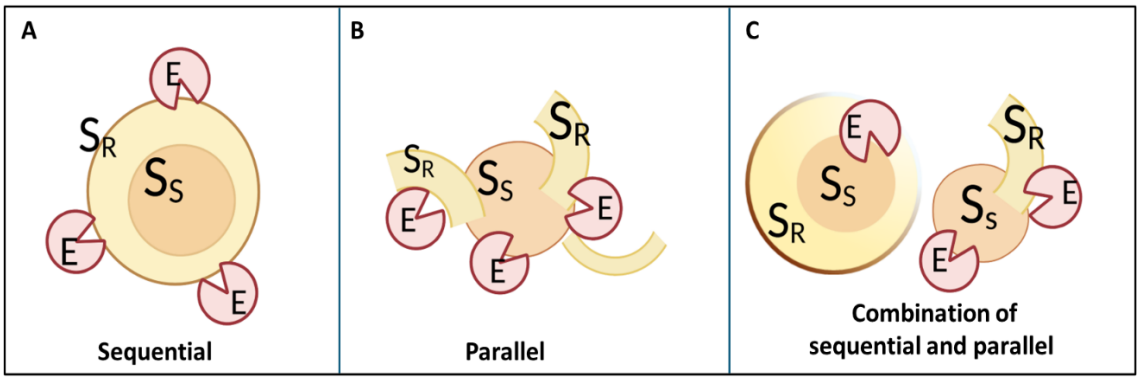


Fig. 2.7. Schematic illustration of the three possible starch digestion patterns in a heterogeneous environment.The image is adapted from Li et al. (2020). (A) sequential pattern, slowly digestible fraction (S_S) digested only after the rapid-digestible fraction (S_R) has been digested. (B) parallel pattern. S_S and S_R are digested simultaneously. (C) combination of sequential and parallel pattern. E: enzyme.

2.7 Recent trends in rice-based food design with a reduced GI potential

2.7.1 Rice varieties with slow starch digestibility

The microstructure characteristics of starch have been the subject of much research over the past few decades (**Section 2.3**), leading to the development of strategies for reducing the RDS in rice-based foods for improved health outcomes and consumer satisfaction. Direct interventions include substituting white rice with low-GI alternatives such as brown rice or mixed grains. However, such alternatives are

not widely accepted at the organoleptic level (Zhang et al., 2010; Mohan et al., 2014). Several approaches to produce white rice varieties with slow starch digestibility have also been explored, including transgenic engineering or precision breeding of varieties high in protein and slowly digestible starch (Cai et al., 2018; Jukanti et al., 2020; Shen et al., 2022), although these last two methods presented trade-offs related to low yield and undesirable textural properties. Several chemical and enzymatic modification approaches have also been used to increase the content of SDS and RS, thereby decreasing the GI value.

Chemical reagents such as esterification with octenyl succinic anhydride, hydroxypropylation, acetylation, and phosphorylation/crosslinking have been reported to significantly reduce the extent of enzyme-catalysed hydrolysis of rice starch, increasing SDS and RS content (Miao et al., 2014; Cai et al., 2020). Single and multiple enzyme-modified (such as β-amylase, transglucosidase, and pullulanase) rice starch was shown to significantly increase SDS and RS content and reduce RDS content and pGI (Li et al., 2020). The possible mechanism is to prevent the digestion of modified starch by blocking enzyme access and forming atypical linkages resistant to enzymatic cleavage.

Physical modification, such as parboiling (a hydrothermal treatment involving soaking, steaming, and drying), is more practical and widely used in manufacturing; it has been shown to reduce the GI by nearly 30 % in the same variety of rice (Larsen et al., 2000). Parboiling alters the starch and protein microstructure irreversibly, forming a peripheral layer of the protein-starch matrices through the hydration of the internal starch granules and their availability to enzymes. Moreover, adding hydrocolloids, such as guar gum, gellan gum, xanthan gum, and carboxymethyl cellulose, may reduce the GI in rice through a similar mechanism to that occurring during parboiling. These two methods could also be coupled, and their application will be discussed in more detail in **Section 2.7.3**.

2.7.2 Imitating the food matrices to reduce starch digestibility

In the seeds of cereals and legumes, starch granules are surrounded by and physically interact with a protein networks, which limits the accessibility of

amylolytic enzymes to starch and reduces the rate of α-amylolysis (Dhital et al., 2016; Bhattarai et al., 2018; Zhou et al., 2018). Imitation of these protein-starch matrices has inspired researchers (academic and industry) to develop healthy foods with low-GI properties. Texturisation of rice starch with rice protein via extrusion was used to imitate the natural protein-starch matrices in native rice grains (Ye et al., 2019). The rice protein networks formed a hydrophobic physical barrier, resistant to water adsorption and restricting granular swelling, leading to a dense packing of encapsulated starches with high SDS content, which could be employed as a food ingredient for glycaemic control. Moreover, rice starch conjugated with several protein isolates (such as rice protein, zein) and their hydrolysates have been used as food ingredients to formulate fortified rice flour, extruded rice grains, and rice-based products with reduced starch digestion rate at the laboratory scale.

It should be noted, however, that the protein may lose its role as a structuring agent and hierarchical barrier in the recomposed rice kernels to prevent enzymes from hydrolysing starch granules. Rice protein is denatured during heated extrusion and no longer appears as a network but as protein assemblies throughout the kernel. The absence of protein-starch matrices makes functional rice more susceptible to degradation during post-processing, such as washing, cooking, and chewing.

2.7.3 Providing low-GI properties to white rice by structuring with hydrocolloids - an example of low acyl gellan gum (LAGG)

Hydrocolloids, polysaccharides with a high molecular weight (especially those obtained from plants, algae, or produced by microorganisms), have attracted particular interest in the food industry (Culetu et al., 2021; Pirsa & Hafezi, 2023). As well as serving as emulsifiers, gelling agents, and stabilisers, these substances also have the ability to slow starch digestion by restricting enzyme access, thereby reducing GI. In the case of rice, Chung et al. (2007) firstly investigated the possibility of slowing starch digestibility by cooking white rice with hydrocolloids, including xanthan gum, guar gum, gellan gum, and sodium alginate. The results showed that cooked rice with a minor number of commercial hydrocolloids (0.3 or 0.7%) has a harder texture and slower starch digestibility. Hydrocolloids have been shown to

slow the rice starch digestibility in either individual or combined forms, by encapsulating starch particles, increasing particle size and weight, as well as increasing viscosity, all of which result in a decreased enzyme accessibility and the release of digested products (Sasaki & Kohyama, 2011; Chen et al., 2017; Ojo et al., 2018).

Among the hydrocolloids evaluated, gellan gum had the greatest effect in reducing the adhesiveness and increasing the SDS content of cooked rice. Several factors contribute to decreased adhesiveness, including the formation of a gel-like matrix with notable degrees of slippage and syneresis, providing a physical barrier to adhesion (Whittaker et al., 1997). In addition, this property is advantageous in reducing the digestibility of starch. The gellan gum gel coating itself is undigestible and interferes with digestive enzyme access to the starch molecules. As starch degradation into glucose becomes slow, a lower glycaemic index may result, contributing to the maintenance of blood glucose homeostasis. (Osmałek et al., 2014; Kanyuck et al., 2022). It has been observed, however, that encapsulation properties are strongly dependent on strength of the gel network (such as polymer concentration, gelling rate, and gelling strategy applied) and stability at different pH levels and soaking times (Ogawa et al., 2006; Stevens et al., 2016). It is therefore necessary to develop a deeper understanding of the gelling profile of gellan gum to manipulate starch digestibility with its effects.

Gellan gum is a water-soluble, linear, and anionic microbial exopolysaccharide produced by the bacterium *Sphingomonas elodea*, which was discovered in 1978. Since then, gellan gum has gained increasing interest in applications due to its physical properties and ease of production through low-cost industrial-scale fermentation with high reproducibility, and it has been widely used in food products as a texturing agent (Bradbeer et al., 2015). When broken down into its simplest form, its tetrasaccharide unit consists of two glucose residues, one glucuronate residue, and one rhamnose residue (**Fig. 2.8**). Its native form contains L-glyceryl and acetyl with one glycerate and a half acetate group present per repeating tetrasaccharide unit. A fermentation broth can be treated with hot alkali to remove

both substituents, producing a low acyl gellan gum (Milivojevic et al., 2019; Sworn & Stouby, 2021).

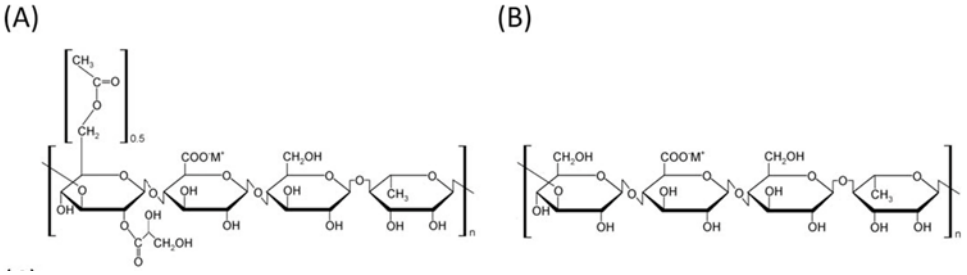


Fig. 2.8. The molecular structure of (A) high acyl gellan gum and (B) low acyl gellan gum. Adopted from Sworn & Stouby (2021)**.**

As for the final application of gelling products, the high acyl gellan gum produces soft, highly elastic and thermoreversible gels. The LAGG gels offer firm, stiff, thermostable gels, making them ideal for hydrogel coatings that require integrity at a temperature as that of the body (37 °C)

Using gellan gum as a food additive is widely accepted in the European Community (under the number E 418), where the daily intake is not specified, and by the American Food and Drug Administration (Code of Federal Regulations 172.665) as safe (Younes et al., 2018; Alam et al., 2014; Palumbo et al., 2020). As shown in **Fig 2.9**, there are three steps involved in the gelation of a hydrogel coating. At low temperatures (30°C), a LAGG dispersion forms an ordered helix of double strands, and at higher temperatures (over 40°C), it forms single stranded coils, which significantly reduces its viscosity. Upon cooling, the gel dispersion undergoes a disorder-to-order transition and forms a stiff structure. Depending on the type of cation present, either monovalent or divalent cations can help develop this structural strength by crosslinking adjacent helices via COO−cation–COO− bridges (salt bridges) (Moritaka et al., 1991; Huang et al., 2021).

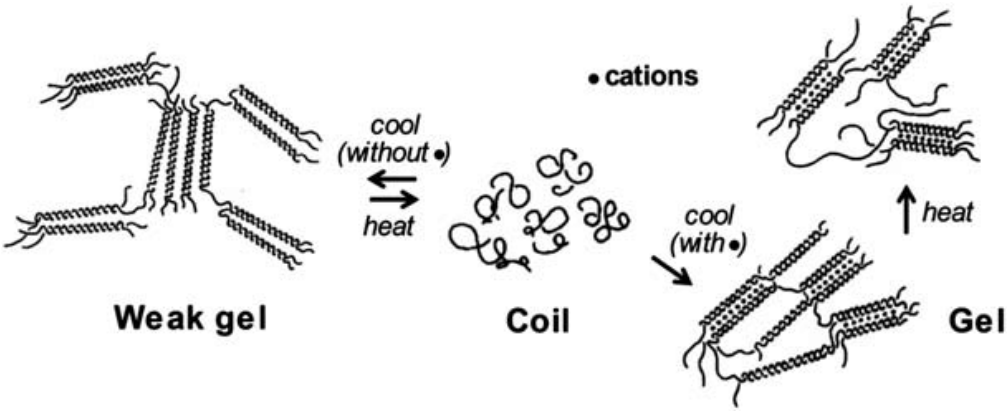


Fig. 2.9. A schematic illustration of how low acyl gellan gum undergoes conformational transitions Gels with and without cations as temperature changes are introduced. Adopted from Ferris et al. (2013)

In terms of decreasing GI values, several pilot studies have explored self-structured LAGG gels and gel-forming behaviours in the presence of rice starch in an acidic environment such as the stomach (Tamura & Ogawa, 2012; Bradbeer et al., 2014; Blanquet-Diot et al., 2021). The findings presented were promising as they demonstrated that the gel had a high resistance to shear force and the capability to increase viscosity at low pH. These characteristics make LAGG a potential option for low-GI and satiety-improving foods. Chung et al. (2007) performed the first study on the texture and *in vitro* digestibility of white rice cooked with LAGG solutions (0.3 and 0.7 %). The results showed that LAGG had the highest impact on the firm texture and SDS content in cooked rice among the six hydrocolloids (Xanthan gum, gellan gum, sodium alginate, locust bean gum, guar gum, and Arabic gum) tested. However, limited information was provided on the potential mechanism responsible for these results. The stability of LAGG hydrogels and their encapsulating strength of starch granules are also unknown as they transit through the digestion stages. Predicting the encapsulation properties of LAGG would provide the required knowledge to formulate and process reduced GI rice-based foods.

2.8 Summary of literature review

This chapter reviewed the literature related to white rice starch digestibility and its respective health impact, together with quantification methods of the GI and solutions explored to decrease it.

The relationship between health and diet is strict. The negative health impact of high-carbohydrate diets and the importance of GI as a health predictor for foods have been extensively covered in the literature. Several *in vivo* and *in vitro* digestion methods to study the impact of foods on health have been developed; however, they have been partially unsuccessful due to the high complexity of human physiological conditions and microstructural changes in food. During digestion, the food matrices disintegrate, i.e., there is a decrease in the structural organisation from the macroscopic to a nanoscopic level of the hierarchical structure at the end of the digestion process. The fashion by which structural disintegration occurs is essential as this ultimately affects the enzyme accessibility and digestion of nutrients. To the best of this thesis author's knowledge, there is still a gap in the literature relating food digestibility to the progressive disintegration of the food matrices; therefore, part of this thesis aims to build knowledge about this relationship.

An aspect of structural disintegration is starch hydrolysis and the related increase in GI, which has been studied by several authors with both *in vitro* and *in vivo* digestion models. Studying the literature about this area of research has been important for designing a suitable digestion model for the rice samples studied in this thesis. Solutions to decrease starch digestibility in rice, e.g. by imitating the structure of rice type with low-GI properties, use of hydrocolloids, and potential techniques to develop rice-based formulation with reduced GI, have been proposed by several researchers. Understanding previous research has been a good starting point for understanding the mechanisms characterising low-GI food manufacturing and proposing potential future innovations.

2.9 References

Alam, M. T., Parvez, N., & Sharma, P. K. (2014). FDA-Approved Natural Polymers for Fast Dissolving Tablets. Journal of Pharmaceutics, 2014(2), 1–6. doi.org/10.1155/2014/952970

Alfenas, R.D.C.G. and Paiva, E., 2007. Effect of glycemic index on satiety and body weight. Revista de Nutrição, 20, pp.197-202. doi.org/10.1590/S1415

Aljahdali, N. & Carbonero, F.(2017) Impact of Maillard reaction products on Nutrition and health: Current knowledge and need to understand their fate in the human digestive

system. Critical Reviews in Food Science and Nutrition, 0 (0): 1–14. doi:10.1080/10408398.2017.1378865.

An, L., Tao, Y., Chen, H., et al. (2020) Embryo-Endosperm Interaction and Its Agronomic Relevance to Rice Quality. Frontiers in Plant Science, 11: 587641. doi:10.3389/FPLS.2020.587641/BIBTEX.

Anderson, C., Milne, G. L., Park, Y. M. M., Sandler, D. P., & Nichols, H. B. (2018). Dietary glycemic index and glycemic load are positively associated with oxidative stress among premenopausal women. Journal of Nutrition, 148(1), 125–130. doi.org/10.1093/jn/nxx022

Anguizola, J., Matsuda, R., Barnaby, O.S., et al. (2013) Review: Glycation of human serum albumin. Clinica chimica acta; International Journal of Clinical Chemistry, 425: 64–76. doi:10.1016/j.cca.2013.07.013.

Arasteh, A., Farahi, S., Habibi-Rezaei, M., et al. (2014) Glycated albumin: an overview of the *In vitro* models of an *In vivo* potential disease marker. Journal of diabetes and metabolic disorders, 13 (1): 49. doi:10.1186/2251-6581-13-49.

Araya, H., Contreras, P., Alviña, M. et al. A comparison between an *in vitro* method to determine carbohydrate digestion rate and the glycemic response in young men. Eur J Clin Nutr 56, 735–739 (2002). doi.org/10.1038/sj.ejcn.1601386

Aravind, N., Sissons, M. & Fellows, C. (2011) Can variation in durum wheat pasta protein and starch composition affect *in vitro* starch hydrolysis? Food Chemistry, 124 (3): 816–821. doi:10.1016/j.foodchem.2010.07.002.

Atkinson, Fiona S., R., Kaye Foser-Powell, Kaye, et al. (2008) International Tables of Glycemic Index and Glycemic: 2008. Diabetes Care, 31 (12): 2281–2283. doi:10.2337/dc08-1239.J.B.M.

Atkinson, F.S., Brand-Miller, J.C., Foster-Powell, K., et al. (2021) International tables of glycemic index and glycemic load values 2021: a systematic review. The American Journal of Clinical Nutrition, 114 (5): 1625–1632. doi:10.1093/AJCN/NQAB233.

Augustin, L.S.A., Kendall, C.W.C., Jenkins, D.J.A., et al. (2015) Glycemic index, glycemic load and glycemic response: ICQC. Nutrition, Metabolism and Cardiovascular Diseases, 25 (9): 795–815. doi:10.1016/J.NUMECD.2015.05.005.

Ball, S.D., Keller, K.R., Moyer-Mileur, L.J., et al. (2003) Prolongation of satiety after low versus moderately high glycemic index meals in obese adolescents. Pediatrics, 111 (3): 488–94. doi: 10.1542/peds.111.3.488.

Bao, J. (2018) “Rice starch.” In Rice: Chemistry and Technology. Elsevier. pp. 55–108. doi:10.1016/B978-0-12-811508-4.00003-4.

Benjamin, O., Silcock, P., Beauchamp, J., et al. (2012) Tongue pressure and oral conditions affect volatile release from liquid systems in a model mouth. Journal of Agricultural and Food Chemistry, 60 (39): 9918–9927. doi:10.1021/jf3028232.

Benmoussa, M., Moldenhauer, K.A.K. & Hamaker, B.R. (2007) Rice Amylopectin Fine Structure Variability Affects Starch Digestion Properties. Journal of Agricultural and Food Chemistry, 55 (4): 1475–1479. doi:10.1021/JF062349X.

Bhavadharini, B., Mohan, V., Dehghan, M., et al. (2020) White Rice Intake and Incident Diabetes: A Study of 132,373 Participants in 21 Countries. Diabetes Care, 43 (11): 2643. doi:10.2337/DC19-2335.

Black, J.L. (2004) animal feed. Encyclopedia of Grain Science, pp. 11–20. doi:10.1016/B0-12-765490-9/00006-9.

Blakeney, A.B. and Matheson, N.K. (1984) Some Properties of the Stem and Pollen Starches of Rice. Starch, 36 (8): 265–269. doi:10.1002/STAR.19840360803.

Blanquet-Diot, S., François, O., Denis, S., et al. (2021) Importance of oral phase *in vitro* starch digestibility related to wholegrain versus refined pastas and mastication impairment. Food Hydrocolloids, 112. doi:10.1016/j.foodhyd.2020.106277.

Boers, H.M., Seijen Ten Hoorn, J. and Mela, D.J. (2015) A systematic review of the influence of rice characteristics and processing methods on postprandial glycaemic and insulinaemic responses. The British Journal of Nutrition, 114 (7): 1035. doi:10.1017/S0007114515001841.

Bohn, T., Carriere, F., Day, L., et al. (2018) Correlation between *in vitro* and *in vivo* data on food digestion. What can we predict with static *in vitro* digestion models? Critical Reviews in Food Science and Nutrition, 58 (13): 2239–2261. doi:10.1080/10408398.2017.1315362.

Boyer, F., Vidot, J.B., Dubourg, A.G., et al. (2015) Oxidative stress and adipocyte biology: Focus on the role of AGEs. Oxidative Medicine and Cellular Longevity, 2015. doi:10.1155/2015/534873.

Bradbeer, J.F., Hancocks, R., Spyropoulos, F., et al. (2014) Self-structuring foods based on acid-sensitive low and high acyl mixed gellan systems to impact on satiety. Food Hydrocolloids, 35 (100): 522. doi:10.1016/J.FOODHYD.2013.07.014.

Brand, J.C., Colagiuri, S., Crossman, S., et al. (1991) Low-Glycemic Index Foods Improve Long-Term Glycemic Control in NIDDM. Diabetes Care, 14 (2): 95 – 101. doi:10.2337/diacare.14.2.95.

Brandon, E.F.A., Oomen, A.G., Rompelberg, C.J.M., et al. (2006) Consumer product *in vitro* digestion model: Bioaccessibility of contaminants and its application in risk assessment. Regulatory Toxicology and Pharmacology, 44 (2): 161–171. doi:10.1016/J.YRTPH.2005.10.002.

Brodkorb, A., Egger, L., Alminger, M., et al. (2019) INFOGEST static *in vitro* simulation of gastrointestinal food digestion. Nature Protocols, 14 (4): 991–1014. doi:10.1038/s41596-018-0119-1.

Butterworth, P.J., Warren, F.J. and Ellis, P.R. (2011) Human α-amylase and starch digestion: An interesting marriage. Starch/Staerke, 63 (7): 395–405. doi:10.1002/star.201000150.

Cai, C., Tian, Y., Yu, Z., et al. (2020) *In vitro* Digestibility and Predicted Glycemic Index of Chemically Modified Rice Starch by One-Step Reactive Extrusion. Starch, 72 (1–2): 1900012. doi:10.1002/STAR.201900012.

Cai, J., Chao, C., Niu, B., et al. (2021) New insight into the interactions among starch, lipid and protein in model systems with different starches. Food Hydrocolloids, 112. doi:10.1016/J.FOODHYD.2020.106323.

Cai, Y., Li, S., Jiao, G., et al. (2018) OsPK2 encodes a plastidic pyruvate kinase involved in rice endosperm starch synthesis, compound granule formation and grain filling. Plant biotechnology journal, 16 (11): 1878–1891. doi:10.1111/PBI.12923.

Carcea, M. (2021) Value of wholegrain rice in a healthy human nutrition. Agriculture (Switzerland), 11 (8). doi:10.3390/agriculture11080720.

Chandel, N.S. (2021) Carbohydrate metabolism. Cold Spring Harbor Perspectives in Biology, 13 (1): 1–15. doi:10.1101/cshperspect.a040568.

Chen, S., Cohen, M.P. and Ziyadeh, F.N. (2000) Amadori-glycated albumin in diabetic nephropathy: Pathophysiologic connections. Kidney International, 58: S40–S44. doi:10.1046/j.1523-1755.2000.07707.x.

Chi, C., Li, X., Feng, T., et al. (2018) Improvement in Nutritional Attributes of Rice Starch with Dodecyl Gallate Complexation: A Molecular Dynamic Simulation and *in vitro* Study. Journal of Agricultural and Food Chemistry, 66 (35): 9282–9290. doi:10.1021/acs.jafc.8b02121.

Chi, C., Li, X., Huang, S., et al. (2021) Basic principles in starch multi-scale structuration to mitigate digestibility: A review. Trends in Food Science and Technology, 109: 154–168. doi:10.1016/J.TIFS.2021.01.024.

Chi, C., Shi, M., Zhao, Y., et al. (2022) Dietary compounds slow starch enzymatic digestion: A review. Frontiers in Nutrition, 9. doi:10.3389/FNUT.2022.1004966.

Chung, H.J., Liu, Q., Lee, L., et al. (2011) Relationship between the structure, physicochemical properties and *in vitro* digestibility of rice starches with different amylose contents. Food Hydrocolloids, 25 (5): 968–975. doi:10.1016/j.foodhyd.2010.09.011.

Chung, H.J., Liu, Q. and Lim, S.T. (2007) Texture and *in vitro* digestibility of white rice cooked with hydrocolloids. Cereal Chemistry, 84 (3): 246–249. doi:10.1094/CCHEM-84-3-0246.

Connor, H., Annan, F., Bunn, E., et al. (2003) The implementation of nutritional advice for people with diabetes. Diabetic medicine : a journal of the British Diabetic Association, 20 (10): 786–807. doi: 10.1046/j.1464-5491.2003.01104.x

Culetu, A., Duta, D. E., Papageorgiou, M., & Varzakas, T. (2021). The Role of Hydrocolloids in Gluten-Free Bread and Pasta; Rheology, Characteristics, Staling and Glycemic Index. Foods 2021, 10(12), 3121. doi.org/10.3390/FOODS10123121

Deferme, S., Annaert, P. and Augustijns, P. (2007) *In vitro* Screening Models to Assess Intestinal Drug Absorption and Metabolism. Drug Absorption Studies, pp. 182–215. doi:10.1007/978-0-387-74901-3_8.

Dhital, S., Warren, F.J., Butterworth, P.J., et al. (2016) Mechanisms of starch digestion by α-amylase—Structural basis for kinetic properties, 57 (5): 875–892. doi:10.1080/10408398.2014.922043.

Dome, K., Podgorbunskikh, E., Bychkov, A., et al. (2020) Changes in the Crystallinity Degree of Starch Having Different Types of Crystal Structure after Mechanical Pretreatment. Polymers, 12 (3). doi:10.3390/polym12030641.

Du, H., Van, D.L. and Feskens, E.J.M. (2006) Dietary glycaemic index: A review of the physiological mechanisms and observed health impacts. Acta Cardiologica, 61 (4): 383–397. doi:10.2143/AC.61.4.2017298.

Dupont, D., Alric, M., Blanquet-Diot, S., et al. (2019) Can dynamic *in vitro* digestion systems mimic the physiological reality? Critical Reviews in Food Science and Nutrition, 59 (10): 1546–1562. doi:10.1080/10408398.2017.1421900.

Egger, L., Schlegel, P., Baumann, C., et al. (2017) Physiological comparability of the harmonized INFOGEST *in vitro* digestion method to *in vivo* pig digestion. Food Research International, 102: 567–574. doi:10.1016/J.FOODRES.2017.09.047.

Elaine T. Champagne (2006) RICE: Chemistry and Technology, Third Edition. Third. doi:10.1094/1891127349.004.

Bertoft, E., 2017. Understanding starch structure: Recent progress. Agronomy, 7(3), p.56.doi.org/10.3390/agronomy7030056

Esfahani, A., Wong, J.M.W., Mirrahimi, A., et al. (2009) The Glycemic Index: Physiological Significance. Journal of the American College of Nutrition, 28 (4): 439S-445S. doi:10.1080/07315724.2009.10718109.

Ferris, C.J., Gilmore, K.J., Wallace, G.G., et al. (2013) Modified gellan gum hydrogels for tissue engineering applications. Soft Matter, 9 (14): 3705–3711. doi:10.1039/c3sm27389j.

Foster-Powell, K., Holt, S.H. and Brand-Miller, J.C. (2002) International table of glycemic index and glycemic load values: 2002. The American Journal of Clinical Nutrition, 76 (1): 5–56. doi:10.1093/ajcn/76.1.5.

Gallant, D.J., Bouchet, B., Buleon, A., et al. (1992) Physical characteristics of starch granules and susceptibility to enzymatic degradation. European Journal of Clinical Nutrition, 46. PMID: 1330527

Ruirui Gao, & Philip D. Chilibeck,(2019) Chapter 10 - Glycemic Index Meal Feeding and Lipid Profiling, Editor(s): Vinood B. Patel, The Molecular Nutrition of Fats, Academic Press,135-149, doi:10.1016/b978-0-12-811297-7.00010-x.

Gibbon, B.C., Wang, X. & Larkins, B.A. (2003) Altered starch structure is associated with endosperm modification in Quality Protein Maize., 100 (26): 15329. doi:10.1073/PNAS.2136854100.

Godber, J.S. and Juliano, B.O. (2004) Chapter 7 - Rice Lipids. RICE: Chemistry and Technology: 163–190. doi:10.1094/1891127349.007.

Goñi, I., Garcia-Alonso, A. and Saura-Calixto, F. (1997) A starch hydrolysis procedure to estimate glycemic index. Nutrition Research, 17 (3): 427–437. doi:10.1016/S0271-5317(97)00010-9.

Greenwood, D.C., Threapleton, D.E., Evans, C.E.L., et al. (2013) Glycemic index, glycemic load, carbohydrates, and type 2 diabetes: Systematic review and dose-response meta-analysis of prospective studies. Diabetes Care, 36 (12): 4166–4171. doi:10.2337/dc13-0325.

Guilbaud, A., Niquet-Leridon, C., Boulanger, E., et al. (2016) How Can Diet Affect the Accumulation of Advanced Glycation End-Products in the Human Body? Foods, 5 (4). doi:10.3390/foods5040084.

Guillén, S., Oria, R. & Salvador, M.L. (2018) Impact of Cooking Temperature on *in vitro* Starch Digestibility of Rice Varieties with Different Amylose Contents. Polish Journal of Food and Nutrition Sciences, 68 (4): 319–325. doi:10.2478/pjfns-2018-0001.

Hamad, S., Zafar, T.A. & Sidhu, J. (2018) Parboiled rice metabolism differs in healthy and diabetic individuals with similar improvement in glycemic response. Nutrition, 47: 43–49. doi:10.1016/J.NUT.2017.09.010.

Huang, Y., Yang, N., Zhang, Y., Hou, J., Gao, Y., Tian, L., Jin, Z., Shen, Y., & Guo, S. (2021). The gelling behavior of gellan in the presence of different sodium salts. International Journal of Biological Macromolecules, 193, 768–777. doi.org/10.1016/J.IJBIOMAC.2021.10.173

He, H., Bian, H., Xie, F., et al. (2021) Different effects of pectin and κ-carrageenan on the multiscale structures and *in vitro* digestibility of extruded rice starch. Food Hydrocolloids, 111. doi:10.1016/J.FOODHYD.2020.106216.

Henning, C. and Glomb, M.A. (2016) Pathways of the Maillard reaction under physiological conditions. Glycoconjugate Journal, 33 (4): 499–512. doi:10.1007/s10719-016-9694-y.

Hoad, C.L., Rayment, P., Spiller, R.C., et al. (2004) *In vivo* Imaging of Intragastric Gelation and Its Effect on Satiety in Humans. The Journal of Nutrition, 134 (9): 2293–2300. doi:10.1093/JN/134.9.2293.

Hussain, M., Bakalis, S., Gouseti, O., et al. (2015) Dynamic and shear stress rheological properties of guar galactomannans and its hydrolyzed derivatives. International Journal of Biological Macromolecules, 72: 687–691. doi.org/10.1016/j.ijbiomac.2014.09.019

Jeevetha, S. (2014) Relationship between Amylose Content and Glycemic Index of Commonly Consumed White Rice. IOSR Journal of Agriculture and Veterinary Science, 7 (9): 12–18. doi:10.9790/2380-07931218.

Jenkins, P.J. and Donald, A.M., 1995. The influence of amylose on starch granule structure. International journal of biological macromolecules, 17(6), pp.315-321.doi.org/10.1016/0141-8130(96)81838-1

Jenkins, D.J., Wolever, T.M., Taylor, R.H., et al. (1981) Glycemic index of foods: a physiological basis for carbohydrate exchange. The American Journal of Clinical Nutrition, 34 (3): 362–366. doi:10.1093/ajcn/34.3.362.

Jenkins, D. J. A., Kendall, C. W. C., McKeown-Eyssen, G.,et al (2008). Effect of a Low–Glycemic Index or a High–Cereal Fiber Diet on Type 2 Diabetes: A Randomized Trial. JAMA, 300(23), 2742–2753.

Jukanti, A.K., Pautong, P.A., Liu, Q., et al. (2020) Low glycemic index rice—a desired trait in starchy staples. Trends in Food Science & Technology, 106: 132–149. doi:10.1016/J.TIFS.2020.10.006.

Kanyuck, K. M., Mills, T. B., Norton, I. T., & Norton-Welch, A. B. (2022). Release of glucose and maltodextrin DE 2 from gellan gum gels and the impacts of gel structure. Food Hydrocolloids, 122, 107090. doi.org/10.1016/J.FOODHYD.2021.107090

Kaur, B., Quek Yu Chin, R., Camps, S., et al. (2016) The impact of a low glycaemic index (GI) diet on simultaneous measurements of blood glucose and fat oxidation: A whole body calorimetric study. Journal of Clinical & Translational Endocrinology, 4: 45. doi:10.1016/J.JCTE.2016.04.003.

Kaur, L. & Singh, J. (2016) "Microstructure, Starch Digestion, and Glycemic Index of Potatoes." In Advances in Potato Chemistry and Technology. Elsevier. pp. 369–402. doi:10.1016/B978-0-12-800002-1.00013-3.

Kong, F. & Singh, R.P. (2010) A Human Gastric Simulator (HGS) to Study Food Digestion in the Human Stomach. Journal of Food Science, 75 (9): E627–E635. doi:10.1111/j.1750-3841.2010.01856.x.

Lambadiari, V., Korakas, E., & Tsimihodimos, V. (2020). The Impact of Dietary Glycemic Index and Glycemic Load on Postprandial Lipid Kinetics, Dyslipidemia and Cardiovascular Risk. Nutrients 2020, Vol. 12, Page 2204, 12(8), 2204. doi.org/10.3390/NU12082204

Langworthy, C.F. and Deuel, H.J. (1922) digestibility of raw rice, arrowroot, canna, cassava, taro, tree-fern, and potato starches. Journal of Biological Chemistry, 52 (1): 251–261. doi:10.1016/S0021-9258(18)85868-9.

Li, C., Gong, B., Hu, Y., et al. (2020) Combined crystalline, lamellar and granular structural insights into *in vitro* digestion rate of native starches. Food Hydrocolloids, 105. doi.org/10.1016/j.foodhyd.2020.105823

Li, H., Gui, Y., Li, J., et al. (2020) Modification of rice starch using a combination of autoclaving and triple enzyme treatment: Structural, physicochemical and digestibility properties. International Journal of Biological Macromolecules, 144: 500–508. doi:10.1016/J.IJBIOMAC.2019.12.112.

Li, N., Zhao, S., Qiao, D., et al. (2021) Multiscale Structural Disorganization of Indica Rice Starch under Microwave Treatment with High Water Contents. ACS Food Science & Technology, 1 (1): 45–53. doi:10.1021/acsfoodscitech.0c00080.

Lucas-González, R., Viuda-Martos, M., Pérez-Alvarez, J.A., et al. (2018) *In vitro* digestion models suitable for foods: Opportunities for new fields of application and challenges. Food Research International, 107 (February): 423–436. doi:10.1016/j.foodres.2018.02.055.

Ludwig, D.S. (2002) The glycemic index: physiological mechanisms relating to obesity, diabetes, and cardiovascular disease. JAMA, 287 (18): 2414–23. doi.org/10.1001/jama.287.18.2414

Madhu, S. (2017) Glycaemic index: challenges in translating concept to practice. International Journal of Diabetes in Developing Countries, 37 (4): 377–378. doi:10.1007/S13410-017-0585-Y

Manful, J.T., Grimm, C.C., Gayin, J., et al. (2008) Effect of variable parboiling on crystallinity of rice samples. Cereal Chemistry, 85 (1): 92–95. doi:10.1094/CCHEM-85-1-0092.

Mann, J., Cummings, J.H., Englyst, H.N., et al. (2007) FAO/WHO Scientific Update on carbohydrates in human Nutrition: conclusions. European Journal of Clinical Nutrition, 61 (S1): S132–S137. doi:10.1038/sj.ejcn.1602943.

Marciani, L., Gowland, P.A., Spiller, R.C., et al. (2001) Effect of meal viscosity and nutrients on satiety, intragastric dilution, and emptying assessed by MRI. American Journal of Physiology-Gastrointestinal and Liver Physiology, 280 (6): G1227–G1233. doi:10.1152/ajpgi.2001.280.6.G1227.

Miao, M., Xiong, S., Jiang, B., et al. (2014) Dual-enzymatic modification of maize starch for increasing slow digestion property. Food Hydrocolloids, 38: 180–185. doi:10.1016/J.FOODHYD.2013.12.006.

Milivojevic, M., Pajic-Lijakovic, I., Bugarski, B., et al. (2019) “Gellan gum in drug delivery applications.” In Natural Polysaccharides in Drug Delivery and Biomedical Applications. Elsevier. pp. 145–186. doi:10.1016/B978-0-12-817055

Miller, J.B., Pang, E. and Bramall, L. (1992) Rice: a high or low glycemic index food? The American Journal of Clinical Nutrition, 56 (6): 1034–1036. doi:10.1093/ajcn/56.6.1034.

Miller, V., Jenkins, D. A., Dehghan, M., et al (2024). Associations of the glycaemic index and the glycaemic load with risk of type 2 diabetes in 127 594 people from 20 countries (PURE): a prospective cohort study. The Lancet Diabetes & Endocrinology, 0(0). doi.org/10.1016/S2213-8587(24)00069-X

Mills, T., Norton, I.T. and Bakalis, S. (2013) Development of tribology equipment to study dynamic processes. Journal of Food Engineering, 114 (3): 384–390. doi.org/10.1016/j.jfoodeng.2012.08.030

Minekus, M., Alminger, M., Alvito, P., et al. (2014) A standardised static *in vitro* digestion method suitable for food – an international consensus. Food Funct., 5 (6): 1113–1124. doi:10.1039/C3FO60702J.

Mirrahimi, A., de Souza, R.J., Chiavaroli, L., et al. (2012) Associations of glycemic index and load with coronary heart disease events: a systematic review and meta-analysis of prospective cohorts. Journal of the American Heart Association, 1 (5): 1–13. doi:10.1161/JAHA.112.000752.

Mohan, V., Spiegelman, D., Sudha, V., et al. (2014) Effect of Brown Rice, White Rice, and Brown Rice with Legumes on Blood Glucose and Insulin Responses in Overweight Asian Indians: A Randomized Controlled Trial. https://home.liebertpub.com/dia, 16 (5): 317–325. doi:10.1089/DIA.2013.0259.

Monro, J.A. & Shaw, M. (2008) Glycemic impact, glycemic glucose equivalents, glycemic index, and glycemic load: Definitions, distinctions, and implications. In American Journal of Clinical Nutrition. 1 January 2008. Narnia. pp. 237S-243S. doi:10.1093/ajcn/87.1.237S.

Mosele, J.I., Macià, A., Romero, M.-P., et al. (2015) Application of *in vitro* gastrointestinal digestion and colonic fermentation models to pomegranate products (juice, pulp and peel extract) to study the stability and catabolism of phenolic compounds. Journal of Functional Foods, 14: 529–540. doi:10.1016/J.JFF.2015.02.026.

Moxon, T.E., Gouseti, O. & Bakalis, S. (2016) In silico modelling of mass transfer & absorption in the human gut. Journal of Food Engineering, 176: 110–120. doi:10.1016/j.jfoodeng.2015.10.019.

Mulet-Cabero, A.I., Rigby, N.M., Brodkorb, A., et al. (2017) Dairy food structures influence the rates of nutrient digestion through different *in vitro* gastric behaviour. Food Hydrocolloids, 67: 63–73. doi:10.1016/j.foodhyd.2016.12.039.

Ngo, T. Van, Kunyanee, K. & Luangsakul, N. (2023) Insights into Recent Updates on Factors and Technologies That Modulate the Glycemic Index of Rice and Its Products. Foods, 12 (19). doi:10.3390/FOODS12193659.

Ojo, Adebowale, F., et al. (2018) The Effect of Dietary Glycaemic Index on Glycaemia in Patients with Type 2 Diabetes: A Systematic Review and Meta-Analysis of Randomized Controlled Trials. Nutrients, 10 (3). doi:10.3390/nu10030373.

Osmałek, T., Froelich, A., & Tasarek, S. (2014). Application of gellan gum in pharmacy and medicine. International Journal of Pharmaceutics, 466(1–2), 328–340. doi.org/10.1016/J.IJPHARM.2014.03.038

Ogawa, E., Takahashi, R., Yajima, H., & Nishinari, K. (2006). Effects of molar mass on the coil to helix transition of sodium-type gellan gums in aqueous solutions. Food Hydrocolloids, 20(2–3), 378–385. doi.org/10.1016/J.FOODHYD.2005.03.016

Palumbo, F. S., Federico, S., Pitarresi, G., Fiorica, C., & Giammona, G. (2020a). Gellan gum-based delivery systems of therapeutic agents and cells. Carbohydrate Polymers, 229, 115430. doi.org/10.1016/J.CARBPOL.2019.115430

Patindol, J., Siebenmorgen, T. & Wang, Y.-J. (2014) Impact of environmental factors on rice starch structure: A review. Starch - Starke, 67. doi:10.1002/star.201400174.

Pawlak, D. B., Bryson, J. M., Denyer, G. S., & Brand-Miller, J. C. (2001). High Glycemic Index Starch Promotes Hypersecretion of Insulin and Higher Body Fat in Rats without Affecting Insulin Sensitivity. The Journal of Nutrition, 131(1), 99–104. doi.org/10.1093/JN/131.1.99

Petitot, M., Abecassis, J. & Micard, V. (2009) Structuring of pasta components during processing: impact on starch and protein digestibility and allergenicity. Trends in Food Science and Technology, 20 (11–12): 521–532. doi:10.1016/j.tifs.2009.06.005.

Pirsa, S., & Hafezi, K. (2023). Hydrocolloids: Structure, preparation method, and application in food industry. Food Chemistry, 399, 133967. doi.org/10.1016/J.FOODCHEM.2022.133967

Puncha-Arnon, S. & Uttapap, D. (2013) Rice starch vs. rice flour: Differences in their properties when modified by heat-moisture treatment. Carbohydrate Polymers, 91 (1): 85–91. doi:10.1016/j.carbpol.2012.08.006.

Reed, M.O., Ai, Y., Leutcher, J.L., et al. (2013) Effects of Cooking Methods and Starch Structures on Starch Hydrolysis Rates of Rice. Journal of Food Science, 78 (7): H1076–H1081.doi.org/10.1111/1750-3841.12165

Rivera Del Rio A , Keppler JK , Boom RM et al.,(2021) . Protein acidification and hydrolysis by pepsin ensure efficient trypsin-catalyzed hydrolysis. Food Function. May 21;12(10):4570-4581. doi: 10.1039/d1fo00413a.

Rondeau, P. & Bourdon, E. (2011) The glycation of albumin: Structural and functional impacts. Biochimie, 93 (4): 645–658. doi:10.1016/j.biochi.2010.12.003.

Salles, C., Tárrega, A., Mielle, P., et al. (2007) Development of a chewing simulator for food breakdown and the analysis of *in vitro* flavor compound release in a mouth environment. Journal of Food Engineering, 82: 189–198. doi:10.1016/j.jfoodeng.2007.02.008.

Salmeron, J., Ascherio, A., Rimm, E.B., et al. (1997) Dietary Fiber, Glycemic Load, and Risk of NIDDM in Men. Diabetes Care, 20 (4): 545–550. doi:10.2337/diacare.20.4.545.

Saneei, P., Larijani, B. & Esmaillzadeh, A. (2017) Rice consumption, incidence of chronic diseases and risk of mortality: Meta-analysis of cohort studies. Public Health Nutrition, 20 (2): 233–244. doi:10.1017/S1368980016002172.

Schwingshackl, L., & Hoffmann, G. (2013). Long-term effects of low glycemic index/load vs. high glycemic index/load diets on parameters of obesity and obesity-associated risks: A systematic review and meta-analysis. Nutrition, Metabolism and Cardiovascular Diseases, 23(8), 699–706. doi.org/10.1016/J.NUMECD.2013.04.008

Sheard, N.F., Clark, N.G., Brand-Miller, J.C., et al. (2004) Dietary carbohydrate (amount and type) in the prevention and management of diabetes: A statement by the American Diabetes Association. Diabetes Care. 27 (9). 2266–2271. doi:10.2337/diacare.27.9.2266.

Shen, L., Li, J. & Li, Y. (2022a) Resistant starch formation in rice: Genetic regulation and beyond. Plant Communications, 3 (3): 100329. doi:10.1016/J.XPLC.2022.100329.

Shen, Y., Hong, S., Singh, G., et al. (2022b) Improving functional properties of pea protein through “green” modifications using enzymes and polysaccharides. Food Chemistry, 385: 132687. doi:10.1016/J.FOODCHEM.2022.132687.

Sivakamasundari, S.K., Moses, J.A. & Anandharamakrishnan, C. (2020) Effect of parboiling methods on the physicochemical characteristics and glycemic index of rice varieties. Journal of Food Measurement and Characterisation, 14 (6): 3122–3137. doi:10.1007/s11694-020-00551-9.

Stevens, L. R., Gilmore, K. J., Wallace, G. G., & In het Panhuis, M. (2016). Tissue engineering with gellan gum. Biomaterials Science, 4(9), 1276–1290. doi.org/10.1039/c6bm00322b

Sujka, M. and Jamroz, J. (2010) Characteristics of pores in native and hydrolyzed starch granules. Starch - Stärke, 62 (5): 229–235. doi:10.1002/STAR.200900226.

Sworn, G. & Stouby, L. (2021) Gellan gum. Handbook of Hydrocolloids. 855–885. doi:10.1016/B978-0-12-820104-6.00009-7.

Syahariza, Z.A., Sar, S., Hasjim, J., et al. (2013) The importance of amylose and amylopectin fine structures for starch digestibility in cooked rice grains. Food Chemistry, 136 (2): 742–749. doi:10.1016/J.FOODCHEM.2012.08.053.

Tamura, M. & Ogawa, Y. (2012) Visualization of the coated layer at the surface of rice grain cooked with varying amounts of cooking water. Journal of Cereal Science, 56 (2): 404–409. doi:10.1016/j.jcs.2012.06.002.

Tang, H., Mitsunaga, T. & Kawamura, Y. (2006) Molecular arrangement in blocklets and starch granule architecture. Carbohydrate Polymers, 63 (4): 555–560. doi.org/10.1016/j.carbpol.2005.10.016

Tappy, L., Lê, K.-A., Abdel-Sayed, A., et al. (2010) Metabolic effects of fructose and the worldwide increase in obesity. Physiological reviews, 90 (1): 23–46. doi:10.1152/physrev.00019.2009.

Tester, R.F., Karkalas, J. & Qi, X. (2004) Starch structure and digestibility Enzyme-Substrate relationship. World's Poultry Science Journal, 60 (2): 186–195. doi:10.1079/WPS200312.

Tharakan, A., Norton, I.T., Fryer, P.J., et al. (2010) Mass transfer and nutrient absorption in a simulated model of small intestine. Journal of Food Science, 75 (6). doi:10.1111/j.1750-3841.2010.01659.x.

Tian, J., Cai, Y., Qin, W., et al. (2018) Parboiling reduced the crystallinity and *in vitro* digestibility of non-waxy short grain rice. Food Chemistry, 257: 23–28. doi:10.1016/j.foodchem.2018.03.005.

Vandeputte, G.E., Derycke, V., Geeroms, J., et al. (2003) Rice starches. II. Structural aspects provide insight into swelling and pasting properties. Journal of Cereal Science, 38 (1): 53–59. doi:10.1016/S0733-5210(02)00141-8.

Vardakou, M., Mercuri, A., Barker, S.A., et al. (2011) Achieving Antral Grinding Forces in Biorelevant *In vitro* Models: Comparing the USP Dissolution Apparatus II and the Dynamic Gastric Model with Human *In vivo* Data. AAPS PharmSciTech, 12 (2): 620–626. doi:10.1208/s12249-011-9616-z.

Vega-López, S., Ausman, L.M., Griffith, J.L., et al. (2007) Interindividual variability and intra-individual reproducibility of glycemic index values for commercial white bread. Diabetes Care, 30 (6): 1412–1417. doi:10.2337/dc06-1598.

Wang, H., Liu, Y., Chen, L., et al. (2018) Insights into the multi-scale structure and digestibility of heat-moisture treated rice starch. Food Chemistry, 242: 323–329. doi:10.1016/J.FOODCHEM.2017.09.014.

Wang, J., Wu, P., Liu, M., et al. (2019) An advanced near real dynamic: *In vitro* human stomach system to study gastric digestion and emptying of beef stew and cooked rice. Food and Function, 10 (5): 2914–2925. doi:10.1039/c8fo02586j.

Wang, K., Wang, W., Ye, R., et al. (2017) Mechanical and barrier properties of maize starch–gelatin composite films: effects of amylose content. Journal of the Science of Food and Agriculture, 97 (11): 3613–3622. doi:10.1002/jsfa.8220.

Wang, S., Chao, C., Cai, J., et al. (2020) Starch–lipid and starch–lipid–protein complexes: A comprehensive review. Comprehensive Reviews in Food Science and Food Safety, 19 (3): 1056–1079. doi:10.1111/1541-4337.12550.

Wang, S. & Copeland, L. (2013) Molecular disassembly of starch granules during gelatinization and its effect on starch digestibility: A review. Food and Function. 4 (11). 1564–1580. doi:10.1039/c3fo60258c.

Wang, S., Li, P., Zhang, T., et al. (2017) *In vitro* starch digestibility of rice flour is not affected by method of cooking. LWT, 84: 536–543. doi:10.1016/J.LWT.2017.06.023.

Wang, S., Zhang, X., Wang, S., et al. (2016) Changes of multi-scale structure during mimicked DSC heating reveal the nature of starch gelatinization. Scientific Reports, 6: 1–9. doi:10.1038/srep28271.

Wang, S., Zheng, M., Yu, J., et al. (2017) Insights into the Formation and Structures of Starch-Protein-Lipid Complexes. Journal of Agricultural and Food Chemistry, 65 (9): 1960–1966. doi:10.1021/ACS.JAFC.6B05772.

Whittaker, L. E., Al-Ruqaie, I. M., Kasapis, S., & Richardson, R. K. (1997). Development of composite structures in the gellan polysaccharide/sugar system. Carbohydrate Polymers, 33(1), 39–46. doi.org/10.1016/S0144-8617(97)00027-1

Whitcomb, E.A., Chiu, C.-J. & Taylor, A. (2015) Dietary glycemia as a determinant of health and longevity. Molecular aspects of medicine, 46: 14–20. doi:10.1016/j.mam.2015.08.005.

Wolever, T.M. & Bolognesi, C. (1996a) Prediction of glucose and insulin responses of normal subjects after consuming mixed meals varying in energy, protein, fat, carbohydrate and glycemic index. The Journal of Nutrition, 126 (11): 2807–12. doi:10.1093/jn/126.11.2807.

Wolever, T. M., & Bolognesi, C. (1996b). The source and amount of carbohydrates affect postprandial glucose and insulin in normal subjects. The Journal of Nutrition, 126(11), 2798–2806. doi.org/10.1093/jn/126.11.2798

Wolever, T.M., Brand-Miller, J.C., Abernethy, J., et al. (2008) Measuring the glycemic index of foods: interlaboratory study. The American Journal of Clinical Nutrition, 87 (1): 247S-257S. doi:10.1093/ajcn/87.1.247S.

Wolever, T.M.S. (2006) Physiological mechanisms and observed health impacts related to the glycaemic index: Some observations. International Journal of Obesity, 30: S72–S78. doi:10.1038/sj.ijo.0803496.

Woolnough, J.W., Monro, J.A., Brennan, C.S., et al. (2008) Simulating human carbohydrate digestion *in vitro*: A review of methods and the need for standardisation. International Journal of Food Science and Technology, 43 (12): 2245–2256. doi:10.1111/j.1365-2621.2008.01862.x.

Wu, P., Deng, R., Wu, X., et al. (2017) *In vitro* gastric digestion of cooked white and brown rice using a dynamic rat stomach model. Food Chemistry, 237: 1065–1072. doi:10.1016/J.FOODCHEM.2017.05.081.

Ye, J., Liu, C., Luo, S., et al. (2019) A simulated gastrointestinal tract study of texturized rice grains: Impact of texturization on starch digestibility. Journal of Cereal Science, 89: 102800. doi:10.1016/j.jcs.2019.102800.

Younes, M., Aggett, P., Aguilar, F., et al. (2018) Re-evaluation of gellan gum (E 418) as food additive. EFSA Journal, 16 (6). doi:10.2903/J.EFSA.2018.5296.

Yu, W., Tao, K. & Gilbert, R.G. (2018) Improved methodology for analyzing relations between starch digestion kinetics and molecular structure. Food Chemistry, 264.284–292. doi:10.1016/j.foodchem.2018.05.049.

Zafar, M.I., Mills, K.E., Zheng, J., et al. (2019) Low glycaemic index diets as an intervention for obesity: a systematic review and meta-analysis. Obesity Reviews, 20 (2): 290–315. doi:10.1111/obr.12791.

Zhang, G., Malik, V.S., Pan, A., et al. (2010) Substituting Brown Rice for White Rice to Lower Diabetes Risk: A Focus-Group Study in Chinese Adults. Journal of the American Dietetic Association, 110 (8): 1216–1221. doi:10.1016/J.JADA.2010.05.004.

Zhang, G., Venkatachalam, M. and Hamaker, B.R. (2006) Structural basis for the slow digestion property of native cereal starches. Biomacromolecules, 7 (11): 3259–3266. doi:10.1021/bm060343a.

Zhang, X., Liao, Z., Wu, P., et al. (2018) Effects of the gastric juice injection pattern and contraction frequency on the digestibility of casein powder suspensions in an *in vitro* dynamic rat stomach made with a 3D printed model. Food Research International, 106 (1): 495–502. doi:10.1016/j.foodres.2017.12.082.

Zhong, Y., Chen, Y., Pan, M., et al. (2023) Insights into the Functional Components in Wheat Grain: Spatial Pattern, Underlying Mechanism and Cultivation Regulation.12 (11): 2192. doi:10.3390/PLANTS12112192.

Zhou, S., Hong, Y., Gu, Z., et al. (2020) Effect of heat-moisture treatment on the *in vitro* digestibility and physicochemical properties of starch-hydrocolloid complexes. Food Hydrocolloids, 104. doi:10.1016/J.FOODHYD.2020.105736.

Zhou, Z., Robards, K., Helliwell, S., et al. (2002) Composition and functional properties of rice. International Journal of Food Science & Technology, 37 (8): 849–868. doi:10.1046/J.1365-2621.2002.00625.X.

Ziaee, A., Afaghi, A. & Sarreshtehdari, M. (2011) Effect of Low Glycemic Load Diet on Glycated Hemoglobin (HbA1c) in Poorly-Controlled Diabetes Patients. Global Journal of Health Science, 4 (1): 211–6. doi:10.5539/gjhs.v4n1p211.

3 Materials and methods

3.1 Materials: sample selection

Six white rice types commercially available in local supermarkets (Nottingham, UK), 2 of which with high-, 2 with medium-, and 2 with low-glycaemic index (GI) (**Tab. 3.1**), were initially chosen as they are commonly consumed in the UK, therefore having a relevant contribution on regulating glucose homeostasis daily. Among these 6, the ones with the highest GI and the lowest GI were selected.

The mean of macronutrient (carbohydrates, proteins, fat, fibre) values listed on the nutrition labels of rice of the same type but of different brands were used as the key nutritional factors associated with the GI (**Tab. 3.1**). GI values reported in this study referred to the international table for GI (Atkinson et al., 2021).

Among the four nutrition components (i.e., carbohydrate, protein, fat, fibre), carbohydrate and protein were identified through principal component analysis (PCA) to be directly responsible for the difference in rice GI values (as shown in **Fig. 3.1**). The carbohydrate (specifically starch) positively correlated with rice GI values, whereas protein negatively correlated with rice GI values; fibre and lipid had an intermediate correlation. Regarding the two selected white rice types, both *Oryza sativa indica*, the high-GI (89) type was Thai Jasmine rice (JR, Green Dragon Thai Hom Mali Aaa, purchase date December 2018; no parboiling involved in the manufacturing process), whereas the low-GI (47) type was easy-cook long grain rice, also called parboiled rice (PR), purchase date January 2019.

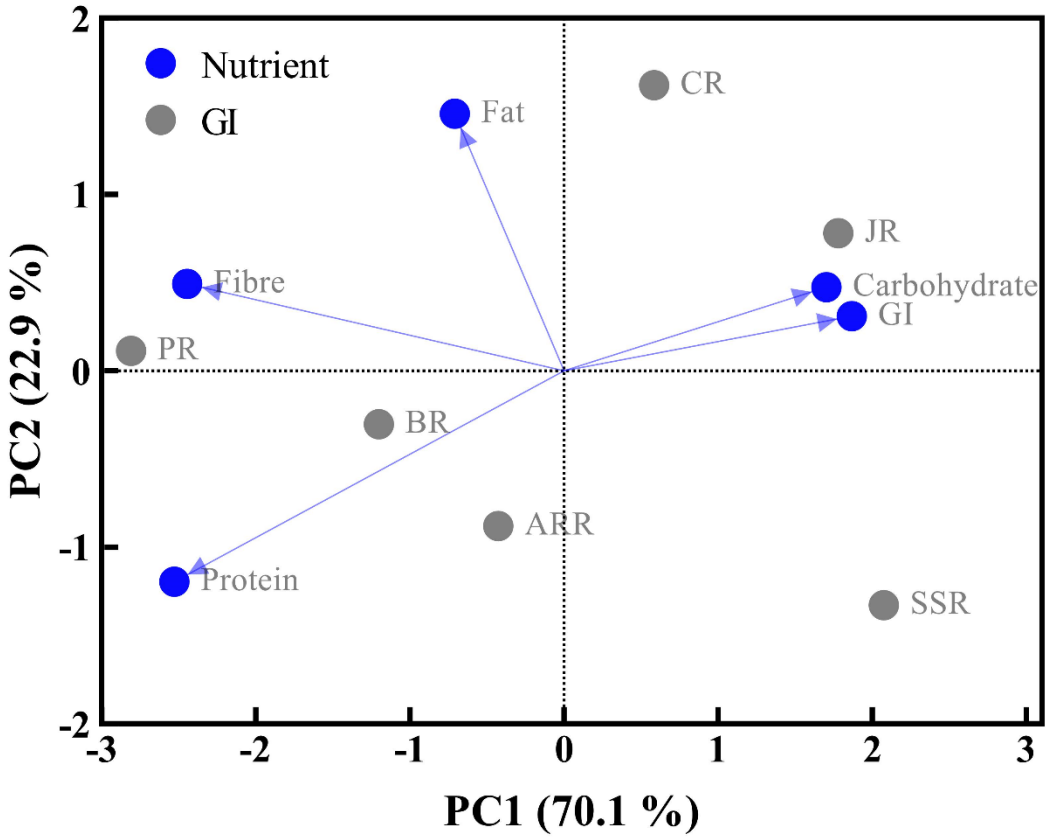


Fig. 3.1. PCA scores and loading plots of GI and main nutrient contents of the six white rice types. The main nutrients are carbohydrates, protein, fat, and fibre. Kaiser-Meyer-Olkin test results are between 0.5 and 1 (0.507), suggesting that the sample quantity is sufficiently high for the analysis. The spherical test results were significant ($p < 0.05$), meaning there was a reasonable correlation between variables to apply a dimension reduction.

Tab. 3.1. Nutritional information (as listed on the food label) and GI of the six commercial white rice types. All values were reported for 100 g of raw rice.

	CR	ARR	BR	PR	JR	SSR
Energy	347.8 ± 2.7[a]	349.9 ± 2.1[a]	354.8 ± 6.1[a]	352.3 ± 0.5[a]	351.8 ± 5.2[a]	357.0 ± 9.9[a]
Fat	1.0 ± 0.1[a]	1.0 ± 0.1[a]	1.1 ± 0.5[a]	1.2 ± 0.5[a]	1.2 ± 0.6[a]	0.9 ± 0.2[a]
Carbohydrates	79.3 ± 0.8[a]	77.5 ± 1.1[a]	78.7 ± 3.4[a]	76.8 ± 0.6[a]	80.5 ± 2.3[a]	79.4 ± 0.9[a]
Of which starch [Φ]	77.8 ± 0.8[a]	76.3 ± 0.9[a]	77.4 ± 1.9[a]	75.2 ± 0.6[a]	79.4 ± 1.3[a]	77.9 ± 0.8[a]
Fibre	1.5 ± 0.8[a]	1.2 ± 0.7[a]	1.3 ± 0.8[a]	1.6 ± 0.1[a]	1.1 ± 0.3[a]	1.5 ± 0.8[a]
Protein	6.7 ± 0.1[a]	7.3 ± 0.3[ab]	7.7 ± 0.3[b]	7.8 ± 0.2[b]	6.9 ± 0.2[a]	6.4 ± 0.1[b]
GI	83 ± 13[a*]	69 ± 7[b*]	55 ± 10 [bc**]	47 ± 6 [c**]	89 ± 6[a*]	70 ± 6[b*]

For each rice type, values are reported as mean ± standard deviation (S.D.) of different commercially available brands. Values in the same row with different superscripts are significantly different from each other ($p < 0.05$). CR (Calrose rice; a paella rice type) - brands: Sunrice, Botan, Sunwhite. ARR (Arborio risotto rice) - brands: Easy C, Morrisons, Coop, Marks & Spencer. BR (Basmati rice) - brands: Ocado Tilda, Laila, Marks & Spencer. PR (Parboiled rice) – brands: Tesco, Tollyboy Tilda, Laila. JR (Jasmine rice) - brands: Tesco Thai Hom Mali, Mali Thai, Tilda, Royal Umbrella, Green Dragon. SSR (Sushi rice) - brands: Tesco Yutaka, Biona, Marks & Spencer. Spanish paella rice, short-grain white rice sold in the UK, was not included in the study as no information is available regarding the rice variety used. It is known that Bomba rice is one of the most common paella rice varieties; however, to the best of our knowledge, only *in vitro* GI results have been reported. Thus, the present study does not include this white rice type.

Symbol * A measurement of the GI was conducted in the UK (Ranawana et al., 2009).

Symbol ** Values from the international table of GI and GL for 2021 (Atkinson et al., 2021).

Symbol Φ Total starch estimated by subtracting the fibre from the total carbohydrate.

3.2 Sample preparation

3.2.1 Rice flour production and respective starch isolation

Samples (100 g) of the two selected rice types, JR and PR, were rinsed three times with distilled water and dried at ambient temperature for 1 h on 500 μm sieves to prepare rice flour. The grains were then ground into flour by using an electrical grinder (KG49, Delonghi, Treviso, Italy) and then passed through a sieve with a mesh size of 500 μm to discard the particles over 500 μm (Zhu et al., 2020). The protein and starch separation process from the rice flour is shown in **Fig 3.2**. Proteins were first extracted under alkaline conditions, as in De Souza et al. (2016). In brief, rice flour was steeped at 30°C for 1 h with sodium hydroxide (NaOH) solution (0.18 %, w/v) to allow protein bodies to be effectively removed with minimal disruption of starch granules (Daiana et al., 2016). Upon centrifugation (4000 rpm, 15 mins), the supernatant (protein-rich fractions) was carefully removed for protein precipitation. The starch-rich pellets were washed with 125 mL 0.18 % NaOH and again centrifuged (4000 rpm, 15 mins). This washing extract was combined with the protein extract obtained previously. The starchy residue was then re-suspended in distilled water (1:1, w/v), neutralised (pH 7.0) with ~30 mL of 0.1 M HCl and dried in a convection oven (MOV-112F, Sanyo, Japan) at 30°C for 36 hs (until constant weight).

Protein precipitation was achieved by adding 0.1 M HCl to the collected supernatant to reach the protein isoelectric point (pH 4.8). After centrifugation (4000 rpm, 15 mins), the protein extract was neutralised with 0.1 M NaOH and dried at 30°C for 24 hs.

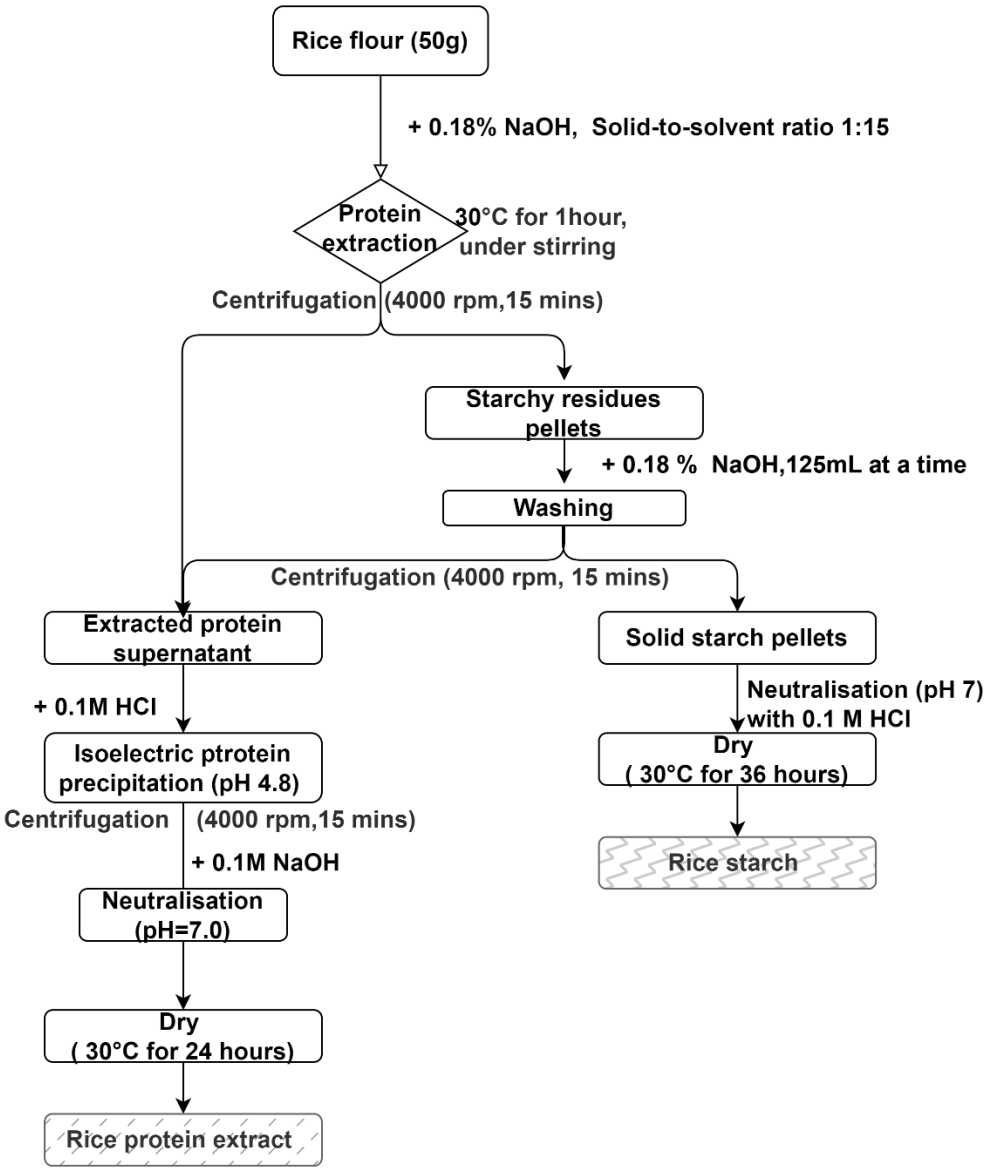


Fig. 3.2. Flowchart of the starch and protein separation process from rice flour used in this study.

3.2.2 Morphological properties of rice flour and starch

The morphological differences (size and shape) between JR and PR flours and the respective starches (JRS and PRS) were observed using the method by Chakraborty et al. (2020). This method utilised an Eclipse Ci microscope (Nikon Instruments Inc., Surrey, UK) equipped with a digital camera (Nikon digital Sight DS-Fi2 camera). The crystalline state (represented by the Maltese cross pattern) was observed under polarised light mode. The Maltese cross is an interference pattern observed in native starch under polarised light due to its ordered, birefringent crystalline structure.

Starch loses its ordered structure following gelatinisation or hydrolysis, thereby its birefringence property. The granule size distribution of JR and PR flours, JRS and PRS was measured using a laser diffraction particle size analyser (LS 13 320, powder system module, Beckman Coulter, Inc., Buckinghamshire, UK). The mean diameter (μm) was reported as an average of triplicate measurements, each measurement from a different sample.

3.3 Physicochemical properties

3.3.1 Pasting properties measured with Rapid Visco Analyser (RVA)

The term "pasting properties" refers to the structural changes occurring in rice samples undergoing a hydrothermal treatment (application of heat in the presence of water) under constant stirring. Structural changes, such as starch swelling and disintegration or the development of a viscose mixture called paste, can alter the viscosity of rice samples. Such viscosity changes could be used as an indicator of the physical behaviour of rice during cooking. A typical RVA experimental curve, with the different thermal transitions occurring in rice flour, is shown in **Fig 3.3**.

Pasting properties are important factors for determining the texture and *in vitro* digestibility of cooked rice (Iwe et al., 2016; Farooq et al., 2021). In this study, the pasting properties of rice samples were examined using an RVA (RVA 4800, PerkinElmer, Buckinghamshire, UK) according to the approved AACC method 61-02 (AACC, 2001). In brief, 3 g of JR or PR (water content 8 %, w/w) were added into an aluminium canister containing 25 g of distilled water, or a dispersion of 0.03, 0.06, or 0.09 g low acyl gellan gum (LAGG) powder in distilled water (these percentages correspond to 1, 2, and 3 % of rice mass, respectively). The JR and PR flour dispersions had a total starch concentration of 8.75 % and 8.54 % (w/w), respectively. To compare the pasting performance in the absence of proteins (contained in rice flour), dispersions at 0 % LAGG were also produced with JRS and PRS (dry starch basis) to the same starch concentration as that in the respective flours. The RVA test of LAGG-water dispersions (without a rice sample) was also

performed. All the dispersion was stirred manually in the canister using a plastic spatula before starting the RVA run.

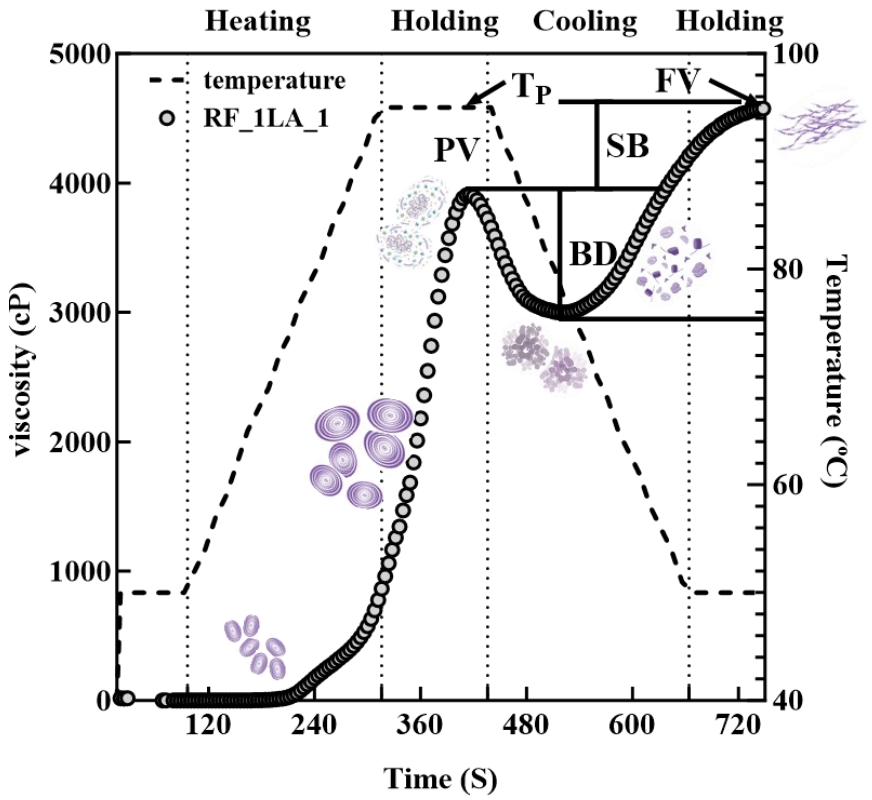


Fig. 3.3. Pasting profile of rice measured using the standard American Association of Cereal Chemists (AACC) method. Image adapted from Balet et al. (2019). PV: peak viscosity, BD: breakdown viscosity, SB: setback viscosity, FV: final viscosity, Tp: peak temperature.

The RVA programme consisted of stirring the sample at 960 rpm for the first 10 s to help homogenise the sample, then at 160 rpm for the remaining part of the procedure. The RVA temperature programme was the following: equilibration at 50°C for 1 min 30 s, heating to 95°C at 12°C/min for 3 min 45 s, holding at 95°C for 2 min 30 s, cooling to 50°C at 12°C/min for 3 min 45 s, holding at 50°C for 1 min. For the pasting properties analysis, the peak viscosity (PV, the maximum viscosity obtained during heating), breakdown viscosity (BD, the degree of disintegration of the granules), final viscosity (FV, viscosity at the end of the run), setback viscosity (SB, the difference between peak and final viscosity), time to peak viscosity (Time), peak temperature (the temperature of the viscosity peak due to starch granule swelling upon the absorption of water) were measured by Thermocline for Windows

software (version 3) supplied with the instrument. All measurements were performed in triplicate.

3.3.2 Thermal properties of rice measured by Differential Scanning Calorimetry (DSC)

The “thermal properties” of rice are related to its ability to conduct heat during the cooking process and are determined by the physicochemical and microstructural characteristics of the grain (Zhu et al., 2020).

Gelatinisation occurs during the cooking process when rice starch is heated in water, and the highly organised structure is disrupted. Upon cooling down to edible temperatures, rice starch undergoes short-term retrogradation, which refers to a process of recrystallisation or reassembly of disaggregated amylose and amylopectin molecules in gelatinised starches (Yan et al., 2021; Yashini et al., 2022; Sahoo et al., 2023). Structural transformations such as starch swelling, melting of crystalline structures, and dissolution of starch molecules involve energy and mass exchange, which can be identified as changes in the heat flow using thermo-analytical techniques such as DSC.

This technique measures the heat flow changes and temperature at which these changes occur when a sample is heated, cooled, or held isothermally for a given amount of time. The DSC instrument consists of two cells, which host two crucibles (or pans), one for the studied sample and one for a reference sample; the reference crucible is usually empty or filled with an inert solvent like water. The heat capacity of the reference is usually known and defined over the whole scanned temperature range (Pungor, 1994). In this thesis, a TGA/DSC 3+ (Mettler Toledo, Leicester, UK) was used. The instrument measures the difference between the heat flow from the sample and the reference, as a function of temperature or time, for both materials to remain at the same temperature upon heating or cooling. The differential heat flow between the sample and reference is used to identify and quantify the sample's physical transformations (e.g., phase transitions) (Usmani et al., 2017).

Upon changing the temperature of both cells, thermally-induced processes in the sample lead to heat being absorbed (endothermic transition) or released (exothermic transition), resulting in a change in the differential heat flow that is recorded as a peak. The direction of the thermal transition, whether endothermic or exothermic and the area under the curve are directly proportional to the enthalpy change.

Exothermic and endothermic transitions are identified by peaks with opposite orientations, either positive (oriented upwards) or negative (oriented downwards). Phase transition (exothermic or endothermic) and corresponding peak orientation depend on the machine. In this thesis, exothermic transitions are identified by negative peaks, whereas endothermic transitions are by positive peaks. A typical DSC experimental curve showing the different thermal transition processes observed in rice starch is shown in **Fig 3.4**.

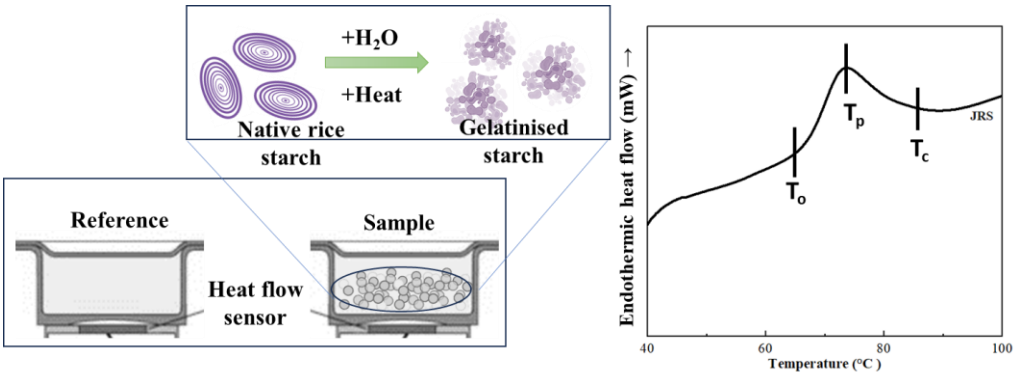


Fig. 3.4. Working mechanism of a DSC instrument. It is adopted from Chakraborty et al. (2022). Right-hand side panel: typical gelatinisation curve of JRS (result from this study reported in Chapter 4). Transition temperatures: onset temperature (To), peak temperature (Tp), conclusion temperature (Tc).

The thermal properties of the rice samples were determined using the method described by Zhu et al. (2019). To simulate the cooking conditions described in **Section 3.4**, 10 mg of rice flour or rice starch were mixed with 15 μL of water (rice-to-water ratio of 1:1.5) or LAGG dispersions containing 0.1, 0.2, or 0.3 mg of LAGG (these values correspond to 1, 2, and 3 % of rice mass, respectively), placed into 40 μL stainless-steel pans, and processed in the DSC with the same thermal programme as that employed for cooking the rice. Specifically, the samples were heated from

30°C to 120°C at 10°C/min, held at 120°C for 15 mins, and cooled at 20°C/min to 60°C, an edible temperature for freshly cooked rice (Yau & Huang, 1996).

The transition temperatures reported were the onset temperature (T_o), peak temperature (T_p), and conclusion temperature (T_c). The enthalpy changes on phase transition (ΔH), expressed as J/g of dry starch, were estimated using the equipped star^e software (Mettler Toledo, Leicester, UK) by integrating the area between the thermograms and a baseline under the peak.

3.3.3 Hydration properties of rice

The term "hydration properties" of rice refers to how rice uptakes and holds water molecules due to the interaction with the grain components, which in turn can damage or disrupt the grain structure, resulting in particle leakage during the cooking process. Since rice hydration is affected by its components and associated structures, differences in hydration properties between rice types can also be related to cooked rice texture and *in vitro* digestibility (Farooq et al., 2018; Boonmeejoy et al., 2019). Hydration behaviour was determined using the swelling power (SP) and water solubility index (WSI) using the method of Farooq et al. (2018). In brief, rice flour (1 g, dry basis) or rice starch (amount corresponding to 1 g of flour, dry basis; **Chapter 3, Section 3.1**) was cooked in 10 mL of distilled water (control) or dispersions containing 10, 20, or 30 mg LAGG (these percentages correspond to 1, 2, and 3 % of rice mass, respectively), at 95°C for 30 min. Measurements were performed in triplicate.

Once cooled to room temperature, the samples were centrifuged at 4000 rpm for 15 mins. The supernatant, containing the soluble fraction, was carefully decanted into pre-weighed glass dishes and dried at 105°C until constant weight. The WSI was calculated using **Eq.3.1**, expressed in % of the dry sample. The residue after centrifuging was weighed for SP determination using **Eq.3.2**.

$$\mathbf{WSI} = \frac{\mathbf{Wr}}{\mathbf{W}} \times \mathbf{100\ \%} \quad \textbf{(Eq.3.1)}$$

$$\mathbf{SP} = \frac{\mathbf{Wt}}{\mathbf{W - Wr}} \times \mathbf{100\ \%} \quad \textbf{(Eq.3.2)}$$

Where:

W_t represents the mass of the wet residues

W_r the mass remained after drying the supernatant

W the initial sample mass (g, dry solid basis)

3.4 Rice cooking method

It has been revealed that the microstructure and texture characteristics of rice can differ significantly between preparation methods (such as pre-soaking and parboiling) (Wu et al., 2021; Shen et al., 2022), as well as cooking methods (such as electric cookers, pressure cookers, stovetop or microwaves) (Chmiel et al., 2018; Ha et al., 2022) . In rice kernels, these effects result in varying degrees of disruption to starch structure and compression protein networks, affecting sensory experience and starch digestibility (*in vivo* and *in vitro*) (Chiu & Stewart, 2013; Boers et al., 2015; Van et al., 2020; Sivakamasundari et al., 2022; Bagchi et al., 2023).

Rice was cooked according to the manufacturer's instructions and previous studies (Chatthongpisut et al., 2015; Liu et al., 2019). A 100 g aliquot of pre-washed rice (JR or PR) was cooked in a rice cooker (NEDIS, Karc06wt-power 300w, Leicester, UK) with 150 g of distilled water (1:1.5 rice-to-water ratio, w/w) for approximately 15 mins (until no excess water was present). The cooked rice was then kept in the rice cooker in warm mode (65-70°C) for 10 mins to fully gelatinise the starch, as determined by visual inspection (no white core in the cooked rice kernels). To do so, randomly selected grains were placed between two microscope slides and squeezed. Cooked grains did not resist deformation under applied force, and no white core could be observed.

JR or PR (100 g) were also cooked in 150 g of distilled water containing 1, 2, or 3 g of LAGG (these percentages correspond to 1, 2, and 3 % of rice mass, respectively) previously dispersed. Samples containing 1, 2, or 3 g of LAGG were coded as JR_1LA, JR_2LA and JR_3LA for JR and PR_1LA, PR_2LA and PR_3LA for PR for all experiments in this thesis.

3.5 Proximate composition analysis

Proximate analysis was used to determine the composition of cooked rice (**Chapters 4**, **5**, and **6**) and cooked orzo (**Chapter 7**). The moisture content was determined using the standard method 934.01 published by the Association of Official Agricultural Chemists (AOAC); the samples were placed in pre-weighed aluminium trays and dried in an oven (MOV-112F, Sanyo, Japan) at 105°C for 24 h (until constant weight). The moisture content was calculated as the difference between the sample weight before and after drying (AOAC, 2005a). A portion of the cooked sample was then lyophilised, ground, and sifted into flour (particles < 500 μm) for chemical composition analysis. The crude protein content was calculated from the nitrogen content of the ground sample according to AOAC 930.29 using a nitrogen-to-protein conversion factor of 5.95 (AOAC, 2005b). The total starch content in the ground samples was measured using the official method 996.11 published by AOAC (2007) with a total starch assay kit (α-amylase/amyloglucosidase) (K-TSTA, Megazyme International Ireland). Briefly, in this method, the starch was first solubilised to maltodextrins in the presence of a thermostable α-amylase, followed by hydrolysis of maltodextrins to glucose by amyloglucosidase. The produced glucose was quantified using a glucose oxidase/peroxidase reagent.

The apparent amylose content of the ground sample was determined using the iodometric method described by Tamura et al. (2014). The ground sample (50 mg) was initially defatted in a 15 mL conical centrifuge tube with 500 μL of 95 % ethanol. Then, 4.5 mL of 1 M NaOH was added, and the tube containing the mix was heated in a boiling water bath for 10 mins to allow amylose to leach out and disperse (Bahdanovich et al., 2022). The total mix volume was adjusted to 10 mL using distilled water. A "blank" with solutions but no sample was also prepared. A 500 μL aliquot of the solution was transferred to another 15 mL tube, diluted with 2 mL distilled water, and neutralised with 500 μL 1 M acetic acid. Subsequently, 1 mL of 0.2 % fresh prepared iodine solution (0.2 g iodine and 2.0 g potassium iodide diluted to 100 mL with distilled water) was added to form the amylose-iodine complex. This final solution was allowed to sit for 10 mins at 30°C to develop colour, and

absorbance was subsequently measured at 620 nm using a UV-visible spectrophotometer (Evolution™ 60S, ThermoFisher, paisley, UK). Potato amylose (A0512, Sigma-Aldrich) was used as the standard material for amylose measurement. A portion of uncooked rice grain and extracted starch was also lyophilised, ground, and sieved to powder to determine the effect of lyophilisation on the composition of raw rice flour and starch. No significant difference in composition was identified in samples with or without lyophilisation. All analyses were performed in triplicate.

Sodium dodecyl sulphate-polyacrylamide gel electrophoresis (SDS-PAGE, 12 % separating gel and 4 % stacking gel) was used for determining the protein profiles, according to the method described by Laemmli et al. (1970). The powdered samples were solubilised in 1x volume of reducing sample buffer (#1610737, 62.5 mM Tris-HCl (pH 6.8), 25 % of glycerol, 2 % of SDS, 5 % of β-mercaptoethanol, 0.01 % of bromophenol blue). Then, the mixture was heated at 95°C for 5 mins. Using the same procedure but without 2-ME, samples were prepared for SDS-PAGE under non-reducing conditions. Using Coomassie Brilliant Blue R-250 (0.05 %) in methanol/acetic acid/water (25:10:65, v/v/v), the gels were stained and then destained in a methanol-water solution containing 10 % acetic acid (1:1:8, v/v/v).

3.6 Microstructural properties

3.6.1 Fourier Transform Infrared Spectroscopy (FTIR)

FTIR is a spectroscopic technique which uses infrared light, mostly the mid-IR region (4000 to 400 cm^{-1}), to analyse the chemical properties of several categories of compounds. These mid-IR region radiations correspond to the vibration frequencies of bonds within functional groups of organic molecules; the molecules absorb those radiations, and the absorbed energy is then released under the form of vibration with increased amplitude (Doyle, 1992). FTIR is a powerful technique used to detect intra- and inter-molecular organisation and interaction among polymers, including rice protein and starch (Guerrero et al., 2014; Frederick et al., 2016; Ying et al., 2017). FTIR is usually combined with X-ray diffraction (XRD) to study the crystalline

structure of molecules such as starch. For starch analysis, FTIR mainly detects the C-OH bending and CH_2-related modes of the α-D-glucopyranose ring in the spectral range between 1050 and 950 cm^{-1}, referred to the short-range order structures of the double-helix (van Soest et al., 1995). For protein analysis, FTIR detects the characteristic bands in the amide I region (1700 to 1600 cm^{-1}) mainly associated with the C=O stretching vibration, directly related to the backbone conformation of the peptide group (Guerrero et al., 2014; Chávez-Murillo et al., 2018).

IR spectra patterns of samples were analysed using a Bruker Tensor 27 FTIR spectrometer equipped with an attenuated total reflectance accessory (Graseby-Space Ltd, Orpington, UK), following the method reported by Garcia-Valle et al. (2021). The FTIR spectra were recorded over the wavenumber range of 4000 to 400 cm^{-1}; 128 full spectrum scans were performed, each scan at 4 cm^{-1} spectral resolution against an empty (air) background reading at room temperature. Four tests were performed for each sample. The collected sample spectra were analysed after considering the background and normalising frequency and scale with OMNIC 6.2 software (Thermos Electron Corporation, Madison, WI, USA) for the peak deconvolution process. The β-sheet (1615-1637 cm^{-1} and 1682-1700 cm^{-1}), random coil (1637-1645 cm^{-1}), α-helix (1646-1664 cm^{-1}) and β-turn (1665-1681 cm^{-1}) were estimated from the amide I region (1700 to 1600 cm^{-1}) according to previous studies (Ellepola et al., 2005; Ying et al., 2017; Fetouhi et al., 2019).

Molecular organisations of starch (including hydrated, amorphous, and ordered structures) were determined from the fingerprint region of polysaccharides (wavenumber 1070 to 950 cm^{-1}) (Pozo et al., 2018). The water-bound state was assessed from the OH-vibration bonding regions between 3600 and 3100 cm^{-1} (Garcia-Valle et al., 2021).

The peak resolution and curve-fitting were performed as follows: peaks of each fingerprint region were first treated by Fourier self-deconvolution and then curve-fitted using the Gauss-Lorentz formula with the OMNIC Peak Resolve analysis software. The area corresponding to each secondary structure was calculated accordingly and expressed as a percentage of the sum of areas.

3.6.2 X-ray diffraction (XRD)

XRD is a diffraction-based technique essential to assess and quantify starch long-range crystalline order, which is related to the packing of the double helices in the crystalline domains. The XRD measurements of samples were carried out using an Advance Bruker AXS powder-diffractometer (D8, Bruker AXS, UK) with a Cu-Kα radiation source (λ = 0.154 nm) running at 40 kV and 25 mA, following the setting described by Choi et al. (2022). A scanning cycle of the diffraction angle (2θ) was conducted from 4° to 45° with a step size of 0.02° at a speed of 2°/min.

A two-phase model is typically used to estimate crystalline order in starch, in which an amorphous halo is subtracted from the ordered parts of the scattering pattern and the ratio of the two phases is used to estimate crystallinity (Wang et al., 2017). It was analysed using the DIFFRAC plus EVA® software equipped within the XRD instrument. The linear baseline correction was applied to the data points of the selected region, and the intensity was normalised between 0 and 1 of arbitrary units (A.U.)

3.6.3 Morphological observations

3.6.3.1 Labelling of LAGG for fluorescence microscopy

Labelling is a type of staining technique that facilitates the detection of specific molecules with fluorescence and confocal microscopy. In this study, labelling was used to observe (labelled) LAGG penetration within rice grains. LAGG was covalently labelled with 5-(4,6-dichlorotriazinyl) aminofluorescein (DTAF) following the procedure described by Khin et al. (2021). In brief, 50 mL of a 20 mg/mL LAGG aqueous dispersion was mixed with 1 mL of 5-DTAF Stock dimethyl sulfoxide (20 mM) solution, followed by a dropwise addition of 15 mL of 10 % (w/v) Na_2SO_4 solution. The mix was adjusted to pH 10 using 1 M NaOH and then allowed to stand at 60°C for 2 hours under continuous stirring. At the end of this period, the reaction was quenched with 200 mL of absolute ethanol. The unbound 5-DTAF was washed under vacuum with 0.055M sodium acetate (pH 5.4)/ethanol (1:2 ratio, w/w) solution through a Buchner funnel fitted with a 0.45 μm PTFE membrane until the

yellow colour on the filter paper disappeared. Afterwards, the precipitate was freeze-dried overnight, and the labelled LAGG was stored in an airtight container, covered with aluminium foil, in the dark at room temperature for further use. For labelling, rice was cooked with DTAF-LAGG with the same procedure adopted with native LAGG and described in **Section 3.4.** The distribution of DTAF-LAGG in rice matrices was visualised using EVOS™ FL microscope with 488 nm excitation wavelength (λ_{Ex}) and 517 nm emission wavelengths (λ_{Em}).

3.6.3.2 Light microscopy

The morphological properties of the protein-starch matrices within cooked samples (reported in **Chapters 4**, **5**, **6**, and **7**) were observed using an Eclipse Ci microscope (Nikon Instruments Inc., Surrey, UK) equipped with a Nikon digital Sight DS-Fi2 camera. Sample slides were prepared based on the method described by Tamura et al. (2016). The cooked samples were exposed to optimum cryo-microtomy embedding medium and cut to 60 μm thickness cross-sections with a microtome (Leica CM 3050s, Leica Microsystems, Milton Keynes, UK). Cross-sections were mounted on gelatine-coated microscope slides, stained with an aqueous solution of 0.1 % fast green FCF acetic acid (1 %) for protein detection, washed with distilled water and stained with Lugol's solution (62650, Sigma-Aldrich, 1:10 dilution) for starch detection. Due to electrostatic bonding between the amino acid side chains and the fast green molecules, protein bodies appeared with a green colour (Steglich et al., 2014), whereas starch appeared blue/purple due to the formation of an amylose/amylopectin-iodine complex (Liu et al., 2009).

3.6.3.3 Environmental scanning electron microscopy (ESEM)

The surface and internal morphology of samples were measured with an ESEM (FEI Quanta 650 with X-Max-150 EDX Detector) equipped with a gaseous secondary electron detector, following the method described by Dang & Copeland (2004). In brief, working conditions were 10 kV accelerating voltage, 1 torr chamber pressure, and the initial working distance was 10 mm. Before imaging, samples were fixed on conductive adhesive tape and were observed at a magnification of 1000x.

3.7 Textural properties

The textural profiles of the freshly cooked sample were evaluated using a texture analyser (TA-XT2, Stable Microsystem, Surrey, England) according to the method described by Boluda-Aguilar et al. (2013). A 2 g aliquot of cooked sample was arranged in a single layer from the centre of the plate to cover an area greater than 35 mm in diameter (circular area of the cylinder applied). The samples were compressed to 75 % of their original thickness by two compression cycles conducted using a stainless-steel cylindrical probe with a diameter of 35 mm and a testing speed of 1 mm/s. The texture profile analysis (TPA) force-time curves determined hardness, adhesiveness, cohesiveness, and chewiness using the Texture Export for Windows software (Stable. Micro Systems, Godalming, UK). Ten technical replicates (compression tests from the same batch of cooked samples) per sample were performed, and the corresponding results were expressed as an average value.

3.8 *In vitro* digestion models

3.8.1 Simulated digestion fluid preparation.

The simulated salivary fluid (SSF), simulated gastric fluid (SGF), and simulated intestinal fluid (SIF) formulations are detailed in **Tab. 3.2**. Each simulated fluid was prepared as a 1.25X concentrated stock solution (400 mL).

Tab. 3.2. Simulated fluid formulations (stocks, 1.25X concentration).

	Volume (mL)		
	SSF (1.25X stock)	SGF (1.25X stock)	SIF (1.25X stock)
KCl (0.5M)	15.1	6.9	6.8
KH_2PO_4 (0.5M)	3.7	0.9	0.8
$NaHCO_3$ (1M)	6.8	12.5	42.5
NaCl (2M)	--	11.8	9.6
$MgCl_2(H_2O)_6$ (0.15M)	0.5	0.4	1.1
$(NH4)_2CO_3$ (0.5M)	0.06	0.5	--
HCl (2M)	~0.3 adjust pH to 7	~3.9 adjust pH to 3	~2.1 adjust pH to 7
MilliQ® water	to 400 mL	to 400 mL	to 400 mL

The solutions were stored at 4°C and used within a week from the day of production.

3.8.2 Oral phase

3.8.2.1 In vitro oral processing and digestion

In this thesis, three types of oral process conditions were applied to simulate only swallowing, normal, and fine *in vivo* oral digestion patterns, according to the method adopted in previous works (Moongngarm et al., 2012; Furuya et al., 2014). To simulate normal and fine oral processing, 120 g of freshly cooked samples were homogenised in a household blender (HB605, Kenwood, Havant, UK) for 10 s or 20 s, respectively. The following *in vitro* digestion step was conducted based on the method described by Fernandes et al. (2020). In brief, 10 g of the non-homogenised (only swallowing, 0 s homogenisation) or homogenised (10 s, 20 s) rice samples were placed in 50 mL conical tubes, followed by the addition of 10 mL of SSF with salivary α-amylase to achieve an activity of 75 U/mL in the digestion mixture. The mixture was incubated for 2 mins at 37°C under constant rotation (50 rpm) in a tube rotator (Fisherbrand™, Thermo Scientific, Hemel Hempstead, UK), then 20 mL of Na_2CO_3 (0.3 M) solution was added to the digested mass to stop amylase activity.

3.8.2.2 Granulometry distribution analysis after in vitro oral digestion

The granulometry distribution of the sample following *in vitro* oral digestion (**Section 3.8.2.1**) was analysed based on the method described by Ranawana et al. (2010). In brief, the digested samples were held in an incubation chamber at 37°C undisturbed for 10 mins to allow residues to sediment. Following filtration through a Buchner funnel, the separated solid particles were carefully removed from the filter paper and oven-dried for 12 h at 70°C until the weight remained constant. Meanwhile, the liquid filtrate was collected for analysis of the digested starch.

The dry residue was weighed once cooled to room temperature and then fractionated using a control sieve shaker (Retsch AS-200, Verder Scientific, Derbyshire, UK) with a vibration height of 0.5 mm for 1 min. The four equipped test sieves (DEBUYER, France) were stacked in descending size order as follows: 2.0 mm, 1.0 mm, 0.5 mm, 0.25 mm, and the base pan. The fractions from each sieve were

carefully collected and weighed. The granulometry distribution was calculated through **Eq.3.3**.

$$\sum \mathbf{R_n}(\%) = \sum \frac{\mathbf{M_n}}{\sum \mathbf{M_n}} \times \mathbf{100}\ \% \quad \textbf{(Eq.3.3)}$$

Where:

M_n is the mass (g) of the fraction retained on each sieve (M_1, M_2, M_3, M_4) and pan (M_p);

ΣM_n is the total mass (g) of grain fractions: $M_1 + M_2 + ... + M_p$;

ΣR_n is the cumulative per cent (%) of mass retained.

The weight loss caused by the particles entrapped within the meshes was negligible.

3.8.3 Rice bolus disintegration

To demonstrate the physical integrity loss of rice bolus in an acidic environment (pH 3), a bolus disintegration experiment was conducted (**Fig 3.5**).

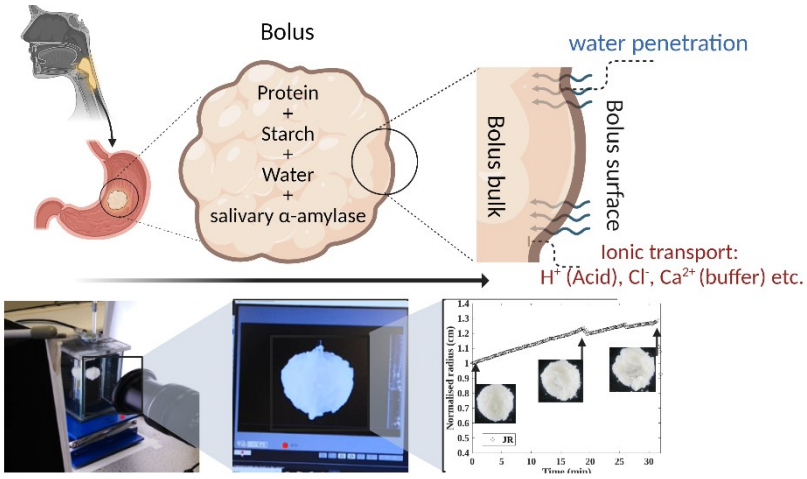


Fig. 3.5. Schematic of bolus disintegration model.

Following 20 s homogenisation of cooked rice (**Section 3.8.2.13.8.2**) and mixing with SSF (1:1, w/w) without salivary amylase, 7 g of this mixture was fixed into a spherical mould (radius = 1 cm, time 0), then a hanger wire was attached to the centre of the spherical bolus. The hung bolus was positioned at the centre of a 500 mL glass cube chamber with a black background. The disintegration process was captured using a Canon digital single-lens reflex 5D, with a 24-100 mm lens and 31 mm macro lens

extender, a high-resolution camera and proper lighting equipment. All experiments were conducted in the same setting and position. Using a tube-connected syringe, 500 mL of SGF pH 3 was gradually added to the chamber to impregnate the bolus sample. The camera recorded the disintegration process of the bolus for 30 mins, starting (time 0) when SGF reached the bottom of the bolus. The video was then converted into frames, and a graph of the bolus radius versus time was produced using Matlab (Matlab® 2023a, MathWorks Inc.). The bolus sphere radius at time 0 was normalised to 1 cm.

3.8.4 Static *in vitro* digestion model

3.8.4.1 Model setting

Working solutions were prepared immediately before performing the digestion experiments. A description of one *in vitro* digestion set, including the electrolyte fluid, is shown in **Tab. 3.3**.

For the preparation of the working solutions, the 1.25X stock solutions were diluted with MilliQ® water to the final volume after adding $CaCl_2(H_2O)_2$ 0.3 M (volumes in **Tab. 3.3**). The working solution was then placed in the incubator at 37°C prior to use. The rice samples, or the digestion mass from the previous phase, were mixed with 80% of the respective working solution, whereas the remaining 20 % was used to dissolve the enzymes before adding it to the sample. This allowed the even distribution of the enzymes throughout the sample. The 20 % fluid aliquot containing enzymes was added to the sample after pH adjustment in the remaining 80 % aliquot. Using the gastric phase as an example, the pH of SGF increased from 3 to 5 after mixing 80 % of the SGF with the “bolus” (the sample mass from the oral phase), then adjusted back to 3 to maintain the pepsin activity, before adding the remaining 20% of fluid containing enzymes (pH 3) and initiate digestion.

Tab. 3.3. Example of a static *in vitro* digestion experimentfor 5 g of cooked rice. (A) Composition of the bolus; (B) composition (volumes) of the working solution (80 % solution mixed with digestion mass + 20 % used for preparation of enzyme solution); (C) Characteristics of the enzyme mix.

(A) JR (example of food model)			
Rice sample (g)	5.00		
Total solid (g)	1.86 (37.2 % of rice mass)		
Total starch (g)	1.62		
Total energy content (kcal) [a]	6.85		
(B) Working solution	Oral (pH 7)[e]	Gastric (pH 3)[e]	Intestinal (pH 7)[e]
Stock solution (mL) (shown in Tab. 3.2)	4 (SSF)	8 (SGF)	16 (SIF)
$CaCl_2(H_2O)_2$ 0.3M (mL)	0.025	0.005	0.08
MilliQ® water (mL)	0.975	1.495	2.92
HCl (5 M) (mL) [b]	--	0.5	--
NaOH (5 M) (mL)[b]	--	--	1
Total fluid volume (mL)	5 (4+1)	10 (8+2)	20 (16+4)
Of which for premixing (mL)	4	8	16
Of which for enzyme solutions (mL)	1	2	4
(C) Enzymes	Salivary α-amylase	Pepsin	Pancreatin
Enzyme activity (unit/mL) in total digestion mix [c]	75	2000	20 [g]
Enzyme-specific activity (unit/mg) [d]	146.2	557.5	31.4
Mass of enzyme (mg) [d]	5.14	71.82	25.48
Digestive mass	5g cooked rice	10mL bolus [f]	20mL of chyme [g]
Final volume (mL)	10	20	40

[a] According to the nutrition information on the food label.

[b] For pH adjustment.

[c] Each batch of enzymes is tested according to standard assays to determine the specific enzyme activity. The amount of pancreatin used is based on the activity of α-amylase. As in the previous trial, the amount of pancreatin based on suggested α-Amylase activity was used, and the starch digestion curve of all samples reached a plateau within 5 mins, which makes it difficult to resolve differences in starch digestion rates. Based on our results, it is recommended to have 0.5-unit amylase per mg starch in the final digestion mixture. This means 20 units/mL amylase is more appropriate to distinguish digestion kinetics for 5g of rice containing around 30 % total starch. The enzyme activity (unit/mL) in the total digestion mix at the distinct phases was calculated as enzyme-specific activity (unit/mg) × enzyme mass (mg) / final volume (mL).

[d] Specific enzyme activity measured for each batch of enzymes according to standard assays.

[e] Final pH means the pH after mixing with the digestive mass accordingly.

[f] The bolus here refers to the food mass (homogenised for 0 s, 10 s, and 20 s) mixed with SSF for 2 mins and ready for gastric digestion.

[g] Chyme refers to the mass that forms after gastric digestion.

3.8.4.2 Procedure

Cooked samples underwent a three-step digestion procedure consisting of an oral, gastric, and intestinal phase. Aliquots of the digesta were collected for protein and starch analysis at the end of the oral and gastric phases and at specific time points during the intestinal phase. Two batch experiments were conducted for each rice sample. Following the oral phase (**Section 3.8.2.1**), the rice bolus sample was processed in the gastric phase.

Gastric phase. SGF (8 mL containing no enzymes) was added to the oral mixture to deactivate the salivary α-amylase. The gastric phase was immediately initiated after adding a further 2 mL of pepsin solution (prepared in SGF) to reach a final volume of 20 mL with 2000 U/mL pepsin activity. The mixture was incubated at 37°C with constant rotation (20 rpm) for 30 mins. The pH of the gastric mixture, measured every 10 mins, was maintained at 3 using HCl 1M. For gastric digestion, 100 μL aliquots of the mixture were withdrawn after 30 mins incubation and dispersed into 1.5 mL microcentrifuge tubes containing 100 μL of "stop solution" (0.3 M Na_2CO_3, pH 9) to inactivate the pepsin. Enzyme blanks contained pepsin and SGF, but no samples were prepared and tested as the samples.

Intestinal phase. At the end of the gastric phase, 16 mL of SIF was added to the gastric chyme and the pH was adjusted to 7 with NaOH 1 M. Subsequently, 4 mL of SIF containing pancreatin (as per equalisation of α-amylase activity 20 U/mL digesta) and mixed to reach a final volume of the intestinal mixture of 40 mL. The mixture was incubated at 37°C under constant rotation (10 rpm) for 180 mins. To study the kinetics of starch digestion (intestine phase), a 100 μL aliquot of digesta was withdrawn from the digestion mixture at 0, 5, 10, 15, 20, 30, 45, 60, 90, 120, and 180 mins. Each aliquot was dispersed into a 1.5 mL microcentrifuge tube containing 100 μL of "stop solution" (0.3 M Na_2CO_3, pH 9) to stop the amylase activity and measure the degree of starch hydrolysis. Meanwhile, a 100 μL aliquot was withdrawn from the digestion mixture at 0, 15, 30, 60, 120, and 180 mins. Each aliquot was dispersed into a 1.5 mL microcentrifuge tube containing 100 μL of a

Bowman-Birk trypsin-chymotrypsin inhibitor solution (0.05 g/L) to stop the trypsin activity and measure the degree of protein hydrolysis.

Blanks containing corresponding enzymes and simulated digestion fluids, but no rice, were run through the same digestion and sampling process to identify the amount of hydrolysed protein belonging to the enzyme. This value was subtracted from the total digested protein measured in the samples to determine the actual digested protein related to the rice.

3.8.5 Semi-dynamic digestion model

3.8.5.1 Model setting

The overall setup of the semi-dynamic model and each function component is illustrated in **Fig. 3.6** and described in **Tab. 3.4**.

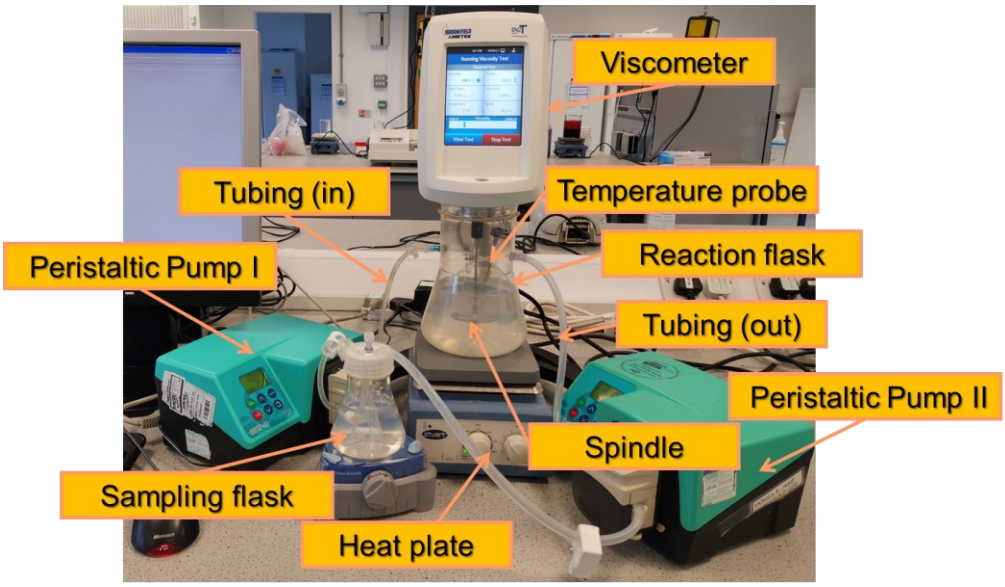
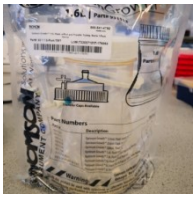
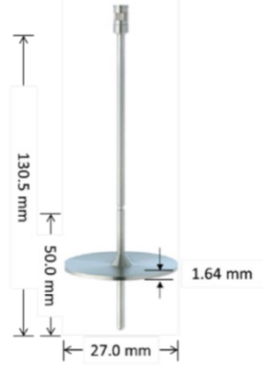


Fig. 3.6. Overview of the semi-dynamic *in vitro* digestion model setup.The image shows blank fluid (solution with enzyme, but no sample) within the system.

Image of component	Identifying name/size	Function
	Multiport flask Height: 240 mm Neck diameter: 96.0 mm Lower circular diameter: 166.0 mm	Simulates the digestion of food in the gastric-intestinal tract. The temperature is maintained at 37°C by a hot plate and monitored by a probe.
 	Viscometer Spindle: RV-04 (04) 1. Multi-point interval data collection for gastric and intestinal phase. 2. Results expressed as mean ± S.D. of viscosity in centipoise (cP)	Monitors the viscosity changes during digestion. It determines the fluid-specific viscosity by measuring the deflection of the spring with a rotary transducer. The DV-III rheometer operates on the principle of rotating the spindle in the test fluid through a calibrated spring. The spring deflection, measured using a rotary transducer, determines the viscous drag of the fluid against the spindle. An aliquot of digesta was injected into the reaction flask and positioned underneath the pivot cup of the rheometer. The rheometer was set up in "controlled shear rate mode," and rotational speed and torque were measured.
	pH waterproof meter	Monitors the solution pH in the sampling flask, which is connected to the reaction flask.
	Peristaltic pump	Assists the enzyme solution delivery with a specific delivery rate, i.e., the volume programmed to be delivered in a given period.
	Hot plate	Maintains the temperature at 37°C.

	C-flex 16 1/4in OD x 1/8in ID x 2ft Long	Fluid transfer in settings. Tubing connects the sampling flask and the reaction flasks in a flow cycle.

3.8.5.2 Procedure

The semi-dynamic *in vitro* digestion model differs from the static model due to the presence of a peristaltic pump, which continuously moves the sample within the system; moreover, there is a controlled bolus-induced gastric pH increase from 2 to 5. The oral phase was instead the one described in **Section 3.8.2**.

Gastric phase. A three-step, block-wise pH profile was used to follow the pH, which increased over a 30-min period, consisting of a linear regression from pH 2 (a fasting state in the stomach) to pH 5 (bolus delivery in the stomach) within 30 mins. The linear pH increase was divided into three blocks of 10 mins each to obtain a representative average pH value for a given period. The reaction flask was filled with 160 mL of SGF (pH 2). The gastric phase was initiated when the rice mass from the oral phase (pH 7, total volume 200 mL) was introduced into the reaction flask via the peristaltic pump I (input) at 20 mL/min.

Once the volume of the reaction flask reached 360 mL, the peristaltic pump II (output) was activated to pump the digested solution into the sampling flask at 20 mL/min for 2 mins. The pH value was then determined (gastric time 0). To reduce bolus-induced pH increase, 20 mL of predetermined SGF was added to the reaction flask every 10 mins (as shown in **Fig. 3.7**) to achieve the target pH, which was adjusted, if necessary, using HCl (2M). The viscosity of the digesta was measured using the Brookfield DV-II rotational rheometer (**Fig. 3.6**). This model was developed based on a previous study in sacrificed pigs (Nadia et al., 2021), where it was observed an average *in vivo* gastric pH increase from 2 to 5 in 30 mins described in **Eq.3.4**.

$$\mathbf{pH_t = 0.1 \times gastric\ digestion\ time\ (min) + pH_{t0}} \quad \textbf{(Eq.3.4)}$$

Where:

pH_t is the stomach pH at a specific time point

pH_{t0} is the stomach pH at time 0 (beginning of digestion time)

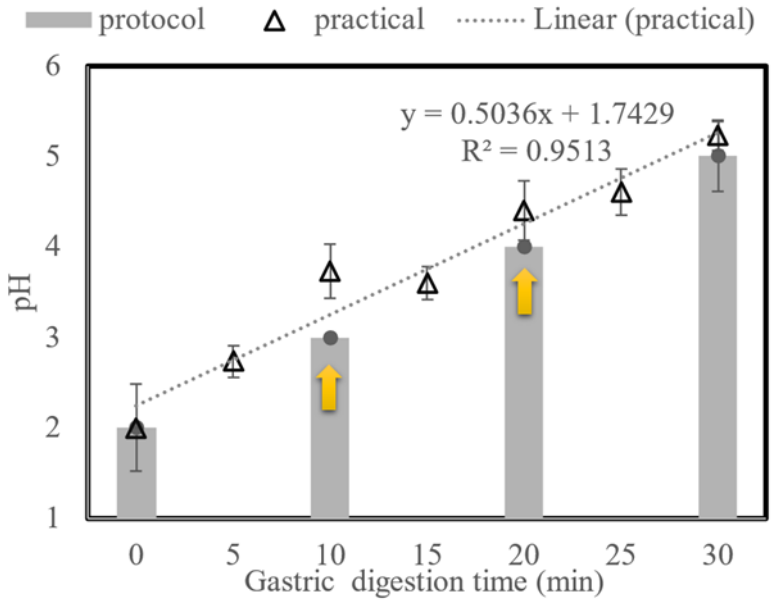


Fig. 3.7. Schematic of the change in gastric pH during semi-dynamic gastric phase. Columns: predicted pH change induced by the bolus, as determined by **Eq. 3.4**. Grey triangles with the linear fitting dashed line: experimental results in our study. Arrows indicate the time points (10th and 20th min) at which block-wise acidification was performed with the addition of SGF (20 mL) and HCl (2 M) to the reaction flask.

Despite the specific time points noted, the in and out tubes remain connected to the reaction flasks and sample flasks to maintain a current of digestion fluids. Pumps continue to operate at a speed of 20 rpm/min. After 30 mins of gastric digestion, 100 μL aliquots were withdrawn in duplicate from the sampling flask and analysed for the static digestion model (**Section3.8.4**).

Intestinal phase. As soon as the gastric phase was completed, 360 mL of SIF (without pancreatin) was pumped into the reaction flask at 50 mL/min to stop pepsin activity. The remaining 40 mL of SIF, containing pancreatin, was added to the reaction flask (final volume 800 mL) to start intestinal digestion. Meanwhile, 100 μL aliquots were withdrawn in duplicate from the sampling flask as time 0. Pumps continue to operate at a speed of 10 rpm/min. Despite the specific time points noted, the in and

out tubes remain connected to the reaction flasks and sample flasks to maintain a current of digestion fluids. The viscosity was measured throughout the intestinal digestion step. Sampling, analysis, and blank testing were performed for the static digestion model (**Section3.8.4**).

3.8.6 Quantitative evaluation of digested starch

Based on the method of Edwards et al. (2019), a colourimetric analysis using a par-hydroxybenzoic acid hydrazide (PAHBAH) assay was conducted on aliquots collected at digestion points to determine the maltose concentration. By referencing the standard curve, the concentration of maltose in each sample was expressed as maltose equivalents. Then, the maltose equivalent concentration units were further converted into the corresponding percentage of starch digested using **Eq.3.5**.

$$\textbf{Digested starch ratio}\ (\%) = \frac{[\textbf{maltose}]_{\textbf{t}}}{[\textbf{maltose}]_{\text{substrate}}} \times \textbf{100}\ \% \quad \textbf{(Eq.3.5)}$$

Where:

$[\text{maltose}]_t$ is the maltose equivalent concentration in the liquid phase of the digesta at a given time.

$[\text{maltose}]_{\text{substrate}}$ is the theoretical concentration of maltose equivalent that would exist at the beginning of the reaction, assuming that total starch (obtained by total starch measurement in **Section 3.5**) within the rice sample could be converted to maltose (360.31 g/mol).

3.8.7 Quantitative evaluation of digested protein

3.8.7.1 Determination of digested soluble protein fragments (DSPF) by Bicinchoninic Acid (BCA) assay

The content of DSPF (including tripeptides and larger polypeptides or proteins) in samples obtained from IVD models was analysed using a BCA protein assay kit (PierceTM BCA Assay, Thermo Fisher Scientific). A 96-well microplate method was used with BSA as a reference standard. Before the analysis, the samples were diluted along the standard curve to determine concentrations within the 20–2000 mg BSA/mL range, mixed with the working reagents, and incubated at 37°C for 30 mins.

As a result of the protein-induced biuret reaction, Cu(I) is formed in a concentration-dependent manner. BCA forms a highly specific chromogenic complex with Cu(I) with an absorbance peak at 562 nm. DSPF concentration was determined by measuring the absorbance at a wavelength of 562 nm (SpectraMax M5 microplate reader, Molecular Devices, US) and calculated using **Eq.3.6.**, as described by Almeida et al. (2015):

$$\mathbf{DSPF} = \left(\frac{\mathbf{P_S} - \mathbf{P_b}}{\mathbf{P_{tot}}}\right) \times \mathbf{100}\ \% \quad \textbf{(Eq.3.6)}$$

Where:

P_S is protein fragment content in digestion fluids

P_b is protein fragment content in blanks

P_{tot} is the concentration of total proteins in the mass before digestion. Protein content was measured as N content × 5.95 (the conversion factor). The obtained DSPF curve (the accumulative increase over time) was evaluated by fitting a first-order association model, as proposed by Bhattarai et al. (2016).

3.8.7.2 Determination of degree of protein hydrolysis (DH by o-phthaldialdehyde (OPA) assay

The degree of protein hydrolysis (DH) was determined by using the o-phthaldialdehyde (OPA) method following the procedure described by Jiménez-Munoz et al. (2021) to determine the proportion of free amino groups (-NH_2) released from rice protein degradation within the supernatant. As suggested by Hall et al. (2022), samples were first filtered using an Amicon® Ultra-4 centrifugal filter device (4000 rpm for 10 mins at room temperature) with a cut-off value of 10 kDa and then washed twice with 150 μL of MilliQ® water. Following centrifugation, it was expected that the molecules present were smaller than 10 kDa under the same dilution. The assay was conducted in 96-well microplates. After derivatisation with OPA and in the presence of 2-mercapto-ethane sulfonic acid, the produced 1-alkylthio-2-alcylisonindol compound was measured using a UV/VIS spectrophotometer (SpectraMax M5 microplate reader, Molecular Devices, US) at

335 nm. The results were calculated using a standard L-glutamic acid curve (0–8 mM in 0.5 M perchloric acid). The enzyme blanks were used as a background, and the obtained OPA values were subtracted from the OPA values of the protein. The DH (%) was calculated with **Eq.3.7**.

$$\mathbf{DH}\ (\%) = \frac{\mathbf{h}}{\mathbf{h_{tot}}} \times \mathbf{100}\ \%\quad (\mathbf{Eq.3.7})$$

Where:

h represents the amount of free amino groups expressed in glutamic acid equivalents (g/L; the molar mass of glutamic acid - 147.13 g/mol - was used as an average molar mass of all amino acids).

h_{tot} is the total rice protein concentration (g/L) in the dispersion.

3.8.8 Analyses of starch digestion kinetics and predicted glycaemic indexes.

The starch digestion curve can be described by a first-order kinetic model as $C_t = C_\infty\left(1 - e^{-kt}\right)$. Here, C_t represents the concentration of maltose (digested starch) at a given time. C_∞ is the estimated maltose concentration at the endpoint of digestion, and k is the digestion rate coefficient. These two values can be calculated by analysing the logarithm of the slope (LoS) plot form as $\ln\left(\frac{dC}{dt}\right) = \ln(C_\infty k) - kt$**,** as reported by Butterworth et al. (2012)**.**

Linearised first-order kinetic models are generally used to describe simple starch substrates digested at a single rate, such as rice starch isolates (Li et al., 2021). For more complex substrates involving lipids and proteins, such as rice or wheat, nonlinear plot modes are more frequently reported (Edwards et al., 2014; Li & Hu, 2020; Zou et al., 2015). Although there could be more phases, biphasic digestogram models with two monophasic digestograms with different rates are commonly used to describe these slope discontinuities. Thus, a first-order equation with a piecewise function (**Eq.3.8**) was used to profile the overall starch digestion curve as proposed by Edwards et al. (2014).

$$C_{(t)} = C_{\infty 1} \times \left(1 - e^{-k1 \times t}\right) + \mathbf{if}\left(t > t_{int}, C_{\infty 2} \times \left(1 - e^{-k2 \times (t - t_{int})}\right), 0\right) \quad \textbf{(Eq.3.8)}$$

Where:

t_{int} is the time of intersection of the two plots

k (k_1 and k_2) are the respective rate constants

C_∞ ($C_{\infty 1}$ and $C_{\infty 2}$) are an estimate of the digested starch proportions at the reaction endpoints of each digestion fraction (referring to the portion of starch digested at rapid - k_1 - or slow - k_2 - rate).

If the digestion curve is a linear phase, t_{int} does not exist, and only the first part applies. The mathematical modelling of *in vitro* starch digestograms used in this study is summarised in **Fig. 3.8**.

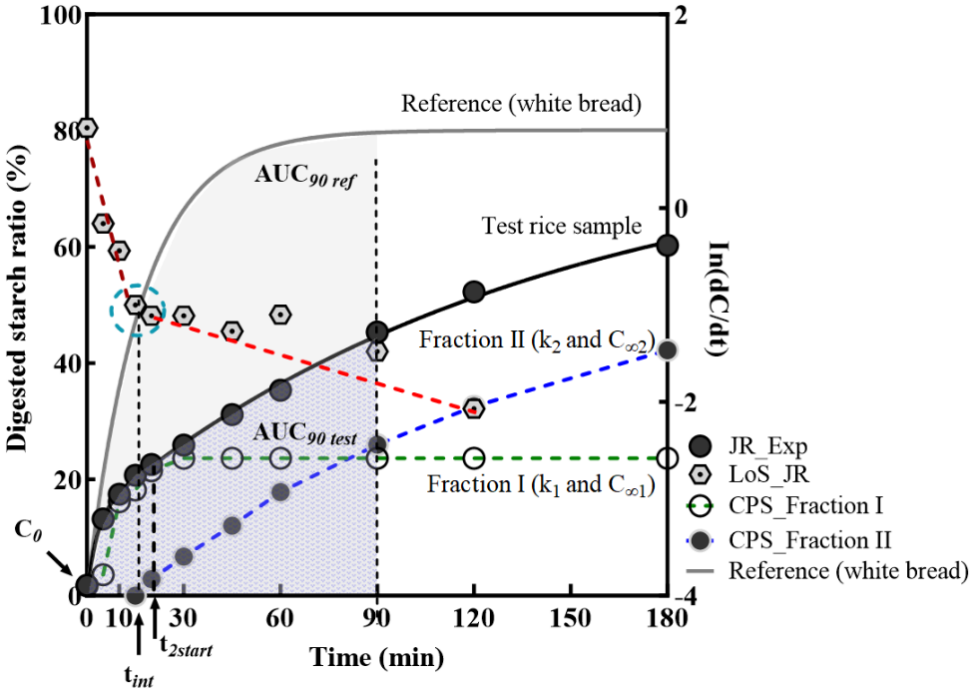


Fig. 3.8. Kinetic models applied on starch digestibility curve. Image adapted from Edwards et al. (2014, 2018). Dots on the starch digestibility curve (black line): proportion of starch digested by enzymes as a function of time. $C_{\infty 1}$ and $C_{\infty 2}$ are the proportion of starch digested at the endpoint of each reaction, obtained with k_1 and k_2. $C_{\infty total}$ is the prediction of digested starch concentrations based on C_0, $C_{\infty 1}$ and $C_{\infty 2}$. HI is calculated by comparing the incremental AUC of the rice sample with reference food (white bread).

Multiple digestible fractions were identified as linear discontinuities after applying a LoS model ($\ln\left(\frac{dC}{dt}\right) = \ln(C_\infty k) - kt$). Thus, the combination of parallel and sequential (CPS) kinetic models proposed by Li et al. (2020) was applied to the digestion curve as in **Eq.3.9**.

$$\mathbf{C_t = C_0 + (C_{\infty 1}) \times \left(1 - e^{-k_1 t}\right) + if(t > t_{2start}, (C_{\infty 2}) \times (1 - e^{-k_2 (t - t_{2start})}, 0)} \quad \textbf{(Eq.3.9)}$$

As for the LoS model, this equation can differentiate digestion phases (e.g., rapid versus slow) with different rate constants (k_1 and k_2) and concentrations at the endpoint of each reaction phase ($C_{\infty 1}$ and $C_{\infty 2}$). CPS model additionally introduces a variable named t_{2start}, which represents sequential or parallel digestion patterns, or a combination of both. When t_{2start} = 0, the parallel digestion pattern is followed. When $t_{int} < t_{2start}$, the sequential digestion pattern is followed. When $0 < t_{2start} \leq t_{int}$, a CPS digestion pattern is followed (Yu et al., 2021).

The predicted glycaemic index (pGI) was calculated using **Eq.3.10**, described by Tamura et al. (2016).

$$\mathbf{pGI = 39.71 + 0.549HI} \quad \textbf{(Eq.3.10)}$$

Where:

HI is the hydrolysis Index, calculated by comparing the area under the curve at 90 mins ($AUC90_{sample}$) of digestibility plots with that obtained for white bread ($AUC90_{reference}$), as shown in **Eq.3.11**.

$$\mathbf{HI = \frac{AUC90_{sample}}{AUC90_{reference}} \times 100} \quad \textbf{(Eq.3.11)}$$

White

3.9 Statistical analysis

Results were calculated as means ± standard deviation. Subsequently, Tukey's test, in conjunction with analysis of variance (ANOVA), was used to determine significant differences among the means at an a priori significance level of $p < 0.05$, using the SPSS software (version 27, Chicago, USA). In the granulometric measurement for the cooked grain after homogenisation, the cumulative Gaussian statistic model was used to calculate the particle size distribution after passing the Shapiro-wilk normality test using Prism (version 9, San Diego, CA) (Blanquet-Diot et al., 2021; Suo et al., 2021).

3.10 References

AACC (2001) Determination of the Pasting Properties of Rice with the rapid Visco-Analyser Official Methods 61-02. American Association of Cereal Chemists. 11th Edition, electronic.

AOAC (2005a) Official methods of analysis of the Association of Analytical Chemists International. Official Methods 934.01: Gaithersburg, MD, USA.

AOAC (2005b) Official methods of analysis of the Association of Analytical Chemists International. Official Methods 933.29: Gaithersburg, MD, USA.

AOAC (2007). Official methods of analysis of Association of Analytical Chemists International. Official Methods 996.11: Gaithersburg, MD, USA.

Atkinson, F.S., Brand-Miller, J.C., Foster-Powell, K., et al. (2021) International tables of glycemic index and glycemic load values 2021: a systematic review. *The American journal of clinical nutrition*, 114 (5): 1625–1632. doi:10.1093/AJCN/NQAB233.

Bahdanovich, P., Axelrod, K., Khlystov, A.Y., et al. (2022) Optimized Spectrophotometry Method for Starch Quantification. *Analytica*, 3 (4): 394–405. doi.org/10.3390/analytica3040027

Balet, S., Guelpa, A., Fox, G., et al. (2019) Rapid Visco Analyser (RVA) as a Tool for Measuring Starch-Related Physiochemical Properties in Cereals: a Review. *Food Analytical Methods*. 12 (10) pp. 2344–2360. doi:10.1007/s12161-019-01581-w.

Blanquet-Diot, S., François, O., Denis, S., et al. (2021) Importance of oral phase *in vitro* starch digestibility related to wholegrain versus refined pastas and mastication impairment. *Food Hydrocolloids*, 112: doi:10.1016/J.FOODHYD.2020.106277.

Boluda-Aguilar, M., Taboada-Rodríguez, A., López-Gómez, A., et al. (2013) Quick cooking rice by high hydrostatic pressure processing. *LWT - Food Science and Technology*, 51 (1): 196–204. doi:10.1016/j.lwt.2012.09.021.

Boonmeejoy, J., Wichaphon, J. and Jiamyangyuen, S. (2019) Classification of rice cultivars by using chemical, physicochemical, thermal, hydration properties, and cooking quality. *Food and Applied Bioscience Journal*, 7 (2): 42–62:org/index.php187071

Butterworth, P.J., Warren, F.J., Grassby, T., et al. (2012) Analysis of starch amylolysis using plots for first-order kinetics. *Carbohydrate Polymers*, 87 (3): 2189–2197. doi.org/10.1016/j.carbpol.2011.10.048

Cardoso, M.B., Putaux, J.L., Samios, D., et al. (2007) Influence of alkali concentration on the deproteinization and/or gelatinization of rice starch. *Carbohydrate Polymers*, 70 (2): 160–165. doi.org/10.1016/j.carbpol.2007.03.014

Chakraborty, I., N, P., Mal, S.S., et al. (2022) An Insight into the Gelatinization Properties Influencing the Modified Starches Used in Food Industry: A review. *Food and Bioprocess Technology 2022 15:6*, 15 (6): 1195–1223. doi:10.1007/S11947-022-02761-Z.

Chakraborty, I., Pallen, S., Shetty, Y., et al. (2020) Advanced microscopy techniques for revealing the molecular structure of starch granules. *Biophysical Reviews*, 12 (1): 105–122. doi:10.1007/S12551-020-00614-7.

Chávez-Murillo, C.E., Veyna-Torres, J.I., Cavazos-Tamez, L.M., et al. (2018) Physicochemical characteristics, ATR-FTIR molecular interactions and *in vitro* starch and protein digestion of thermally-treated whole pulse flours. *Food Research International*, 105 (November 2017): 371–383. doi:10.1016/j.foodres.2017.11.029.

Chmiel, T., Saputro, I. E., Kusznierewicz, B., & Bartoszek, A. (2018). The impact of cooking method on the phenolic composition, total antioxidant activity and starch digestibility of rice (Oryza sativa L.). Journal of Food Processing and Preservation, 42(1), e13383. doi.org/10.1111/JFPP.13383/SUPPINFO

Choi, H.W. and Kim, H.S. (2022) Hydroxypropylation and acetylation of rice starch: effects of starch protein content. *Food Science and Biotechnology*, 31 (9): 1169. doi:10.1007/S10068-022-01106-Y.

Dang, J. and Copeland, L. (2004) Studies of the fracture surface of rice grains using environmental scanning electron microscopy. *Journal of the Science of Food and Agriculture*, 84: 707–713. doi:10.1002/jsfa.1671.

de Souza, D., Sbardelotto, A.F., Ziegler, D.R., Marczak, L.D.F. and Tessaro, I.C., 2016. Characterization of rice starch and protein obtained by a fast alkaline extraction method. *Food Chemistry*, *191*, pp.36-44.doi.org/10.1016/j.foodchem.2015.03.032

Edwards, C.H., Cochetel, N., Setterfield, L., et al. (2019) A single-enzyme system for starch digestibility screening and its relevance to understanding and predicting the glycaemic index of food products. *Food and Function*, 10 (8): 4751–4760. doi:10.1039/c9fo00603f.

Edwards, C.H., Maillot, M., Parker, R., et al. (2018) A comparison of the kinetics of *in vitro* starch digestion in smooth and wrinkled peas by porcine pancreatic alpha-amylase. *Food Chemistry*, 244 (June 2017): 386–393. doi:10.1016/j.foodchem.2017.10.042.

Edwards, C.H., Warren, F.J., Milligan, P.J., et al. (2014) A novel method for classifying starch digestion by modelling the amylolysis of plant foods using first-order enzyme kinetic principles. *Food and Function*, 5 (11): 2751–2758. doi:10.1039/c4fo00115j.

Farooq, A.M., Li, C., Chen, S., et al. (2018) Particle size affects structural and *in vitro* digestion properties of cooked rice flours. *International Journal of Biological Macromolecules*, 118: 160–167. doi:10.1016/J.IJBIOMAC.2018.06.071.

Farooq, M.A., Murtaza, M.A., Aadil, R.M., et al. (2021) Investigating the structural properties and *in vitro* digestion of rice flours. *Food Science & Nutrition*, 9 (5): 2668. doi:10.1002/FSN3.2225.

Fernandes, J.M., Madalena, D.A., Pinheiro, A.C., et al. (2020) Rice *in vitro* digestion: application of INFOGEST harmonized protocol for glycemic index determination and starch morphological study. *Journal of Food Science and Technology*, 57 (4): 1393. doi:10.1007/S13197-019-04174-X.

Furuya, J., Hara, A., Nomura, T., et al. (2014) Volitional chewing with a conscious effort alters and facilitates swallowing during the feeding sequence. *Journal of Oral Rehabilitation*, 41 (3): 191–198. doi:10.1111/JOOR.12140.

Garcia-Valle, D.E., Bello-Pérez, L.A., Agama-Acevedo, E., et al. (2021) Effects of mixing, sheeting, and cooking on the starch, protein, and water structures of durum wheat semolina and chickpea flour pasta. *Food Chemistry*, 360: 129993. doi:10.1016/J.FOODCHEM.2021.129993.

Guerrero, P., Kerry, J.P. and De La Caba, K. (2014) FTIR characterization of protein-polysaccharide interactions in extruded blends. *Carbohydrate Polymers*, 111: 598–605. doi:10.1016/j.carbpol.2014.05.005.

Ha, M., Jeong, H. Y., Lim, S. T., & Chung, H. J. (2022). The cooking method features controlling eating quality of cooked rice: An explanation from the view of starch structure in leachate and morphological characteristics. Food Research International, 162, 111980. doi.org/10.1016/J.FOODRES.2022.111980

Iwe, M.O., Onyeukwu, U. and Agiriga, A.N. (2016) Proximate, functional and pasting properties of FARO 44 rice, African yam bean and brown cowpea seeds composite flour. *Carbohydrate Polymers* 2 (1). doi:10.1080/23311932.2016.1142409.

Jiménez-Munoz, L., Brodkorb, A., and Gómez-Mascaraque, L.G. (2021) Effect of heat treatment on the digestion behaviour of pea and rice protein dispersions and their blends studied using the semi-dynamic INFOGEST digestion method. *Food and Function*, 12 (18): 8747–8759. doi:10.1039/d1fo01223a.

Khin, M.N., Ahammed, S. and Zhong, F. (2021) Development of DTAF-labelled polysaccharides for characterization of microstructure and phase distribution of composite hydrogel visualization of hydrogels using CLSM. *Food Bioscience*, 41: 100909. doi:10.1016/J.FBIO.2021.100909.

Laemmli, U.K., 1970. Cleavage of structural proteins during the assembly of the head of bacteriophage T4. Nature, 227(5259), pp.680-685. doi.org/10.1038/227680a0

Li, C. & Hu, Y. (2020) Combination of parallel and sequential digestion kinetics reveals the nature of digestive characteristics of short-term retrograded rice starches. *Food Hydrocolloids*, 108: 106071. doi:10.1016/J.FOODHYD.2020.106071.

Li, C., Hu, Y., Gu, F., et al. (2021) Causal relations among starch fine molecular structure, lamellar/crystalline structure and *in vitro* digestion kinetics of native rice starch. *Food & Function*, 12 (2): 682–695. doi:10.1039/D0FO02934C.

Liu, J., Fei, L., Maladen, M., et al. (2009) Iodine binding property of a ternary complex consisting of starch, protein, and free fatty acids. *Carbohydrate Polymers*, 75 (2): 351–355. doi:10.1016/J.CARBPOL.2008.08.015.

Moongngarm, A., Bronlund, J., Grigg, N., et al. (2012) Chewing Behavior and Bolus Properties as Affected by Different Rice Types. *International Journal of Medical and Biological Sciences*, 6. doi.org/10.5281/zenodo.1079550

Nadia, J., Olenskyj, A.G., Stroebinger, N., et al. (2021) Tracking physical breakdown of rice- and wheat-based foods with varying structures during gastric digestion and its influence on gastric emptying in a growing pig model. *Food and Function*, 12 (10): 4349–4372. doi:10.1039/d0fo02917c.

Pozo, C., Rodríguez-Llamazares, S., Bouza, R., et al. (2018) Study of the structural order of native starch granules using combined FTIR and XRD analysis. *Journal of Polymer Research*, 25 (12): 1–8. doi:10.1007/S10965-018-1651-Y

Ranawana, D. V, Henry, C.J.K., Lightowler, H.J., et al. (2009) Glycaemic index of some commercially available rice and rice products in Great Britain. *International journal of food sciences and nutrition*, 60 Suppl 4: 99–110. doi:10.1080/09637480802516191.

Ranawana, V., Monro, J.A., Mishra, S., et al. (2010) Degree of particle size breakdown during mastication may be a possible cause of interindividual glycemic variability. *Nutrition research (New York, N.Y.)*, 30 (4): 246–254. doi:10.1016/J.NUTRES.2010.02.004.

Sahoo, B., Kumari, A., Sarkhel, S., et al. (2023) Rice Starch Phase Transition and Detection During Resistant Starch Formation. doi:10.1080/87559129.2022.2163498.

Van Soest, J.J.G., Tournois, H., de Wit, D., et al. (1995) Short-range structure in (partially) crystalline potato starch determined with attenuated total reflectance Fourier-transform IR spectroscopy. *Carbohydrate Research*, 279 (C): 201–214. doi.org/10.1016/0008-6215(95)00270-7

De Souza, D., Sbardelotto, A.F., Ziegler, D.R., et al. (2016) Characterization of rice starch and protein obtained by a fast alkaline extraction method. *Food Chemistry*, 191: 36–44. doi:10.1016/J.FOODCHEM.2015.03.032.

Steglich, T., Bernin, D., Röding, M., et al. (2014) Microstructure and water distribution of commercial pasta studied by microscopy and 3D magnetic resonance imaging. *Food Research International*, 62: 644–652. doi:10.1016/J.FOODRES.2014.04.004.

Suo, X., Mosca, A.C., Pellegrini, N., et al. (2021) Effect of pasta shape and gluten on pasta cooking quality and structural breakdown during mastication. *Food & Function*, 12 (22): 11577–11585. doi:10.1039/D1FO02339J.

Tamura, M., Nagai, T., Hidaka, Y., et al. (2014) Changes in nonwaxy Japonica rice grain textural-related properties during cooking. *Journal of Food Quality*, 37 (3): 177–184. doi:10.1111/jfq.12085.

Tamura, M., Singh, J., Kaur, L., et al. (2016) Impact of structural characteristics on starch digestibility of cooked rice. *Food Chemistry*, 191: 91–97. doi:10.1016/j.foodchem.2015.04.019.

Warren, F.J., Gidley, M.J. and Flanagan, B.M. (2016) Infrared spectroscopy as a tool to characterise starch ordered structure--a joint FTIR-ATR, NMR, XRD and DSC study. *Carbohydrate polymers*, 139: 35–42. doi:10.1016/j.carbpol.2015.11.066.

Wu, Z., He, Y., Yan, W., Zhang, W., Liu, X., Hui, A., Wang, H., & Li, H. (2021). Effect of high-pressure pre-soaking on texture and retrogradation properties of parboiled rice. Journal of the Science of Food and Agriculture, 101(10), 4201–4206. doi.org/10.1002/JSFA.11058

Yan, W., Yin, L., Zhang, M., et al. (2021) Gelatinization, Retrogradation and Gel Properties of Wheat Starch–Wheat Bran Arabinoxylan Complexes. *Gels*, 7 (4). doi:10.3390/GELS7040200.

Yashini, M., Khushbu, S., Madhurima, N., et al. (2022) Thermal properties of different types of starch: A review, Critical Reviews in Food Science and Nutrition. doi:10.1080/10408398.2022.2141680.

Yau, N.J.N. and Huang, J.J. (1996) Sensory analysis of cooked rice. *Food Quality and Preference*, 7 (3): 263–270. doi.org/10.1016/S0950-3293(96)00010-9.

Ying, D., Hlaing, M.M., Lerisson, J., et al. (2017) Physical properties and FTIR analysis of rice-oat flour and maize-oat flour based extruded food products containing olive pomace. *Food Research International (Ottawa, Ont.)*, 100 (Pt 1): 665–673. doi:10.1016/j.foodres.2017.07.062.

Yu, W., Zhou, X. and Li, C. (2021) Application of first-order kinetics modelling to reveal the nature of starch digestion characteristics. *Food & Function*, 12 (15): 6652–6663. doi:10.1039/D1FO00450F.

Zhu, L., Bi, S., Wu, G., et al. (2020) Comparative analysis of the texture and physicochemical properties of cooked rice based on the adjustable rice cooker. *LWT*, 130: 109650. doi.org/10.1016/j.lwt.2020.109650.

Zhu, L., Wu, G., Cheng, L., et al. (2019) Effect of soaking and cooking on structure formation of cooked rice through thermal properties, dynamic viscoelasticity, and enzyme activity. *Food Chemistry*, 289: 616–624. doi.org/10.1016/j.foodchem.2019.03.082.

Zou, W., Sissons, M., Gidley, M.J., et al. (2015) Combined techniques for characterising pasta structure reveal how the gluten network slows enzymic digestion rate. *Food Chemistry*, 188: 559–568. doi:10.1016/j.foodchem.2015.05.032.

4 The physicochemical and microstructural effects of low acyl gellan gum on the protein-starch matrices of cooked white rice: Impact on textural properties

Qingsu Liu[1], Vincenzo Di Bari[2], Nicholas James Watson[3*]

[1] Food, Water, Waste Research Group, Faculty of Engineering, The University of Nottingham, University Park Campus NG7 2RD, UK

[2] Division of Food Sciences, The University of Nottingham, Sutton Bonington Campus, Loughborough LE12 5RD, UK

[3] School of Food Science and Nutrition, University of Leeds, Leeds, LS2 9JT, UK

***Corresponding author:** n.j.watson@leeds.ac.uk

(Manuscript prepared for Submission)

Abstract

This study explores the impact of low acyl gellan gum on the physicochemical and microstructural attributes of cooked non-parboiled and parboiled rice. The findings reveal distinctive effects of low acyl gellan gum on the viscosity and thermal properties of non-parboiled rice, while parboiled rice exhibits limited responsiveness, providing evidence of the complex interactions between low acyl gellan gum and rice's characteristics, composition and structure. The presence of low acyl gellan gum induces observable shifts in structural composition, such as the formation of β-sheet structures and V-type starch-low acyl gellan gum complexes. Microscopic analysis confirms the formation of a coating on the rice grain surface, which alters the textural characteristics of cooked, non-parboiled rice. Parboiled rice exhibits a lower susceptibility to acyl gellan gum-induced changes due to its distinct microstructure. Additionally, variations in pre-homogenisation time and the addition of Low acyl gellan gum significantly impact starch digestibility in oral phase simulation, highlighting the intricate relationship between rice grain composition and microstructure. This study provides valuable insights into the manipulation of *in vitro* starch digestibility through Low acyl gellan gum incorporation during the cooking process.

Highlights

- The addition of a low acyl gellan gum affected cooked white rice's physicochemical and microstructural properties to a different extent according to the rice types (non-parboiled vs parboiled).
- Low acyl gellan gum increases rice dispersion's pasting properties during cooking and reduces starch retrogradation during cooling.
- Low acyl gellan gum forms a coating at the rice grain's peripheral region and retains the cooked grain's compact protein-starch matrices.
- The effect of low acyl gellan gum on the physicochemical and textural properties of white rice is more evident in the non-parboiled rather than parboiled type.
- Upon oral processing simulation, intact or pre-homogenised rice significantly decreases oral starch digestibility when using low acyl gellan gum.

Keywords: white rice, low acyl gellan gum, protein-starch matrices; *in vitro* starch digestibility.

4.1 Introduction

Rice continues to gain importance in the human diet as an essential source of carbohydrates and energy for more than half of the world's population, providing nearly 20 % of calorie intake (OECD-FAO. 2021). White rice is the predominantly consumed rice type, in which the grain is refined by milling out the bran and germ, which contain the major proportion of total fat and fibre, to leave the starchy endosperm (Van Dam, 2020). The refining process affects the grain's composition, especially starch (up to 90 % dry weight), protein (4-11 % dry weight) and fat (0.5-2 % dry weight), and their configurations (Toutounji et al., 2019) in addition to facilitating the cooking process and improving the cooked rice's texture and taste. Oral recognition of starch occurs when it is broken down into maltose by the α-amylase in the saliva. Therefore, the degree of starch degradation in the oral cavity could be of nutritional importance (Peyrot & Breslin, 2016; Toutounji et al., 2019). Both characteristics contributed to white rice's popularity and profitability, as evidenced by the market success of white jasmine rice (Jarma et al., 2020; Jirapornvaree et al., 2021). The gluten-free nature of rice makes it an ideal choice for individuals who suffer from gluten sensitivity or follow a low-fat diet. It is also versatile as it can be served whole, ground into flour, or fermented into desserts and yoghurt (Alvarez-Jubete et al., 2010; Kamlesh & Prakash, 2010; Toutounji et al., 2019).

Due to its popularity, white rice now plays a key role in health management. Ingestion of rice containing a high amount of rapidly digestible starch (RDS) is associated with an acute glycaemic response. It is considered a risk factor for hyperglycaemia and insulin resistance (Kaur et al., 2016). Involving 132,373 participants in 21 countries, a long-term (9.5 years) cohort study was conducted to understand the correlation between white rice consumption and diabetes. Higher intakes of cooked white rice (450 g per day, around 3 cups of cooked rice, compared to lower < 150 g/day, around 1 cup) were associated with a significant increase in diabetes development (Carcea et al., 2021). Conversely, rice containing slowly

digestible starch (SDS) or resistant starch (RS) was associated with significant nutritional and health benefits (Jukanti et al., 2020).

Therefore, exploring strategies for reducing the RDS in white rice has gained interest and importance among researchers from multiple disciplines. To be effective, proposed interventions with rice must consider health impacts and consumer satisfaction. One option is replacing white rice containing SDS/RS sources with brown rice or mixed grains. However, these alternatives are not widely accepted at the organoleptic level. Several approaches to producing SDS rice products have also been explored, including crossbreeding (Suklaew et al., 2020), chemical and enzymatic modification (Dupuis, Liu and Yada, 2014; Nguyen Doan et al., 2019), and hydrothermal treatments such as parboiling (Kiatponglarp et al., 2015; Rocha-Villarreal, Serna-Saldivar & García-Lara, 2018). Parboiling is a treatment that involves soaking, pressure steaming, and drying. It is applied before dehulling in conventional grain processing. Parboiling has been reported to contribute to better rice quality by increasing milling yields, nutritional value and reducing the effects of insect damage (Paiva et al., 2016). Aside from being easy-cook and preserving the traditional taste, parboiled rice (PR) contains more SDS than non-parboiled rice, making it a healthier option for glucose-sensitive customers. This can be attributed to changes in the starch's physical state following the parboiling process. Rice starch after parboiling achieves more ordered structures than those found in non-parboiling (Larsen et al., 2000; Cheng, Chen & Yeh, 2019). The protein networks enclosing the starch granules, forming the characteristic protein-starch matrices, become more compact due to parboiling. This prevents the starch granules from gelatinising upon cooking and potentially reduces starch digestibility during digestion (Tian et al., 2018; Cheng et al., 2019; Sivakamasundari et al., 2020). Specifically, the more compact protein network likely depends on heat-denatured protein forming a gel matrix that enhances the integrity of starches and restricts the water-absorbing capability of rice grains (Fitzgerald et al., 2003).

Cooking rice in hydrocolloid dispersion has been proposed as a simple method to reduce the starch digestibility of cooked rice. These hydrocolloids could inhibit the

enzymatic hydrolysis either through single or combined effects, e.g., encapsulating starch granules, increasing the particle size and viscosities of digesta (Sasaki & Kohyama, 2011; Chen et al., 2017; Ojo et al., 2018). One such hydrocolloid is Low acyl gellan gum (LAGG). It is a water-soluble, anionic polysaccharide produced by the bacterium Sphingomonas elodea, and it has been widely used in food products as a texturing agent (Bradbeer et al., 2015). This material forms a liquid gel that can withstand 120°C and solidifies into a brittle gel texture under quiescent cooling. In terms of increasing SDS content, several pilot studies have explored self-structured LAGG gels and gel-forming behaviour in the presence of rice starch in an acidic environment such as the stomach (Bradbeer et al., 2015; Tamura et al., 2017; S Blanquet-Diot et al., 2021). The findings presented were promising as they demonstrated high resistance to shear force and the capability to increase viscosity at low pH. An increased viscosity or a gel network impedes the mass transfer of the food materials (increases satiation) and enzymes (slows the digestion rate) (Kanyuck et al., 2022). These characteristics make this polysaccharide a potential option for SDS-containing foods while providing satiety. Chung et al. (2008) performed the first study on the texture and *in vitro* digestibility of white rice cooked with LAGG dispersions at two concentrations (0.3 and 0.7 %). The results showed that among six different hydrocolloids tested, LAGG had the most significant impact on the texture and SDS content in cooked rice (Srikaeo & Paphonyanyong, 2020). However, limited information was provided on the potential mechanism responsible for these. Establishing the physicochemical and microstructural effects of LAGG on the protein-starch matrices of cooked white rice would provide the required knowledge to produce high SDS-based foods.

Therefore, this study aims to investigate the physicochemical and microstructural effects of LAGG on the protein-starch matrices of two types of cooked white rice (non-parboiled vs parboiled). Several physicochemical properties of rice were analysed. The rice pasting and thermal properties were evaluated with a rapid visco analyser (RVA) and a differential scanning calorimeter (DSC). The hydration properties were instead evaluated with swelling power and solubility index

measurements. The microstructural properties at multi-scales were studied by Fourier transform infrared (FTIR), X-ray diffraction (XRD) and microscopic observations. The resulting textural properties of cooked rice were analysed using a textural property analyser (TPA). An *in vitro* oral process was also performed to assess the cooked grain disintegrations and oral starch digestibility.

4.2 Materials and methods

4.2.1 Materials

Two types of *Indica* rice were used in this study: a non-parboiled type - Thai Jasmine rice (JR, Green Dragon Thai Hom Mali Aaa, purchase date December 2018), and an easy-cook long grain rice, also called parboiled rice (PR), purchase date January 2019). Low acyl gellan gum (LAGG) was purchased from CP Kelco, UK. Human salivary α-amylase (Sigma A-1031, batch number SLBX2637) was purchased from Sigma-Aldrich. Enzyme activity was determined in the lab using the procedure by Brodkorb et al. (2019). The enzyme activity was 145.98 U/mg, where 1 unit/mg represented the capability of liberating 1 mg of maltose from soluble potato starch (S2630, Sigma-Aldrich) in 3 mins at a pH of 6.9 at 20°C. Unless otherwise stated, all reagents were of analytical grade and supplied from Sigma-Aldrich, UK.

4.2.2 Rice flour production and extraction of starch

Rice (100 g) was rinsed thrice with distilled water and then dried at ambient temperature for 1 h. To produce the rice flour, cleaned JR or PR grains were ground using an electric grinder (KG49, Delonghi, Treviso, Italy) and the powder was passed through a sieve with a 500 μm mesh size; the particles larger than 500 μm were discarded. Rice starch was recovered based on the method described by Singh et al. (2003). In brief, rice flour (50 g) was mixed with 0.18 % (w/v) NaOH solution to a flour-to-solution ratio of 1:15 (w/v) while stirring at 30°C for 1 h. After centrifuging (4000 rpm, 15 mins), the protein-rich supernatant was separated from the starchy residue pellet, and the latter was washed using 125 mL of with 0.18 % NaOH and centrifuged (4000 rpm, 15 mins) again. The starchy residue was neutralised with 0.1 M HCl (~30 mL) to pH 7.0 and dried in an oven (MOV-112F, Sanyo, Japan) at 30°C for

24 h (until constant weight). It was then blended and sifted as for the rice flour. The starchy powders produced from JR and PR are defined as jasmine rice starch (JRS) and parboiled rice starch (PRS).

4.2.3 Morphological Properties of rice flour and starch

Rice flour and starch produced using the methodology in **Section 4.2.2** were examined under brightfield and polarised light microscopy to observe the differences in their morphological attributes (size and shape) and native crystalline states (represented by Maltese cross). Light microscopy was performed using an Eclipse Ci microscope (Nikon Instruments Inc., Surrey, UK) equipped with a digital camera (Nikon digital Sight DS-Fi2 camera). Samples were prepared as described by Chakraborty et al. (2020). A drop of the starch or flour-water mixture (1 % w/v) was placed on the microscope slide and covered with a cover slip. The images were viewed and captured at 20 times magnification using NIS-Elements software (Nikon Instruments Inc., Surrey, UK).

The particle size distribution of rice flour or starch was measured with a laser diffraction particle size analyser (LS 13 320, powder system module Beckman Coulter, Inc., Buckinghamshire, UK). The mean diameter over volume (μm) was reported as an average of three measurements.

4.2.4 Preparation of cooked rice with and without LAGG

Rice samples were cooked following the manufacturer's instructions and previous studies (Chatthongpisut et al., 2015; Liu et al., 2019). Pre-washed JR or PR (100 g) were cooked in a rice cooker (NEDIS, Karc06wt-power 300w, Leicester, UK) with 150 g of distilled water (1:1.5 rice-to-water ratio, w/w) until no excess water was present (approximately 15 mins). After cooking, the rice was kept in the rice cooker in warm mode (65-70°C) for 10 mins to cook the grains fully. The grains were visually determined to be fully cooked using the glass slide method described by Singh et al. (2005). The kernels of cooked rice were randomly selected and loaded between two microscopes. The rice was considered cooked if it had softened without hard centres or a white core during the shredding process. JR or PR (100 g) were also cooked in

150 g of distilled water containing 1, 2, or 3 g of pre-dispersed LAGG (corresponding to 1, 2, and 3 % of rice mass, respectively). Samples containing 1, 2, or 3 g of LAGG were coded as JR_1LA, JR_2LA and JR_3LA for JR and PR_1LA, PR_2LA and PR_3LA for PR.

The moisture content was determined using standard method 934.01 published by the Association of Official Agricultural Chemists (AOAC). The samples were dried in an oven (MOV-112F, Sanyo, Japan) at 105°C for 24 h (until constant weight). The moisture content was represented by the difference in the sample weight before and after drying (AOAC, 2005a). Aliquots of the cooked rice samples were lyophilised, ground, and sifted into flour (particles < 500 μm) before chemical composition analysis. The nitrogen content in samples was measured with the Kjeldahl method according to AOAC 930.29, and respective crude protein content was calculated using a nitrogen-to-protein conversion factor of 5.95 (AOAC, 2005b). The total starch content in each sample was measured using method 996.11 by AOAC with a total starch assay kit (α-amylase/amyloglucosidase) (K-TSTA, Megazyme, Ireland). The apparent amylose content of the rice samples was determined using the iodometric method described by Tamura et al. (2014). In brief, each sample (50 mg) was initially defatted in a 15 mL conical centrifuge tube with 500 μL of 95 % ethanol, then mixed with 1 M NaOH (4.5 mL) and heated in a boiling water for 10 mins to allow amylose to leach and disperse (Bahdanovich et al., 2022). The total mix volume was adjusted to 10 mL using distilled water, 500 μL of the solution was withdrawn, diluted with 2 mL distilled water, and then neutralised with 500 μL 1 M acetic acid into another 15 mL tube. 1 mL of 0.2 % fresh prepared iodine solution (0.2 g iodine and 2.0 g potassium iodide diluted to 100 mL with distilled water) was then added to form an amylose-iodine complex, and the mix was rested for 10 mins at 30°C to develop colour. The mix absorbance was subsequently measured at 620 nm using a UV-visible spectrophotometer (Evolution™ 60S, ThermoFisher, paisley, UK), using potato amylose (A0512, Sigma-Aldrich) as the standard. A portion of uncooked rice grain and extracted starch was also lyophilised, ground, and sieved to a powder to determine the effect of lyophilisation on the

composition of raw rice flour and starch. No significant difference in composition was identified in samples with or without lyophilisation. Rice protein profiles were determined by sodium dodecyl sulphate-polyacrylamide gel electrophoresis (SDS-PAGE, 12 % separating gel and 4 % stacking gel) according to the method described by Laemmli et al. (1970). The powdered samples were solubilised in one time volume of reducing sample buffer (1610737, 62.5 mM Tris-HCl (pH 6.8), 25 % of glycerol, 2 % of SDS, 5 % of β-mercaptoethanol, 0.01 % of bromophenol blue). Then, the mixture was heated at 95°C for 5 mins. The samples for SDS-PAGE under non-reducing conditions were prepared using the same process, just without 2-ME. Gels were stained with Coomassie Brilliant Blue R-250 and destained in a methanol-water solution containing 10 % acetic acid (methanol/acetic acid/water = 1:1:8, v/v/v).

The pasting properties of rice samples cooked with and without LAGG were evaluated using an RVA (4800, PerkinElmer, Buckinghamshire, UK) following AACC 61-02 (AACC, 2001). In brief, 3 g of JR or PR flour (based on 8 % water content) was added into an aluminium canister containing 25 g of 0, 0.03, 0.06 or 0.09 g (w/w) LAGG dispersion, corresponding to 0 %, 1 %, 2 % and 3 % of the flour mass (3 g), respectively. LAGG was initially dispersed in distilled water to prepare the mixtures and equilibrated at ambient temperature for 1 h. After stirring the dispersions and loading into the RVA instrument, the samples were mixed at 960 rpm for the first 10 s, then at 160 rpm for the remaining procedure. The heating profile was as follows: holding at 50°C for 1 min 30 s, heating to 95°C in 3 mins 45 s, holding at 95°C for 2 mins 30 s, and cooling to 50°C in 3 mins 45 s and holding at 50°C for 1 min. The pasting properties parameters, i.e., peak (PV), breakdown (BD), final (FV), and setback viscosity (SB), peak time (P_t), peak temperature, were calculated with Thermocline for Windows software (version 3) supplied with the instrument. Following the RVA test, the corresponding proportions of JRS and PRS (dry starch basis) were added to 25 g of distilled water (0 % LAGG) to assess the difference in starch pasting behaviour without protein. The RVA test of LAGG-water dispersions (without a rice sample) was also performed. All measurements were performed in triplicate.

4.2.5 Thermal properties

The thermal properties of the samples were determined using DSC (Dsc 3+, Mettler Toledo, Leicester, UK) based on the method described by Zhu et al. (2020). The rice flour/rice starch (10 mg) was mixed with 15 μL distilled water to achieve the same rice-to-water ratio used in cooking and placed into stainless-steel pans (40 μL). Pre-prepared LAGG dispersion (1-3 %, w/w) were added (15 μL). To prepare rice in LAGG dispersion, 0.1, 0.2, or 0.3 mg of LAGG powder was mixed with 15 μL distilled water, then added to the rice flour as control (without LAGG). A temperature profile simulating the rice cooker was used to analyse the samples, as described by Zhu et al. (2020). In brief, the sample and reference (empty) pans were heated at 10°C/min from 30°C to 120°C and kept at 120°C for 15 mins. The samples were then cooled at 20°C/min to 60°C to match an edible temperature for freshly cooked rice (Yau & Huang, 1996). Onset temperature (T_o), peak temperature (P_T), conclusion temperature (T_c), and enthalpy of phase transition (ΔH) were calculated from the curve area (under the peak of the thermograms with a baseline) using star^e software (Mettler Toledo, Leicester, UK). Enthalpy was expressed as J/g of dry starch.

4.2.6 Hydration properties

The hydration properties of cooked rice included water solubility index (WSI) and swelling power (SP). These were determined using the method described by Farooq et al. (2018). Briefly, rice flour (1 g) mixed with 10 mL LAGG (0, 1, 2, or 3 mg/mL) dispersion was boiled in a water bath (95°C, 30 mins). For the added rice flour, the corresponding starch proportions of JRS and PRS were mixed with 10 mL of distilled water (0 % LAGG) to assess the difference in starch hydration behaviour without protein.

Upon cooling to ambient temperature, the samples were centrifuged (4000 rpm, 15 mins). The supernatant (containing the soluble fraction) was removed and placed in pre-weighed glass dishes dried at 105°C until the weight was constant and weighed to calculate the WSI using **Eq. 4.1**, expressed in % of dry sample. The residue after centrifuging was weighed for SP determination using **Eq. 4.2**.

$$\mathbf{WSI} = \frac{\mathbf{Wr}}{\mathbf{W}} \times \mathbf{100\ \%} \quad \textbf{(Eq. 4.1)}$$

$$\mathbf{SP} = \frac{\mathbf{Wt}}{\mathbf{W-Wr}} \times \mathbf{100\ \%} \quad \textbf{(Eq.4.2)}$$

Where:

W_t represents the mass of the wet residues

W_r the mass remained after drying the supernatant

W the initial mass of the sample (g, dry solid basis)

4.2.7 Microstructural properties

4.2.7.1 Fourier transform infrared (FTIR) spectra

To identify chemical bonds that characterise functional groups present in the protein and starch of rice before and after cooking, the infrared spectra patterns of samples were recorded using a Bruker Tensor 27 FTIR spectrometer equipped with an attenuated total reflectance accessory (Graseby-Space Ltd, Orpington, UK), following the method reported by Garcia-Valle et al. (2021). Spectra were recorded in the 4000 - 400 cm^{-1} range (128 scans, 4 cm^{-1}), and ambient air was used as a background reading. Data analysis was done using OMNIC software (version 6.2, Thermos Electron Corporation). Following a baseline correction and deconvolution of IR spectra, the secondary structure of rice proteins (amide I region, 1700 cm^{-1} to 1600 cm^{-1}) was quantitatively evaluated by fitting peaks with Gaussian models based on the procedure described by Fetouhi et al. (2019). Assigning secondary structure of protein was on the peaks centred in the region at 1615-1637 cm^{-1} and 1682-1700 cm^{-1} for β-sheet, 1637-1645 cm^{-1} for random coil, 1646-1664 cm^{-1} for α-helix and 1665-1681 cm^{-1} for β-turn, as reported previously (Ellepola et al., 2005; Ying et al., 2017; Fetouhi et al., 2019). The results were expressed as a percentage contribution of each secondary structure, calculated by dividing the relative areas under the curves by the sum of the fitted model. Absorption intensity ratios at 995/1022 (R995/1022) and 1047/1022 (R1047/1022) were used to assess the short-range molecular structure of rice starch, according to Wang et al. (2020).

4.2.7.2 XRD

The crystalline structure patterns of the rice sample were analysed using an X-ray diffractometer (D8, Bruker AXS, Congleton, UK) with a Cu-Kα source (λ = 0.154 nm) running at 40 kV and 25 mA, based on the setting described by Choi et al. (2022). Samples scanned in the 2θ angle range of 4° to 45°, with a step size of 0.02° (2θ) and a scan speed of 2°/min. The relative crystallinity was quantified as the ratio of the crystalline area peak to the total area diffraction peaks (both amorphous and crystalline) evaluated using the DIFFRAC plus EVA® software provided with the XRD instrument.

4.2.7.3 Morphological properties of cooked rice

4.2.7.3.1 Morphological analysis of cooked rice kernel

The cooked samples were imaged using a digital single-lens reflex camera with a 64 mm macro lens (5D, Canon, Tokyo, Japan). Based on the International Rice Research Institute's procedures, ten freshly prepared grains were randomly selected within the central region of the pot for visual quality assessment (Graham et al., 2002). The parameters used for describing kernel morphology, including grain length, thickness, and width, were repeatedly measured with a digital vernier calliper with a resolution of 0.01 mm (PGA1001, Modelcraft, Hereford, UK). The measurement results were expressed in millimetres (means ± standard deviations).

4.2.7.3.2 Light microscopy

The microstructure of the cooked rice grains, especially the protein-starch matrices, was observed under a brightfield microscope (Eclipse Ci microscope, Nikon Instruments, Surrey, UK) equipped with a digital camera (Nikon digital Sight DS-Fi2 camera) based on the method described by Juntunen et al. (2002). In brief, cooked samples were placed in an optimum-cryo-microtomy embedding medium and sectioned into 60 μm thicknesses with a microtome (Leica CM 3050s, Leica Microsystems, Milton Keynes, UK). The tissue sections were then mounted on gelatine-coated microscopic slides. A double stain was applied to the rice sections for light microscopy. A 0.1 % (w/v) fast green 1 % acetic acid aqueous solution was

used to stain the first protein for 1 min and was then washed twice with distilled water to remove the unacted dye. The 1:10 diluted Lugol's iodine solution was added to stain the starch. Micrographs of the samples were taken using the digital camera. The images showed that the protein was observed in green due to its basic amino acid chains' electrostatic bonding with fast green (Steglich et al., 2014). Starch was shown in blue/purple due to the amylase-iodine (blue) and amylopectin-iodine (purple) complex. To track the hydrogel penetration towards the rice grains, the LAGG was covalently labelled using 5-(4,6-dichlorotriazinyl) amino fluorescein (DTAF), following the procedure described by Khin et al. (2021). As with the native LAGG shown in **Section 4.2.4**, the cooked rice samples with DTAF-LAGG were visualised using an EVOS™ FL microscope with 488 nm excitation wavelengths of 488 nm excitation wavelength and 517 nm emission wavelength.

4.2.7.3.3 ESEM

The microstructure of the surface and cross-sections of cooked rice samples were captured using an ESEM (FEI Quanta 650 with Oxford Instruments X-Max-150 EDX Detector) with a gaseous detection device detector. The equipment settings were based on the method described by Dang & Copeland (2004). The micrographs were captured at a magnification of 1000x.

4.2.8 Textural properties of cooked rice samples

4.2.8.1 Textural profile analysis

The textural properties of freshly cooked rice samples were evaluated using a two-cycle compression test using a texture analyser (TA-XT2, Stable. Microsystem, Surrey, England) based on the procedure described by Boluda-Aguilar et al. (2013). In brief, A 2 g aliquot of cooked rice was arranged in a single layer from the centre of the plate to cover an area greater than 35 mm in diameter. It was then compressed using a cylindrical probe with a diameter of 35 mm. Two compression cycles were performed at 1.0 mm/s to 75 % deformation. By analysing the force-time curve, hardness, cohesiveness, gumminess, and springiness were calculated

using the Texture Export for Windows software provided by the instrument. Ten technical measurements were repeated for each rice sample.

4.2.8.2 Oral in vitro digestion

The oral process simulation of cooked rice samples was conducted based on the method described by Tamura et al. (2017). In brief, an aliquot of cooked rice sample (120 g) was homogenised using a household blender (HB605, Kenwood, Havant, UK) for 0 s, 10 s or 20 s to simulate the swallowing, normal and fine mastication conditions. The following *in vitro* digestion step was conducted based on the method described by Fernandes et al. (2020). In brief, an aliquot of the non-homogenised and homogenised (10 s, or 20 s) sample (10 g) was weighed in a conical tube (50 mL), adding 10 mL simulated salivary fluid containing salivary α-amylase (75 U/mL). The mixture was incubated (37°C) for 2 mins under constant rotation (50 rpm). A 20 mL Na_2CO_3 (0.3 M) solution was added to stop the enzyme activity. The samples were then held at 37°C undisturbed for 10 mins to allow the residues to sediment. Following filtration through a Buchner funnel, the filtrate was collected for the evaluation of oral (*in vitro*) starch digestion, and separated particles were carefully removed from the filter paper and placed in the oven to dry for 12 h at 70°C until constant weight. To determine the digestibility of starch during the oral phase, the concentration of reducing sugars in the liquid filtrate produced from starch amylolysis was measured using a par-hydroxybenzoic acid hydrazide (PAHBAH) assay as described by Edwards et al. (2019).

The granulometry distribution of the digested rice mass was evaluated based on the method described by Ranawana et al. (2010). The total weight of dried residues was recorded first, and the residues were then screened through four test sieves stacked in descending order of size (2.0 mm, 1.0 mm, 0.5 mm, and 0.25 mm) and a base pan. This was conducted using a Retsch AS 200 control sieve shaker (Verder Scientific, Derbyshire, UK) with a vibration height of 0.5 mm and a duration of 1 min. The fragments isolated over each sieve were collected and weighed. In this study, these will be referred to as distributed grain fragments. The weight loss caused by the

particles entrapped within the meshes was negligible. The distribution was calculated using **Eq. 4.3**.

$$\sum \mathbf{R_n}(\%)=\sum \frac{\mathbf{M_n}}{\sum \mathbf{M_n}} \quad (\mathbf{Eq.4.3})$$

Where:

M_n is the mass (g) of the fraction retained on each sieve (M_1, M_2, M_3, M_4) and pan (M_p)

ΣM_n is the total mass (g) of grain fractions: $M_1 + M_2 +...+ M_p$

ΣR_n is the cumulative per cent (%) of mass retained

4.2.9 Statistical analysis

Results were calculated as mean ± standard deviation. Subsequently, Tukey's test, in conjunction with analysis of variance (ANOVA), was used to determine significant differences among the means at an a priori significance level of $p < 0.05$, using the SPSS software (version 27, Chicago, USA). In the granulometric measurement for cooked grain after homogenisation, the cumulative Gaussian statistic model was used to calculate the particle size distribution after passing the Shapiro-wilk normality test using Prism (version 9, San Diego, CA) based on a reported method (Blanquet-Diot et al., 2021; Suo et al., 2021).

4.3 Results

4.3.1 Proximate composition and morphological properties of raw rice

As shown in **Tab. 4.1**, PR contained significantly higher protein and amylose levels than JR, whereas their total starch and moisture content were similar. The recovered starchy residues (JRS, PRS) had a total starch content of 95 %, significantly higher than that in JR and PR flours, and a lower protein and water content than the flours. The results agree with those previously reported on the starch composition isolated from milled rice flour (Puncha-Arnon & Uttapap, 2013). The percentage of amylose in JRS and PRS was similar to that in rice flour, suggesting that the protein extraction process did not significantly alter the proportion of amylose.

Tab. 4.1.Chemical composition of raw JR and PR flour and their isolated starch (g/100g).

	Moisture content	Total starch	Amylose	Protein
JRS	2.43 ± 0.35 [b]	95.60 ± 1.32 [a]	18.03 ± 1.79 [b]	0.62 ± 0.03 [c]
JR	8.59 ± 0.04 [a]	83.63 ± 1.68 [b]	17.19 ± 0.08 [b]	6.66 ± 0.58 [b]
PRS	2.60 ± 0.39 [b]	95.02 ± 0.58 [a]	28.84 ± 1.68 [a]	0.65 ± 0.02 [c]
PR	8.24 ± 0.02 [a]	81.68 ± 1.32 [b]	27.01 ± 0.78[a]	8.52 ± 0.26[a]

Mean ± SD. calculated from triplicate measurements. Values in each column with different superscript letters are significantly different ($p < 0.05$)

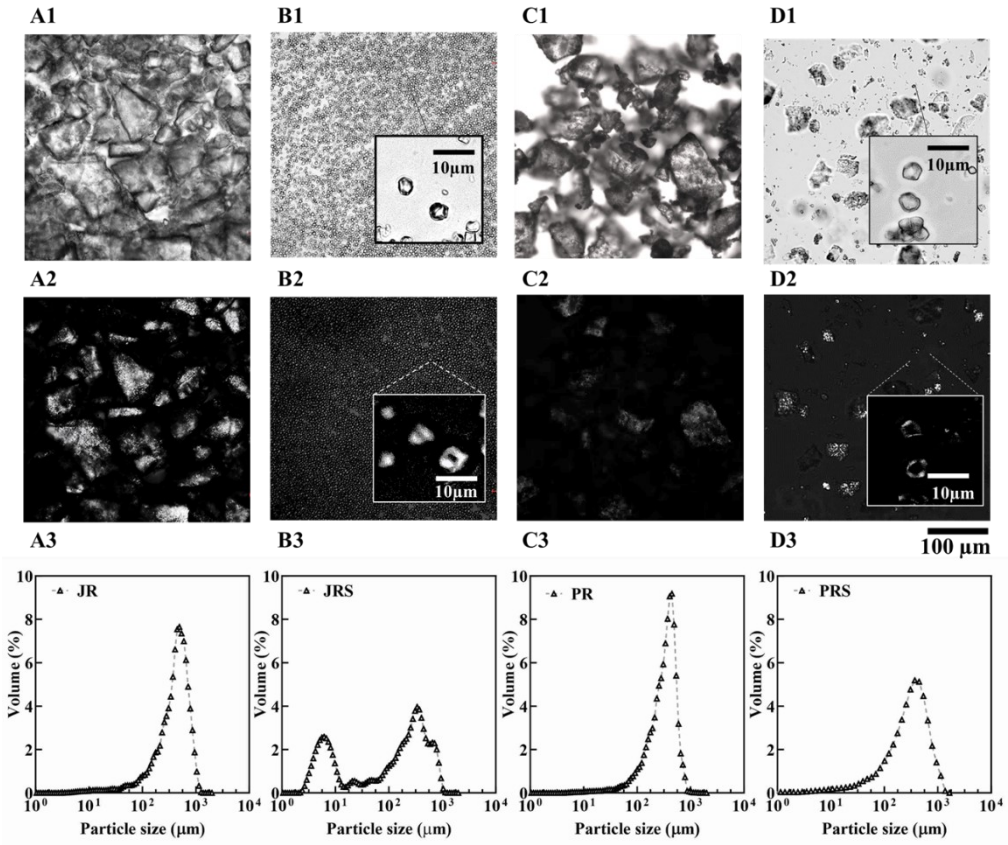


Fig. 4.1. Morphology of raw flour and starch isolates. JR flour (A), JRS (B), PR flour (C), and PRS (D) were observed under both bright (A1-D1) and polarised light (A2-D2) field microscopy. Scale bar 100 μm. A3-D3: the particle size distribution of each sample.

observed between JR and PR, which could affect the rice's physicochemical properties during cooking and, thus, the texture of the cooked rice. Under brightfield and polarised light microscopy, raw JR, PR, JRS, and PRS were characterised for their morphology (**Fig. 4.1A1-D1**) and crystalline structure (**Fig. 4.1A2-D2**). As part of the morphological description, rice samples' particle size distribution patterns were also examined (**Fig. 4.1A3-D3**).

Both flours contained particles predominantly with cubic or polygonal shape. The size ranges from 374.5 µm to 514.2 µm, consisting of tightly packed starch granules approximately 8.5 µm in size. The starch granules of JR flour showed a clear birefringence as observed under polarised light, with the characteristic Maltese cross, and were densely packed (**Fig. 4.1A2**). In contrast, the starch granules of PR flour displayed a lower degree of birefringence intensity than that of JR flour (**Fig. 4.1C2**). This was in line with the work of Sittipod & Shi (2016), who examined the morphological differences between starch granules of parboiled and non-parboiled rice. Parboiled rice exhibited a lower level of birefringence, attributed to starch gelatinisation (loss of molecular order) caused by the parboiling. As for the particle size distribution, this was unimodal for both flours (**Fig. 4.1A3** and **C3**), with a mean diameter *d*(50) of 487.5 μm for JR and 435.6 μm for PR. Upon removal of protein by alkaline-mediated treatment, the distribution curve of the JRS sample appeared to have a peak range of 7-9 μm (Fig. 4.1B3), suggesting the presence of individual rice starch granules as previously reported (Jang et al., 2016; Vandeputte & Delcour, 2004). Under polarised light, the Maltese cross of JRS flour appeared more defined than that of JR flour (**Fig. 4.1A2)**.

A large number of PRS granules remained clustered following the removal of the protein network. No increase in birefringence was observed, suggesting the presence of gelatinised starch, which was absent in JRS (**Fig. 4.1D2).** The size distribution curve showed a single peak supporting the microscopic observation as presence of starch clusters with lower *d*(50) (310.3 μm) than PR flour, and no distinct peaks indicated individual starch release (**Fig. 4.1D3)**.

4.3.2 Pasting properties of rice dispersion with and without LAGG

The RVA profiles of JR and PR are shown in **Fig. 4.2**, and the pasting parameters are presented in **Tab. 4.2**.

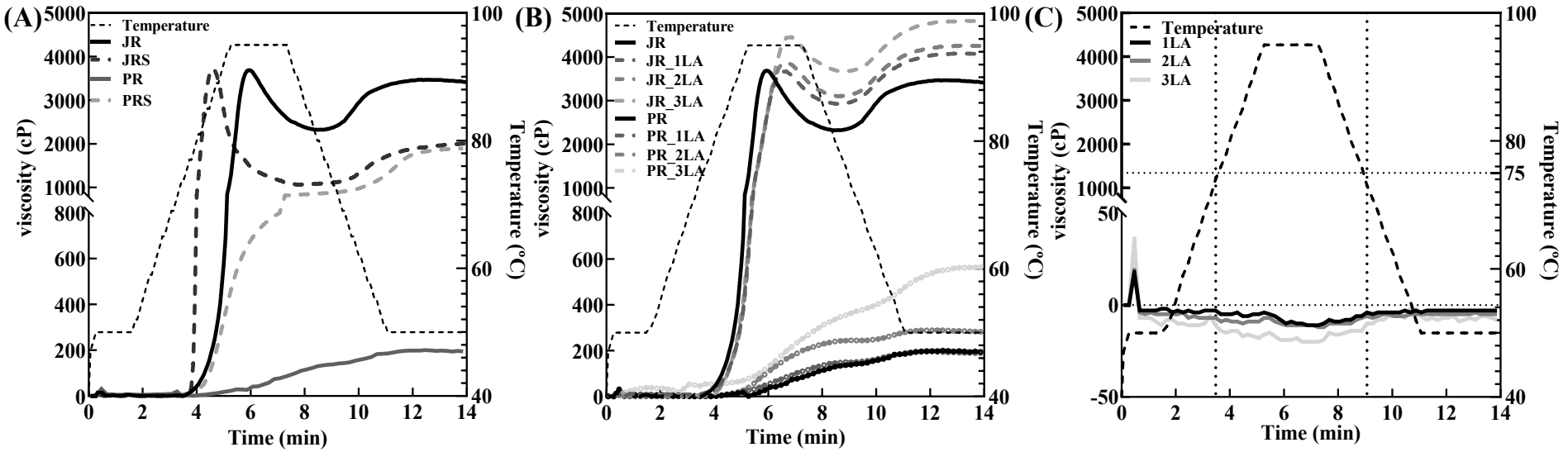


Fig. 4.2. RVA profiles of rice with and without 1-3 % LAGG.

(A) JR flour, PR flour, JRS, or PRS in distilled water; (B) JR and PR flour dispersed in 0, 0.12, 0.24, or 0.36 % LAGG dispersion, and (C) 0.12, 0.24, 0.36 % LAGG dispersion only. The LAGG addition corresponds to 0-3 % of the rice flour mass.

Tab. 4.2. Pasting properties of rice starch and rice flour with and without LAGG addition.

Rice type	PV (cP)	BD (cP)	FV (cP)	SB (cP)	Time (min)	P_T (°C)
JRS	3791.7 ± 31.9 [b]	2683.0 ± 74.7 [a]	2026.3 ± 54.3 [e]	1763.3 ± 31.8 [a]	4.6 ± 0.0 [a]	78.0 ± 0.4 [b]
JR	3468.3 ± 18.6 [c]	1140.0 ± 23.1 [b]	3157.7 ± 19.2 [d]	544.0 ± 40.6 [c]	6.2 ± 0.3 [b]	88.1 ± 0.3 [a]
JR_1LA	3856.7 ± 46.0 [b]	741.3 ± 18.0 [c]	3849.0 ± 34.4 [c]	186.3 ± 12.6 [d]	6.6 ± 0.1 [b]	88.4 ± 0.3 [a]
JR_2LA	3938.7 ± 45.0 [b]	776.7 ± 5.5 [c]	4221.3 ± 26.0 [b]	183.0 ± 13.5 [d]	6.7 ± 0.0 [b]	88.6 ± 0.1 [a]
JR_3LA	4434.7 ± 28.9 [a]	792.3 ± 6.7 [c]	4679.7 ± 38.9 [a]	179.0 ± 4.6 [d]	6.8 ± 0.1 [bc]	88.7 ± 0.1 [a]
PRS	795.3 ± 26.0 [d]	10.3 ± 2.3 [d]	1796.0 ± 53.7 [e]	1067.3 ± 15.9 [b]	7.0 ± 0.0 [c]	89.5 ± 0.4 [a]
PR	74.0 ± 7.59 [e]	4.0 ± 1.5 [de]	187.0 ± 17.6 [g]	112.7 ± 24.7 [e]	7.0 ± 0.0 [c]	--
PR_1LA	101.0 ± 16.3 [e]	3.7 ± 1.9 [de]	181.0 ± 28.3 [g]	82.0 ±14.3 [e]	7.0 ± 0.0 [c]	--
PR_2LA	192.0 ± 15.9 [f]	7.0 ± 1.8 [d]	275.5 ± 45.5 [fg]	84.0 ± 12.5 [e]	7.0 ± 0.1 [c]	--
PR_3LA	229.0 ± 48.8 [e]	12.3 ± 5.3 [d]	552.0 ± 92.9 [f]	323.0 ± 54.2 [e]	7.0 ± 0.0 [c]	--

Mean ± S.D. values in the same column with a different superscript are significantly different from each other ($p < 0.05$).

Here the abbreviations include PV: peak viscosity; BD: breakdown viscosity; FV, final viscosity; SB setback viscosity; P_T peak temperature.

The JR dispersion showed typical RVA curves of starchy foods (**Fig. 4.2A**). Upon heating with excess water under shear force, a rapid increase in viscosity to the peak value was observed, likely resulting from the starch granules' complete gelatinisation to the point of structural disruption (shown as PV). The subsequent reduction in viscosity (BD) can be attributed to the starch granules structural loss during continuous heating and shearing. This is due to reduced interaction between the starch molecules with decreased resistance to the flow as they tend to align to it. Upon cooling, the viscosity increased (SB) mainly due to starch retrogradation, as the gelatinised starch molecules restructured. Unlike JR, PR did not display a clear viscosity peak and maintained constant viscosity during cooling. The lack of viscosity development in PR could be due to the fact that part of the starch was already gelatinised due to parboiling. Therefore, starch granule integrity in PR was already compromised, resulting in lower swelling and lower resistance to shear force upon heating in RVA.

JRS and PRS (**Fig. 4.2A**) illustrate the starch pasting profiles without the protein network role in the matrices. Compared with JR, the JRS had a significant increase in PV, BD, and SB, a significant decrease in FV and an earlier peak time (shorter P_t). The PRS showed a significant increase in viscosities (including PV, FV and SB) compared to PR. A similar pasting profile was observed in legume flours and their starch isolates reported by Do et al. (2019). The results suggested that the protein network may serve as a physical barrier that prevents the gelatinisation and disruption of starch granules during the heating and holding phases and starch retrogradation during the cooling phase.

In addition, JRS viscosity values were significantly higher than in PRS. This can be attributed to the proportional ratio of amylose to amylopectin and the resultant crystalline structure, affecting the degree of starch gelatinisation, swelling, and retrogradation (You et al., 2015; Cornejo-Ramírez et al., 2018). Compared to JR, PR has a higher proportion of amylose, which acts both as a diluent (by reducing the amount of hydrogen bonds amylopectin can form with water molecules) and as an

inhibitor of swelling (amylopectin), restricting viscosity development (Cornejo-Ramírez et al., 2018; Vamadevan & Bertoft, 2020).

Pasting profiles of JR and PR flour with and without the presence of 1-3 % LAGG dispersions are shown in **Fig. 4.2B.** In the initial holding stage (50°C), no significant differences were observed in the viscosity of the flour-LAGG dispersion compared to the control (flour alone). With the increase in LAGG addition, the viscosity peak of JR was delayed during the heating phase. Moreover, with an increase in LAGG addition (from 0 to 3%), JR displayed an increased trend in PV and FV. PR exhibited similar changes to JR in the viscosity profile upon increased LAGG additions, although to a lower extent.

Additionally, individual RVA profiles of 1-3 % LAGG dispersions were evaluated to determine if LAGG addition provided a higher threshold in viscosity than only water, as observed in guar gum or xanthan gum (Zhang et al., 2020). As shown in **Fig. 4.2C**, the LAGG dispersions had low viscosities (around 20 cP), and at above 75°C, their viscosities decreased to near zero, suggesting no viscosifying effect from only LAGG. Therefore, it is suggested that the effect of LAGG addition in rice paste occurs synergistically rather than cumulatively on increasing viscosity.

A combination of phase separations and intermolecular interactions is widely regarded as the cause of the synergetic increase in starch viscosity upon adding hydrocolloids (Fang et al., 2018; Zhang et al., 2020). Without LAGG, the gelatinisation phase of starch can be described as a two-phase system composed of dispersed granules gradually swelling and a continuous phase of leached amylose. When LAGG is present, its concentration in the continuous phase will increase upon swelling of the starch granules, resulting in an increased viscosity of the mixed system. LAGG also undergoes gel-to-liquid-like conformational changes when heated above 75°C, transitioning from a double-helix (cohesive solution state) to a random coil structure (liquid state). During the transformation process of LAGG, water molecules may migrate at a slower rate, which leads to a delay in reaching the viscosity peak (**Fig. 4.2C**). Additionally, the observed increase in viscosity of rice flour-LAGG dispersions may be caused primarily by entanglement between leached

amylose and conformationally disordered 'random coils' of LAGG, as evidenced by similar results reported previously (Song et al., 2006; Saha & Bhattacharya, 2010; Zheng et al., 2021). When the temperature was above 75°C, the individual molecules of hydrocolloids could move freely (A reduction in the viscosity of 1-3% LAGG dispersion can be seen in **Fig. 4.2C**). This could facilitate crosslinking with released amylose via structural interpenetration and electrostatic interactions (especially hydrogen bonding) induced by carboxyl groups on glucuronic acid residues of LAGG (Fang et al., 2018). As a result of the gel formation, the gel system shows greater resistance to shear forces applied, which is reflected in its increased viscosity.

Upon cooling, the viscosity again increased and reached the FV of gel pastes mainly due to starch molecules retrogradation (realignment of amylose and amylopectin chains upon cooling, resulting in reordered structures accompanied by water expulsion). The SB (difference between PV and FV) values decreased with increasing LAGG concentrations, suggesting that LAGG-containing pastes have a lower retrogradation tendency. Similar results were reported in rice starch-LAGG mixtures and other hydrocolloids, such as guar gum and locust bean gum (Fang et al., 2018; Zhang et al., 2020). The reduced starch retrogradation is probably due to structural changes of LAGG, consequently affecting the reticulation state within amylose-LAGG copolymers. LAGG undergoes a coil-to-helix transition, which acts as a steric hindrance to the reorganisation of amylose and prevents water molecules from exiting (Milas et al., 1990; Morris et al., 2012).

4.3.3 Thermal properties of rice dispersion with and without LAGG

The thermal properties of the JR and PR dispersions containing 0 to 3 % LAGG were determined using DSC (**Fig. 4.3**).

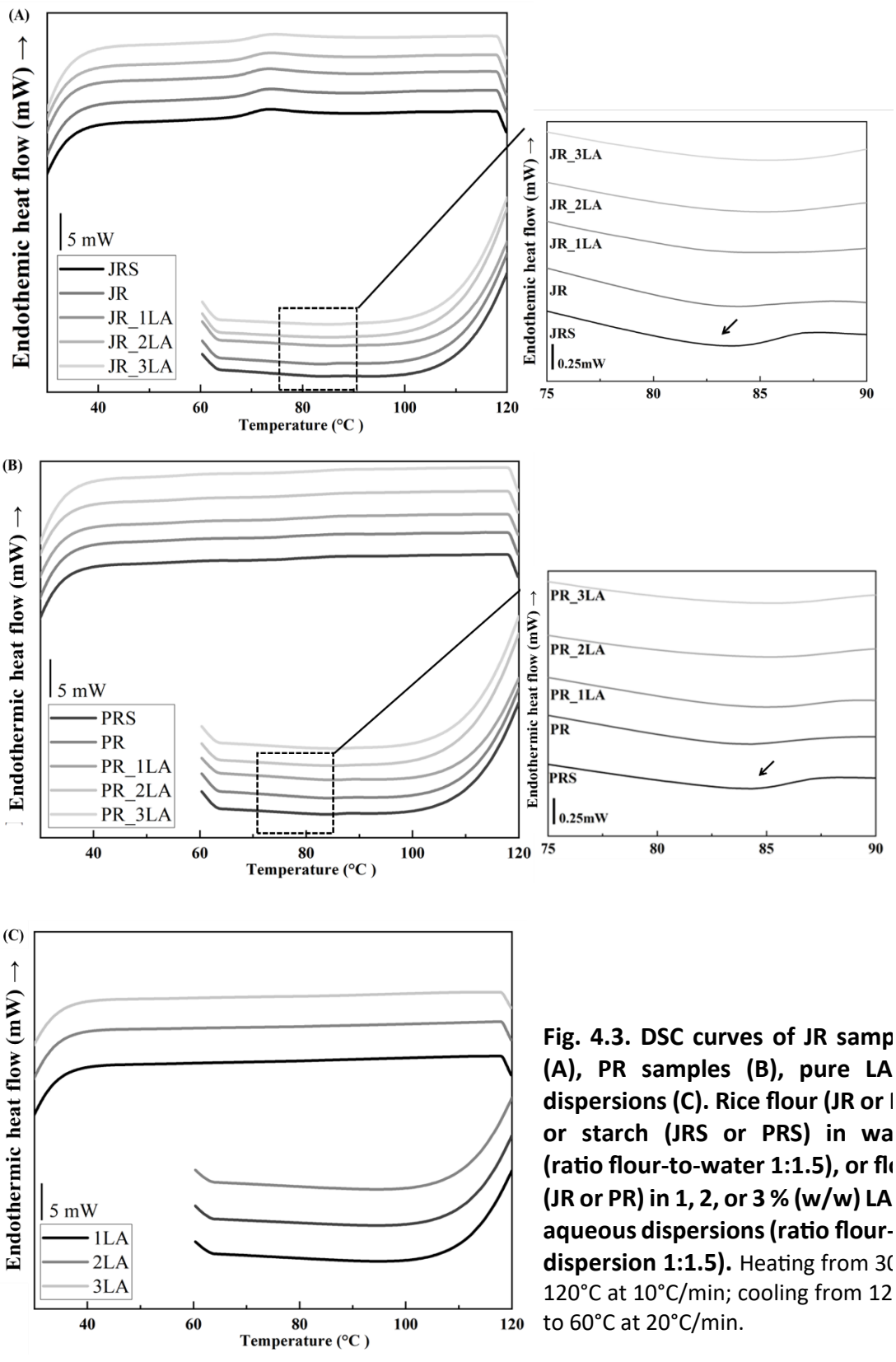


Fig. 4.3. DSC curves of JR samp (A), PR samples (B), pure LA dispersions (C). Rice flour (JR or or starch (JRS or PRS) in wa (ratio flour-to-water 1:1.5), or fl (JR or PR) in 1, 2, or 3 % (w/w) LA aqueous dispersions (ratio flour- dispersion 1:1.5). Heating from 3(120°C at 10°C/min; cooling from 12 to 60°C at 20°C/min.

JRS and PRS dispersions in water were also tested to study starch gelatinisation without protein networks. JR and PR exhibited different gelatinisation patterns. In JR samples, an endothermic peak was observed between 65 and 84°C, which indicates the melting of rice starch crystalline layers. In PR samples, a small peak was detected between 50 and 70°C, suggesting the melting of retrograded amylopectin, which had gelatinised during the parboiling process, as reported previously (Bhattacharya, 1985; Islam et al., 2002).

The onset (T_o), peak (T_p), and conclusion (T_c) temperatures and the phase transition enthalpy (ΔH) are reported in **Tab. 4.3**. Upon normalising ΔH by the starch content, JRS and PRS showed higher enthalpy than the respective JR and PR and slightly lower T_o and T_p. This difference, although not statistically significant, may suggest that starch gelatinisation can occur at lower temperature and higher extent without a protein network, which aligns with their RVA profiles. Ma et al. (2022) and Puncha-Arnon & Uttapap (2013) reported similar findings regarding the changes in the thermal properties of rice flour before and after removing granule-associated proteins.

The phase transition temperature range (65.84-82.67°C) of JR flour, which contains 6.66 % protein and 83.63 % starch, appears to be restricted compared to that of starch gelatinisation (64.25-83.63°C; **Tab. 4.3**). This may again be explained by the presence of proteins, which would delay the onset of starch gelatinisation and result in a longer time for total gelatinisation to complete. It is likely that glutelin, the major protein in white rice (as confirmed by SDS-PAGE in **Section 4.3.7**), denatured at temperatures towards the end of starch gelatinisation, e.g., 78.8°C (Ju et al., 2001) or 82.2°C (Wang et al., 2015).

In PR, the phase transition peaks were not substantial. The protein-starch matrices that is formed during parboiling involved protein denaturation and partial starch gelatinisation (Lii et al., 2018), thus decreasing the extent of phase transition occurring upon cooking. Moreover, protein denaturation and unfolding during parboiling, facilitated the formation of intermolecular disulfide bonds, which make the protein network more rigid and resistant to heat (Zavareze et al., 2010; Silva et

al., 2017). Furthermore, this network encapsulates starch granules, which are also restructured during parboiling. The thermal behaviour of rice starch provides further evidence of the structural reorganisation effects on phase transitions. PRS showed a lower ΔH than JRS, which is in line with results reported previously (Kong et al., 2015; Puncha-Arnon & Uttapap, 2013; Wang et al., 2018). Combined, these results indicate that PRS contains a less ordered and/or thermally stable starch structure than JRS.

With increasing LAGG concentration (0 to 3 %), transition temperatures (T_o, T_p, and T_c) and ΔH increased for both rice types, although this was not statistically significant.

Tab. 4.3. Thermal properties upon heating (Section 4.2.5) of JR and PR flours in 0-3 % LAGG dispersions and of JRS and PRS in water.

Rice type	T_o (°C)	T_p (°C)	T_c (°C)	ΔH (J/g of starch)
JRS	64.25 ± 0.32 ^{a}	71.27 ± 0.80 ^{a}	83.63 ± 1.01 ^{a}	9.14 ± 1.02 ^{a}
JR	65.84 ± 0.19 ^{a}	72.38 ± 0.76 ^{a}	82.67 ± 1.30 ^{a}	8.20 ± 0.50 ^{a}
JR_1LA	65.94 ± 0.24 ^{a}	72.49 ± 0.56 ^{a}	84.18 ± 1.07 ^{a}	8.23 ± 0.45 ^{a}
JR_2LA	65.79 ± 0.65 ^{a}	72.89 ± 0.27 ^{a}	86.37 ± 1.26 ^{a}	8.28 ± 0.31 ^{a}
JR_3LA	65.86 ± 0.23 ^{a}	72.93 ± 0.14 ^{a}	86.40 ± 1.83 ^{a}	8.45 ± 0.33 ^{a}
PRS	49.53 ± 1.16 ^{d}	59.51 ± 0.63 ^{c}	71.97 ± 1.37 ^{b}	0.91 ± 0.11 ^{b}
PR	50.68 ± 1.18 ^{cd}	59.74 ± 1.40 ^{c}	68.32 ± 1.41 ^{d}	0.86 ± 0.15 ^{b}
PR_1LA	51.78 ± 0.96 ^{c}	60.19 ± 0.95 ^{bc}	69.70 ± 0.96 ^{cd}	0.89 ± 0.25 ^{b}
PR_2LA	52.68 ± 0.72 ^{c}	60.50 ± 0.39 ^{bc}	71.43 ± 1.08 ^{bcd}	1.01 ± 0.10 ^{b}
PR_3LA	54.39 ± 0.81 ^{b}	61.80 ± 0.72 ^{b}	73.35 ± 1.67 ^{b}	1.16 ± 0.14 ^{b}

T_o is onset temperature; T_p is peak temperature; T_c is conclusion temperature; ΔH is the enthalpy change (J/g of starch on dry weight based). Mean ± S.D. values in the same column with a different superscript are significantly different from each other ($p < 0.05$).

Cooling rice from 120°C to 60°C (edible temperature), as reported by Yau and Huang (1996), may cause starch short-term retrogradation (mainly amylose retrogradation), reorganisation of the protein-starch matrices, and water expulsion, eventually affecting the freshly cooked rice texture (Wang et al., 2020). As shown in **Tab. 4.4**, JRS and PRS showed a clear exothermic peak in the 90-70°C range, indicating that starch retrogradation occurred. The JR and PR flours did not exhibit obvious exothermic peaks, either with or without LAGG. A reduction in the phase transition enthalpy during cooling was observed in the presence of protein networks and LAGG in conjunction with the resulting gelatinised starch. The first two factors

likely contributed to the enthalpy reduction by interfering with amylose movement and recrystallisation (Wang et al., 2020). This agrees with the reduced SB in RVA (**Section 4.3.2**) and with similar results reported previously (Yu et al., 2009; Puncha-Arnon & Uttapap, 2013; Eom et al., 2018). Upon increasing LAGG concentrations, both rice types did not show significant variations in ΔH during cooling.

Tab. 4.4. Thermal properties upon cooling (Section 4.2.5) of JR and PR flours in 0-3 % LAGG dispersions and of JRS and PRS in water.

Rice type	T_o (°C)	T_p (°C)	T_c (°C)	ΔH (J/g of starch)
JRS	90.60 ± 0.48 ^{ab}	84.00 ± 0.18 ^{a}	71.98 ± 0.87 ^{c}	1.22 ± 0.04 ^{a}
JR	89.60 ± 0.10 ^{b}	84.24 ± 0.76 ^{a}	73.81 ± 0.10 ^{bc}	0.83 ± 0.04 ^{b}
JR_1LA	90.94 ± 0.24 ^{ab}	84.28 ± 0.35 ^{a}	72.20 ± 0.24 ^{bc}	0.87 ± 0.02 ^{b}
JR_2LA	91.00 ± 0.54 ^{ab}	84.74 ± 0.27 ^{a}	74.10 ± 0.20 ^{b}	0.90 ± 0.07 ^{b}
JR_3LA	92.26 ± 0.43 ^{a}	86.67 ± 0.43 ^{a}	76.65 ± 1.83 ^{a}	0.90 ± 0.10 ^{b}
PRS	90.84 ± 0.48 ^{ab}	85.03 ± 0.18 ^{a}	77.53 ± 0.87 ^{a}	1.09 ± 0.04 ^{a}
PR	89.63 ± 0.20 ^{b}	85.05 ± 0.33 ^{c}	77.54 ± 0.32 ^{a}	0.73 ± 0.03 ^{b}
PR_1LA	90.92 ± 0.20 ^{ab}	85.05 ± 0.33 ^{c}	77.54 ± 0.32 ^{a}	0.78 ± 0.03 ^{b}
PR_2LA	91.78 ± 0.89 ^{a}	85.15 ± 0.56 ^{bc}	76.94 ± 0.45 ^{a}	0.82 ± 0.08 ^{b}
PR_3LA	92.73 ± 1.81 ^{a}	84.61 ± 0.44 ^{b}	74.62 ± 0.31 ^{b}	0.81 ± 0.14 ^{b}

T_o is onset temperature; T_p is peak temperature; T_c is conclusion temperature; ΔH is the enthalpy change (J/g of starch on dry weight based) during the cooling stage. Mean ± S.D. values in the same column with different superscripts are significantly different from each other ($p < 0.05$).

4.3.4 Hydration properties of rice dispersion with and without LAGG

Tab. 4.5 presents the values of SP (g/g) and WSI (%) for JR and PR dispersions containing 0 to 3 % LAGG measured after boiling. In PR, SP and WSI were significantly lower than in JR. Upon protein removal, JRS showed significant increases in SP and WSI compared to JR. Yu et al. (2012) reported found identical results in their study on the increase in SP and WSI of rice starch derived from four varieties of rice flour. Similar results were also observed by Wani et al. (2016) for legume starches, which had a higher SP and WSI than their respective flours. It is suggested that removing protein networks can facilitate starch accessibility to water and increase starch swelling space.

Tab. 4.5. Hydration properties, SP (g/g) and WSI (%), of JR and PR flours in 0-3 % LAGG dispersions and JRS and PRS in water.

Rice sample	SP (g/g)	WSI (%)
JRS	12.26 ± 0.69 [a]	41.18 ± 5.92 [a]
JR	9.77 ± 0.34 [b]	32.03 ± 2.79 [b]
JR_1LA	8.95 ± 0.12 [c]	30.34 ± 0.63 [bc]
JR_2LA	8.61 ± 0.12 [c]	26.31 ± 0.22 [cd]
JR_3LA	8.31 ± 0.13 [c]	25.25 ± 0.51[cd]
PRS	6.31 ± 0.28 [c]	22.12 ± 1.24 [d]
PR	6.04 ± 0.42 [c]	11.47 ± 0.77 [e]
PR_1LA	5.91 ± 0.07 [c]	10.23 ± 0.54 [e]
PR_2LA	5.45 ± 0.22 [c]	9.09 ± 0.44 [e]
PR_3LA	5.54 ± 0.39 [c]	8.68 ± 0.62 [e]

Mean ± S.D. values in the same column with different superscripts are significantly different from each other ($p < 0.05$).

In PRS, WSI was significantly higher than PR, but not SP. This is in line with parboiling facilitating starch solubility in water and easy-cook properties reported by Unnikrishnan & Bhattacharya (1988) and in accordance with the lower gelatinisation capacity of PRS shown in RVA and DSC, and the microscopic observation (in **Section 4.3.1**) also indicated a limited space for swelling within the starch clusters.

As a result of the addition of LAGG, significant reductions were observed in SP and WSI values of JR samples. The WSI of JR decreases with the concentration of LAGG. In addition, PR observed a reduction in SP and WSI values with LAGG addition, although it was not statistically significant. Similar results were reported previously by Song et al. (2006) on rice starch/LAGG mixture and rice starch/xanthan mixture by Su et al. (2018). The reduced SP and WSI in rice-LAGG mixtures may be attributed to the interaction of gum with water and leached amylose. The higher number of OH groups in LAGG makes it more hydrophilic, limiting water availability for starch granules, which inhibit swelling. Moreover, leached amylose and LAGG in continuous phases can also cause a film to develop around the granules, preventing further amylose exudation, and thereby reducing the WSI.

4.3.5 The secondary structure of rice protein and the short-range ordered structure of starch

Identifying the role of proteins and starch in determining rice microstructure is important to understanding the textural properties of cooked rice, which can be identified and characterised with FTIR spectroscopy by analysing specific spectral regions of these two components, as described in **Section 4.2.9.1**.

The FTIR spectra of samples obtained from raw and cooked rice with and without 1-3% LAGG added are shown in **Fig. 4.4.** Upon a baseline correction and deconvolution of the IR spectra curve, four sub-peaks were identified from the amide I region (1600-1700 cm^{-1}). They referred to the secondary structure components of proteins as β-sheets (1615-1637 and 1682-1700 cm^{-1}), random coils (RC, 1637-1645 cm^{-1}), α-helix (1646-1664 cm^{-1}) and β-turns (1665-1681 cm^{-1}), as described in previous studies (Guerrero et al., 2014; Chávez-Murillo et al., 2018; Hu et al., 2019). Each substructure's contribution to percentage is presented in **Tab. 4.6**. Raw PR shows a greater RC and lower α-helix proportion than JR. A similar difference on the protein structure before and after the thermal treatment has been reported by Heydari et al. (2022) for lentil proteins and by Wang et al. (2019) for rice glutelin. Combined, a high proportion of disordered conformations and intermolecular β-sheet aggregates is indicative of the presence of denatured protein. The position of the main amide I peak band changed in the cooked JR and PR compared to their raw counterparts. As discussed previously by Kubelka et al. (2001) and Barth et al. (2007), peak upshifts may be related to a decrease in the molecular mass of the proteins. It can also be observed the lower molecular mass band shown in cooked rice sample compared to the raw sample in the native SDS-PAGE (**Section 4.3.7**, **Fig. 4.6**).Meanwhile, cooked rice shown significant increases in the percentage of ordered structure A significant increase in ordered structures (β-sheet of cooked JR and α-helix of cooked PR) and a concomitant decrease in RC content was evident after cooking (**Table 5**).

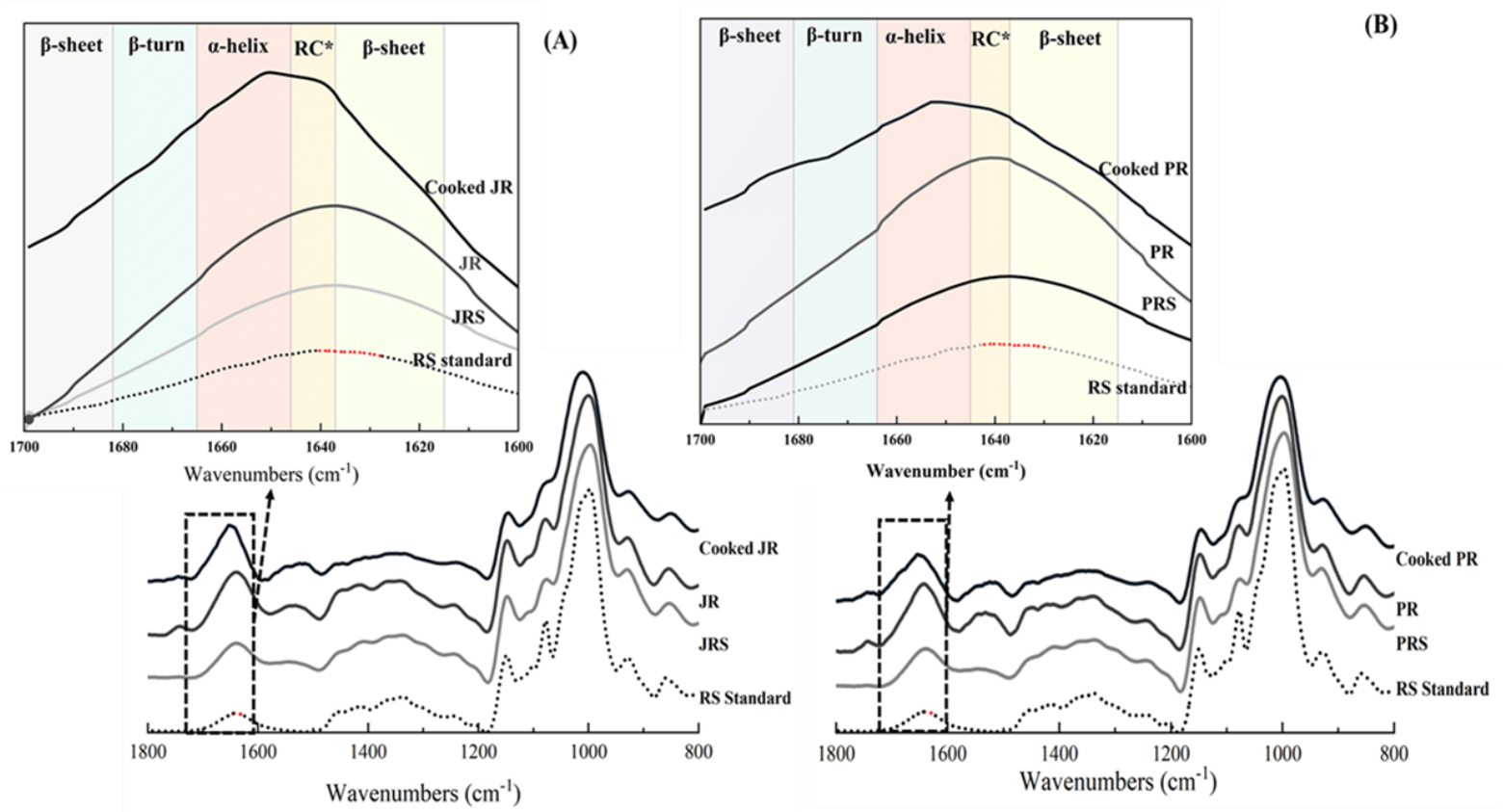


Fig. 4.4 (Part I). The amide I and starch fingerprint region spectra taken from the FTIR spectra. (A) JRS, JR before and after cooking, rice starch standard as a reference; (B) PRS, PR before and after cooking, rice starch standard as a reference, respectively (Figure part II at Page 141).

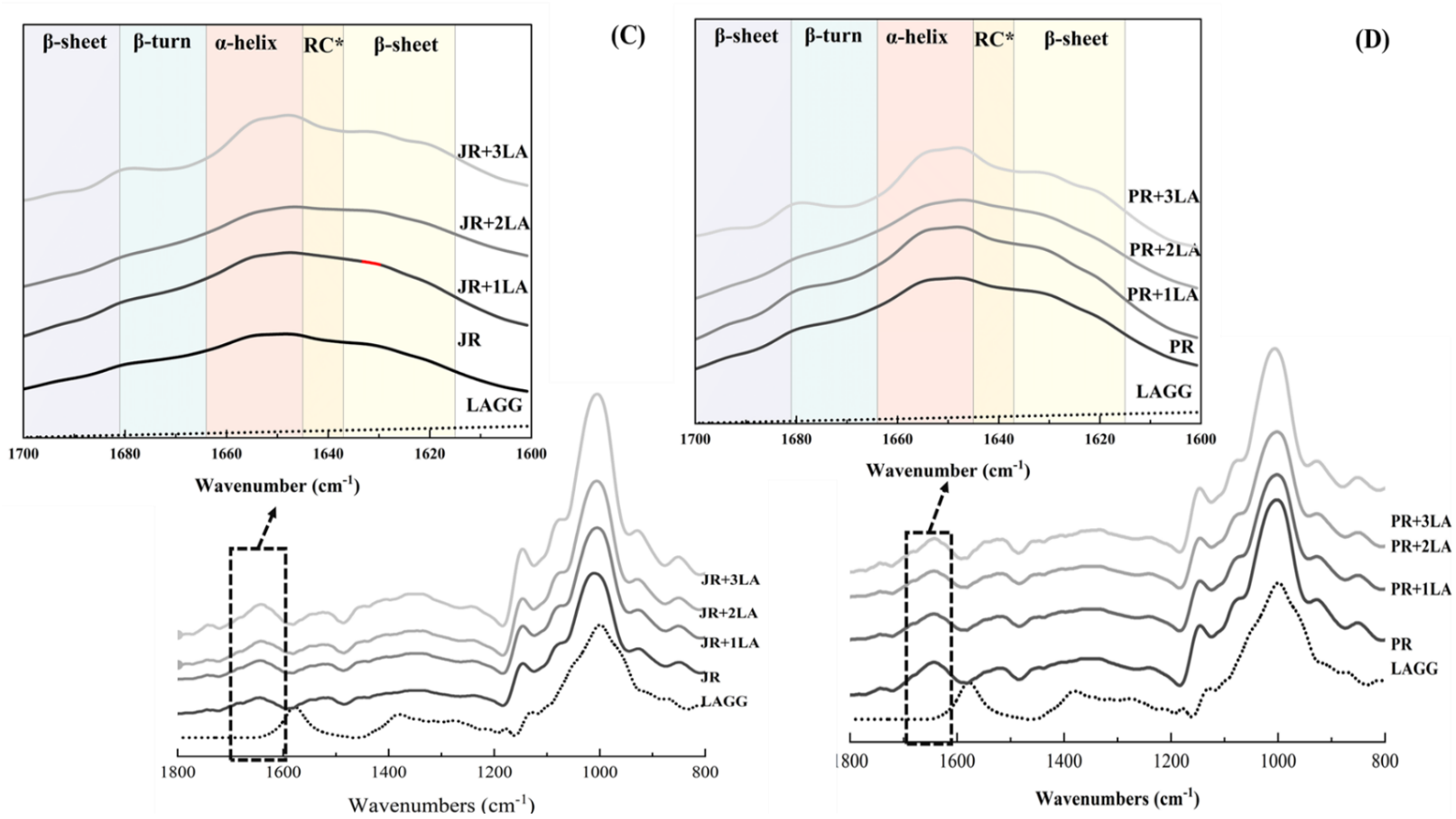


Fig. 4.5 (Part II). The amide I and starch fingerprint region spectra taken from the FTIR spectra.

(C) cooked JR with and without 1-3 % LAGG, respectively; (D) cooked PR with and without 1-3 % LAGG, respectively (Figure part I at Page 140).

Cooking rice in LAGG dispersions increased the β-sheets content for both rice types (**Fig. 4.4C** and **D**), suggesting that protein aggregation occurred. When rice was cooked in a LAGG dispersion with increased content, the proportion of β-sheets increased in both rice types while decreasing the RC concentration. The results suggested that rice protein can transition from a random structure ("loops", relatively flexible) to a more ordered structure ("train", relatively stable) in the presence of LAGG. A similar result has been reported for guar gum-gluten mixtures by Linlaud et al. (2010) and guar gum/gum Arabic-pea protein by Shen et al. (2022). The occurrence of this phenomenon may be due to two factors. First, introducing LAGG caused rice protein to aggregate, possibly due to electrostatic repulsion between protein and LAGG, which are negatively charged at native pH. Additionally, heating induces the protein structure to loosen and rearrange. Hydrophobic and polar groups inside the protein were exposed to the surface, which may further enhance the effect between rice protein and LAGG.

By observing the starch fingerprint region (900-1200 cm^{-1}) in three specific absorbance bands at 995 cm^{-1}, 1022 cm^{-1} and 1047 cm^{-1}, which are linked to the intramolecular hydrogen bonding among C6 hydroxyl groups, amorphous and crystalline starch structures, respectively. Therefore, the ratios of 995/1022 cm^{-1} (R995/1022) and 1047/1022 cm^{-1} (R1047/1022) were calculated and listed in **Tab.4.6** to evaluate short-range order of starch (primarily the local arrangement of helices into crystalline arrays) (Nhouchi et al., 2022; Yang et al., 2022). Raw JR had a higher R1047/1022 than PR, indicating a great level of ordered structure in their external region, which was very similar to their isolated starch (0.71±0.01 of JRS and 0.71±0.01 of PRS, respectively)

Compared to the raw samples, both cooked rice types showed reduced R1047/1022 and R995/1022, indicating that cooking damaged the short-range ordered structure of starch and caused the distribution of the double helices and starch chains. LAGG also contributes to the above absorption peaks in the polysaccharide region (**Fig. 4.4**). Subtracting the contribution of LAGG on the intensities of the peaks, R1047/1022 and R995/1022 showed a downward trend but not a significant

decrease when LAGG concentration increased (**Tab. 4.6**). It appears that LAGG inhibits the formation of short-range ordered structures within starch, possibly by interfering with the formation of hydrogen bonds between released amylose, thus delaying the short-term retrogradation of rice starch. These results align with the pasting and thermal properties reported in **Section 4.3.2** and **Section 4.3.3** and in accordance with the rice starch/β-glucan mixture system reported by Zhao et al. (2023).

Tab. 4.6 Secondary protein and starch structure values taken from normalised FTIR spectra of cooked JR and PR with and without 1-3 % LAGG (w/w). Values for uncooked rice samples (raw JR and raw PR) are also reported as control.

Rice sample	β-Sheet (1615-1637)/ (1682-1700)	Unordered (Random coil) 1637-1645	α-Helix 1646-1664	β-Turn 1665-1681	995/1022	1047/1022
Raw JR	32.17 ± 2.62 ^{f}	9.27 ± 3.44 ^{b}	38.17 ± 2.62 ^{a}	18.70 ± 3.04 ^{b}	0.98 ± 0.02 ^{c}	0.35 ± 0.01 ^{a}
JR	38.29± 3.73 ^{e}	5.55 ± 1.31 ^{bcd}	36.08 ± 2.13 ^{a}	17.40 ± 2.18 ^{bcd}	0.88 ± 0.02 ^{de}	0.33 ± 0.02 ^{ab}
JR_1LA	42.54 ± 2.19 ^{cd}	3.57 ± 1.31 ^{cd}	37.07 ± 1.12 ^{a}	13.81 ± 0.37 ^{cde}	0.87 ± 0.01 ^{e}	0.29 ± 0.04 ^{abc}
JR_2LA	46.30 ± 2.92 ^{b}	2.86 ± 0.37 ^{d}	36.54 ± 1.08 ^{a}	13.47 ± 0.70 ^{de}	0.82 ± 0.07 ^{e}	0.26 ± 0.08 ^{abc}
JR_3LA	48.30 ± 2.01^{a}	2.33 ± 0.45 ^{d}	38.02 ± 0.83 ^{a}	11.73 ± 0.55 ^{e}	0.80 ± 0.04 ^{e}	0.24 ± 0.01 ^{abc}
Raw PR	37.29 ± 1.18 ^{e}	15.74 ± 1.80 ^{a}	28.61 ± 5.92 ^{b}	24.21 ± 2.29 ^{a}	1.44 ± 0.02 ^{a}	0.25 ± 0.03 ^{abc}
PR	37.92 ± 1.40 ^{e}	7.38 ± 1.16 ^{bc}	35.49 ± 1.03 ^{a}	17.82 ± 0.58 ^{bc}	1.27 ± 0.03 ^{b}	0.20 ± 0.07 ^{bc}
PR_1LA	40.42 ± 3.70 ^{de}	6.16 ± 0.65 ^{bc}	36.89 ± 1.03 ^{a}	16.79 ± 0.36 ^{bcd}	1.23 ± 0.02 ^{b}	0.18 ± 0.03 ^{c}
PR_2LA	42.76 ± 1.24 ^{cd}	5.19 ± 0.48 ^{cd}	35.37 ± 2.97 ^{a}	15.49 ± 1.60 ^{bcde}	1.20 ± 0.03 ^{b}	0.17 ± 0.03 ^{c}
PR_3LA	45.17 ± 1.50 ^{bc}	4.96 ± 0.43 ^{cd}	34.45 ± 1.44 ^{a}	14.91 ± 0.53 ^{bcde}	1.01 ± 0.04 ^{c}	0.15 ± 0.02 ^{c}

Mean ± S.D. values in the same column with different superscripts are significantly different from each other ($p < 0.05$).

4.3.6 Crystalline structure

The X-ray diffractograms of rice samples, describing their crystalline structure, are shown in **Fig. 4.5**.

The crystal structure of the starch component in raw JR and PR and their respective starch isolates presented an A-type pattern and A+V tape pattern, which is common in cereals. A-type pattern with single peaks at 15.5°, 23.5° with unresolved peaks at 17.1° and 18.2°, and V-type pattern with a peak at 20.2° were observed, which matched the results in previous studies on JR and PR (Dhital et al., 2015). Raw JR samples had a higher degree of crystallinity (DOC), calculated from the XRD pattern, than raw PR samples (11.3 % in JR and 8.0 % in PR). Similar differences between waxy rice (contains < 0.5% amylose) and high-amylose (contains > 33.3% amylose) rice have also been reported by Luo et al. (2021). When most of the protein bodies were removed, JRS and PRS showed similar DOC (12.4 % in JRS, 8.5 % in PRS) compared to JR and PR flour. In raw rice, starch is a semicrystalline material containing both amorphous and crystalline regions, mainly composed of linear amylose and branched amylopectin molecules, respectively (Vandeputte & Delcour, 2004). Therefore, JRS contain a higher proportion of amylopectin, leading to higher crystallinity than PR and PRS.

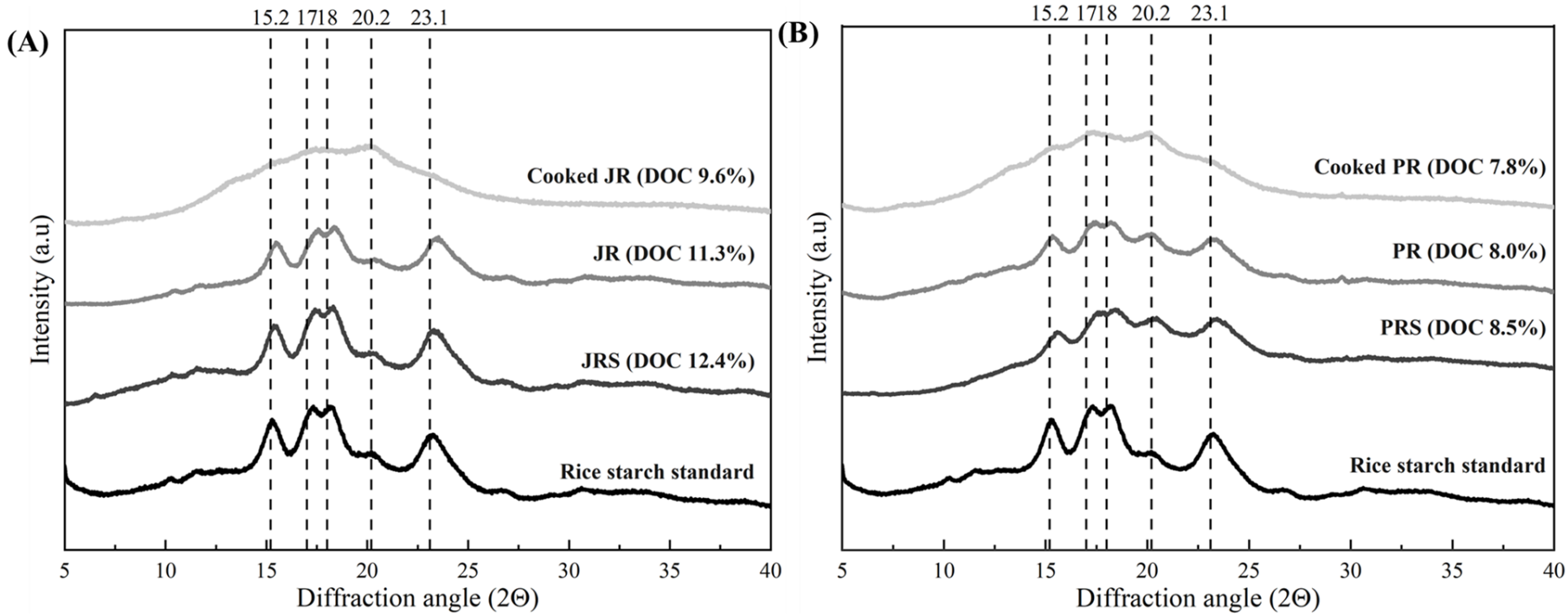


Fig. 4.6 (Part I). XRD diffraction patterns.(A) JRS, JR and cooked JR, and the rice starch standard as a reference; (B) PRS, PR and cooked PR and the rice starch standard as a reference, following by P148.The labelled guideline is a typical A-type crystalline starch at 15.2°, 20.2°, and 23.1° with an unresolved peak at 17° and 18°. Fig. 4.5 Part II at page 146

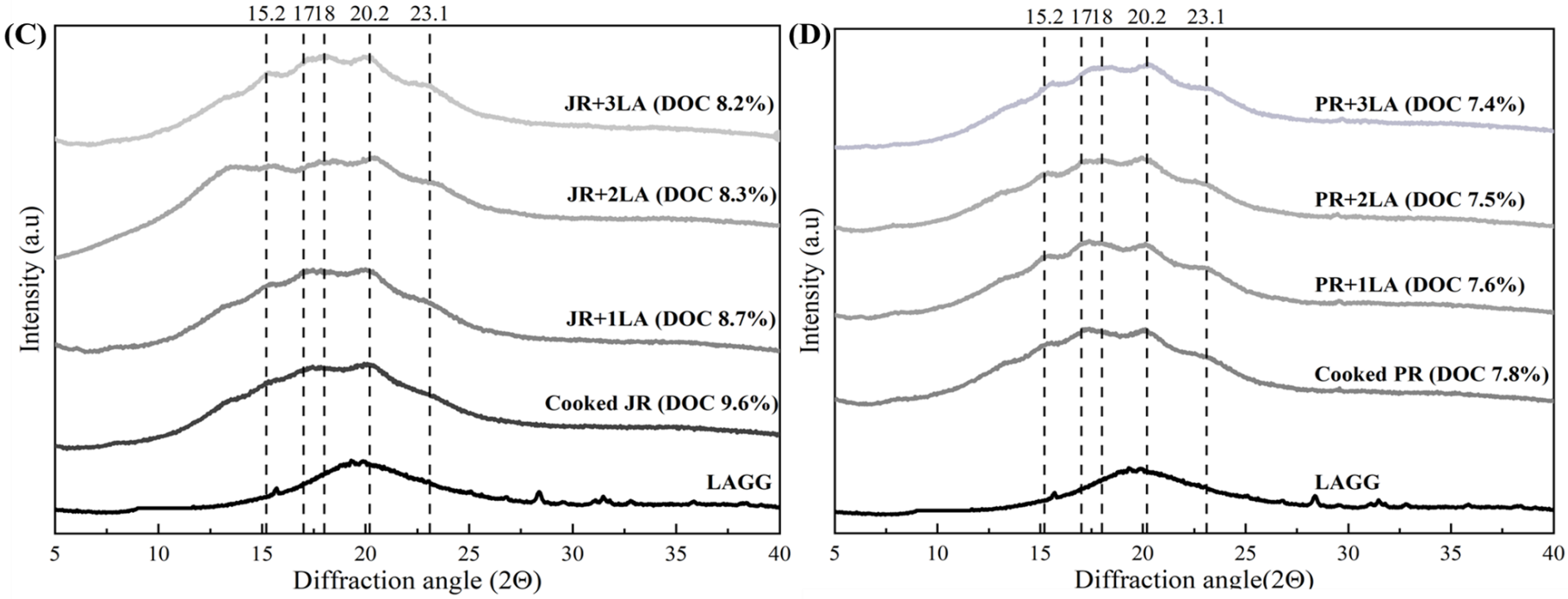


Fig. 4.7 (Part II). XRD diffraction patterns (following by P147).(C) cooked JR with 0-3 % LAGG addition, respectively; (D) cooked PR with 0-3 % LAGG, respectively. The labelled guideline is a typical A-type crystalline starch at 15.5°, 20.2°, and 23.5° with an unresolved peak at 17.1° and 18.2°.**Fig.4.5** Part I at page 145

Cooked rice flour no longer exhibits specific A-type diffraction peaks, suggesting that rice starch crystallites have been disrupted in the cooking process. A presence of a prominent peak at 20°, indicating the presence of V-type patterns (Farooq et al., 2018). In fact, the V-type, formed after cooking, results from complex interactions between the amylose and other compounds, including proteins and lipids. A similar decrease in A-type structure along with the formation of V-type complexes was reported in cooked rice, pre-gelatinised rice dispersions, and other novel cereal products (Farooq et al., 2018; Cai et al., 2021; Hirata et al., 2023). A V-type pattern, associated modest decrease in DOC, were also evident in both JR and PR cooked with LAGG. These results are consistent with the findings of Zhou et al. (2020) on corn starch-hydrocolloid (including gum Arabic, xanthan gum or guar gum) complexes under the heat-moisture treatment.

4.3.7 Proximate composition and morphological properties of cooked rice

As in raw rice (**Section 4.3.1**), the protein and amylose contents remained significantly different between cooked JR and PR and adding LAGG had a limited effect on the proximate composition (**Tab. 4.7**).

Tab. 4.7. Proximate composition (g/100 g total sample) and morphological properties of cooked JR and PR with and without 1-3 % (w/w) LAGG.

	JR	JR_1LA	JR_2LA	JR_3LA	PR	PR_1LA	PR_2LA	PR_3LA
Moisture content	57.77 ± 2.81 [a]	60.10 ± 2.06 [a]	61.20 ± 1.54 [a]	62.26 ± 1.43 [a]	59.54 ± 2.60 [a]	61.92 ± 1.85 [ab]	61.78 ± 1.17 [a]	62.37 ± 1.81 [a]
Total starch	35.86 ± 1.92 [a]	35.39 ± 2.17 [a]	34.45 ± 3.46[a]	35.11 ± 2.61[a]	33.18 ± 2.27[a]	31.81 ± 1.56[a]	32.68 ± 2.42[a]	32.57 ± 3.32[a]
In which amylose (%)	14.26 ± 1.06 [b]	13.73 ± 0.99 [b]	14.12 ± 2.18 [b]	14.69 ± 1.64 [b]	20.19 ± 0.43 [a]	19.48 ± 0.57 [a]	20.13 ± 1.82 [a]	18.89 ± 2.01 [a]
Protein	2.64 ± 0.04 [b]	2.65 ± 0.04 [b]	2.63 ± 0.40 [b]	2.57 ± 0.04 [b]	3.42 ± 0.12 [a]	3.36 ± 0.08 [a]	3.50 ± 0.09 [a]	3.44 ± 0.14 [a]
Length (cm)	1.00 ± 0.03 [a]	1.03 ± 0.05 [a]	0.97 ± 0.05 [a]	1.00 ± 0.06 [a]	1.09 ± 0.03 [a]	0.98 ± 0.07 [a]	0.92 ± 0.03 [a]	0.98 ± 0.04 [a]
Width (cm)	0.30 ± 0.02[a]	0.30 ± 0.02[a]	0.30 ± 0.01[a]	0.32 ± 0.04 [a]	0.32 ± 0.02 [a]	0.28 ± 0.02 [a]	0.30 ± 0.04 [a]	0.28 ± 0.03 [a]
Thickness (cm)	0.09 ± 0.01 [a]	0.09 ± 0.01 [a]	0.09 ± 0.01 [a]	0.10 ± 0.02 [a]	0.09 ± 0.01 [a]	0.08 ± 0.01 [a]	0.10 ± 0.03 [a]	0.08 ± 0.02 [a]
Sphericity	0.29 ± 0.02 [a]	0.29 ± 0.02 [a]	0.31 ± 0.01 [a]	0.32 ± 0.04 [a]	0.29 ± 0.02 [a]	0.29 ± 0.02 [a]	0.32 ± 0.05 [a]	0.28 ± 0.03 [a]
Surface area (cm^2)	0.53 ± 0.02 [a]	0.57 ± 0.05 [a]	0.54 ± 0.05 [a]	0.60 ± 0.10 [a]	0.64 ± 0.05 [a]	0.50 ± 0.06 [a]	0.52 ± 0.08 [a]	0.50 ± 0.06 [a]
Roundness	0.22 ± 0.02 [a]	0.22 ± 0.02 [a]	0.24 ± 0.01 [a]	0.24 ± 0.01 [a]	0.22 ± 0.01 [a]	0.22 ± 0.01 [a]	0.25 ± 0.05 [a]	0.22 ± 0.03 [a]

Mean ± S.D. values in the same row with different superscripts are significantly different from each other ($p < 0.05$).

Morphological properties include length, width, thickness, sphericity, surface area and roundness.

The protein profile, analysed by SDS-PAGE, of raw and cooked rice with 0-3 % LAGG is shown in **Fig. 4.6**. For both JR and PR, four major protein bands, prolamins (15 kDa), glutelin's basic subunits (19 - 25 kDa), glutelin's acidic subunits (35 - 39 kDa) and pro glutelin (45 - 57 kDa), were identified both under native (no 2-Mercaptoethanol) and reducing SDS-PAGE conditions. Specifically, a higher weight band at 70 kDa was only noticed in JR (raw and cooked) under native conditions, indicating glutelin presence. This band nearly vanished in the presence of 2-Mercaptoethanol, along with enhanced intensities of the smaller weight bands, representing the glutelin basic subunit (19-25 kDa) and acidic subunit (35-39 kDa), initially linked via disulfide bonds. Compared with raw rice (**Fig. 4.6A**; lane 1), the protein pattern did not appear to differ significantly after cooking. An interesting observation is that the 70 kDa and 50 kDa bands gradually lose intensity with increasing LAGG concentrations, possibly due to proteins with higher molecular weight being encapsulated in the LAGG domain (500 kDa) and being too large to penetrate the gel matrix.

For JR under reducing conditions (**Fig. 4.6B**), the band at 50 kDa, supposed to be glutelin precursor, visible in raw rice, was barely observed in cooked rice (lanes 2-5), suggesting that disulfide bonds within rice protein were ruptured by cooking. When the rice is cooked with LAGG, the protein pattern is similar to that of the rice control (no LAGG), suggesting that LAGG does not alter the configuration of rice protein during cooking.

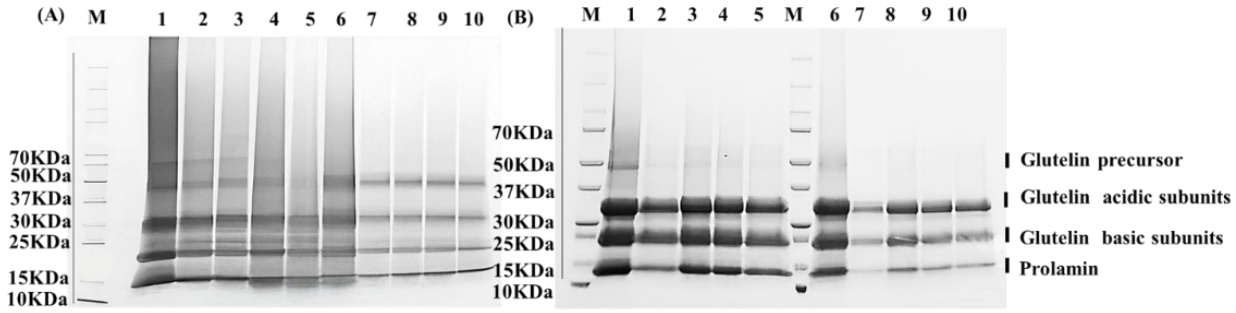


Fig. 4.8. SDS-PAGE profile of JR and PR proteins from rice raw and cooked with 0-3 % LAGG. (A) native conditions, (B) reducing conditions. M: markers, 1 uncooked JR; 2 cooked JR; 3-5 cooked JR with 1-3 % LAGG; 6 uncooked PR; 7 cooked PR; 8-10 cooked PR with 1-3 % LAGG.

Fig. 4.7 and **Fig. 4.8** show the morphological properties of JR and PR, respectively. It can be observed how those properties are nearly identical between the two rice types (e.g., similar size and shape of kernels); moreover, the properties did not change in the presence of LAGG. However, a structure with a "fabric string" appearance was observed on the surface of cooked JR and PR cooked with 2 and 3 % LAGG, most likely due to the formation of self-structured hydrogels at the peripheral region of the rice grain.

In PR, a thin protein layer adhering to and encircling the starch granules was visible (**Fig. 4.8C1**) in the cross-sections (pericarp-endosperm) of the double-stained grain; this led to an orderly structure, characterised by separate subgranules, which was not apparent in JR (**Fig. 4.7C1**). Similar structural characteristics of the protein-starch matrices have also been found in brown rice and other cereal crops, including sorghum, corn, and kidney beans (Bugusu et al., 2002; Xu and Wei, 2020). Additionally, ESEM images revealed that granule units were deformed in cooked JR and PR, showing axial fissures and gluey outer surfaces with loose granules attached (**Fig. 4.7D1** and **E1**). The cross-section of cooked PR revealed a loose fracture plane and exposed fused granule agglomerates (**Fig. 4.8D1** and **E1**).

The cross-sections of LAGG-labelled cooked rice grains illustrate how LAGG dispersion coats the grain. Upon cooking with 1 % LAGG, a coating appears along

the pericarp of rice grains, with increasing penetration depth at higher LAGG concentrations, especially at 3 % concentrations (**Fig. 4.7B** and **Fig. 4.8B**). The double-stained cooked JR and PR with also revealed a greater amount of intact protein networks and packed starch granules compared to the no LAGG control. As LAGG concentration increases, opalescent rings, perhaps formed by the LAGG-coating, appear around the outer layers of grains where stain solution penetration is limited (**Fig. 4.7C** and **Fig. 4.8C**). Compared to JR and PR, which displayed obvious pores and tunnels, JR_1LA and PR_1LA displayed smoother surfaces (**Fig. 4.7E** and **Fig. 4.8E**).

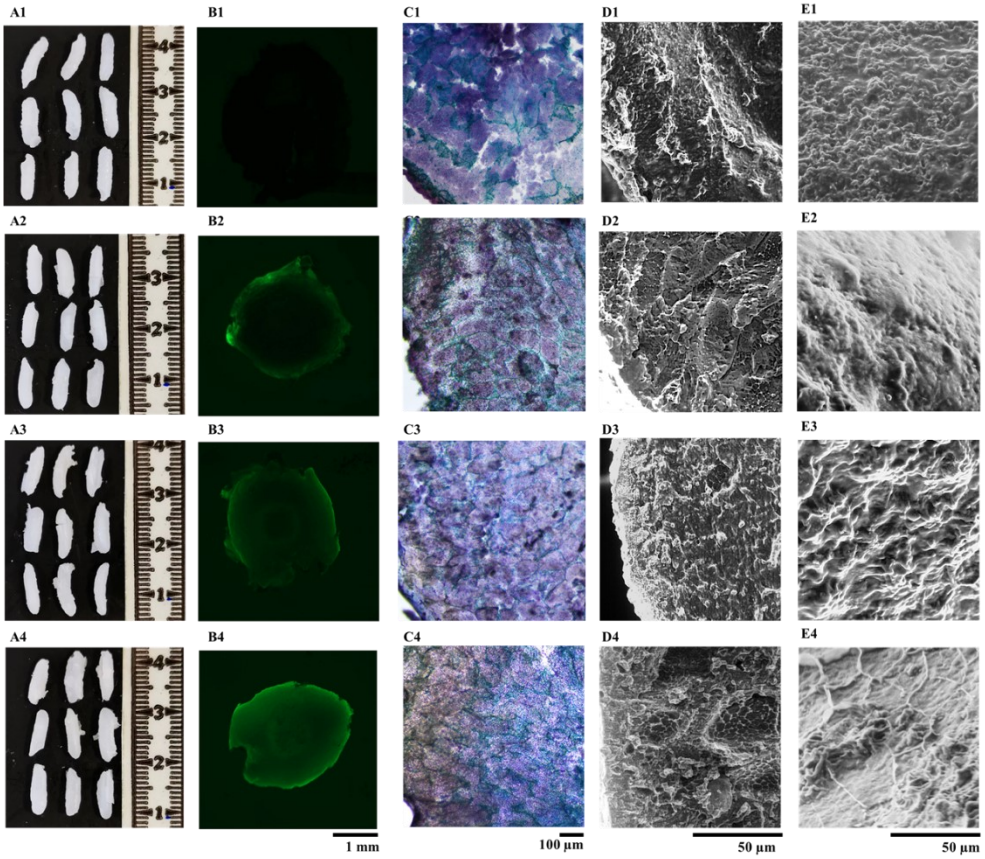


Fig. 4.9. Morphology of JR cooked with 0-3 %LAGG.

Morphology of the whole cooked grain (Scale bar = 1 cm) (A1-4); Fluorescence observation of cooked rice containing DTAF labelled LAGG (Scale bar =1 mm) (B1-4); Microtone section of cooked grain viewed under light microscope (C1-4). Protein bodies appeared green with fast green staining, starch exhibited a blue-purple stain from Lugol's solution, amylopectin-rich regions were purple, and amylose-rich regions were blue. (Scale bar = 100 μm); cross-section (D1-4) and (E1-4) surface of cooked grain under ESEM (Scale bar =50 μm)

A filamentous structure appeared on the surface of both JR_2LA and PR_2LA and agglomerated into clusters shown in JR_3LA and PR_3LA, which were suspected to be self-structured gel masses, as reported previously (Rupenthal et al., 2011). Under ESEM (**Fig. 4.7D** and **Fig. 4.8D**), the shuttle-shaped protein-starch matrices were even more visible in cooked rice containing LAGG, confirming that LAGG application can preserve the integrity of cooked rice.

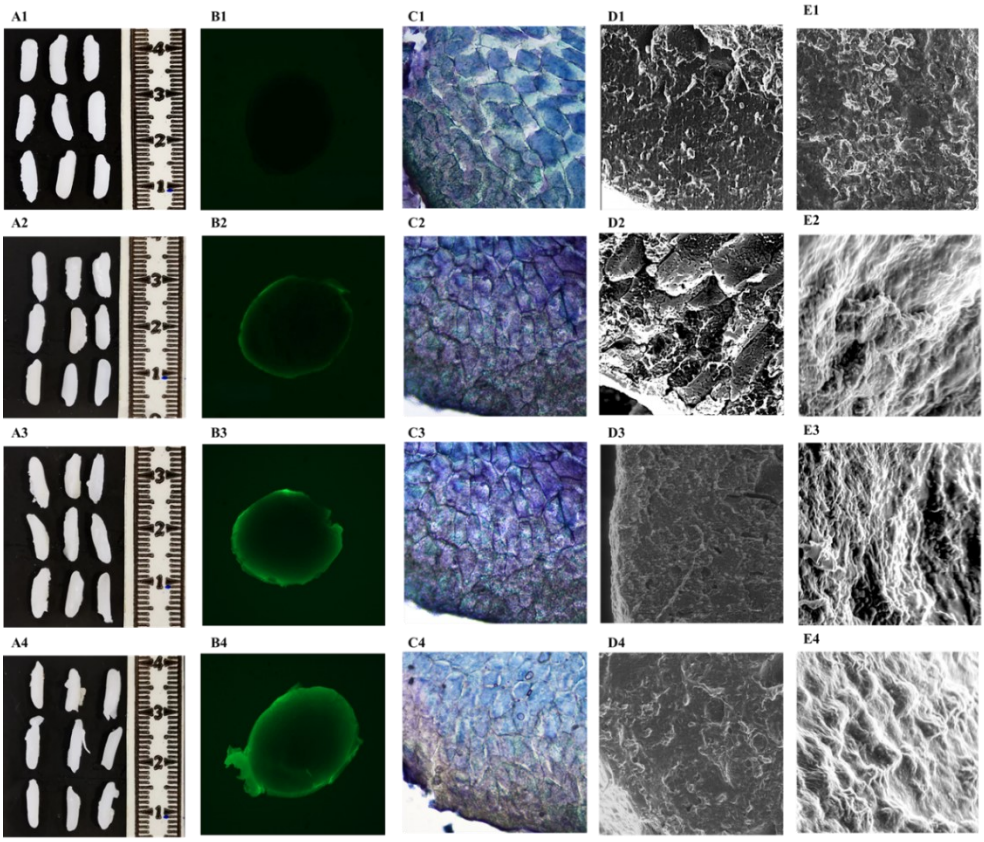


Fig. 4.10. Morphology of PR cooked with 0-3 %LAGG.

Morphology of the whole cooked grain (Scale bar = 1 cm) (A1-4); Fluorescence observation of cooked rice containing DTAF labelled LAGG (Scale bar = 1 mm) (B1-4); Microtone section of cooked grain viewed under light microscope (C1-4). Protein bodies appeared green with fast green staining, starch exhibited a blue-purple stain from Lugol's solution, amylopectin-rich regions were purple, and amylose-rich regions were blue. (Scale bar = 100 μm); cross-section (D1-4) and (E1-4) surface of cooked grain under ESEM (Scale bar = 50 μm)

4.3.8 Textural profile and oral digestion (*in vitro*) of cooked rice.

4.3.8.1 Textural profile

The textural properties (hardness, adhesiveness, cohesiveness, and chewiness) of JR and PR cooked in water or 1-3 % LAGG dispersions, determined by TPA, are shown in **Fig. 4.9**.

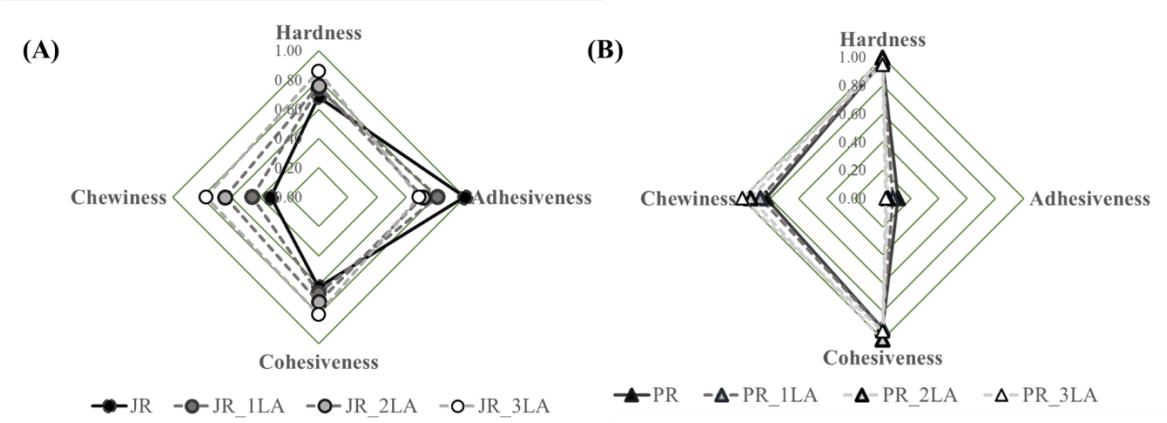


Fig. 4.11. Textural properties (hardness, cohesiveness, adhesiveness, and chewiness) of JR (A) and PR (B) cooked in 0-3 % (w/w) LAGG dispersions in water.

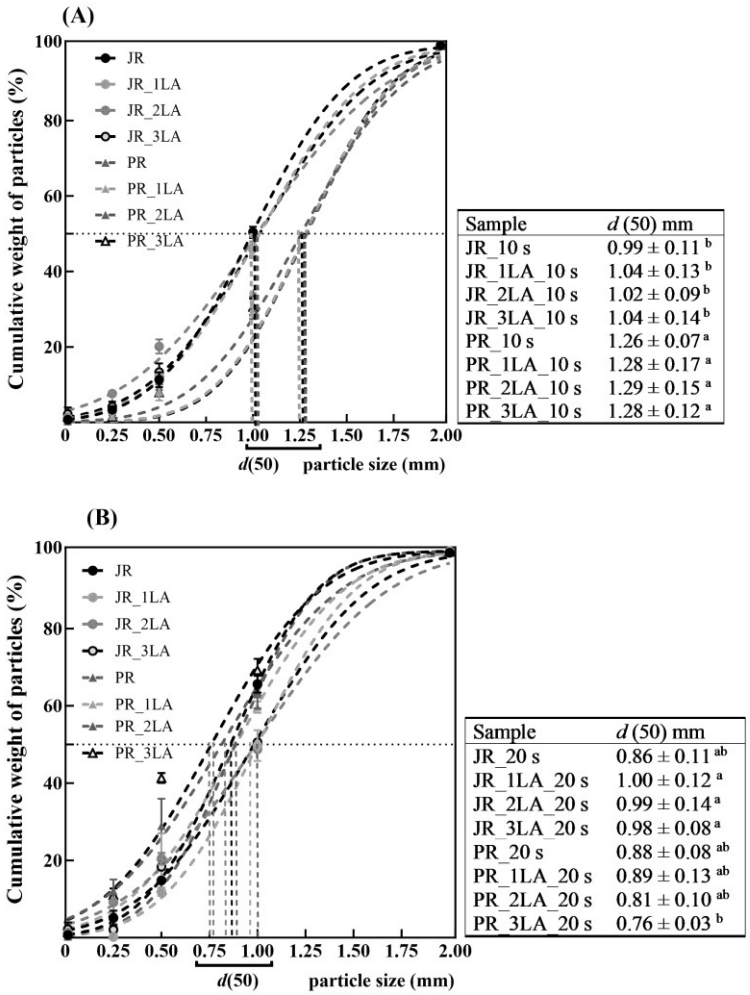
Hardness is a measure of the force required to compress a rice grain initially, and it describes its first "bite" (Yau &Huang, 1996; Tao et al., 2020). The cohesiveness indicates the inner strength of the specimen, i.e., its resistance to deformation over chewing. Chewiness is a measure of energy needed to masticate foods, which are normally solid, whereas adhesiveness indicates the sample's tendency to stick to the probe lifting after the first compression (Windham et al., 1997; Li et al., 2019). Compared with cooked PR, cooked JR exhibited lower hardness, cohesiveness, and chewiness but higher adhesion. Similar textural characteristics were reported previously for PR, suggesting that parboiling strengthens the protein-starch matrices rice (Ong & Blanshard, 1995; Zhang et al., 2022). As illustrated in the current study, the more thermally stable protein network in PR would allow the starch granules to remain compact during cooking, making the cooked PR microstructure more difficult to rupture. Additionally, due to the resultant structure, fewer amylopectin molecules leached out. Thus, the PR grain exhibited lower adhesive properties due to the lack of amylopectin on the grain surface.

Increased LAGG concentration resulted in increased hardness, cohesiveness and chewiness in both rice types, and a reduce in adhesiveness in cooked JR. The difference in chewiness and adhesiveness becomes significant between JR and JR_3LA. Comparable results were also reported by Srikaeo et al. (2020) for waxy rice cooked in 0.3, 0.5, or 0.7 % of LAGG - or other hydrocolloid (guar gum, xanthan gum, sodium alginate) - dispersions. Also, similar texture modification effects of food polysaccharides (gum Arabic and soybean soluble polysaccharides) on cooked rice were reported by Ishihara et al. (2010). It is possible to attribute these changes to the rigid textural nature of LAGG, which coated or filled pores and tunnels in the kernels, retarding amylopectin leaching. Moreover, LAGG interacted with starch chains (shown as a V-type starch crystalline structure) within the cooked rice grains to enhance their cohesiveness.

4.3.8.2 Oral digestion (in vitro) of cooked rice

To assess the effects of "chewing" time, rice type, and LAGG addition (1-3%) during cooking, on the bolus properties (particle size distribution and starch digestibility) *in vitro* (i.e., simulating swallowable food mass in vivo), rice samples were homogenised using a grinder for 10 or 20 seconds, to produce normal and fine "chewed" rice (Jalabert-Malbos et al., 2007; Moongngarm et al., 2012; Sethupathy et al., 2021). As shown in **Fig. 4.10**, JR and PR boluses had different particle size distributions following 10 second of homogenisation (simulating normal mastication pattern), as evidenced by the significantly higher *d*(50) value of PR (1.26 ± 0.07 mm) compared with JR (0.99 ± 0.11 mm). This may be explained by a harder PR texture, which makes it more resistant to the breaking effect of mastication. However, after 20 s homogenisation (simulating the fine mastication), PR and JR particles no longer significantly differed in *d*(50) values (0.88 ± 0.08 mm for PR and 0.86 ± 0.11 mm for JR), indicating that further 10 s of chewing has a more disruptive effect on PR as its particle size decreased to a larger extent. The explanation for this may again depend on the more brittle (harder and less adhesive, **Section 4.3.7.1**) texture of PR, which may tend to fragment into smaller pieces than JR, a more "plastic" material if sufficient disruptive energy (prolonged chewing) is applied. Similar results were

reported for pasta, where wholegrain pasta produced smaller particles than refined pasta after normal mastication simulation (Blanquet-Diot et al., 2021).



Sample	*d* (50) mm
JR_10 s	0.99 ± 0.11 [b]
JR_1LA_10 s	1.04 ± 0.13 [b]
JR_2LA_10 s	1.02 ± 0.09 [b]
JR_3LA_10 s	1.04 ± 0.14 [b]
PR_10 s	1.26 ± 0.07 [a]
PR_1LA_10 s	1.28 ± 0.17 [a]
PR_2LA_10 s	1.29 ± 0.15 [a]
PR_3LA_10 s	1.28 ± 0.12 [a]

Sample	*d* (50) mm
JR_20 s	0.86 ± 0.11 [ab]
JR_1LA_20 s	1.00 ± 0.12 [a]
JR_2LA_20 s	0.99 ± 0.14 [a]
JR_3LA_20 s	0.98 ± 0.08 [a]
PR_20 s	0.88 ± 0.08 [ab]
PR_1LA_20 s	0.89 ± 0.13 [ab]
PR_2LA_20 s	0.81 ± 0.10 [ab]
PR_3LA_20 s	0.76 ± 0.03 [b]

Fig. 4.12.Distribution of particle sizes in bolus of cooked JR and PR with 0-3 % (w/w) LAGG addition after homogenization for 10 s (A) or 20 s (B).

The LAGG additions did not significantly change particle size distribution in the respective JR and PR bolus following 10 s homogenisation. After 20 s homogenisation, cooked JR samples containing LAGG displayed slightly larger *d*(50) than JR with no LAGG. Conversely, among the four PR samples, the sample with the highest LAGG concentration presented a lower *d*(50) compared to the others. LAGG addition may generally increase the hardness of rice samples. However, although a clear trend in the particle size distribution among the samples cannot be defined,

LAGG might affect the texture properties of JR and PR to different levels. At 3 % LAGG, PR becomes more brittle and more easily fragmented after 20 s homogenisation. In contrast, in JR, there might be a restructuring of the fragments caused by an interaction between LAGG and the JR amylopectin (more abundant than in PR), which resulted in a larger particle size.

The starch digestibility in the oral phase of cooked rice with 0-3 % LAGG was evaluated after three homogenisation times (0 s, 10 s, 20 s), simulating three different eating behaviours, i.e., swallow, normal chewing, and fine chewing, respectively (Moongngarm et al., 2012; Tamura et al., 2017; Mandalari et al., 2018).

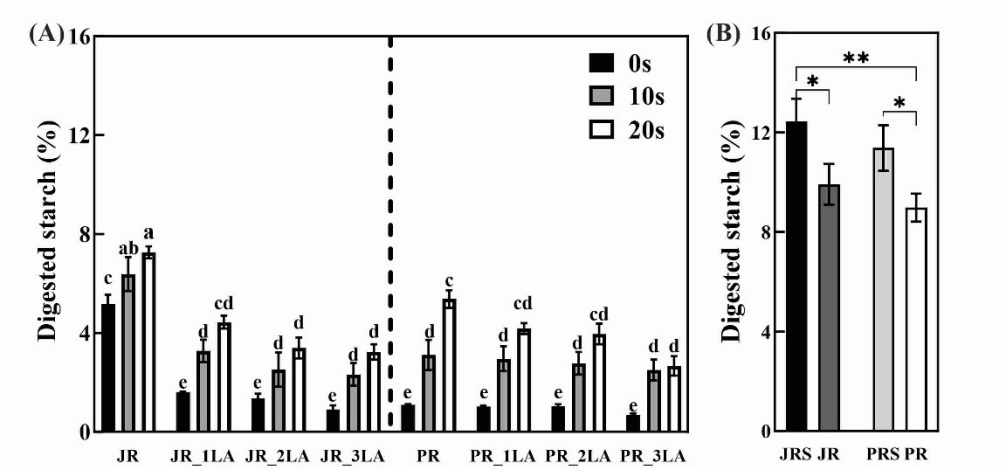


Fig. 4.13. Starch digestibility after the *in vitro* oral phase(**Section 4.2.8.2**). (A) rice samples cooked in 0-3 % LAGG, digested after 0 s (no homogenisation), 10 s, or 20 s homogenisation. The dashed line separates JR from PR samples. (B) Starch digestibility of JR and PR flours and their respective starch isolates. The asterisk (*) and lines displayed in (B) represents P-value for which selected comparisons. * $P < 0.05$; ** $P < 0.01$.

As shown in **Fig. 4.11**, the starch digestibility of all samples increased with prolonged homogenisation, suggesting that maintaining grain integrity, especially protein-starch matrices, plays a key role in controlling oral starch digestion. Starch digestibility further increases in JR and PR flours, due to the extensive grain physical disruption, consequently of the protein-starch matrices (**Fig. 4.11B**). This effect is even more evident in JRS and PRS samples, as the protein had been previously removed.

It was found that cooking with LAGG significantly reduced starch digestibility for intact JR. This could be due to the physical barrier of the LAGG-coating, which prevents the penetration of amylase in the intact grain form. Upon homogenisation, starch digestibility increases due to physical disruption of the grain, but in presence of LAGG, the physical barrier is partially retained on the rice fragments, resulting in reduce starch digestibility in the LAGG-coated JR samples. There could also be a reduction in accessibility to salivary amylase due to the fragment retains its larger size than rice control, which has also investigated and shown in terms of the particle size distributions. No evidence of reduction was instead observed in intact PR compared with PR with LAGG, perhaps due to the already low starch digestibility of PR control (<5 %) (**Fig. 4.11A**). However, 20 s homogenised LAGG-coated PR had lower starch digestibility than the 20 s homogenised PR control.

4.4 Conclusions

This study showed how physicochemical (pasting, thermal and hydration) and microstructural (infrared spectra patterns, X-ray diffraction patterns and morphology) properties of two types of cooked rice (JR – non-parboiled, PR – parboiled) can be influenced by adding low acyl gellan gum (LAGG) in cooking water.

PR and JR had similar total starch contents, but PR had higher protein levels and higher amylose/amylopectin ratio. Upon cooking raw rice, then cooling it to edible state, a two-phase transition was observed as evidenced by the viscosity (determined by RVA) and thermal profile (determined by DSC). It was observed that with increasing LAGG concentration, the peak and final viscosities increased, while the setback viscosity decreased. A trend of increasing enthalpy was also observed for both endothermic and exothermic processes, although not significant.

For rice proteins, the molecular structure was unaffected by LAGG, as demonstrated by the SDS-PAGE. The FTIR analysis showed that as LAGG concentration increased, more β-sheet and less random coils were detected in cooked JR. This indicates that cooking in LAGG dispersion promoted rice protein structural rearrangement to a more stable form. In combination, these results suggest an interaction between

LAGG and certain leached molecules, primarily amylose during cooking, resulting in starch-LAGG complexes (XRD confirmed the formation of the V-type crystalline structure) with decreased swelling power and water solubility. Microscopic observation of cooked rice with LAGG revealed a core-shell structure with a protein-starch matrices of cooked JR that remains more ordered than without LAGG. With the increase in LAGG addition, cooked rice did not undergo significant changes in its composition. However, the resultant structural changes led to increased hardness, cohesiveness, chewiness, reduced adhesiveness, and significantly lower *in vitro* starch digestibility in the oral phase. As a result, digested starch was below 5% even with higher homogenisation times (to simulate finer chewing conditions). Conversely, PR was less susceptible to LAGG-induced microstructural changes, which could be due to the difference in protein-starch matrices with the presence of denatured proteins along with pre-gelatinised starch. As a future work, the potential on reducing starch digestibility of cooked rice with LAGG will be systematically studied in the gastric and intestinal *in vitro* phases.

4.5 References

Alvarez-Jubete, L., Auty, M., Arendt, E.K., et al. (2010) Baking properties and microstructure of pseudocereal flours in gluten-free bread formulations. *European Food Research and Technology*, 230 (3): 437–445. doi:10.1007/s00217-009-1184-z.

AACC (2001) Determination of the Pasting Properties of Rice with the Rapid Visco Analyser. AACC St. Paul, Minn.: EUA (9).

AOAC (2005a) Official methods of analysis of the Association of Analytical Chemists International. Official Methods 934.01: Gaithersburg, MD, USA.

AOAC (2005b) Official methods of analysis of the Association of Analytical Chemists International. Official Methods 933.29: Gaithersburg, MD, USA.

AOAC (2007). Official methods of analysis of Association of Analytical Chemists International. Official Methods 996.11: Gaithersburg, MD, USA.

Bahdanovich, P., Axelrod, K., Khlystov, A.Y., et al. (2022) Optimized Spectrophotometry Method for Starch Quantification. *Analytica*, 3 (4): 394–405. doi:10.3390/3040027/S1.

Battacharya, K.R., (1985). Parboiling of rice, in rice chemistry and technology. St. Paul mina America Association of Cereal Chemists, 285-348.

Blanquet-Diot, S., François, O., Denis, S., et al. (2021) Importance of oral phase *in vitro* starch digestibility related to wholegrain versus refined pastas and mastication impairment. *Food Hydrocolloids*, 112: 106277. doi.org/10.1016/j.foodhyd.2020.106277.

Boluda-Aguilar, M., Taboada-Rodríguez, A., López-Gómez, A., et al. (2013) Quick cooking rice by high hydrostatic pressure processing. *LWT - Food Science and Technology*, 51 (1): 196–204. doi:10.1016/j.lwt.2012.09.021.

Bradbeer, J.F., Hancocks, R., Spyropoulos, F., et al. (2015) Low acyl gellan gum fluid gel formation and their subsequent response with acid to impact on satiety. *Food Hydrocolloids*, 43: 501–509. doi.org/10.1016/j.foodhyd.2014.07.006

Brodkorb, A., Egger, L., Alminger, M., et al. (2019) INFOGEST static *in vitro* simulation of gastrointestinal food digestion. *Nature Protocols 2019 14:4*, 14 (4): 991–1014. doi:10.1038/s41596-018-0119-1.

Bugusu, B.A., Hamaker, B.R. and Rajwa, B. (2002) Interaction of maize zein with wheat gluten in composite dough and bread as determined by confocal laser scanning microscopy. *Scanning*, 24 (1): 1–5. doi.org/10.1002/sca.4950240101

Cai, J., Chao, C., Niu, B., et al. (2021) Effects of Debranching on the Formation of Maize Starch-Lauric Acid-β-Lactoglobulin Complexes. *Journal of Agricultural and Food Chemistry*, 69 (32): 9086–9093. doi.org/10.1021/acs.jafc.0c07230

Carcea, M. (2021) Value of wholegrain rice in a healthy human nutrition. *Agriculture (Switzerland)*, 11 (8). doi:10.3390/agriculture11080720.

Chávez-Murillo, C.E., Veyna-Torres, J.I., Cavazos-Tamez, L.M., et al. (2018) Physicochemical characteristics, ATR-FTIR molecular interactions and *in vitro* starch and protein digestion of thermally-treated whole pulse flours. *Food Research International*, 105: 371–383. doi:10.1016/j.foodres.2017.11.029.

Chen, L., Tian, Y., Zhang, Z., et al. (2017) Effect of pullulan on the digestible, crystalline and morphological characteristics of rice starch. *Food Hydrocolloids*, 63: 383–390. doi:10.1016/j.foodhyd.2016.09.021.

Cheng, K.C., Chen, S.H. and Yeh, A.I. (2019) Physicochemical properties and *in vitro* digestibility of rice after parboiling with heat moisture treatment. *Journal of Cereal Science*, 85: 98–104. doi.org/10.1016/j.jcs.2018.11.016

Cornejo-Ramírez, Y.I., Martínez-Cruz, O., Del Toro-Sánchez, C.L., et al. (2018) The structural characteristics of starches and their functional properties. *CYTA - Journal of Food*, 16 (1): 1003–1017. doi:10.1080/19476337.2018.1518343.

Van Dam, R.M. (2020) A Global Perspective on White Rice Consumption and Risk of Type 2 Diabetes. *Diabetes Care*, 43 (11): 2625–2627. doi:10.2337/DCI20-0042.

Dang, J. & Copeland, L. (2004) Studies of the fracture surface of rice grains using environmental scanning electron microscopy. *Journal of the Science of Food and Agriculture*, 84: 707–713. doi:10.1002/jsfa.1671.

Dhital, S., Dabit, L., Zhang, B., et al. (2015) *In vitro* digestibility and physicochemical properties of milled rice. *Food Chemistry*, 172: 757–765. doi:10.1016/J.FOODCHEM.2014.09.138.

Do, D.T., Singh, J., Oey, I., et al. (2019) Modulating effect of cotyledon cell microstructure on *in vitro* digestion of starch in legumes. *Food Hydrocolloids*, 96: 112–122. doi:10.1016/J.FOODHYD.2019.04.063.

Dupuis, J.H., Liu, Q. & Yada, R.Y. (2014) Methodologies for Increasing the Resistant Starch Content of Food Starches: A Review. *Comprehensive Reviews in Food Science and Food Safety*, 13 (6): 1219–1234. doi:10.1111/1541-4337.12104.

Edwards, C.H., Cochetel, N., Setterfield, L., et al. (2019) A single-enzyme system for starch digestibility screening and its relevance to understanding and predicting the glycaemic index of food products. *Food and Function*, 10 (8): 4751–4760. doi:10.1039/c9fo00603f.

Ellepola, S.W., Siu, M.C. and Ma, C.Y. (2005) Conformational study of globulin from rice (Oryza sativa) seeds by Fourier-transform infrared spectroscopy. *International Journal of Biological Macromolecules*, 37 (1–2): 12–20. doi:10.1016/J.IJBIOMAC.2005.07.008.

Eom, H., Chang, Y., Lee, E. et al. (2018). Development of a starch/gum-based edible coating for rice cakes to retard retrogradation during storage. LWT, 97, 516–522. doi.org/10.1016/J.LWT.2018.07.044

Fang, S., Wang, J., Xu, X., et al. (2018) Influence of Low Acyl and High Acyl Gellan Gums on Pasting and Rheological Properties of Rice Starch Gel. *Food Biophysics*, 13. doi:10.1007/s11483-018-9517-8.

Farooq, A.M., Li, C., Chen, S., et al. (2018) Particle size affects structural and *in vitro* digestion properties of cooked rice flours. *International Journal of Biological Macromolecules*, 118: 160–167. doi:10.1016/J.IJBIOMAC.2018.06.071.

Fetouhi, A., Benatallah, L., Nawrocka, A., et al. (2019) Investigation of viscoelastic behaviour of rice-field bean gluten-free dough using the biophysical characterization of proteins and starch: a FT-IR study. *Journal of food science and technology*, 56 (3): 1316—1327. doi:10.1007/s13197-019-03602-2.

Fitzgerald, M.A., Martin, M., Ward, R.M., et al. (2003) Viscosity of rice flour: A rheological and biological study. *Journal of Agricultural and Food Chemistry*, 51 (8): 2295–2299. doi:10.1021/jf020574i.

Garcia-Valle, D.E., Bello-Pérez, L.A., Agama-Acevedo, E., et al. (2021) Effects of mixing, sheeting, and cooking on the starch, protein, and water structures of durum wheat semolina and chickpea flour pasta. *Food Chemistry*, 360: 129993. doi:10.1016/J.FOODCHEM.2021.129993.

Guerrero, P., Kerry, J.P. and De La Caba, K. (2014) FTIR characterization of protein-polysaccharide interactions in extruded blends. *Carbohydrate Polymers*, 111: 598–605. doi:10.1016/j.carbpol.2014.05.005.

Heydari, M.M., Najib, T. and Meda, V. (2022) Investigating starch and protein structure alterations of the processed lentil by microwave-assisted infrared thermal treatment and their correlation with the modified properties. *Food Chemistry Advances*, 1: 100091. doi:10.1016/J.FOCHA.2022.100091.

Hirata, Y., Nakagawa, H., Yamauchi, H., et al. (2023) Effect of starch retrogradation on molecular dynamics of cooked rice by quasi-elastic neutron scattering. *Food Hydrocolloids*, 141: 108728. doi:10.1016/J.FOODHYD.2023.108728.

Hu, Y., Sun-Waterhouse, D., Liu, P. Zhan, et al. (2019) Modification of rice protein with glutaminase for improved structural and sensory properties. *International Journal of Food Science and Technology*, 54 (7): 2458–2467. doi:10.1111/IJFS.14161.

Ishihara, S., Nakauma, M., Funami, T., et al. (2010) Functions of gum arabic and soybean soluble polysaccharide in cooked rice as a texture modifier. *Bioscience, Biotechnology and Biochemistry*, 74 (1): 101–107. doi:10.1271/BBB.90605.

Islam, M.R., Shimizu, N. & Kimura, T. (2002) Effect of Processing Conditions on Thermal Properties of Parboiled Rice. *Food Science and Technology Research*, 8 (2): 131–136. doi:10.3136/FSTR.8.131.

Jalabert-Malbos, M. L., Mishellany-Dutour, A., Woda, A., & Peyron, M. A. (2007). Particle size distribution in the food bolus after mastication of natural foods. Food Quality and Preference, 18(5), 803–812. doi.org/10.1016/J.FOODQUAL.2007.01.010

Jang, E.H., Lee, S.J., Hong, J.Y., et al. (2016) Correlation between physicochemical properties of japonica and indica rice starches. *LWT - Food Science and Technology*, 66: 530–537. doi:10.1016/J.LWT.2015.11.001.

Jarma Arroyo, S.E., Hogan, V., Wisdom, D.A., et al. (2020) Effect of geographical indication information on consumer acceptability of cooked aromatic rice. *Foods*, 9 (12): 9–11. doi:10.3390/foods9121843.

Jirapornvaree, I., Suppadit, T. & Kumar, V. (2021) Assessing the economic and environmental impact of jasmine rice production: Life cycle assessment and Life Cycle Costs analysis. *Journal of Cleaner Production*, 303: 127079. doi:10.1016/j.jclepro.2021.127079.

Ju, Z.Y., Hettiarachchy, N.S. & Rath, N. (2001) Extraction, denaturation and hydrophobic properties of rice flour proteins. *Journal of Food Science*, 66 (2): 229–232. doi:10.1111/j.1365-2621.2001.tb11322.x.

Jukanti, A.K., Pautong, P.A., Liu, Q., et al. (2020) Low glycemic index rice—a desired trait in starchy staples. *Trends in Food Science & Technology*, 106: 132–149. doi:10.1016/J.TIFS.2020.10.006.

Juntunen, K.S., Niskanen, L.K., Liukkonen, K.H., et al. (2002) Postprandial glucose, insulin, and incretin responses to grain products in healthy subjects. *The American Journal of Clinical Nutrition*, 75 (2): 254–262. doi:10.1093/AJCN/75.2.254.

Prasad, K.,& Prakash, P. (2010) Rice-based functional cookies for celiac: Studies on its formulation. *LAP Lambert Academic Publishing: Saarbrucken, Germany*, p.128.

Kanyuck, K.M., Mills, T.B., Norton, I.T., et al. (2022) Release of glucose and maltodextrin DE 2 from gellan gum gels and the impacts of gel structure. *Food Hydrocolloids*, 122: 107090. doi:10.1016/J.FOODHYD.2021.107090.

Kasarda, D.D., Dupont, F.M., Vensel, W.H., et al. (2008) Surface-Associated Proteins of Wheat Starch Granules: Suitability of Wheat Starch for Celiac Patients. *Journal of Agricultural and Food Chemistry*, 56 (21): 10292–10302. doi:10.1021/JF801575S.

Kaur, B., Ranawana, V. and Henry, J. (2016) The Glycemic Index of Rice and Rice Products: A Review, and Table of GI Values. *Critical Reviews in Food Science and Nutrition*, 56 (2): 215–236. doi:10.1080/10408398.2012.717976.

Khin, M.N., Ahammed, S. & Zhong, F. (2021) Development of DTAF-labelled polysaccharides for characterization of microstructure and phase distribution of composite hydrogel visualization of hydrogels using CLSM. *Food Bioscience*, 41: 100909. doi:10.1016/J.FBIO.2021.100909.

Kiatponglarp, W., Tongta, S., Rolland-Sabaté, A., et al. (2015) Crystallization and chain reorganization of debranched rice starches in relation to resistant starch formation. *Carbohydrate Polymers*, 122: 108–114. doi.org/10.1016/j.carbpol.2014.12.070

Kong, X., Qiu, D., Ye, X., Bao, J., Sui, Z., Fan, J., & Xiang, W. (2015). Physicochemical and crystalline properties of heat-moisture-treated rice starch: Combined effects of moisture and duration of heating. Journal of the Science of Food and Agriculture, 95(14), 2874–2879. doi.org/10.1002/jsfa.7028

Larsen, H.N., Rasmussen, O.W., Rasmussen, P.H., et al. (2000) Glycaemic index of parboiled rice depends on the severity of processing: Study in type 2 diabetic subjects. *European Journal of Clinical Nutrition*, 54 (5): 380–385. doi:10.1038/sj.ejcn.1600969.

Li, H., Yang, J., Yan, S., et al. (2019) Molecular causes for the increased stickiness of cooked non-glutinous rice by enzymatic hydrolysis of the grain surface protein. *Carbohydrate Polymers*, 216: 197–203. doi:10.1016/J.CARBPOL.2019.04.031.

Lii, E., Mauromoustakos, A. & Wang, Y.J. (2018) Effects of cultivar and ageing on parboiled rice properties. *Cereal Chemistry*, 95 (5): 689–698. doi:10.1002/CCHE.10082.

Linlaud, N., Ferrer, E., Puppo, M.C., et al. (2010) Hydrocolloid Interaction with Water, Protein, and Starch in Wheat Dough. *Journal of Agricultural and Food Chemistry*, 59 (2): 713–719. doi:10.1021/JF1026197.

Lu, X., Ma, R., Qiu, H., et al. (2021) Mechanism of the effect of endogenous/exogenous rice protein and its hydrolysates on rice starch digestibility. *International Journal of Biological Macromolecules*, 193: 311–318. doi:10.1016/J.IJBIOMAC.2021.10.140.

Luo, X., Cheng, B., Zhang, W., et al. (2021) Structural and functional characteristics of Japonica rice starches with different amylose contents. *CYTA - Journal of Food*, 19 (1): 532–540. doi:10.1080/19476337.2021.1927194.

Ma, M., Chen, X., Zhou, R., et al. (2021) Surface microstructure of rice starch is altered by removal of granule-associated proteins. *Food Hydrocolloids*, 121:107038. doi:10.1016/j.foodhyd.2021.107038.

Man, J., Lin, L., Wang, Z., et al. (2014) Different Structures of Heterogeneous Starch Granules from High-Amylose Rice. *Journal of Agricultural and Food Chemistry*, 62 (46): 11254–11263. doi:10.1021/jf503999r.

Mandalari, G., Merali, Z., Ryden, P., et al. (2018) Durum wheat particle size affects starch and protein digestion *in vitro*. *European Journal of Nutrition*, 57 (1): 319–325. doi:10.1007/s00394-016-1321-y.

Milas, M., Shi, X. & Rinaudo, M. (1990) On the physicochemical properties of gellan gum. *Biopolymers*, 30 (3–4): 451–464. doi:10.1002/BIP.360300322.

Moongngarm, A., Bronlund, J., Grigg, N., et al. (2012) Chewing Behavior and Bolus Properties as Affected by Different Rice Types. *International Journal of Medical and Biological Sciences*, 6.doi.org/10.1016/j.crfs.2021.11.018

Morris, E.R., Nishinari, K. and Rinaudo, M. (2012) Gelation of gellan - A review. *Food Hydrocolloids*. 28 (2) pp. 373–411. doi:10.1016/j.foodhyd.2012.01.004.

Nguyen Doan, H.X., Song, Y., Lee, S., et al. (2019) Characterization of rice starch gels reinforced with enzymatically-produced resistant starch. *Food Hydrocolloids*, 91:76–82. doi:10.1016/j.foodhyd.2019.01.014.

Nhouchi, Z., Botosoa, E.P., Chèné, C., et al. (2022) Mid-infrared as a tool to study the conformational structure of starch and proteins with oil addition during gelatinization. *LWT*, 157: 113093. doi:10.1016/J.LWT.2022.113093.

Organisation for Economic Co-operation and Development (OECD), Food and of the United Nations, A.O. (2021) Rice projections: Consumption, food", in *OECD-FAO Agricultural Outlook 2023-2032*, OECD Publishing, Paris. doi.org/10.1787/1372eb0d-en

Oh, I.K., Bae, I.Y. and Lee, H.G. (2018) Complexation of high amylose rice starch and hydrocolloid through dry heat treatment: Physical property and *in vitro* starch digestibility. *Journal of Cereal Science*, 79: 341–347. doi.org/10.1016/j.jcs.2017.11.017

Ong, M.H. and Blanshard, J.M.V. (1995) Texture determinants of cooked, parboiled rice. II: Physicochemical properties and leaching behaviour of rice. *Journal of Cereal Science*, 21 (3): 261–269. doi:10.1006/jcrs.1995.0029.

Paiva, F.F., Vanier, N.L., Berrios, J.D.J., et al. (2016) Polishing and parboiling effect on the nutritional and technological properties of pigmented rice. *Food Chemistry*, 191: 105–112. doi:10.1016/j.foodchem.2015.02.047.

Peyrot des Gachons, C. & Breslin, P.A.S. (2016) Salivary Amylase: Digestion and Metabolic Syndrome. *Current diabetes reports*, 16 (10): 102. doi:10.1007/S11892-016-0794-7.

Puncha-Arnon, S. & Uttapap, D. (2013) Rice starch vs. rice flour: Differences in their properties when modified by heat–moisture treatment. *Carbohydrate Polymers*, 91 (1): 85–91. doi:10.1016/J.CARBPOL.2012.08.006.

Ranawana, V., Monro, J.A., Mishra, S., et al. (2010) Degree of particle size breakdown during mastication may be a possible cause of interindividual glycemic variability. *Nutrition research (New York)*, 30 (4): 246–254. doi:10.1016/J.NUTRES.2010.02.004.

Rocha-Villarreal, V., Serna-Saldivar, S.O. and García-Lara, S. (2018) Effects of parboiling and other hydrothermal treatments on the physical, functional, and nutritional properties of rice and other cereals. *Cereal Chemistry*, 95 (1): 79–91. doi:https://doi.org/10.1002/cche.10010.

Rupenthal, I.D., Green, C.R. and Alany, R.G. (2011) Comparison of ion-activated in situ gelling systems for ocular drug delivery. Part 1: Physicochemical characterisation and *in vitro* release. *International Journal of Pharmaceutics*, 411 (1–2): 69–77. doi:10.1016/J.IJPHARM.2011.03.042.

Saha, D., & Bhattacharya, S. (2010). Hydrocolloids as thickening and gelling agents in food: a critical review. Journal of Food Science and Technology, 47(6), 587. doi.org/10.1007/S13197-010-0162-6

Saneei, P., Larijani, B. and Esmaillzadeh, A. (2017) Rice consumption, incidence of chronic diseases and risk of mortality: Meta-analysis of cohort studies. *Public Health Nutrition*, 20 (2): 233–244. doi:10.1017/S1368980016002172.

Sasaki, T. & Kohyama, K. (2011) Effect of non-starch polysaccharides on the *in vitro* digestibility and rheological properties of rice starch gel. *Food Chemistry*, 127 (2): 541–546. doi:10.1016/j.foodchem.2011.01.038.

Sethupathy, P., Sivakamasundari, S.K., Moses, Jeyan.A., et al. (2021) Effect of varietal differences on the oral processing behaviour and bolus properties of cooked rice. *International Journal of Food Engineering*, 17 (3): 177–188. doi:10.1515/ijfe-2020-0097.

Shen, Y., Hong, S., Singh, G., et al. (2022) Improving functional properties of pea protein through “green” modifications using enzymes and polysaccharides. *Food Chemistry*, 385: 132687. doi:10.1016/J.FOODCHEM.2022.132687.

Silva, W. M. F., Biduski, B., Lima, K. O., Pinto, V. Z., Hoffmann, J. F., Vanier, N. L., & Dias, A. R. G. (2017). Starch digestibility and molecular weight distribution of proteins in rice grains subjected to heat-moisture treatment. Food Chemistry, 219, 260–267. doi.org/10.1016/J.FOODCHEM.2016.09.134

Sittipod, S. & Shi, Y.-C. (2016) Changes of starch during parboiling of rice kernels. *Journal of Cereal Science*, 69: 238–244. doi.org/10.1016/j.jcs.2016.03.015.

Sivakamasundari, S.K., Moses, J.A. & Anandharamakrishnan, C. (2020) Effect of parboiling methods on the physicochemical characteristics and glycemic index of rice varieties. *Journal of Food Measurement and Characterization*, 14 (6): 3122–3137. doi:10.1007/s11694-020-00551-9.

Song, J. Y., Kwon, J. Y., Choi, J., Kim, Y. C., & Shin, M. (2006). Pasting Properties of Non-waxy Rice Starch-Hydrocolloid Mixtures. Starch - Stärke, 58(5), 223–230. doi.org/10.1002/STAR.200500459

Srikaeo, K. & Paphonyanyong, W. (2020) Texture, microstructure and *in vitro* starch digestibility of waxy rice cooked with hydrocolloids. *Food Research*, 4 (4): 1089–1097. doi:10.26656/fr.2017.4(4).026.

Steglich, T., Bernin, D., Röding, M., et al. (2014) Microstructure and water distribution of commercial pasta studied by microscopy and 3D magnetic resonance imaging. *Food Research International*, 62: 644–652. doi:10.1016/J.FOODRES.2014.04.004.

Su, J., Chotineeranat, S., Laoka, B., et al. (2018) Effect of Dry Heat Treatment With Xanthan Gum on Physicochemical Properties of Different Amylose Rice Starches. *Starch - Stärke*, 70 (3–4): 1700142. doi:10.1002/STAR.201700142.

Suklaew, P.O., Chusak, C. & Adisakwattana, S. (2020) Physicochemical and functional characteristics of rd43 rice flour and its food application. *Foods*, 9 (12). doi.org/10.3390/foods9121912

Suo, X., Mosca, A.C., Pellegrini, N., et al. (2021) Effect of pasta shape and gluten on pasta cooking quality and structural breakdown during mastication. *Food & Function*, 12 (22): 11577–11585. doi:10.1039/D1FO02339J.

Tamura, M., Nagai, T., Hidaka, Y., et al. (2014) Changes in nonwaxy Japonica rice grain textural-related properties during cooking. *Journal of Food Quality*, 37 (3): 177–184. doi:10.1111/jfq.12085.

Tamura, M., Okazaki, Y., Kumagai, C., et al. (2017) The importance of an oral digestion step in evaluating simulated *in vitro* digestibility of starch from cooked rice grain. *Food Research International*, 94: 6–12. doi:10.1016/j.foodres.2017.01.019.

Tao, K., Yu, W., Prakash, S., et al. (2020) Investigating cooked rice textural properties by instrumental measurements. *Food Science and Human Wellness*, 9 (2): 130–135. doi:10.1016/J.FSHW.2020.02.001.

Tian, J., Cai, Y., Qin, W., et al. (2018) Parboiling reduced the crystallinity and *in vitro* digestibility of non-waxy short-grain rice. *Food Chemistry*, 257: 23–28. doi:10.1016/j.foodchem.2018.03.005.

Toutounji, M.R., Farahnaky, A., Santhakumar, A.B., et al. (2019a) Intrinsic and extrinsic factors affecting rice starch digestibility. *Trends in Food Science and Technology*. 88 pp. 10–22. doi:10.1016/j.tifs.2019.02.012.

Unnikrishnan, K. R., & Bhattacharya, K. R. (1981). Swelling and solubility behaviour of parboiled rice flour. International Journal of Food Science & Technology, 16(4), 403–408. doi.org/10.1111/J.1365-2621.1981.TB01831.X

Vamadevan, V. and Bertoft, E. (2020) Observations on the impact of amylopectin and amylose structure on the swelling of starch granules. *Food Hydrocolloids*, 103: 105663. doi:10.1016/J.FOODHYD.2020.105663.

Vandeputte, G.E. and Delcour, J.A. (2004) From sucrose to starch granule to starch physical behaviour: A focus on rice starch. *Carbohydrate Polymers*, 58 (3): 245–266. doi:10.1016/j.carbpol.2004.06.003.

Wang, C., Xu, F., Li, D., et al. (2015) Physico-chemical and structural properties of four rice bran protein fractions based on the multiple solvent extraction method. 33 (3): 283–291. doi:10.17221/462/2014-CJFS.

Wang, H., Liu, Y., Chen, L., Li, X., Wang, J., & Xie, F. (2018). Insights into the multi-scale structure and digestibility of heat-moisture treated rice starch. Food Chemistry, 242, 323–329. doi.org/10.1016/j.foodchem.2017.09.014

Wang, L., Zhao, S., Kong, J., et al. (2020) Changing cooking mode can slow the starch digestion of colored brown rice: A view of starch structural changes during cooking.

International Journal of Biological Macromolecules, 155: 226–232. doi:10.1016/J.IJBIOMAC.2020.03.203.

Wang, Y.R., Yang, Q., Fan, J.L., et al. (2019) The effects of phosphorylation modification on the structure, interactions and rheological properties of rice glutelin during heat treatment. *Food Chemistry*, 297: 124978. doi:10.1016/J.FOODCHEM.2019.124978.

Wani, I.A., Sogi, D.S., Hamdani, A.M., et al. (2016) Isolation, composition, and physicochemical properties of starch from legumes: A review. *Starch - Stärke*, 68 (9–10): 834–845. doi:10.1002/STAR.201600007.

Windham, W.R., Lyon, B.G., Champagne, E.T., et al. (1997) Prediction of Cooked Rice Texture Quality Using Near-Infrared Reflectance Analysis of Whole-Grain Milled Samples. *Cereal Chemistry*, 74 (5): 626–632. doi:10.1094/CCHEM.1997.74.5.626.

Xu, A. and Wei, C. (2020) Comprehensive comparison and applications of different sections in investigating the microstructure and histochemistry of cereal kernels. *Plant Methods*, 16 (1): 1–13. doi.org/10.1186/s13007-020-0558-x

Yang, T., Wang, P., Zhou, Q., et al. (2022) Effects of Different Gluten Proteins on Starch's Structural and Physicochemical Properties during Heating and Their Molecular Interactions. *International Journal of Molecular Sciences*, 23 (15). doi:10.3390/IJMS23158523.

Yau, N.J.N. and Huang, J.J. (1996a) Sensory analysis of cooked rice. *Food Quality and Preference*, 7 (3): 263–270 doi.org/10.1016/S0950

Ying, D., Hlaing, M.M., Lerisson, J., et al. (2017) Physical properties and FTIR analysis of rice-oat flour and maize-oat flour based extruded food products containing olive pomace. *Food Research International*, 100 (Pt 1): 665–673. doi:10.1016/j.foodres.2017.07.062.

Yu, S., Ma, Y., & Sun, D. W. (2009). Impact of amylose content on starch retrogradation and texture of cooked milled rice during storage. Journal of Cereal Science, 50(2), 139–144. doi.org/10.1016/J.JCS.2009.04.003

Yu, S., Ma, Y., Menager, L., & Sun, D. W. (2012). Physicochemical Properties of Starch and Flour from Different Rice Cultivars. Food and Bioprocess Technology, 5(2), 626–637. doi.org/10.1007/S11947-010-0330-8/TABLES/8

You, S. Y., Oh, S. K., Kim, H. S., et al. (2015). Influence of molecular structure on physicochemical properties and digestibility of normal rice starches. International Journal of Biological Macromolecules, 77, 375–382. doi.org/10.1016/J.IJBIOMAC.2015.02.054

Zavareze, E. da R., Storck, C. R., de Castro, L. A. S., Schirmer, M. A., & Dias, A. R. G. (2010). Effect of heat-moisture treatment on rice starch of varying amylose content. Food Chemistry, 121(2), 358–365. doi.org/10.1016/J.FOODCHEM.2009.12.036

Zhang, W., Cheng, B., Zeng, X., et al. (2022) Physicochemical and Digestible Properties of Parboiled Black Rice With Different Amylose Contents. *Frontiers in Nutrition*, 9: 934209 doi:10.3389/FNUT.2022.934209.

Zhang, Y., Li, M., You, X., et al. (2020a) Impacts of guar and xanthan gums on pasting and gel properties of high-amylose corn starches. *International Journal of Biological Macromolecules*, 146: 1060–1068. doi:10.1016/J.IJBIOMAC.2019.09.231.

Zhao, L., Jin, X., Wu, J., et al. (2023) Effects of Qingke β-glucan with different molecular weights on pasting, gelation, and digestive properties of rice starch. *Food Chemistry: X*, 19: 100803. doi:10.1016/J.FOCHX.2023.100803.

Zheng, J., Huang, S., Zhao, R et al. (2021). Effect of four viscous soluble dietary fibers on the physicochemical, structural properties, and in vitro digestibility of rice starch: A comparison study. Food Chemistry, 362, 130181. doi.org/10.1016/J.FOODCHEM.2021.130181

Zhou, S., Hong, Y., Gu, Z., et al. (2020) Effect of heat-moisture treatment on the *in vitro* digestibility and physicochemical properties of starch-hydrocolloid complexes. *Food Hydrocolloids*, 104: 105736. doi:10.1016/J.FOODHYD.2020.105736.

Zhu, L., Wu, G., Cheng, L., et al. (2019) Effect of soaking and cooking on structure formation of cooked rice through thermal properties, dynamic viscoelasticity, and enzyme activity. *Food Chemistry*, 289: 616–624. doi:https://doi.org/10.1016

5 An evaluation of *in vitro* digestion of protein-starch matrices in cooked rice containing low acyl gellan gum using a multi-enzyme approach

Qingsu Liu[1], Vincenzo Di Bari[2], Nicholas James Watson[3*]

[1] Food, Water, Waste Research Group, Faculty of Engineering, The University of Nottingham, University Park Campus NG7 2RD, UK

[2] Division of Food, Nutrition and Dietetics, The University of Nottingham, Sutton Bonington Campus, Loughborough LE12 5RD, UK

[3] School of Food Science and Nutrition, University of Leeds, Leeds, LS2 9JT, UK

***Corresponding author:** n.j.watson@leeds.ac.uk

(Manuscript prepared for Submission)

Abstract

Rice kernel comprises starch granules encased in protein networks, critical in controlling starch structural disintegration, digestibility, and related glycaemic response upon consumption. In this study, we investigated: i) modes of protein-starch matrices disintegration in two indica rice types, jasmine (not-parboiled) and parboiled type, and how this affects cooked rice starch digestibility in a simulated upper gastrointestinal environment. ii) The impact of *in vitro* oral fragmentation (homogenisation) on starch digestibility, measured using modified digestion models incorporating gradual protein hydrolysis. iii) The rice structure–digestibility profile was evaluated using empirical kinetic models. The same methodology was applied for rice cooked in low acyl gellan gum dispersions (1 % of the rice mass, w/w) to evaluate the hydrogel's potential protective coating role in reducing starch digestibility.

Results showed that multi-enzyme systems progressively removed rice protein networks from the matrices. The starch digestograms of the intestinal phase revealed two-phase digestion patterns (i.e., digestion fractions) with fast-to-slow rates, demonstrating differences in enzyme accessibility towards digestible fractions as digestion progressed. Parboiled rice exhibited a lower starch digestibility than jasmine rice, although the physical disintegration of parboiled rice grain significantly increased starch digestibility. Low acyl gellan gum showed promising results in reducing starch digestibility in intact and homogenised rice models, playing an encapsulating role similar to that of a protein network.

These findings can be a reference point for the food industry and consumers to develop strategies for rice-based foods with reduced starch digestibility. *In vitro* digestion models with multi-enzymes may help to gain a more comprehensive understanding of the role of the protein-starch matrices in regulating enzymatic hydrolysis on digestion.

Highlights

- Intact rice is less digestible from protein and starch than homogenised rice.
- *In vitro* oral processing of cooked rice induces microstructure heterogeneity, which affects starch and protein digestion kinetics.
- Starch hydrolysis is facilitated by food disintegration and the presence of salivary α-amylase.
- An increase in the rate and extent of starch digestion was observed in conjunction with a higher level of protein digestion.
- Rice cooked with low acyl gellan gum exhibits reduced starch digestibility.

Keywords: protein-starch matrices, *in vitro* digestion, cooked rice digestibility, low acyl gellan gum

5.1 Introduction

White rice is a major component of the human diet, particularly in Asian cultures. As a result of the manufacturing practices and cooking methods, its starch becomes highly digestible, causing a spike in blood sugar levels. This has been linked to several health risks, especially for individuals suffering from hyperglycaemia and diabetes (Boers et al., 2015; Bhavadharini et al., 2020). In these terms, determining and mediating the rate and extent of rice starch digestion profoundly impacts health management. Although complex, starch digestion of cooked rice undergoes three fundamental steps *in vivo*: i) enzymatic diffusion (mainly α-amylases) and adsorption, 2) formation of the enzyme-substrate complex, 3) catalytic event (Butterworth et al., 2011). Several factors in grain structure affect enzyme accessibility. In addition to the structural characteristics of rice starch (such as the ratio of amylose to amylopectin and crystallite types), other components, such as proteins (whose structural net encapsulates the starch granules), also contribute to the starch digestion process (Hasjim et al., 2013; Dhital et al., 2015). Several recent studies have demonstrated the mechanisms by which rice protein and its hydrolysates play a role in controlling starch digestion(Chi et al., 2018; Li et al., 2021; Lu et al., 2022). The rice protein networks can stabilise the starch structure as physical barriers, thereby reducing starch gelatinisation and enzymatic accessibility. Besides, rice protein is subjected to different stages of proteolysis upon consumption, including gastric digestion by pepsin followed by further hydrolysis simultaneously with starch by pancreatin during the interstitial phase. The water-soluble peptide fragments from digested protein showed a substantial inhibitory effect on starch digestibility. Meanwhile, residues of the water-insoluble protein fractions remain bound to starch granules, reducing enzyme accessibility due to steric hindrances (Yu et al., 2018).

Different researchers have explored methods to develop rice-based products with slowly digestible starch. These include increasing resistant starch (RS) by transgenic engineering(Cai et al., 2018) and precisely breeding rice varieties high in protein and RS. However, some trade-offs are related to low yield and undesirable textural

properties. In addition, several plant-based protein isolates and their hydrolysates have been used as food ingredients to formulate fortified rice flour extruded rice grains and are related rice-based products with reduced starch digestion rate at a laboratory scale (Na-Nakorn et al., 2019; He et al., 2021; Shen et al., 2022). It should be noted, however, that the protein may lose its role as a structuring agent and hierarchical barrier in the recomposed rice kernels to prevent enzymes from attacking starch granules. Rice protein is denatured during heated extrusion and no longer appears as a network but as protein assemblies throughout the kernel. The absence of protein-starch matrices makes functional rice more susceptible to degradation during post-processing, like washing, cooking, and chewing (Sivakamasundari et al., 2022). There is evidence that using a physical modification such as parboiling (a hydrothermal treatment involving soaking, steaming, and drying) can reduce starch digestibility and GI, and a significant reduction can be observed when pressure parboiling is applied (Larsen et al., 2000; Gunaratne et al., 2013). Parboiling causes starch retrogradation and denaturation of protein bodies and irreversibly alters the biopolymer's microstructure (Hapsari et al., 2016). During the cooking of parboiled rice, the denatured proteins also interact with gelatinised starch through hydrophobic interactions and hydrogen bonding, forming peripheral layers of the protein-starch matrices. The structure inhibits the hydration of the internal starch granules and their enzyme availability (López-Barón et al., 2017). Similar strategies can be adopted to modify domestic cooking-storage methods (Hapsari et al., 2016; Liu et al., 2019). A further approach for developing rice formulations with low-glycaemic index (GI) is by addition of hydrocolloids, such as guar gum and gellan gum, which would embed the starch substrates of foods in hydrocolloid networks, reducing their exposure to the enzymatic processes (Chung et al., 2007; He et al., 2020).

Determining GI in *in vivo* conditions is crucial. Still, it can be challenging to do so reproducibly and accurately due to inherent differences among individuals, particularly human subjects. Monitoring food behaviour in the gastrointestinal tract is technically demanding, and ethical and financial concerns must also be

considered. Therefore, a growing interest has been in modelling digestion as an alternative technique to understand starch digestibility from a food perspective to improve consumer health through better-informed food product design. Digestion systems exhibit a high level of physical-chemical complexity, but they are still based on mechanical movements similar to those already available in food processing (Bornhorst et al., 2016). For example, chewing, blending, and mixing food in the upper digestive pathway is analogous to the food process's crushing, grinding, and homogenising processes. A majority of previous studies have been conducted using simple models such as rice starch and slurry to assess the starch digestion of cooked rice as well as evaluating the catalytic activity of enzymes directly influenced by proteins or their hydrolysates (Amin et al., 2018; Chi et al., 2018; Li & Hu, 2020). However, a need remains to investigate howthe textural properties of protein-starch matrices in cooked rice grains and their breakdown during digestion contribute to starch digestibility. For example, Tamura et al.(2016) investigated the necessity of simulating oral processing for starch digestion of cooked rice. They found that the rate of starch digestion increased significantly in correlation with grain damage intensity. Hardness-induced differences in bolus (chewed food mass before swallowing) have been demonstrated to affect starch and digestion kinetics in wheat (Wu & Warren, 2023), sorghum flour (Xu et al., 2022), and pasta (Blanquet-Diot et al., 2021; Li et al., 2021), yet such evidence of cooked rice remains limited.

The hypothesis underpinning this research posits that cooked rice can have a lower starch digestibility if the protein network is preserved. Additionally, it is postulated that this effect can be augmented by utilising low acyl gellan gum to maintain the integrity of the rice grain by hydrogel coating. To do so, two food model cases were considered in this study: intact (case 1) and homogenised (case 2) rice. In case 1, the protein-starch matrices were mainly intact at the beginning of the digestion process, whereas in case 2, the matric structure had been damaged by homogenisation, which simulated oral processing. A modified *in vitro* digestion model series incorporating gradual protein hydrolysis was developed to assess 1) how protein-starch matrices affect protein and starch digestion behaviour; 2) how *in vitro* oral

fragmentation (case 2) impacts protein and starch digestibility; 3) empirical kinetic models were used to evaluate rice structure–digestibility profile. In addition, the above methodology was applied to rice cooked in low acyl gellan gum dispersions (1 %, w/w) to determine if the formed hydrogel could have a protective coating role in reducing starch digestibility.

5.2 Materials and methods

5.2.1 Material

Two white rice types in this work were selected for their different glycaemic index (GI). The GI of a food refers to the % of starch digested in a defined amount of time (usually 2 h), compared with a reference (glucose or white bread, with 100 % relative starch digestibility, i.e., GI equal to 100). Foods are normally classified as high (≥70) and low (≤55) GI, according to their starch digestibility (Atkinson et al., 2021). In this study, high-GI rice type (89 > 70), Thai Jasmine rice (JR, Green Dragon Thai Hom Mali Aaa, non-parboiled, purchased date: December 2018), and low-GI rice type, easy-cook long grain white rice (also known as parboiled rice, PR, purchased date January 2019) were from a local supermarket in Nottingham, UK. Both rice (*Oryza sativa*) are indica varieties. Low acyl gellan gum (LAGG) powder was purchased from CPKelco, UK. The reagents used to produce simulated salivary fluid (SSF), simulated gastric fluid (SGF), and simulated intestinal fluid (SIF) were prepared as reported in the INFOGEST method (Brodkorb et al., 2019). In the present study, the bile salt of the intestinal phase was not included, as the fat content in white rice is negligible. All reagents used for digestive solutions, including enzymes, were of analytical grade and supplied from Sigma-Aldrich, UK. Enzyme activity (**Tab. 5.1**) was determined using the procedures by Brodkorb et al. (2019).

Tab. 5.1. Product code and experimentally measured activity for salivary α-amylase, pepsin, pancreatic α-amylase, trypsin, and pancreatin (consisting of pancreatic α-amylase and trypsin) used in this study. Different superscripts indicate the activity of different enzymes in the same enzyme complex.

	salivary α-amylase	pepsin	pancreatic α-amylase	pancreatin (α-amylase/trypsin)	trypsin
Product code (Sigma-Aldrich)	A1031a	P7000	A3176	P1750, 4×USP specification	T0303
Enzyme activity (U/mg)	146.21	557.52	15.281/0.243	31.41 1/2.30 3	4.52 3

[1] 1 unit/mg represents the capability of liberating 1 mg of maltose from soluble potato starch (S2630, Sigma-Aldrich) in three mins at a pH of 6.9 at 20°C.

[2] 1 unit/mg represents the capability of liberating 1 mg of Tyrosine from the haemoglobin digestion at pH 2.0 at 37°C.

[3] 1 unit/mg represents the capability of hydrolysing 1 μmole of p-toluene-sulfonyl-L-arginine methyl ester (TAME) per min at pH 8.1 at 25°C.

5.2.2 Preparation of cooked rice samples

Rice was cooked according to the manufacturer's instructions and previous studies (Chatthongpisut et al., 2015; Liu et al., 2019). JR or PR (100 g), pre-washed in water and dried at room temperature, were cooked in a rice cooker (NEDIS, Karc06wt-power 300w, Leicester, UK) with 150 g of distilled water (1:1.5 rice-to-water ratio; w/w) for approximately 15 mins (until no excess water was present). The cooked rice was then kept in the rice cooker in warm mode (65-70°C) for 10 mins to fully gelatinise the starch in the grain, as determined by visual inspection (no white core in the cooked rice kernels) (Srikaeo et al., 2020). Besides pure water, JR and PR were also cooked in a 1 % (w/w of raw rice) aqueous LAGG dispersion using the same cooking method; samples produced in this dispersion were coded as JR_1LA and PR_1LA, respectively.

5.2.3 Proximate analysis of cooked rice samples with and without LAGG

A moisture analyser (MB120, OHAUS, New Jersey, USA) was used to measure the moisture content of cooked rice samples at 105°C with air circulation according to AOAC Official Method 934.01 (AOAC, 2005a). The cooked rice crude protein content (dry matter) was measured using the official AOAC method 930.29 with a nitrogen-to-protein conversion factor of 5.95 (AOAC, 2005b). The protein profile was

estimated by sodium-dodecyl-sulphate polyacrylamide gel electrophoresis (SDS-PAGE), with and without β-mercaptoethanol as a reducing agent. The total starch was measured using AOAC 996.11 with a total starch assay kit (AA/AMG, Megazyme, Co. Wicklow, Ireland). The amylose content of the cooked sample was estimated using the iodine colourimetric method, as described by Tamura et al. (2014). All analyses were performed in triplicate.

5.2.4 *In vitro* digestion experiments

These experiments were performed to gain a better understanding of how protein networks affect the starch digestibility of cooked rice *in vitro* by simulating *in vivo* conditions where proteins were progressively digested under the action of pepsin, pancreatin and trypsin. According to INFOGEST static *in vitro* protocols, a series of three-phase *in vitro* digestion (IVD) models with multiple enzyme conditions were developed to analyse the digestion of proteins and starches in cooked rice (**Fig. 5.1,** description in **Tab. S1**). (Brodkorb et al., 2019).

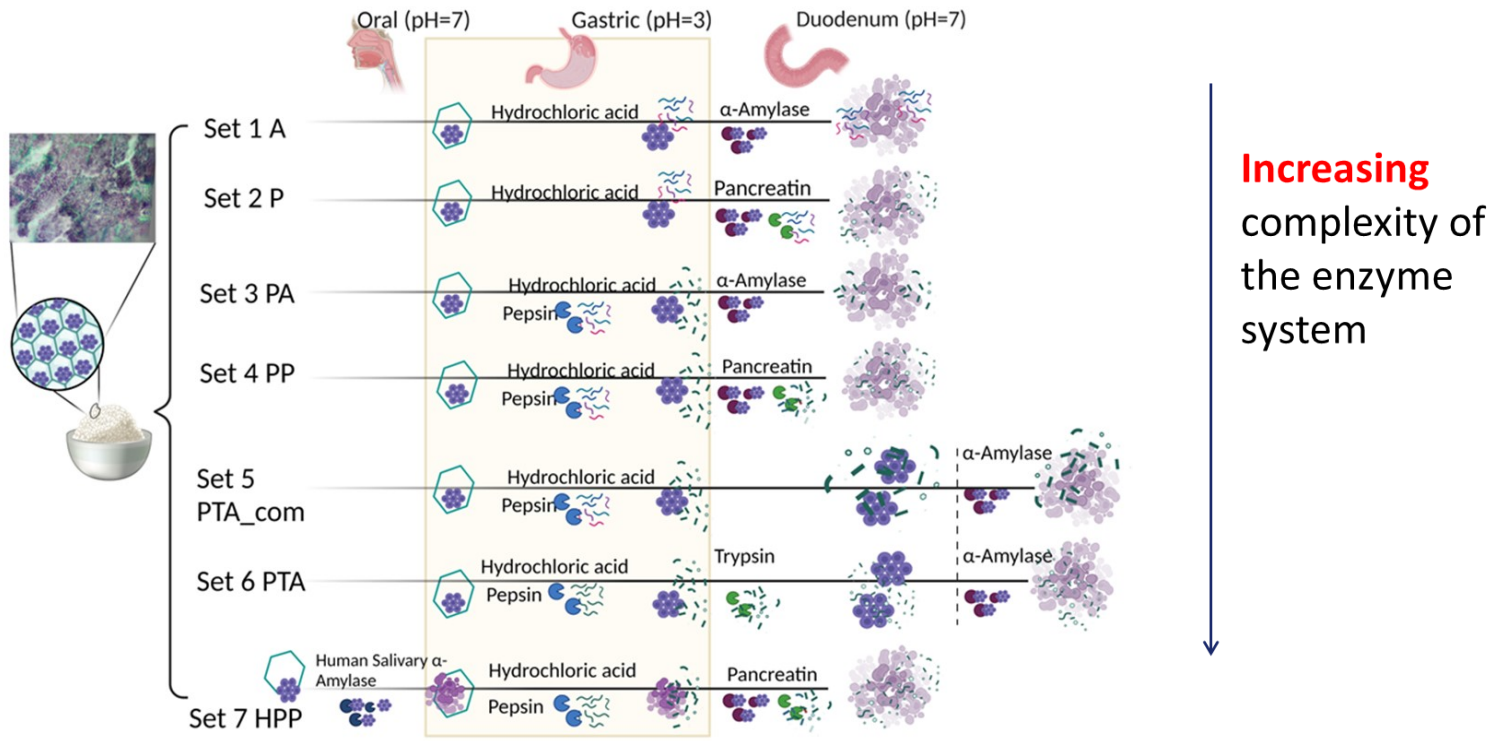


Fig. 5.1. Schematic representation of the seven static *in vitro* digestion sets. Each set consists of oral, gastric, and intestinal phases, containing the respective simulated digestion fluids and different combinations of digestive enzymes.

In vitro digestion experiments were independently performed on two aliquots (5 g) of each rice sample type, cooked as described in **Section 5.2.2**. A quantitative evaluation of digested protein and starch was conducted in duplicate for each aliquot.

5.2.4.1 Oral phase

To understand the effect of structural integrity on starch digestibility, *in vitro* digestion was performed on samples of cooked rice (120 g, wet weight) pre-homogenised in a household blender (HB605, Kenwood, Havant, UK) for 20 s and compared with non-homogenised (intact; 0 s homogenisation) cooked rice samples. Oral phase digestion was conducted by Fernandes et al. (2020). In brief, rice samples (5 g) were mixed with 5 mL of simulated salivary fluid (SSF). For Set 7, add the SSF containing salivary α-amylase to achieve an activity of 75 U/mL in the digestion mixture. The mixture was incubated for 2 min at 37°C under constant rotation (50 rpm) in a tube rotator (Fisherbrand™, Thermo Scientific, Hemel Hempstead, UK). Then, aliquots (100 μL) of the mixture were withdrawn and dispersed into 1.5 mL microcentrifuge tubes containing 100 μL of "stop solution" (0.3 M Na_2CO_3, pH 9) to inactivate the enzyme, which will later be used to determine the starch digestibility (oral phase).

5.2.4.2 Gastric phase

The simulated gastric fluid (SGF; 8 mL) was added to the oral mixture to deactivate the salivary α-amylase. The gastric phase was then initiated by adding 2 mL of SGF to reach a final volume of 20 mL. From Set 3 to Set 7, 2 mL of pepsin solution (prepared in SGF) was added to reach a final volume of 20 mL with 2000 U/mL pepsin activity. Enzyme blanks containing pepsin and SGF, but no sample, were also performed as samples. The mixture was incubated at 37°C for 30 mins under constant rotation (20 rpm). The pH of the gastric mixture was measured every 10 mins and maintained at 3 using 1M HCl. Aliquots (100 μL) of the mixture were withdrawn after 30 min incubation and dispersed into 1.5 mL microcentrifuge tubes containing 100 μL of "stop solution" (0.3 M Na_2CO_3, pH 9) to inactivate the pepsin, which will later be used to determine the starch digestibility (gastric phase).

5.2.4.3 Intestinal phase

Following the gastric phase, 16 mL of simulated intestinal fluid (SIF) was added to the gastric chyme and the pH was adjusted to 7 with NaOH (1 M). Subsequently, 4 mL of SIF containing pancreatic α-amylase (20 U/mL digesta) or pancreatin (α-amylase activity 20 U/mL digesta as per pancreatic α-amylase, automatically achieving 1.5 U/mL trypsin activity), were added to the mix to reach a final volume of the intestinal mixture of 40 mL. The mixture was incubated at 37°C under constant rotation (10 rpm) for 180 mins.

In addition, protein degradation occurring within the intestine phase due to trypsin proteolysis was also investigated. As in Set 6_PTA, after the gastric phase with pepsin, the first 19 mL of SIF with trypsin is added to the chyme (20 mL) to achieve the 1.5 U/mL total digesta as trypsin activity as having in pancreatin (like Set 2_P) for 180 mins, before starting starch digestion by adding final 1 mL SIF with α-amylase to reach the 20 U/mL total digesta. A subsequent period of protein digestion was monitored over specified times. A control (Set 5_PTA con) with the same conditions but without trypsin was used to examine the effect of the 3-hour incubation step on dispersing the protein network. While adding pancreatic α-amylase or pancreatin, a 100 μL aliquot of digesta was withdrawn from the digestion mixture at 0, 5, 10, 15, 20, 30, 45, 60, 90, 120, and 180 mins to study the kinetics of starch digestion (intestine phase). Each aliquot was mixed with 100 μL of "stop solution" (0.3 M Na_2CO_3, pH 9) to stop the amylase activity and measure the degree of starch hydrolysis. Moreover, other 100 μL aliquots were withdrawn from the digestion mixture at 0, 15, 30, 60, 120, 180 mins, each time mixed with 100 μL of a Bowman-Birk trypsin-chymotrypsin inhibitor solution (0.05 g/L) to stop the trypsin activity and measure the degree of protein hydrolysis.

Blanks corresponding to the enzymes and simulated digestion fluids, but no rice, were run through the same digestion and sampling process to identify the amount of hydrolysed protein belonging to the enzyme. This value was subtracted from the total digested protein measured in the samples to determine the actual digested rice protein.

5.2.5 Quantitative evaluation of starch and protein digestion

Soluble molecules released in the digestion fluids over time were quantified as described in **Sections 5.2.4.1**, **5.2.4.2** and **5.2.4.3** for starch and proteins, respectively. Digested proteins were quantified as the amount of soluble hydrolysed protein fractions (DSPF) and free amino groups in the digestion fluids. The DSPF was quantified using two methods to cover a wider spectrum of peptide size, as suggested by Hall et al. (2022): Two methods were conducted using i) bicinochinic acid (BCA) for fractions ranging from 10 kDa to tripeptides and o-phthaldialdehyde (OPA) for fractions ranging from 6 kDa to free amino acids, including bioaccessible hydrolysate fractions (tripeptides to amino acids). Prior to the BCA test, digested protein samples were filtered using an Amicon® Ultra-4 centrifugal filter device (4000 rpm for 10 mins at room temperature) with a cut-off value of 10 kDa**.** After centrifugation, the digesta were washed with 75 μL of MilliQ® water and centrifuged twice, allowing protein fractions (< 10 kDa) trapped in the filter membrane to be collected.

5.2.5.1 Determination of digested starch

A colourimetric analysis, par-hydroxybenzoic acid hydrazide (PAHBAH) assay, was performed to determine the amount of digested starch, following the method described by Edwards et al. (2019). Aliquots were collected at various points to determine the concentration of maltose in the samples. By referring to the standard curve produced with the maltose standard, maltose equivalents were calculated for each sample. Then, the maltose equivalent concentration units can be further converted into the corresponding percentage of digested starch using **Eq.5.1**.

$$\textbf{Digested starch} = \frac{[\textbf{maltose}]_t}{[\textbf{maltose}]_{\textbf{substrate}}} \times \textbf{100}\ \% \quad \textbf{(Eq.5.1)}$$

Where:

$[maltose]_t$ is the maltose equivalent concentration in the liquid phase of the digesta at a given time.

$[maltose]_{substrate}$ is the concentration of maltose equivalent (starch yet not hydrolysed to maltose) in the food sample at the beginning of the reaction.

This is based on the theoretical assumption that all the starch in the sample will be converted to maltose.

5.2.5.2 Determination of digested soluble protein fragment (DSPF) by BCA assay

A BCA protein assay kit (Pierce™ BCA Assay, Thermo Fisher Scientific, Waltham, MA, USA) with standard 96-well microplates method was used to analyse digested samples at each time point using bovine serum albumin (BSA) as a reference standard. The samples were diluted to determine concentrations within the standard curve of 20–2000 mg BSA/mL, mixed with the working reagents, and incubated at 37°C for 30 min before analysis. DSPF concentration was determined by measuring the absorbance at a wavelength of 562 nm (absorbance wavelength of the complex bicinchoninic acid-Cu(I), used in the BCA protein method) (SpectraMax M5 microplate reader, Molecular Devices, US) and calculated using **Eq.5.2**, as described by Almeida et al. (2015):

$$\mathbf{DSPF} = \left(\frac{\mathbf{P_S - P_b}}{\mathbf{P_{tot}}}\right) \times \mathbf{100}\ \% \quad \textbf{(Eq5.2)}$$

Where:

P_S is protein fragment content in digestion fluids

P_b is protein fragment content in blanks (**Section 5.2.4**)

P_{tot} is the concentration of total proteins in the mass before digestion. Protein content measured as N content × 5.95 (the conversion factor)

The obtained DSPF curve (the accumulative increase over time) was evaluated by fitting a first-order association model, as proposed by Bhattarai et al. (2016).

5.2.5.3 Determination of degree of protein hydrolysis by o-phthaldialdehyde (OPA) method

The OPA method measures the percentage of free amino groups (-NH2), and it can be used to determine the degree of hydrolysis (DH) resulting from rice protein degradation. Following the procedure described by Jiménez-Munoz et al. (2021), the assay was conducted in 96-well microplates. The digested protein samples were

derivatised with OPA in the presence of 2-mercapto-ethane sulfonic acid, which produced 1-alkylthio-2-alcylisonindol compound, whose concentration was measured using a UV/VIS spectrophotometer (SpectraMax M5 microplate reader, Molecular Devices, US) at 335 nm. Digested fluids containing enzymes, but no samples were used as blanks, and the obtained OPA values were subtracted from the OPA values of the sample. The results were calculated using a standard L-glutamic acid curve (0–8 mM in 0.5M perchloric acid). The resulting absorbance values were converted to free amino groups (mmol/L as mmol of glutamic acid equivalents). The DH (%) was calculated with **Eq.5.3**.

$$\mathbf{DH} = \frac{\mathbf{h}}{\mathbf{h_{tot}}} \times \mathbf{100}\,\% \quad \textbf{(Eq. 5.3)}$$

Where:

h is the amount of free amino groups expressed in glutamic acid equivalents (g/L; based on 147.13 g/mol glutamic acid molar mass, used as an average mass for the amino acid population).

h_{tot} is the total concentration of rice protein in the original dispersion (g/L).

5.2.6 Analyses of starch digestion kinetics and predicted glycaemic index

Starch digestibility curves (in **Section 5.2.5.1**) can be used to estimate and predict key nutritional indices (Edwards et al., 2014, 2018). The kinetic models used in this study are the same illustrated and summarised in **Fig. 5.2.**

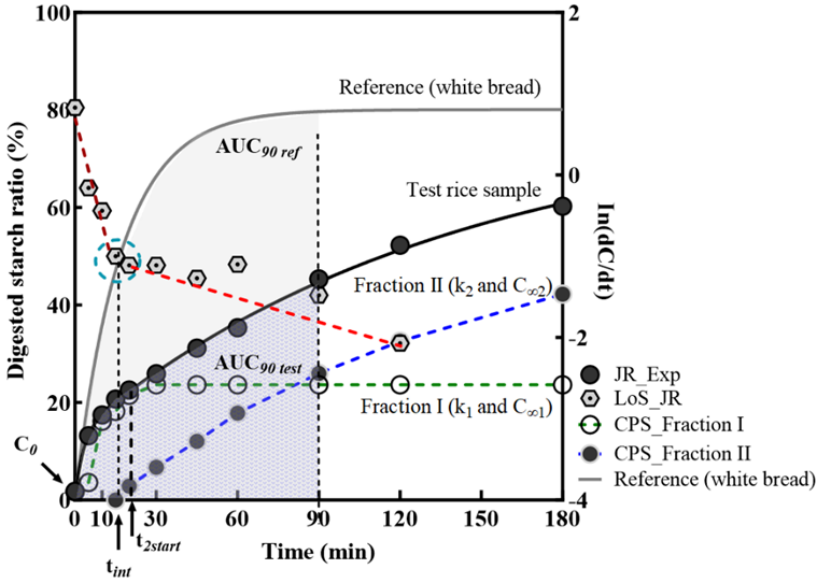


Fig. 5.2. Schematic of kinetic models applied on starch digestibility curve. According to the starch digestibility curve, the dots represent the proportion of starch digested by enzymes as a function of time. On the starch digestibility curve (black line), the dots indicate the percentage of starch digested by enzymes over time. The percentage of starch digested at the endpoint of each reaction is calculated with k_1 and k_2. The $C_{\infty total}$ is calculated by combining C_0, $C_{\infty 1}$ and $C_{\infty 2}$. By comparing the incremental AUC of the rice sample with that of the reference food (white bread), HI is calculated. Figure adapted from Edwards et al. (2014, 2018).

5.2.6.1 Logarithm of slope (LoS) fitting of starch digestion curve

A first-order kinetic model can describe the starch digestion curve as $C_t = C_\infty\left(1 - e^{-kt}\right)$. Here, C_t represents the concentration of maltose (digested starch) at a given time. C_∞ is the estimated concentration at the endpoint of digestion, and k is the digestion rate constant. These two values can be calculated by analysing the logarithm of the slope (LoS) plot form as $\ln\left(\frac{dC}{dt}\right) = \ln(C_\infty k) - kt$, as Butterworth et al. (2012) reported.

Linearised first-order kinetic models generally describe simple starch substrates digested at a single rate, such as rice starch isolates (Li et al., 2021). For more complex substrates involving lipids and proteins, such as rice or wheat, nonlinear plot modes are more frequently reported (Edwards et al., 2014; Zou et al., 2015; Li & Hu, 2020). Although there could be more phases, biphasic digestogram models with two monophasic digestograms with different rates are commonly used to describe these slope discontinuities. Thus, a first-order equation with a piecewise

function was used to profile the overall starch digestion curve as proposed by Edwards et al. (2014), as shown in **Eq. 5.4**.

$$\mathbf{C_{(t)} = C_{\infty 1} \times \left(1 - e^{-k1 \times t}\right)} + \mathbf{if(t > t_{int}, (C_{\infty 2} \times (1 - e^{-k2 \times (t - t_{int})}), 0)} \quad \textbf{(Eq.5.4)}$$

Where:

t_{int}, the time of intersection of the two plots

k (k_1 and $k_{2)}$ are the respective rate constants

C_∞ ($C_{\infty 1}$ and $C_{\infty 2}$) is the predicted digested starch proportion at the reaction endpoint of each digestion fraction.

If the digestion curve is a linear phase, t_{int} does not exist, and only the first part of this **Eq. 5.4** applies.

5.2.6.2 Combination of parallel and sequential (CPS) kinetic model fitting starch digestion curve

The combination of parallel and sequential (CPS) kinetic model proposed by Li et al. (2020) was applied in the digestion curve, as shown **Eq. 5.5**.

$$\mathbf{C_{(t)} = C_{\infty 1} \times \left(1 - e^{-k1 \times t}\right)} + \mathbf{if(t > t_{2start}, (C_{\infty 2} \times (1 - e^{-k2 \times (t - t_{2start})}). 0)} \quad \textbf{(Eq. 5.5)}$$

The CPS kinetic model utilises some of the parameters used in the LoS model (C_0, $C_{\infty 1}$, $C_{\infty 2}$, k_1 and k_2), with the addition of a parameter called t_{2start}. When t_{2start} = 0, it follows the parallel digestion pattern (fractions I and II digest simultaneously). If $t_{2start} > t_{int}$, the sequential digestion pattern (fraction II follows fraction I) is followed. If $0 < t_{2start} \leq t_{int}$, a combination of parallel and sequential digestion patterns (as in parallel, but fraction II continues while fraction I become negligible) occurs (Li et al., 2020).

5.2.6.3 Predicted glycaemic index

Predicted glycaemic index (pGI) is an approach to estimate a food's impact on the glycaemic index based on its digestibility. This work simulated the digestion of

cooked rice samples in a three-stage static *in vitro* digestion model with enzyme complexes (human α-amylase, pepsin, and pancreatin) (Set 7, **Section 5.2.4**).

The hydrolysis index (HI, as shown in **Fig. 5.2**) was the ratio (%) as the area under the digestibility curve up to 90 mins ($AUC90_{sample}$) of the test sample compared with white bread as the reference food ($AUC90_{reference}$). The pGI was calculated based on **Eq. 5.6** (Tamura, 2016).

$$\mathbf{pGI} = \mathbf{39.71} + \mathbf{0.549HI} \quad \textbf{(Eq.5.6)}$$

5.2.8 Measurement of the particle size distribution in digested fluid

After finishing Set 7 (**Section 5.2.4**), 5mL of digested fluid was withdrawn and mixed with 5mL of stop solution (1:1 v/v). The mixture was then kept at ambient temperature without interruption for 10 mins for segmentation. The particle size distribution of the digested fluid from the segmented digested sample was measured using a laser diffraction particle size analyser with a liquid system module (LS 13 320, Beckman Coulter, Inc., Buckinghamshire, UK).

5.2.9 Statistical analysis

Using Statistical Package for Social Science Software (version 27, Chicago, USA), a one-way ANOVA was used to determine the difference between samples. Tukey's test was used to determine the significance of the average ($p < 0.05$) when there were any differences between samples.

5.3 Results

5.3.1 Sample condition

The main composition and texture properties of cooked JR and PR, with/without 1 % LAGG, are reported in **Tab. 5.2**. Both JR and PR, cooked with and without LAGG, had similar moisture content - ~60 % (w/w) - as reported previously (Dibba et al., 1991; Felix et al., 2013). The total starch content did not differ among all four samples, whereas amylose and protein content were significantly higher in PR and PR_1LA than in JR and JR_1LA. The higher amylose content in PR than in JR agrees with previous studies (Ong & Blanshard, 1995; Gong et al., 2019).

As for texture characteristics, PR had a higher hardness but a lower adhesiveness than JR, which might be due to the increased strength of the protein-starch matrices in rice obtained through parboiling (Gong et al., 2019). Moreover, JR_1LA and PR_1LA had lower adhesiveness than JR, possibly due to the LAGG-coating effect (Chung et al., 2007).

After homogenisation for 20 s, the proportion of grain fragments that passed through the sieve (< 1mm) in PR and PR_1LA was significantly higher than in JR and JR_1LA (values in **Tab. 5.2**), indicating a tendency for the more brittle grain (PR) to break into smaller fragments under certain processing condition. Similar results were also shown for *in vivo* masticated cooked rice (Jalabert-Malbos et al., 2007; Kataoka et al., 2013).

Tab. 5.2. Proximate analysis (g/100g) and mechanical properties of cooked JR, JR_1LA, PR, and PR_1LA.

Rice type	JR	JR_1LA	PR	PR_1LA
Moisture content	62.85 ± 2.81[a]	62.80 ± 2.06[a]	62.54 ±0.60[a]	62.92 ± 0.85[a]
Protein	2.64 ± 0.32[b]	2.64 ± 0.24[b]	3.32 ± 0.53[a]	3.30 ± 0.77 [a]
Total starch	32.33 ± 1.92[a]	32.00 ± 0.99[a]	30.25 ± 1.62 [a]	30.28 ± 1.70[a]
In which amylose	5.49 ± 0.99[b]	5.70 ± 1.06[b]	8.08± 0.43 [a]	7.79 ± 0.51[a]
Hardness (N)	42.69 ± 1.09[a]	47.12 ± 1.67 [a]	51.20 ± 1.81 [a]	50.47 ± 1.3[a]
Adhesiveness (N/s)	9.88 ± 0.39[a]	10.31 ± 0.43 [a]	10.92 ± 0.26[a]	9.80 ± 0.60[a]
d(50)* (mm)	0.86 ± 0.11[b]	1.00 ± 0.12 [a]	0.88 ± 0.08[b]	0.89± 0.13[b]

Mean ± S.D. values in the same row with different superscripts are significantly different from each other ($p < 0.05$).

*Median particle size *d*(50) refers to the theoretical mesh size through which 50 % of the rice mass after 20 s homogenisation could pass)

Protein compositions of the four rice samples before and after cooking were analysed using non-reducing and reducing SDS-PAGE, as shown in **Fig. 5.3A** and **B**.

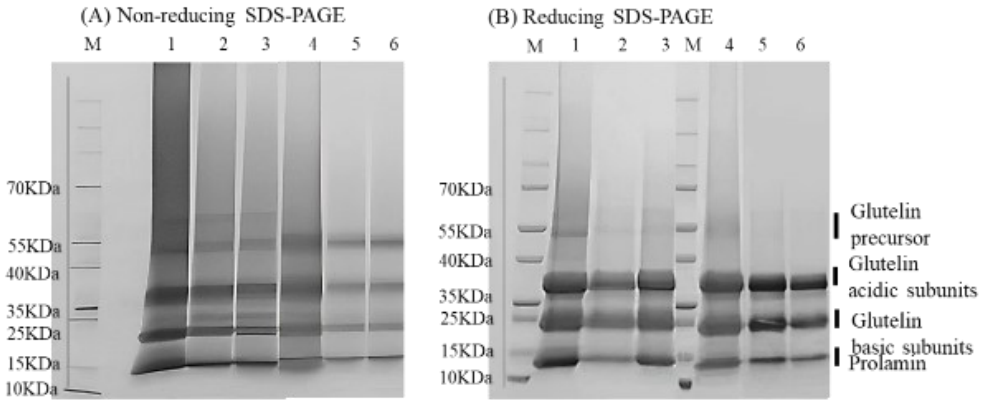


Fig. 5.3. SDS-PAGE patterns of rice proteins under (A) non-reducing and (B) reducing conditions. M: Molecular weight marker proteins. For both (A) and (B), lines 1–3 represent raw JR, cooked JR and cooked JR_1LA, respectively; lines 4-6 represent raw PR, cooked PR and cooked PR_1LA, respectively.

With SDS-PAGE under the non-reducing conditions (**Fig. 5.3A**), high molecular weight proteins over 55 kDa were detected in JR and JR_1LA but not in PR and PR_1LA. The absence of the high molecular weight band in PR may be attributed to the disruption of disulfide bonds during the parboiling process (Derycke et al., 2005). Moreover, the JR rice protein profile appears not to have been altered by cooking since the same band pattern was observed in raw and cooked rice with and without 1 % LAGG. With SDS-PAGE under reducing conditions (**Fig. 5.3B**), the bands > 55 kDa in JR samples (lines 1-3) tended to disappear after cooking (especially for JR) with

two low-weight protein bands at 22-23 kDa and 37-39 kDa becoming more visible (**Fig. 5.3B**), indicating the initial presence of a polymeric form stabilised by disulfide bonds in JR samples. The results also suggest that the LAGG did not interfere with the protein extraction process. The absence of further bands in rice protein with LAGG suggested that complexes of LAGG covalently bound to protein fractions were not detectable.

5.3.2 Protein digestion

The protein digestion during the gastric and intestinal phases from non-homogenised (intact grains), and homogenised rice samples, both cooked, under 6 different proteolysis conditions (Set 1 to Set 6), is presented in this section. The quantitative description of protein digestion kinetics was performed using a first-order kinetic model (Bhattarai et al., 2016).

5.3.2.1 The effects of different proteolysis conditions

In **Fig. S1**, the DSPF (%) and DH (%) for Set 1 to Set 6 are presented as time functions. The estimated kinetic parameters are shown in **Tab. 5.3**. The analysis first point (t= 0) corresponds to the end of the gastric phase and simultaneously to the beginning of the intestinal phase after adding the SIF (pH=7) to terminate the existing pepsin activity (Pletsch & Hamaker, 2018; Wang et al., 2017). The oral phase is not included, as protein digestion is negligible in this phase.

For Set 1_A and Set 2_P, as shown by Y_0 (i.e., the percentage of digested protein at the beginning of the intestinal phase), most protein remains undigested in all samples in the gastric phase (digested protein less than 2 %; **Tab 5.3**), suggesting the acidic environment without pepsin cannot induce sufficient protein digestion. During the intestinal phase, though, the presence of protease (pancreatin) in Set 2_P allowed substantial release of DSPF, and hydrolysates compared to Set 1_A (control), where only α-amylase was used, which is known to be responsible for starch digestion primarily. Despite the absence of protease, DSPF and DH increased over time, although to a much lower extent than for the other sets. The increase in DSPF and DH in Set 1_A could depend on the diffusion of the digestion solution and starch digestion, which would both promote the dissolution of protein networks. Trypsin remaining active in the α-amylase product may also contribute to releasing protein fragments.

When pepsin was included in the digestion model (Set 3 to Set 6), significantly higher DSPF and DH were observed in comparison with Set 1_A and Set 2_P (**Fig 5.4**), as also shown by the Y_0 values in **Tab 5.3**, which also increased intestinal protein digestion rates and extents. Kinetic analysis of the intestinal phase revealed significantly higher K and Span values in the presence of pancreatin (Set 4_PP) compared to only α-amylase (Set 3_PA). Results showed that both DSPF and DH rates and extent in Set 6_PTA were significantly higher than any other digestion conditions. In rice grains treated with trypsin, the increased hydrolysis may be caused by the degradation of the protein networks, which is detectable in the control but barely visible after treatment with trypsin, in accordance with microscopy observation (**Fig. 5.4A** and **B**).

Tab. 5.3. Kinetic parameters of DSPF (BCA method) and DH (OPA method) in cooked rice digested under different conditions, evaluated by fitting a pseudo-first-order association model (Case 1: intact rice).

		DSPF					DH				
		K_{DSPF} (min^{-1})	$Y_{\infty DSPF}$ (%)	$Y_{0\ DSPF}$ (%)	$Span_{DSPF}$ (%)	R^2	K_{DH} (min^{-1})	$Y_{\infty DH}$ (%)	$Y_{0\ DH}$ (%)	$Span_{DH}$ (%)	R^2
JR	A	0.004±0.001 ^{c}	7.38 ± 1.18^{c}	1.66 ± 0.07^{c}	5.71 ± 1.15 ^{c}	0.9544	0.004 ± 0.001^{a}	6.41 ± 0.34^{c}	1.38 ± 0.30^{c}	5.03 ± 0.14^{c}	0.9544
	P	0.009 ± 0.001 ^{b}	11.96 ± 3.01^{b}	1.50 ± 0.09 ^{c}	10.46 ± 2.52^{b}	0.9823	0.008 ± 0.002^{b}	15.57 ± 1.84^{b}	1.44 ± 0.27^{c}	14.12 ± 1.57^{a}	0.9823
	PA	0.007 ± 0.003 ^{b}	15.61 ± 1.25^{bc}	8.99 ± 0.37 ^{b}	6.62 ± 1.28^{c}	0.9243	0.007 ± 0.003^{b}	15.31 ± 0.29^{b}	5.72 ± 0.24^{b}	9.58 ± 0.15^{bc}	0.9243
	PP	0.013 ± 0.004 ^{b}	19.75 ± 1.11^{b}	9.17 ± 0.49 ^{b}	10.57 ± 0.91^{b}	0.9678	0.014 ± 0.001^{b}	16.51 ± 0.24^{b}	6.39 ± 0.35^{b}	10.12 ± 0.20^{b}	0.9678
	PTA_con	0.009 ± 0.001 ^{b}	22.38 ± 0.57^{b}	9.74 ± 0.10 ^{b}	12.64 ± 0.66^{c}	0.9954	0.010 ± 0.003^{b}	16.01 ± 1.04^{b}	7.30 ± 0.10^{b}	8.71 ± 1.13^{bc}	0.9954
	PTA	0.027 ± 0.002 ^{a}	39.10 ± 0.75^{a}	18.64 ± 0.16^{a}	20.46 ± 0.65^{a}	0.9416	0.024 ± 0.001^{a}	31.91 ± 2.41^{a}	17.05 ± 1.34^{a}	14.86 ± 0.64^{a}	0.9416
From Set 1_A to Set 6_PTA in JR, different letters over each column indicate significant differences ($p < 0.05$)											
		K_{DSPF} (min^{-1})	$Y_{\infty DSPF}$ (%)	$Y_{0\ DSPF}$ (%)	$Span_{DSPF}$(%)	R^2	K_{DH} (min^{-1})	$Y_{\infty DH}$ (%)	$Y_{0\ DH}$ (%)	$Span_{DH}$ (%)	R^2
JR-1LA	A	0.004 ± 0.002 ^{c}	4.46 ± 0.65 ^{c}	1.38 ± 0.12 ^{c}	3.08 ± 0.69 ^{c}	0.9361	0.004 ± 0.001 ^{c}	3.93 ± 0.75 ^{c}	0.51 ± 0.05 ^{c}	3.42 ± 0.74^{c}	0.9444
	P	0.008 ± 0.001 ^{bc}	13.10 ± 1.70 ^{bc}	1.19 ± 0.17 ^{c}	11.90 ± 1.63 ^{b}	0.9928	0.007 ± 0.001 ^{bc}	12.21 ± 0.60 ^{b}	0.46 ± 0.12 ^{c}	11.75 ± 0.63^{b}	0.9933
	PA	0.007 ± 0.001 ^{bc}	10.93 ± 1.69 ^{c}	3.78 ± 1.12 ^{b}	7.15 ± 1.73 ^{bc}	0.9790	0.005 ± 0.002 ^{c}	6.90 ± 1.85 ^{c}	1.84 ± 0.10 ^{b}	5.06 ± 1.75^{c}	0.9495
	PP	0.013 ± 0.002 ^{b}	17.97 ± 0.25 ^{b}	5.19 ± 1.08 ^{b}	12.78 ± 1.30 ^{b}	0.9325	0.013 ± 0.002 ^{b}	13.23 ± 2.23 ^{b}	2.01 ± 0.31^{b}	11.22 ± 2.51^{b}	0.9325
	PTA_con	0.011 ± 0.003 ^{b}	9.46 ± 1.16 ^{c}	4.07 ± 1.23 ^{b}	5.39 ± 0.93 ^{c}	0.9645	0.010 ± 0.002 ^{b}	8.59 ± 7.09 ^{b}	2.62 ± 0.32 ^{b}	5.97 ± 6.79^{bc}	0.9656
	PTA	0.024 ± 0.002 ^{a}	24.73 ± 0.40 ^{a}	6.21 ± 0.97 ^{a}	18.51 ± 0.78 ^{a}	0.9811	0.022 ± 0.001 ^{a}	23.02 ± 1.66 ^{a}	6.21 ± 0.66 ^{a}	16.81 ± 1.04^{a}	0.9610
From Set 1_A to Set 6_PTA in JR_1LA, different letters over each column indicate significant differences ($p < 0.05$)											

K_{DSPF} and K_{DH} represent the reaction rate constants; Y_{0DSPF} and Y_{0DH} are the DSPF and DH at time 0; $Y_{\infty DSPF}$ and $Y_{\infty DH}$ are the estimated DSPF and DH at the end of the digestion process; $Span_{DSPF}$ and $Span_{DH}$ are DSPF and DH in the intestinal phase, calculated as $Y_{\infty DSPF}$ - Y_{0DSPF} and $Y_{\infty DH}$- $Y_{0DH,}$ respectively.

		DSPF					DH				
		K_{DSPF} (min^{-1})	$Y_{\infty DSPF}$ (%)	$Y_{0\ DSPF}$ (%)	$Span_{DSPF}$(%)	R^2	K_{DH} (min^{-1})	$Y_{\infty DH}$ (%)	$Y_{0\ DH}$ (%)	$Span_{DH}$ (%)	R^2
PR	A	0.003 ± 0.001^{c}	6.09 ± 1.44^{c}	1.49 ± 0.02^{c}	4.61 ± 1.43^{c}	0.9919	0.004 ± 0.001^{c}	3.93 ± 0.75^{d}	0.51 ± 0.05^{c}	3.42 ± 0.74^{c}	0.9444
	P	0.007 ± 0.001^{bc}	9.97 ± 0.53^{c}	1.03 ± 0.02^{c}	8.94 ± 0.56^{b}	0.9518	0.007 ± 0.002^{c}	13.21 ± 0.60^{b}	0.46 ± 0.12^{c}	12.75 ± 0.63^{b}	0.9933
	PA	0.009 ± 0.003^{bc}	8.63 ± 0.95^{c}	4.05 ± 0.17^{b}	5.58 ± 0.78^{bc}	0.9095	0.005 ± 0.002^{c}	6.90 ± 1.85^{c}	1.84 ± 0.10^{b}	5.06 ± 1.75^{c}	0.9495
	PP	0.014 ± 0.001^{b}	18.19 ± 1.35^{b}	4.37 ± 1.11^{b}	13.83 ± 1.39^{a}	0.9908	0.013 ± 0.002^{b}	13.23 ± 2.23^{b}	2.01 ± 0.31^{b}	11.22 ± 2.51^{b}	0.9325
	PTA_con	0.009 ± 0.001^{bc}	16.91 ± 1.11^{b}	4.38 ± 1.11^{b}	12.53 ± 1.20^{a}	0.9818	0.010 ± 0.002^{b}	12.59 ± 7.09^{b}	2.62 ± 0.32^{b}	9.97 ± 6.79^{b}	0.9656
	PTA	0.026 ± 0.004^{a}	29.24 ± 0.26^{a}	13.63 ± 0.22^{a}	15.61 ± 0.45^{a}	0.9385	0.022 ± 0.001^{a}	23.02 ± 1.66^{a}	6.21 ± 0.66^{a}	16.81 ± 1.04^{a}	0.9610
From Set 1_A to Set 6_PTA in PR, different letters (a–d) over each column indicate significant differences ($p < 0.05$)											
	A	K_{DSPF} (min^{-1})	$Y_{\infty DSPF}$ (%)	$Y_{0\ DSPF}$ (%)	$Span_{DSPF}$(%)	R^2	K_{DH} (min^{-1})	$Y_{\infty DH}$ (%)	$Y_{0\ DH}$ (%)	$Span_{DH}$ (%)	R^2
PR_1LA	P	0.003 ± 0.001^{c}	2.30 ± 0.41^{c}	0.35 ± 0.04^{c}	1.95 ± 0.37^{c}	0.9581	0.003 ± 0.001^{c}	2.43 ± 0.41^{d}	0.19 ± 0.01^{d}	2.25 ± 0.37^{d}	0.9664
	PA	0.006 ± 0.002^{bc}	9.54 ± 3.20^{bc}	0.35 ± 0.06^{c}	9.19 ± 3.14^{b}	0.9909	0.006 ± 0.002^{bc}	9.83 ± 1.75^{b}	0.32 ± 0.14^{d}	9.51 ± 1.67^{b}	0.9912
	PP	0.010 ± 0.002^{bc}	6.64 ± 0.36^{c}	2.64 ± 0.57^{b}	4.00 ± 0.39^{c}	0.9530	0.005 ± 0.001^{c}	6.89 ± 1.30^{c}	1.74 ± 0.13^{c}	5.15 ± 0.24^{c}	0.9836
	PTA_con	0.014 ± 0.003^{b}	11.99 ± 0.80^{b}	3.66 ± 0.72^{b}	8.32 ± 0.69^{b}	0.9499	0.010 ± 0.002^{b}	12.00 ± 0.87^{b}	1.41 ± 0.43^{c}	10.59 ± 1.44^{ab}	0.9761
	PTA	0.011 ± 0.003^{b}	12.66 ± 1.13^{b}	5.34 ± 1.27^{b}	7.32 ± 0.86^{b}	0.9636	0.012 ± 0.001^{b}	10.14 ± 0.23^{b}	3.50 ± 0.43^{b}	6.64 ± 0.57^{c}	0.9456
	A	0.018 ± 0.000^{a}	22.87 ± 0.25^{a}	8.87 ± 0.14^{a}	14.00 ± 0.25^{a}	0.9961	0.023 ± 0.001^{a}	20.49 ± 0.83^{a}	7.10 ± 0.45^{a}	13.40 ± 1.17^{a}	0.9841
From Set 1_A to Set 6_PTA in PR_1LA, different letters (a–d) over each column indicate significant differences ($p < 0.05$)											

K_{DSPF} and K_{DH} represent the reaction rate constants; Y_{0DSPF} and Y_{0DH} are the DSPF and DH at time 0; $Y_{\infty DSPF}$ and $Y_{\infty DH}$ are the estimated DSPF and DH at the end of the digestion process; $Span_{DSPF}$ and $Span_{DH}$ are DSPF and DH in the intestinal phase, calculated as $Y_{\infty DSPF}$ - Y_{0DSPF} and $Y_{\infty DH}$- $Y_{0DH,}$ respectively.

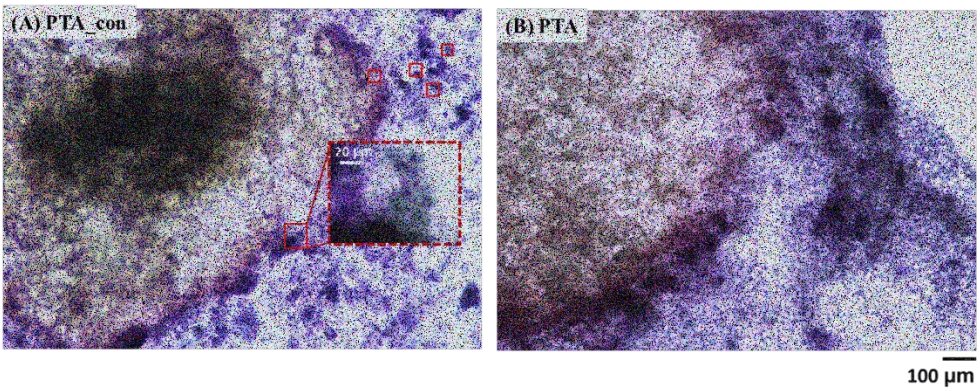


Fig. 5.4. Microstructural comparison of JR grain (upon gastric digestion with pepsin) following 2h incubation with (B) (Set 6_PTA) or without (A) (Set 5_PTA_con) trypsin proteolysis. In (A), it is observed in the disintegrated grain factions that the remaining protein networks (green) embed the starch granules (purple) but not in (B). Trypsin hydrolyses proteins, decreasing the matrix effect and revealing more individual starch granules.

5.3.2.2 Protein digestion differs by rice type.

Although PR displayed similar protein digestion behaviour to JR under different conditions, differences could be identified by kinetic analysis (shown in **Tab 5.3**). Similar to JR, as the complexity of the digestion set systematically increased from Set 1_A to Set 6_PTA, the rate and extent of DSPF release and DH in PR gradually increased and became significantly higher under Set 4_PP and Set 6_PTA than Set 1_A. Unlike JR, PR has comparable Span values for Set 4_PP and Set 6_PTA. Set 6_PTA with pre-proteolysis with trypsin, DSPF and DH reached a plateau at 60 mins after α-amylase was introduced (**Fig. S1**). As a result, although the digestion rate in PR differs from Set 4-5 (linear increase) and Set 6 (increase with plateau), the amount of digested protein at the end of digestion (Span, %) was similar. This suggests that pre-proteolysis can be more effective than increasing the total amount of digestible protein.

5.3.2.3 The effect of LAGG-coating

The digestibility of proteins in the cooked rice with and without LAGG was similar when the digestion sets were identical, as shown in **Fig. S1A2**, **B2**, **A4**, and **B4**. Based on the kinetic modelling (shown in **Tab. 5.3**), there were no significant differences in the K of DSPF and DH in both JR and PR with and without LAGG, digested with the

same set. However, under similar K_{DSPF} and K_{DH}, Y_∞ of DSPF and DH were lower when LAGG was present, particularly when pepsin was involved, as in Set 3_P, Set 4_PP and Set 6_PTA.

As shown in **Tab. 5.3,** Y_0 of JR_1LA and PR_1LA is less than half compared to those in JR and PR, suggesting that LAGG suppresses protein digestion with pepsin under gastric conditions. This is likely a result of the more compact microstructure of rice due to the presence of a LAGG gel coating, whose strength would be enhanced at pH 3 and further restrict the diffusion of pepsin (gastric conditions) (Bradbeer et al., 2015). This is in line with the results reported by Santos & Cunha (2018); self-structured gels are known to exhibit greater cohesiveness (higher rupture stresses) at acidic conditions due to hydrogen ions bounding to available anionic sites on the LAGG, causing decreased distance between the helices of LAGG.

During the intestinal phase, hydrolysis continued with trypsin for 180 mins. DSPF and DH were lower in JR_1LA and PR_1LA than in JR and PR (values in **Tab. 5.3**), perhaps due to the physical barrier provided by LAGG remaining stable in the intestinal phase and reducing the accessibility of trypsin to proteins. These findings are supported by a study by de Silva et al. (2015) on the degradation behaviour of LAGG hydrogel after immersion in trypsin solution for 42 days. LAGG gel swelling was observed (swelling ratio of 45 %) due to hydration, but the gel structure remained stable with a mass loss of less than 10 %. A further possibility could be a reduced trypsin activity due to a shortage of calcium ions previously cross-linked with LAGG gel. By preventing the formation of inert enzyme aggregates during digestion, calcium ions in SIF solution ensure that trypsin activity is maintained (Bergmeyer et al., 1983). In the presence of LAGG, calcium ions can reduce the negative charge of LAGG to a greater degree than hydrogen ions due to their ability to cross-link one pair of helices (Morris et al., 2012; Santos & Cunha, 2018).

However, the suppression effect of LAGG was diminished when α-amylase was present (Set 6_PTA). As shown in **Tab. 5.3**, there was no significant difference in Span and K in both rice types with and without LAGG. One explanation is that digested starch released from the matrix exposed more proteins, thus proteolytic

sites for trypsin. Reactivating inert trypsin is another possibility when the α-amylase is added to the system. Pancreatic α-amylase contains calcium and can be hydrolysed by trypsin, providing external calcium ions to provoke more trypsin activity (Hsiu et al., 1964; Granger et al., 1975).

5.3.2.4 The effect of homogenisation

After undergoing homogenisation (**Fig. S8**), all rice samples, regardless of their types and whether LAGG was added, had higher protein digestibility than their intact counterparts, as showed by the higher Y_{0DSPF}, K_{DSPF} and $Y_{\infty DSPF}$ in the homogenised samples (**Tab. 5.4**), especially from Sets 2_P to 6_PTA, i.e., when proteinase was involved in the digestion. The higher DSPF in homogenised rice could result from grain structure disintegration due to homogenisation. However, for the homogenised samples, DH from Set 1_A and Set 2_P does not significantly differ from the intact samples, whereas a significant increase in DH was observed following the introduction of the pepsin in the digestion protocol (from Set 3_PA onward). This suggests that a proteolytic enzyme is still the initial factor for protein hydrolysis. Moreover, introducing a trypsin incubation step further increases DSPF and DH, as shown in Set 6_PTA. Besides trypsin hydrolysis, an increase in protein digestion was also observed in Set 5_PTA_con, which may be due to the dissolution effect of the digestive solution after three hours of incubation. In fact, at Y_0, Set 5_PTA_con had slightly higher DSPF and DH than Set 3_PA, which has the same enzyme composition as Set 5_PTA_con but no incubation step. Interestingly, by comparing those two sets, the protein digestion increase was only observed after introducing the α-amylase into the system. The results indicate that α-amylase can also assist in protein digestion during incubation by facilitating protease dissolution.

In homogenised PR, DSPF reached a similar final digestion amount as DH and followed a similar protein digestion rate (**Fig. S8C1** and **C2**, and **Tab. 5.4**). $Y_{\infty DSPF}$ and $Y_{\infty DH}$ values of homogenised PR remained lower than those of homogenised JR. Given the similar composition of proteins in JR and PR, as shown by SDS-PAGE in **Fig. 5.3**, this indicates a more ordered structure of the protein-starch matrices, which may limit the accessibility of enzymes.

Tab. 5.4. Kinetic parameters of DSPF (BCA method) and DH (OPA method) in cooked rice digested under different conditions, evaluated by fitting a pseudo-first-order association model (Case 2: homogenised rice).

		DSPF					DH				
		K_{DSPF} (min^{-1})	$Y_{\infty DSPF}$ (%)	$Y_{0\ DSPF}$ (%)	$Span_{DSPF}$ (%)	R^2	K_{DH} (min^{-1})	$Y_{\infty DH}$ (%)	$Y_{0\ DH}$ (%)	$Span_{DH}$ (%)	R^2
JR	A	0.005 ± 0.001 ^{d}	14.23 ± 0.24 ^{e}	3.27 ± 0.25 ^{c}	10.96 ± 1.49 ^{d}	0.9689	0.007 ± 0.003 ^{c}	8.05 ± 1.71 ^{d}	1.45 ± 0.24 ^{d}	6.60 ± 1.47 ^{c}	0.9630
	P	0.013 ± 0.001 ^{c}	21.92 ± 2.28 ^{d}	3.69 ± 0.16 ^{c}	18.24 ± 1.26 ^{c}	0.9793	0.013 ± 0.003 ^{b}	16.51 ± 1.85 ^{c}	2.64 ± 0.59 ^{d}	12.87 ± 0.77 ^{b}	0.9664
	PA	0.011 ± 0.002 ^{c}	13.72 ± 1.80 ^{e}	8.89 ± 0.37 ^{b}	5.47 ± 0.86 ^{e}	0.9672	0.012 ± 0.002 ^{b}	14.56 ± 1.53 ^{c}	5.44 ± 0.40 ^{c}	11.13 ± 1.39 ^{b}	0.9751
	PP	0.028 ± 0.003 ^{b}	33.65 ± 2.79 ^{b}	9.64 ± 1.35 ^{b}	24.02 ± 2.59 ^{b}	0.9820	0.028 ± 0.003 ^{a}	21.32 ± 1.29 ^{b}	7.24 ± 0.38 ^{c}	14.08 ± 2.21 ^{b}	0.9224
	PTA_con	0.024 ± 0.002 ^{b}	27.10 ± 0.74 ^{c}	11.22 ± 1.19 ^{b}	15.21 ± 2.19 ^{c}	0.9543	0.016 ± 0.001 ^{b}	25.04 ± 2.35 ^{b}	11.15 ± 0.04 ^{b}	13.90 ± 1.33 ^{b}	0.9917
	PTA	0.033 ± 0.002 ^{a}	54.65 ± 1.28 ^{a}	21.51 ± 0.30 ^{a}	33.16 ± 0.30 ^{a}	0.9804	0.036 ± 0.005 ^{a}	41.22 ± 0.39 ^{a}	19.15 ± 1.24 ^{a}	22.08 ± 2.15 ^{a}	0.9473
From Set 1_A to Set 6_PTA in JR, different letters over each column indicate significant differences ($p < 0.05$)											
		K_{DSPF} (min^{-1})	$Y_{\infty DSPF}$ (%)	$Y_{0\ DSPF}$ (%)	$Span_{DSPF}$(%)	R^2	K_{DH} (min^{-1})	$Y_{\infty DH}$ (%)	$Y_{0\ DH}$ (%)	$Span_{DH}$ (%)	R^2
JR_1LA	A	0.005 ± 0.002 ^{c}	9.16 ± 2.28 ^{c}	2.52 ± 0.09 ^{d}	6.64 ± 2.22 ^{c}	0.9362	0.005 ± 0.00 ^{c}	5.58 ± 0.35 ^{c}	1.16 ± 0.05 ^{c}	4.42 ± 0.30 ^{c}	0.9511
	P	0.012 ± 0.001 ^{b}	19.52 ± 1.42 ^{b}	2.69 ± 0.16 ^{d}	16.88 ± 1.45 ^{b}	0.9886	0.008 ± 0.002 ^{bc}	21.52 ± 3.70 ^{b}	1.47 ± 0.41 ^{c}	20.06 ± 3.29 ^{a}	0.9747
	PA	0.010 ± 0.000 ^{b}	10.46 ± 0.15 ^{c}	4.21 ± 0.37 ^{c}	6.25 ± 1.20 ^{c}	0.9831	0.005 ± 0.001 ^{c}	19.56 ± 5.13 ^{b}	1.37 ± 0.37 ^{c}	18.19 ± 4.65 ^{b}	0.9673
	PP	0.012 ± 0.003 ^{b}	22.20 ± 2.08 ^{b}	6.81 ± 1.35 ^{b}	21.14 ± 2.45 ^{a}	0.9740	0.014 ± 0.003 ^{b}	25.06 ± 1.63 ^{b}	1.56 ± 0.79 ^{c}	23.50 ± 1.46 ^{a}	0.9751
	PTA_con	0.013 ± 0.001 ^{b}	19.53 ± 1.42 ^{b}	9.78 ± 1.19 ^{b}	12.20 ± .43 ^{b}	0.9962	0.010 ± 0.001 ^{b}	19.26 ± 2.60 ^{b}	4.52 ± 0.12 ^{b}	14.74 ± 2.71 ^{b}	0.9948
	PTA	0.031 ± 0.004 ^{a}	35.00 ± 0.81 ^{a}	19.49 ± 3.30 ^{a}	22.54 ± 1.98 ^{a}	0.9664	0.032 ± 0.002 ^{a}	33.08 ± 1.37 ^{a}	10.65 ± 0.25 ^{a}	22.43 ± 0.41 ^{a}	0.9811
From Set 1_A to Set 6_PTA in JR_1LA, different letters over each column indicate significant differences ($p < 0.05$)											

K_{DSPF} and K_{DH} represent the reaction rate constants; Y_{0DSPF} and Y_{0DH} are the DSPF and DH at time 0; $Y_{\infty DSPF}$ and $Y_{\infty DH}$ are the estimated DSPF and DH at the end of the digestion process; $Span_{DSPF}$ and $Span_{DH}$ are DSPF and DH in the intestinal phase, calculated as $Y_{\infty DSPF}$ - Y_{0DSPF} and $Y_{\infty DH}$- $Y_{0DH,}$ respectively.

		DSPF					DH				
		K_{DSPF} (min^{-1})	$Y_{\infty DSPF}$ (%)	$Y_{0\ DSPF}$ (%)	$Span_{DSPF}$ (%)	R^2	K_{DH} (min^{-1})	$Y_{\infty DH}$ (%)	$Y_{0\ DH}$ (%)	$Span_{DH}$ (%)	R^2
PR	A	0.007±0.001 ^{d}	10.26±0.52 ^{c}	1.93±0.09 ^{c}	8.33±0.44 ^{a}	0.9495	0.006±0.002 ^{c}	7.54±0.13 ^{e}	0.87±0.13 ^{c}	6.67±1.13 ^{c}	0.9908
	P	0.015±0.002 ^{c}	21.10±1.38 ^{c}	2.15±0.55 ^{c}	18.95±0.55 ^{c}	0.9656	0.019±0.005 ^{b}	18.62±2.78 ^{c}	0.74±0.52 ^{c}	17.88±2.30 ^{b}	0.9549
	PA	0.010±0.001 ^{d}	13.30±1.25 ^{c}	5.60±0.74 ^{b}	7.70±0.26 ^{a}	0.9027	0.009±0.002 ^{c}	13.20±2.07 ^{d}	3.13±0.14 ^{b}	10.07±2.04 ^{c}	0.9605
	PP	0.023±0.001 ^{b}	29.06±1.26 ^{b}	5.95±0.73 ^{b}	23.11±0.54 ^{a}	0.9607	0.016±0.003 ^{b}	27.62±1.06 ^{b}	3.89±0.55 ^{b}	23.73±1.60 ^{a}	0.9701
	PTA_con	0.016±0.001 ^{c}	20.49±2.31^{c}	7.31±1.19 ^{b}	13.17±0.33 ^{b}	0.9335	0.015±0.003 ^{b}	18.02±3.32 ^{c}	5.60±1.35 ^{b}	12.42±2.97 ^{bc}	0.9818
	PTA	0.030±0.001 ^{a}	37.04±1.17 ^{a}	17.63±2.12 ^{a}	19.41±1.18 ^{a}	0.9658	0.027±0.003 ^{a}	34.70±2.21 ^{a}	16.36±2.62 ^{a}	18.35±0.47 ^{b}	0.9385
From Set 1_A to Set 6_PTA in JR, different letters over each column indicate significant differences ($p < 0.05$)											
		K_{DSPF} (min^{-1})	$Y_{\infty DSPF}$ (%)	$Y_{0\ DSPF}$ (%)	$Span_{DSPF}$(%)	R^2	K_{DH} (min^{-1})	$Y_{\infty DH}$ (%)	$Y_{0\ DH}$ (%)	$Span_{DH}$ (%)	R^2
PR_1LA	A	0.003±0.001 ^{d}	7.09±1.44 ^{c}	0.49±0.02 ^{d}	6.61±1.43 ^{c}	0.9919	0.004±0.001 ^{d}	3.19±0.75 ^{d}	0.38±0.05 ^{c}	2.80±0.74^{c}	0.9843
	P	0.007±0.001 ^{c}	9.97±0.53 ^{c}	1.03±0.02 ^{d}	8.94±0.56 ^{b}	0.9518	0.006±0.001 ^{c}	10.60±0.60 ^{c}	0.56±0.12 ^{c}	10.71±0.63^{b}	0.9606
	PA	0.009±0.003 ^{c}	8.63±0.95 ^{c}	4.05±0.17 ^{b}	4.58±0.78 ^{c}	0.9095	0.008±0.002 ^{c}	10.08±1.85 ^{c}	3.04±0.10 ^{b}	7.04±1.75^{b}	0.9116
	PP	0.014±0.001 ^{ab}	18.19±1.35 ^{b}	4.37±1.11 ^{b}	13.83±1.39 ^{a}	0.9908	0.011±0.002 ^{b}	16.89±2.23 ^{b}	3.52±0.31 ^{b}	13.39±2.51^{a}	0.9869
	PTA_con	0.009±0.002 ^{c}	16.91±1.11 ^{b}	4.38±1.27 ^{b}	12.53±1.20 ^{a}	0.9818	0.006±0.002 ^{c}	16.51±7.09 ^{b}	4.69±0.32 ^{b}	14.81±6.79^{a}	0.9592
	PTA	0.018±0.002 ^{a}	22.87±0.25 ^{a}	8.87±0.14 ^{a}	14.00±0.25 ^{a}	0.9961	0.023±0.001 ^{a}	20.49±0.83 ^{a}	7.10±0.45 ^{a}	13.40±1.17^{a}	0.9772
From Set 1_A to Set 6_PTA in JR_1LA, different letters over each column indicate significant differences ($p < 0.05$)											

K_{DSPF} and K_{DH} represent the reaction rate constants; Y_{0DSPF} and Y_{0DH} are the DSPF and DH at time 0; $Y_{\infty DSPF}$ and $Y_{\infty DH}$ are the estimated DSPF and DH at the end of the digestion process; $Span_{DSPF}$ and $Span_{DH}$ are DSPF and DH in the intestinal phase, calculated as $Y_{\infty DSPF}$ - Y_{0DSPF} and $Y_{\infty DH}$- $Y_{0DH,}$ respectively.

During the parboiling process (soaking-steaming-drying), proteins undergo structural modification via intermolecular interactions, aggregation, and network formation, resulting in compact protein aggregates with reduced surface area, which reflects a reduced number of cleavage sites for pepsin exposed to the gastric phase (Derycke et al., 2005; Pal et al., 2018). Since SDS-PAGE profiles did not reveal bands at larger molecular weights in PR, these aggregates are probably caused by hydrophobic interactions between the proteins denatured by heat treatment rather than covalent bonds. During parboiling, the proteins may have unfolded, exposing the hydrophobic residues, then rearranged in a way to reduce exposure of hydrophobic residues, which are the ones preferred by pepsin (Ahn et al., 2013), thus decreasing protein digestibility.

5.3.3 Food model case 1: starch digestibility of cooked grain

5.3.3.1 The effect of protein digestion on starch digestibility

As shown in **Fig. 5.5**, the starch digestion curves of intact JR grains and the relative LoS kinetics (**Section 5.2.6**) are plotted under progressive protein digestion (Sets 1 to 6). As shown in **Tab. 5.5**, the model produced an acceptable fitting of the digestograms (R^2 > 0.9). The model could distinguish between the various starch digestible fractions present within the system, and the observed trend can be explained using the first-order kinetic models (Edwards et al., 2014; Butterworth et al., 2022). In JR, a single digestion pattern was observed in Set 1_A, which agreed with previous studies on rice starch (Li & Hu, 2020) and rice flour (Li et al., 2021). This suggests that most of the starch present in JR is structurally homogeneous, which facilitates its hydrolysis by α-amylase. A significant increase in digested starch was observed during pancreatin digestion (Set 2_P), occurring simultaneously with protein hydrolysis. In Set 2_P, a two-phase digestion pattern was identified, demonstrated by LoS fitting with discontinuity in a linear correlation pattern, suggesting the appearance of heterogeneous digestible fractions. Similar starch digestion patterns have been reported previously in pasta (Zou et al., 2015), cooked wheat noodles (Li et al., 2021), and retrograded rice starch (Gong et al., 2019).

As observed, a first-reaction phase corresponds to a rapidly digestible starch phase (k_1, $C_{\infty 1}$; **Section 5.2.6**), followed by a second reaction phase, which refers to a slowly digestible starch phase (k_2, $C_{\infty 2}$). There was a nearly eight-fold higher digestion rate for the rapid reaction (k_1) compared to the second reaction (k_2). The intersection between the two linear phases of the LoS plot reveals that the slower phase dominates after 20 mins of hydrolysis under the digestibility conditions (pancreatin) used in the experiment. The results are in line with the definition of Englyst et al. (1992) for rapidly digestible starch, which is described as starch types that quickly break down into glucose within 20 mins. The rate constant for the second phase, k_2, is slightly lower than that obtained for single-phase amylolysis (0.015 for Set 2_P vs. 0.019 for Set 1_A).

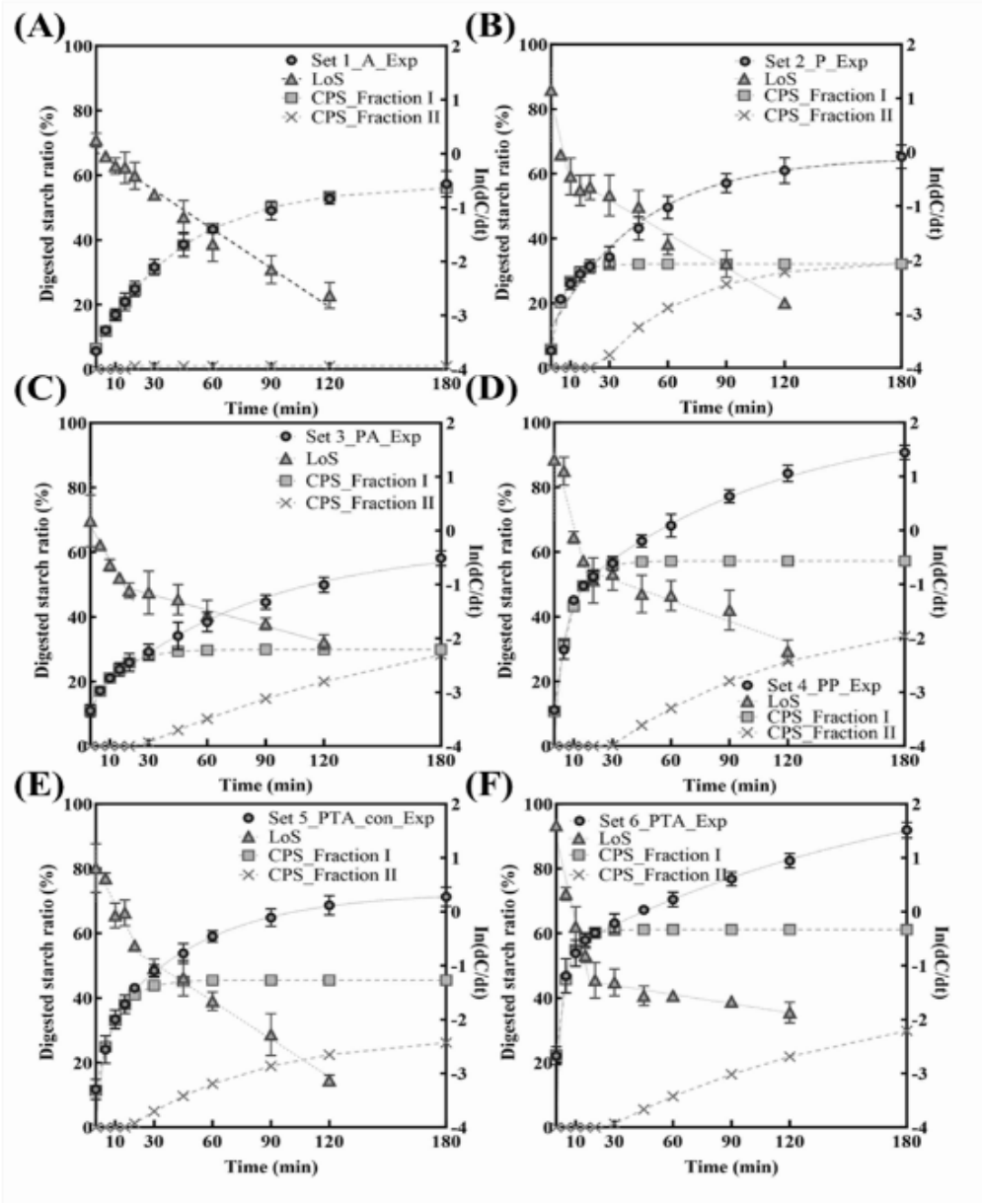


Fig. 5.5. *In vitro* starch digestion of cooked JR grains. Circles correspond to the experimental values; all error bars represent standard deviations (n = 4). Letters A to F represent from Set 1_A to Set 6_PTA; triangles with dashed lines correspond to LoS plots. Squares and crosses correspond to digestible fractions I and II of starch based on CPS kinetics model fittings for the digestion curves.

Tab. 5.5. Kinetic fitting (LoS and CPS) with constant rates fitting for JR and PR with and without 1 % LAGG addition (intact rice).

		C_0 (%)	k_1 (min^{-1})	$C_{\infty 1}$ (%)	t_{int} (min)	k_2 (min^{-1})	$C_{\infty 2}$ (%)	R^2	k_1 (min^{-1})	$C_{\infty 1}$ (%)	t_{2start} (min)	k_2 (min^{-1})	$C_{\infty 2}$ (%)	R^2
JR	A	5.60±0.72^{c}	0.019±0.002^{d}	62.25±0.96^{a}	—	—	—	0.9762	0.021±0.000^{d}	50.49±2.31^{a}	—	—	—	0.9992
	P	5.36±0.10^{c}	0.122±0.002^{c}	26.77±1.83^{d}	14.5±0.0^{a}	0.015±0.002^{a}	34.56±1.98^{a}	0.9806	0.123±0.009^{b}	29.04±3.61^{c}	19.04±1.21^{a}	0.017±0.001^{a}	41.58±2.93^{a}	0.9990
	PA	10.75±0.79^{b}	0.071±0.002^{c}	19.62±3.52^{d}	15.0±0.0^{a}	0.008±0.002^{b}	27.85±3.12^{c}	0.9905	0.079±0.001^{c}	22.07±3.86^{d}	23.37±0.93^{a}	0.009±0.001^{c}	35.86±5.11^{b}	0.9999
	PP	11.17±1.33^{b}	0.138±0.007^{b}	44.54±2.01^{b}	15.0±0.0^{a}	0.015±0.003^{a}	34.18±1.26^{b}	0.9736	0.135±0.012^{b}	45.67±2.38^{a}	24.50±2.29^{a}	0.017±0.001^{a}	44.43±5.18^{a}	0.9991
	PTA_con	11.47±1.55^{b}	0.124±0.007^{b}	42.04±3.56^{b}	15.0±0.5^{a}	0.016±0.001^{a}	32.41±3.86^{b}	0.9449	0.114±0.007^{c}	38.57±0.14^{b}	25.04±1.05^{a}	0.015±0.001^{b}	34.58±3.36^{b}	0.9995
	PTA	22.04±2.24^{a}	0.155±0.002^{a}	46.23±2.80^{c}	15.0±1.0^{a}	0.015±0.001^{a}	31.78±5.67^{ab}	0.9841	0.175±0.007^{a}	47.50±0.97^{a}	21.59±1.27^{a}	0.017±0.001^{a}	38.44±1.07^{b}	0.9991
From Set 1_A to Set 6_PTA in JR, different letters over each column indicate significant differences ($p < 0.05$)														
JR_1LA	A	1.36±0.46 ^{a}	0.013±0.001^{c}	29.73±0.69^{c}	—	—	—	0.9494	0.012±0.001^{c}	36.20±0.69^{c}	—	—	—	0.9985
	P	5.70±0.64 ^{b}	0.016±0.002^{b}	54.41±1.83^{b}	—	—	—	0.9047	0.015±0.001^{c}	60.03±2.80^{b}	—	—	—	0.9992
	PA	6.06±1.46 ^{b}	0.014±0.001^{c}	52.93±2.97^{b}	—	—	—	0.9484	0.013±0.002^{c}	56.06±1.81^{b}	—	—	—	0.9994
	PP	5.91±0.56 ^{b}	0.018±0.000^{b}	65.13±3.69^{a}	—	—	—	0.9304	0.017±0.001^{c}	73.93±2.99^{a}	—	—	—	0.9988
	PTA_con	9.15±1.77 ^{b}	0.072±0.012^{a}	32.21±3.03^{b}	15.00±0.00^{a}	0.020±0.002^{a}	37.49±2.40^{a}	0.9479	0.081±0.012^{a}	32.86±2.35^{c}	16.50±2.45^{a}	0.005±0.001^{a}	24.86±3.03^{a}	0.9987
	PTA	11.23±1.38 ^{a}	0.110±0.008^{a}	36.56±1.34^{b}	14.83±0.29^{b}	0.013±0.001^{a}	38.19±4.38^{a}	0.9426	0.162±0.010^{a}	49.59±2.48^{c}	15.00±0.14^{a}	0.010±0.001^{a}	36.80±1.74^{a}	0.9982
From Set 1_A to Set 6_PTA in JR_1LA, different letters over each column indicate significant differences ($p < 0.05$)														

Mean ± S.D. calculated from triplicate measurements. For each parameter (column), the different superscript letters indicate values among the four samples are statistically different ($p < 0.05$). Values presented here are: the concentration of digested starch (C_0, %) at the beginning of intestinal digestion phase; starch digestion rate constants of rapid (k_1) and slow phase (k_2), corresponding estimated percentage of digested starch ($C_{\infty 1}$ and $C_{\infty 2}$, %), t_{int} is defined as the time intersection of two distinct digestion phase (estimated from LoS model), and t_{2start} is defined as the time intersection of two distinct digestion phase (estimated from CPS model). The goodness of curve-fitting (reflected by R^2).

		C_0 (%)	k_1 (min^{-1})	$C_{\infty 1}$ (%)	t_{int} (min)	k_2 (min^{-1})	$C_{\infty 2}$ (%)	R^2	k_1 (min^{-1})	$C_{\infty 1}$ (%)	t_{2start} (min)	k_2 (min^{-1})	$C_{\infty 2}$ (%)	R^2
PR	A	2.35±0.98 [b]	0.043±0.001 [c]	16.13±1.68[a]	16.80±0.32 [b]	0.008±0.001 [b]	35.09±3.53[c]	0.9474	0.037±0.017 [c]	12.03±0.23 [c]	21.92±3.58 [a]	0.006±0.001[b]	35.16±4.52 [c]	0.9995
	P	1.15±0.31 [b]	0.052±0.002 [b]	21.56±1.85 [a]	20.92±0.92 [a]	0.003±0.000 [c]	30.88±5.17 [c]	0.9310	0.047±0.007 [b]	27.37±1.96 [b]	25.33±2.00 [a]	0.002±0.000 [c]	31.54±2.37 [c]	0.9976
	PA	3.48±0.50 [a]	0.053±0.001 [b]	28.87±2.72[a]	16.50±3.04 [b]	0.004±0.000 [c]	33.43±2.98 [c]	0.9325	0.047±0.02 [b]	22.14±2.50 [b]	23.86±1.97 [a]	0.004±0.001 [b]	37.31±5.19 [c]	0.9757
	PP	3.68±2.19 [a]	0.101±0.007[a]	47.19±0.24 [a]	14.50±0.00 [b]	0.010±0.001 [a]	45.75±1.85 [a]	0.9448	0.089±0.007 [a]	19.25±1.28 [b]	26.07±1.53 [a]	0.008±0.002 [a]	44.66±2.35 [ab]	0.9918
	PTA_con	2.04±0.64 [b]	0.088±0.004 [a]	31.19±2.61 [a]	14.70±0.51 [b]	0.07±0.001 [a]	46.59±3.43 [a]	0.9641	0.092±0.014 [a]	21.96±2.74 [b]	22.52±2.50 [a]	0.008±0.002 [a]	50.55±5.61 [a]	0.9996
	PTA	4.95±1.06 [a]	0.093±0.004 [a]	40.82±0.27 [a]	14.05±0.07 [b]	0.010±0.004 [a]	50.32±1.40 [a]	0.9608	0.094±0.004 [a]	27.10±0.48 [a]	25.00±1.00 [a]	0.009±0.001 [b]	49.89±2.48 [a]	0.9982
From Set 1_A to Set 6_PTA in PR, different letters over each column indicate significant differences ($p < 0.05$)														
R_1LA	A	1.02±0.08[a]	0.029±0.008[d]	11.58±2.24[c]	14.70±1.48[a]	0.006±0.001[a]	20.58±1.48[c]	0.9455	0.028±0.002[c]	19.72±0.19[b]	24.14±1.74[a]	0.003±0.000[c]	23.36±1.15[c]	0.9992
	P	1.50±0.12[a]	0.049±0.001[c]	15.31±0.44[b]	15.07±0.99[a]	0.006±0.001[a]	26.62±3.68[b]	0.9482	0.051±0.032[b]	25.57±2.59[a]	25.73±0.46[a]	0.007±0.001[b]	29.44±2.19[bc]	0.9997
	PA	3.14±0.75[b]	0.059±0.006[b]	20.73±0.69[a]	15.38±2.01[a]	0.008±0.000a	30.19±2.71[b]	0.9279	0.061±0.015[b]	26.31±1.34[a]	25.49±0.85[a]	0.005±0.001[b]	32.95±6.88[b]	0.9996
	PP	2.83±0.32[b]	0.066±0.008[a]	24.45±1.19[a]	15.23±0.23[a]	0.011±0.001[a]	48.85±3.73[b]	0.9310	0.070±0.006[a]	29.87±1.11[a]	24.91±1.74[a]	0.009±0.000[b]	39.41±5.57[b]	0.9997
	PTA_con	4.45±0.11[a]	0.050±0.007[c]	23.19±3.69[a]	15.01±0.02[a]	0.009±0.002[a]	46.93±2.70[b]	0.9552	0.56±0.028[b]	28.81±2.40[a]	23.46±2.51[a]	0.009±0.001[b]	40.22±0.86[b]	0.9999
	PTA	5.37±0.20[a]	0.075±0.008[a]	26.64±4.87[a]	15.00±0.00[a]	0.012±0.002[a]	56.24±2.12[a]	0.9883	0.080±0.003[a]	31.35±3.28[a]	26.86±1.49[a]	0.011±0.001[a]	56.15±2.65[a]	0.9996
From Set 1_A to Set 6_PTA in PR_1LA, different letters over each column indicate significant differences ($p < 0.05$)														

Mean ± S.D. calculated from triplicate measurements. For each parameter (column), the different superscript letters indicate values among the four samples are statistically different ($p < 0.05$). Values presented here are: the concentration of digested starch (C_0, %) at the beginning of intestinal digestion phase; starch digestion rate constants of rapid (k_1) and slow phase (k_2), corresponding estimated percentage of digested starch ($C_{\infty 1}$ and $C_{\infty 2}$, %), t_{int} is defined as the time intersection of two distinct digestion phase (estimated from LoS model), and t_{2start} is defined as the time intersection of two distinct digestion phase (estimated from CPS model). The goodness of curve-fitting (reflected by R^2).

Furthermore, two successive increases in protein hydrolysis were observed due to both gastric (pepsin) and pancreatic proteases (primarily trypsin). Upon treatment with pepsin, which reduced the protein content in the food system, a nearly two-fold increase in starch was observed in digestion fluids at time 0, as shown in **Fig. 5.5C** (Set 3_PA) and **D** (Set 4_PP). An exponential association pattern was also observed, as in the presence of pancreatin only (Set 2_P). This corresponds to k_1 being nearly eight times higher than k_2, contributing to one-third of the maximum digestion ratio in 20 mins. During pepsin-pancreatin digestion (Set 4_PP), k_1 significantly increased, while K_2 remained similar to pancreatin only (Set 2_P), leading to a higher starch digestibility (90.62 %) than rice digestion without pepsin treatment (65.27 %) (Set 2_P). Set 6_PTA combines pepsin and trypsin to remove proteins at maximum levels. A two-phase digestion of starch follows. The rates of the rapid phase have increased to their highest levels, while k_2 remained similar to other sets.

The estimate for $C_{\infty 1}$ and $C_{\infty 2}$ indicates each amylolysis phase's contribution to the total starch degradation. With simultaneous digestion of protein and starch with pancreatin (Set 2_P), the $C_{\infty 1}$ contributes less than $C_{\infty 2}$ to total starch digestion than that in the pre-treatment with pepsin followed by α-amylase (Set 3_PA). A combination of pepsin-pancreatin digestion (Set 4_PP) resulted in a fairly even contribution of the two reaction phases to the estimation of total starch digestion extent. It can also be noticed that when protein is predigested by pepsin-trypsin, $C_{\infty 1}$ contributes more than $C_{\infty 2}$ to the total amount of starch digestion. The results indicated that when intrinsic protein was enzymatically removed from the rice structure, there was an increase in both the rate and percentage of starch hydrolysis. Similar results have been reported in pasta and wheat (Zou et al., 2015; Bhattarai et al., 2016).

5.3.3.2 Starch digestibility differs by rice types

Cooked PR was digested by the same six sets used to assess JR to understand how rice type affected rice digestibility. PR had slower starch digestibility than JR in each digestion set, as confirmed by the kinetic model fitting (**Tab. 5.5**), with lower k_1 and

$C_{\infty 1}$ in PR than in JR. Aside from having a higher protein content with lower digestibility and high-amylose content, the protein-starch matrices configuration in cooked PR can also contribute to slowing down digestion. By microscopic observation (**Fig. 5.6**) of cooked rice samples prior to digestion, JR appears to have a less ordered microstructure (damaged protein networks with highly swollen starch form homogeneous protein-starch matrices) than PR (a denser protein network surrounding a limited number of swollen starch granules). Accordingly, JR may be more enzymatically accessible than PR (Ong & Blanshard, 1995; Derycke et al., 2005).

When rice protein digestion was sequentially proteased, JR and PR showed similar digestion rates (K_{DSPF} and K_{DH}), resulting in similar intestinal protein digestion ($Span_{DSPF}$ and $Span_{DH}$) and slightly lower protein digestion in PR concerning higher PR protein content. Relative protein digestibility for both JR and PR followed the trend: Set 1_A < Set 2_P < Set 3_PA < Set 4_PP < Set 5_PTA_con < Set 6_PTA. PR exhibited two distinguished digestion phases in all sets (as shown in **Fig. S2**). As protein was removed from the rice grain, the k_1 values increased in PR, similar to JR (although to a lower extent for PR), which indicates that a reduction in native protein networks correlates with an increase in starch digestion (Zou et al., 2015; Tamura et al., 2017). Also, PR starch is less digestible, which may be attributed to the more ordered crystalline structure produced by parboiling, providing greater resistance to enzymatic hydrolysis (Tian et al., 2018; Sivakamasundari et al., 2020).

5.3.3.3 The effect of LAGG addition on starch digestion

The starch *in vitro* digestion patterns for JR_1LA and PR_1LA are presented in **Fig. S2** and **Fig. S4**. The kinetic parameters are summarised in **Tab. 5.5**. In both rice types, LAGG reduced the starch digestibility, although to different extents. Compared to JR, a slower digestion phase was observed during the first hour of digestion for JR_1LA, which gradually reached a plateau by the end of the test (**Fig. S2**). The LoS plot of JR_1LA revealed more single-phase digestion patterns from Set 1_A to Set 4_PP, with lower k than those of JR (**Tab. 5.5**). As in Set 6_PTA and Set 5_PTA_con, the starch hydrolysis is again divided into two phases, and LAGG remains effective

in reducing starch digestibility, as JR_1LA has much lower k_1 and $C_{\infty 1}$ than JR. LAGG reduces starch digestibility in PR during the rapid phase, as evidenced by the lower k_1 but not k_2 in starch hydrolysis of PR from Set 4_PP to Set 6_PTA.

A difference between PR and JR grain structures may affect LAGG's ability to decrease starch digestibility. **Fig 5.7** shows the surface microstructure of rice samples before and after amylase hydrolysis (as Set 1_A) (rows 1 and 3). Cooked JR exhibits protuberances with concave regions under ESEM, whereas in the presence of LAGG, a smoother surface with thin filament aggregates is observed in JR_1LA; the cooked, non-hydrolyzed PR surface shows visible pores and tunnels (C), which are masked and filled by the hydrogel in PR_1LA (D).

After α-amylase hydrolysis (Fig. 5.6row 3), JR (A) and PR (C) showed a more damaged surface, with open pores and enlarged tunnels, whereas JR_1LA (B) and PR_1LA (D) showed a smoother surface, with less evident damage. As LAGG may have been present in the tunnels of hydrolysed JR_1LA (B) and PR_1LA (D), it sealed up the intergranular spaces and fissures on the grain, thus serving as a physical barrier to enzymatic degradation. As observed in **Fig. 5.6** rows 2 and 4, showing the respective cross-section imaging of rows 1 and 3, the rice grain morphology seems to change also to a certain distance (~100 μm) from the surface, suggesting a degree of penetration of LAGG, in JR_1LA and PR_1LA, compared to the respective non-LAGG samples.

In summary, imaging suggests a protective effect by LAGG, which would limit enzyme accessibility to starch and prevent starch from leaching out of the rice grain, resulting in lower starch digestibility.

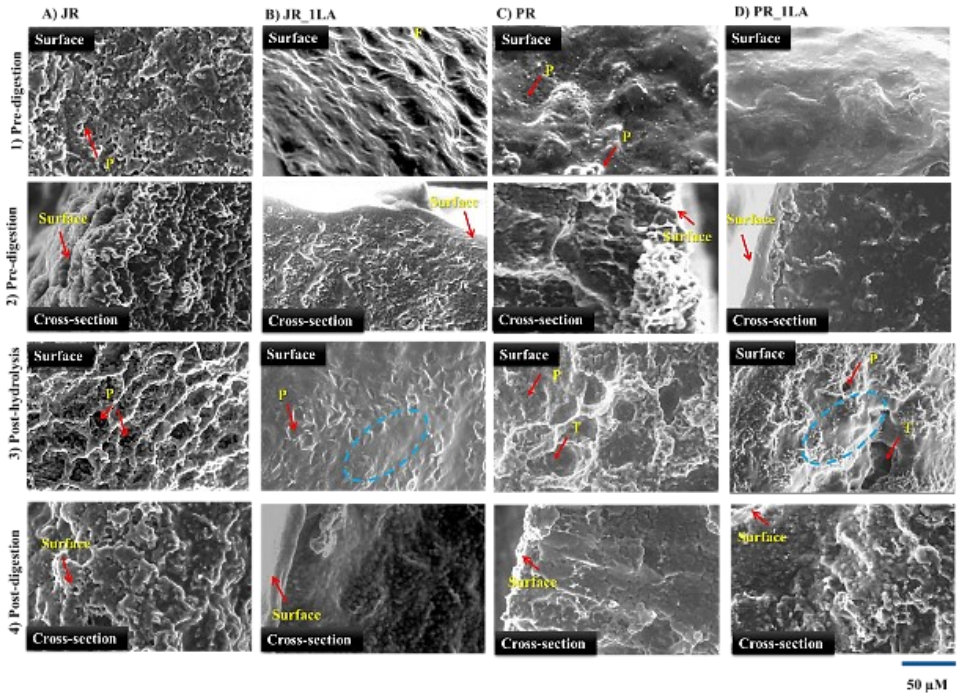


Fig. 5.6. Scanning electron micrograph of (A) JR, (B) JR_1LA, (C) PR and (D) PR_1LA. Row 1 (surface) and 2 (cross-section): cooked pre-digested samples. Row 3 (surface) and 4 (cross-section): respective digested (Set 1_A) samples.

Even though the hydrogel began to fade and lose strength during the intestinal phase (pH 7) in Set 5_PTA_con and Set 6_PTA, a reduced starch digestibility of LAGG-coated samples was still expected due to the encapsulating effect of LAGG. These results are consistent with those described previously for LAGG gel stability changes during digestion (Santos & Cunha, 2018).

5.3.4 Food model case 2: Protein and starch digestibility of cooked and homogenised rice

5.3.4.1 Effect of protein digestion on starch digestibility

The kinetic parameters related to starch digestion of the homogenised JR, JR_1LA, PR, and PR_1LA (**Fig. S5** to **Fig. S8**) are summarised in **Tab. S2**. The rapid phase was reduced to less than 15 min with protein hydrolysis (Set 2_P to Set 6_PTA). Compared to the intact samples, starch in homogenised rice samples digested at a faster rate (higher k_1), especially when the proteinase was involved. It can be hypothesised that homogenisation directly impacted the starch availability towards α-amylase, especially when proteins were removed enzymatically. These results align with previous findings, which showed that the starch digestibility of white rice increased following a 120 s homogenisation step (Tamura et al., 2016, 2017).

5.3.4.2 Starch digestibility differs by rice types

As a result of homogenisation, the differences between JR and PR are less evident than those in intact grains (**Section 5.3.2**). In fact, within the first 20 minutes of digestion, PR still displays a lower rate of starch digestion than JR (lower k_1). Afterwards, a second phase of digestion occurred at a slightly higher rate (k_2) than JR (**Fig. S5** to **Fig. S8**; **Tab. S2**). These factors result in comparable starch digestibility for JR and PR at the end of the digestion cycle.

5.3.4.3 The effect of LAGG addition on starch digestion

JR_1LA and PR_1LA had lower k_1 but similar k_2 compared to JR and PR (**Tab. S2**). Overall extent of digested starch was similar at the end of the sets. It suggests that the attenuating effect of LAGG on starch digestibility was more related to the rate than the extent of digestibility. This mitigating effect (albeit limited) on starch digestibility by LAGG may be explained by a physical barrier role of residual LAGG contained in a population of the aggregates forming the homogenised rice mass. Aggregates with LAGG may entrap aggregates without LAGG and reorganise into larger clusters due to the presence of cations (mono- and di-valent) in the gastric phase, which would facilitate interaction between LAGG chains from different

aggregates (Funami et al., 2008; Kohyama et al., 2021). Due to their lower specific surface area, these larger clusters would require a longer time to disintegrate. Thus, the digestion rate in the rapid phase would be slowed down, with a more segmented digestion pattern.

5.3.5 Starch digestibility profiles and predicted GI

5.3.5.1 Starch digestibility profiles

The LoS and CPS fittings (methods in **Section 5.2.6.1** and **5.2.6.2**, respectively) are presented, and the results are summarised in **Tab. 5.5** and **Tab. S2.** All CPS fittings appeared satisfactory ($R^2 > 0.99$), with two distinct kinetic components in the starch digestograms of most of the intact JR and PR samples. Also, in the samples with $t_{2start} > t_{int}$, the sequential digestion pattern was related to the characteristic structure of cooked grain, wherein the rapid-digestible fraction located at the perimeter surrounds the slowly digestible fraction (Li & Hu, 2020).

As explained earlier in **Section 5.2.6.2**, the t_{2start} within the range of 0 to t_{int} ($0 < t_{2start} \leq t_{int}$), a more complex digestion profile (combination of parallel and sequential digestion pattern) was observed in homogenised rice samples as compared to non-homogenised samples (sequential digestion pattern).

In homogenised JR, $t_{2start} = 0$ in Set 1_A, suggesting coexisting rapid and slow digestion (parallel digestion pattern). Thus, the results support previously reported findings concerning the importance of oral processing in the starch digestion of cooked rice (Tamura et al., 2017). The relationship between rice structure and digestion must be considered carefully when the oral processing step is applied before digestion, as it leads to more complex digestion profiles than when intact grains are involved.

5.3.5.2 Predicted glycaemic index (pGI)

Set 7_HPP represents the results of *in vitro* oral-gastrointestinal digestion of starch. It has been suggested that a three-phase digestion process is more relevant to evaluate the pGI value (using **Eq. 5.6** in **Section 5.2.6.3**) when it is referred to the GI value for a healthy diet (Odenigbo, 2014; Cai et al., 2020; Bagchi et al., 2023).

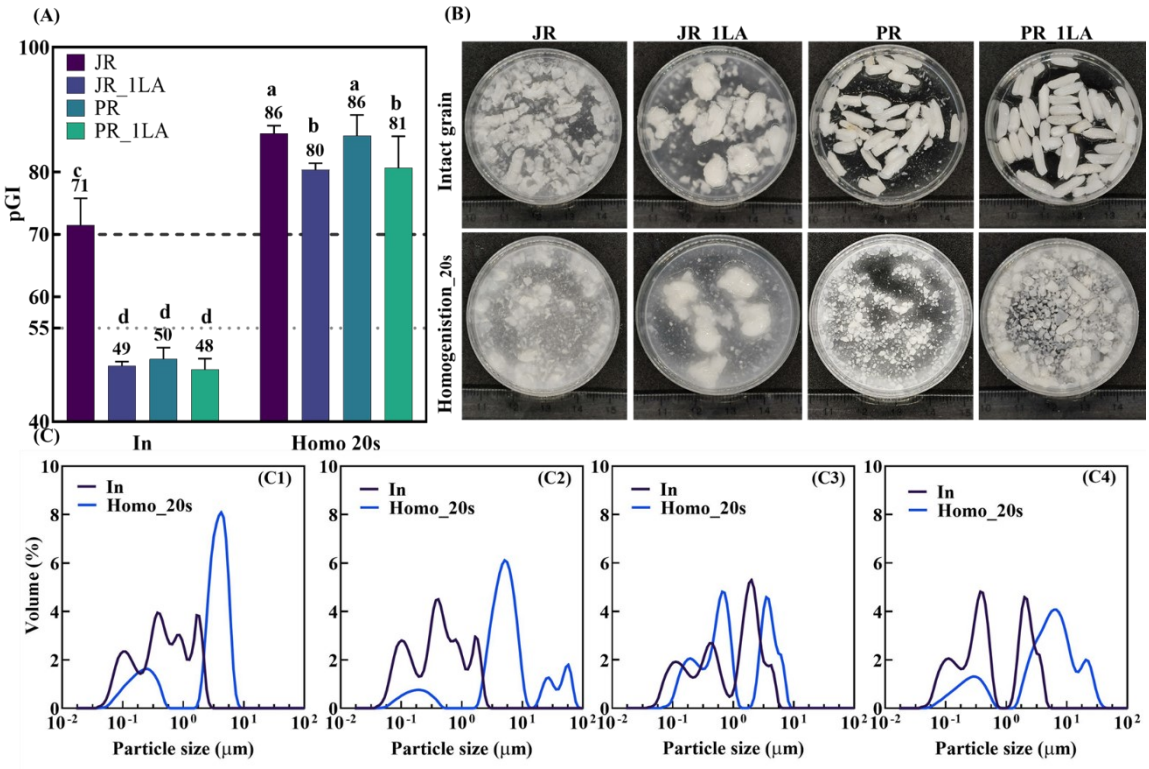


Fig. 5.7. pGI (A), imaging (B), and particle size distribution (C) of cooked digested rice, non-homogenised or homogenised for 20 seconds, as evaluated after Set 7_HPP. In (B) non-homogenised (top row) and homogenised for 20 s (bottom row). (1) JR, (2) JR_1LA, (3) PR, (4) PR_1LA.

In the case of non-homogenised cooked JR, *in vitro* pGI was the highest (71) and classified as a high-GI food (pGI ≥70), which is much lower than practical GI (89 as an average) obtained from *in vivo* studies (Truong et al., 2014; Atkinson et al., 2021). Unlike JR, PR had a pGI of 50 and was classified as low-GI food (pGI < 55). *In vivo* evaluations also reveal that parboiling reduces the GI of rice compared to non-parboiled rice of the same variety (Wolever et al., 1986; Hasbullah et al., 2017). Upon addition of LAGG, pGI in JR_1LA were significantly lower than in JR, whereas no significant differences between PR and PR_1LA were observed, and this could correlate with the less damaged grain structure showed by JR_1LA, PR and PR_1LA (**Fig. 5.7B**). The particle size distribution in the supernatant of digested rice samples is shown in **Fig. 5.7C**. Non-homogenised and homogenised (In and Homo_20 s, respectively, in **Fig 5.7**) rice samples exhibit distinct particle size distributions. The

non-homogenised rice samples display a multimodal distribution, with particle sizes ranging from 0.05 to 3 μm. These particles correspond to liberated starch granules and protein bodies (Vandeputte et al., 2003; Amagliani et al., 2017). In addition to the sediment with large clusters (shown in **Fig. 5.7B**), the distribution pattern suggests non-homogenised samples have not undergone extensive breakdown, leaving larger particles intact. The homogenised JR samples showed a major peak at size <10 μm and a smaller peak at around 0.1 μm. There is a noticeable increase of the particle size as a consequence of homogenisation, suggesting that homogenisation can facilitate the release and distribution of larger clusters from rice to the digestion fluids, promoting the enzyme accessibility. This could contribute to the substantial increase in pGI of homogenised JR, which reached 86.

It is also interesting that the pGI of PR upon homogenisation increased from 50 to 86, which is a high-GI value. The particle size distribution of the homogenised PR exhibited a similar bimodal pattern to that of intact PR, but with a greater proportion of smaller particles (0.1-1 μm). There seems to be an increase in the proportion of particles <1 μm as a consequence of homogenisation in non-coated PR (**Fig. 5.7C3**), likely due to disruption of larger aggregates present in the non-homogenised PR.

Therefore, smaller particles and more uniform distribution can enhance the accessibility of starch to digestive enzymes, accelerating the starch hydrolysis process in homogenised PR. As reported in the literature, the *in vivo* GI of PR varies from 39 to 79. The GI difference has been attributed to the extent to which the grain has been broken down by chewing (Pathiraje et al., 2011; Kataoka et al., 2013).

A significant effect of LAGG on regulating pGI was observed in both rice types after homogenisation. The pGI values decreased by 11.6 % and 10.4 %, respectively, compared to JR and PR control (no LAGG). This could be caused by a reduction in surface area exposed to the digestion solution, perhaps due to the larger fractions remaining after homogenisation of the LAGG-containing samples. The peaks located at larger diameters, i.e., 10-100 μm in JR (**Fig. 5.7C2**) and 10-50 μm in PR (**Fig. 5.7C4**), may be segmented LAGG-starch conjugates or small protein-starch-LAGG fragments.

From the data in this section, simulating oral processing by homogenisation is important as it accounts for its disruptive effects on rice microstructure, leading to higher pGI. In return, food models would respond differently to oral processing, e.g., in the extent of protein and starch digestibility, according to their structural characteristics (in this case, represented by rice type and addition of LAGG).

5.4 Conclusion

The glycaemic index (GI) of two rice types, jasmine rice (JR) and parboiled rice (PR), were determined using *in vitro* digestion protocols using a multi-enzyme approach. Kinetic analysis was conducted to study the relationship between digestibility and microstructure in rice samples. PR showed significantly lower starch digestibility and pGI than JR in this study, perhaps due to higher amylose levels and a compact and less digestible protein network. The effect of *in vitro* oral processing (homogenisation for 20 s) on protein and starch digestibility was also considered. Homogenisation caused higher pGI in PR and JR (with an overall decrease in the pGI difference between PR and JR) due to the physical disintegration of the grains, which would have facilitated enzyme accessibility. Also, the effect of rice cooking in a 1 % low acyl gellan gum (LAGG) dispersion was evaluated to reduce GI. LAGG had a mitigation effect on GI in both non-homogenised and homogenised samples, which could depend on a reduced enzyme penetration through the rice material due to a barrier action of LAGG and to a larger segmentation of the homogenised materials containing LAGG. As a summary of the findings, the digestion behaviour of protein and starch is interdependent. This method provided a way to understand the importance of protein digestibility on starch digestibility and how microstructural variables are part of the determining factors of digestive patterns. Characterising the physicochemical properties of proteins and applying LAGG to develop low-GI food would be beneficial in future work.

5.5 References

Ahn, J., Cao, M.J., Yu, Y.Q., et al. (2013) Accessing the Reproducibility and Specificity of Pepsin and other Aspartic Proteases. *Biochimica et biophysica acta*, 1834 (6): 1222. doi:10.1016/J.BBAPAP.2012.10.003.

Almeida, C.C., Monteiro, M.L.G., Costa-Lima, B.R.C. da, et al. (2015) *In vitro* digestibility of commercial whey protein supplements. *LWT - Food Science and Technology*, 61 (1): 7–11. doi:10.1016/j.lwt.2014.11.038.

Amagliani, L., O'Regan, J., Kelly, A.L., et al. (2017) The composition, extraction, functionality and applications of rice proteins: A review. *Trends in Food Science and Technology*. 64 pp. 1–12. doi:10.1016/j.tifs.2017.01.008.

Amin, T., Naik, H.R., Hussain, S.Z., et al. (2018) *In vitro* digestion, physicochemical and morphological properties of low glycemic index rice flour prepared through enzymatic hydrolysis. *International Journal of Food Properties*, 21 (1): 2632–2645. doi:10.1080/10942912.2018.1545789.

AACC (2001) Determination of the Pasting Properties of Rice with the Rapid Visco Analyser. AACC St. Paul, Minn.: EUA (9).

AOAC (2005a) Official methods of analysis of the Association of Analytical Chemists International. Official Methods 934.01: Gaithersburg, MD, USA.

AOAC (2005b) Official methods of analysis of the Association of Analytical Chemists International. Official Methods 933.29: Gaithersburg, MD, USA.

AOAC (2007). Official methods of analysis of Association of Analytical Chemists International. Official Methods 996.11: Gaithersburg, MD, USA.

Bagchi, T. B., Das, B., Kumar, A., et al. (2023). Impact of cooking, parboiling and fermentation on nutritional components, predicted glycemic index and pasting properties of rice. Journal of Cereal Science, 114, 103763. doi.org/10.1016/J.JCS.2023.103763

Bergmeyer, H.U., Bergmeyer, J. & Grassl, M. (1983) Methods of enzymatic analysis: Samples, reagents, assessment of results. p. 539.

Bhattarai, R.R., Dhital, S. and Gidley, M.J. (2016) Interactions among macronutrients in wheat flour determine their enzymic susceptibility. *Food Hydrocolloids*, 61: 415–425. doi:10.1016/j.foodhyd.2016.05.026.

Bhavadharini, B., Mohan, V., Dehghan, M., et al. (2020) White Rice Intake and Incident Diabetes: A Study of 132,373 Participants in 21 Countries. *Diabetes Care*, 43 (11): 2643. doi:10.2337/DC19-2335.

Blanquet-Diot, S., François, O., Denis, S., et al. (2021) Importance of oral phase *in vitro* starch digestibility related to wholegrain versus refined pastas and mastication impairment. *Food Hydrocolloids*, 112: 106277. doi:10.1016/J.FOODHYD.2020.106277.

Boers, H.M., Seijen Ten Hoorn, J. and Mela, D.J. (2015) A systematic review of the influence of rice characteristics and processing methods on postprandial glycaemic and insulinaemic responses. *The British Journal of Nutrition*, 114 (7): 1035. doi:10.1017/S0007114515001841.

Bornhorst, G.M., Gouseti, O., Wickham, M.S.J., et al. (2016) Engineering Digestion: Multiscale Processes of Food Digestion. *Journal of Food Science*, 81 (3): R534–R543. doi:10.1111/1750-3841.13216.

Bradbeer, J.F., Hancocks, R., Spyropoulos, F., et al. (2015) Low acyl gellan gum fluid gel formation and their subsequent response with acid to impact on satiety. *Food Hydrocolloids*, 43: 501–509. doi.org/10.1016/j.foodhyd.2014.07.006.

Brodkorb, A., Egger, L., Alminger, M., et al. (2019) INFOGEST static *in vitro* simulation of gastrointestinal food digestion. *Nature Protocols 2019 14:4*, 14 (4): 991–1014. doi:10.1038/s41596-018-0119-1.

Butterworth, P.J., Bajka, B.H., Edwards, C.H., et al. (2022) Enzyme kinetic approach for mechanistic insight and predictions of *in vivo* starch digestibility and the glycaemic index of foods. *Trends in Food Science and Technology*, 120 (November 2021): 254–264. doi:10.1016/j.tifs.2021.11.015.

Butterworth, P.J., Warren, F.J. and Ellis, P.R. (2011) Human α-amylase and starch digestion: An interesting marriage. *Starch/Staerke*, 63 (7): 395–405. doi:10.1002/star.201000150.

Butterworth, P.J., Warren, F.J., Grassby, T., et al. (2012) Analysis of starch amylolysis using plots for first-order kinetics. *Carbohydrate Polymers*, 87 (3): 2189–2197. doi.org/10.1016/j.carbpol.2011.10.048

Cai, Y., Li, S., Jiao, G., et al. (2018) OsPK2 encodes a plastidic pyruvate kinase involved in rice endosperm starch synthesis, compound granule formation and grain filling. *Plant Biotechnology Journal*, 16 (11): 1878–1891. doi:10.1111/PBI.12923.

Cai, C., Tian, Y., Yu, Z., et al. (2020). In Vitro Digestibility and Predicted Glycemic Index of Chemically Modified Rice Starch by One-Step Reactive Extrusion. Starch - Stärke, 72(1–2), 1900012. doi.org/10.1002/STAR.201900012

Chatthongpisut, R., Schwartz, S.J. and Yongsawatdigul, J. (2015) Antioxidant activities and antiproliferative activity of Thai purple rice cooked by various methods on human colon cancer cells. *Food Chemistry*, 188: 99–105. doi.org/10.1016/j.foodchem.2015.04.074.

Chi, C., Li, X., Zhang, Y., et al. (2018) Understanding the mechanism of starch digestion mitigation by rice protein and its enzymatic hydrolysates. *Food Hydrocolloids*, 84: 473–480. doi:10.1016/j.foodhyd.2018.06.040.

Chung, H.J., Liu, Q. and Lim, S.T. (2007) Texture and *in vitro* digestibility of white rice cooked with hydrocolloids. *Cereal Chemistry*, 84 (3): 246–249. doi:10.1094/CCHEM-84-3-0246.

Derycke, V., Veraverbeke, W., Vandeputte, G., et al. (2005a) Impact of Proteins on Pasting and Cooking Properties of Nonparboiled and Parboiled Rice. *Cereal Chemistry*, 82: 468–474. doi:10.1094/CC-82-0468.

Dhital, S., Dabit, L., Zhang, B., et al. (2015) *In vitro* digestibility and physicochemical properties of milled rice. *Food Chemistry*, 172: 757–765. doi:10.1016/j.foodchem.2014.09.138.

Dibba, D., Weaver, L.T. and Hudson, G.J. (1991) Water content of cooked rice is related to variety and cooking method. *Nutrition Research*, 11 (12): 1397–1402. doi:10.1016/S0271-5317(05)80472-5.

Edwards, C.H., Cochetel, N., Setterfield, L., et al. (2019) A single-enzyme system for starch digestibility screening and its relevance to understanding and predicting the glycaemic index of food products. *Food and Function*, 10 (8): 4751–4760. doi:10.1039/c9fo00603f.

Edwards, C.H., Grundy, M.M.L., Grassby, T., et al. (2015) Manipulation of starch bioaccessibility in wheat endosperm to regulate starch digestion, postprandial glycemia, insulinemia, and gut hormone responses: a randomized controlled trial in healthy ileostomy participants. *The American journal of clinical nutrition*, 102 (4): 791–800. doi:10.3945/AJCN.114.106203.

Edwards, C.H., Maillot, M., Parker, R., et al. (2018) A comparison of the kinetics of *in vitro* starch digestion in smooth and wrinkled peas by porcine pancreatic alpha-amylase. *Food Chemistry*, 244 (June 2017): 386–393. doi:10.1016/j.foodchem.2017.10.042.

Edwards, C.H., Warren, F.J., Milligan, P.J., et al. (2014a) A novel method for classifying starch digestion by modelling the amylolysis of plant foods using first-order enzyme kinetic principles. *Food and Function*, 5 (11): 2751–2758. doi:10.1039/c4fo00115j.

Felix, A., Trinidad, T., Tuaño, A.P., et al. (2013) Short-Term Satiety of Cooked Philippine Rices of Varying Apparent Amylose Content and Glycemic Index. *Philippine Agricultural Scientist*.api.semanticscholar.org

Fernandes, J.M., Madalena, D.A., Pinheiro, A.C., et al. (2020) Rice *in vitro* digestion: application of INFOGEST harmonized protocol for glycemic index determination and starch morphological study. *Journal of Food Science and Technology*, 57 (4): 1393. doi:10.1007/S13197-019-04174-X.

Funami, T., Noda, S., Nakauma, M., et al. (2008) Molecular Structures of Gellan Gum Imaged with Atomic Force Microscopy in Relation to the Rheological Behavior in Aqueous Systems in the Presence or Absence of Various Cations. *Journal of Agricultural and Food Chemistry*, 56 (18): 8609–8618. doi:10.1021/jf8007713.

Gong, B., Cheng, L., Gilbert, R.G., et al. (2019) Distribution of short to medium amylose chains are major controllers of *in vitro* digestion of retrograded rice starch. *Food Hydrocolloids*, 96: 634–643. doi:10.1016/J.FOODHYD.2019.06.003.

Granger, M., Abadie, B. and Marchis-Mouren, G. (1975) Limited action of trypsin on porcine pancreatic amylase: characterization of the fragments. *FEBS letters*, 56 (2): 189–193. doi:10.1016/0014-5793(75)81088-X.

Gunaratne, A., Kao, W., Ratnayaka, J., et al. (2013) Effect of parboiling on the formation of resistant starch, digestibility and functional properties of rice flour from different varieties grown in Sri Lanka. *Journal of the Science of Food and Agriculture*, 93 (11): 2723–2729. doi:10.1002/jsfa.6091.

Hall, A.E. and Moraru, C.I. (2022) Comparative effects of high-pressure processing and heat treatment on *in vitro* digestibility of pea protein and starch. *NPJ Science of Food*, 6 (1). doi:10.1038/S41538-021-00116-0.

Hapsari, A.H., Kim, S.J. and Eun, J.B. (2016) Physical characteristics of parboiled Korean glutinous rice (Olbyeossal) using a modified method. *LWT - Food Science and Technology*, 68: 499–505. doi:10.1016/J.LWT.2015.12.066.

Hasbullah, R., Pujantoro, L., Koswara, S., et al. (2017) Steaming process of paddy to improve quality and reduce the glycemic index of parboiled rice. *Acta Horticulturae*, 1152 (March): 375–379. doi:10.17660/ActaHortic.2017.1152.50.

Hasjim, J., Li, E. and Dhital, S. (2013) Milling of rice grains: Effects of starch/flour structures on gelatinization and pasting properties. *Carbohydrate Polymers*, 92 (1): 682–690. doi.org/10.1016/j.carbpol.2012.09.023

He, H., Bian, H., Xie, F., et al. (2021) Different effects of pectin and κ-carrageenan on the multiscale structures and *in vitro* digestibility of extruded rice starch. *Food Hydrocolloids*, 111. doi:10.1016/J.FOODHYD.2020.106216.

He, H., Chi, C., Xie, F., et al. (2020) Improving the *in vitro* digestibility of rice starch by thermomechanically assisted complexation with guar gum. *Food Hydrocolloids*, 102. doi:10.1016/J.FOODHYD.2019.105637.

Hsiu, J., Fischer, E.H. and Stein, E.A. (1964) Alpha-Amylases as Calcium-Metalloenzymes. II. Calcium and the Catalytic Activity. *Biochemistry*, 3 (1): 61–66. doi.org/10.1021/bi00889a011

Jalabert-Malbos, M.L., Mishellany-Dutour, A., Woda, A., et al. (2007) Particle size distribution in the food bolus after mastication of natural foods. *Food Quality and Preference*, 18 (5): 803–812. doi:10.1016/J.FOODQUAL.2007.01.010.

Jiménez-Munoz, L., Brodkorb, A., Gómez-Mascaraque, L.G., et al. (2021) Effect of heat treatment on the digestion behaviour of pea and rice protein dispersions and their blends studied using the semi-dynamic INFOGEST digestion method. *Food and Function*, 12 (18): 8747–8759. doi:10.1039/d1fo01223a.

Kataoka, M., Venn, B.J., Williams, S.M., et al. (2013) Glycaemic responses to glucose and rice in people of Chinese and European ethnicity. *Diabetic medicine : a journal of the British Diabetic Association*, 30 (3). doi:10.1111/DME.12080.

Kohyama, K., Ishihara, S., Nakauma, M., et al. (2021) Fracture phenomena of soft gellan gum gels during compression with artificial tongues. *Food Hydrocolloids*, 112 (August 2019): 106283. doi:10.1016/j.foodhyd.2020.106283.

Larsen, H.N., Rasmussen, O.W., Rasmussen, P.H., et al. (2000) Glycaemic index of parboiled rice depends on the severity of processing: Study in type 2 diabetic subjects. *European Journal of Clinical Nutrition*, 54 (5): 380–385. doi:10.1038/sj.ejcn.1600969.

Li, C., Cao, P., Wu, P., et al. (2021a) Effects of endogenous proteins on rice digestion during small intestine (*in vitro*) digestion. *Food Chemistry*, 344 (June 2020): 128687. doi:10.1016/j.foodchem.2020.128687.

Li, C. & Hu, Y. (2020) Combination of parallel and sequential digestion kinetics reveals the nature of digestive characteristics of short-term retrograded rice starches. *Food Hydrocolloids*, 108: 106071. doi:10.1016/J.FOODHYD.2020.106071.

Li, C., Hu, Y., Gu, F., et al. (2021) Causal relations among starch fine molecular structure, lamellar/crystalline structure and *in vitro* digestion kinetics of native rice starch. *Food & Function*, 12 (2): 682–695. doi:10.1039/D0FO02934C.

Li, H.T., Li, Z., Fox, G.P., et al. (2021) Protein-starch matrix plays a key role in enzymic digestion of high-amylose wheat noodle. *Food Chemistry*, 336 (March 2020): 127719. doi:10.1016/j.foodchem.2020.127719.

Liu, K., Zheng, J. and Chen, F. (2019) Effect of domestic cooking on rice protein digestibility. *Food Science and Nutrition*, 7 (2): 608–616. doi:10.1002/FSN3.884.

López-Barón, N., Gu, Y., Vasanthan, T., et al. (2017) Plant proteins mitigate *in vitro* wheat starch digestibility. *Food Hydrocolloids*, 69: 19–27. doi:10.1016/j.foodhyd.2017.01.015.

Lu, X., Ma, R., Zhan, J., et al. (2022) Mechanism of peptides from rice hydrolyzed proteins hindering starch digestion subjected to hydrothermal treatment. *npj Science of Food 2022 6:1*, 6 (1): 1–8. doi:10.1038/s41538-022-00153-3.

McGrane, Cornell and Rix (1998) A simple and rapid colourimetric method for the determination of amylose in starch products. *Stärke*, 50 (4): 158–163.

Minekus, M., Alminger, M., Alvito, P., et al. (2014) A standardised static *in vitro* digestion method suitable for food- an international consensus. *Food and Function*, 5 (6): 1113–1124. doi:10.1039/c3fo60702j.

Morris, E.R., Nishinari, K. and Rinaudo, M. (2012) Gelation of gellan - A review. *Food Hydrocolloids*. 28 (2) pp. 373–411. doi:10.1016/j.foodhyd.2012.01.004.

Na-Nakorn, K., Kulrattanarak, T., Hamaker, B.R., et al. (2019) Starch digestion kinetics of extruded reformed rice is changed in different ways with added protein or fibre. *Food and Function*, 10 (8): 4577–4583. doi:10.1039/c9fo00521h.

Nooshkam, M. and Varidi, M. (2021) Physicochemical stability and gastrointestinal fate of β-carotene-loaded oil-in-water emulsions stabilized by whey protein isolate-low acyl gellan gum conjugates. *Food Chemistry*, 347. doi:10.1016/j.foodchem.2021.129079.

Odenigbo, A. (2014). Nutrient Composition and Predicted Glycemic Index of Rice Varieties from Nigeria. British Journal of Applied Science & Technology, 4(2), 302–318. doi.org/10.9734/bjast/2014/6203

Ong, M.H. and Blanshard, J.M.V. (1995a) Texture determinants in cooked, parboiled rice. I: Rice starch amylose and the fine structure of amylopectin. *Journal of Cereal Science*, 21 (3): 251–260. doi:10.1006/JCRS.1995.0028.

Pal, P., Singh, N., Kaur, P., et al. (2018) Effect of Parboiling on Phenolic, Protein, and Pasting Properties of Rice from Different Paddy Varieties. *Journal of Food Science*, 83 (11): 2761–2771. doi:10.1111/1750-3841.14347.

Pathiraje, P., Madhujith, W., Chandrasekara, A., et al. (2011) The Effect of Rice Variety and Parboiling on *in vivo* Glycemic Response. *Tropical Agricultural Research*, 22 (1): 26. doi:10.4038/tar.v22i1.2667.

Santos, T.P. and Cunha, R.L. (2018) Role of process variables on the formation and *in vitro* digestion of gellan gels. *Carbohydrate polymers*, 192: 111–117. doi:10.1016/J.CARBPOL.2018.03.062.

Shen, L., Li, J. and Li, Y. (2022) Resistant starch formation in rice: Genetic regulation and beyond. *Plant Communications*, 3 (3): 100329. doi:10.1016/J.XPLC.2022.100329.

Sivakamasundari, S.K., Moses, J.A. & Anandharamakrishnan, C. (2020) Effect of parboiling methods on the physicochemical characteristics and glycemic index of rice varieties. *Journal of Food Measurement and Characterization*, 14 (6): 3122–3137. doi:10.1007/s11694-020-00551-9.

Sivakamasundari, S.K., Priyanga, S., Moses, J.A., et al. (2022) Impact of processing techniques on the glycemic index of rice. *Critical Reviews in Food Science and Nutrition*. 62 (12) pp. 3323–3344. doi:10.1080/10408398.2020.1865259.

Tamura, M., Okazaki, Y., Kumagai, C., et al. (2017) The importance of an oral digestion step in evaluating simulated *in vitro* digestibility of starch from cooked rice grain. *Food Research International*, 94: 6–12. doi:10.1016/j.foodres.2017.01.019.

Tamura, M., Singh, J., Kaur, L., et al. (2016) Impact of structural characteristics on starch digestibility of cooked rice. *Food Chemistry*, 191: 91–97. doi:10.1016/j.foodchem.2015.04.019.

Tian, J., Cai, Y., Qin, W., et al. (2018) Parboiling reduced the crystallinity and *in vitro* digestibility of non-waxy short-grain rice. *Food Chemistry*, 257: 23–28. doi:10.1016/j.foodchem.2018.03.005.

Truong, T.H., Yuet, W.C. & Hall, M.D. (2014). The glycemic index of American-grown jasmine rice is classified as high. *http://dx.doi.org/10.3109/09637486.2013.869797*, 65 (4): 436–439. doi:10.3109/09637486.2013.869797.

Vandeputte, G.E., Derycke, V., Geeroms, J., et al. (2003) Rice starches. II. Structural aspects provide insight into swelling and pasting properties. *Journal of Cereal Science*, 38 (1): 53–59. doi:10.1016/S0733-5210(02)00141-8.

Wolever, T.M.S., Jenkins, D.J.A., Kalmusky, J., et al. (1986) Comparison of regular and parboiled rice: explanation of discrepancies between reported glycemic responses to rice. *Nutrition Research*, 6 (4): 349–357. doi:10.1016/S0271-5317(86)80175-0.

Wu, J. & Warren, F.J. (2023) The impact of the soluble protein fraction and kernel hardness on wheat flour starch digestibility. *Food Chemistry*, 406: 135047. doi:10.1016/J.FOODCHEM.2022.135047.

Xu, X., Bean, S., Wu, X., et al. (2022) Effects of protein digestion on *in vitro* digestibility of starch in sorghum differing in endosperm hardness and flour particle size. *Food Chemistry*, 383: 132635. doi:10.1016/J.FOODCHEM.2022.132635.

Yu, W., Zhou, X. and Li, C. (2021) Application of first-order kinetics modelling to reveal the nature of starch digestion characteristics. *Food & Function*, 12 (15): 6652–6663. doi:10.1039/D1FO00450F.

Yu, W., Zou, W., Dhital, S., et al. (2018) The adsorption of α-amylase on barley proteins affects the *in vitro* digestion of starch in barley flour. *Food Chemistry*, 241: 493–501. doi:10.1016/J.FOODCHEM.2017.09.021.

Zou, W., Sissons, M., Gidley, M.J., et al. (2015a) Combined techniques for characterising pasta structure reveal how the gluten network slows enzymic digestion rate. *Food Chemistry*, 188: 559–568. doi:10.1016/j.foodchem.2015.05.032.

5.6 Supplementary material

Tab. S1. Description of digestion objects in each set.

Set	Description
Set 1_A	digest only starch by the intestinal α-amylase.
Set 2_P	digest starch and protein in a sentient manner by using intestinal pancreatin.
Set 3_PA	digest proteins with pepsin in the gastric phase, followed by digesting starch alone with intestinal α-amylase
Set 4_PP	digest the protein first with pepsin in the gastric phase, then digest starch and protein with pancreatin.
Set 5_PTA_con and Set 6_PTA	Digest the protein first with pepsin in the gastric phase, and further intestinal proteolysis with trypsin for 180mins (as a control, incubate without trypsin to assess the effect of water diffusion)
Set 7 HPP	A complete set of three-stage IVD experiments was carried out to predict the glycaemic index using salivary α-amylase(oral), gastric proteolysis (pH 3, pepsin), and protein-starch digestion using pancreatin.

Tab. S2. Kinetic fitting (LoS and CPS) with constant rates fitting the JR and PR with and without 1 % LAGG addition (20s homogenisation).

		C_0 (%)	k_1 (min^{-1})	$C_{\infty 1}$ (%)	t_{int} (min)	k_2 (min^{-1})	$C_{\infty 2}$ (%)	R^2	k_1 (min^{-1})	$C_{\infty 1}$ (%)	t_{2start} (min)	k_2 (min^{-1})	$C_{\infty 2}$ (%)	R^2
JR	A	1.69±0.83^{c}	0.114±0.006^{b}	22.74±0.37^{c}	14.17±0.29^{a}	0.009±0.001^{c}	35.77±4.59^{c}	0.9618	0.128±0.017^{b}	27.70±2.51^{b}	12.33±2.02^{a}	0.007±0.001^{c}	39.47±6.86^{cd}	0.9993
	P	2.66±0.54^{bc}	0.128±0.018^{b}	28.50±3.82^{c}	14.52±0.03^{a}	0.015±0.003^{b}	46.94±1.87^{b}	0.9174	0.121±0.012^{b}	32.13±3.43^{b}	11.87±2.17^{a}	0.015±0.005^{ab}	48.04±2.82^{b}	0.9995
	PA	3.23±0.61^{b}	0.085±0.001^{c}	23.63±2.09^{d}	10.21±0.21^{b}	0.022±0.002^{a}	64.18±3.44^{a}	0.9794	0.122±0.026^{b}	22.01±1.52^{b}	11.26±1.25^{a}	0.019±0.001^{a}	67.73±1.60^{a}	0.9988
	PP	3.51±0.54^{b}	0.142±0.013^{b}	37.75±1.70^{b}	13.04±2.61^{a}	0.017±0.001^{b}	53.76±2.10^{b}	0.9169	0.114±0.021^{bc}	28.59±2.74^{b}	10.21±0.36^{a}	0.016±0.001^{ab}	63.62±5.35^{a}	0.9979
	PTA_con	9.75±0.45^{a}	0.135±0.034^{b}	38.28±2.36^{b}	14.50±0.00^{a}	0.007±0.000^{c}	29.74±2.96^{c}	0.9899	0.103±0.013^{c}	24.54±3.90^{b}	13.18±2.30^{a}	0.009±0.002^{c}	30.29±1.34^{d}	0.9992
	PTA	9.00±0.66^{a}	0.199±0.002^{a}	46.84±1.04^{a}	14.50±0.00^{a}	0.014±0.003^{b}	32.29±2.02^{c}	0.9290	0.207±0.011^{a}	45.85±0.63^{a}	9.98±0.02^{a}	0.011±0.002^{c}	31.61±2.81^{d}	0.9993
From Set 1_A to Set 6_PTA in JR, different letters over each column indicate significant differences ($p < 0.05$)														
JR_1LA	A	0.55±0.10^{a}	0.112±0.002^{a}	19.02±1.10^{a}	15.60±0.00^{a}	0.012±0.001^{a}	29.03±1.83^{c}	0.9092	0.114±0.005^{a}	24.61±0.42^{d}	0.00±0.00^{b}	0.012±0.001^{a}	31.67±1.62^{a}	0.9997
	P	1.30±0.12^{c}	0.106±0.001^{a}	17.71±1.20^{d}	15.00±0.00^{a}	0.015±0.001^{a}	48.15±1.80^{b}	0.9081	0.118±0.003^{a}	32.28±2.77^{c}	14.75±0.22^{a}	0.14±0.001^{a}	45.67±0.80^{b}	0.9986
	PA	3.21±0.68^{b}	0.015±0.001^{c}	90.19±1.80^{a}	--	--	--	0.9586	0.016±0.001^{c}	86.38±1.87^{a}	--	--	--	0.9996.
	PP	1.76±0.42^{c}	0.113±0.001^{a}	21.77±3.04^{c}	14.50±0.50^{a}	0.010±0.001^{c}	63.94±1.26^{a}	0.9439	0.114±0.005^{a}	20.54±0.78^{d}	10.00±0.00^{a}	0.010±0.001^{a}	67.71±1.19^{c}	0.9991
	PTA_con	13.05±0.34^{a}	0.027±0.000^{b}	75.60±3.23^{b}	--	--	--	0.9604	0.031±0.001^{b}	74.75±1.35^{b}	--	--	--	0.9982
	PTA	13.85±2.42^{a}	0.113±0.001^{a}	22.99±2.94^{c}	15.04±1.00^{a}	0.009±0.001^{c}	50.67±4.27^{b}	0.9189	0.114±2.014^{a}	20.46±2.12^{d}	10.67±0.58^{a}	0.008±0.000^{b}	54.38±4.48^{d}	0.9988
From Set 1_A to Set 6_PTA in JR_1LA, different letters over each column indicate significant differences ($p < 0.05$)														

Mean ± S.D. calculated from triplicate measurements. For each parameter (column), the different superscript letters indicate values among the four samples are statistically different ($p < 0.05$). Values presented here are: the concentration of digested starch (C_0, %) at the beginning of intestinal digestion phase; starch digestion rate constants of rapid (k_1) and slow phase (k_2), corresponding estimated percentage of digested starch ($C_{\infty 1}$ and $C_{\infty 2}$, %), t_{int} is defined as the time intersection of two distinct digestion phase (estimated from LoS model), and t_{2start} is defined as the time intersection of two distinct digestion phase (estimated from CPS model). The goodness of curve-fitting (reflected by R^2).

		C_0 (%)	k_1 (min^{-1})	$C_{\infty 1}$ (%)	t_{int} (min)	k_2 (min^{-1})	$C_{\infty 2}$ (%)	R^2	k_1 (min^{-1})	$C_{\infty 1}$ (%)	t_{2start} (min)	k_2 (min^{-1})	$C_{\infty 2}$ (%)	R^2
PR	A	1.69±0.83^{c}	0.114±0.006^{b}	22.74±0.37^{c}	14.17±0.29^{a}	0.009±0.001^{c}	35.77±4.59^{c}	0.9618	0.128±0.017^{b}	27.70±2.51^{b}	12.33±2.02^{a}	0.007±0.001^{c}	39.47±6.86^{cd}	0.9993
	P	2.32±0.33^{c}	0.127±0.005^{c}	47.09±1.70^{a}	16.50±0.78^{a}	0.017±0.004^{a}	46.27±1.55^{b}	0.9913	0.155±0.007^{c}	43.61±1.77^{a}	14.50±0.00^{a}	0.015±0.001^{b}	51.56±4.01^{c}	0.9993
	PA	8.04±1.28^{ab}	0.080±0.005^{e}	22.92±2.29^{c}	12.50±1.10^{b}	0.018±0.001^{b}	56.95±5.45^{a}	0.9555	0.087±0.003^{d}	18.70±1.53^{d}	10.17±0.28^{b}	0.017±0.002^{c}	63.29±0.36^{a}	0.9989
	PP	10.26±1.48^{a}	0.096±0.001^{d}	35.79±3.24^{b}	14.50±1.31^{a}	0.022±0.004^{a}	58.40±4.44^{b}	0.9679	0.221±0.001^{a}	35.57±3.70^{b}	12.20±0.30^{ab}	0.029±0.003^{a}	71.31±3.12^{c}	0.9982
	PTA_con	6.90±2.39^{b}	0.195±0.006^{b}	39.90±1.83^{b}	15.50±0.50^{b}	0.009±0.001^{c}	49.67±5.28^{b}	0.9553	0.210±0.009^{ab}	30.24±2.91^{c}	12.00±1.43^{ab}	0.011±0.001^{c}	55.83±1.85^{a}	0.9989
	PTA	7.54±0.43^{b}	0.223±0.002^{a}	34.26±3.06^{b}	15.20±0.70^{b}	0.020±0.003^{a}	56.05±2.92^{a}	0.9613	0.223±0.017^{a}	28.25±0.74^{d}	12.50±0.20^{ab}	0.021±0.002^{c}	60.27±4.00^{a}	0.9995
From Set 1_A to Set 6_PTA in PR, different letters over each column indicate significant differences (p < 0.05)														
PR_1LA	A	1.89±0.20^{c}	0.080±0.005^{c}	32.13±4.12^{a}	14.25±0.16^{a}	0.019±0.002^{b}	61.80±4.12^{b}	0.9474	0.142±0.005^{c}	31.08±2.75^{b}	13.20±1.30^{a}	0.018±0.001^{c}	52.37±4.25^{a}	0.9984
	P	2.06±0.25^{bc}	0.125±0.003^{a}	32.63±2.79^{a}	12.50±0.29^{b}	0.029±0.001^{a}	64.07±6.16^{b}	0.9630	0.157±0.006^{b}	27.45±1.20^{b}	12.50±0.00^{a}	0.027±0.002^{a}	64.65±1.51^{b}	0.9997
	PA	5.67±1.80^{b}	0.017±0.002^{d}	89.71±3.47^{b}	--	--	--	0.9283	0.018±0.005^{d}	87.01±1.45^{a}	--	--	--	0.9991
	PP	3.42±1.46^{bc}	0.114±0.008^{b}	36.23±1.51^{a}	14.00±0.50^{a}	0.018±0.001^{b}	57.60±0.17^{a}	0.9494	0.177±0.002^{a}	28.37±2.49^{b}	12.80±0.30^{a}	0.018±0.000^{b}	58.58±1.03^{c}	0.9991
	PTA_con	10.87±0.35^{a}	0.026±0.003^{d}	86.61±2.14^{c}	--	--	--	0.9383	0.028±0.005^{d}	88.48±0.53^{a}	--	--	--	0.9979
	PTA	9.79±1.20^{a}	0.127±0.003^{a}	30.24±3.43^{a}	12.50±0.96^{b}	0.019±0.002^{b}	58.15±3.11^{a}	0.9773	0.177±0.000^{a}	28.45±1.93^{b}	12.00±0.89^{a}	0.022±0.001^{c}	61.78±0.75^{c}	0.9999
From Set 1_A to Set 6_PTA in PR_1LA, different letters over each column indicate significant differences (p < 0.05)														

Mean ± S.D. calculated from triplicate measurements. For each parameter (column), the different superscript letters indicate values among the four samples are statistically different (p < 0.05). Values presented here are: the concentration of digested starch (C_0, %) at the beginning of intestinal digestion phase; starch digestion rate constants of rapid (k_1) and slow phase (k_2), corresponding estimated percentage of digested starch ($C_{\infty 1}$ and $C_{\infty 2}$, %), t_{int} is defined as the time intersection of two distinct digestion phase (estimated from LoS model), and t_{2start} is defined as the time intersection of two distinct digestion phase (estimated from CPS model). The goodness of curve-fitting (reflected by R^2).

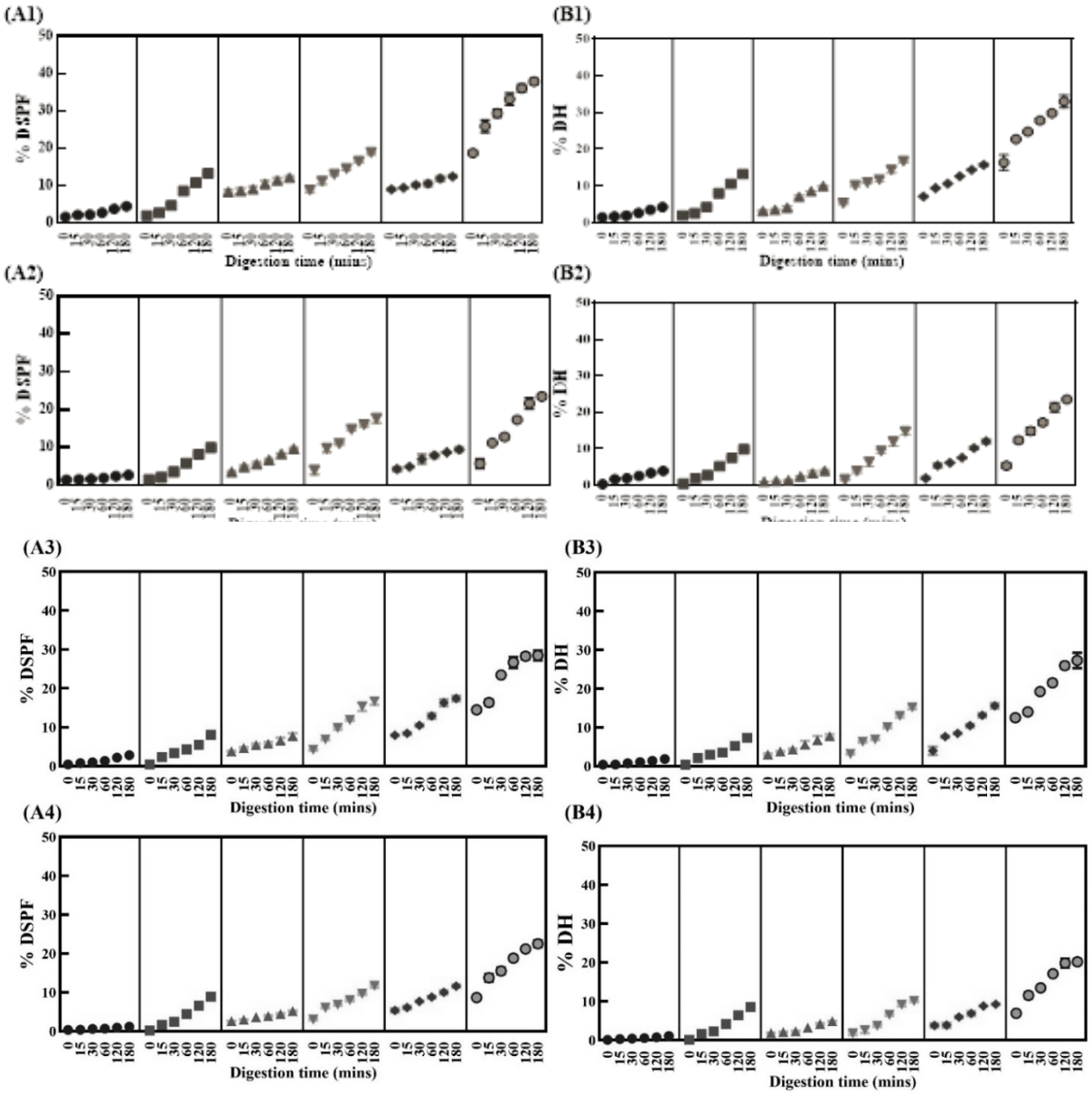


Fig. S1. DSPF (%) and DH (%) in cooked rice samples (intact grain) determined by BCA (A) and OPA (B) assays, respectively. (1) JR, (2) JR_1LA, (3) PR, (4) PR_1LA.

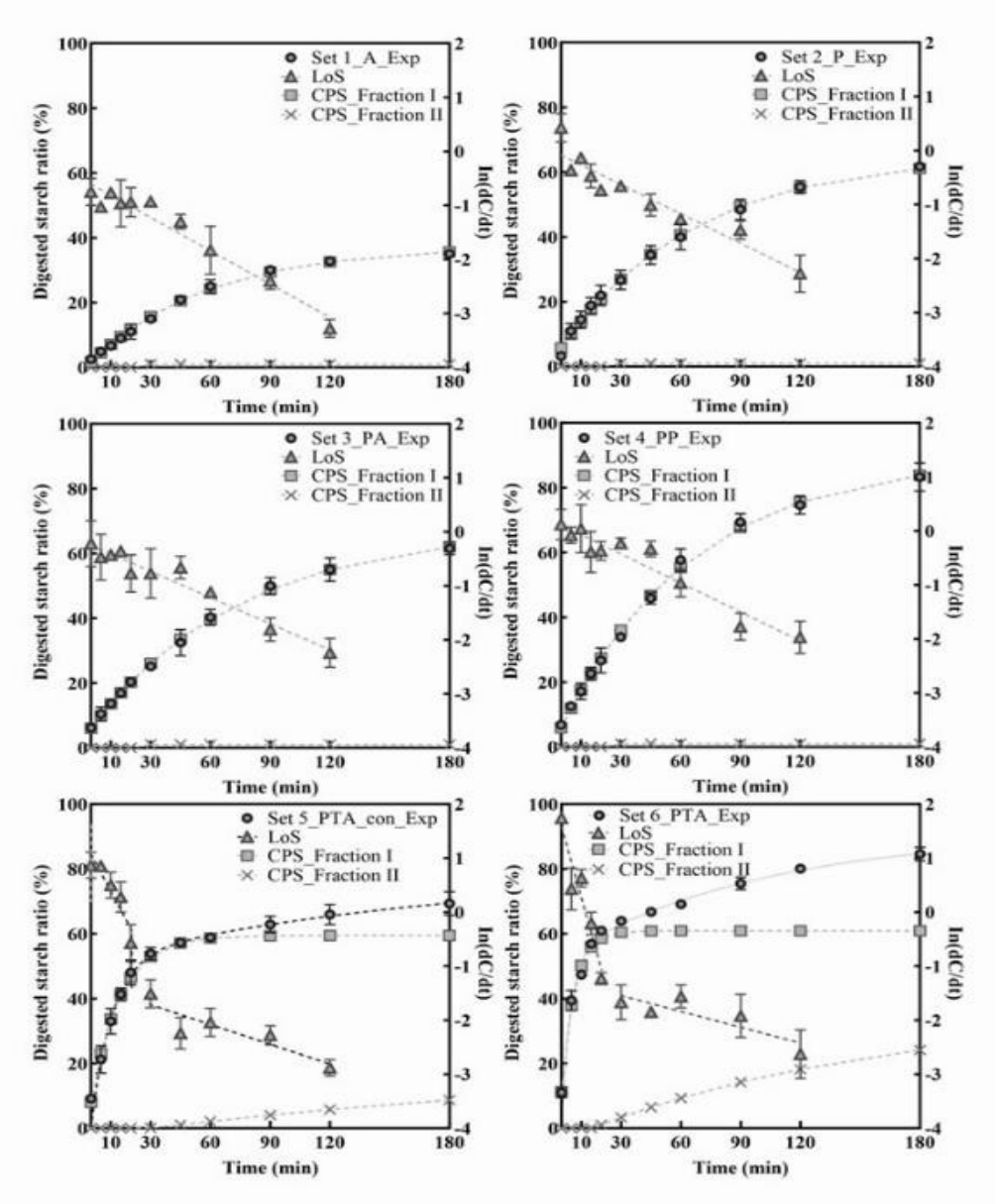


Fig. S2. *In vitro* starch digestion of cooked JR_1LA grains.

Circles correspond to the experimental values; all error bars represent standard deviations (n = 4). Letters A to F represent from Set 1_A to Set 6_PTA; Triangles with dashed lines correspond to LoS plots. Squares and crosses corresponded to digestion fractions I and II of starch based on CPS kinetics model fittings for the digestion curves.

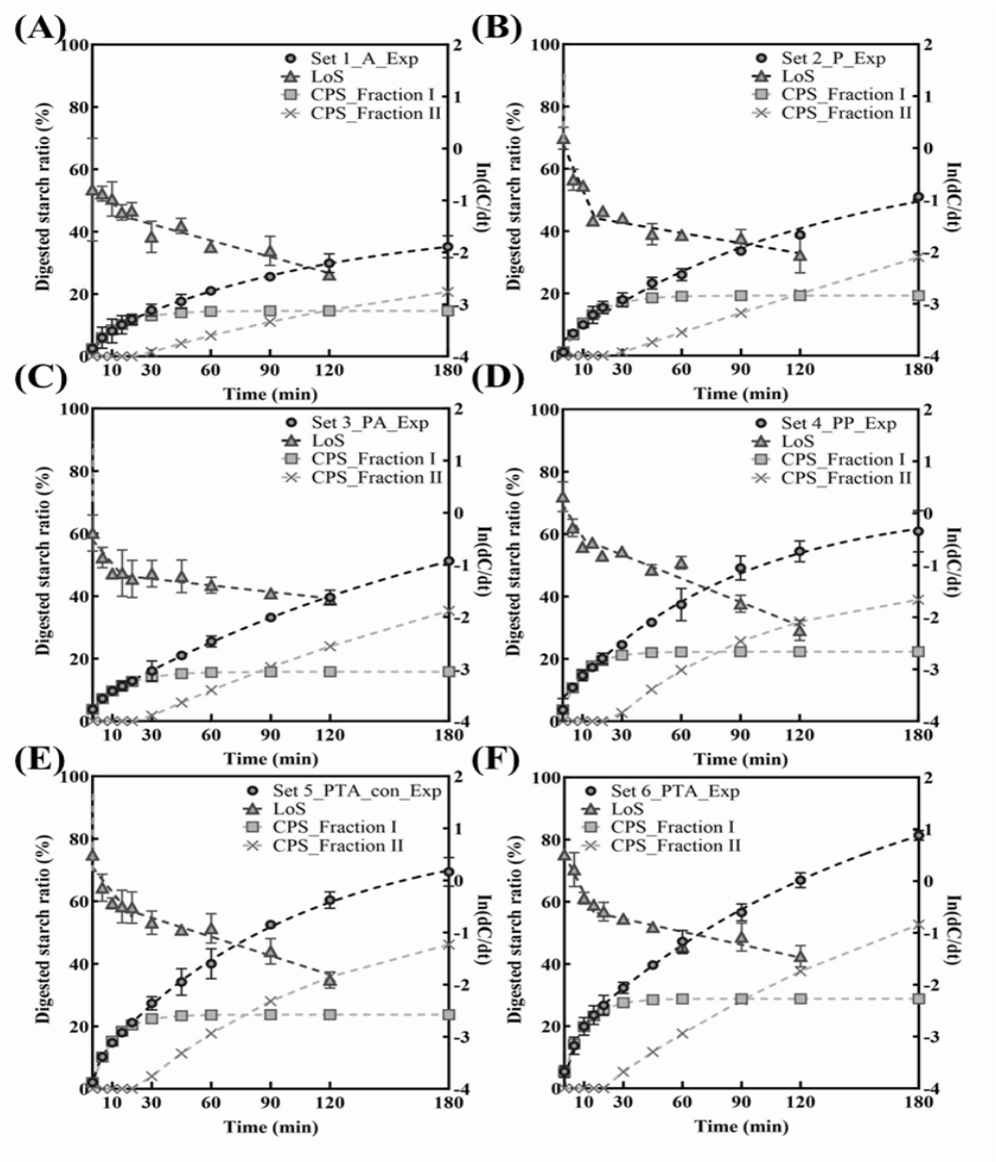


Fig. S3. *In vitro* starch digestion of cooked PR grains.

Circles correspond to the experimental values; all error bars represent standard deviations (n = 4). Letters A to F represent from Set 1_A to Set 6_PTA; Triangles with dashed lines correspond to LoS plots. Squares and crosses corresponded to digestion fractions I and II of starch based on CPS kinetics model fittings for the digestion curves.

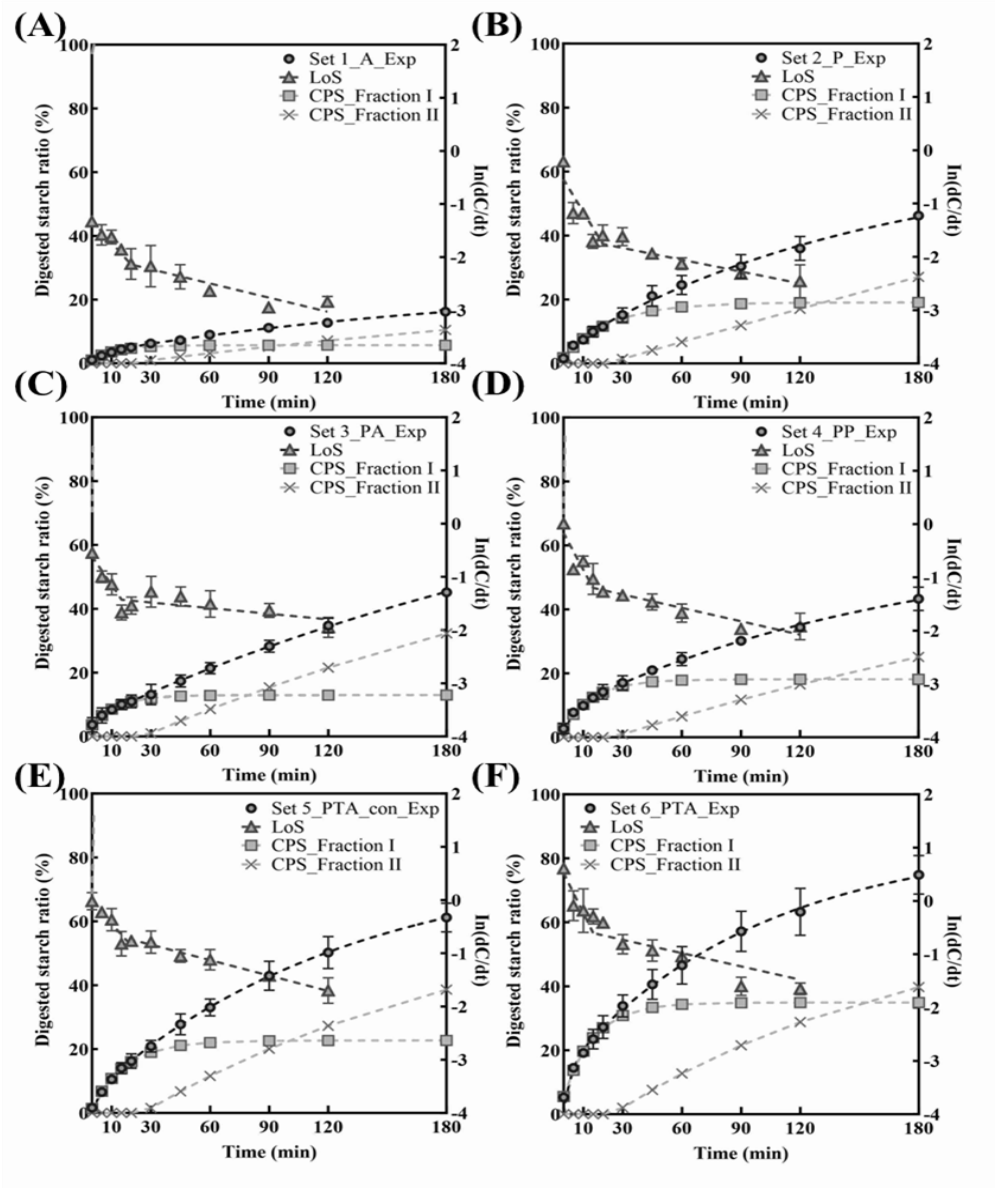


Fig. S4.*In vitro* starch digestion of cooked PR_1LA grains.

Circles correspond to the experimental values; all error bars represent standard deviations (n = 4). Letters A to F represent from Set 1_A to Set 6_PTA; Triangles with dashed lines corresponded to LoS plots. Squares and crosses corresponded to digestion fractions I and II of starch based on CPS kinetics model fittings for the digestion curves.

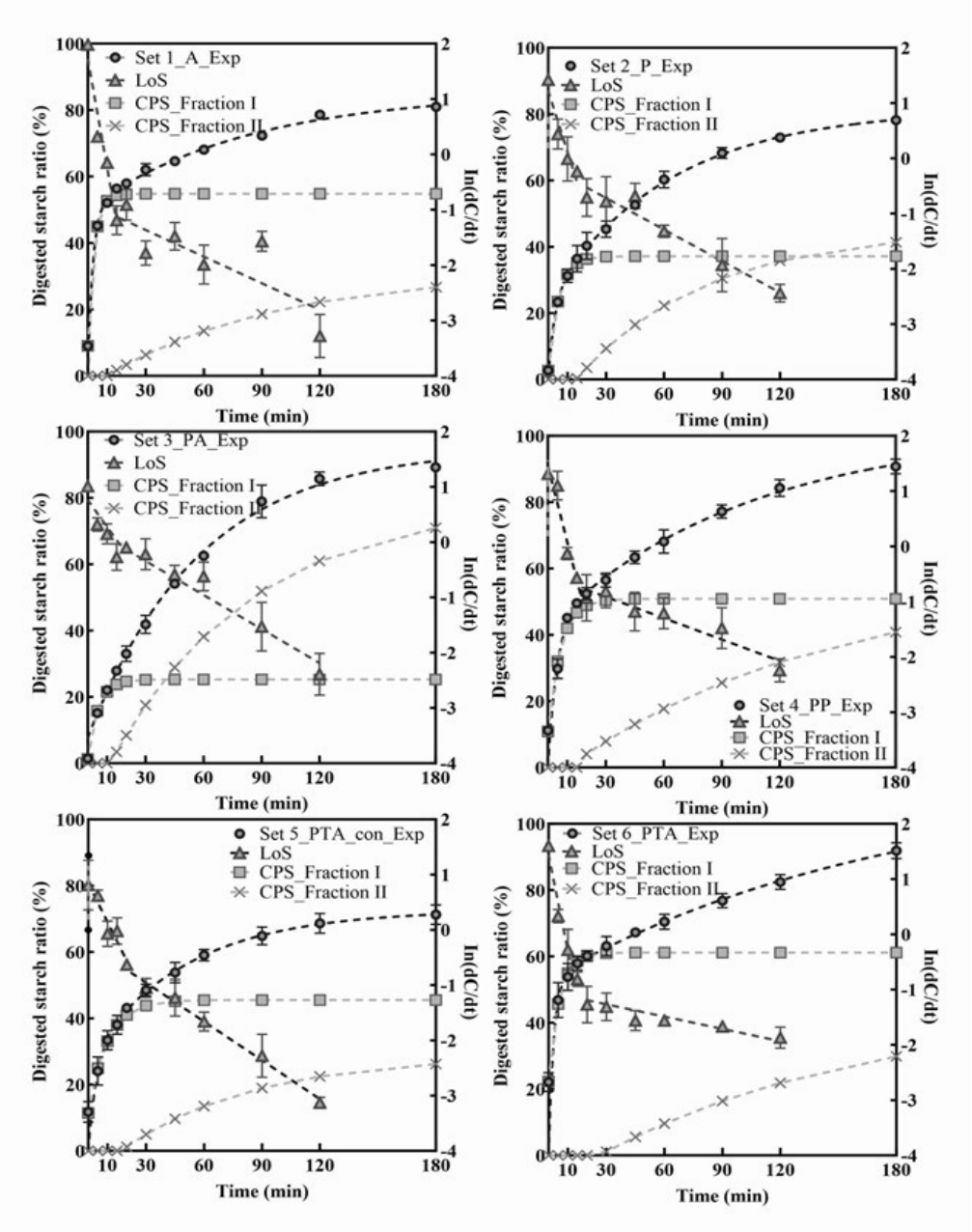


Fig. S5 *In vitro* starch digestion of homogenised (20s) JR samples.

Circles correspond to the experimental values; all error bars represent standard deviations (n = 4). Letters A to F represent from Set 1_A to Set 6_PTA; Triangles with dashed lines corresponded to LoS plots. Squares and crosses corresponded to digestion fractions I and II of starch based on CPS kinetics model fittings for the digestion curves.

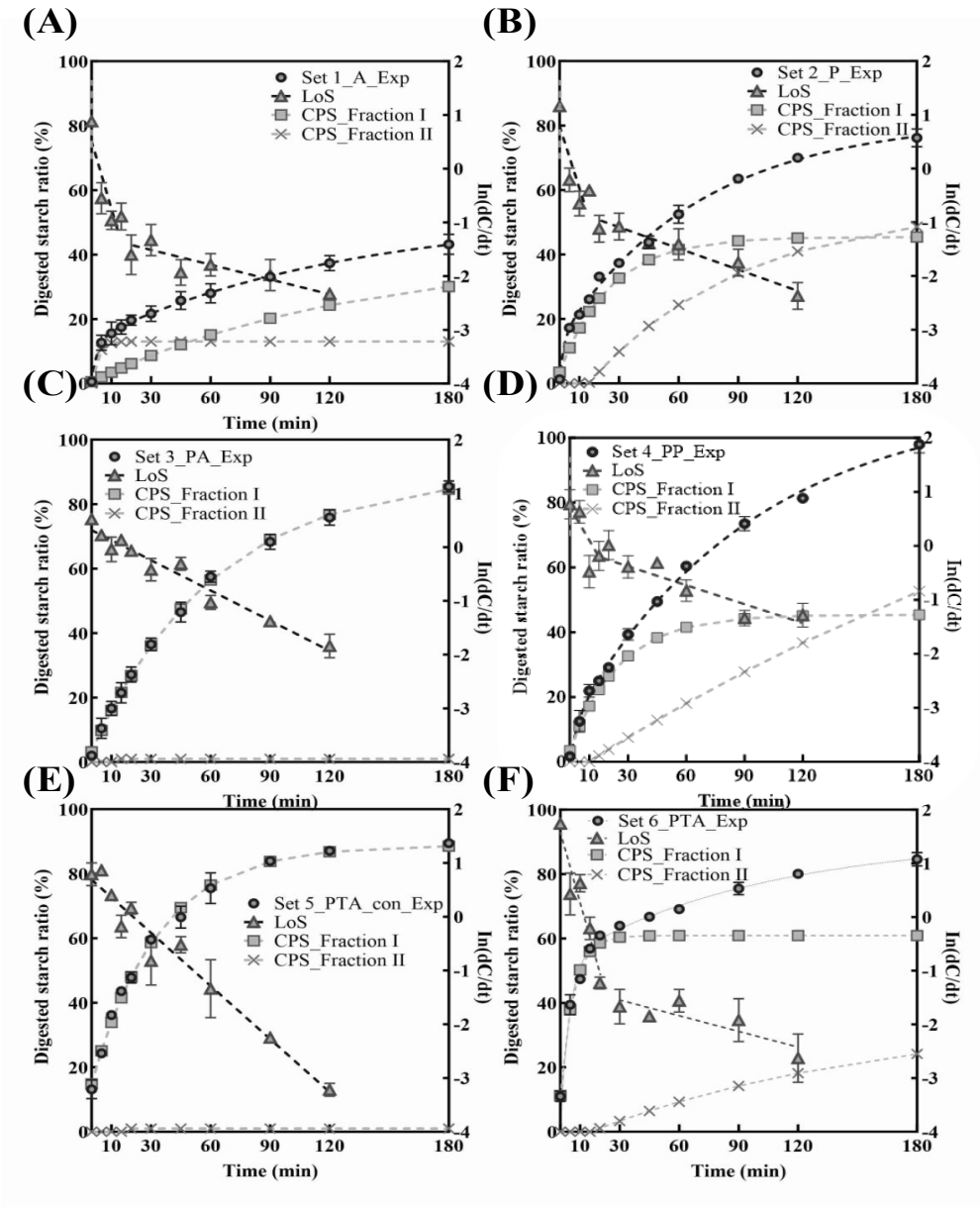


Fig. S6. *In vitro* starch digestion of homogenised (20s) JR_1LA samples.

Circles correspond to the experimental values; all error bars represent standard deviations (n = 4). Letters A to F represent from Set 1_A to Set 6_PTA. Triangles with dashed lines. corresponded to LoS plots. Squares and crosses corresponded to digestion fractions I and II of starch based on CPS kinetics model fittings for the digestion curves.

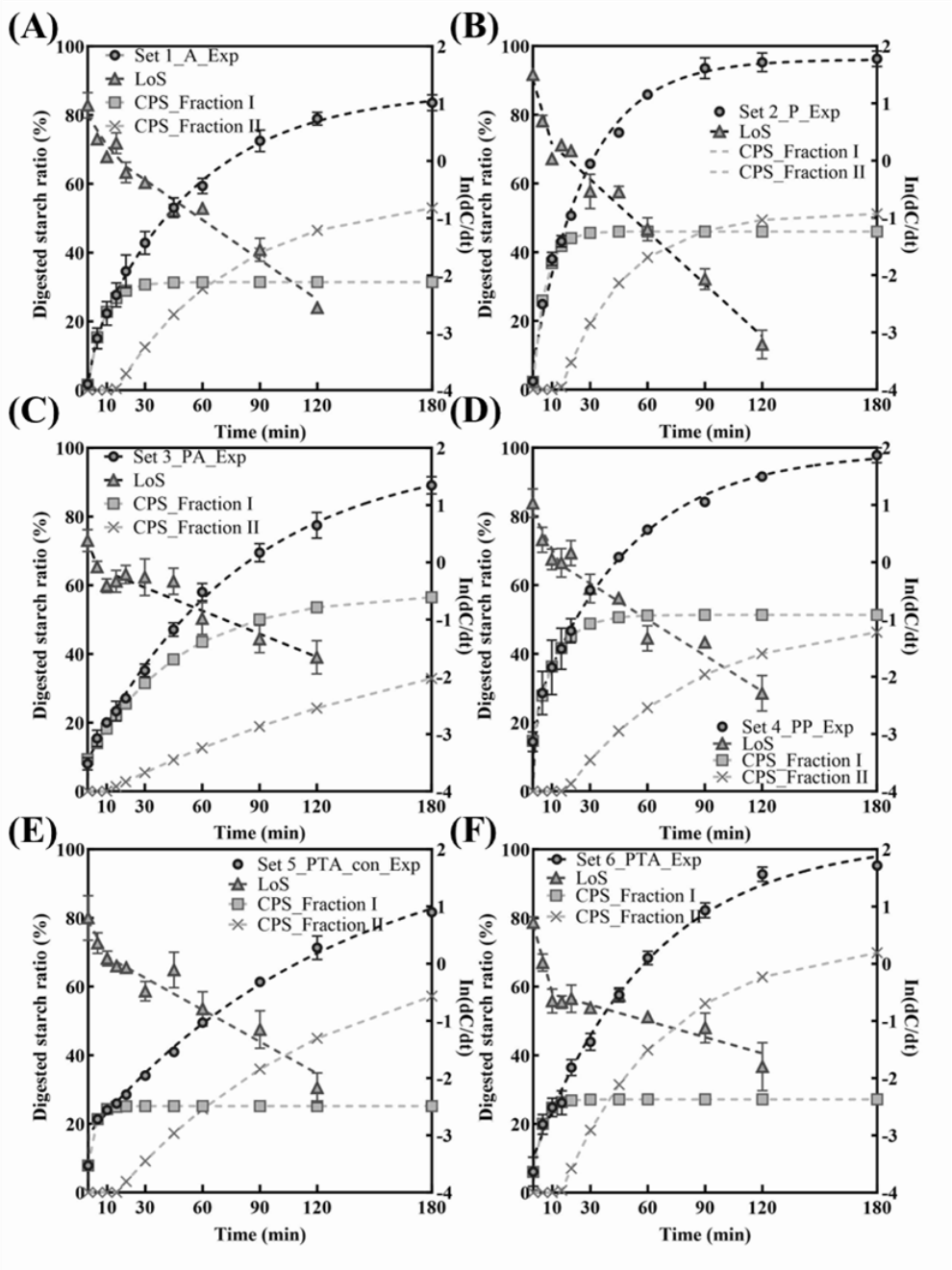


Fig. S7. *In vitro* starch digestion of homogenised (20s) PR samples.

Circles correspond to the experimental values; all error bars represent standard deviations (n = 4). Letters A to F represent from Set 1_A to Set 6_PTA; triangles with dashed lines corresponded to LoS plots. Squares and crosses corresponded to digestion fractions I and II of starch based on CPS kinetics model fittings for the digestion curves.

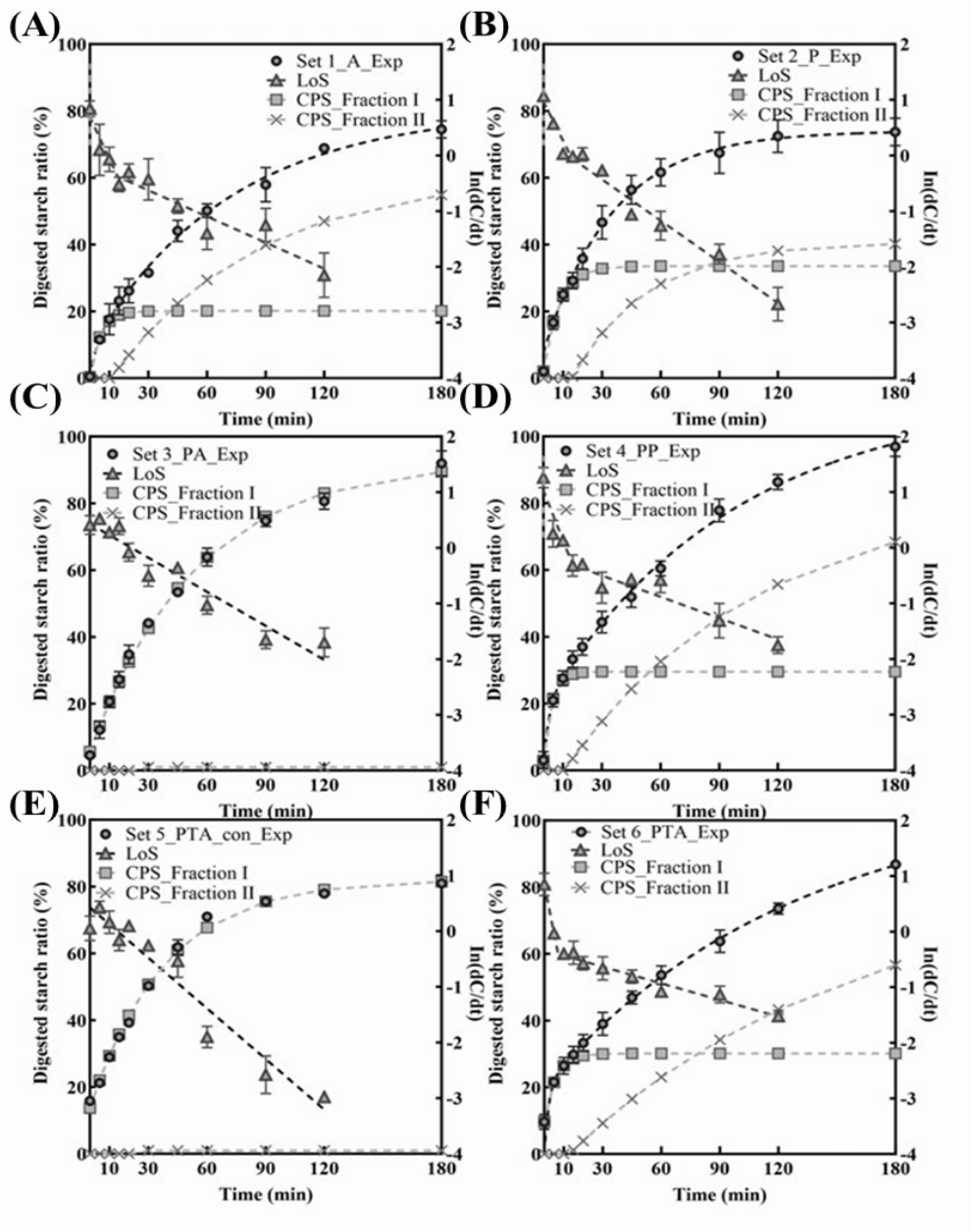


Fig. S8. *In vitro* starch digestion of homogenised (20s) PR_1LA samples.

Circles correspond to the experimental values; all error bars represent standard deviations (n = 4). Letters A to F represent from Set 1_A to Set 6_PTA; triangles with dashed lines corresponded to LoS plots. Squares and crosses corresponded to digestion fractions I and II of starch based on CPS kinetics model fittings for the digestion curves.

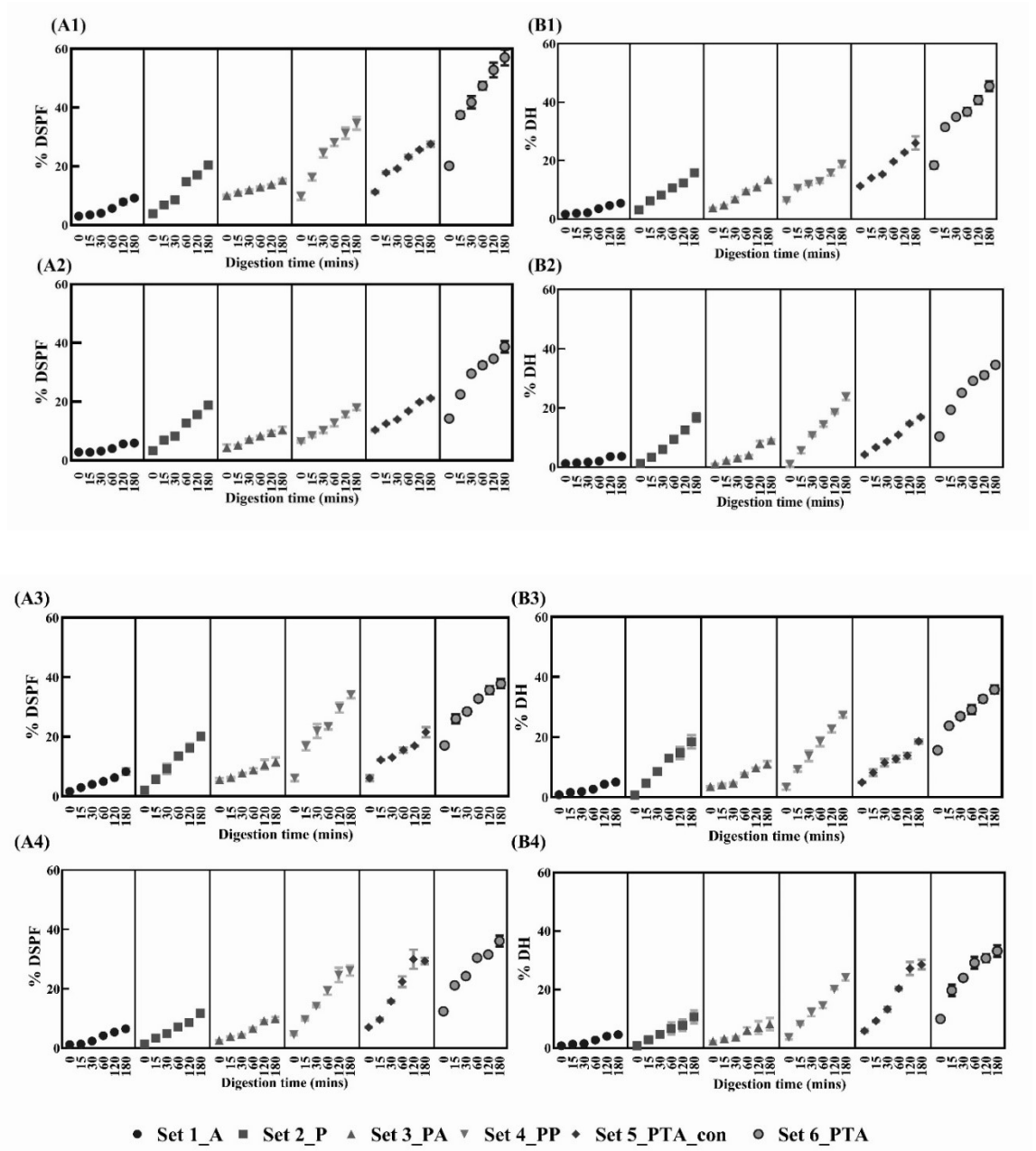


Fig. S9. DSPF (%) and DH (%) in cooked rice samples (homogenised sample) as determined by BCA (A) and OPA (B) assays, respectively. (1) JR, (2) JR_1LA, (3) PR, (4) PR_1LA.

6 An *in vitro* study of protein and starch digestibility in rice cooked with low acyl gellan gum evaluated using static and semi-dynamic digestion models

Qingsu Liu[1], Vincenzo di Bari[2], Nicholas J. Watson[3*]

[1] Food, Water, Waste Research Group, Faculty of Engineering, The University of Nottingham, University Park Campus, NG7 2RD, UK.

[2]Division of Food, Nutrition and Dietetics, School of Biosciences, The University of Nottingham, Sutton Bonington Campus, Loughborough, LE12 5RD, UK.

[3] School of Food Science and Nutrition, University of Leeds, Leeds, LS2 9JT, UK.

*Corresponding author: n.j.watson@leeds.ac.uk

(Manuscript prepared for Submission)

Abstract

The role of structural disintegration on starch digestibility during *in vitro* oral processing of cooked white rice was investigated. For the *in vitro* oral phase, rice was homogenised for 0 s, 10 s, or 20 s, corresponding to three different extents of oral processing (only swallowing, normal, or fine chewing, respectively). Two rice types, parboiled rice (PR) and jasmine non-parboiled rice (JR), were compared for their different microstructure. JR and PR were cooked either in only water or in water containing 1 % low acyl gellan gum (LAGG). For the non-homogenised (0 s) rice samples, JR showed a higher predicted glycaemic index (pGI) (71.4) than PR (50.0). Microstructure analysis suggested that the lower pGI in PR could be attributed to its more ordered protein-starch matrices, which preserved the structural integrity of starch accessible by enzymes. The impact of rice type on pGI became less pronounced with increasing homogenisation time. When homogenised JR and PR were compared, particle size differences decreased after homogenisation, and PR reached a similar pGI level to JR. The impact of pre-homogenisation of rice on starch digestibility is less apparent under the semi-dynamic digestion model. It is possible to attribute the grain disintegration in the semi-dynamic model to the mechanical movements involved, such as continuous mixing and compressing, which simulate the contractions of the digestive system. When JR and PR were cooked in LAGG dispersion, they showed lower starch digestibility and pGI than the respective water-cooked samples under the three homogenisation conditions. Several factors have been attributed to this, including a physical barrier effect of LAGG, which allows cooked rice to retain some structural integrity (as indicated by microscopy and bolus swelling imaging), as well as a greater viscosity in the intestinal phase of digestion. Overall, this work suggests that, as more complex digestive conditions were applied (homogenisation step, semi-dynamic digestion system), LAGG exhibited multi-functionality in mitigating starch digestibility of cooked rice, which could be used as a potential approach towards developing starch-based foods with reduced GI.

Highlights

- A static and semi-dynamic digestion model was employed for the first time to investigate the characteristics of starch digestibility on cooked rice with or without low acyl gellan gum in response to three homogenisation levels (non-, 10 s and 20 s).
- *In vitro* oral processing combined with a semi-dynamic model appeared to be a more reproducible method to determine the starch digestibility of cooked rice than when combined with a static model.
- PR is harder and less sticky than JR, showing higher fragmentation upon homogenisation.
- Rice cooked with low acyl gellan gum (LAGG) displayed a reduction in starch digestibility and pGI. The mitigating effect of LAGG diminished when homogenisation was applied.
- The mitigating effect of LAGG on pGI was lower when *in vitro* digestion was applied to pre-homogenised rice samples.

Keywords: white rice, **low acyl gellan gum**, **static *in vitro* digestion**, **semi-dynamic *in vitro* digestion**.

6.1 Introduction

Nowadays, there is a strong interest in understanding the modulating effects of food digestion on improving human health. In particular, replacing high glycaemic index (GI) foods (such as refined cereal products) with foods that contain slowly digestible starch (SDS) and resistant starch (RS) has been recommended as an intervention method for managing glycaemic response in clinics with multiple health benefits, including those for obese (Jimenez-Cruz et al., 2003), people with diabetes (Rave et al., 2007) and cardiovascular disease (Amano et al., 2004). The research approaches in this field have changed from *in vivo* to a hybrid approach incorporating *in vitro* due to many limitations of the *in vivo* method alone, such as time consumption, high cost, invasive sampling, inter-individual variability, and ethical concerns. *In vitro* models would enhance the reproducibility and the acquisition of more detailed information, such as specific nutrient digestibility on food microstructural changes (like structure disintegration viscosity) (Villemejane et al., 2015, 2016). Prediction of the GI of starchy foods by *in vitro* method is a classic example of *in vitro* method application as a pilot trial prior to *in vivo* test in food product development with a low-GI (Argyri et al., 2016).

Most *in vitro* digestion systems focus on the gastric and intestinal phases by developing a series of mechanical, chemical, and enzymatic processes to simulate digestion. Conversely, simulated oral processes have yet to be widely implemented due to the short duration compared to the entire digestion process. For example, chewing normally takes less than 10 seconds for swallowing, and salivary enzymes are exposed for less than 2 mins before becoming inactive shortly after entering the stomach. However, the oral phase dramatically affects food digestibility due to the reduction in particle size and increasing surface area that happens during this phase. The importance of the oral phase for the digestion of starchy foods has been highlighted in relation to the food's structural integrity (Blanquet-Diot et al., 2021). Decreasing the food particle size by mastication increases the surface area exposure, allowing higher enzyme accessibility and thus higher starch digestion, as observed in wheat (Heaton et al., 1988), corn (Panouillé et al., 2016), oats and rice (Tamura et

al., 2017). Corresponding to *in vitro* results, Read et al. (1986) showed that thorough chewing of rice, potato, or sweet corn induced a postprandial increase in glucose while swallowing those foods without chewing significantly reduced the blood glucose response. In Ranawana et al. (2010a, 2010b), particle size was found to relate significantly to the *in vivo* glycaemic response to chewed cooked rice. However, differences in individuals' chewing may lead to differences in the glycaemic response.

In addition, food that supplies health benefits via digestion should also be valued based on its physical domain, referred to as "food matrices". This is a system that includes and interacts with specific constituents in a way that provides different functionalities and behaviours than those exhibited by the components alone (Aguilera, 2019). In particular, many researchers have explored the possibility of lowering GI of cereal products, like white rice, through genetic, chemical, and physical approaches. These techniques have considered starch microstructure, and non-starch components, including protein, lipids, and dietary fibres. It was found that modified starch had reduced starch digestibility and several structural characteristics, including a higher amylose content and an orderly multiscale organisation within the cell, slowing enzyme-catalysed reactions. It has also been found that protein networks and amylose-lipid complexes reduce starch digestion by providing physical barriers against enzyme access to starch (Guraya et al., 1997; Sagum & Arcot, 2000; Toutounji et al., 2019). Substituting a high-GI with a low-GI staple food, such as multigrain or cereals with a high protein/lipid content, has shown a minor but clinically meaningful effect on glycaemic control *in vivo* (Bornhorst et al., 2013).

Likewise, the addition of non-digestible fibres such as guar gum, xanthan gum, pullulan, and low acyl gellan gum (LAGG) could potentially reduce starch digestibility by reducing enzyme accessibility, as demonstrated by the *in vitro* system (Chen et al., 2017; Choi et al., 2010; Gouseti et al., 2014; Norton et al., 2011). Hydrocolloids still need to be better understood regarding how they influence starch digestion throughout the digestive system.

In this study, the effects of both the food matrices and the addition of dietary fibre on the starch digestibility of cooked rice throughout the oral-gastrointestinal tract were assessed. Two types of rice, white jasmine rice (high-GI) and parboiled rice (low-GI), whose effects on the glycaemic response have been demonstrated *in vivo* (Hamad et al., 2018), were tested. LAGG was used as a non-digestible fibre and hydrocolloid. Three mastication conditions (swallowing, normal, and fine) were considered and analysed using two *in vitro* digestion models, static and semi-dynamic, providing a more holistic analysis of the starch digestibility of cooked rice. The impact of rice type with different characteristics of the protein-starch matrices and mastication performance were analysed in terms of food bolus properties and level of starch digestibility undergoing mastication and gastrointestinal digestion.

6.2 Materials and methods

6.2.1 Materials

Two white rice types, one belonging to a high glycaemic index (GI) category (> 70) and one to a low-GI category (< 55), were selected (Atkinson et al., 2021; Ranawana et al., 2009). The high-GI type (89) was Thai Jasmine rice (JR, Green Dragon Thai Hom Mali Aaa, purchase date December 2018), whereas the low-GI (47) was parboiled rice (PR, easy-cook long grain rice, purchase date January 2019). The two white rice varieties are *Oryza sativa* indica, and for JR, no parboiling is involved in the manufacturing process. Low acyl gellan gum (LAGG) powder was purchased from CPKelco, UK. The enzymes used were purchased from Sigma-Aldrich, UK. Enzyme activity (**Tab. 6.1**) was determined using the procedures by Brodkorb et al. (2019). Unless otherwise stated, all other reagents were of analytical grade and supplied from Sigma-Aldrich, UK.

Tab. 6.1. Product code, batch number and activity (measured in our labs) for salivary α-amylase, pepsin, and pancreatin (consisting of α-amylase and trypsin) used in this study.

	salivary α-amylase	pepsin	Pancreatin (α-amylase / trypsin)
Product code (Sigma-Aldrich)	A1031[a]	P7000	P1750, 4×USP
batch number	SLBX2637	BCBZ7879	SLCD1114
Enzyme activity (U/mg)	146.2 [1]	557.5 [2]	31.4 [1]/2.3 [3]

[1] 1 unit/mg represented the capability of liberating 1 mg of maltose from soluble potato starch (S2630, Sigma-Aldrich) in three mins at a pH of 6.9 at 20°C.

[2] 1 unit/mg represented the capability of liberating the amount of Tyrosine produced from the haemoglobin decomposition at pH 2.0 at 37°C.

[3] 1 unit/mg represented the capability of hydrolysing 1 μmole of p-toluene-sulfonyl-L-arginine methyl ester (TAME) per min at 25°C, pH 8.1.

The reagents used to produce simulated salivary fluid (SSF), simulated gastric fluid (SGF), and simulated intestinal fluid (SIF) were prepared as in Brodkorb et al. (2019). The details have been included in **Chapter 3**, **Section 3.8.4.1**. In the present study, the bile salt was not included in the intestinal phase, as fat in white rice is negligible (<0.5%). The 5-(4,6-Dichlorotriazinyl) amino fluorescein (5-DTAF, CAS No. 51306−35−5, Sigma-Aldrich) was used as a labelling agent for LAGG.

6.2.2 Preparation of cooked rice samples

Rice was cooked as per previous studies (Chatthongpisut et al., 2015; Liu et al., 2019). In brief, JR or PR (100 g) were rinsed three times with distilled water and placed on 0.5 mm sieves at ambient temperature for an hour to dry. Rice samples were then placed in the cooking pot with 150 g of distilled water (1:1.5 rice-to-water mass ratio; w/w) and cooked using a rice cooker (NEDIS, Karc06wt-power 300W, Leicester, UK) for approximately 15 mins (until no excess water was present), after which the device automatically turned into a warm mode (65-70°C). The cooked rice was then kept in the rice cooker in warm mode for 10 mins to fully gelatinase the grain, as determined by visual inspection (no white core in the cooked rice kernels). Besides pure water, rice was also cooked in the 1 % LAGG dispersion (w/w of raw rice) using the same cooking method used with pure water. As demonstrated in **Chapter 4**, *in vitro* oral phase, 1 % LAGG can mitigate starch digestibility, with lower

differences between LAGG addition and control (non-LAGG) than at higher concentrations (2 and 3 %). Cooked rice was evaluated for moisture content and texture profile under the same serving conditions (intact grain, at 65°C) as those reported for *in vivo* trials in literature (Lu et al., 2017).

6.2.3 Proximate composition of cooked rice with and without LAGG

The moisture content of cooked rice grain was measured in triplicate using a moisture analyser (MB120, OHAUS, New Jersey, USA) at 105°C with air circulation according to AOAC Official Method 934.01(AOAC, 2005a). The crude protein content of cooked rice (dry matter) was determined according to the official AOAC method 930.29 using a nitrogen-to-protein conversion factor of 5.95 (AOAC, 2005b). The total starch content was determined using a total starch assay kit (AA/AMG, Megazyme, Wicklow, Ireland) following AOAC Official Method 996.11 (AOAC, 2007). The apparent amylose content of cooked rice was estimated using the iodine colourimetric method, as described by Mcgrane et al. (1998). All analyses were performed in triplicate.

6.2.4 Morphological structure of cooked rice with and without LAGG

Cooked rice kernel size (length, width, and thickness) was measured using a Vernier calliper with 0.01 mm accuracy. The shape (sphericity, surface area, and roundness) of cooked rice kernels was calculated using the method described by Mohsenin et al. (1987). The morphology of the protein-starch matrices within cooked rice was observed using an Eclipse Ci microscope (Nikon Instruments Inc., Surrey, UK) equipped with a Nikon digital Sight DS-Fi2 camera. Sample slides were prepared using a method adapted from Tamura et al. (2016). The cooked samples were exposed to optimum cryo-microtomy embedding medium and cut into 60 μm thick-sections with a microtome (Leica CM 3050s, Leica Microsystems, Milton Keynes, UK). Cross-sections were mounted on gelatine-coated microscope slides, stained with 0.1 % fast green FCF acetic acid (1 %) solution for protein detection, washed with distilled water, and stained with Lugol's solution (62650, Sigma-Aldrich1:10 dilution) for starch detection. Due to electrostatic bonding between the amino acid side chains and the fast green molecules, protein bodies appeared with a green

colour (Steglich et al., 2014), whereas starch appeared purple due to the formation of an amylose/amylopectin-iodine complex. LAGG was covalently labelled with 5-(4,6-dichlorotriazinyl) aminofluorescein (DTAF) following the procedure described by Khin et al. (2021). For labelling, rice was cooked with DTAF-LAGG with the same procedure adopted with native LAGG and described in **Section 6.2.2**. The distribution of DTAF-LAGG in rice matrices was visualised using an EVOS™ FL microscope. The excitation and emission spectra for DTAF were 488 nm and 517 nm.

The surface and internal morphology of cooked rice were observed with an ESEM (FEI Quanta 650 with X-Max-150 EDX Detector) equipped with a gaseous secondary electron detector by using the method of Dang & Copeland (2004). Working conditions were 10 kV accelerating voltage, 1 torr chamber pressure, and the initial working distance was 10 mm. Before imaging, samples were fixed on conductive adhesive tape and were observed at a magnification of 1000x.

6.2.5 Oral *in vitro* digestion of cooked rice with and without LAGG

6.2.5.1 In vitro oral digestion simulation of cooked rice

To simulate oral (only swallowing, normal and fine) processing conditions, 120g of cooked rice were homogenised in a household blender (HB605, Kenwood, Havant, UK) for 0, 10 or 20 s (Moongngarm et al., 2012; Furuya et al., 2014). The following *in vitro* digestion step was conducted based on the method described by Fernandes et al. (2020). In brief, 10 g of the homogenised (0 s, 10 s, 20 s) rice samples were placed in 50 mL conical tubes, followed by the addition of 10 mL of SSF containing salivary α-amylase to achieve an activity of 75U/mL in the digestion mixture. The mixture was incubated for 2 mins at 37°C under constant rotation (50 rpm) in a tube rotator (Fisherbrand™, Thermo Scientific, Hemel Hempstead, UK).

6.2.5.2 Granulometry distribution analysis of digested rice bolus

Following *in vitro* oral processing, 20 mL of Na_2CO_3 (0.3 M) solution was added to the digested mass to stop amylase activity. The granulometry distribution of the rice bolus was analysed based on the method by Ranawana et al. (2010). In brief, the digested samples were held in an incubation chamber at 37°C undisturbed for 10

mins to allow residual sedimentation. Following filtration through a Buchner funnel, the separated solid particles were carefully removed from the filter paper (H14632, Bel-Art, 3 μm pore size) used in the funnel and oven-dried for 12 h at 70°C until the constant weight. The liquid filtrate was collected for starch digestibility.

The residue was weighed after drying and then fractionated using a sieve shaker (Retsch AS 200 control, Verder Scientific, Derbyshire, UK) with a vibration height of 0.5 mm and duration of 1 min. The four equipped test sieves (DEBUYER, France) were stacked in descending size order as follows: 2.0 mm, 1.0 mm, 0.5 mm, 0.25mm and the base pan. A granulometry distribution can calculated via **Eq. 6.1,** following the collection and weighing of fractions from each sieve.

$$\sum \mathbf{R_n}(\%) = \sum \frac{\mathbf{M_n}}{\sum \mathbf{M_n}} \times \mathbf{100}\ \% \quad \textbf{(Eq. 6.1)}$$

Where:

M_n is the mass (g) of the fraction retained on each sieve (M_1, M_2, M_3, M_4) and pan (M_p);

ΣM_n is the total mass (g) of grain fractions: $M_1 + M_2 + ... + M_p$;

ΣR_n is the cumulative per cent (%) of mass retained.

The weight loss caused by the particles entrapped within the meshes was negligible.

6.2.6 *In vitro* digestion models

Two models, static and semi-dynamic, were used to study the *in vitro* digestion of cooked rice following oral processing. The static model was based on the INFOGEST protocol for rice, as described by Fernandes et al. (2020). The semi-dynamic model was developed during this project. Details about the models and protocols are described in **Chapter 3**.

6.2.6.1 Simulated digestion fluid preparation

The SSF, SGF and SIF formulations are detailed in **Tab 3.2**, **Section 3.8.1**. Each simulated fluid was prepared as a 1.25x concentrated stock solution (400 mL).

6.2.6.2 Static in vitro digestion model setting

Working solutions were prepared soon before performing the digestion experiments. A description of one set of *in vitro* digestion, including the electrolyte fluid, is shown in **Tab. 6.2.**

For the preparation of the working solutions, the 1.25× stock solutions were diluted with MilliQ® water to the final volume after adding $CaCl_2(H_2O)_2$ (0.3 M) (volumes in **Tab. 6.2**). The working solution was then placed in the incubator at 37°C prior to use. The rice samples, or the digestion mass from the previous phase, were mixed with 80 % of the respective working solution, while the remaining 20 % was used to dissolve the enzymes before adding them to the sample. This allowed enzymes throughout the sample to be evenly distributed. After pH adjustment, the 20 % fluid aliquot containing enzymes was added to the sample. Using the gastric phase as an example, the pH of SGF increased from 3 to 5 after mixing 80 % of the SFG with the "bolus" (the sample mass from the oral phase); therefore, it was adjusted back to 3 to keep the pepsin activity, before adding the remaining 20 % of fluid containing enzymes (pH 3) and initiate digestion. An example set of static *in vitro* digestion experiments has been illustrated in **Tab. 6.2**.

Tab. 6.2. Example of a static *in vitro* digestion experiment for 5 g of cooked sample. A) Composition of the bolus; B) Composition (volumes) of the working solution (80 % solution mixed with digestion mass + 20 % used for the preparation of enzyme solution); C) Characteristics of the enzyme mix.

A. JR as an example of the food model			
Rice sample (g)	5.00		
Total solid (g)	1.86 (dry matter, 37.2 %)		
Total starch (g)	1.62		
Total energy content (Kcal) [a]	6.85		
B. Working solution	Oral (pH[e] 7)	Gastric (pH[e] 3)	Intestinal (pH[e] 7)
Stock solution (mL) (Tab. 3.2)	4 (SSF)	8 (SGF)	16 (SIF)
$CaCl_2(H_2O)_2$ (0.3 M) (mL)	0.025	0.005	0.08
MilliQ® water (mL)	0.975	1.495	2.92
HCl (5 M) (mL) [b]	--	0.500	--
NaOH (5 M) (mL)[b]	--	--	1.00
Total fluid volume (mL)	5 (4+1)	10 (8+2)	20 (16+4)
For premixing, the volume used is (mL)	4	8	16
To prepare enzyme solutions, use (mL)	1	2	4
C. Enzymes	Salivary α-amylase	Pepsin	Pancreatin [f]
Enzyme activity (unit/mL) in total digestion mix [c]	75	2000	20 [g]
Enzyme-specific activity (unit/mg) [d]	146.2	557.5	31.4
Mass of enzyme (mg) [d]	5.14	71.82	25.48
Digestive mass	5g of cooked rice	10mL of bolus	20mL of chyme [g]
Final volume (mL)	10	20	40

[a]: According to the nutrition information on the food label.

[b]: For pH adjustment.

[c]: Each batch of enzymes is tested according to standard assays to determine the specific enzyme activity. The amount of pancreatin used is based on the activity of α-amylase. As in the previous trial, the amount of pancreatin based on suggested α-amylase activity was used, and the starch digestion curve of all samples reached the plateau within 5 mins, which makes it difficult to resolve differences in starch digestion rates. Based on our results, it is recommended that the 0.5-unit amylase per mg starch be in the final digestion mixture. This means 20 units/mL amylase is more proper to distinguish digestion kinetics for 5g of rice containing around 30% total starch. The enzyme activity (unit/mL) in total digestion mix at the separate phases was calculated as follows: Enzyme activity (unit/mg) × enzyme mass (mg)/final volume (mL).

[d] Specific enzyme activity measured for each batch of enzymes according to standard assays.

[e] Final pH means the pH after mixing with the digestive mass for each phase.

[f] The bolus here refers to the food mass (homogenised for 0s, 10 s, and 20 s) mixed with SSF for 2 mins before gastric digestion.

[g] Chyme refers to the mass that forms after gastric digestion.

Using the gastric phase as an example, the pH of SGF increased from 3 to 5 after mixing 80 % of the SFG with the "bolus" (the sample mass from the oral phase); therefore, it was adjusted back to 3 to keep the pepsin activity, before adding the remaining 20 % of fluid containing enzymes (pH 3) and initiate digestion. An example set of static *in vitro* digestion experiments has been illustrated in **Tab. 6.2**.

6.2.6.3 Static in vitro digestion model of cooked rice

Cooked rice samples underwent a three-step digestion procedure consisting of an oral, gastric, and intestinal phase. Aliquots of the digesta were collected for protein and starch analysis at the end of the oral and gastric phases and at specific time points during the intestinal phase. Two batch experiments were conducted for each rice sample. Following the oral phase (**Section 6.2.5.1**), the rice bolus sample was processed in the gastric phase as follows.

Gastric phase: SGF (8 mL; containing no enzymes) was added to the oral mixture to deactivate the salivary α-amylase. The gastric phase was immediately initiated after adding a further 2 mL of pepsin solution (prepared in SGF) to reach a final volume of 20 mL with 2000 U/mL pepsin activity. The mixture was incubated in a shaking incubator at 37°C with constant rotation (20 rpm) for 30 mins. The pH of the gastric mixture, measured every 10 mins, was maintained at 3 using HCl (1 M). For gastric digestion kinetics, 100 μL aliquots of the mixture were withdrawn after 30 mins incubation and dispersed into 1.5 mL microcentrifuge tubes containing 100 μL of "stop solution" (0.3 M Na_2CO_3, pH 9) to inactivate the pepsin. Enzyme blanks containing pepsin and SGF, but no samples were prepared and evaluated as the sample.

Intestinal phase: following the gastric phase, 16 mL of SIF was added to the gastric chyme and the pH was adjusted to 7 with NaOH (1 M). Subsequently, 4 mL of SIF containing pancreatin (as per equalisation of α-amylase activity 20 U/mL digesta) and mixed to reach a final volume of the intestinal mixture of 40 mL. The mixture was incubated at 37°C under constant rotation (10 rpm) for 180 mins. To study the kinetics of starch digestion in the intestine phase, a 100 μL aliquot of digesta was withdrawn from the digestion mixture at 0, 5, 10, 15, 20, 30, 45, 60, 90, 120, and

180 mins, respectively. Each aliquot was dispersed into a 1.5 mL microcentrifuge tube containing 100 μL of "stop solution" (0.3 M Na_2CO_3, pH 9) to stop the amylase activity and measure the degree of starch digestion. Meanwhile, 100 μL aliquots were withdrawn from the digestion mixture at 0, 15, 30, 60, 120, and 180 mins. Each aliquot was dispersed into a 1.5 mL microcentrifuge tube containing 100 μL of a Bowman-Birk trypsin-chymotrypsin inhibitor solution (0.05 g/L) to stop the trypsin activity and measure the degree of protein digestion. Blanks containing corresponding enzymes and simulated digestion fluids, but no rice, were run through the same digestion and sampling process to identify the amount of hydrolysed protein belonging to the enzyme. This value was subtracted from the total digested protein measured in the samples to determine the actual digested protein related to the rice.

6.2.6.4 Semi-dynamic digestion model setting

The overall setup of the semi-dynamic model and each function component is illustrated in **Fig. 6.1**Fig. 6.1 and described in **Tab. 6.3.**

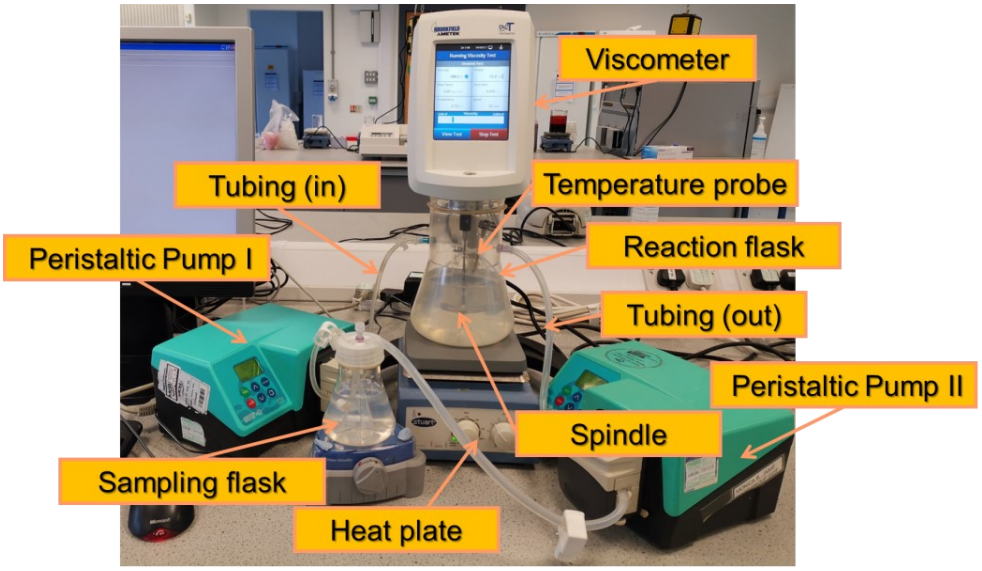
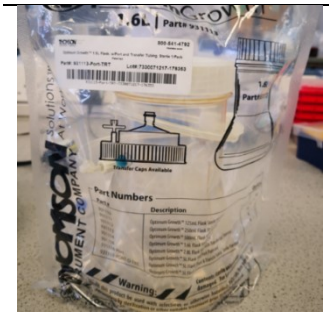
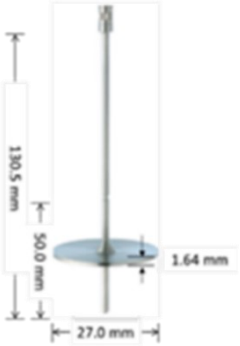


Fig. 6.1. Overview of the semi-dynamic *in vitro* digestion model setup. The image shows blank fluid (solution with enzyme, but no sample) within the system.

Tab. 6.3. Description of the semi-dynamic digestion model components.

Image of component	Identifying name/size	Function
	Multiport flask Hight:240 mm Neck diameter: 96.0 mm Bottom diameter: 166.0 mm	Simulates the digestion of food in the gastric-intestinal tract. A temperature probe monitors the temperature and keeps it at 37°C on a hot plate.
 	Viscometer Spindle: RV-04 (04) 1. multi-point interval data collection for gastric and intestinal phase. 2. Results expressed as mean ± standard deviation of viscosity (cP)	Monitors the viscosity changes during digestion. The DV-III rheometer operates on the principle of rotating the spindle in the test fluid through a calibrated spring. The spring deflection, measured using a rotary transducer, is used to determine the specific viscosity of the fluid. An aliquot of digesta was injected into the reaction flask and positioned underneath the pivot cup of the rheometer. The rheometer was set up in "controlled shear rate mode," and rotational speed and applied torque were measured.
	pH waterproof meter	Monitors the solution pH in the sampling flask, which is connected to the reaction flask.

	Peristaltic pump	Assists the enzyme solution delivery with a specific delivery rate, i.e., the volume programmed to be delivered in a given period.
	Hot plate	Maintains the temperature at 37°C.
	C-flex 16 1/4in OD x 1/8in ID x 2ft Long	Fluid transfer in settings. Tubing connects the sampling flask and the reaction flasks in a flow cycle.

6.2.6.4.1 Introduction of semi-dynamic in vitro digestion conditions.

The semi-dynamic *in vitro* digestion model differs from the static model due to the presence of a peristaltic pump, which continuously moves the sample within the system; moreover, there is a controlled bolus-induced gastric pH increase from 2 to 5. The oral phase was instead equal to that in the static model (**Section 6.2.5.1**).

Gastric phase: to follow the pH increase over a 30-min period, a three-step, block-wise pH profile was used, consisting of a linear regression from pH 2 (a fasting state in the stomach) to pH 5 (bolus delivery in the stomach) within 30 mins. This model was developed based on a previous *in vivo* study conducted by Nadia et al. (2021), where it was observed that an average *in vivo* gastric pH increased from 2 to 5 in 30 mins in sacrificed pigs. The model is described by **Fig.6.2** and **Eq.6.2.**

$$\mathbf{pH_t = 0.1 \times gastric\ digestion\ time\ (min) + pH_{t0}} \quad \textbf{(Eq. 6.2)}$$

Where:

pH_t is the stomach pH at a specific time point

pH_{t0} is the stomach pH at time 0 (beginning of digestion time)

To obtain a representative average pH value for a given period, the linear pH increase was divided into three blocks of 10 mins each. The reaction flask was filled with 160 mL of SGF (pH 2) to simulate the fasting state of the stomach. The gastric phase was initiated when the rice mass from the oral phase (pH 7, total volume 200 mL) was introduced into the reaction flask via the peristaltic pump I (input) at 25 mL/min.

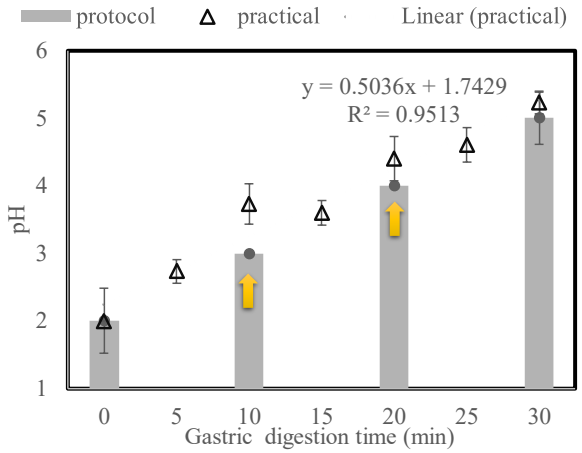


Fig. 6.2. An illustration of the gradual change in gastric pH during the semi-dynamic gastric phase Column: predicted pH change induced by the bolus, as determined by **Eq. 6.2**. Grey triangles with the linear fitting dashed line: experimental results in this study. Arrows indicate the time points (10^{th} min and 20^{th} min) at which block-wise acidification was performed with the addition of SGF (20 mL) and HCl (2M) to the reaction flask.

Once the volume of the reaction flask reached 360 mL, the peristaltic pump II (output) was activated to pump the digested solution into the sampling flask at a rate of 20 mL/min for 2 mins. Next, the pH value was determined (gastric time 0). To reduce bolus-induced pH increases, 20 mL of predetermined SGF was added to the reaction flask every 10 mins (see **Fig. 6.2**) to achieve the target pH, which was adjusted if necessary, using HCl (2M). The viscosity of the digesta was measured

using the Brookfield DV-II rotational rheometer, as described in **Fig. 6.1.** Despite the specific time points noted, the in and out tubes remain connected to the reaction flasks and sample flasks to maintain a current of digestion fluids. Pumps continue to operate at a speed of 20 rpm/min. After 30 mins of gastric digestion, 100 μL of the sampling flask was withdrawn in duplicate into 1.5 mL microcentrifuge tubes containing 100 μL of "stop solution" (0.3 M Na_2CO_3, pH=9) to inactivate the pepsin and further analyse digestion kinetics in the gastric phase.

Intestinal phase: As soon as the gastric phase was completed, 360 mL of SIF (without pancreatin) was pumped into the reaction flask at 50 mL/min to stop pepsin activity. After mixing, the peristaltic pump II (out) was activated to pump the digested solution into the sampling flask at a rate of 20 mL/min for 2 mins. The remaining 40 mL of SIF, containing pancreatin, was added to the reaction flask (final volume 800 mL) to start intestinal digestion. Meanwhile, 100 μL of the sampling flask was withdrawn in duplicate into 1.5 mL microcentrifuge tubes containing 100 μL of "stop solution" (intestinal time 0). Despite the specific time points noted, the in and out tubes remain connected to the reaction flasks and sample flasks to maintain a current of digestion fluids. Pumps continue to operate at a speed of 10 rpm/min. The viscosity was measured throughout the intestinal digestion step. Sampling, analysis, and blank testing were performed for the static digestion model (**Section 6.2**).

6.2.7 Quantitative evaluation of digested starch

Based on the method of Edwards et al. (2019), a colourimetric analysis using a par-hydroxybenzoic acid hydrazide (PAHBAH) assay was conducted on aliquots collected at various time points to determine the concentration of maltose in the samples. By referencing the standard curve, the concentration of maltose in each sample was expressed as maltose equivalents, which were further converted into the corresponding proportion of starch digested using **Eq.6.3**.

$$\textbf{Digested starch ratio}\ (\%) = \frac{[\textbf{maltose}]_{\textbf{t}}}{[\textbf{maltose}]_{\textbf{substrate}}} \times \textbf{100}\ \%\quad \textbf{(Eq.6.3)}$$

Where:

$[maltose]_t$ is the maltose equivalent concentration in the liquid phase of the digesta at a given time.

$[maltose]_{substrate}$ is the theoretical concentration of maltose equivalent that would exist at the beginning of the reaction, assuming all starch within the food sample converted to maltose (360.31 g/mol).

6.2.8 Quantitative evaluation of digested protein

Samples were first filtered using an Amicon® Ultra-4 centrifugal filter device (4000 rpm for 10 mins at room temperature) with a cut-off value of 10 kDa to collect the sedimented particles (< 10 kDa). The material remaining within the filter (particles > 10 kDa) was washed twice with 150 μL of MilliQ® water and re-centrifuged to collect the remaining particles < 10 kDa; this operation was repeated once more, as suggested by Hall et al. (2022). The degree of protein hydrolysis (DH) was determined by using the o-phthaldialdehyde (OPA) method following the procedure described by Jiménez-Munoz et al. (2021) to determine the proportion of free amino groups ($-NH_2$) released from rice protein degradation into supernatant.

The assay was conducted in 96-well microplates. After derivatisation with OPA and in the presence of 2-mercapto-ethane sulfonic acid, the produced 1-alkylthio-2-alcylisonindol compound was measured using a UV/VIS spectrophotometer (SpectraMax M5 microplate reader, Molecular Devices, US) at 335 nm. The results were calculated using a standard L-glutamic acid curve (0–8 mM in 0.5 M perchloric acid). The enzyme blanks were used as a background, and the obtained OPA values were subtracted from the OPA values of the protein. The DH (%) was calculated using **Eq. 6.4.**

$$\mathbf{DH}\ (\%) = \frac{\mathbf{h}}{\mathbf{h_{tot}}} \times \mathbf{100}\ \%\ \textbf{(Eq.6.4)}$$

Where:

h represents the amount of free amino groups, expressed in glutamic acid equivalents (g/L according to a 147.13 g/mol average molar mass of amino acids)

h_{tot} is the total protein concentration in the initial dispersion (g/L).

6.2.9 Analyses of starch digestion kinetics and predicted glycaemic indexes.

The mathematical modelling of digestograms used was summarised in **Fig. 3.8** (**Chapter 3**). Multiple digestible fractions (referred to the portion of starch digested at rapid- k_1 - or slow - k_2 - rate) were identified as the linear discontinue by applying a logarithmic of slope (LoS) port form of a first-order kinetic model. Here. The time at which two linear plots intersect is named t_{int}, used to identify the time required to complete a rapid-digestible fraction. The combination of parallel and sequential (CPS) kinetic model proposed by Li et al. (2020) was applied in the digestion curve, as shown in **Eq.6.5.**

$$\mathbf{C_t} = \mathbf{C_0} + (\mathbf{C_{\infty 1}}) \times \left(\mathbf{1} - \boldsymbol{e}^{-\boldsymbol{k_1 t}}\right)$$

$$+\text{if } (\mathbf{t} > \mathbf{t_{2start}}, (\mathbf{C_{\infty 2}}) \times \left(\mathbf{1} - \mathbf{e}^{-\mathbf{k_2}(\mathbf{t}-\mathbf{t_{2start}})}\right), 0) \quad \textbf{(Eq. 6.5)}$$

This model, similar to the LoS model, can differentiate digestion phases (e.g., rapid vs. slow) with different rate constants (k_1 and k_2) and concentration at the endpoint of each reaction phase ($C_{\infty 1}$ and $C_{\infty 2}$). CPS model additionally introduces a variable named as t_{2start}, which represents digestion patterns either sequentially, parallelly, or a combination of both. $t_{2start} = 0$ follows the parallel digestion pattern. If $t_{2start} > t_{int}$, then the sequential digestion pattern is followed. Otherwise, $t_{int} > t_{2start} > 0$ refers to a CPS digestion pattern (Li & hu., 2021). The predicted glycaemic index (pGI) was calculated using **Eq. 6.6,** described by Tamura et al. (2016).

$$\mathbf{pGI} = \mathbf{39.71} + \mathbf{0.549HI} \quad \textbf{(Eq. 6.6)}$$

Here, the hydrolysis Index (HI) was calculated by comparing the area under the curve at 90 mins (AUC90) of digestibility plots for the rice samples with that of white bread

($AUC90_{reference}$), also measured in this work. Three pGI levels were classified as high (≥70), medium (56-69), and low (≤55) (Kaur et al., 2016).

6.2.10 Rice bolus disintegration

To demonstrate the physical integrity loss of rice bolus in an acidic environment (pH 3), a rice bolus disintegration experiment was conducted as follows (demonstrated in **Fig. 6.3**). Following 20 s homogenisation (**Section 6.2.5**) and mixing with SSF (1:1, w/w) without salivary amylase, 7g of rice-SSF mixture was fixed into a spherical mould (radius 1 cm, time 0), then hanger wire was attached to the centre of the spherical bolus. The hung bolus was positioned at the centre of a 500 mL glass cube chamber with a black background. The disintegration process was recorded using a Canon digital single-lens reflex 5D, with a 24-100 mm lens and 31 mm macro lens extender, a high-resolution camera and lighting equipment. All experiments were conducted in the same setting and position. Using a tube-connected syringe, 500 mL of SGF pH 3 was added gradually to the chamber and impregnated the bolus sample. The camera started recording (time 0) when SGF reached the bottom of the bolus. The video was then converted into frames, and a graph of the radius versus time was produced using Matlab (Matlab® 2023a, MathWorks Inc.).

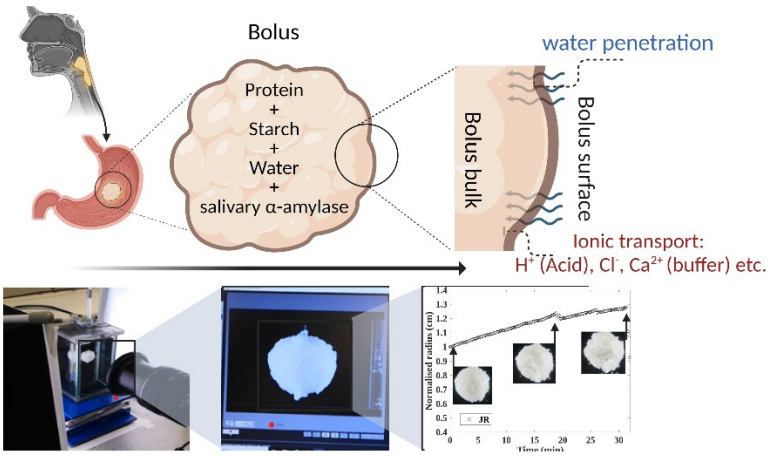


Fig. 6.3. Schematic representation of bolus disintegration model.

6.2.11 Statistical analysis

Results were calculated as means ± standard deviations of three replicates. Tukey's test, in conjunction with analysis of variance (ANOVA), was used to determine

significant differences among samples at a significant level of $p < 0.05$, using the SPSS software (version 27, Chicago, USA). In the granulometric measurement for cooked grain after homogenisation, the cumulative Gaussian statistic model was used to calculate the particle size distribution after passing the Shapiro-wilk normality test, used to confirm whether the distribution is normal, using Prism (version 9, San Diego, CA) based on the method by Blanquet-Diot et al. (2021).

6.3 Results

6.3.1 Proximate composition and granular morphology of cooked grains

The nutritional composition data for cooked JR and PR are shown in **Tab. 6.4**. PR's protein and amylose content were significantly higher than those of JR, but the total starch content was similar. The protein and starch content results were consistent with the nutritional values reported on the rice food labels. JR and PR grain shape was representative of indica rice varieties, and no significant difference was observed in the apparent morphology between both cooked rice samples (shape parameter data in **Tab. 6.4** and **Fig. 6.4A1** and **A3**). As a result of cooking rice with LAGG dispersion, no statistically significant differences were detected in the nutrition composition, kernel size or shape (**Tab. 6.4**, **Fig. 6.4A)**.

Tab. 6.4. Nutritional composition of cooked rice with and without 1 % LAGG (g/100g).

Rice type	JR	JR_1LA	PR	PR_1LA
Moisture content	62.85 ±2.81^{a}	62.80 ±2.06 ^{a}	62.54 ±0.60 ^{a}	62.92 ±0.85^{a}
Total starch content	32.33 ± 1.92^{a}	32.00 ± 0.99 ^{a}	30.25 ± 1.62 ^{a}	30.28 ± 1.70^{a}
In which amylose	5.49 ± 0.99^{a}	5.70± 1.06^{a}	8.08± 0.43 ^{b}	7.79 ± 0.51^{b}
Protein content	2.64 ± 0.39^{a}	2.64 ± 0.20 ^{a}	3.22 ± 0.08^{b}	3.09 ± 0.47^{b}
Length (L, mm);	9.88± 0.39^{a}	10.31± 0.43^{a}	10.92 ± 0.26^{a}	9.80± 0.60^{a}
Width (W, mm)	2.86± 0.12^{a}	3.02± 0.14^{a}	3.17± 0.15^{a}	2.80± 0.16^{a}
Thickness (T, mm)	0.83± 0.10^{a}	0.89± 0.08^{a}	0.92± 0.08^{a}	0.80± 0.07^{a}
sphericity	0.29± 0.02^{a}	0.29± 0.02^{a}	0.29± 0.01^{a}	0.29± 0.01^{a}
Surface area (mm^2)	25.91± 1.71^{a}	28.78± 2.90^{a}	31.90± 2.68 ^{a}	25.03± 3.22^{a}
Roundness (mm)	2.30± 0.22^{a}	2.24± 0.14^{a}	2.22± 0.11^{a}	2.18± 0.12^{a}

Mean ± S.D. calculated from triplicate measurements. For each parameter (first column), the different superscript letters indicate values among the four samples are statistically different ($p < 0.05$). For moisture content, total starch content, protein content are calculated as a percentage of weight on the fresh cooked sample basis. Sphericity calculated from sphericity=$(L*W*T)^{1/3}/L$ (Thakur & Gupta, 2006), Surface area, SA = $(\pi*B*L)^2/(2L-B)$ where, B = $(W*T)^{0.5}$ Roundness = (W/L+T/W+T/L)/3 as reported previously (Karababa & Coşkuner, 2007).

6.3.2 Morphology of cooked rice with and without LAGG

Fig. 6.4 shows the microstructural organisation and phase distribution of LAGG and protein-starch matrices in cooked rice. As observed under fluorescence light (panels B in **Fig. 6.4**), the black region in **Fig. 6.4** represented the cooked rice grain (cross-

section), while the highlighted green halo represented the DTAF-labelled LAGG, indicating that LAGG has been coated along the grain periphery regions of the grain.

JR revealed discontinued protein networks, and the starch granules exhibited considerable deformation and fused at the exterior layer of the grain. In contrast, towards the centre of the grain, amylopectin-rich regions (staining in purple with the iodine) can still be recognisable in the intergranular space (**Fig. 6.4C1**). PR contains protein-starch matrices units with shuttle-like shapes, where proteins enclosed starch granules in netlike arrangements (**Fig. 6.4C3**). Interestingly, the LAGG layer in the external region of the grain was less stained than in the uncovered area, indicating that LAGG-coating can limit the penetration of the stain solution (**Fig. 6.4C2** and **C4**). The ESEM images of JR revealed granule units that were deformed with intergranular fissures and loose granules attached to the edge (**Fig. 6.4D1**), indicative of starch granules leaching. In PR, granule agglomerates and inner tunnels were also observed, indicating a loose fracture plane (**Fig. 6.4D3**). Cooked in LAGG dispersion, both grains developed a thin gel-like coating around the pericarpic region, showing the adhesive properties of LAGG gel coating. As a result, both LAGG-coated rice grains still had recognisable intact starch granules, suggesting that LAGG mitigates starch gelatinisation by obstructing kernel pores and channels and hindering water penetration (**Fig. 6.4D2** and **D4**).

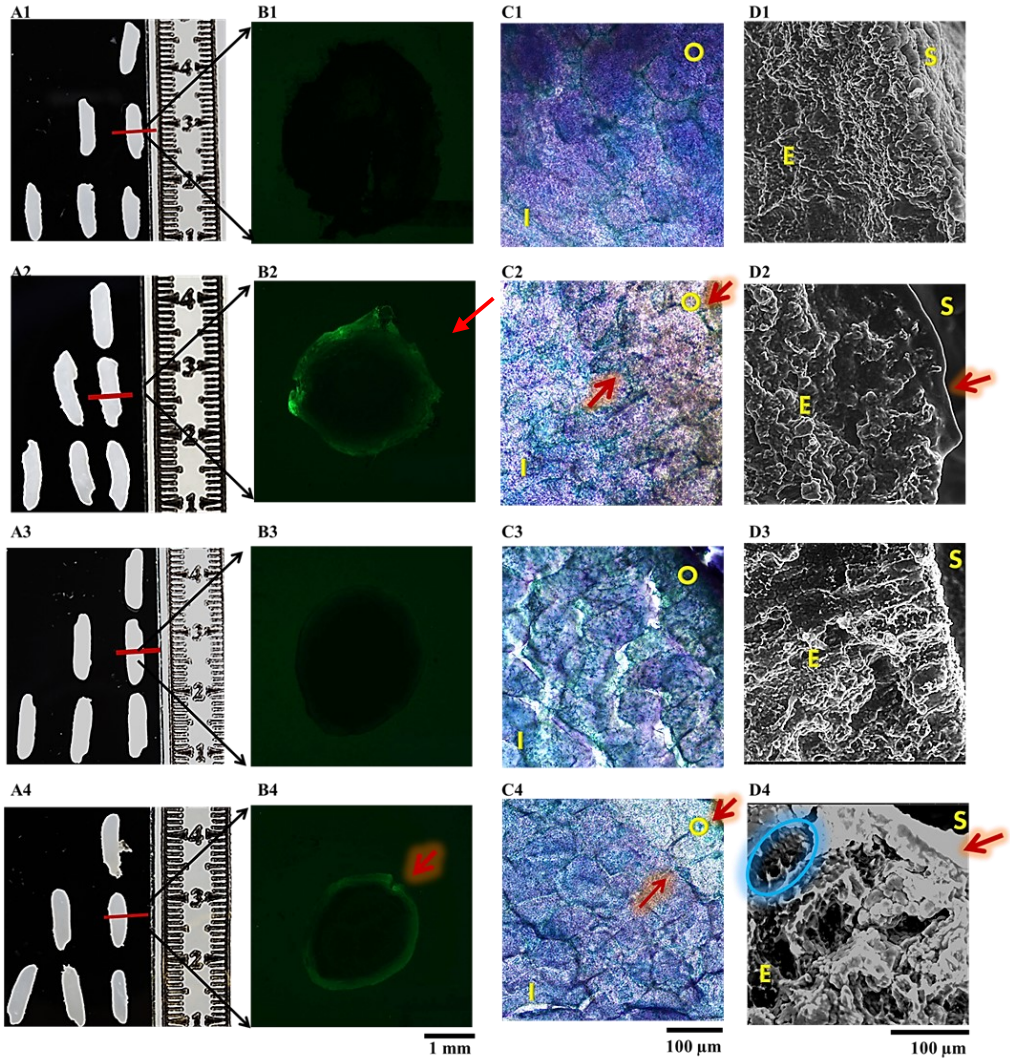


Fig. 6.4. Morphology of cooked rice grains. Numbers 1 to 4 refer to JR, JR_1LA, PR, and PR_1LA, respectively. (A) apparent morphology of cooked grain (ruler scale =1 cm); B) cross-section of DTAF-labelled LAGG-coatings on cooked rice observed under a fluorescence microscope at 2X magnification; C) Cross-section of cooked grain under a light microscope. Protein bodies appeared green with fast green staining, starch exhibited a purple stain from Lugol's solution, amylopectin-rich regions were purple, and amylose-rich regions were blue. Scale bar =100 μm, O: outer endosperm and I: inner endosperm. D) Cross-section of cooked grain under ESEM (Scale bar =100 μm). Red arrows in (B), (C), and (D) indicate LAGG-coating. E: endosperm; S: surface of the grain.

6.3.3 Texture properties of cooked rice with and without LAGG

Aside from determining eating quality, the texture profile of cooked rice affects particle size reduction and starch digestion initiation in response to mastication. The resultant bolus (swallowable chewed mass) could further accelerate and facilitate starch digestion (Tamura et al., 2017; Choy et al., 2021; Sethupathy et al., 2021).

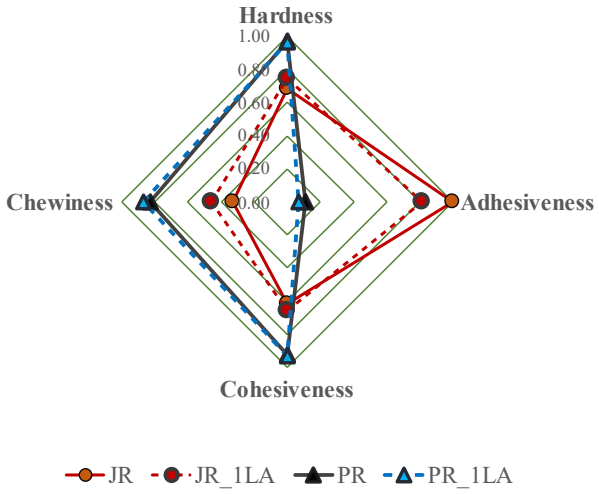


Fig. 6.5. Radar charts showing the textural characteristics of cooked rice with and without LAGG. The texture parameters are hardness, adhesiveness ,cohesiveness ,and chewiness. For each textural characteristic, a factor was calculated by dividing the measured value by the highest value (set to 1) among the four samples (JR, JR_1LA, PR and PR_1LA) measured.

As demonstrated by the results of the double-cycle compression TPA (**Fig. 6.5**), differences were observed among the grains with and without LAGG-coating. Hardness relates to the force required to break the grain during the first bite. The physical and chemical characteristics of rice grains (the leaching materials during cooking) are likely to be the major determinants of the adhesiveness (degree of stickiness) between rice grains and “teeth” (probe interfaces). Through continuous oral processing, the degree of deformation and resistance of the rice is reflected through its cohesiveness and chewiness (Yau & Huang, 1996; Han, Lee & Meullenet, 2017; Hong, 2017; Tao et al., 2020). As shown in **Fig. 6.5**, The texture profiles of PR differ from those of JR, PR exhibited higher hardness, cohesiveness, and chewiness but less adhesiveness than JR. This could be attributed to PR's high protein and amylose content, combined with its compact microstructure, ensuring starch structural retention (Martin & Fitzgerald, 2002) and preventing gelatinisation (Ong & Blanshard, 1995).

Similarly, Nawaz et al. (2016) found that alkali treatment increases the stickiness of cooked rice after protein removal. Also, Li et al. (2019) reported that non-glutenous

rice kernels were stickier after surface protein removal. Regarding starch molecular structure, higher amylopectin content, a branched polymer of starch, features more shear and extension viscosities than linear polymers like amylose. As cooked rice (120°C) cools to serving temperature (65°C), rice starch undergoes a short-term retrogradation. The linear structure of amylose facilitates its re-association faster than that of amylopectin (Hu et al., 2020). Therefore, a greater amount of amylose in cooked PR, which leads to a faster formation of an amylose network that restricts the movement of amylopectin, thereby decreasing its flexibility and increasing cooked rice rigidity (Riva et al., 2000; Bertoft et al., 2004). Combined with the denatured protein networks generated by the parboiling process, the resulting protein-starch matrices exhibited a rigid texture while having difficulty recovering from distortion, thereby reducing adhesiveness.

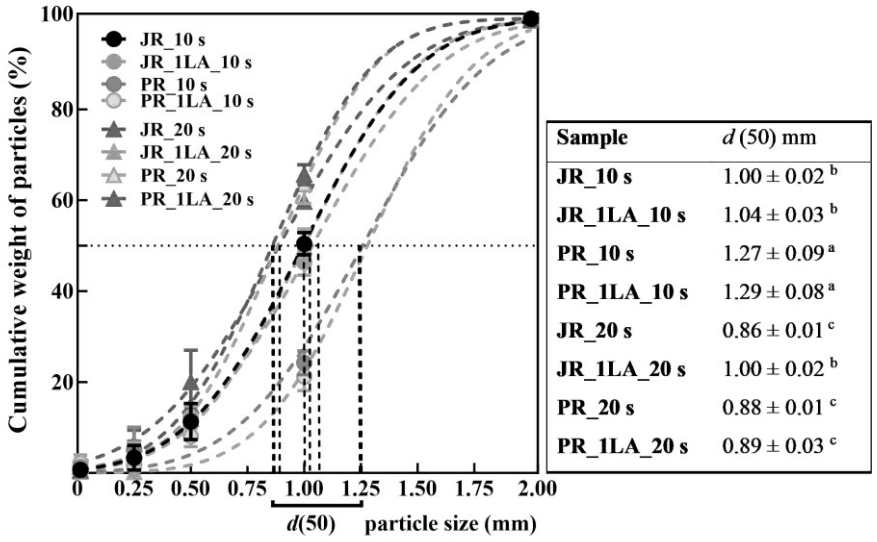
No significant differences were observed in PR_1LA and PR texture properties, whereas JR_1LA had reduced adhesiveness compared to JR. This suggests that cooking in LAGG dispersion results in greater rigidity for JR_1LA than for PR_1LA. Similarly, Chung et al. (2007) reported that applying LAGG at a concentration of 0.7 % significantly reduced the adhesion of cooked white rice. This can be attributed to the change in surface characteristics caused by gum additions affecting water penetration and leaching of starch molecules, especially amylopectin, during cooking. Additionally, LAGG gel may have formed an elastic and brittle gel when cooled (Sworn & Stouby, 2021).

6.3.4 *In vitro* oral digestion of cooked rice with and without LAGG

The GI of the same rice types varies significantly *in vivo* because of differences in particle size distribution caused by individual differences (such as chewing time, efficiency, and salivary enzyme activity). Moreover, the characteristics of the rice itself may affect GI (Kataoka et al., 2013; Liu et al., 2020). Rice disintegration has been studied using various *in vitro* methods, including grinding, blending, and cut-and-pestle, with the former two approaches providing similar physical characteristics as *in vivo* mastication (Tamura et al., 2017). Additionally, different simulation times for default (7.7 s) and normal (14.8 s) chewing scenarios on the

starch digestion of refined and wholegrain pasta under unified "masticatory" efficiency (shear stress) conditions were also used (Blanquet-Diot et al., 2021).

Thus, simulated procedures for oral processing of cooked PR and JR were developed following previous work by Moongngarm et al. (2012) to investigate how homogenised rice particles degrade over time, including the factors that may be affected by rice's texture differences. Homogenisation for 10 s is considered to be a simulation of normal mastication, which is half the simulation duration recommended for fine oral processing (Moongngarm et al., 2012; Mandalari et al., 2018) The median particle size *d*(50), defined as the theoretical sieve through which 50 % of the mass could pass, is shown in **Fig. 6.6**. In the boluses collected following 10 s homogenisation, there were significant differences in particle size distribution between PR and JR, evidenced in *d*(50) values of 1.26 ± 0.07 mm and 0.99 ± 0. 11 mm, respectively.



Sample	*d* (50) mm
JR_10 s	1.00 ± 0.02 [b]
JR_1LA_10 s	1.04 ± 0.03 [b]
PR_10 s	1.27 ± 0.09 [a]
PR_1LA_10 s	1.29 ± 0.08 [a]
JR_20 s	0.86 ± 0.01 [c]
JR_1LA_20 s	1.00 ± 0.02 [b]
PR_20 s	0.88 ± 0.01 [c]
PR_1LA_20 s	0.89 ± 0.03 [c]

Fig. 6.6. The particle size distribution of cooked rice with and without LAGG after oral processing *in vitro* simulation. Particle size distribution curves were obtained after 10 or 20 seconds of homogenisation (in imitation of normal and fine mastication, respectively). Curves were presented as the mean cumulative weight (3 replicates) of particles passing through each sieve of four sieves in total. A homogenised mass containing particles larger than the greater sieve aperture or particles remaining in the sieve's mesh did not reach 100 % cumulative weight.

The constituent particles of both boluses became smaller after the 20 s homogenisation, and no significant differences were observed in their *d*(50) values

(0.88 ± 0.01 mm for PR and 0.86 ± 0.01 mm for JR). Similar results have been noted for middle-scale foods like pasta, where wholegrain pasta had a smaller particle size distribution when compared with refined pasta after normal mastication simulation (Blanquet-Diot et al., 2021).

Cooking in LAGG dispersion did not lead to significant changes in particle size in the PR bolus after 10 s and 20 s oral processing, whereas a significantly larger *d*(50) value was observed in JR_1LA compared to JR control after 20 s homogenisation. This might be ascribed to the interaction between leached starch molecules and small gel nuclei under the applied shear mixing (Fang et al., 2018). Like practical mastication (fragmentation and salivation), the liquid phase of an *in vitro* oral process consists primarily of maltose, with small amounts of dextrin, maltotriose, and glucose (Blanquet-Diot et al., 2021). As such, the amount of maltose released from "chewed" rice mass is a measure of oral starch digestibility (converted total starch of rice samples into maltose), as shown in **Fig. 6.7**. The oral starch digestibility differed among rice types. Intact JR had significantly higher starch digestibility than PR, which remained highest under both homogenisation processes. This suggests that when rice is consumed as whole grains (swallowing), its compact structure is important in limiting starch digestion. The role of particle size on digestibility could be more clearly understood by considering that rice flour (physical dispersion of rice grains) shows a significantly higher starch digestibility than rice grains, even when pre-homogenised. Starch digestibility in rice starch isolates was even higher than in flour as protein networks were removed. These results suggest that a greater degree of structural disintegration may be associated with a more rapid rise in rice starch digestibility.

For JR, LAGG-coating significantly reduced starch digestibility. Although starch digestibility increased under homogenisation, it was still less than rice control, with digested starch below 5 %. This might be due to LAGG partially coating rice fragments, limiting amylase accessibility. Moreover, the larger rice fragment size at 20 s homogenisation would further contribute to the reduced starch digestibility in JR, due to a lower surface area available for enzyme attack (shown in **Fig. 6.6**). For

PR, starch digestibility was lower than JR at any homogenisation time, but LAGG-coating did not significantly reduce the digestibility, possibly due to the already low starch digestibility in this rice type. Furthermore, no significant increase in particle size after homogenisation was observed in LAGG-coated samples compared with the non-coated.

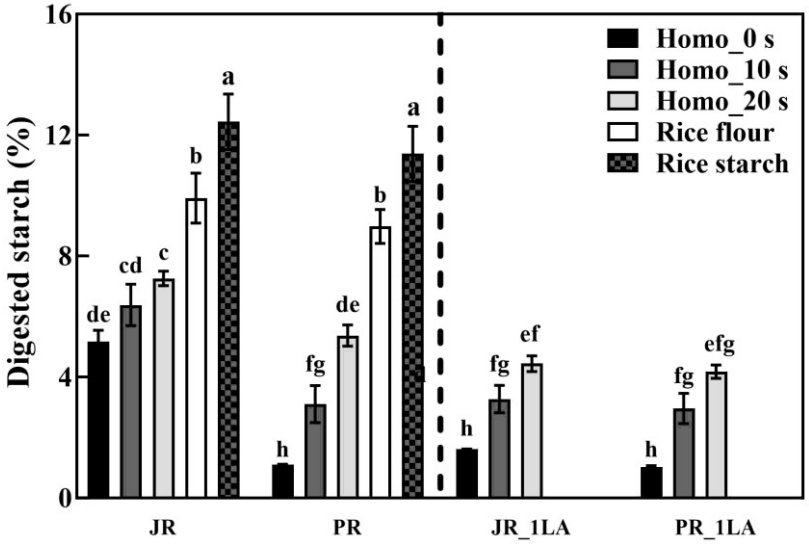


Fig. 6.7. *In vitro* oral phase starch digestibility of cooked rice grain with and without 1 % LAGG after homogenisation (0 s, 10 s and 20 s). The starch digestion of water-cooked JR and PR flour, as well as JR and PR starch isolates, were also included as references.

6.3.5 Rice bolus disintegration behaviour

By exposing LAGG hydrogel to an acidic gastric-like environment, the gel structure can be reinforced through intra- and intermolecular associations with univalent or divalent cations with ionic bonding and electrostatic forces of attraction (Norton et al., 2011; Tako et al., 2016). The stronger LAGG gel, formed at low pH, may, in turn, contrast the disintegration of rice boluses, as demonstrated by imaging modelling shown in **Fig. 6.8**. To achieve this, a standardised bolus (based on weight and shape) was immersed in SGF without pepsin. An analysis of the changes in the bolus size over time was performed. Physiologically, the formation of rice bolus is related to the cohesiveness of rice mass, whereby the resulting compression forces of the oesophagus cause chewed rice fractions to adhere to each other and form a solid mass (Peyron et al., 2011). Under the influence of digestion solution penetration

(inducing swelling) and degradation (decomposition) of acids and enzymes, the bolus is disintegrated into small particles in the gastric phase (Drechsler & Bornhorst, 2018). As a result, studying this process (structural changes in bolus and time) can indicate the rate of gastric emptying and the likelihood of rice chyme exposure to enzymes that have smaller particle sizes and larger surface areas, resulting in a faster digestion rate (Bornhorst & Singh, 2012).

When immersed in SGF (no pepsin), the JR bolus experienced swelling three times greater than the initial bolus. As shown in **Fig. 6.8A**, the radius of the bolus increased and began to disintegrate at the 17th min, as small peripheral pieces began to peel off, resulting in a reduction in radius. In the following 5 mins, two occasions of swelling and disintegration were observed in JR boluses, with a reduced swelling extent on the radius. The remaining bolus fell from the test site after 30 mins, signalling the end of the disintegration test, which coincided with that of the static gastric phase in the current study and reported previously (Tamura et al., 2017). Under current experimental conditions, the JR_1LA bolus exhibited a similar swelling but no piecewise disintegration pattern (**Fig. 6.8B**). Within 20 mins, the JR_1LA bolus radius gradually increases by approximately 20 % to the initial radius. The presence of a higher proportion of rapid-digestible starch (RDS) in masticated rice has been reported to facilitate the formation of a bolus *in vivo* compared to rice with lower RDS (Ranawana et al., 2010), consistent with the findings in **Section 6.3.4**.

It is possible that inner starch digestion and acid penetration account for bolus disintegration differences. Although salivary amylase deactivates on the surface of rice bolus at low pH, starch digestion still occurs since amylase inside the bolus remains active (Nadia et al., 2022). During this process, the cohesive force of the starch particles and the structural barriers for water penetration were reduced. The rice bolus containing LAGG showed expansion without piece peeling, indicating that LAGG-coating delays the process of disintegration under gastric conditions. This may be due to the increased strength of the coating gel at pH 3, which can hinder the diffusion of the solution. In agreement with these findings, Norton et al. (2011) reported that exposing LAGG fluid gels to an acidic gastric-like environment

increased the gel's strength. A similar result has been reported by Santos et al. (2018) that self-structured gels exhibit greater hardness (represented by higher rupture stresses) due to hydrogen ions bonding to available anionic sites, resulting in distance reduction between the helices of the LAGG, creating a more compact gel structure. Meanwhile, the textural characteristics of PR may contribute to its fast disintegration. The PR bolus disintegrated much faster and dissolved within 1 min (**Fig. 6.8C**), and the same deformation pattern was also observed in the PR_1LA bolus (**Fig. 6.8D**).The rigid structure of cooked PR showed a high hardness and low stickiness, suggesting that the rice grain may be difficult to deform and challenging to reshape as a bolus due to its lack of cohesion linkages.

A gravity-induced disintegration of the bolus in an acidic environment would occur using this experiment setup, although this does not reflect the *in vivo* digestion process occurring in the stomach. In fact, it is important to consider the mechanical, chemical, and enzymatic limitations encountered when developing the next experimental strategy. Some techniques are being developed to investigate the effect of dynamic changes in pH and forces on rice bolus disintegration. The adhesive texture of JR promoted saliva impregnation and enhanced particle cohesion. JR was less resistant to structure disintegration than PR, especially during the gastric phase.

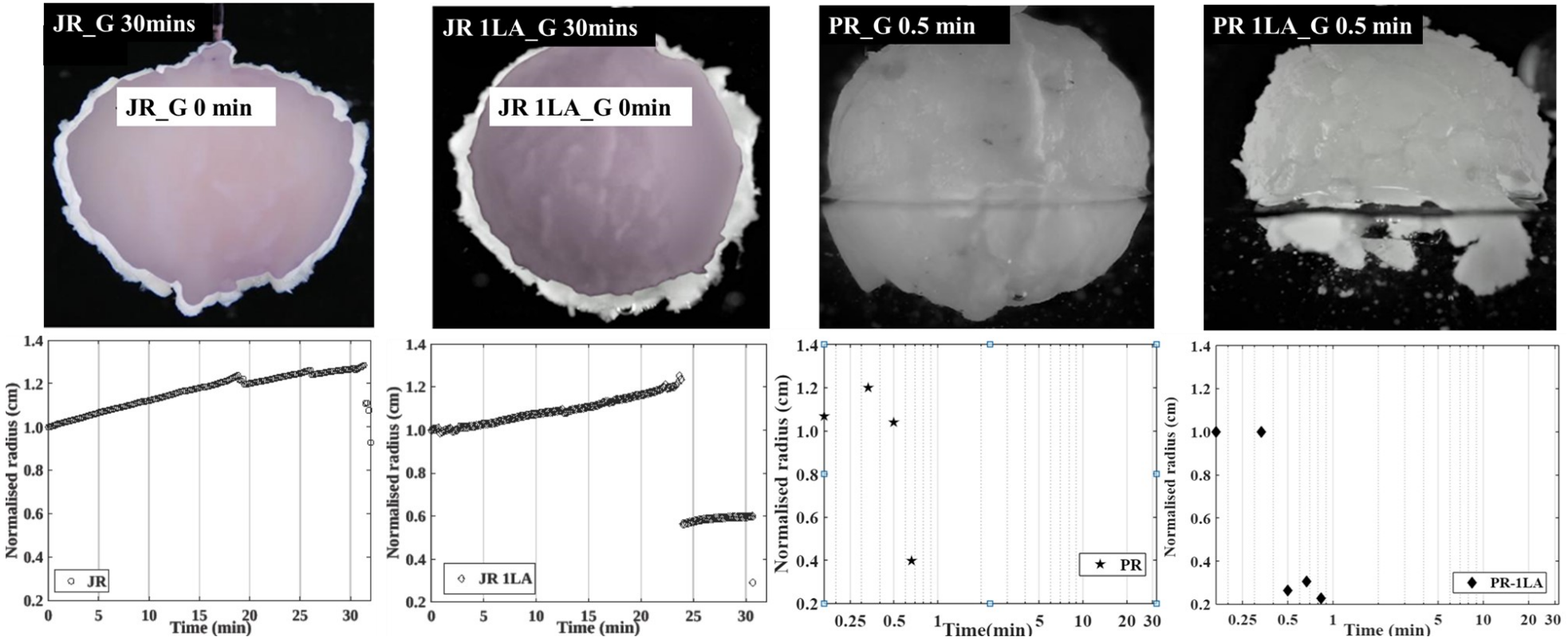


Fig. 6.8. Rice bolus disintegration of cooked rice with and without LAGG in the simulated acidic (pH 3) gastric-like environment. The overlaid images of the bolus were captured at the beginning and end of the stay in the experiment site before falling off. In PR, the process of dissolving occurs within a short period following the immersion of the rice bolus into the SGF. In this case, the image shown represented the partially dissolved state of the rice bolus in the solution.

6.3.6 *In vitro* digestion of cooked rice with and without LAGG

To understand whether there is a microstructure (protein-starch matrices) effect on the digestibility of rice cooked with or without LAGG, *in vitro* static and semi-dynamic digestion experiments were performed. In both digestion models, α-amylase had 50 units of activity per 100 mg of starch, which is 10-fold higher than that suggested for cooked rice flour, allowing sufficient starch digestion over time (Farooq et al., 2018). A digestogram is a curve illustrating the increase in hydrolysed starch (mainly maltose) released in the supernatant with time. The free amino groups produced by protein hydrolysis under corresponding trypsin activity were also evaluated.

6.3.6.1 Static model

The starch digestibility (%) in cooked rice grain following three homogenisation conditions (0 s, 10 s, or 20 s) is shown in **Fig. 6.9.**

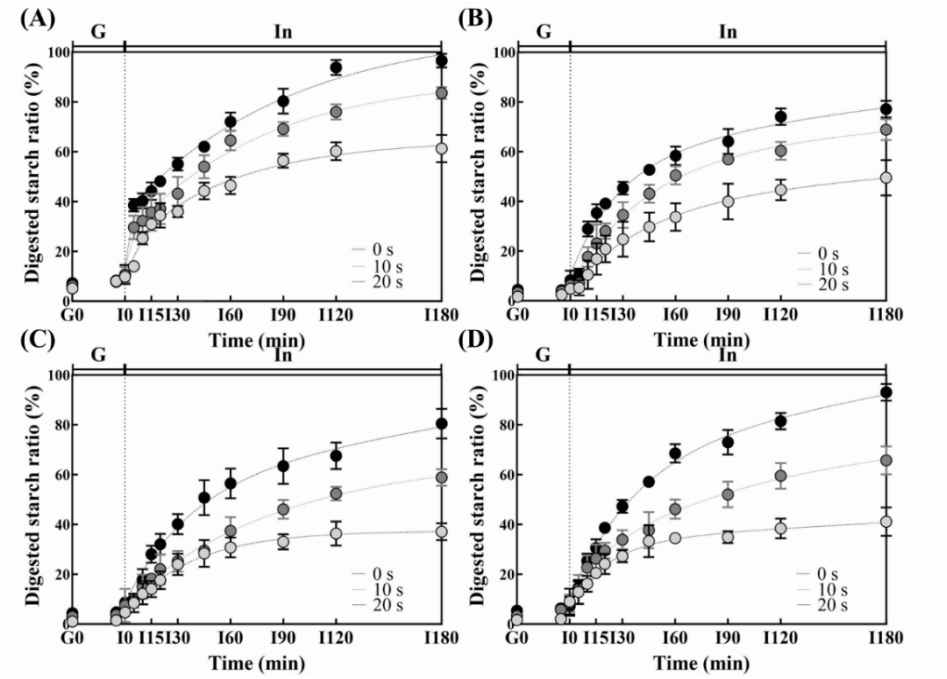


Fig. 6.9. Starch digestibility of cooked grains with and without LAGG. The starch digestibility was evaluated under three different structural conditions: non-homogenised (0 s), homogenised 10 s, and 20 s. (A) JR; (B) JR_1LA; (C) PR; (D) PR_1LA. The dot points correspond to the experiment-measured values; all error bars represent standard deviations (n = 4), and dashed lines correspond to the kinetic model fittings for the digestion curves. G: gastric phase, In intestinal phase.

Each rice sample's starch digestion curve displayed an increase at the function of time following the order specified: intact grain < 10 s homogenisation < 20 s homogenisation. There is a good agreement between these findings and those reported in the literature demonstrating that the degree of starch digestion in rice grains is related to the homogenisation degree of rice grains (1 s or 120 s) (Tamura et al., 2017). Protein digestion increased, as well as starch digestion, in response to the extent of oral processing, as shown in **Fig. 6.10**.

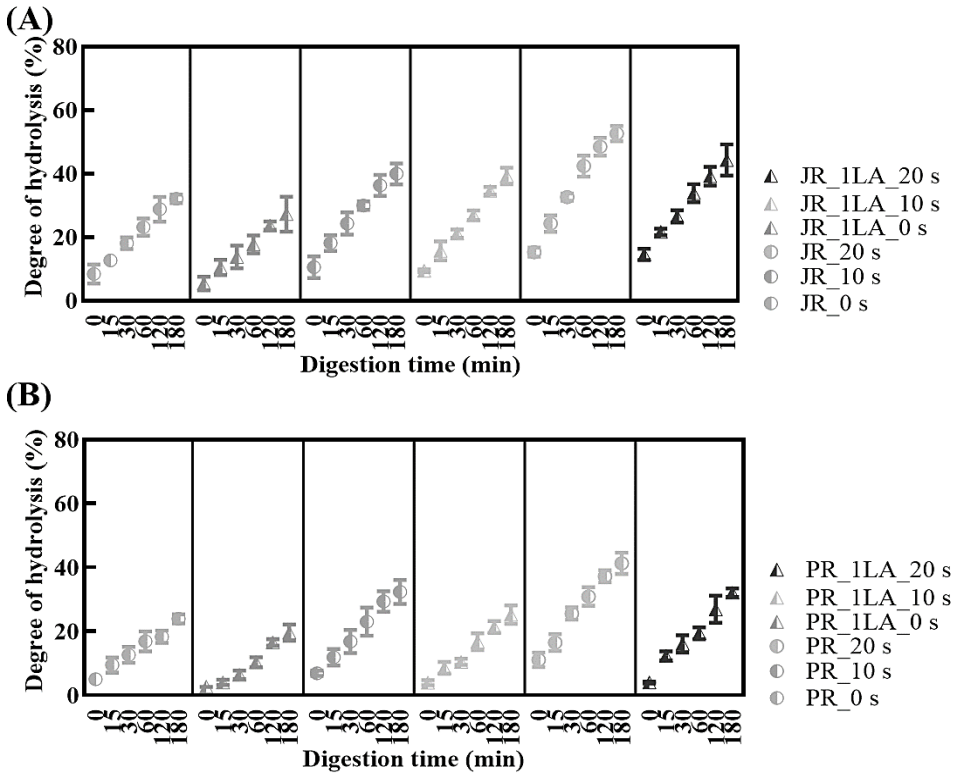


Fig. 6.10. Protein digestion in cooked rice grains with and without LAGG. The protein digestibility was evaluated under three different structural conditions: non-homogenised (0 s), homogenised 10 s, and 20 s. (A) JR and JR_1LA, (B) PR and PR_1LA, respectively.

When both rice types were homogenised for 20 s, about double the amount of hydrolysed protein was released compared with intact grains by the beginning of the intestinal phase (15.3 % vs 8.5 % for JR_20 s and JR_0 s, and 11.1 % vs 5.0 % for PR_20 s and PR_0 s, respectively). Both types of rice were also found to have the highest amount of protein digestion at each time point following homogenisation for 20 s. This suggests that the extent of homogenisation can facilitate protein digestion. Under three homogenisation conditions, PR exhibits a lower degree of

protein digestion than JR. This could be due to the heat-induced changes in rice physicochemical properties and the formation of new bonds in the protein network, such as hydrophobic interactions and intramolecular disulfide bonds, resulting in lower protein digestibility. Similarly, reduced protein digestibility was reported in heat-treated rice protein suspension than in control (non-heat treatment) (Liu et al., 2021).

All digestion profiles resulted in acceptable (**Tab. 6.5**, R^2 > 0.99) after data transformation fitting into the CPS kinetic model (**Section 6.2.9**). It has also been observed that there were two distinct linear fractions involved in the digestion of starch in samples: nearly 20 % of the starch was digested in the first phase with a faster rate constant (k_1), whereas the remaining was digested in the second phase, with a slower rate constant (k_2). The rapid digestion phase of all the samples was completed within 20 mins after they were introduced into the digestion solution. This is consistent with the RDS definition by Englyst et al. (1992), indicating the presence of RDS in the rice samples. After homogenisation, the two rice types exhibited different patterns of reaching the slow stage. The starch digestion of intact JR reached the slow stage after 15 mins, with 21.6 % of digested starch ($C_{\infty 1}$) at k_1 of 0.136. As a result of the 10 s and 20 s homogenisation, k_1 increased nearly by twofold and 2.5-fold, respectively. The rapid digestion phase of the 10 s and 20 s homogenised JR samples was also extended to over 15 mins, resulting in significantly higher $C_{\infty 1}$ than that of intact JR, which were 24.7 ± 3.4 and 27.5 ± 0.9, respectively. Compared with intact JR, intact PR's starch digestion curve showed more flattened contours, resulting in a significantly lower k_1 (0.044 versus 0.136, respectively). As homogenisation time increased from 0 s to 10 s to 20 s, PR reached a similar amount of starch digestion at a faster rate, with about 18-21% ($C_{\infty 1}$, **Tab. 6.5**) of starch digested in 15 min, 10 min and 5 min, respectively (k_1 increased from 0.04 to 0.15). There was a significant reduction in rice starch and protein digestibility in both rice types when LAGG was added. However, there may be a difference in LAGG's ability to mitigate starch digestion between the two types of rice. For JR, the kinetic fitting results revealed that rice with LAGG had a two-phase digestion pattern similar to

rice control but at a lower rate and extent (**Tab. 6.5**). When the extent of homogenisation increases, the LAGG mediation effect on JR starch digestion remained effective, as the initial concentration (C_0), constant rate (k_1), experimental extent ($C_{\infty 1}$), and period of rapid digestion phase (t_{int}) (parameter details in **Section 6.2.9**) exhibited a non-significant increase. For PR, the $C_{\infty 1}$ reached a similar concentration at the end of the rapid digestion phase for intact and homogenised samples, while a faster digestion rate (k_1, **Tab. 6.5**) was observed in the 10 s and 20 s homogenised samples.

While the rate constant (k_2) for the slow stage was at least five times lower than that for the rapid stage (k_1), the longer duration of the slow stage (160 mins compared to 20 mins) resulted in a greater amount of starch degradation in the slow stage as $C_{\infty 2}$ was nearly twice as $C_{\infty 1}$. This indicates that the slow digestion stage is an essential step in starch digestion in cooked rice. Upon homogenisation, no significant increase was observed in k_2, which could because the role of particle size for slowly digestible starch is less important than for rapidly digestible starch, and it may be instead related to the higher proportion of in slowly digestible starch. The expected total amount of hydrolysed starch ($C_{\infty total} = C_0 + C_{\infty 1} + C_{\infty 2}$) was lower in intact grains than in homogenised grains.

The insignificant k_2 increase after homogenisation of JR grains suggests that homogenisation was associated with increased RDS (**Tab. 6.5**). Homogenisation caused disruption of the grain, exposing more starch to enzymes. In the presence of LAGG-coating, grain fragments may still be partially coated by the hydrocolloid, which hindered enzyme accessibility.

Regarding PR, the impact of homogenisation on the rapidly digestible starch (RDS) portion appeared to be more significant on the digestion rate (k_1) than on the amount of starch digested ($C_{\infty 1}$). Compared to JR, PR contains a higher proportion of slowly digestible starch (SDS), which is the pregelatinised starch produced during parboiling (Hasbullah et al., 2017). It is possible that the RDS fraction is formed at the periphery of kernels because of damaged protein networks (that prevent starch from digestion) and swelling starch granules formed during cooking (Li & Hu, 2020;

Zou et al., 2015). After RDS digestion, SDS becomes more easily attacked by digestive enzymes, and the digestion rate of the SDS fraction is accelerated.

The pGI is shown in **Tab. 6.5**. The pGI of intact JR was significantly greater and characterised as high-GI (71.4 ± 3.8 > 70), while the mean pGI of intact PR was 50.0 ± 2.6 < 55 and classified as low-GI group. These values are in line with most published *in vitro* and *in vivo* studies (Ranawana et al., 2009; Sivakamasundari et al., 2020; Truong et al., 2014; Wolever et al., 1986). After cooked rice samples were homogenised, the pGI of PR increased significantly. Both are classified as high-GI food, which is also comparable with those reported by Wolever et al. (1986) and the results from the Chinese group reported by Kataoka et al. (2012) (PR's GI of the Chinese group ranges 63–82 in and 50-64 in European group using glucose solution as a reference). The addition of LAGG significantly reduced the pGI of JR in both homogenisation conditions, showing a decrease of approximately 20.89 ± 1.35 % and 17.27 ± 1.89 %, respectively. LAGG had a significant impact on lowering the pGI of 20 s homogenised PR (80.7±1.5) compared to the respective 20 s homogenised PR control (85.8±1.2) (**Tab. 6.5**).

Tab. 6.5. Fitting of the kinetic models for *in vitro* digestion (static model) cooked rice with and without LAGG after oral-gastrointestinal processing simulations (0 s, 10 s, 20 s).

	time	C_0 (%)	k_1 (min^{-1})	$C_{\infty 1}$ (%)	t_{int} (min)	k_2 (min^{-1})	$C_{\infty 2}$ (%)	C_{total} (%)	C_{180} (%)	pGI	R^2
	0 s	9.0 ± 0.8 ^{a}	0.136 ± 0.020 ^{cd}	21.6 ± 3.3 ^{ab}	15.0 ± 0.8 ^{a}	0.014 ± 0.002 ^{ab}	39.4 ± 0.6 ^{de}	71.0 ± 4.7 ^{bc}	61.3 ± 5.5 ^{c}	71.5 ± 3.8 ^{c}	0.9993
JR	10 s	10.6 ± 3.1 ^{a}	0.269 ± 0.033 ^{b}	24.7 ± 3.4^{ab}	15.4 ± 0.3 ^{a}	0.016 ± 0.002 ^{ab}	50 0.1 ± 5.1 ^{c}	84.8 ± 0.8 ^{b}	83.6 ± 1.4^{b}	82.8 ± 2.0	0.9990
	20 s	10.8 ± 2.5 ^{a}	0.353 ± 0.015 ^{a}	27.5 ± 0.9 ^{a}	15.7 ± 0.9 ^{a}	0.017 ± 0.001 ^{a}	61.0 ± 1.9 ^{b}	98.5 ± 0.5 ^{a}	96.6 ± 1.4^{a}	86.2 ± 1.3 ^{a}	0.9993
	0 s	3.7 ± 1.9 ^{b}	0.055 ± 0.011^{ef}	22.8 ± 4.1 ^{ab}	10.0 ± 1.0 ^{bc}	0.011 ± 0.001 ^{b}	39.8 ± 2.8 ^{de}	66.3 ± 4.4 ^{c}	56.6 ± 7.1 ^{c}	48.9 ± 0.6 ^{e}	0.9993
JR_1LA	10 s	6.2 ± 1.3 ^{ab}	0.070 ± 0.007 ^{e}	23.7 ± 3.1 ^{ab}	11.9 ± 2.2^{ab}	0.014 ± 0.001 ^{ab}	45.7 ± 4.7 ^{cd}	75.6 ± 4.1 ^{c}	68.9 ± 1.1 ^{b}	72.5 ± 1.9 ^{cd}	0.9990
	20 s	6.7 ± 1.2 ^{ab}	0.080 ± 0.005 ^{e}	25.5 ± 2.3 ^{ab}	15.0 ± 0.6 ^{ab}	0.013 ± 0.002 ^{ab}	49.7 ± 7.1 ^{c}	81.9 ± 6.0 ^{b}	77.1 ± 1.4 ^{b}	80.9 ± 2.3 ^{ab}	0.9993
	0 s	7.3 ± 2.9 ^{ab}	0.044 ± 0.001 ^{f}	20.9 ± 2.2 ^{ab}	15.7 ± 2.4 ^{a}	0.009 ± 0.002 ^{c}	25.5 ± 3.6 ^{f}	53.7 ± 4.6^{d}	46.1 ± 5.7 ^{d}	50.0 ± 1.6 ^{e}	0.9990
PR	10 s	7.6 ± 3.1 ^{ab}	0.129 ± 0.019 ^{cd}	18.7 ± 1.1 ^{b}	10.0 ± 0.5 ^{c}	0.012 ± 0.001 ^{b}	47.3 ± 0.9 ^{cd}	73.6 ± 5.6 ^{b}	65.7 ± 5.6 ^{c}	76.4 ± 1.4 ^{bc}	0.9919
	20 s	8.0 ± 3.3 ^{ab}	0.150 ± 0.008 ^{c}	18.3 ± 0.6 ^{b}	5.0 ± 0.5 ^{d}	0.014 ± 0.001 ^{ab}	71.8 ± 1.5 ^{a}	98.1 ± 0.8 ^{a}	93.0 ± 1.4 ^{a}	85.8 ± 1.2 ^{a}	0.9967
	0 s	4.7 ± 0.8 ^{b}	0.041 ± 0.005 ^{f}	13.9 ± 1.6 ^{c}	10.0 ± 1.0 ^{c}	0.010 ± 0.002 ^{c}	21.5 ± 2.8 ^{f}	40.1 ± 3.7^{e}	37.1 ± 1.4 ^{e}	48.3 ± 1.5 ^{e}	0.9996
PR_1LA	10 s	6.6 ± 0.2 ^{ab}	0.072 ± 0.002 ^{e}	16.7 ± 2.1 ^{bc}	10.8 ± 1.2 ^{c}	0.011 ± 0.003 ^{bc}	36.8 ± 1.1 ^{e}	60.1 ± 4.8 ^{cd}	58.8 ± 3.3 ^{c}	68.9 ± 1.9 ^{d}	0.9988
	20 s	6.8 ± 1.2 ^{ab}	0.100 ± 0.005 ^{d}	14.3 ± 1.0 ^{c}	5.5 ± 0.7 ^{d}	0.013 ± 0.002 ^{ab}	60.5 ± 1.6 ^{b}	81.6 ± 3.2 ^{b}	80.5 ± 6.0 ^{b}	80.7 ± 1.5 ^{ab}	0.9928

Mean ± S.D. calculated from triplicate measurements. For each parameter (column), the different superscript letters indicate values among the four samples are statistically different ($p < 0.05$). Values presented here are: the concentration of digested starch (C_0, %) at the beginning of intestinal digestion phase; starch digestion rate constants of rapid (k_1) and slow phase (k_2), corresponding estimated percentage of digested starch ($C_{\infty 1}$ and $C_{\infty 2}$, %), t_{int} is defined as the time intersection of two distinct digestion phase. The percentage of digested starch at the end of experiment predicted (C_{total}, %) and practical (C_{180}, %), predicted glycemic index (pGI), and the goodness of curve-fitting (reflected by R^2). 0 s, 10 s, 20 s refer to different homogenisation time

6.3.6.2 Semi-dynamic model

To gain more detailed information about starch digestibility under *in vivo* conditions, the effect of changing gastric pH (to simulate chemical changes in the gastric phase *in vivo*) and peristaltic compression forces (to simulate mechanical effects through digestion fate) was evaluated using a semi-dynamic model. Besides the LAGG-coating ability to inhibit starch digestion, the role of LAGG viscosity in the *in vitro* digestibility of cooked rice has been highlighted in this thesis. Hence, during *in vitro* digestion, the mixture's viscosity was monitored (**Section 6.3.6.2**). **Fig. 6.11** and **Fig. 6.12** shows the *in vitro* semi-dynamic starch and protein digestibility of cooked grains

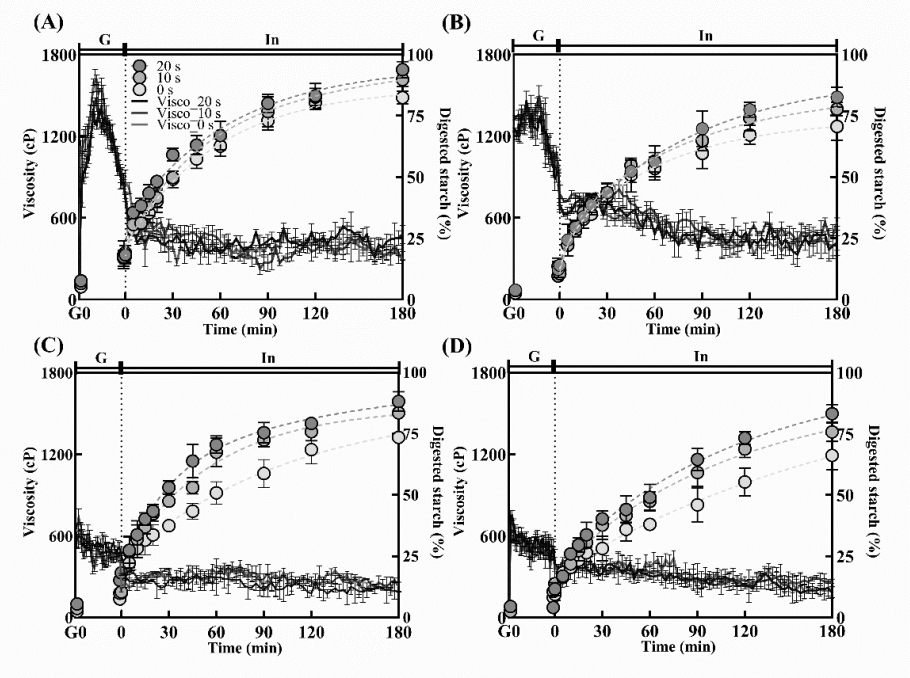


Fig. 6.11. *In vitro* semi-dynamic starch digestibility of cooked grains with and without LAGG. The starch digestibility was evaluated under three different structural conditions: non-homogenised (0 s), homogenised 10 s, and 20 s. Panels A to D correspond to starch digestion of JR, JR_1LA, PR and PR_1LA, respectively, during the gastric phase (G; 30 mins), followed by the intestinal phase (In; 180 mins). Sample legend in panel A. Light grey, grey and black circles correspond to starch digestibility (measured values) from samples homogenised for 0 s (intact grain), 10 s and 20 s, respectively. The dashed lines correspond to kinetics model fittings for the digestion curves of each sample. Light grey,

grey, and black lines refer to the respective viscosities. Error bars represent standard deviations (n = 4).

As shown in **Fig. 6.11**, the viscosity in the gastric phase was between 2 and 3 times the viscosity in the intestinal phase, possibly due to the dilution caused by the SIF. While semi-dynamic model results were similar to the digestion trends (a general increase in the degree of hydrolysis as the digestion time progresses) in starch and protein (**Fig. 6.11** and **Fig. 6.12**) obtained from the static model (**Fig. 6.9** and **Fig. 6.10**). This indicates that starch and protein hydrolysis continue over time under both digestion systems. For Protein digestion, there is a clear differentiation in the degree of hydrolysis among the different homogenising time. For instance, JR_20 s appears to have a higher degree of hydrolysis compared to JR_0 s, indicating that physical disruption of granular structures enhances starch and protein digestion efficiency.

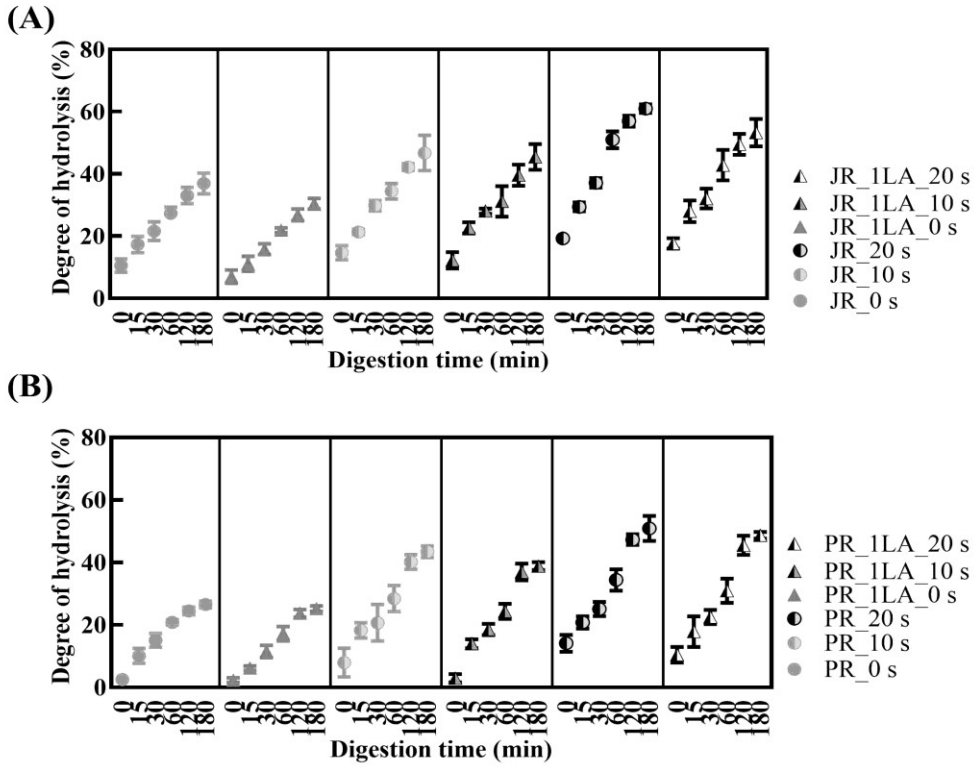


Fig. 6.12. *In vitro* semi-dynamic protein digestibility of cooked grains with and without LAGG The protein digestibility was evaluated under three different structural

conditions: non-homogenised (0 s), homogenised 10 s, and 20 s. Panels A and B correspond to protein digestion of JR and JR_1LA, PR and PR_1LA, respectively.

Further for starch digestion, during the intestinal phase, the extent of digested starch increased and appeared to slow down, reaching equilibrium in all samples after 120 mins, similar to the digestion curve obtained from the static model. With an R^2 > 0.99, the kinetic model accurately fitted the whole digestion curve. In agreement with what was observed in static models during digestion, two distinct digestion fractions (rapid to slow) were identified among the rice samples. The fitting parameters are shown in **Tab. 6.6**. As predicted, the digestion rates of rapidly digestible fractions (k_1) were significantly higher than those of slowly digestible fractions (k_2), in agreement with the results of static digestion. Among the rapid digestion phases (within 20 mins), the rapid digestion extent accounted for 20 % of the total digestion amount, while the slow digestion phase was the major contributor (80 %) to the total amount of digested starch. These parameters were in good agreement with the rate constants and digestion extents observed in static models and published in the literature for regular and retrograded starches (Edwards et al., 2014; Gong et al., 2019; Li et al., 2019).

The increase in the extent of homogenisation in JR was consistent with the increase in k_1, $C_{\infty 1}$ and intersection times (t_{2start}), which indicated that oral processing to the food model like rice grain had a substantial impact on starch digestibility *in vitro*, in agreement with the static model results. It was interesting to note that the k_1, $C_{\infty 1}$, and t_{2start} values were not significantly different for PR under different homogenisation extents. The PR's textural characteristics may be responsible for the behaviour in response to the compression force applied in the semi-dynamic system. The PR observed a hard and less sticky texture in **Section 6.3.3**, rapid disintegration data in **Section 6.3.5** and low viscosity in the semi-dynamic model. It can be hypothesised that PR grain has a rigid structure that makes it difficult for rice fractions to form a compact bolus. The simulated peristalsis compression in the semi-dynamic model facilitated the PR structure breaching, resulting in a closer particle size distribution and starch digestibility to JR than that observed with the static model (**Tab. 6.6**).

Rice cooked in LAGG dispersion produced a more viscous system on digestion. A significant increase was observed in the intestinal phase of JR_1LA, increasing from 470 cP to 650 cP in response to the increase in homogenisation. It was also observed in JR_1LA that starch digestibility and pGI were lower than the JR control. These results suggest that the LAGG provides an external resistance (via viscosity increase) to enzyme diffusion, which may contribute to digestion restriction. Similar phenomena have been noted when modulating the viscosity of starch gels by the addition of hydrocolloids (such as guar gum and xanthan gum), attributed to the difficulty of enzymes in accessing starch (He et al., 2020a; Santamaria et al., 2022).

Tab. 6.6. Fitting of the kinetic models for *in vitro* digestion (semi-dynamic model) cooked rice samples with and without LAGG under different oral processing simulations (0 s, 10 s, 20 s).

	time	C_0 (%)	k_1 (min $^{-1}$)	$C_{\infty 1}$ (%)	t_{int} (min)	k_2 (min^{-1})	$C_{\infty 2}$ (%)	C_{total} (%)	C_{180} (%)	G_{visco} (cP)	In_{visco} (cP)	pGI	R^2
JR	0 s	16.0 ± 4.7 ^{ab}	0.185 ± 0.049 ^{bc}	20.3 ± 6.6 ^{ab}	14.1 ± 2.1 ^{bc}	0.015 ± 0.001 ^{a}	56.4 ± 3.5 ^{ab}	92.7 ± 1.6 ^{ab}	86.4 ± 2.7 ^{ab}	1230 ± 220 ^{a}	390 ± 60 ^{b}	73.9 ± 1.9 ^{b}	0.9962
	10 s	19.1 ± 2.1 ^{a}	0.224 ± 0.061 ^{ab}	24.0 ± 4.4^{a}	13.1 ± 2.2 ^{bc}	0.016 ± 0.006 ^{a}	55.3 ± 4.0 ^{ab}	98.3 ± 1.0 ^{a}	84.9 ± 4.6 ^{ab}	1110 ± 210 ^{a}	400 ± 90 ^{b}	77.3 ± 2.7 ^{a}	0.9927
	20 s	17.6 ± 3.1 ^{ab}	0.269 ± 0.041^{a}	26.8 ± 1.3 ^{a}	11.7 ± 1.4 ^{c}	0.014 ± 0.001 ^{a}	55.1 ± 2.2 ^{ab}	99.4 ± 0.5 ^{a}	93.8 ± 3.3^{a}	1130 ± 190 ^{a}	430 ± 50 ^{b}	78.4 ± 1.1 ^{a}	0.9991
JR_ 1LA	0 s	12.0 ± 1.0 ^{b}	0.085 ± 0.021 ^{d}	24.5 ± 3.9 ^{a}	20.0 ± 1.0 ^{a}	0.012 ± 0.001 ^{ab}	34.8 ± 2.5 ^{d}	71.3 ± 3.3 ^{c}	70.6 ± 5.7 ^{d}	1200 ± 210 ^{a}	470 ± 70 ^{b}	65.0 ± 1.9 ^{d}	0.9968
	10 s	16.5 ± 3.5 ^{ab}	0.088 ± 0.012 ^{d}	22.2 ± 2.8 ^{ab}	18.3 ± 2.4 ^{ab}	0.015 ± 0.001 ^{a}	44.2 ± 3.1 ^{c}	82.9 ± 2.9 ^{b}	78.9 ± 3.1 ^{bc}	1210 ± 180 ^{a}	570 ± 120 ^{ab}	70.7 ± 1.0 ^{bc}	0.9929
	20 s	14.0 ± 1.0 ^{b}	0.095 ± 0.025 ^{d}	24.8 ± 1.6 ^{a}	12.2 ± 3.0 ^{bc}	0.017 ± 0.002 ^{a}	48.6 ± 3.6 ^{bc}	87.4 ± 6.5 ^{ab}	77.5 ± 2.0 ^{bc}	1210 ± 160 ^{a}	650 ± 100 ^{a}	73.3 ± 0.9 ^{b}	0.9961
PR	0 s	11.5 ± 0.6 ^{bc}	0.150 ± 0.003 ^{c}	22.0 ± 2.1 ^{ab}	15.0 ± 0.5 ^{b}	0.006 ± 0.001 ^{c}	46.5 ± 1.6 ^{c}	80.0 ± 4.6 ^{bc}	73.5 ± 2.2 ^{cd}	460 ± 90 ^{b}	290 ± 40 ^{cd}	63.5 ± 1.2 ^{d}	0.9998
	10 s	13.6 ± 2.3 ^{b}	0.153 ± 0.005 ^{c}	25.6 ± 0.4 ^{a}	15.0 ± 1.0 ^{b}	0.009 ± 0.003 ^{bc}	54.1 ± 9.0 ^{bc}	93.4 ± 5.4 ^{ab}	85.7 ± 2.6 ^{ab}	490 ± 100 ^{b}	270 ± 40 ^{cd}	69.3 ± 1.9 ^{c}	0.9984
	20 s	18.3 ± 1.6 ^{a}	0.174 ± 0.00 ^{bc}	24.1 ± 3.5 ^{a}	12.7 ± 2.7 ^{bc}	0.013 ± 0.004 ^{ab}	50.9 ± 4.9 ^{c}	92.7 ± 5.5 ^{ab}	84.2 ± 1.0 ^{ab}	530 ± 60 ^{b}	240 ± 30 ^{d}	75.7 ± 1.8 ^{a}	0.9998
PR_ 1LA	0 s	9.4 ± 2.0 ^{c}	0.110 ± 0.014 ^{cd}	13.9 ± 2.5 ^{c}	13.3 ± 2.4 ^{bc}	0.010 ± 0.002 ^{bc}	52.0 ± 2.7 ^{bc}	75.4 ± 2.1^{c}	66.2 ± 5.8 ^{d}	490 ± 110 ^{b}	300 ± 60 ^{cd}	56.8 ± 1.9 ^{e}	0.9969
	10 s	13.8 ± 0.7 ^{b}	0.090 ± 0.026 ^{d}	17.1 ± 4.2 ^{b}	15.2 ± 1.2 ^{b}	0.008 ± 0.001 ^{c}	60.8 ± 6.0^{ab}	91.7 ± 7.5 ^{ab}	75.7 ± 3.9 ^{bc}	520 ± 60 ^{b}	310 ± 60 ^{cd}	64.7 ± 1.7 ^{c}	0.9979
	20 s	11.7 ± 0.6 ^{bc}	0.119 ± 0.022 ^{cd}	15.7 ± 1.0 ^{bc}	5.0 ± 0.5 ^{d}	0.010 ± 0.005 ^{bc}	65.4 ± 3.9 ^{a}	92.8 ± 5.2 ^{ab}	83.2 ± 3.8 ^{b}	600 ± 80 ^{b}	290 ± 70 ^{cd}	71.5 ± 1.8 ^{b}	0.9971

Mean ± S.D. calculated from triplicate measurements. For each parameter (column), the different superscript letters indicate values among the four samples are statistically different ($p < 0.05$). Values presented here are: the concentration of digested starch (C_0, %) at the beginning of intestinal digestion phase; starch digestion rate constants of rapid (k_1) and slow phase (k_2), corresponding estimated percentage of digested starch ($C_{\infty 1}$ and $C_{\infty 2}$, %), t_{int} is defined as the time intersection of two distinct digestion phase. The percentage of digested starch at the end of experiment predicted (C_{total}, %) and practical (C_{180}, %), gastric (G_{visco}) and intestinal (In_{visco}) viscosity changes; predicted glycemic index (pGI), and the goodness of curve-fitting (reflected by R^2). 0 s, 10 s, 20 s refer to different homogenisation time

6.4 Conclusions

By using static and semi-dynamic digestion models, this study demonstrated LAGG's ability to reduce starch digestibility in cooked rice when subjected to three levels of oral breakdown simulations (non, normal, fine). The findings of this study support and demonstrate the importance of oral processing of cooked rice in initiating *in vitro* starch digestion assessment, especially in static models, since it affects particle size reduction and enzyme exposure. Compared to chewed rice, swallowed rice (intact grains) was less digestible. A compact grain structure may prevent starch from leaching into the matrices and being exposed to amylase. As a result, the increased digestibility of orally processed rice is expected to depend on the formation of rice fragments, which are more easily impregnated with digestion solutions. It is also important to consider the texture characteristics of the food model, such as cooked rice, as the food model could respond differently to oral processing in terms of grain fracturability and starch digestion performance. Rice cooked with LAGG showed promising results for delaying starch digestion. This may be due to physical barriers, structural integrity preservation, and viscosity enhancement.

6.5 References

Aguilera, J.M. (2019) The food matrix: implications in processing, nutrition and health. *Critical reviews in food science and nutrition*, 59 (22): 3612–3629. doi:10.1080/10408398.2018.1502743.

Amano, Y., Kawakubo, K., Lee, J.S., et al. (2004) Correlation between dietary glycemic index and cardiovascular disease risk factors among Japanese women. *European Journal of Clinical Nutrition 2004 58:11*, 58 (11): 1472–1478. doi:10.1038/sj.ejcn.1601992.

AOAC (2005a) Official methods of analysis of the Association of Analytical Chemists International. Official Methods 934.01: Gaithersburg, MD, USA.

AOAC (2005b) Official methods of analysis of the Association of Analytical Chemists International. Official Methods 933.29: Gaithersburg, MD, USA.

AOAC (2007). Official methods of analysis of Association of Analytical Chemists International. Official Methods 996.11: Gaithersburg, MD, USA.

Argyri, K., Athanasatou, A., Bouga, M., et al. (2016) The Potential of an *in vitro* Digestion Method for Predicting Glycemic Response of Foods and Meals. *Nutrients*, 8 (4). doi:10.3390/NU8040209.

Atkinson, F.S., Brand-Miller, J.C., Foster-Powell, K., et al. (2021) International tables of glycemic index and glycemic load values 2021: a systematic review. *The American Journal of Clinical Nutrition*, 114 (5): 1625–1632. doi:10.1093/AJCN/NQAB233.

Bertoft, E. (2004) On the nature of categories of chains in amylopectin and their connection to the super helix model. *Carbohydrate Polymers*, 57 (2): 211–224. doi:10.1016/J.CARBPOL.2004.04.015.

Blanquet-Diot, S., François, O., Denis, S., et al. (2021) Importance of oral phase *in vitro* starch digestibility related to wholegrain versus refined pastas and mastication impairment. *Food Hydrocolloids*, 112: 106277. doi.org/10.1016/j.foodhyd.2020.106277.

Bornhorst, G.M. & Singh, R.P. (2012) Bolus Formation and Disintegration during Digestion of Food Carbohydrates. *Comprehensive Reviews in Food Science and Food Safety*, 11 (2): 101–118. doi:10.1111/j.1541-4337.2011.00172.x.

Brodkorb, A., Egger, L., Alminger, M., et al. (2019) INFOGEST static *in vitro* simulation of gastrointestinal food digestion. *Nature Protocols 2019 14:4*, 14 (4): 991–1014. doi:10.1038/s41596-018-0119-1.

Chatthongpisut, R., Schwartz, S.J. & Yongsawatdigul, J. (2015) Antioxidant activities and antiproliferative activity of Thai purple rice cooked by various methods on human colon cancer cells. *Food Chemistry*, 188: 99–105. doi.org/10.1016/j.foodchem.2015.04.074.

Chen, L., Tian, Y., Zhang, Z., et al. (2017) Effect of pullulan on the digestible, crystalline and morphological characteristics of rice starch. *Food Hydrocolloids*, 63: 383–390. doi:10.1016/j.foodhyd.2016.09.021.

Choi, H.J., Lee, C.J., Cho, E.J., et al. (2010) Preparation, digestibility, and glucose response in mice of rice coated with resistant starch type 4 using locust bean gum and agar. *International Journal of Food Science and Technology*, 45 (12): 2612–2621. doi:10.1111/j.1365-2621.2010.02434.x.

Choy, J.Y.M., Goh, A.T., Chatonidi, G., et al. (2021) Impact of food texture modifications on oral processing behaviour, bolus properties and postprandial glucose responses. *Current Research in Food Science*, 4 (November): 891–899. doi:10.1016/j.crfs.2021.11.018.

Dang, J. and Copeland, L. (2004) Studies of the fracture surface of rice grains using environmental scanning electron microscopy. *Journal of the Science of Food and Agriculture*, 84: 707–713. doi:10.1002/jsfa.1671.

Drechsler, K.C. & Bornhorst, G.M. (2018) Modeling the softening of carbohydrate-based foods during simulated gastric digestion. *Journal of Food Engineering*, 222: 38–48. doi:10.1016/J.JFOODENG.2017.11.007.

Edwards, C.H., Cochetel, N., Setterfield, L., et al. (2019) A single-enzyme system for starch digestibility screening and its relevance to understanding and predicting the glycaemic index of food products. *Food and Function*, 10 (8): 4751–4760. doi:10.1039/c9fo00603f.

Edwards, C.H., Maillot, M., Parker, R., et al. (2018) A comparison of the kinetics of *in vitro* starch digestion in smooth and wrinkled peas by porcine pancreatic alpha-amylase. *Food Chemistry*, 244 (June 2017): 386–393. doi:10.1016/j.foodchem.2017.10.042.

Edwards, C.H., Warren, F.J., Milligan, P.J., et al. (2014) A novel method for classifying starch digestion by modelling the amylolysis of plant foods using first-order enzyme kinetic principles. *Food and Function*, 5 (11): 2751–2758. doi:10.1039/c4fo00115j.

Fang, S., Wang, J., Xu, X., et al. (2018) Influence of Low Acyl and High Acyl Gellan Gums on Pasting and Rheological Properties of Rice Starch Gel. *Food Biophysics*, 13 (2): 116–123. doi:10.1007/s11483-018-9517-8.

Farooq, A.M., Li, C., Chen, S., et al. (2018) Particle size affects structural and *in vitro* digestion properties of cooked rice flours. *International Journal of Biological Macromolecules*, 118: 160–167. doi:10.1016/j.ijbiomac.2018.06.071.

Fernandes, J.M., Madalena, D.A., Pinheiro, A.C., et al. (2020) Rice *in vitro* digestion: application of INFOGEST harmonized protocol for glycemic index determination and starch morphological study. *Journal of Food Science and Technology*, 57 (4): 1393. doi:10.1007/S13197-019-04174-X.

Fitzgerald, M.A., Martin, M., Ward, R.M., et al. (2003) Viscosity of rice flour: A rheological and biological study. *Journal of Agricultural and Food Chemistry*, 51 (8): 2295–2299. doi:10.1021/jf020574i.

Furuya, J., Hara, A., Nomura, T., et al. (2014) Volitional chewing with a conscious effort alters and facilitates swallowing during the feeding sequence. *Journal of Oral Rehabilitation*, 41 (3): 191–198. doi:10.1111/JOOR.12140.

Gouseti, O., Jaime-Fonseca, M.R., Fryer, P.J., et al. (2014) Hydrocolloids in human digestion: Dynamic *in vitro* assessment of the effect of food formulation on mass transfer. *Food Hydrocolloids*, 42 (P3): 378–385. doi:10.1016/j.foodhyd.2014.06.004.

Guraya, H. S., Kadan, R. S., & Champagne, E. T. (1997). Effect of rice starch-lipid complexes on in vitro digestibility, complexing index, and viscosity. Cereal Chemistry, 74(5), 561–565. doi.org/10.1094/CCHEM.1997.74.5.561

Hamad, S., Zafar, T.A. & Sidhu, J. (2018) Parboiled rice metabolism differs in healthy and diabetic individuals with similar improvement in glycemic response. *Nutrition*, 47: 43–49. doi:10.1016/J.NUT.2017.09.010.

Han, A., Lee, Y. and Meullenet, J.F. (2017) Comparison of a double compression test for the prediction of sensory texture attributes of cooked rice to a single compression test. *Emirates Journal of Food and Agriculture*, 29 (8): 643–650. doi:10.9755/ejfa.2017-03-544.

Hasbullah, R., Pujantoro, L., Koswara, S., et al. (2017) Steaming process of paddy to improve quality and reduce the glycemic index of parboiled rice. *Acta Horticulturae*, 1152 (March): 375–379. doi:10.17660/ActaHortic.2017.1152.50.

He, H., Chi, C., Xie, F., et al. (2020) Improving the *in vitro* digestibility of rice starch by thermomechanically assisted complexation with guar gum. *Food Hydrocolloids*, 102. doi:10.1016/J.FOODHYD.2019.105637.

Li Hongyan (2017) Understanding the texture of cooked rice from the molecular, instrumental and sensory levels. PhD Thesis, Queensland Alliance for Agriculture and Food Innovation, The University of Queensland.doi.org/10.14264/uql.2017.868

Jimenez-Cruz, A., Bacardi-Gascon, M., Turnbull, W.H., et al. (2003) A Flexible, Low-Glycemic Index Mexican-Style Diet in Overweight and Obese Subjects With Type 2 Diabetes Improves Metabolic Parameters During a 6-Week Treatment Period. *Diabetes Care*, 26 (7): 1967–1970. doi:10.2337/DIACARE.26.7.1967.

Jiménez-Munoz, L., Brodkorb, A., Gómez-Mascaraque, L.G., et al. (2021) Effect of heat treatment on the digestion behaviour of pea and rice protein dispersions and their blends

studied using the semi-dynamic INFOGEST digestion method. *Food and Function*, 12 (18): 8747–8759. doi:10.1039/d1fo01223a.

Karababa, E. & Coşkuner, Y. (2007) Moisture-dependent physical properties of dry sweet corn kernels. *International Journal of Food Properties*, 10 (3): 549–560. doi:10.1080/10942910601003981.

Kataoka, M., Venn, B.J., Williams, S.M., et al. (2013) Glycaemic responses to glucose and rice in people of Chinese and European ethnicity. *Diabetic medicine : a journal of the British Diabetic Association*, 30 (3): e101-7. doi:10.1111/dme.12080.

Kaur, B., Ranawana, V. and Henry, J. (2016) The Glycemic Index of Rice and Rice Products: A Review, and Table of GI Values. *Critical Reviews in Food Science and Nutrition*. 56 (2) pp. 215–236. doi:10.1080/10408398.2012.717976.

Khin, M.N., Ahammed, S. and Zhong, F. (2021) Development of DTAF-labelled polysaccharides for characterization of microstructure and phase distribution of composite hydrogel visualization of hydrogels using CLSM. *Food Bioscience*, 41: 100909. doi:10.1016/J.FBIO.2021.100909.

Hu, X., Huang, Z., Zeng, Z., et al. (2020). Improving resistance of crystallized starch by narrowing molecular weight distribution. Food Hydrocolloids, 103, 105641. doi.org/10.1016/J.FOODHYD.2020.105641

Li, C. & Hu, Y. (2020) Combination of parallel and sequential digestion kinetics reveals the nature of digestive characteristics of short-term retrograded rice starches. *Food Hydrocolloids*, 108. doi:10.1016/j.foodhyd.2020.106071.

Li, H., Yang, J., Yan, S., et al. (2019) Molecular causes for the increased stickiness of cooked non-glutinous rice by enzymatic hydrolysis of the grain surface protein. *Carbohydrate Polymers*, 216 (3): 197–203. doi:10.1016/j.carbpol.2019.04.031.

Liu, K., Zheng, J. & Chen, F. (2019) Effect of domestic cooking on rice protein digestibility. *Food Science and Nutrition*, 7 (2): 608–616. doi:10.1002/FSN3.884.

Liu, K., Zheng, J. & Chen, F. (2021) Heat-induced changes in the physicochemical properties and *in vitro* digestibility of rice protein fractions. *Journal of Food Science and Technology*, 58 (4): 1368. doi:10.1007/S13197-020-04648-3.

Liu, Ren, X., Asimi, S., et al. (2020) Changes in oral processing parameters of three rice varieties. *Journal of Texture Studies*. doi:10.1111/jtxs.12526.

Lu, L.W., Venn, B., Lu, J., et al. (2017) Effect of Cold Storage and Reheating of Parboiled Rice on Postprandial Glycaemic Response, Satiety, Palatability and Chewed Particle Size Distribution. *Nutrients*, 9 (5). doi:10.3390/NU9050475.

Mandalari, G., Merali, Z., Ryden, P., et al. (2018) Durum wheat particle size affects starch and protein digestion *in vitro*. *European Journal of Nutrition*, 57 (1): 319–325. doi:10.1007/s00394-016-1321-y.

Martin, M. and Fitzgerald, M.A. (2002) Proteins in Rice Grains Influence Cooking Properties! *Journal of Cereal Science*, 36 (3): 285–294. doi.org/10.1006/jcrs.2001.0465.

Moongngarm, A., Bronlund, J., Grigg, N., et al. (2012) Chewing Behavior and Bolus Properties as Affected by Different Rice Types. *International Journal of Medical and Biological Sciences*, 6.doi.org/10.5281/zenodo.1079550

Nadia, J., Olenskyj, A.G., Stroebinger, N., et al. (2021) Tracking physical breakdown of rice- and wheat-based foods with varying structures during gastric digestion and its influence on gastric emptying in a growing pig model. *Food and Function*, 12 (10): 4349–4372. doi:10.1039/d0fo02917c.

Nadia, J., Olenskyj, A.G., Subramanian, P., et al. (2022) Influence of food macrostructure on the kinetics of acidification in the pig stomach after the consumption of rice- and wheat-based foods: Implications for starch hydrolysis and starch emptying rate. *Food Chemistry*, 394: 133410. doi:10.1016/J.FOODCHEM.2022.133410.

Nawaz, M.A., Fukai, S. & Bhandari, B. (2016) Effect of Different Cooking Conditions on the Pasting Properties of Flours of Glutinous Rice Varieties from Lao People's Democratic Republic. *International Journal of Food Properties*, 19 (9): 2026–2040. doi:10.1080/10942912.2015.1092163.

Norton, A.B., Cox, P.W. & Spyropoulos, F. (2011) Acid gelation of low acyl gellan gum relevant to self-structuring in the human stomach. *Food Hydrocolloids*, 25 (5): 1105–1111. doi:10.1016/j.foodhyd.2010.10.007.

Ong, M.H. & Blanshard, J.M.V. (1995) Texture determinants in cooked, parboiled rice. I: Rice starch amylose and the fine structure of amylopectin. *Journal of Cereal Science*, 21 (3): 251–260. doi:10.1006/JCRS.1995.0028.

Panouillé, M., Saint-Eve, A. & Souchon, I. (2016) Instrumental methods for bolus characterization during oral processing to understand food perceptions. *Current Opinion in Food Science*, 9: 42–49. doi:10.1016/j.cofs.2016.05.002.

Peyron, M.A., Gierczynski, I., Hartmann, C., et al. (2011) Role of Physical Bolus Properties as Sensory Inputs in the Trigger of Swallowing. *PLoS ONE*, 6 (6). doi:10.1371/JOURNAL.PONE.0021167.

Ranawana, D. V, Henry, C.J.K., Lightowler, H.J., et al. (2009) Glycaemic index of some commercially available rice and rice products in Great Britain. *International journal of food sciences and nutrition*, 60 Suppl 4: 99–110. doi:10.1080/09637480802516191.

Ranawana, V., Monro, J.A., Mishra, S., et al. (2010) Degree of particle size breakdown during mastication may be a possible cause of interindividual glycemic variability. *Nutrition Research*, 30 (4): 246–254. doi:10.1016/J.NUTRES.2010.02.004.

Rave, K., Roggen, K., Dellweg, S., et al. (2007) Improvement of insulin resistance after diet with a whole-grain based dietary product: results of a randomized, controlled cross-over study in obese subjects with elevated fasting blood glucose. *The British journal of nutrition*, 98 (5): 929–936. doi:10.1017/S0007114507749267.

Riva, M., Fessas, D. and Schiraldi, A. (2000) Starch retrogradation in cooked pasta and rice. *Cereal Chemistry*, 77 (4): 433–438. doi:10.1094/CCHEM.2000.77.4.433.

Sagum, R., & Arcot, J. (2000). Effect of domestic processing methods on the starch, non-starch polysaccharides and in vitro starch and protein digestibility of three varieties of rice with varying levels of amylose. Food Chemistry, 70(1), 107–111. doi.org/10.1016/S0308-8146(00)00041-8

Santamaria, M., Montes, L., Garzon, R., et al. (2022) Unraveling the impact of viscosity and starch type on the *in vitro* starch digestibility of different gels. *Food & Function*, 13 (14): 7582–7590. doi:10.1039/D2FO00697A.

Santos, T.P. and Cunha, R.L. (2018) Role of process variables on the formation and *in vitro* digestion of gellan gels. *Carbohydrate Polymers*, 192: 111–117. doi:10.1016/J.CARBPOL.2018.03.062.

Sethupathy, P., Sivakamasundari, S.K., Moses, Jeyan.A., et al. (2021) Effect of varietal differences on the oral processing behaviour and bolus properties of cooked rice. *International Journal of Food Engineering*, 17 (3): 177–188. doi:10.1515/ijfe-2020-0097.

Sivakamasundari, S.K., Moses, J.A. & Anandharamakrishnan, C. (2020) Effect of parboiling methods on the physicochemical characteristics and glycemic index of rice varieties. *Journal of Food Measurement and Characterization*, 14 (6): 3122–3137. doi:10.1007/s11694-020-00551-9.

Steglich, T., Bernin, D., Röding, M., et al. (2014) Microstructure and water distribution of commercial pasta studied by microscopy and 3D magnetic resonance imaging. *Food Research International*, 62: 644–652. doi:10.1016/J.FOODRES.2014.04.004.

Sworn, G. & Stouby, L. (2021) Gellan gum. *Handbook of Hydrocolloids*, pp. 855–885. doi:10.1016/B978-0-12-820104-6.00009-7.

Tamura, M. (2016) Impact of structural characteristics on starch digestibility of cooked rice. *Food Chemistry*, 191: 91–97. doi:10.1016/J.FOODCHEM.2015.04.019.

Tamura, M., Okazaki, Y., Kumagai, C., et al. (2017) The importance of an oral digestion step in evaluating simulated *in vitro* digestibility of starch from cooked rice grain. *Food Research International*.94: 6–12. doi:10.1016/j.foodres.2017.01.019.

Tao, K., Yu, W., Prakash, S., et al. (2020) Investigating cooked rice textural properties by instrumental measurements. *Food Science and Human Wellness*, 9 (2): 130–135. doi:10.1016/j.fshw.2020.02.001.

Thakur, A.K. & Gupta, A.K. (2006) Water absorption characteristics of paddy, brown rice and husk during soaking. *Journal of Food Engineering*, 75 (2): 252–257. doi:10.1016/J.JFOODENG.2005.04.014.

Toutounji, M. R., Farahnaky, A., Santhakumar, A. B et al. (2019). Intrinsic and extrinsic factors affecting rice starch digestibility. In Trends in Food Science and Technology (Vol. 88, pp. 10–22). Elsevier Ltd.doi.org/10.1016/j.tifs.2019.02.012

Truong, T.H., Yuet, W.C. & Hall, M.D. (2014). The glycemic index of American-grown jasmine rice is classified as high. 65 (4): 436–439. doi:10.3109/09637486.2013.869797.

Villemejane, C., Denis, S., Marsset-Baglieri, A., et al. (2016) *In vitro* digestion of short-dough biscuits enriched in proteins and/or fibres using a multi-compartmental and dynamic system (2): Protein and starch hydrolyses. *Food Chemistry*, 190: 164–172. doi:10.1016/J.FOODCHEM.2015.05.050.

Wolever, T.M.S., Jenkins, D.J.A., Kalmusky, J., et al. (1986) Comparison of regular and parboiled rice: explanation of discrepancies between reported glycemic responses to rice. *Nutrition Research*, 6 (4): 349–357. doi:10.1016/S0271-5317(86)80175-0.

Yau, N.J.N. & Huang, J.J. (1996) Sensory analysis of cooked rice. *Food Quality and Preference*, 7 (3–4): 263–270. doi:10.1016/S0950-3293(96)00010-9.

Yu, W., Zhou, X. & Li, C. (2021) Application of first-order kinetics modelling to reveal the nature of starch digestion characteristics. *Food & Function*, 12 (15): 6652–6663. doi:10.1039/D1FO00450F.

7 Understanding the structure, texture, and digestion of rice-based formulations incorporated with rice protein and low acyl gellan gum.

Qingsu Liu[1], Vincenzo Di Bari[2], Nicholas James Watson[3*]

[1] Food, Water, Waste Research Group, Faculty of Engineering, The University of Nottingham, University Park Campus NG7 2RD, UK.

[2] Division of Food Sciences, The University of Nottingham, Sutton Bonington Campus, Loughborough LE12 5RD, UK.

[3] School of Food Science and Nutrition, University of Leeds, Leeds, LS2 9JT, UK

***Corresponding author:** n.j.watson@leeds.ac.uk

(Manuscript prepared for Submission)

Abstract

Rice is an essential food alternative for individuals with gluten sensitivities or allergies. However, high in rapidly digestible starch and can potentially cause health complications for those with diabetes. These concerns may be mitigated by the development of rice-based products on a reduced glycaemic index. This study proposes a rice-based pasta possessing this desirable characteristic.

The effect of rice protein and low acyl gellan gum addition on the physicochemical properties, microstructural modification, *in vitro* starch digestibility and predicted glycaemic index of cooked gluten-free orzo pasta was investigated. Gluten-free orzo pasta formulations consisted of 100 % rice flour or rice flour partially replaced with rice protein (9 %, w/w) and/or low acyl gellan gum (1 %, w/w). Another approach was to add the same amount (1 %, w/w) of low acyl gellan gum to the cooking water rather than to the formulation itself.

In rice protein and low acyl gellan gum-incorporated formulations, orzo pasting properties showed distinct viscosity profiles and a greater tendency to short-term retrogradation (setback viscosity) than the rice flour control. The resulting cooked orzo from modified formulations had a lower cooking loss and higher structural ordering than the control. Rice protein enrichment resulted in cooked orzo with a soft, extensible texture. Low acyl gellan gum addition increased the orzo texture strength to a different extent, whether in formulation or cooking water. The rice flour and low acyl gellan gum-incorporated formulations had intermediate texture properties. In rice protein and/or low acyl gellan gum-incorporated orzo, starch digestion rate and predicted glycaemic index decreased under the static *in vitro* digestion model, whereas this reduction was less noticeable under the semi-dynamic digestion model. Rice-based orzo incorporated with rice protein and low acyl gellan gum showed the lowest starch digestibility and predicted glycaemic index in the semi-dynamic digestion model. This suggests that rice protein and low acyl gellan gum are promising for producing low-glycaemic index orzo with improved cooking quality and texture.

Highlights

- Rice-based orzo formulations with rice protein and/or low acyl gellan gum were tested for their cooking quality (optimal cooking time, cooking loss, rehydration), microstructural and textural properties, and *in vitro* starch digestibility.
- Rice-based orzo pasta containing 1 % low acyl gellan gum showed reduced starch digestibility and a low predicted glycaemic index.
- A positive effect of producing orzo with rice protein and low acyl gellan gum on reducing starch digestibility was also observed under a semi-dynamic *in vitro* digestion model.
- Orzo incorporated with 9g/100g of rice protein and/or 1g/100 g of low acyl gellan gum improved cooking quality with less cooking loss.
- Orzo incorporated with rice protein showed a hybrid A+V crystalline starch structure type, indicating the presence of slowly digestible starch.

Keywords: rice-based orzo pasta, rice protein, low acyl gellan gum, *in vitro* digestion model

7.1 Introduction

Worldwide rice consumption is 530.54 kcal/per capita/day (FAOSTAT, 2020), nearly one-quarter of the recommended daily calorie intake (2000 kcal/day) for adult individuals (WHO, 2019). In Asia, rice is so important in diets that cooking procedures (soaking, rice-water-ratio setting, and timing) and equipment (such as rice cookers and pressure cookers) improves precision to achieve the finest texture and taste possible (Zhu et al., 2020; Tamura et al., 2021). Its gluten-free, low-fat, and versatile nature has also made rice a much more prevalent food in Western diets as a wheat alternative.

Two concerns about rice's nutritional value in gluten-free food products have been raised. Intrinsically, rice is low in protein but high in rapidly digestible starch content, producing a high *in vivo* glycaemic response, which could pose a significant health risk to diabetics (Bhavadharini et al., 2020; Hu et al., 2012; Khosravi-Boroujeni et al., 2013; Truong et al., 2014). Extrinsically, the cooking method adopted in Western countries is characterised by boiling the rice in excess water (similar to pasta cooking), whereas the Asian style involves a rice cooker that cooks rice in a closed chamber with limited water and no stirring required. To our knowledge, only a few studies have investigated the impact of the two above cooking methods on starch digestibility in rice grains. Tamura et al. (2017) observed faster starch hydrolysis in rice grains when cooked in limited water rather than excess water. This partially agrees with Yi et al. (2022), who reported the correlation between starch digestibility in rice flour and the starch molecular structure in several rice varieties. However, this disappeared at high water-to-rice ratios (over 4:1). Conversely, Wang et al. (2017) found that the rate of starch hydrolysis in cooked rice flour was not affected by pressure, soaking, or water-to-rice ratio but rather varied by rice varieties. These different results may be attributed to the native structure of rice flour, which undergo varying degrees of changes when exposed to water at specific amounts while heating. The impact of the cooking method is more complex at the grain-scale level, including molecular compositions (amylose and amylopectin ratio and size), supramolecular organisation (crystalline-amorphous structure types),

starch granule morphology (size and shape), surface features (pores and channels), as well as their packing pattern in cells with assistance from other non-starch compositions such as proteins, lipids, and fibres in cells (Michelle et al., 2019). The structural integrity of rice under excess water cooking conditions is also associated with problematic issues such as kernel disintegration, high cooking loss, and excessive moisture content, which is not generally accepted by consumers (Yu et al., 2017).

Orzo, a rice-shaped pasta, may provide a solution against high starch digestibility and structural disintegration. Besides playing a key role in the Mediterranean diet, pasta has been described as a healthy, sustainable, and quality food model by the WHO and the FAO (Food and Agriculture Organisation) of the United Nations. The pasta market has recently expanded worldwide due to an increase in available choices (pulse or vegetable-enriched, or gluten-free - GF) and improvements from a sensory and nutritional perspective, including postprandial glycaemic control (Zavitsanou et al., 2019). Rice is currently one of the most common cereal sources for commercial GF pasta; however, rice-based pasta has been associated with a poor nutritional profile as it is low in protein concentration, dietary fibres, and micronutrients and high in rapidly digestible starch (Morreale et al., 2019; Suo et al., 2022). Therefore, food-derived complexing agents, particularly protein, fibre, and hydrocolloids, are commonly added to reduce starch digestion and improve rice pasta cooking and nutritional quality. Strategies and opportunities for producing functional pasta have been widely reviewed in the last ten years. What these studies have in common is the awareness that pasta can be considered an important and interesting carrier for functional nutrients, such as protein and dietary fibres. Typically, wheat pasta has a low-glycaemic index (47-50 < 50) due to the presence of gluten, a protein network of glutenin and gliadin that entraps starch, forming protein-starch matrices, from which starch release is controlled (Zou et al., 2015b; Atkinson et al., 2021a). The compact gluten structure also reduces enzyme accessibility and restricts the amount of starch gelatinisation and swelling, resulting in higher crystalline starch content upon cooking, further reducing enzyme

accessibility. For this study, rice protein (RP) was selected because it has a higher biological value and protein efficiency ratio compared to that of the other commercially available cereal proteins, such as corn and wheat proteins (Wang et al., 1999). Rice is regarded as one of the best gluten-free plant proteins due to its hypoallergenic and multiple health benefits (Amagliani et al., 2017b). More importantly, RP and its hydrolysate have been shown to reduce rice starch digestibility (Chi, Li, Zhang, et al., 2018b; Khatun, Waters and Liu, 2020).

Despite improved protein content, GF pasta enriched with proteins still faces challenges in achieving comparable viscoelasticity and extensibility (beneficial for texture and sensory properties and to slow down starch digestibility) as gluten-containing pasta (Alvarez-Jubete et al., 2010; Hospital, 2017; Phongthai et al., 2017a; Rudra et al., 2020). As a result, several studies have added hydrocolloids, such as guar gum (He et al., 2020b) or xanthan gum (Cai et al., 2016a), to improve the GF pasta cooking quality and texture and reduce starch digestibility. Cooking quality parameters are moisture content, cooking loss (amount of matter lost from the orzo during cooking) and rehydration (evaluation of the water absorption and holding capacity during cooking); they are important as related to the structural integrity of the pasta, which in turn determines the starch digestibility.

A further way to reduce the structural weakness (e.g., cracks or breakage) of GF pasta is by producing small-sized pasta shapes, such as orzo. Moreover, due to its similar grain shape, orzo could be an ideal low-GI rice substitute. Low acyl gellan gum (LAGG) is a food-grade hydrocolloid and non-digestible carbohydrate, which could be potentially used to produce GF and low-GI pasta. It is a linear, anionic exopolysaccharide with a molecular weight of 500 kDa. It has a tetrasaccharide repeating sequence consisting of 1,3-d-glucose, 1,4-d-glucuronic acid, 1,4-d-glucose, and 1,4-n-l-rhamnose. LAGG is obtained by deacylating native gellan gum under alkali conditions (Morris et al .,2012). When dissolved in water, a reversible conformational transition occurs from a mixed single coil/double-stranded helix at low temperature (forming a weak gel) to a disordered single-stranded coil at a temperature above 70°C (Milas & Rinaudo, 1996). This transition could, therefore,

be observed during the cooking and cooling process of formulations incorporated with LAGG. As a result, LAGG could be employed as a gel coating layer either by self-structuring upon cooling or by forming a matrix by entwining with other components. Both gel models can be strengthened by interacting with divalent ions such as Ca^{2+} and Mg^{2+} through ionic bonding or by exposure to an acidic environment (pH 3), similar to digestion in the gastric phase (Bradbeer et al., 2015; Santos and Cunha, 2018). Therefore, LAGG has the potential to mediate starch digestion by maintaining matric integrity and reducing enzyme accessibility.

Considering what is described above, it could be hypothesised that adding RP and/or LAGG to rice flour (RF) could reduce the *in vitro* starch digestibility in rice-based orzo pasta.

This study aimed to determine the starch digestibility in a rice-based orzo pasta containing RP and LAGG by investigating their role in orzo cooking quality, structure, and texture. The *in vitro* starch digestibility of orzo was evaluated using static and semi-dynamic digestion systems. The cooking quality was evaluated by measuring the pasting properties using a rapid visco analyser (RVA), cooking loss and rehydration using standardised methods published by the American Association of Clinical Chemistry (AACC). The orzo microstructure was studied using X-ray diffractometry (XRD), Fourier Transform Infrared Spectroscopy (FTIR), and Environmental Scanning Electron Microscopy (ESEM), and the resulting texture properties were determined by Texture Profile Analysis (TPA).

7.2 Materials and Methods

7.2.1 Materials

Thai white jasmine rice (Green dragon Thai Hom Mali Aaa), used to prepare gluten-free orzo (GFO) pasta, and commercial orzo pasta (reference material), were purchased from a local supermarket (Nottingham, UK). The macronutrient information of the Thai jasmine rice (protein 7.2 g, fat 0.9 g, and carbohydrate 79.8g /100g) and orzo reference (converted from 75g of cooked pasta, protein 11.7 g, fat 2 g, and carbohydrate 74.9g /100g) was initially acquired from the food label. The

LAGG was kindly provided by Kelco, UK. Rice protein (RP) concentrates were purchased from Myprotein (THG plc., Manchester, UK), with a protein content of 81.41 ± 2.37 % (based on dry mass).

7.2.2 Preparation of rice flour (RF)

Rice grains were washed to remove impurities and left at room temperature for 24 hours to allow the remaining water to evaporate. The cleaned grains were then milled into flour using an electrical grinder (KG49, Delonghi, Treviso, Italy) and sifted through a 0.5 mm sieve; the particles over 0.5 mm were discarded. The resulting RF was measured for protein (6.66 ± 0.58 g/100g) and starch content (83.63 ± 1.68 g/100g).

7.2.3 Preparation of orzo pasta using a Rice-based formula

The preparation of cooked orzo pasta requires four steps: dough production, pasta formation, drying, and cooking in distilled water. **Tab. 7.1** reports the four different formulations used to produce orzo and coded with code 1, 2, 3, and 4. For the second cooking media, 0.1 % LAGG dispersion in distilled water (w/w) was used, with codes 5. RF_1LA_2 and 6. RFRP_1LA_2. Regardless of whether LAGG was added to the flour or the cooking water, its mass remains 1 % of the total dry mass. The ratio of the orzo-to-cooking medium was always 1:10 (w/w); therefore, the ratio of LAGG-to-water was always 0.1 % (w/w).

In formulation 3. RFRP, part of the RF, was substituted by an amount of rice protein concentrate to equal the protein content of the commercial orzo. The amount of protein reduced by removing part of the flour was compensated for by adding protein concentrate, as confirmed in **Section 7.3.1.**

Tab. 7.1. Formulation design of the experiment.

Sample code	Dry material mass ratio (RF:RP: LAGG)	RP g	RF %	LA %	Water %
1. RF (control)	100:0:0	--	63.0	--	37.0
2. RF_1LA_1	100:0:1 (dispersion)	--	62.5	0.6	36.9
3. RFRP	91:9:0	5.7	57.3	--	37.0
4. RFRP_1LA_1	91:9:1 (dispersion)	5.6	56.9	0.6	36.9
5. RF_1LA_2	Cooking 1. RF in 0.1 % LAGG (w/w) dispersion. Ratio RF-to-water 1:10 (w/w)				
6. RFRP_1LA_2	Cooking 4. RFRP in 0.1 % LAGG (w/w) dispersion. Ratio RF-to-water 1:10 (w/w)				

RF: rice flour; RP: rice protein; 1LA: 1% (w/w flour based) of low acyl gellan gum (LAGG). RF_1LA_1 and RFRP_1LA_1 means LAGG addition via dough-making and cooked in water; RF_1LA_2 and RFRP_1LA_2 means RF and RFRP sample cooked in the LAGG-water dispersion.

Fig. 7.1 outlines the orzo formation process; the cooking step (**Section 7.2.5**) is also shown. For dough preparation, 200 g of formulations that are reported in **Tab. 7.1** were mixed with 118g of heated (80°C) water or 1 % LAGG-water dispersion (w/w to total flour). The mixtures were kneaded with a stand mixer (KMX754ABK, Kenwood, Leicestershire, UK) for 10 mins to form a dough. The dough was then shaped into sheets of 2.0 ± 0.1 mm thickness with a pasta-making machine (Sailnovo, Dover, UK). The sheets were cut into a tagliatelle shape, then cut into orzo-shaped pieces with a length of 10.0 ± 0.1 mm and width 3.0 ± 0.1 mm. Subsequently, the fresh orzo (water content 37 %) was dried in an oven at 45°C for 4 h to reach 8 %, corresponding to the commercial products' water content. In this way, the final weight after cooking should reflect the differences in the water-holding capacity of the different orzo formulations.

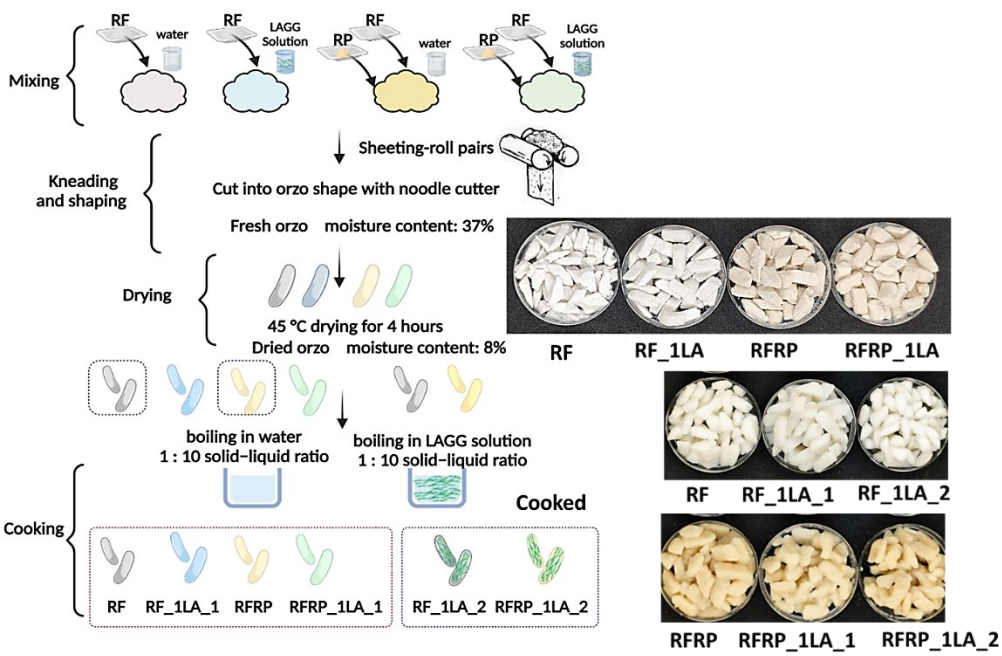


Fig. 7.1. Schematic of the orzo formation and cooking process

7.2.4 Pasting properties of orzo pasta

The pasting properties were examined using a RVA (RVA 4800, Perten Instruments, Sweden) under the method 61-02 approved by the American Association of Cereal Chemists (AACC, 2000). Powdered Orzo raw samples (particle size < 0.5 mm, 3.0 g, 8 % water content) from formulation 1 to 4 were mixed with distilled water (25 g) to prepare a dispersion with 9.55 % (w/w) total solids. Using the same method, orzo formulations 1 and 4 dissolved in a 0.1 % (w/w) LAGG dispersion instead of distilled water. To facilitate sample dispersion, the mixtures were stirred manually with a plastic spatula before loading into the RVA instrument. The system was further set to stir the sample at 960 rpm for 10 s and 160 rpm for the remainder of the test. The temperature profile consisted of equilibrating the samples at 50°C for 1 min 30 s, heating to 95°C at 12°C/ min (3 min 45 s), holding at 95°C for 2 min 30 s, cooling to 50°C at 12°C /min (3 min 45 s), and finally holding at 50°C for 1 min. All measurements were performed in triplicate. The pasting properties: peak temperature, peak viscosity (PV), breakdown viscosity (BD), final viscosity (FV) and setback viscosity (SB) were calculated from the pasting curve using the Thermocline software (version 3 Newport Scientific, Warriewood, Australia).

7.2.5 Orzo pasta cooking method and evaluation of cooking quality

The orzo pasta was cooked following the AACC-approved 66.50 guideline (AACC, 2000). An orzo from each formulation was cooked in boiling distilled water (1:10 w/v). Orzo formulations 1 (RF) and 3 (RFRP) were also cooked in 0.1 % (w/w) LAGG dispersions. In both cases, cooking practices were conducted in triplicates. For all samples, the optimal cooking time (OCT) was determined by the disappearance of the white core inside the orzo. To do so, individual orzo pieces were collected from cooking water at 30 s intervals, starting from cooking min 7, and squeezed between two microscope slides to visually determine the presence of the white core; the process continued until the disappearance of the white core, and the corresponding sampling time was defined as OCT.

The OCT-cooked pasta was drained, rinsed with 100 mL of distilled water at room temperature for 10 s, blotted with paper to remove surface water, and finally weighed. A portion of cooked orzo was immediately used to determine moisture content (measured using the standard AOAC method 934.01). The moisture content was calculated as the difference between the sample weight before and after drying (AOAC, 2005a). The cooking loss (CL) and rehydration (RH) using **Eq.7.1** and **Eq.7.2** as described by Garcia-Valle et al. (2021).

$$\mathbf{CL}\ (\%) = \frac{\mathbf{Weight\ of\ dry\ matter\ left\ in\ cooking\ water\ (g)}}{\mathbf{Weight\ of\ dry\ orzo\ (g)}} \times\ \mathbf{100}\ \%\ \textbf{(Eq. 7.1)}$$

$$\mathbf{RH}\ (\%) = \frac{\mathbf{Weight\ of\ cooked\ orzo\ (g) - Weight\ of\ uncooked\ orzo (g)}}{\mathbf{Weight\ of\ uncooked\ orzo\ (g)}} \times\ \mathbf{100}\%\ \textbf{(Eq.7.2)}$$

7.2.6 Proximate analysis of cooked orzo pasta

A portion of cooked orzo was then lyophilised, ground, and sifted into flour (particles < 500 µm) for chemical composition analysis. The crude protein content of cooked orzo was calculated from the nitrogen content according to AOAC 930.29, using a nitrogen-to-protein conversion factor of 5.95 (AOAC, 2005b). The total starch contents and the apparent amylase content in the ground samples were measured according to the official AOAC (2007) method 996.11 using a total starch assay kit (K-TSTA, Megazyme, Wicklow, Ireland). All analyses were performed in triplicate.

7.2.7 Structural properties of cooked orzo pasta

7.2.7.1 Infra-red (IR) characterisation

IR spectra patterns of cooked samples were analysed using a Bruker Tensor 27 FTIR spectrometer equipped with an attenuated total reflectance accessory (Graseby-Space Ltd, Orpington, UK), following the method reported by Garcia-Valle et al. (2021). The FTIR spectra were recorded in the wavenumber range of 4000 to 400 cm^{-1} 128 full spectrum scans were performed, each scan at 4 cm^{-1} spectral resolution against an empty (air) background reading at room temperature. Four spectra were recorded for each sample. The collected sample spectra were analysed after considering the background and normalizing frequency and scale with the OMNIC software (version 6.2; Thermos Electron Corporation) for the peak deconvolution process. The β-sheet (1615-1637 cm^{-1} and 1682-1700 cm^{-1}), random coil (1637-1645 cm^{-1}), α-helix (1646-1664 cm^{-1}) and β-turn (1665-1681 cm^{-1}) were estimated from the amide I region (1700 to 1600 cm^{-1}) according to previous studies (Ellepola et al., 2005; Ying et al., 2017; Fetouhi et al., 2019). The area corresponding to each secondary structure was calculated accordingly and expressed as a percentage of the sum of areas. Molecular organisations of starch were determined from the fingerprint region (wavenumber 1070 to 950 cm^{-1}); the absorbance intensity ratio of 1047/1022 (R1047/1022) and 995/1022 (R995/1022) was calculated to evaluate the short-range order of starch (Zhu et al., 2020). The water-bound state was assessed from the OH-vibration bonding regions between 3600 and 3100 cm_{-1} (Garcia-Valle et al., 2021).

7.2.7.2 XRD

The XRD patterns of rice samples were analysed using an Advance Bruker AXS powder-diffractometer (D8, Bruker AXS, Congleton, UK) with a Cu-Kα source (λ = 0.154 nm) running at 40 kV and 25 mA, following the setting described by Choi et al. (2022). A scanning cycle was conducted from 4° to 45° (2θ) with a step size of 0.02° at a speed of 2°/min. The relative crystallinity was quantified as the ratio of the crystalline area peak to the total diffraction peak analysed using the DIFFRAC plus EVA® software equipped with the XRD instrument.

7.2.7.3 Morphological properties of cooked orzo

7.2.7.3.1 Light microscopy

The morphological properties of the protein-starch matrices within cooked orzo were observed using an Eclipse Ci microscope (Nikon Instruments Inc., Surrey, UK) equipped with a Nikon digital Sight DS-Fi2 camera. Sample slides were prepared using a method adapted from Tamura et al. (2016). The cooked orzo samples were exposed to optimum cryo-microtomy embedding medium and cut into 60 μm thick-sections with a microtome (Leica CM 3050s, Leica Microsystems, Milton Keynes, UK). Cross-sections were mounted on gelatine-coated microscope slides, stained with 0.1 % fast green FCF acetic acid (1 %) solution for protein detection, washed with distilled water, and stained with Lugol's solution (62650, Sigma-Aldrich. 1:10 dilution) for starch detection. Due to electrostatic bonding between the amino acid side chains and the fast green molecules, protein bodies appeared with a green colour (Steglich et al., 2014). In comparison, starch appeared blue/purple due to the formation of an amylose/amylopectin-iodine complex. LAGG was covalently labelled with 5-(4,6-dichlorotriazinyl) amino fluorescein (DTAF) following the procedure described by Khin et al. (2021). The DTAF-LAGG was then applied as a native LAGG addition (via dough-making or cooking) to prepare cooked orzo. The actual phase distribution of LAGG in orzo matrices was visualized using an EVOS™ FL microscope. DTAF excitation and emission wavelengths are 488 nm and 517 nm, respectively.

7.2.7.3.2 ESEM

The surface and internal morphology of cooked orzo were measured with an ESEM (FEI Quanta 650 with X-Max-150 EDX Detector) equipped with a gaseous secondary electron detector using the method described by Dang & Copeland (2004). Working conditions were 10 kV accelerating voltage, 1 torr chamber pressure, and the initial working distance was 10 mm. Before imaging, the sample was fixed on conductive adhesive tape and was observed at a magnification of 1000x.

7.2.8 Texture properties of cooked orzo

The textural profiles of the cooked orzo were evaluated using a texture analyser (TA-XT2, Stable. Microsystem, Surrey, England) according to the method described by Boluda-Aguilar et al. (2013). Cooked orzo (2 g) was evenly arranged on the plate groove in a single layer. The orzo grains were compressed to 75% of their original thickness by two compression cycles conducted using a stainless-steel cylindrical probe with a diameter of 35 mm and a testing speed of 1 mm/s. From the TPA force-time curves, hardness, adhesiveness, cohesiveness, and chewiness were determined. Ten technical replicates (compression tests from the same batch of cooked orzo grains) per sample were performed, and the corresponding results were expressed as an average value.

7.2.9 Oral processing simulation and granulometry distribution analysis

Fine oral processing of cooked orzo was simulated based on established methods reported by Suo et al. (2021). Specifically, 25 g of cooked orzo was homogenised for 20 s using a household blender (HB605, Kenwood, Havant, UK). The subsequent in vitro digestion step followed the method described by Fernandes et al. (2020). After homogenisation, a 10 g aliquot of each sample was transferred into 50 mL conical tubes. To initiate oral digestion, 10 mL of simulated salivary fluid (SSF) containing salivary α-amylase (75 U/mL activity) was added to each sample. The mixture was incubated for 2 mins at 37°C with constant rotation at 50 rpm using a tube revolver (Thermo Scientific TM). After the incubation, 10 mL of 0.3 M Na2CO3 solution was added to halt the amylase activity. The granulometry distribution of the cooked orzo post in vitro oral processing was analysed using the method described by Ranawana et al. (2010). Digested samples were held in an incubation chamber at 37°C for 10 mins to allow sedimentation of residues. The samples were then filtered through a Buchner funnel. The separated solid particles were carefully removed from the filter paper and oven-dried at 70°C for 12 hours until the weight stabilised. The liquid filtrate was collected for starch digestion analysis.

Once dried and cooled to room temperature, the residue was weighed and fractionated using a Retsch AS 200 control sieve shakers (Verder Scientific,

Derbyshire, UK) with a vibration height of 0.5 mm for 1 min. Four test sieves (DEBUYER, France) were used, stacked in descending order of mesh size: 2.0 mm, 1.0 mm, 0.5 mm, and 0.25 mm, with a base pan underneath. The fractions from each sieve were carefully collected and weighed. The granulometry distribution was calculated using **Eq. 7.3**.

$$\sum R_n(\%) = \sum \frac{M_n}{\sum M_n} \times 100\ \% \quad \textbf{(Eq. 7.3)}$$

Where,

M_n is the mass (g) of the fraction retained on each sieve (M_1, M_2, M_3, M_4) and pan (M_p);

ΣM_n is the total mass (g) of grain fractions: $M_1 + M_2 + ... + M_p$;

ΣR_n is the cumulative per cent (%) of mass retained.

The weight loss caused by the particles entrapped within the meshes was negligible.

7.2.10 *In vitro* digestion and quantitative evaluation of protein and starch digestion

Two *in vitro* models, static and semi-dynamic, were used to study the digestion of homogenised samples.

7.2.10.1 Static digestion model

Orzo was subjected to static *in vitro* digestion with a method adapted from the INFOGEST protocol (Fernandes et al., 2020). A 5.0 g aliquot of homogenised sample underwent continuous oral, gastric, and intestinal digestion for 2 mins, 30 mins, and 180 mins, respectively. A 30-min incubation time, rather than the 120-min of the INFOGEST protocol, was used for the gastric phase, as previous works investigating starch digestion in grain material (Tamura et al., 2016; Wang et al., 2017) identified this as a more suitable time. The gastric 30-min incubation time corresponds to the interval between the first feed and the first blood sampling *in vivo* for the GI test (Ranawana et al., 2011).

Simulated intestinal fluid (SIF) was added to the chyme to the ratio of chyme-to-SIF 1:1 (v/v). The INFOGEST method suggests using trypsin (100 U/mL) or pancreatic α-amylase (200 U/mL) for starch-rich samples (starch isolates) to indicate the enzyme activity of pancreatin. In this study, pancreatin prepared in SIF was added to achieve a pancreatic α-amylase activity of 20 U/mL in the digestion mixture containing 40 mg/mL of starch, a comparable value to that in Edwards et al. (2019) (16 U/mL pancreatic α-amylase for 40 mg/mL of starch in the digestion mixture).

7.2.10.2 Semi-dynamic digestion model

For the semi-dynamic model, further details about the model and protocol are described in **Section 3.8.5**, **Chapter 3**. Compared to the static, the semi-dynamic digestion model provides a more comprehensive representation of humans. The *in vivo* digestion model includes 1) food-induced pH change in the gastric phase, 2) use of a peristaltic pump to mimic the physical breakdown in the digestive tract, and 3) viscosity changes monitored with a rheometer during digestion.

7.2.11 Quantification of digested protein and starch

From each sample, 2 x 5g aliquots were used to run two static *in vitro* digestion cycles (technical reps), whereas 2 x 100 g aliquots were used to run two semi-dynamic *in vitro* digestion cycles (technical reps). Two sets of hydrolysed starch for each aliquot were quantitatively evaluated in duplicate after collection at different time points. The concentration of maltose produced from starch amylolysis in aliquots recovered in various time intervals was determined using the p-hydroxybenzoic acid hydrazide (PAHBAH) assay described by Edwards et al.(2018).

According to Edwards et al. (2014), digestibility curves were analysed by applying the Logarithm of Slope (LoS) method and fitting the piecewise pesto-first-order enzyme kinetic model described in **Eq. 7.4**. to identify and quantify starch fractions with different nutritional values.

$$\mathbf{C_{(t)} = C_0 + (C_{\infty 1}) \times \left(1 - e^{-k_1 \times t}\right)} \\ \mathbf{+ if (t > t_{int,} (C_{\infty 2}) \times (1 - e^{-k_2 \times (t - t_{int})}, 0)} \quad \textbf{(Eq.7.4)}$$

Where:

t_{int} is defined as the time intersection of two distinct linear LoS plots.

C_{int} is the product concentration at t_{int} and is calculated by letting t = t_{int} using substituted values for $C_{1\infty}$ and k_1. Thus, it was added to the second term to describe the final product formation.

The hydrolysis index (HI) is the area under the digestibility curve up to 90 mins (AUC90) of the test sample expressed relative to a reference food ($AUC90_{reference}$), as shown in **Eq. 7.5**. In this case, white bread following the same *in vitro* digestion protocols were used as the reference food.

$$\mathbf{HI} = \frac{\mathbf{AUC90_{sample}}}{\mathbf{AUC90_{reference}}} \times \mathbf{100}\ \% \quad \textbf{(Eq. 7.5)}$$

The predicted glycaemic index (pGI) can, therefore, be determined from the HI using **Eq. 7.6**.

$$\mathbf{pGI} = \mathbf{39.71} + \mathbf{0.549HI} \quad \textbf{(Eq. 7.6)}$$

7.2.12 Statistical analysis

All results were calculated as means ± standard deviations of three replicates. Subsequently, Tukey's honestly significant difference test in conjunction with analysis of variance (ANOVA) was used to determine significant differences among the means, at an a priori significance level of $p < 0.05$, using the SPSS software (version 28, IBM, Armonk, NY, USA). In the granulometric measurement for cooked grain after homogenisation, the cumulative Gaussian statistic model was used to calculate the particle size distribution after passing the Shapiro-Wilk normality test using Prism (version 9, San Diego, CA) based on the reported method.

7.3 Results

7.3.1 Proximate composition and cooking quality of orzo pasta

The chemical composition of cooked GFO made from the six formulations described in **Section 7.2.3** is presented in **Tab. 7.2.** Significant differences in protein and total starch with and without the addition of RP were observed. The protein in the RFRP samples was comparable with that of commercial wheat orzo. Meanwhile, no

significant difference was seen in the RFRP sample with and without the addition of LAGG. The cooking properties were also evaluated (**Tab. 7.2**). OCT ranged from 6.5 to 7.2 mins, and no significant differences were detected between the orzo samples. The results agree with those reported for GF faba bean pasta and GF pasta enriched with rice bran protein. However, they are slightly higher than those reported for GF pasta enriched with animal protein (e.g., egg albumen, whey protein concentrate) (Rosa-Sibakov et al., 2016; Phongthai et al., 2017).

Furthermore, GFO had a shorter OCT than the commercial wheat orzo. Similar findings were reported previously (Phongthai et al., 2017), demonstrating that GF pasta requires less cooking time than commercial durum wheat pasta. This could be attributed to the absence of a compact structure provided by the gluten network, which allows water to enter the orzo more readily.

The RF control showed a CL of 10.97 %, which was considered low quality (Özyurt et al., 2015). All samples incorporated with RP and LAGG displayed lower CL, ranging between 6.90 and 8.53, indicating a higher capability of the orzo to resist structural disintegration. The rehydration values for RP-enriched orzo were significantly lower than those of the RF control but were comparable to those of the orzo reference. Similarly, Sofi et al. (2020) reported a decrease in rehydration after additional chickpea protein isolate was added to rice noodles, as did Detchewa et al. (2022) after adding RP to rice spaghetti. Low CL and rehydration could be due to the protein network entrapping the starch granules, limiting water intake, and swelling. Moreover, RP could affect the rehydration through its different water-holding capacity than starch. When pasta is made and cooked, RP undergoes a partial structural change from an ordered to a disordered/less flexible structure, resulting in more hydrophobic residues on the pasta surface and a low water-binding capacity (Jayaprakash et al., 2022).

As a result of adding LAGG during the pasta-making process, significantly higher rehydration values were observed in both RF_1LA_1 and RFRP_1LA_1. However, no observed changes were found when LAGG was added during cooking. A possible explanation is that LAGG chains undergo reversible random coil-helix transitions (via

intramolecular hydrogen bonds) during dough preparation. The helices assemble into clusters trapped within the protein-starch matrices via hydrophobic interactions that might occur between the methyl groups and Van der Waals interactions between the hemiacetal oxygen atoms on different molecules. The hydrophilic portion of the gel remains bound with water molecules throughout the cooking process, thus maintaining its hygroscopic properties (Bacelar et al., 2016; Tako et al., 2016).

In summary, RP and/or LAGG addition help to reduce CL and increase rehydration in GFO. The effect of LAGG on modifying the CL and rehydration was different when added to the dough or in the cooking water. As reported by Kraithong & Rawdkuen (2020) and Sofi et al. (2020), low CL and high rehydration have been positively correlated with increased firmness, sensory acceptability, and reduced pGI in rice noodles either prepared with hydrocolloids (such as guar gum and xanthan gum) or enriched with chickpea protein isolate.

Tab. 7.2. Proximate composition (g/100 g total weight) and cooking quality of GFO made with studied formulas. Here, commercial orzo is evaluated as a reference for protein content in the GFO formulation.

Sample code	Protein	Total starch	In which amylose	Moisture content	OCT (min)	CL (%)	Rehydration
RF	6.31 ± 0.24 ^{b}	32.15 ± 1.29 ^{a}	4.58 ± 0.15 ^{b}	59.03 ± 1.76 ^{a}	6.5 ± 0.5 ^{a}	10.97 ± 1.32 ^{a}	141.74 ± 7.45 ^{a}
RF_1LA_1	6.26 ± 0.36 ^{b}	30.72 ± 1.95 ^{a}	4.22 ± 0.22 ^{b}	61.48 ± 0.56 ^{a}	7.0 ± 0.5 ^{a}	8.53 ± 0.14 ^{ab}	240.03 ± 6.28 ^{b}
RF_1LA_2	6.30 ± 0.34 ^{b}	30.44 ± 0.96 ^{a}	4.18 ± 0.11 ^{b}	62.27 ± 0.56 ^{a}	6.6 ± 0.5 ^{a}	7.49 ± 0.18 ^{b}	144.10 ± 12.52 ^{a}
RFRP	13.54 ± 0.57 ^{a}	22.63 ± 0.57 ^{b}	3.23 ± 0.17 ^{c}	59.83 ± 3.83 ^{a}	6.8 ± 0.5 ^{a}	7.65 ± 0.40 ^{b}	102.35 ± 3.29 ^{c}
RFRP_1LA_1	13.15 ± 0.34 ^{a}	22.20 ± 2.64 ^{b}	3.05 ± 0.30 ^{c}	62.03 ± 1.54 ^{a}	7.0 ± 0.5 ^{a}	7.10 ± 0.20 ^{b}	174.05 ± 8.49 ^{d}
RFRP_1LA_2	13.19 ± 0.59 ^{a}	22.00 ± 0.88 ^{b}	3.02 ± 0.10 ^{c}	60.63 ± 2.66 ^{a}	7.2 ± 0.5 ^{a}	6.90 ± 0.80 ^{b}	134.89 ± 1.67 ^{a}
Orzo (commercial)	13.48 ± 0.34 ^{a}	21.57 ± 1.95 ^{c}	5.83 ± 0.43 ^{a}	58.14 ± 1.07 ^{a}	8.8 ± 0.5 ^{b}	7.70 ± 1.31 ^{b}	119.06 ± 7.47 ^{c}

Results are mean ± S.D. of three replicates. In each column, values with different letters indicate a significant difference ($p < 0.05$). RF - rice flour (control); RF_1LA_1 - RF with 1% LAGG in dough; RF_1LA_2 - RF with 1% LAGG in cooking water; RFRP – RF + rice protein (RP); RFRP_1LA_1 - RF + RP with 1% LAGG in dough; RFRP_1LA_2 - RF + RP with 1% LAGG in cooking water. For more details, see Section 7.2.3.

7.3.2 Pasting properties of rice-based formulations

The pasting curves for orzo made from four formulations and two LAGG addition methods were determined by RVA, as shown in **Fig. 7.2**. The pasting profiles are presented in **Tab. 7.3**. The RF control reached PV at 72.2°C in 6 mins, consistently with previous studies on RF (Zhu et al., 2018). Starch granules are suggested to reach their rupture point when a sufficiently large amount of swelling occurs along with destabilisation of the crystal structure and resulting breakage into smaller fractions. Under constant shearing at 95°C, further disruption of the granules occurred, which decreased the paste viscosity (i.e., BD). Amylose molecules leached into the solution, possibly aligning with each other. Upon cooling, retrogradation occurred as amylose molecules were reassociated, increasing the apparent viscosity (i.e., SB) (Balet et al., 2019).

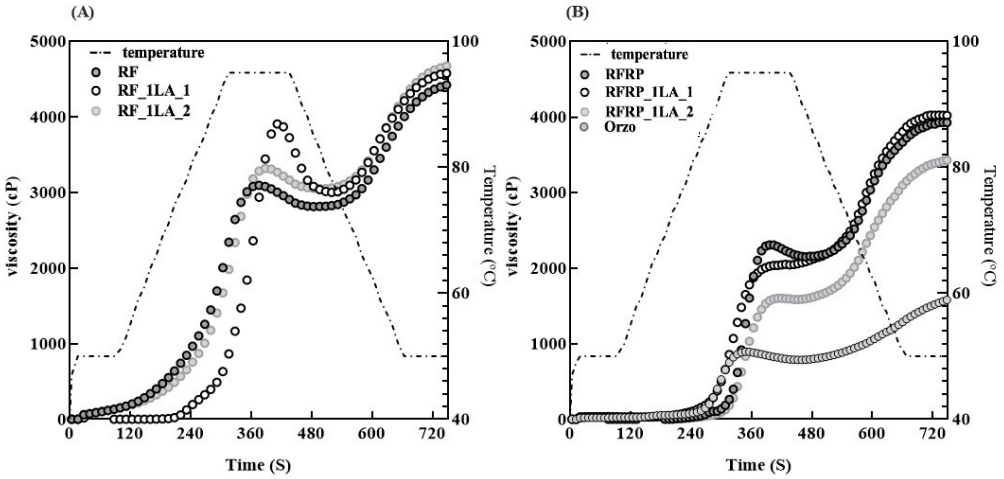


Fig. 7.2 Pasting profile (cP) of rice-based formulations incorporated with RP and LAGG as a function of time (s). Commercial orzo is also presented as a reference.

Tab. 7.3. Pasting properties of rice-based formulations incorporated with RP and LAGG through dough preparation (RF_1LA_1 and RFRP_1LA_1) and cooking (RF_1LA_2 and RFRP_1LA_2). The commercial orzo was also presented as a reference.

Sample code	PV (cP)	BD (cP)	FV (cP)	SB (cP)	Time (min)	P_T (°C)
RF	3094.7 ± 108.4 ^{b}	283.3 ± 24.3 ^{b}	4420.3 ± 98.1 ^{ab}	1325.7 ± 10.5 ^{c}	6.2 ± 0.2 ^{ab}	75.2 ± 1.0 ^{d}
RF_1LA_1	3918.3 ± 177.4 ^{a}	918.0 ± 50.8 ^{a}	4575.3 ± 235.9 ^{a}	657.0 ± 116.7 ^{d}	6.8 ± 0.1 ^{a}	82.0 ± 3.5 ^{c}
RF_1LA_2	3321.3 ± 280.9 ^{b}	275.7 ± 50.0 ^{b}	4672.3 ± 96.1 ^{a}	1350.7 ± 108.4 ^{c}	6.6 ± 0.1 ^{ab}	79.4 ± 6.3 ^{c}
RFRP	2308.3 ± 172.9 ^{c}	159.7 ± 27.4 ^{c}	3925.7 ± 111.4 ^{b}	1617.3 ± 64.7 ^{b}	6.6 ± 0.2 ^{ab}	91.1 ± 3.4 ^{ab}
RFRP_1LA_1	2048. ± 60.5 ^{c}	14.0 ± 4.0 ^{d}	4018.5 ± 63.5 ^{b}	1970.0 ± 53.5 ^{a}	6.8 ± 0.1 ^{a}	94.6 ± 0.1 ^{a}
RFRP_1LA_2	1604.0 ± 36.0 ^{d}	20.0 ± 5.5 ^{d}	3192.0 ± 15.8 ^{c}	1588.0 ± 51.0 ^{b}	6.9 ± 0.3 ^{a}	94.7 ± 0.3 ^{a}
Orzo (commercial)	895.7 ± 28.7 ^{e}	111.3 ± 14.4 ^{c}	1578.3 ± 57.6 ^{d}	682.7 ± 32.4 ^{d}	5.9 ± 0.2 ^{b}	93.1 ± 1.1 ^{a}

Results are mean ± SD of three replicates. In each column, values with different letters are significantly different from each other ($p < 0.05$). The pasting properties includes peak viscosity (PV), breakdown viscosity (BD), final viscosity (FV), setback viscosity (SB) and peak temperature (P_T).

As a result of adding LAGG, a delayed onset of gelatinisation was observed in RF_1LA_1 and RF_1LA_2, possibly because LAGG slows down water mobility and delays gelatinisation. A significantly higher PV BD but lower SB was observed in RF_1LA_1 compared with RF. As a result of phase separations and intermolecular interactions, rice starch, LAGG, and water were predicted to exhibit synergistic effects. Song et al. (2006) investigated the pasting properties of non-waxy rice starch and LAGG mixtures. It has been found that when the mixture was heated, the inner LAGG was also excluded from the system in addition to the starch granules gradually swelling. Due to the increased LAGG concentrations in the continuous phase, the hot paste became thicker and more viscous. Similar increases in PV and BD were reported by Cai et al. (2016) for glutinous RF hydrothermally treated (510 rpm, 90°C, 30 mins) along with 1 % xanthan gum. The interaction between xanthan gum and gelatinised starch granules could have resulted in the formation of a viscous gel mixture during the hydrothermal treatment, which could also occur during the pasta-making process, as investigated by Hu et al. (2019). The resulting mixture may display enhanced resistance to degradation, requiring longer heating and continuous shearing forces. A second contributing factor to the PV and FV increases observed in RF_1LA_1 compared to RF control (no LAGG) was LAGG interaction with solubilised/leached starch (primarily amylose) molecules. As demonstrated in waxy corn starch-LAGG mixtures, the gel networks surround swollen and disrupted starch granules, enhancing the viscosity (Rodríguez-Hernández et al., 2006). This can also explain the higher FV observed for RF_1LA_2 compared to the RF control.

RFRP achieved a lower PV at a higher PT than the RF control, which could be related to a lower swelling of starch granules and/or the reduced starch content. Comparable results have been reported for rice starch-modified RP blends (Wu et al., 2022) and protein-enriched RF (Wang et al., 2020). Apart from the starch substituted by RP, the protein network formed during processing could be a physical barrier to prevent starch from swelling. Under hydrothermal and homogenisation conditions, like dough-making and sheeting in this study, the water-holding capacity

could be enhanced, limiting the amount of water available for starch gelatinisation and reducing its swelling (Likitwattanasade & Hongsprabhas, 2010).

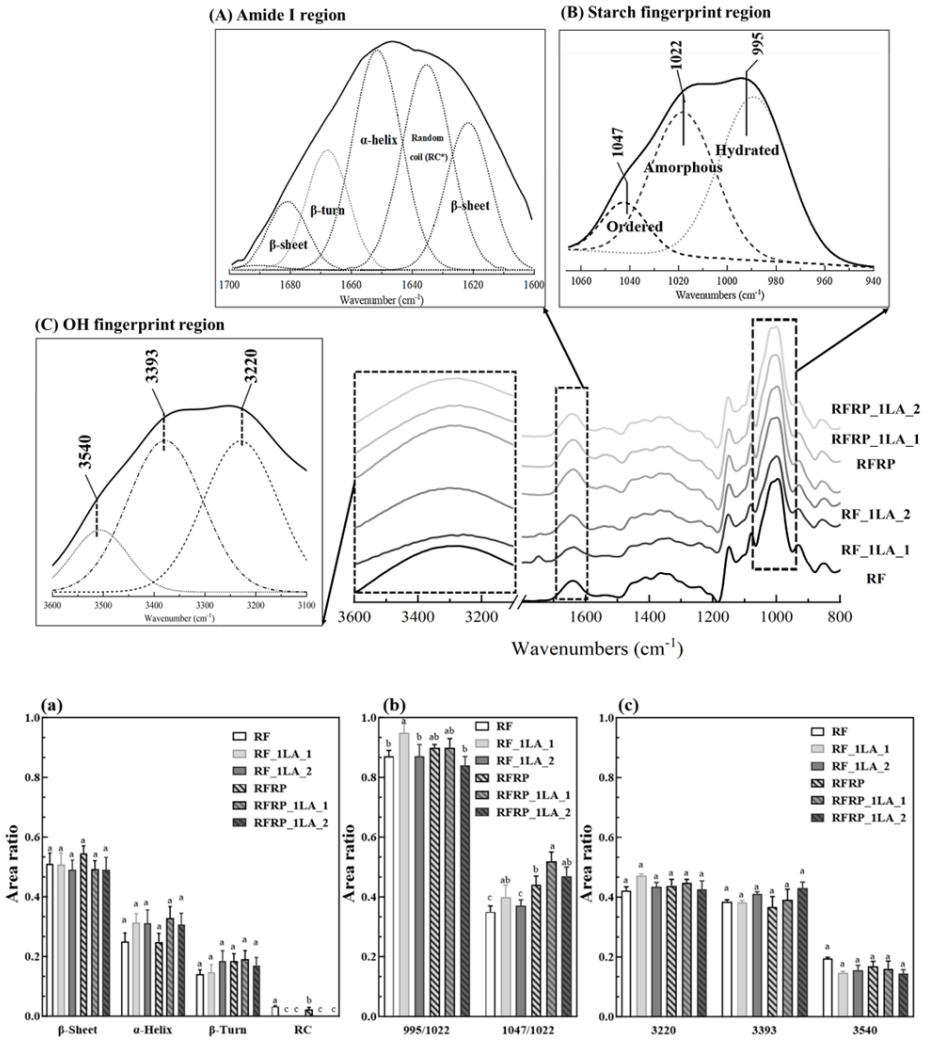
When RF was incorporated with RP and LAGG (RFRP-1LA-1), the pasting profile did not significantly differ from that of RPRF. When cooking with LAGG, however, RRFRP_1LA_2 exhibited a more flattened viscosity curve, as indicated by the lowest PV and FV. This could be attributed to the synergistic effect between the RP (internal) and LAGG (external) networks, which further impeded starch granule access to water (Guo et al., 2014; Almeida & Sato, 2019).

In the cooling process, the realignment of particles within the hot paste may cause an increase in viscosity, referred to as a "setback" viscosity (SB), which is calculated as the difference between PV and FV. A higher SB indicates that the disaggregated amylose and amylopectin molecules are more likely to re-crystallise (starch retrogradation) or associate with non-starch components, which has the potential to produce starch with reduced *in vitro* digestibility by increasing type-3 and/or type-5 resistant starch (Dupuis et al., 2014; Balet et al., 2019). The decrease in BD value observed in RF_1LA_1 suggested that LAGG could delay short-term retrogradation by adding it to the dough-making process. With RP-enrichment, a higher SB was observed than in RF control. Similarly, higher SB in a mixture of RP and rice starch (1:9 ratio) has been previously reported by Wu et al. (2022), which indicated that protein-starch interactions and network formation were more resistant to shear force upon cooling. It was possible that under constant shearing force, unfolded protein chains derived from denatured RP and leached amylose may result in a stronger and more ordered structure. The stronger gel mixture was also observed with further combination with LAGG (RFRP_1LA_1). No noticeable change was observed when adding LAGG during cooking.

Despite having comparable protein and starch contents, wheat orzo had a viscosity nearly 2.5 times lower than rice-based orzo, except for the BD, which was 1.4 times lower. This could be expected because of the differences in the protein structure, starch structure formations, and the resulting protein-starch matrices.

7.3.3 IR characterisation of structural differences in cooked orzo

As white rice is naturally low in lipid and fibre, a determinant of the quality of rice-based GFO is in the microstructure and interaction of proteins, starch, and moisture. The spatial distribution of these major components can be studied using FTIR microscopy. **Fig 7.3** shows the FTIR spectra of cooked GFO formulations produced in this study.



9

Fig. 7.3 The characteristic FTIR spectra patterns of cooked GFO made with rice-based formula incorporated with RP and LAGG (D). Example of numerical deconvolution of amide I (A) and variation of the ratios (a), starch fingerprint region (B) and variation of the ratios on R995/1022 and R1047/1022 (b), OH-stretching region (C) and variation of the ratios (c). Small letters marked on the columns in the same group (within the same horizontal axis symbols) indicated statistically significant differences ($p < 0.05$).

The characteristic spectrum regions for protein, starch and including amide I (1600 to 1700 cm^{-1}, **Fig. 7.3A**), starch fingerprint bands (940 to 1060 cm^{-1}, **Fig. 7.3B**), and OH-stretching (3200–3600 cm^{-1}, **Fig. 7.3C**) region for hydrogen bonding were evaluated to understand their roles in determining the microstructural characters of cooked GFO incorporated with RP and LAGG (Yang et al., 2017; Garcia-Valle et al., 2021).

An analysis of the amide I region of the FTIR spectrum can provide information regarding the secondary structure of proteins, which can inform their functionality and interaction with the textural properties of cooked GFO. From the fitting of the experimental data, four peaks could be identified from the numerical deconvolution of the amide I region. As illustrated in **Fig. 7.3A**, these peaks corresponded to β-sheets (1615-1637 and 1682-1700 cm^{-1}), random coils (1637-1645 cm^{-1}), α-helix (1637-1645 cm^{-1}) and β-turns (1665-1681 cm^{-1}), following the study of Wang et al. (2019). As shown in **Fig. 7.3a**, β-sheets were the largest component for cooked GFO (over 44 %), followed by α-helix (25-33 %) and β-turn (14-24 %). The content ratio of GFO made with RFPR showed higher β-sheets and lower β-Turn than the other samples, but the difference was insignificant. A difference in the β-sheet structure ratio is thought to be associated with dough viscoelasticity after hydration and textural characteristics after cooking. In a study by Jeong et al. (2017), a rice-based dough complex with zein (> 5 %, w/w) exhibited a 28 % increase in β-sheets intensity and could form long noodles. In contrast, pasta made from a chickpea-wheat blend (50:50) has been reported to have a lower β-sheet and higher β-turn ratio and exhibit less elastic, chewy, and harder (but not significantly) characteristics than wheat pasta after cooking (Garcia-Valle et al., 2021). As also supported by the results from the present study, RFRP exhibits a higher β-sheets ratio and higher cohesiveness and chewiness than the RF control. The RFRP was, however, noted to have low hardness, which was different from previous studies, which could be due to less fibre and the lack of gluten network compared to pea flour and wheat flour.
As illustrated (**Fig. 7.3B**)**,** the FTIR spectrum of starch reveals a complex sequence of intensive peaks (940-1060 cm^{-1}) mainly arising from coupled C-O and C-O-H

vibrational modes (Frederick et al., 2016). Several studies on starch, including wheat, corn and rice, have revealed that the bands at 1022 cm^{-1} appear to increase in amorphous samples, whereas the bands at 995 cm^{-1} (e.g., intramolecular hydrogen bonds formed between the hydroxyl groups) and 1047 cm^{-1} (e.g., formation of double helices) appear more clearly defined in crystallised samples (Ubeyitogullari et al. 2018; Cao et al. 2020; Zhang et al. 2023). As a result, the ratio of 995/1022 (R995/1022) and 1047/1022 (R1047/1022) was used to evaluate the alignment of helices and quantify the short-range order of starch structures. As shown in **Fig. 7.3b**, the R1047/1022 of the RFRP were significantly higher than the RF control, indicating a higher ratio of ordered to amorphous starch structure when RP is present at higher concentrations. The results were similar to those of enzymatically modified RF containing an increased protein content (8 % to 13 %) reported by Zhai et al. (2023). As suggested, RP possibly contributed to this by providing an encasing effect, inhibiting the gelatinisation of the starch granules, thereby remaining in a more starch ordered structure. This also corresponds to the results of this thesis, as a significantly lower PV and rehydration level was observed. It was shown in this study that the protein was forming a more stable/orderly secondary structure (e.g., higher in β-sheets), although the difference was insignificant.

Additionally, the interaction with unfolded protein chains could contribute to the recrystallisation of leached amylose by affecting water migration (Wu et al., 2023). It was also reflected in the higher SB viscosity and degree of crystallinity (reported in **Section 7.3.4**) shown in RFRP than in RF control. When the starch has more crystallised components, i.e., a more organised structure, the glucose hydroxyl groups form hydrogen bonds between themselves, whereas when the starch is more amorphous, there will be more hydrogen bonds between starch and water, which would explain the higher water-bonding capacity than the control. Comparably, other water-binding constituents within the food matrices, such as LAGG used in the current study, also showed an effect on starch retrogradation. For LAGG added via dough-making, higher R995/1022 of R1047/1022 were observed in

RFRP_1LA_1 than RFRP, and both became significantly higher in RF_1LA_1 than the RF control. The addition of LAGG via cooking did not differ in either case. The findings indicate that the LAGG addition in the formulation plays a key role in water mobility through hydrogen bonding and electrostatic interactions within the starch matrices.

For these reasons, the water state, which the OH-stretching groups can reflect, is important in GFO's texture and digestion behaviour in this study. Following Gaussian fitting analyses, it was found that a series of three overlapping OH-stretching bands that occurred from high frequencies to low frequencies peaks at 3540, 3393, and 3220 cm $^{-1}$ corresponded to water-water interactions (free water), and the interaction between water molecules and GFO constituents. It should be noted that if the OH peak position shifts to a lower wavenumber, it could be due to the hydrogen bonding weakening the OH bond strength, which results in a lower stretching frequency (Janardhnan & Sain, 2011; Lee et al., 2015). As shown in the **Fig. 7.3C**, lower-frequency components (peaking at 3220 and 3393 cm^{-1}) were dominant, with combined contents ranging from 78 % to 86 %, while free water (3540 cm^{-1}) contributed only to 13-18 % **Fig. 7.3c**). The results suggest that OH-stretching was linked to their protein-starch matrices via intra- and intermolecular bonds. Based on similar findings reported by Garcia-Valle et al. (2021), they suggested that water molecules within pasta exhibited strong and moderate linkage bonds with their surrounding environment. As recommended by the International Union of Pure and Applied Chemistry, the term "strong hydrogen bonds" results in the red shifting of the frequency (lower wavenumber) of infrared OH-stretching (Arunan et al., 2011). This study observed the deshielding of the proton for H in O–H, which may require further verification by nuclear magnetic resonance analysis. As shown in **Fig. 7.3C**, due to the substitution with RP and addition of LAGG, 3220 and 3393 cm-1 ratios were higher, while not significant compared with RF control. It has been reported that cooked chickpea pasta exhibits similar absorbance patterns to wheat pasta (Garcia-Valle et al., 2021). The same pattern was observed in sweet potato vermicelli containing white protein and hydrocolloids such as xanthan gum (Feng et al., 2020). These results suggested that higher protein and

hydrocolloid levels might facilitate the formation of more complex hydrogen bonds between water molecules and various pasta components.

7.3.4 XRD pattern of cooked orzo

The XRD patterns of GFO samples are presented (**Fig. 7.4**)**.** RF control displayed a V-type diffraction pattern with 13.2 and 20°(2θ) peaks. The findings were consistent with the previous results reported by Farooq et al. (2021) on cooked RF and Thuengtung et al. (2019) on cooked rice using two different methods (microwave and steaming). Both suggested that the interaction between starch and other components, like protein, could form helical inclusion complexes with amylose during heat-moisture treatment (cooking). As a result of LAGG addition, either via processing (RF_1LA_1) or cooking (RF_1LA_2), both resulting samples also exhibited V-type crystalline structures, indicating that LAGG did not alter starch crystallisation type. Comparable results were also reported by Huang et al. (2022) in rice noodles complexed with xanthan gum (0 and 2.5 %, flour-based), as well as by He et al. (2020) on rice starch-guar gum complexes with thermomechanical treatment. The crystallisation degree of RF_1LA_1 was higher than that of RF, while the degree of crystallinity (DOC) of RF_1LA_2 remained similar to the RF control (as shown in **Fig. 7.4)**. The difference possibly resulted from the stronger intrinsic LAGG-AM interaction than AM-AM, which prevented starch molecules from reorganising (retrogradation). Results in this chapter were consistent with the low setback values observed in **Section 7.3.2**. The DOC has also been observed to increase in starch mixtures containing an increased concentration (0-10 %) of guar gum, as reported by He et al. (2020).

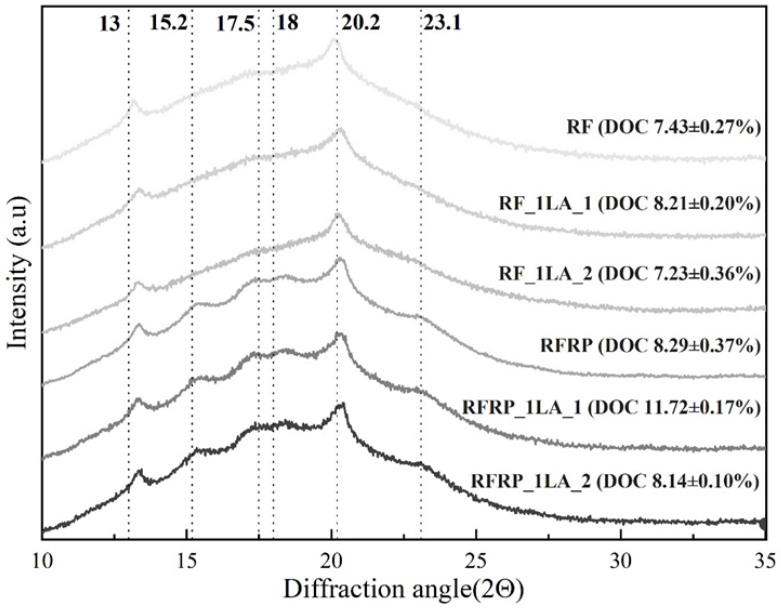


Fig. 7.4. XRD patterns for cooked GFO incorporated with RP and/or LAGG samples.

The GFO enriched with RP (RFRP) and its further combination with LAGG (RFRP_1LA_1 and RFRP_1LA_2) revealed hybrid A+V crystalline structures as demonstrated by the simultaneous appearance of both peak sets at 15°, 17°, 18°, and 23° (characterised as A-type), as well as at 13° and 20° (characterised as V-type). Neither LAGG addition method showed an apparent alteration in crystallinity. However, LAGG addition via dough-making resulted in a significantly higher DOC than the control (no LAGG) or addition via cooking. Rice starch typically has A-type crystalline structures, characterised by self-assembled debranched starches via crystallisation and parallel-stranded double helices arranged in monoclinic unit cells (Dome et al., 2020). Meanwhile, the V-type structure may vary depending on the structure of the guest (protein and/or LAGG) and its interactions with the host structure (starch).

7.3.5 Morphology of cooked orzo

The microscopic structure of cooked GFO samples is depicted in **Fig. 7.5**. In all samples, starch granules (coloured bluish-purple) were surrounded by a protein network (stained green). A gradual microstructural change from the pasta surface to its core was not evident, which differed from wheat pasta enriched with gluten, faba or egg protein reported by Laleg et al. (2016). As samples have been cooked to

their optional cooking time (as completely cooked without a white raw core appearance), the heterogeneous structure regions showed in wheat pasta, which can be distinguished by the degree of starch swelling decreasing towards the core, may be difficult to identify in GFO at this scale. The damaged protein networks were observed in the RF control, while a portion of the starch granule units were partially preserved (**Fig. 7.5A1**). There were notable increases in protein content in cooked GFO samples. Large RP aggregates (green) surrounded by starch (dark blue) were readily apparent.

As a result of adding LAGG during dough-making (RF_1LA_1, **Fig. 7.5A2**), the cellular units of the protein-starch matrices disintegrated and were replaced by a gel-like starch mixture surrounded by protein layers. A similar structure was also observed at the periphery region of RF orzo cooked in LAGG desperation (RF_1LA_2, **Fig. 7.5A3**). The RF_1LA_1 and RFRP_1LA_1 fluorescence micrograph further demonstrated that adding LAGG via dough-making promoted the formation of LAGG-derived networks exhibiting sponge-like ordered structures (**Fig. 7.5B2 and B5**). Upon cooking in a LAGG dispersion, the resultant orzo developed a hydrogel coating (**Fig. 7.5B3 and B6**). ESEM images showed that in the RF control (without LAGG), starch granules leached and adhered to the orzo surface while protein-starch matric units were still visible (**Fig. 7.5D1**).

Compared to the control sample, LAGG promoted a textured but intact structure on the surface of cooked GFO samples. An inner fibrous network structure was observed in the cross-section of RF_1LA_1, which showed a similar structure pattern as gluten-free pasta with xanthan gum, as demonstrated by Ertaş et al. (2022). The RFRP, on the other hand, presented a smooth surface with protein-starch matrices surrounded by flocculant masses, suggesting the formation of RP aggregates. Following cooking in LAGG dispersion, the RF_1LA_2 and RFRP_1LA_2 also showed similar smooth surfaces. The observed linear fabric strands adhering to the surface may represent a self-assembled hydrogel, similar to a structure reported in the LAGG hydrogel system for ocular medicine (Rupenthal et al., 2011). From the outer to the central region of these two GFO types, two distinct regions were observed

based on their textural differences, which may indicate the presence of hydrogel penetration and embedding to the GFO.

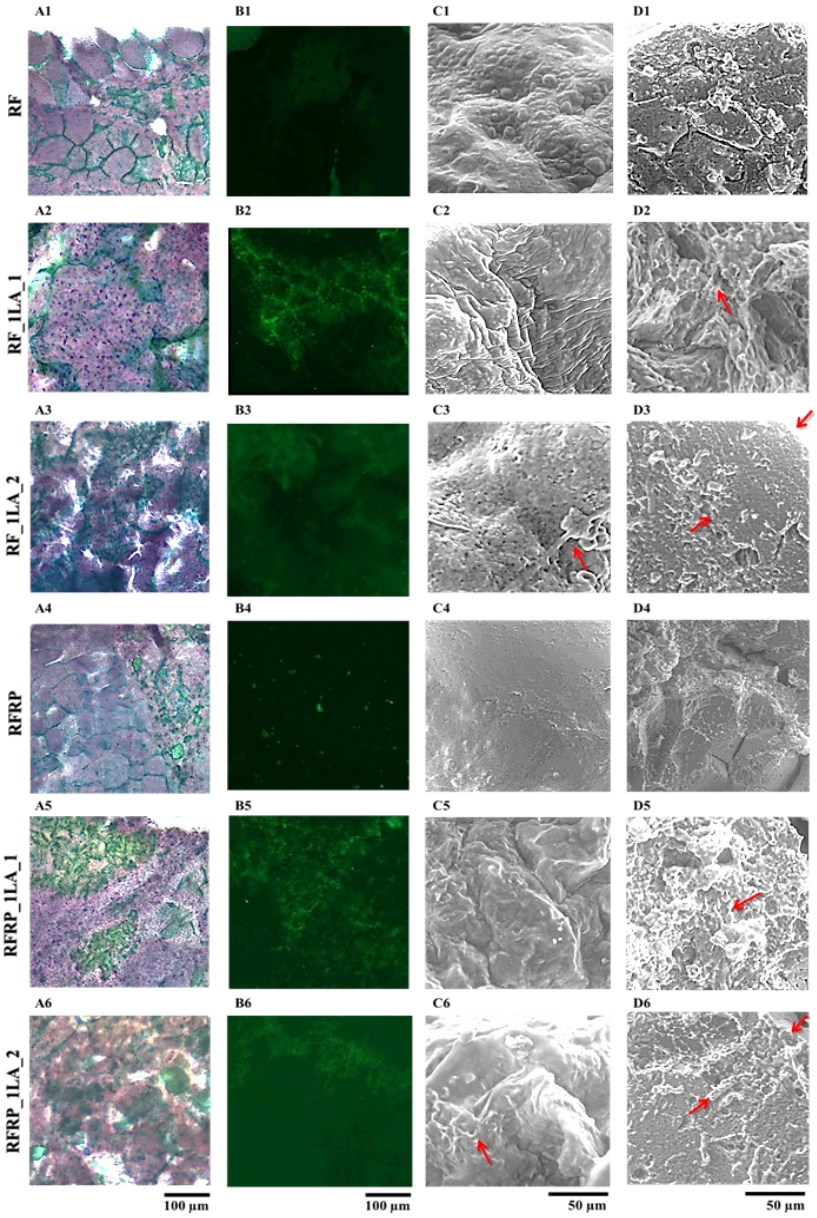


Fig. 7.5. Morphology of cooked GFO incorporated with RP and/or LAGG. Brightfield (A, cross-section), fluorescence (B, cross-section), and ESEM (C, surface; D, cross-section). Under brightfield micrographs show protein in green (stained with Fast Green) and starch in blue–purple (stained with 10 % Lugol's iodine solution); scale bars 100 μm. In fluorescence micrographs, 5DTAF labelled LAGG is shown in green; scale bars 100 μm. In ESEM, the fabric structure is observed (pointed by arrows); scale bars 50 μm.

7.3.6 Textural properties of cooked orzo

Besides being an important characteristic for consumers, the texture profiles (hardness, resilience, cohesiveness, springiness, chewiness, and adhesiveness) of cooked GFO also contribute to oral digestion. Texture results from this work are presented in **Fig. 7.6**. RP-enrichment (RFRP) displayed significant reductions in hardness ($p < 0.05$) but increased cohesiveness and chewiness ($p < 0.05$) than the RF control. No significant difference was found in adhesiveness and springiness ($p > 0.05$), indicating that RFRP has a softer and more extensible texture than RF control. These results agree with the work of previous results obtained with RP-enriched rice pasta, in which replacing RF with RP (0.0-7.5 %) resulted in a significant decrease in hardness while increasing adhesiveness, and similar pasting properties to those found in this thesis (Detchewa et al., 2022). As a result of RP-enrichment, RFRP showed a lower FV and a higher SB than the RF control. A rice noodle with comparable pasting properties had been reported to have a similar texture profile (Han et al., 2011). In this case, since proteins are integrated within the starch structure organisation, the resulting textural changes are more complex than they would be as single components. Due to this textural profile, particle size distributions in RFRP boluses collected *in vitro* for oral processing were not significantly different from those in the RF control, with $d(50)$ values of 0.68 ± 0.08 mm and 0.67 ± 0.04 mm for RFRP and RF, respectively (shown in **Fig. 7.7**).

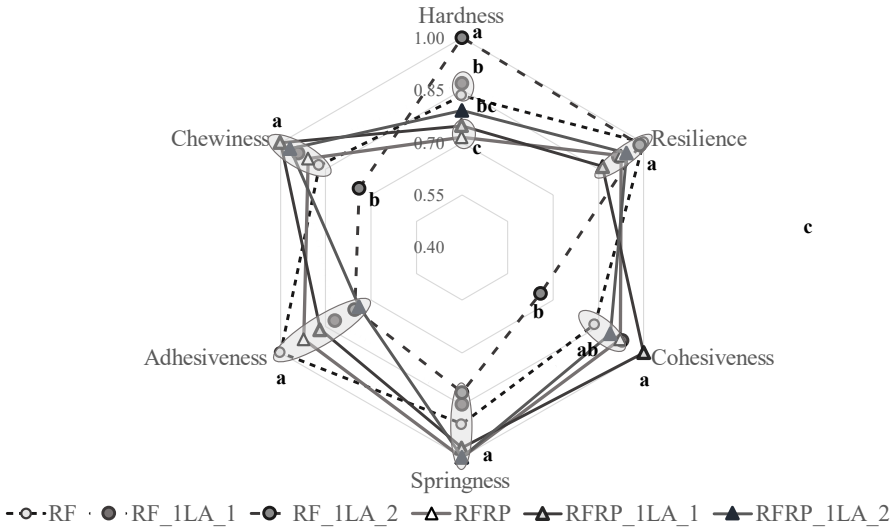
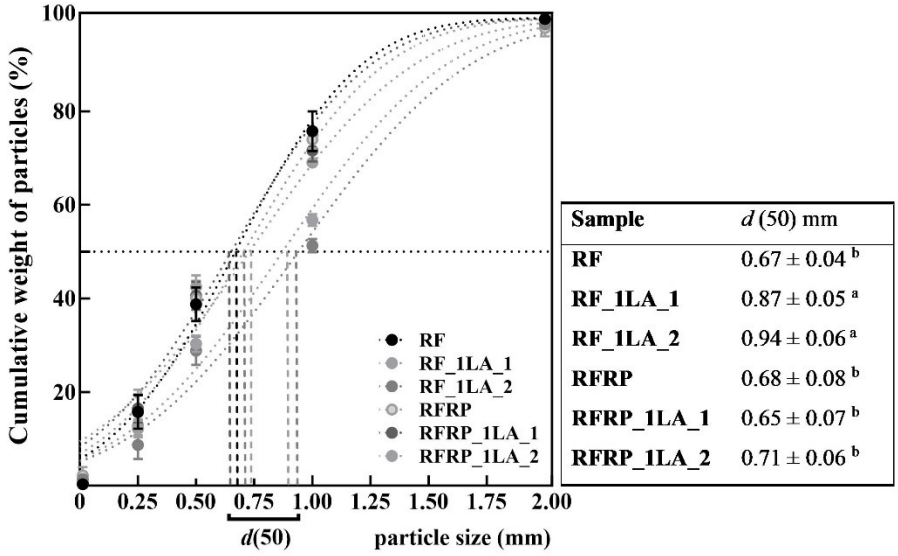


Fig. 7.6 Radar chart of the texture profiles of GFO made with rice-based formula incorporated with RP and LAGG. In the grey cycle, textural factors followed by a lower letter presented in the cycle are not significantly different ($p > 0.05$).



Sample	*d* (50) mm
RF	0.67 ± 0.04 [b]
RF_1LA_1	0.87 ± 0.05 [a]
RF_1LA_2	0.94 ± 0.06 [a]
RFRP	0.68 ± 0.08 [b]
RFRP_1LA_1	0.65 ± 0.07 [b]
RFRP_1LA_2	0.71 ± 0.06 [b]

Fig. 7.7 Particle size distribution curves of cooked rice-based GFO pasta obtained after 20 s homogenisation (*in vitro* oral process simulation). The curves are presented as the mean cumulative weight of particles passing through each sieve (n = 4). Boluses containing particles larger than the greater sieve aperture did not achieve 100 % cumulative weight. The median size *d*(50) was obtained by graphical projection for each curve. The shift towards larger particles in the RF control with the addition of LAGG was accompanied by a higher *d*(50) value. This was not observed in the RP-enriched sample.

Selected characteristics of the cooked GFO were found to change due to the LAGG addition. Increased hardness was observed in cooked RF and RFRP with added LAGG, and the increase became significant when LAGG was added during cooking.

As a result of LAGG addition (both methods), the adhesiveness, resilience, and springiness decreased slightly, but the differences in these values were not significant (p > 0.05) compared with RF and RFRP controls (without LAGG). Comparable results have been reported by Huang et al. (2022) on cooked rice noodles formulated with xanthan gum and by Hanet al. (2011) on rice starch noodles with gellan gum, both of which increased hardness but reduced adhesiveness when the hydrocolloids were added. Several factors may have contributed to textural differences. These include the intramolecular interactions between the LAGG helix chains themselves, providing LAGG with a brittle structure, and intermolecular interactions with proteins and/or starch, which would have increased the complexity of cooked GFO microstructure, along with its overall structural rigidity. Therefore, different methods of adding LAGG to cooked GFO were expected to result in different textural characteristics. As shown in **Fig. 7.6**, RF_1LA_1 and RFRP_1LA_1 (addition via dough-making) showed higher cohesiveness and chewiness than the RF and RFRP controls. However, these differences were not statistically significant (p > 0.05), apart from the RF_1LA_2 (addition via cooking), which displayed significantly lower adhesiveness and chewiness (p < 0.05). This result suggested that adding LAGG during dough preparation might facilitate the restructuring of the protein-starch and hydrocolloid in the matrices during cooking, resulting in a structured GFO with a stronger or more interconnected microstructure and a more cohesive texture. A similar result has been observed with xanthan-formulated rice noodles (Huang et al., 2022). As a result of the cooking with LAGG, the results in this current study revealed that the hydrogel coating the periphery of GFO (observed in DTAF-labelled LAGG in **Fig. 7.5B3 and B6**) provided a binding effect to the leached amylose by hydrocolloids (significantly lower in the CL compared to the RF control), resulting in a rigid surface layer. In this manner, the GFO hardness increased (in response, its hardness increased in the first compression cycle), whereas no significant changes were observed in the RF_1LA_2 in the following compression (in response as no significant difference in cohesiveness and chewiness compared to RF and RFRP, respectively). After oral processing simulation, the LAGG-

incorporated GFO bolus consisted of a higher proportion of larger particles (50 % > 0.94 mm) than the RF control bolus (shown in **Fig. 7.7**)

7.3.7 *In vitro* digestion (static model)

After *in vitro* digestion, the starch digestibility of cooked GFO was evaluated by measuring the amount of reducing sugar (primarily maltose) released from the starch hydrolysis into the liquid phase of the bolus (after oral processing), chyme (after gastric phase) and digested mass during intestinal phase (at each digestion time point).The amount of digested starch in the gastric phase was higher than in the oral phase for all samples, except for RF and RF_LA_1 (not statistically different) (Shown in **Fig. 7.8**).

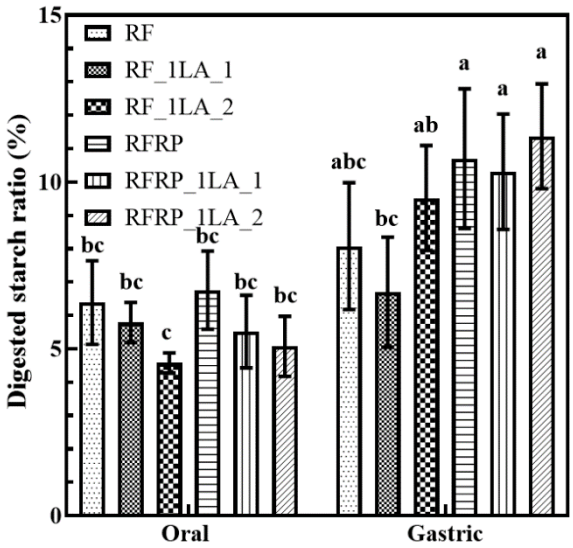


Fig. 7.8. Oral and gastric starch digestibility of cooked orzo evaluated after 20 s homogenisation. Digestibility was expressed as % (w/w) of digested starch (maltose in the liquid phase) of the bolus before and after gastric digestion.

Regarding the intestinal phase **(Fig. 7.9**), it was observed that starch hydrolysis began to increase rapidly after 30 mins and then gradually increased at a slow and steady rate for 180 mins. The RP-enrichment and/or addition of LAGG (via dough-making or addition in cooking water) slowed down starch digestion, resulting in 2.5-14.5 % less digested starch at the end of the experiment period compared to the RF control (shown in **Fig.7.9**). The results were consistent with micro-extruded rice starch prepared with guar gum, as reported by He et al. (2020). The deceleration

effect of LAGG addition in starch digestion of RFRP samples was not clearly observed in the digestion period. Also, adding LAGG via dough-making slowed down the process more than adding LAGG through cooking, although the difference was insignificant (**Tab. 7.4**).

The digestion change as a function of time can be quantitatively described by certain key parameters following the application of piecewise first-order kinetic models established by Goñi et al. (1997) and further developed by other researchers (Patel et al., 2014; Edwards et al. 2018; Li and Hu, 2020; Yu et al., 2021; Butterworth et al., 2022). These factors include time identifiers, which indicate the time intervals for each consecutive reaction. An example in this study is the intersection of the different phases shown in the LoS plot, representing the point at which the rapid phase is about to reach a plateau, and the slower phase begins to emerge; digestion rate coefficients (k_1 and k_2); and estimated starch digested percentages ($C_{\infty 1}$and $C_{\infty 2}$), which is the estimated concentration of each digestion phase. As shown in **Tab. 7.4**, the model applied agrees with the experimental data, as indicated by R^2 over 0.99. All samples showed a two-phase digestion pattern. For example, the RF control samples digested rapidly in the first 20 mins and reached equilibrium with over 50 % of the starch digested as expected ($C_{\infty 1}$+ C_0). Afterwards, digestion slowed down, with a ten times lower rate constant (k_2) than k_1. It fits the concept of rapid starch digestion. Both methods of adding LAGG to RF samples significantly reduced the k_1 values in the rapid phase of the experiment. Meanwhile, $C_{\infty 1}$ showed a reduction in estimated concentrations to 30 % digested starch, indicating that LAGG mediated starch digestion rate and a reduction in RDS concentration. The mediating effect appeared to diminish in the later slow phase, as their k_2 became higher than that of RF control, although the difference was insignificant ($p < 0.05$).

The RP-enriched GFO showed a small but significant increase in C_0 compared to the RF control. It is possible that the smaller particle size following oral fragmentation, coupled with a reduced amount of entrapment due to the protein network's hydrolysation in the gastric phase, may lead to greater exposure of starch granules to pancreatic amylase attack. As the rapid phase progressed, a decrease in k_1 from

0.087 to 0.046 min^{-1} was observed in RFRP, resulting in a decreased $C_{\infty 1}$ after 20 mins digestion. The digestion subsequently slowed down with a slightly lower k_2 than the RF control, leading to a lower, but not significant, final concentration of digested starch. A similar reduction in digestion rate and extent has been reported in wheat protein hydrolysates (pepsin hydrolysis for 30 mins as used in this study)-rice starch complexes under co-gelatinisation, reduced starch digestibility also shown in hydrothermally treated rice starch-rice peptide (pepsin hydrolysis for 120 mins) mixtures (Lu et al., 2022, 2023).

There are several possible explanations for this phenomenon: 1) the amino acid sequences with different molecular weights (< 10 kDa) of hydrolysed RP peptide chains entangled with hydrolysed starch chains, sterically hindering enzyme contact; 2) peptides derived from digested RP are likely to form complexes with starch at neutral pH, inhibiting starch hydrolysis; 3) the remaining hybrid A+V-type protein-starch complexes with a higher crystallinity hinder the enzymatic degradation of starch.

Further addition of LAGG to RPRF reduced starch digestibility at a similar level to the RFRP control with no significant differences amongst the three pGI values (as shown in **Tab. 7.4**). The RF control had a pGI of 78, considered a high-GI food (GI over 70 *in vivo*, over 75 *in vitro*) (Truong et al., 2014; Chi et al., 2019). The pGI of RF with LAGG addition was lower at an intermediate GI level (below 70). LAGG addition via dough-making displayed the lowest PGI (67) but did not differ significantly from LAGG addition via cooking. Although RFRP and LAGG additions observed lower pGI than RF control, they were considered high-GI (GI > 70) foods according to *in vivo* categorisation. Notably, the methods used in this study yielded an effective reduction of pGI, demonstrating the potential of these methods to modulate the digestibility of starch and the development of low pGI rice-based GF pasta.

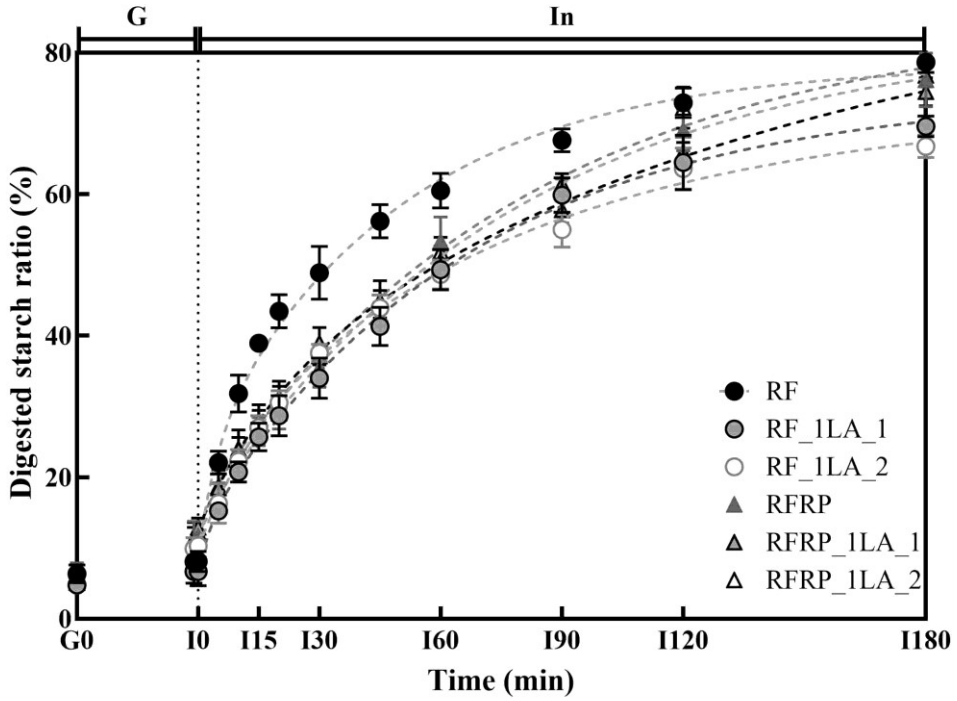


Fig. 7.9 *In vitro* digestion curves (the concentration of digested starch over time) obtained for cooked rice-based GFO incorporated with RP and LAGG (via dough-making or cooking). Data points are mean values with error bars as S.D. (n = 4).

Tab. 7.4. Kinetic models for *in vitro* digestion (static model) of cooked orzo incorporated with RP and LAGG under oral processing simulations (20s homogenisation).

Sample code	C_0 (%)	k_1 (min^{-1})	$C_{\infty 1}$ (%)	t_{int} (min)	k_2 (min^{-1})	$C_{\infty 2}$ (%)	C_{total} (%)	C_{180} (%)	pGI	R^2
RF	8.1 ± 2.4 ^{bc}	0.087 ± 0.004^{a}	42.5 ± 1.5 ^{a}	20.0 ± 1.5 ^{a}	0.015 ± 0.001 ^{ab}	44.2 ± 1.0 ^{b}	94.9 ± 2.9 ^{ab}	78.7 ± 1.5 ^{a}	78.4 ± 3.5 ^{a}	0.9998
RF_1LA_1	6.7 ± 1.1 ^{c}	0.043 ± 0.002 ^{b}	30.9 ± 1.8 ^{bc}	23.0 ± 2.4 ^{a}	0.017 ± 0.001 ^{a}	47.9 ± 4.2 ^{b}	88.5 ± 4.9 ^{b}	69.1 ± 1.3 ^{b}	67.7 ± 2.2 ^{b}	0.9971
RF_1LA_2	6.3 ± 1.3 ^{c}	0.049 ± 0.003 ^{b}	34.7 ± 1.5 ^{b}	20.0 ± 2.8 ^{a}	0.017 ± 0.001 ^{a}	43.6 ± 1.3 ^{b}	88.7 ± 1.4 ^{b}	69.8 ± 3.0 ^{b}	68.9 ± 3.4 ^{b}	0.9978
RFRP	11.7 ± 0.5 ^{ab}	0.046 ± 0.005^{b}	28.6 ± 3.4 ^{c}	20.0 ± 1.0 ^{a}	0.013 ± 0.002 ^{b}	58.5 ± 1.7 ^{a}	98.8 ± 1.5 ^{a}	76.2 ± 1.0 ^{a}	71.8 ± 1.7 ^{ab}	0.9981
RFRP_1LA_1	12.9 ± 1.4 ^{a}	0.045 ± 0.002 ^{b}	32.5 ± 2.2 ^{bc}	20.0 ± 0.7 ^{a}	0.014 ± 0.001 ^{ab}	45.7 ± 0.5 ^{b}	91.2 ± 1.4 ^{b}	72.5 ± 2.8 ^{ab}	70.0 ± 3.0 ^{b}	0.9991
RFRP_1LA_2	12.2 ± 1.0 ^{a}	0.051 ± 0.002 ^{b}	27.2 ± 2.2 ^{c}	20.0 ± 1.0 ^{a}	0.015 ± 0.001 ^{ab}	54.8 ± 2.2 ^{a}	94.3 ± 1.9 ^{ab}	76.8 ± 3.2 ^{a}	71.1 ± 2.9 ^{ab}	0.9879

Mean ± SD calculated from triplicate measurements. For each parameter (named in the first row), the different superscript letters indicate values among the 6 samples are statistically different ($p < 0.05$). Values presented here are: the concentration of digested starch (C_0, %) at the beginning of intestinal digestion phase; starch digestion rate constants of rapid (k_1) and slow phase (k_2), corresponding estimated percentage of digested starch ($C_{\infty 1}$ and $C_{\infty 2}$, %), t_{int} is defined as the time intersection of two distinct digestion phase. The percentage of digested starch at the end of experiment predicted (C_{total}, %) and practical (C_{180}, %), predicted glycemic index (pGI), and the goodness of curve-fitting (reflected by R^2). 0 s, 10 s, 20 s refer to different homogenisation time

7.3.8 *In vitro* digestion (semi-dynamic model)

With the change in pH (from 3 to 5) and mechanical stresses and fluid flows provided by the peristaltic pumps, detailed simulations of the digestive tract were developed to assess the reproducibility of results obtained from a static model and to gather comprehensive information on digestion behaviour, such as digesta viscosity. The real-time viscosity of the solution was monitored, as well as its digestibility, to evaluate viscosity changes while starch digestion occurred. **Fig. 7.10** illustrates the evolution of the apparent viscosity and starch digestibility of the bolus in the gastric phase and the chyme in the intestinal phase during *in vitro* digestion of cooked GFO incorporated with RP and/or LAGG.

With 30 mins of gastric digestion, the RF control demonstrated low mean viscosity values, gradually reducing from 978 to 820 cP. Similar trends were observed in the samples (RF and RFRP) when LAGG was added via cooking. The gastric viscosity of samples (RF and RFRP) incorporated with LAGG remained fairly stable. The viscosity stability may be attributed to the hydrolysis of protein networks by pepsin. Homogenised orzo with smaller particles facilitates dispersion in liquid. As a result of gastric movements and the environment (acidity and enzyme activity), particle size is further reduced, and pepsin facilitates the release of peptides and entrapped starch granules from the food matrices, maintaining the viscosity level of the dispersion (Villemejane et al., 2015). Viscosity stability could also be explained by reinforcing the cross-links in the inner hydrocolloid chains resulting from acid exposure (Bradbeer et al., 2014).

In the intestinal phase, RP-enrichment appears to contribute to the increase in orzo digesta viscosity, but the increase is not significant, with viscosities up to 530 ±164 compared to RF control as 377 ± 161 (shown in **Fig. 7.10A1 and B1**). For the same method of adding LAGG via cooking, RFRP_1LA_2 also displayed a higher viscosity than RF_1LA_2 (**Fig. 7.10A3 and B3**). It suggests that protein enrichment has a facilitating effect on viscosity development. Adding LAGG via dough-making also impacted the viscosity of digesta in the intestinal phase. Regardless of the RP-enrichment, digesta viscosity was higher for RF_1LA_1 and RFRP_1LA_1 than for the

control and adding LAGG via cooking. The results are consistent with the theory that LAGGs are not degraded in intestinal phases and keep their viscosifying properties and interpenetrating network structure (Bradbeer et al., 2014; Xu et al., 2023).

Further fitting parameters for digestion plots of all samples using the piecewise first-order kinetic model were presented in **Tab. 7.5**. The R^2 value of 0.99 indicates that the model fits well into the digestion curve. As observed in the static model, the sample digested in the semi-dynamic model also showed multiple digestion phases (rapid to slow) and approximately 50 % of starch was digested at the end of the rapid phase, which suggests that the amount of rapidly digestible starch is largely determined by the food characteristics rather than digestion process.

Unlike the static model results, a significant increase was observed in the C0 of the RF control as an example, and it reached its first equilibrium at a faster rate (k_1 = 0.099 for DDM > 0.087 for static) within 20 mins. As in the static model, the RF with LAGG addition demonstrated similar retarding effects on starch digestion both during dough-making and during cooking, although both k_1 was significantly increased.

Interestingly, the trend of $C_{\infty 1}$ and k_1 did not fully coincide with one another. This means the k value of RF_1LA_2 was lower than those of RF control and RF_1LA_1, but the former had a much higher $C_{\infty 1}$ than those of the latter two. Comparable results have been reported previously and indicate that the initial starch digestion (here in the case of C_o) is determined more by the starch hierarchical structure, while $C_{\infty 1}$ is further influenced by other factors, such as enzyme activity (Chi et al., 2019). Hence, the k_1 and $C_{\infty 1}$ changes for starch-LAGG formulations reflect the synergistic effects of starch gel structure and LAGG inhibitory activity against α-amylase.

Under the semi-dynamic model, the k_1 values were significantly decreased with RP-enrichment and LAGG addition (via dough-making and cooking) compared to the RF control, and the first equilibrium took a longer time to reach, which indicated their mitigation effect was more on digestion rate than extent with a slightly elevated k_2, the final digestion extent reached similar levels to the RF control, ranging between 82.0 ± 1.5 and 76.3 ± 0.9.

It is also important to note that RFRP_1LA_1 showed the lowest k_1 and k_2 values and the lowest digested starch content (72.0±2.8) at the end of the digestion period. As a result of the complex nature of the semi-dynamic digestion model, the formulation of rice-based GF pasta consisting of RF incorporated with RP and LAGG demonstrated more promising results in retarding starch digestion, suggesting that further exploration of relative food production development with reduced GI.

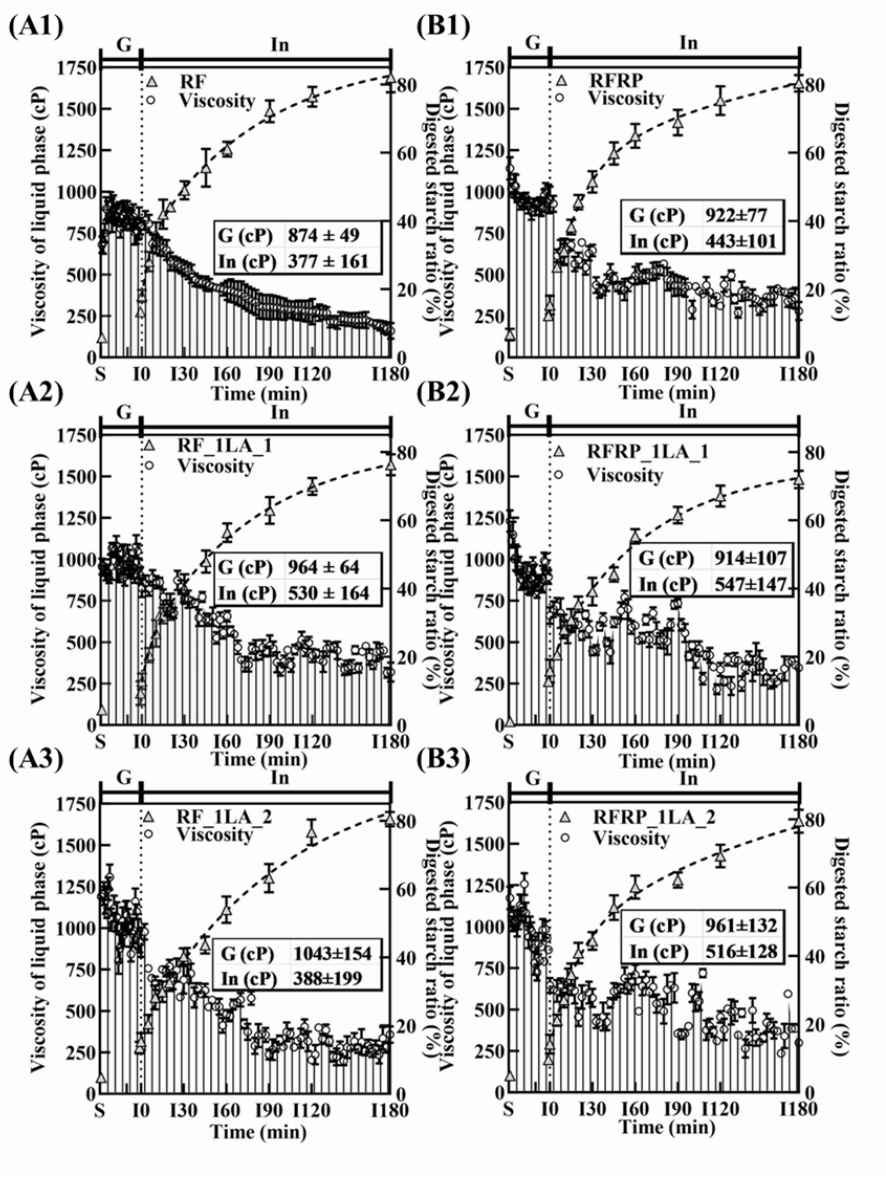


Fig. 7.10 Evolution of the digesta viscosity and *in vitro* starch digestion versus time in the gastric and intestinal phase. A1-3 showed RF and/or with LAGG addition via dough-making RF_1LA_1 and via cooking RF_1LA_2; B1-3 showed RP-enriched RF and/or with LAGG addition via dough-making RFRP_1LA_1 and via cooking RFRP_1LA_2.

Tab. 7.5. Kinetic models for *in vitro* digestion (semi-dynamic digestion model) of cooked orzo incorporated with RP and LAGG under oral processing simulations (20s homogenisation).

Sample code	C_0 (%)	k_1 (min $^{-1}$)	$C_{1\infty}$ (%)	t_{int} (min)	k_2 (min $^{-1}$)	$C_{2\infty}$ (%)	C_{total} (%)	C_{180} (%)	pGI	R^2
RF	18.0±0.8 ^{a}	0.099±0.006^{a}	30.7±1.5^{a}	16.8±2.0 ^{a}	0.014±0.002 ^{a}	36.3±1.1 ^{c}	85.0±1.4 ^{c}	82.0±1.5 ^{a}	78.5±2.8 ^{a}	0.9978
RF_1LA_1	12.8±0.5 ^{c}	0.069±0.003 ^{b}	29.3±3.1^{a}	17.8±1.2^{a}	0.013±0.001 ^{a}	49.2±3.8 ^{a}	91.3±1.0 ^{b}	76.3±0.9 ^{ab}	72.6±1.2 ^{ab}	0.9984
RF_1LA_2	15.3±0.5 ^{bc}	0.052±0.001^{cd}	34.3±2.3 ^{a}	20.0±2.0 ^{a}	0.014±0.001 ^{a}	47.6±1.6 ^{a}	97.2±3.2 ^{a}	80.5±3.0 ^{a}	73.4±1.0 ^{ab}	0.9986
RFRP	15.3±1.9 ^{bc}	0.058±0.002 ^{c}	30.5±3.6 ^{a}	18.5±2.0 ^{a}	0.016±0.001 ^{a}	44.4±3.2 ^{ab}	96.5±2.4 ^{ab}	80.3±1.0 ^{a}	77.6±3.2 ^{ab}	0.9985
RFRP_1LA_1	15.8±0.6 ^{ab}	0.045±0.004 ^{d}	30.8±1.4 ^{a}	19.2±2.0 ^{a}	0.013±0.002 ^{a}	37.7±1.4 ^{bc}	84.3±2.6 ^{c}	72.0±2.8 ^{b}	70.5±1.5 ^{b}	0.9981
RFRP_1LA_2	14.9±0.7 ^{bc}	0.050±0.003 ^{cd}	33.9±4.0 ^{a}	18.0±2.4 ^{a}	0.015±0.002^{a}	49.7±4.2 ^{a}	98.5±2.4 ^{a}	79.4±2.3 ^{a}	74.0±4.3 ^{ab}	0.9983

Mean ± SD calculated from triplicate measurements. For each parameter (named in the first row), the different superscript letters indicate values among the 6 samples are statistically different ($p < 0.05$). Values presented here are: the concentration of digested starch (C_0, %) at the beginning of intestinal digestion phase; starch digestion rate constants of rapid (k_1) and slow phase (k_2), corresponding estimated percentage of digested starch ($C_{\infty 1}$ and $C_{\infty 2}$, %), t_{int} is defined as the time intersection of two distinct digestion phase. The percentage of digested starch at the end of experiment predicted (C_{total}, %) and practical (C_{180}, %), predicted glycemic index (pGI), and the goodness of curve-fitting (reflected by R^2). 0 s, 10 s, 20 s refer to different homogenisation time.

7.4 Conclusion

In this study, rice-based gluten-free orzo (GFO) pasta was produced with formulations enriched with rice protein (RP) and/or low acyl gellan gum (LAGG) to improve cooking quality and reduce starch digestibility.

The results showed that RP and/or LAGG addition to GFO pasta formulations reduced CL and pGI. The GFO formulation with LAGG showed greater ordering, crystallinity, and homogeneity of structure, larger bolus sizes and the lowest starch digestibility among all the formulations under static *in vitro* digestion conditions. Under semi-dynamic digestion conditions, characterised by a pH increase from 3 to 5 in the gastric phase and simulated peristaltic movements (both not produced in the static digestion model), GFO incorporated with both RP and LAGG exhibited the lowest starch digestibility and pGI, which the high ordering structure and viscosity of the intestinal phase could explain.

The results presented in this study may contribute to developing new formulations of gluten-free pasta with low-GI, characterised by desirable texture properties.

7.5 References

Alvarez-Jubete, L., Auty, M., Arendt, E.K., et al. (2010) Baking properties and microstructure of pseudocereal flours in gluten-free bread formulations. *European Food Research and Technology*, 230 (3): 437–445. doi:10.1007/s00217-009-1184-z.

Amagliani, L., O'Regan, J., Kelly, A.L., et al. (2017) The composition, extraction, functionality and applications of rice proteins: A review. *Trends in Food Science & Technology*, 64: 1–12. doi:10.1016/J.TIFS.2017.01.008.

Arunan, E., Desiraju, G.R., Klein, R.A., et al. (2011) Definition of the hydrogen bond (IUPAC Recommendations 2011). *Pure and Applied Chemistry*, 83 (8): 1637–1641. https://doi.org/10.1351/PAC-REC-10-01-02

AOAC (2005a) Official methods of analysis of the Association of Analytical Chemists International. Official Methods 934.01: Gaithersburg, MD, USA.

AOAC (2005b) Official methods of analysis of the Association of Analytical Chemists International. Official Methods 933.29: Gaithersburg, MD, USA.

AOAC (2007). Official methods of analysis of Association of Analytical Chemists International. Official Methods 996.11: Gaithersburg, MD, USA.

Atkinson, F.S., Brand-Miller, J.C., Foster-Powell, K., et al. (2021) International tables of glycemic index and glycemic load values 2021: a systematic review. *The American journal of clinical nutrition*, 114 (5): 1625–1632. doi:10.1093/AJCN/NQAB233.

Bacelar, A.H., Silva-Correia, J., Oliveira, J.M., et al. (2016) Recent progress in gellan gum hydrogels provided by functionalization strategies. *Journal of Materials Chemistry B*, 4 (37): 6164–6174. doi:10.1039/C6TB01488G.

Balet, S., Guelpa, A., Fox, G., et al. (2019) Rapid Visco Analyser (RVA) as a Tool for Measuring Starch-Related Physiochemical Properties in Cereals: a Review. *Food Analytical Methods*. 12 (10) pp. 2344–2360. doi:10.1007/s12161-019-01581-w.

Bhavadharini, B., Mohan, V., Dehghan, M., et al. (2020) White Rice Intake and Incident Diabetes: A Study of 132,373 Participants in 21 Countries. *Diabetes Care*, 43 (11): 2643. doi:10.2337/DC19-2335.

Boluda-Aguilar, M., Taboada-Rodríguez, A., López-Gómez, A., et al. (2013) Quick cooking rice by high hydrostatic pressure processing. *LWT - Food Science and Technology*, 51 (1): 196–204. doi:10.1016/j.lwt.2012.09.021.

Bradbeer, J.F., Hancocks, R., Spyropoulos, F., et al. (2014) Self-structuring foods based on acid-sensitive low and high acyl mixed gellan systems to impact on satiety. *Food Hydrocolloids*, 35 (100): 522. doi:10.1016/J.FOODHYD.2013.07.014.

Bradbeer, J.F., Hancocks, R., Spyropoulos, F., et al. (2015) Low acyl gellan gum fluid gel formation and their subsequent response with acid to impact on satiety. *Food Hydrocolloids*, 43: 501–509. doi.org/10.1016/j.foodhyd.2014.07.006.

Brodkorb, A., Egger, L., Alminger, M., et al. (2019) INFOGEST static *in vitro* simulation of gastrointestinal food digestion. *Nature Protocols 2019 14:4*, 14 (4): 991–1014. doi:10.1038/s41596-018-0119-1.

Butterworth, P.J., Bajka, B.H., Edwards, C.H., et al. (2022) Enzyme kinetic approach for mechanistic insight and predictions of *in vivo* starch digestibility and the glycaemic index of foods. *Trends in Food Science and Technology*, 120: 254–264. doi:10.1016/J.TIFS.2021.11.015.

Cai, J., Chiang, J.H., Tan, M.Y.P., et al. (2016) Physicochemical properties of hydrothermally treated glutinous rice flour and xanthan gum mixture and its application in gluten-free noodles. *Journal of Food Engineering*, 186: 1–9. doi:10.1016/J.JFOODENG.2016.03.033.

Chi, C., Li, X., Zhang, Y., et al. (2018) Understanding the mechanism of starch digestion mitigation by rice protein and its enzymatic hydrolysates. *Food Hydrocolloids*, 84: 473–480. doi:10.1016/j.foodhyd.2018.06.040.

Chi, C., Li, X., Zhang, Y., et al. (2019) Modulating the *in vitro* digestibility and predicted glycemic index of rice starch gels by complexation with gallic acid. *Food Hydrocolloids*, 89: 821–828. doi:10.1016/J.FOODHYD.2018.11.016.

Choi, H.W. and Kim, H.S. (2022) Hydroxypropylation and acetylation of rice starch: effects of starch protein content. *Food Science and Biotechnology*, 31 (9): 1169. doi:10.1007/S10068-022-01106-Y.

Dang, J. and Copeland, L. (2004) Studies of the fracture surface of rice grains using environmental scanning electron microscopy. *Journal of the Science of Food and Agriculture*, 84: 707–713. doi:10.1002/jsfa.1671.

Detchewa, P., Prasajak, P., Phungamngoen, C., et al. (2022) Substitution of rice flour with rice protein improved quality of gluten-free rice spaghetti processed using single screw extrusion. *LWT*, 153: 112512. doi:10.1016/J.LWT.2021.112512.

Dome, K., Podgorbunskikh, E., Bychkov, A., et al. (2020) Changes in the Crystallinity Degree of Starch Having Different Types of Crystal Structure after Mechanical Pretreatment. *Polymers 2020, Vol. 12, Page 641*, 12 (3): 641. doi:10.3390/POLYM12030641.

Dupuis, J.H., Liu, Q. and Yada, R.Y. (2014) Methodologies for Increasing the Resistant Starch Content of Food Starches: A Review. *Comprehensive Reviews in Food Science and Food Safety*, 13 (6): 1219–1234. doi:10.1111/1541-4337.12104.

Edwards, C.H., Cochetel, N., Setterfield, L., et al. (2019) A single-enzyme system for starch digestibility screening and its relevance to understanding and predicting the glycaemic index of food products. *Food and Function*, 10 (8): 4751–4760. doi:10.1039/c9fo00603f.

Edwards, C.H., Maillot, M., Parker, R., et al. (2018) A comparison of the kinetics of *in vitro* starch digestion in smooth and wrinkled peas by porcine pancreatic alpha-amylase. *Food Chemistry*, 244 (June 2017): 386–393. doi:10.1016/j.foodchem.2017.10.042.

Edwards, C.H., Warren, F.J., Milligan, P.J., et al. (2014) A novel method for classifying starch digestion by modelling the amylolysis of plant foods using first-order enzyme kinetic principles. *Food and Function*, 5 (11): 2751–2758. doi:10.1039/c4fo00115j.

Ellepola, S.W., Siu, M.C. and Ma, C.Y. (2005) Conformational study of globulin from rice (Oryza sativa) seeds by Fourier-transform infrared spectroscopy. *International Journal of Biological Macromolecules*, 37 (1–2): 12–20. doi:10.1016/J.IJBIOMAC.2005.07.008.

Ertaş, N., Aslan, M. and Çevik, A. (2022) Improvement of Structural and Nutritional Quality of Gluten Free Pasta. *https://doi.org/10.1080/15428052.2021.2020198*. doi:10.1080/15428052.2021.2020198.

FAOSTAT (2023), Food and Agricultural Organization of the United Nations, Statistics Division (FAOSTAT).Available at: https://www.fao.org/faostat/en/#data/FBS (Accessed: 3 August 2023).

Farooq, M.A., Murtaza, M.A., Aadil, R.M., et al. (2021) Investigating the structural properties and *in vitro* digestion of rice flours. *Food Science & Nutrition*, 9 (5): 2668–2675. doi:10.1002/FSN3.2225.

Feng, Y.Y., Mu, T.H., Zhang, M., et al. (2020) Effects of ionic polysaccharides and egg white protein complex formulations on dough rheological properties, structure formation and *in vitro* starch digestibility of wet sweet potato vermicelli. *International Journal of Biological Macromolecules*, 149: 1170–1179. doi:10.1016/J.IJBIOMAC.2020.02.020.

Fernandes, J.M., Madalena, D.A., Pinheiro, A.C., et al. (2020) Rice *in vitro* digestion: application of INFOGEST harmonized protocol for glycemic index determination and starch morphological study. *Journal of Food Science and Technology*, 57 (4): 1393. doi:10.1007/S13197-019-04174-X.

Fetouhi, A., Benatallah, L., Nawrocka, A., et al. (2019) Investigation of viscoelastic behaviour of rice-field bean gluten-free dough using the biophysical characterization of proteins and starch: a FT-IR study. *Journal of Food Science and Technology*, 56 (3): 1316–1327. doi:10.1007/s13197-019-03602-2.

Garcia-Valle, D.E., Bello-Pérez, L.A., Agama-Acevedo, E., et al. (2021a) Effects of mixing, sheeting, and cooking on the starch, protein, and water structures of durum wheat semolina and chickpea flour pasta. *Food Chemistry*, 360: 129993. doi:10.1016/J.FOODCHEM.2021.129993.

Goñi, I., Garcia-Alonso, A. and Saura-Calixto, F. (1997) A starch hydrolysis procedure to estimate glycemic index. *Nutrition Research*, 17 (3): 427–437. doi:10.1016/S0271-5317(97)00010-9.

Guo, J., Liu, Y.C., Yang, X.Q., et al. (2014) Fabrication of edible gellan gum/soy protein ionic-covalent entanglement gels with diverse mechanical and oral processing properties. *Food Research International*, 62: 917–925. doi:10.1016/J.FOODRES.2014.05.014.

Han, H.M., Cho, J.H. and Koh, B.K. (2011) Processing properties of Korean rice varieties in relation to rice noodle quality. *Food Science and Biotechnology*, 20 (5): 1277–1282. doi:10.1007/S10068-011-0176-5/METRICS.

He, H., Chi, C., Xie, F., et al. (2020) Improving the *in vitro* digestibility of rice starch by thermomechanically assisted complexation with guar gum. *Food Hydrocolloids*, 102. doi:10.1016/j.foodhyd.2019.105637.

Jones, A.L., 2017. The gluten-free diet: fad or necessity? Diabetes Spectrum, 30(2), pp.118-123. doi.org/10.2337/ds16-0022

Hu, E.A., Pan, A., Malik, V., et al. (2012) White rice consumption and risk of type 2 diabetes: Meta-analysis and systematic review. *BMJ (Online)*, 344 (7851): 1–9. doi:10.1136/bmj.e1454.

Huang, S., Chi, C., Li, X., et al. (2022) Understanding the structure, digestibility, texture and flavour attributes of rice noodles complexation with xanthan and dodecyl gallate. *Food Hydrocolloids*, 127: 107538. doi:10.1016/J.FOODHYD.2022.107538.

Janardhnan, S. and Sain, M. (2011) Isolation of cellulose nanofibers: Effect of biotreatment on hydrogen bonding network in wood fibres. *International Journal of Polymer Science*, 2011. doi:10.1155/2011/279610.

Jayaprakash, G., Bains, A., Chawla, P., et al. (2022) A Narrative Review on Rice Proteins: Current Scenario and Food Industrial Application. *Polymers*. 14 (15). doi:10.3390/polym14153003.

Jeong, S., Kim, H.W. and Lee, S. (2017) Rheological and secondary structural characterization of rice flour-zein composites for noodles slit from the gluten-free sheeted dough. *Food Chemistry*, 221: 1539–1545. doi:10.1016/J.FOODCHEM.2016.10.139.

Khatun, A., Waters, D.L.E. and Liu, L. (2020) The impact of rice protein on *in vitro* rice starch digestibility. *Food Hydrocolloids*, 109: 106072. doi:10.1016/J.FOODHYD.2020.106072.

Khin, M.N., Ahammed, S. and Zhong, F. (2021) Development of DTAF-labelled polysaccharides for characterization of microstructure and phase distribution of composite hydrogel visualization of hydrogels using CLSM. *Food Bioscience*, 41: 100909. doi:10.1016/J.FBIO.2021.100909.

Khosravi-Boroujeni, H., Sarrafzadegan, N., Mohammadifard, N., et al. (2013) White rice consumption and CVD risk factors among Iranian population. *Journal of Health, Population and Nutrition*, 31 (2): 252–261. doi:10.3329/jhpn.v31i2.16390.

Kraithong, S. and Rawdkuen, S. (2020) Effects of food hydrocolloids on quality attributes of extruded red Jasmine rice noodle. *PeerJ*, 8. https://doi.org/10.7717/peerj.10235

Laleg, K., Barron, C., Santé-Lhoutellier, V., et al. (2016) Protein enriched pasta: structure and digestibility of its protein network. *Food & function*, 7 (2): 1196–1207. doi:10.1039/C5FO01231G.

Lee, C.M., Kubicki, J.D., Fan, B., et al. (2015) Hydrogen-Bonding Network and OH Stretch Vibration of Cellulose: Comparison of Computational Modeling with Polarized IR and SFG Spectra. *Journal of Physical Chemistry B*, 119 (49): 15138–15149. doi.org/10.1021/acs.jpcb.5b08015

Li, C. & Hu, Y. (2020) Combination of parallel and sequential digestion kinetics reveals the nature of digestive characteristics of short-term retrograded rice starches. *Food Hydrocolloids*, 108. doi:10.1016/j.foodhyd.2020.106071.

Likitwattanasade, T. & Hongsprabhas, P. (2010) Effect of storage proteins on pasting properties and microstructure of Thai rice. *Food Research International*, 43 (5): 1402–1409. doi:10.1016/J.FOODRES.2010.04.011.

Lu, X., Ma, R., Zhan, J., et al. (2022) Mechanism of peptides from rice hydrolyzed proteins hindering starch digestion subjected to hydrothermal treatment. *npj Science of Food 2022 6:1*, 6 (1): 1–8. doi:10.1038/s41538-022-00153-3.

Lu, X., Ma, R., Zhan, J., et al. (2023) Starch digestion retarded by wheat protein hydrolysates with different degrees of hydrolysis. *Food Chemistry*, 408. doi:10.1016/j.foodchem.2022.135153.

Milas, M. & Rinaudo, M., 1996. The gellan sol-gel transition. Carbohydrate Polymers, 30(2-3), pp.177-184. doi.org/10.1016/S0144-8617(96)00090-2

Morreale, F., Boukid, F., Carini, E., et al. (2019) An overview of the Italian market for 2015: cooking quality and nutritional value of gluten-free pasta. *International Journal of Food Science & Technology*, 54 (3): 780–786. doi:10.1111/IJFS.13995.

Morris, E.R., Nishinari, K. and Rinaudo, M. (2012) Gelation of gellan - A review. *Food Hydrocolloids*. 28 (2) pp. 373–411. doi:10.1016/j.foodhyd.2012.01.004.

Özyurt, G., Uslu, L., Yuvka, I., et al. (2015) Evaluation of the Cooking Quality Characteristics of Pasta Enriched with Spirulina Platensis. *Journal of Food Quality*, 38 (4): 268–272. doi:10.1111/JFQ.12142.

Patel, H., Day, R., Butterworth, P.J., et al. (2014) A mechanistic approach to studies of the possible digestion of retrograded starch by α-amylase revealed using a log of slope (LOS) plot. *Carbohydrate Polymers*, 113: 182–188. doi:10.1016/j.carbpol.2014.06.089.

Phongthai, S., D'Amico, S., Schoenlechner, R., et al. (2017) Effects of protein enrichment on the properties of rice flour-based gluten-free pasta. *LWT*, 80: 378–385. doi:10.1016/j.lwt.2017.02.044.

Ranawana, V., Clegg, M.E., Shafat, A., et al. (2011) Postmastication digestion factors influence glycemic variability in humans. *Nutrition Research*, 31 (6): 452–459. doi:10.1016/J.NUTRES.2011.05.006.

Ranawana, V., Monro, J.A., Mishra, S., et al. (2010) Degree of particle size breakdown during mastication may be a possible cause of interindividual glycemic variability. *Nutrition research.*30 (4): 246–254. doi:10.1016/J.NUTRES.2010.02.004.

Rodríguez-Hernández, A.I., Durand, S., Garnier, C., et al. (2006) Rheology-structure properties of waxy maize starch–gellan mixtures. *Food Hydrocolloids*, 20 (8): 1223–1230. doi:10.1016/J.FOODHYD.2006.01.007.

Rosa-Sibakov, N., Heiniö, R.L., Cassan, D., et al. (2016) Effect of bioprocessing and fractionation on the structural, textural and sensory properties of gluten-free faba bean pasta. *LWT - Food Science and Technology*, 67: 27–36. doi:10.1016/J.LWT.2015.11.032.

Rudra, S.G., Anand, V., Kaur, C., et al. (2020) Hydrothermal Treatment to Improve Processing Characteristics of Flour for Gluten-Free Pasta. *Starch/Staerke*, 72 (9–10). doi:10.1002/star.201900320.

Rupenthal, I.D., Green, C.R. & Alany, R.G. (2011) Comparison of ion-activated in situ gelling systems for ocular drug delivery. Part 1: physicochemical characterisation and *in vitro* release. *International journal of pharmaceutics*, 411 (1–2): 69–77. doi:10.1016/J.IJPHARM.2011.03.042.

Santos, T.P. and Cunha, R.L. (2018) Role of process variables on the formation and *in vitro* digestion of gellan gels. *Carbohydrate Polymers*, 192: 111–117. doi:10.1016/J.CARBPOL.2018.03.062.

Sofi, S.A., Singh, J., Chhikara, N., et al. (2020) Quality characterization of gluten-free noodles enriched with chickpea protein isolate. *Food Bioscience*, 36: 100626. doi:10.1016/J.FBIO.2020.100626.

Song, J.Y., Kwon, J.Y., Choi, J., et al. (2006) Pasting Properties of Non-waxy Rice Starch-Hydrocolloid Mixtures. *Starch - Stärke*, 58 (5): 223–230. doi:10.1002/STAR.200500459.

Souza Almeida, F. and Kawazoe Sato, A.C. (2019) Structure of gellan gum–hydrolyzed collagen particles: Effect of starch addition and coating layer. *Food Research International*, 121: 394–403. doi:10.1016/j.foodres.2019.03.057.

Steglich, T., Bernin, D., Röding, M., et al. (2014) Microstructure and water distribution of commercial pasta studied by microscopy and 3D magnetic resonance imaging. *Food Research International*, 62: 644–652. doi:10.1016/J.FOODRES.2014.04.004.

Suo, X., Dall'Asta, M., Giuberti, G., et al. (2022) The effect of chickpea flour and its addition levels on quality and *in vitro* starch digestibility of corn–rice-based gluten-free pasta. 73 (5): 600–609. doi:10.1080/09637486.2022.2040008.

Suo, X., Mosca, A.C., Pellegrini, N., et al. (2021) Effect of pasta shape and gluten on pasta cooking quality and structural breakdown during mastication. *Food & Function*, 12 (22): 11577–11585. doi:10.1039/D1FO02339J.

Tako, M., kitajima, S., Yogi, T., et al. (2016) Structure-Function Relationship of a Gellan Family of Polysaccharide, S-198 Gum. *Advances in Biological Chemistry*, 6 (3): 55–69. doi:10.4236/ABC.2016.63007.

Tamura, M., Kumagai, C., Kaur, L., et al. (2021) Cooking of short, medium and long-grain rice in limited and excess water: Effects on microstructural characteristics and gastro-small intestinal starch digestion *in vitro*. *LWT*, 146: 111379. doi:10.1016/J.LWT.2021.111379.

Tamura, M., Nagai, T., Hidaka, Y., et al. (2014) Changes in nonwaxy Japonica rice grain textural-related properties during cooking. *Journal of Food Quality*, 37 (3): 177–184. doi:10.1111/jfq.12085.

Tamura, M., Okazaki, Y., Kumagai, C., & Ogawa, Y. (2017). The importance of an oral digestion step in evaluating simulated *in vitro* digestibility of starch from cooked rice grain. In *Food Research International* (Vol. 94). Elsevier Ltd. doi.org/10.1016/j.foodres.2017.01.019

Tamura, M., Singh, J., Kaur, L., et al. (2016) Impact of structural characteristics on starch digestibility of cooked rice. *Food Chemistry*, 191: 91–97. doi:10.1016/j.foodchem.2015.04.019.

Thuengtung, S., Matsushita, Y. & Ogawa, Y. (2019) Comparison between microwave-cooking and steam-cooking on starch properties and *in vitro* starch digestibility of cooked pigmented rice. *Journal of Food Process Engineering*, 42 (6): e13150. doi:10.1111/JFPE.13150.

Toutounji, M.R., Farahnaky, A., Santhakumar, A.B., et al. (2019) Intrinsic and extrinsic factors affecting rice starch digestibility. *Trends in Food Science and Technology*. 88 pp. 10–22. doi:10.1016/j.tifs.2019.02.012.

Truong, T.H., Yuet, W.C. and Hall, M.D. (2014). The glycemic index of American-grown jasmine rice is classified as high. International Journal of Food Sciences and Nutrition*.2013.869797*, 65 (4): 436–439. doi:10.3109/09637486.2013.869797.

Villemejane, C., Wahl, R., Aymard, P., et al. (2015) *In vitro* digestion of short-dough biscuits enriched in proteins and/or fibres, using a multi-compartmental and dynamic system (1): Viscosity measurement and prediction. *Food Chemistry*, 182: 55–63. doi:10.1016/J.FOODCHEM.2015.02.125.

Wang, L., Zhang, L., Wang, H., et al. (2020) Insight into protein-starch ratio on the gelatinization and retrogradation characteristics of reconstituted rice flour. *International Journal of Biological Macromolecules*, 146: 524–529. doi:10.1016/j.ijbiomac.2020.01.048.

Wang, M., Hettiarachchy, N.S., Qi, M., et al. (1999) Preparation and functional properties of rice bran protein isolate. *Journal of agricultural and food chemistry*, 47 (2): 411–416. doi:10.1021/JF9806964.

Wang, S., Li, P., Zhang, T., et al. (2017a) *In vitro* starch digestibility of rice flour is not affected by the method of cooking. *LWT*, 84: 536–543. doi:10.1016/J.LWT.2017.06.023.

Wang, S., Li, P., Zhang, T., et al. (2017b) Trypsin and chymotrypsin are necessary for *in vitro* enzymatic digestion of rice starch. *RSC Advances*, 7 (7): 3660–3666. doi:10.1039/C6RA24816K.

Wang, Y.R., Yang, Q., Fan, J.L., et al. (2019) The effects of phosphorylation modification on the structure, interactions and rheological properties of rice glutelin during heat treatment. *Food Chemistry*, 297: 124978. doi:10.1016/J.FOODCHEM.2019.124978.

Warren, F.J., Gidley, M.J. and Flanagan, B.M. (2016) Infrared spectroscopy as a tool to characterise starch ordered structure—a joint FTIR–ATR, NMR, XRD and DSC study. *Carbohydrate Polymers*, 139: 35–42. doi:10.1016/J.CARBPOL.2015.11.066 .

Wu, J., Xu, S., Yan, X., et al. (2022) Effect of Homogenization Modified Rice Protein on the Pasting Properties of Rice Starch. *Foods 2022, Vol. 11, Page 1601*, 11 (11): 1601. doi:10.3390/FOODS11111601.

Xu, J., Wang, R., Liu, W., et al. (2023) The specificity of ten non-digestible carbohydrates to enhance butyrate-producing bacteria and butyrate production *in vitro* fermentation. *Food Science and Human Wellness*, 12 (6): 2344–2354. doi:10.1016/J.FSHW.2023.03.038.

Yang, X., Li, Y., Li, S., et al. (2018) Effects of ultrasound-assisted α-amylase degradation treatment with multiple modes on the extraction of rice protein. *Ultrasonics Sonochemistry*, 40 (August 2017): 890–899. doi:10.1016/j.ultsonch.2017.08.028.

Yi, X., Li, E., Yu, S., et al. (2022) Combined effects of starch fine molecular structures and water content on starch digestibility of cooked white rice. *International Journal of Biological Macromolecules*, 215: 192–202. doi:10.1016/J.IJBIOMAC.2022.06.116.

Ying, D., Hlaing, M.M., Lerisson, J., et al. (2017) Physical properties and FTIR analysis of rice-oat flour and maize-oat flour based extruded food products containing olive pomace. *Food Research International (Ottawa)*, 100 (Pt 1): 665–673. doi:10.1016/j.foodres.2017.07.062.

Yu, L., Turner, M.S., Fitzgerald, M., et al. (2017) Review of the effects of different processing technologies on cooked and convenience rice quality. *Trends in Food Science & Technology*, 59: 124–138. doi:10.1016/J.TIFS.2016.11.009.

Yu, W., Zhou, X. and Li, C. (2021) Application of first-order kinetics modelling to reveal the nature of starch digestion characteristics. *Food & Function*, 12 (15): 6652–6663. doi:10.1039/D1FO00450F.

Zavitsanou, S., Massa, J., Deshpande, S., et al. (2019) The Effect of Two Types of Pasta Versus White Rice on Postprandial Blood Glucose Levels in Adults with Type 1 Diabetes: A Randomized Crossover Trial. Diabetes Technology & Therapeutics.,21 (9): 485–492. doi:10.1089/DIA.2019.0109.

Zhai, J., Li, X., Svensson, B., et al. (2023) Increasing Protein Content of Rice Flour with Maintained Processability by Using Granular Starch Hydrolyzing Enzyme. *Molecules*, 28 (8). doi:10.3390/molecules28083522.

Zhu, B., Zhan, J., Chen, L., et al. (2020a) Amylose crystal seeds: Preparation and their effect on starch retrogradation. *Food Hydrocolloids*, 105: 105805. doi:10.1016/J.FOODHYD.2020.105805.

Zhu, L., Wu, G., Zhang, H., et al. (2018) Using RVA-full pattern fitting to develop rice viscosity fingerprints and improve type classification. *Journal of Cereal Science*, 81: 1–7. doi:10.1016/J.JCS.2018.02.013.

Zou, W., Sissons, M., Gidley, M.J., et al. (2015) Combined techniques for characterising pasta structure reveal how the gluten network slows enzymic digestion rate. *Food Chemistry*, 188: 559–568. doi:10.1016/j.foodchem.2015.05.032.

8 General discussions, conclusions, and recommendations for future work

8.1 General discussions and conclusions

The aim of this PhD thesis was to evaluate potential methods to modify starch in rice to decrease its starch digestibility, and to formulate low-glycaemic index (low-GI) rice-based products by understanding the composition, structure and function of rice protein-starch matrices. This aligns with the principles of biomimetic design (Do et al., 2018), where the configuration of starch-entrapped matrices in low-GI rice varieties (whether naturally occurring or created through physical means - parboiling) was replicated. The findings of this thesis could help develop several types of low-GI foods with health potential.

The principle upon which low-GI food could be effectively produced is to preserve the functional properties (i.e. slowing starch enzymatic digestion) of starch-entrapped matrices when subjected to digestion (resulting in structural disruption, enzyme attack, and pH change).

Therefore, knowing the mechanisms by which digestion affects the rice microstructure is a key element to understand how to preserve the protein-starch matrices. To understand the relationship microstructure-digestion, it may be useful to refer to foods with already proven health effects, such as parboiled rice.

An important contribution to preserve the protein-starch matrices microstructure and control rice starch digestion rate could come from low acyl gellan gum (LAGG), an indigestible hydrocolloid. LAGG was chosen in this thesis as a representative hydrocolloid because it is widely used in the food industry as a thickener, emulsifier, gelling agent, and stabiliser (Norton et al., 2011; Fang et al., 2018; Nooshkam & Varidi, 2021). It also exhibits medical and nutritional values as an encapsulation medium for functional compounds that require extended-time release (Omoto et al., 1999; Ferris et al., 2013; Bacelar et al., 2016; Milivojevic et al., 2019;). There has been limited discussion of LAGG's effects on mitigating starch digestibility and their

underlying mechanisms, and this study attempts to fill the gap. The work discussed in the four experimental chapters (4 to 7) was focused on the following objectives:

- Understand the effect of cooking on the characteristics of the protein networks concerning starch digestibility in white rice (**Chapter 4**).
- Understand the effect of protein hydrolysis on the impact of starch digestibility in white rice (**Chapter 5**).
- Utilise a semi-dynamic digestion system to create a complex digestion scenario to understand the digestive response of cooked white rice (**Chapter 6**).
- Study the role of low acyl gellan gum in preserving the microstructure of white rice upon cooking (**Chapters 4** to **7**).
- Based on the results of chapters 4, 5, and 6, develop a formulation to bio-mimic the protein-starch matrices and create food with low-GI properties (**Chapter 7**).

8.1.1 The protein-starch matrices play a role in regulating rice starch digestibility *in vitro*

In this study, the influence of protein-starch matrices on rice starch digestibility *in vitro* was investigated. Rice grain, like many cereals (such as corn and wheat), contains protein, which can encapsulate starch granules on a micron scale. Same as many cereals, rice also requires hydrothermal treatment (such as boiling) and cooling until it is suitable for consumption (Jamilah et al., 2009; Bravo-Núñez et al., 2019; Zheng et al., 2021). During cooking, physicochemical changes in proteins (denaturation) and starches (gelatinisation and retrogradation) occur, causing changes in the matrix organisation and interaction between these two components. Therefore, the primary research questions focused on understanding the physiochemical changes and structural interactions between proteins and starches during cooking and their subsequent effects on starch digestibility. Among the most consumed types of white rice with clinic-confirmed GI values, a high-and low-GI rice variety were selected, namely Jasmine white rice (JR; high-GI) and parboiled white rice (PR; low-GI).

The results demonstrated that changes in the proteins present in the matrices contributed to the inhibitory effects on starch digestibility in cooked rice. As a result of the absence of protein (protein extraction), JR starch showed individual starch granules were released (morphology). The JR starch molecule was characterised by a large number of branched helices that grouped neatly into crystalline arrays (shown by FTIR), identified with an A-type pattern with high relative crystallinity (shown by XRD). However, the crystallinity was easily lost during cooking, causing the starch to be highly digestible. Comparable results have been reported in high-GI basmati rice varieties by Gunathilaka and Ekanayake (2015), and in cooked RF by Wang et al. (2017). These results suggested that the high concentration of amylopectin was favourable for water penetration upon heating, thus promoting the role of α-amylase during digestion, thereby explaining the high digestibility of JR starch.

In contrast, protein networks act as a barrier to starch gelatinisation by limiting water access and swelling space, and by decreasing amylase accessibility to starch. This results in decreased starch digestion in JR flour, and even further reduction in JR grain, due to the higher density of the protein-starch matrices in the grain.

Researchers have previously demonstrated that the starch-protein interactions in the matrices are multi-scale (e.g., molecular orders, nanoscale structure and morphology), and occur through different types of bonds (e.g., hydrogen bonds, Van der Waals forces, hydrophobic interactions, etc.) (Scott & Awika, 2023; Shi et al., 2020; J. Wang et al., 2021; Zhang et al., 2022). In the presence of heat and water during cooking, these interactions can be disrupted. As shown in this study, protein denaturation occurs during cooking, with change in their three-dimensional structure (observed in FTIR). Denaturation affects protein interaction with water (solubility), other proteins (aggregation), and starch (V-type complex); these interactions are all vital to determine the initial digestion of starch. Due to the more compact microstructure of rice grains, the level of intrinsic interactions within the protein-starch matrices remains higher than that of JR flour and starch, resulting in an increasingly challenging amylase degradation process.

8.1.2 Disruption of the macroscopic-scale structure in rice increased starch digestibility during *in vitro* digestion.

A novelty of this study was to understand how increasing starch digestibility along with (*in vitro*) digestion, was related to a progressive rice grain microstructure degradation. This effect became larger when an oral digestion simulation step (homogenisation) was included. More extensive homogenisation (20 s) caused higher starch digestibility than less extensive homogenisation (10 s).The static *in vitro* digestion models with a multi-enzyme system revealed a progressive hydrolysis of the rice protein networks. During gastric phase, the protein-starch matrices are degraded due to the acidic environment (pH=3), causing protein denaturation and higher exposure to enzymatic cleavage. Changes in ionic strength can also affect the electrostatic interactions and binding properties of the matrix components, potentially affecting its ability to inhibit starch digestion.

Findings in this thesis (**Chapter 5**) suggest that the enzymatic removal of proteins from the matrices during gastric (pepsin) and intestinal (trypsin from pancreatin) makes starch more digestible, as also reported by Ma et al. (2020) and Ye et al. (2019). However, the peptides released upon digestion may also have an important role in promoting or inhibiting starch digestibility. This role is not clear yet, and future research may focus on the effect of peptides on regulating starch digestibility.

The possible reasons for increased starch digestibility upon digestion may be: i) loss of matrix physical barrier function between starch and amylase, ii) disruption of stabilising interactions (e.g., hydrogen bonds, hydrophobic interactions) between protein and starch during cooking, promoting binding of digestive enzymes to starch.

8.1.3 Modifying the protein-starch matrices microstructure may affect *in vitro* starch digestibility.

In this thesis, the lower starch digestibility and pGI in cooked PR compared with JR grains, was explained by differences in the protein-starch matrices. Compared to JR, PR partially contains denatured proteins and pre-gelatinised starch, which may

create a stronger and more compact matrices, which can act as a physical barrier and inhibit the activity of digestive enzymes (Hasbullah et al., 2017; Tian et al., 2018). Moreover, PR contains slow-digestible starch and characteristic protein-starch complexes, which decrease the amount of glycosidic bonds exposed to amylase. The presence of peptides and amino acids generated from denatured protein has been reported to exhibit inhibited function on α-amylose by bonding to active site of the enzyme or interacting with the complex of enzyme-substrates (Chi et al., 2018).

8.1.4 LAGG addition decreased starch digestibility.

An important finding in this thesis was the reduced starch digestibility (and pGI) in cooked rice containing LAGG than in that without LAGG, both in intact and homogenised rice. Various mechanism occurring during rice cooking and digestion could be responsible for this mitigating action of LAGG. i) LAGG-coating of the grain periphery, masking the pores and tunnels, acting as a physical barrier to enzymes from the external, and preventing starch leaching from the inside of the grain. ii) Water competition with starch, reducing the amount of free water available for starch gelatinisation. iii) Starch-LAAG complex formation, preventing starch granules from being accessible to enzymes. iv) Enhanced LAGG gel cohesiveness in acidic gastric environment, due to LAGG ionisation and more effective interaction with cations (Norton et al., 2011; Bradbeer et al., 2015). v) Increased digesta viscosity, which hinders the movement of starch and enzymes in the digestive tract. vi) Larger particle size of the homogenised samples containing LAGG compared with the ones without LAGG, perhaps exposing less starch surface area for the possible interactions with enzymes.

8.1.5 A food model system (rice-based orzo pasta) with reduced pGI was produced based on the findings in this thesis

In **Chapter 7**, a pasta-type (orzo shape) food model was developed and appraised, based on the findings from **Chapter 4**, **5**, and **6**. The microstructure of this food consisted of starch granules entrapped by a protein and/or protein-LAGG matrices. Orzo samples were prepared using four formulas: only RF, single and binary blends

of RPs and LAGG (illustrated in **Fig. 8.1**). Two media were used for cooking orzo: water and aqueous LAGG dispersion.

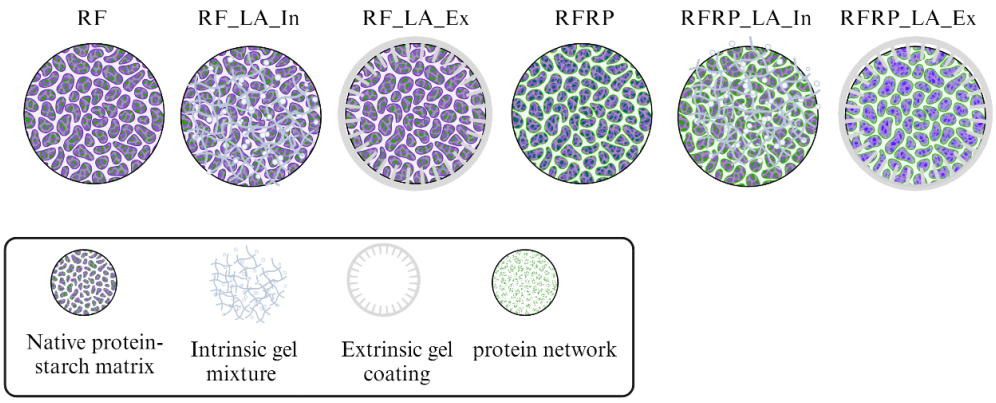


Fig. 8.1. Schematic of the orzo pasta microstructure, inspired by PR and cooked with LAGG in six different formulations. Legend: RF, rice flour; RF_LA_In, RF with the addition of LAGG via dough-making (intrinsic addition); RF_LA_Ex, cooking RF pasta in LAGG dispersion (extrinsic addition); RFRP, RF with the addition of rice protein (RP) via dough-making (intrinsic addition); RFRP_LA_In, RF with the addition of RP and LAGG via dough-making (intrinsic addition); RFRP_LA_Ex, cooking RFRP pasta in LAGG dispersion (extrinsic addition).

Results showed that LAGG addition to the orzo formulation creates the matrices that can function as a physical barrier against α-amylase access to entrapped starch, similar to cooked PR. This effect can be enhanced by protein addition.

Orzo-shaped pasta containing RP and LAGG in the matrices exhibited the lowest starch digestibility and pGI. The higher ordering structure and viscosity of the intestinal phase could explain this.

8.2 Novelty of the research

This research is grounded in the principles of biomimetic design, which involves replicating and enhancing the structural configurations characterised in low-GI rice varieties. The work presented here offers potential in both the fundamental understanding of rice practical applications and nutritional contribution for food industries and consumers. Specifically, the novelty contribution consists of the following features:

i). Biomimetic design approach: By employing biomimetic principles, the study seeks to better understand and reproduce the protein-starch matrices that are more promising for reducing starch digestibility, offering innovative ways of developing foods with health benefits.

ii) Role of LAGG: Demonstrating the effectiveness of LAGG in reducing starch digestibility, and potentially increasing satiety. The addition methods explored in this study are simple additions in domestic cooking and more complex additions in a rice-based product formulation.

iii).Semi-dynamic digestion model: Introduction of a new dynamic *in vitro* digestion model that simulates more complex digestion conditions related to in vivo, providing better insights into how food structure affects starch digestibility and pGI in response dynamic digestion conditions.

iv) Low-GI rice-based formulation: Development of a novel rice-based formulation that combines rice flour, RP, and LAGG to achieve low-GI properties, expanding the applications of low-GI formulations.

By leveraging the principles of biomimetic design and the functional properties of LAGG, we have introduced novel methods to enhance the structural and digestibility characteristics of rice. The introduction of a semi-dynamic digestion model and the creation of rice-based orzo pasta further illustrate the practical applications and potential impact of this work. These contributions provide a foundation for future research and innovation in the field of food science, with the potential to improve public health through the development of healthier carbohydrate-based foods.

8.3 Recommendation of future work

Work in this thesis showed the possibility of controlling the glycaemic index of rice/rice-based products by understanding the role of protein-starch matrices and LAGG. Despite the global importance of rice as a staple food, and the promising results shown by LAGG in decreasing starch digestibility, the field of exploration in the near future could be expanded.

Potential areas to be explored are here reported:

i) Use of other proteins and starches from different plant-based materials, and hydrocolloids (e.g., xanthan or blends), to manufacture low-GI foods. This would generalise the findings to a broader range of food applications.

ii) Enhanced oral processing simulation: The oral processing simulation using a household blender does not perfectly replicate the complex mechanical and enzymatic processes occurring during mastication. While this method provides a practical approximation, it lacks the nuanced movements and varying pressures of human chewing, which may influence the breakdown and initial digestion of food. Therefore, this can be improved by the use of dynamic oral simulators developed by the University of Leeds or other oral mastication simulators.

iii) Weight and size changes during digestion: This study did not account for the weight and size changes in the rice samples during digestion due to water absorption, enzymatic breakdown, and response to mixing. These changes can all affect the concentration and distribution of digestive enzymes and the accessibility of starch granules, potentially influencing the overall digestibility results. Future studies can develop methods to monitor weight and size changes during digestion. These include water absorption by measuring water content before and after digestion using gravimetric analysis or moisture analysers. The reduction of particle weight/size due to enzymatic breakdown can be monitored using size-exclusion chromatography with multi-angle light scattering.

iv) Interaction between protein and starch: The study focused on the microstructural encapsulation of starch by the protein matrices but did not extensively explore the chemical interactions (e.g., hydrogen bonding, hydrophobic and charge-dipole interactions), which can significantly influence starch digestibility. Analytical techniques like FTIR and Raman spectroscopy could provide insights into these interactions by identifying specific functional groups involved in the bonding. Nuclear Magnetic Resonance Spectroscopy can be used to investigate the changes of double helices, single helix and amorphous fractions, respectively, which can be affected by presence and interactions with protein and hydrocolloids. Additionally, methods like zeta potential measurements can be used to study the surface charge

interactions of protein-starch complexes, revealing how these interactions affect the stability and digestibility of starch. Rheological studies can understand changes in viscosity and texture of the digested matrices, which can be correlated with physical state and strength of matrices in the digested samples.

v) Developing the semi-dynamic digestion system and expanding its applications, to better simulate the human gastrointestinal tract. This can be achieved by incorporating more advanced control of digestive parameters, such as pH, enzyme concentrations, and peristaltic movements. Additionally, the application of this system could be expanded to study the digestibility of a broader range of foods, including different grains, legumes, and processed foods. Future work can first include improvement of the simulated gastric and intestinal phases by using enzyme mixtures with progressive additions (incremental secretion), and pH profiles that change over time, and mimic gastric emptying conditions. Secondly, a model for nutrient absorption could be included to study how different food components affect the bioavailability of nutrients. The third aspect is to develop personalised model-based digestion systems that can account for differences in chewing conditions, enzyme levels, and transit times in infants, senior adults, and other digestive physiology variations. It is possible to tailor dietary recommendations based on this information.

By addressing these limitations and exploring these specific future work avenues, research in this field can advance the understanding of starch digestibility and contribute to the development of healthier, low-GI food products. These experiments will not only validate the protective mechanisms of the protein-LAGG network but also guide the formulation of rice products with improved health benefits.

8.4 References

Aleixandre, A., Benavent-Gil, Y. & Rosell, C.M. (2019) Effect of bread structure and *in vitro* oral processing methods in bolus disintegration and glycemic index. *Nutrients*, 11 (9). doi.org/10.3390211092105

Bacelar, A.H., Silva-Correia, J., Oliveira, J.M., et al. (2016) Recent progress in gellan gum hydrogels provided by functionalization strategies. *Journal of Materials Chemistry B*, 4 (37): 6164–6174. doi:10.1039/C6TB01488G.

Blanquet-Diot, S., François, O., Denis, S., et al. (2021) Importance of oral phase *in vitro* starch digestibility related to wholegrain versus refined pastas and mastication impairment. *Food Hydrocolloids*, 112. doi:10.1016/j.foodhyd.2020.106277.

Bradbeer, J.F., Hancocks, R., Spyropoulos, F., et al. (2015) Low acyl gellan gum fluid gel formation and their subsequent response with acid to impact on satiety. *Food Hydrocolloids*, 43: 501–509. doi.org/10.1016/j.foodhyd.2014.07.006

Bravo-Núñez, Á., Garzón, R., Rosell, C.M., et al. (2019) Evaluation of starch-protein interactions as a function of pH. *Foods*, 8 (5): 2–11. doi:10.3390/foods8050155.

Brodkorb, A., Egger, L., Alminger, M., et al. (2019) INFOGEST static *in vitro* simulation of gastrointestinal food digestion. *Nature Protocols 2019 14:4*, 14 (4): 991–1014. doi.org/10.1038/s41596-018-0119-1

Cassanelli, M., Prosapio, V., Norton, I., et al. (2018). Acidified/basified gellan gum gels: The role of the structure in drying/rehydration mechanisms. Food Hydrocolloids, 82, pp.346-354. doi:10.1016/j.foodhyd.2018.04.024.

Chen, Y., Stieger, M., Capuano, E., et al. (2022) Influence of oral processing behaviour and bolus properties of brown rice and chickpeas on *in vitro* starch digestion and postprandial glycaemic response. *European Journal of Nutrition*, 61 (8): 3961–3974. doi.org/10.1007/s00394-022-02935-7

Ferris, C.J., Gilmore, K.J., Wallace, G.G., et al. (2013) Modified gellan gum hydrogels for tissue engineering applications. *Soft Matter*, 9 (14): 3705–3711. doi:10.1039/c3sm27389j.

Guo, J., Liu, Y.C., Yang, X.Q., et al. (2014) Fabrication of edible gellan gum/soy protein ionic-covalent entanglement gels with diverse mechanical and oral processing properties. *Food Research International*, 62: 917–925. doi:10.1016/J.FOODRES.2014.05.014.

Halford, J.C.G. and Harrold, J.A. (2012) Satiety-enhancing products for appetite control: Science and regulation of functional foods for weight management. *Proceedings of the Nutrition Society*, 71 (2): 350–362. doi:10.1017/S0029665112000134.

Hiolle M, Floury J, Boulier-Monthéan N, et al. (2019) *In vitro* digestion of complex foods: How microstructure influences food disintegration and micronutrient bioaccessibility. Food Research International, 128,.108817.doi.org/10.1016/j.foodres.2019.108817

Hoad, C.L., Rayment, P., Spiller, R.C., et al. (2004) *In vivo* Imaging of Intragastric Gelation and Its Effect on Satiety in Humans. *The Journal of Nutrition*, 134 (9): 2293–2300. doi:10.1093/JN/134.9.2293.

Jamilah, B., Mohamed, A., Abbas, K.A., et al. (2009) Protein-starch interaction and their effect on thermal and rheological characteristics of a food system: A review. *Journal of Food, Agriculture and Environment*, 7 (2): 169–174.api.semanticscholar.org

Jiménez-Munoz, L., Brodkorb, A., Gómez-Mascaraque, L.G., et al. (2021) Effect of heat treatment on the digestion behaviour of pea and rice protein dispersions and their blends studied using the semi-dynamic INFOGEST digestion method. *Food and Function*, 12 (18): 8747–8759. doi:10.1039/d1fo01223a.

Kugimiya, M. (1990) Separation of Cotyledon Cells of Legumes by Successive Treatments with Acid and Alkali., Nippon Shokuhin Kogyo Gakkaishi, 37 (11): 867–871. doi:10.3136/NSKKK1962.37.11_867.

Milivojevic, M., Pajic-Lijakovic, I., Bugarski, B., et al. (2019) "Gellan gum in drug delivery applications." In *Natural Polysaccharides in Drug Delivery and Biomedical Applications*. Elsevier. pp. 145–186. doi:10.1016/B978-0-12-817055-7.00006-6.

Nadia, J., Bronlund, J., Singh, R.P., et al. (2021) Structural breakdown of starch-based foods during gastric digestion and its link to glycemic response: *In vivo* and *in vitro* considerations. *Comprehensive Reviews in Food Science and Food Safety*, 20 (3): 2660–2698. doi:10.1111/1541-4337.12749.

Niwano, Y., Adachi, T., Kashimura, J., et al. (2009) Is the glycemic index of food a feasible predictor of appetite, hunger, and satiety? *Journal of Nutritional Science and vitaminology*, 55 (3): 201–7.doi.org/10.3177/jnsv.55.201

Omoto, T., Uno, Y. & Asai, I. (1999) The latest technologies for the application of gellan gum. *Physical Chemistry and Industrial Application of Gellan Gum*, pp. 123–126. doi:10.1007/3-540-48349-7_18.

Osmałek, T., Froelich, A. & Tasarek, S. (2014) Application of gellan gum in pharmacy and medicine. *International Journal of Pharmaceutics*, 466 (1–2): 328–340. doi:10.1016/J.ijpharm.2014.03.038.

Santamaria, M., Montes, L., Garzon, R., et al. (2022) Unraveling the impact of viscosity and starch type on the *in vitro* starch digestibility of different gels. *Food & Function*, 13 (14): 7582–7590. doi:10.1039/D2FO00697A.

Sasaki, T. & Kohyama, K. (2012) Influence of non-starch polysaccharides on the *in vitro* digestibility and viscosity of starch suspensions. *Food Chemistry*, 133 (4): 1420–1426. doi:10.1016/J.FOODCHEM.2012.02.029.

Sworn, G. & Stouby, L. (2021) Gellan gum. *Handbook of Hydrocolloids*, 855–885. doi:10.1016/B978-0-12-820104-6.00009-7.

Tako, M., kitajima, S., Yogi, T., et al. (2016) Structure-Function Relationship of a Gellan Family of Polysaccharide, S-198 Gum, Produced by Alcaligenes *Advances in Biological Chemistry*, 6 (3): 55–69. doi:10.4236/ABC.2016.63007.

Tucker, R. M., & Mattes, R. D. (2013). Satiation, satiety: The puzzle of solids and liquids. Satiation, satiety and the control of food intake, 182-201. doi:10.1533/9780857098719.3.182.

Villemejane, C., Wahl, R., Aymard, P., et al. (2015) *In vitro* digestion of short-dough biscuits enriched in proteins and/or fibres, using a multi-compartmental and dynamic system (1): Viscosity measurement and prediction. *Food Chemistry*, 182: 55–63. doi:10.1016/j.foodchem.2015.02.125.

Wang, T., Yang, Y., Feng, W., et al. (2019) Co-folding of hydrophobic rice proteins and shellac in hydrophilic binary microstructures for cellular uptake of apigenin. *Food Chemistry*, 309 (October 2019): 125695. doi:10.1016/j.foodchem.2019.125695.

Zheng, M., Ye, A., Singh, H., et al. (2021) The *in vitro* digestion of differently structured starch gels with different amylose contents. *Food Hydrocolloids*, 116. doi:10.1016/j.foodhyd.2021.106647.